

Sheffield Hallam University

Plasto-hydrodynamic die-less strip drawing.

MEMON, Abdul Hameed.

Available from the Sheffield Hallam University Research Archive (SHURA) at:

<http://shura.shu.ac.uk/20055/>

A Sheffield Hallam University thesis

This thesis is protected by copyright which belongs to the author.

The content must not be changed in any way or sold commercially in any format or medium without the formal permission of the author.

When referring to this work, full bibliographic details including the author, title, awarding institution and date of the thesis must be given.

Please visit <http://shura.shu.ac.uk/20055/> and <http://shura.shu.ac.uk/information.html> for further details about copyright and re-use permissions.

6989

TELEPEN

100228570 4



17. NOV. 19.30

20/11/95 16:32.

29/1/95 19.55

30/1 17.48

30 JAN 1995

20.59

~~8 FEB~~
17.11

9 FEB
18.33.

10 FEB 1995

20:59

13/2/95
4pm.

15/2 - 20:59

16/2 - 16.51

23 FEB 1995

20:59

30.4.95

7.59pm

2 MAY 2008

6/5 - 17.00

~~10 MAY 95~~

16.14

11/5/95
16.51

12/5 17.59

19/5 - 17.59

28/5

20.00

16/6 17.59.

ProQuest Number: 10697362

All rights reserved

INFORMATION TO ALL USERS

The quality of this reproduction is dependent upon the quality of the copy submitted.

In the unlikely event that the author did not send a complete manuscript and there are missing pages, these will be noted. Also, if material had to be removed, a note will indicate the deletion.



ProQuest 10697362

Published by ProQuest LLC (2017). Copyright of the Dissertation is held by the Author.

All rights reserved.

This work is protected against unauthorized copying under Title 17, United States Code
Microform Edition © ProQuest LLC.

ProQuest LLC.
789 East Eisenhower Parkway
P.O. Box 1346
Ann Arbor, MI 48106 – 1346

PLASTO-HYDRODYNAMIC DIE-LESS STRIP DRAWING

by

ABDUL HAMEED MEMON B Eng

A Thesis submitted to the COUNCIL FOR NATIONAL ACADEMIC AWARDS

in partial fulfilment for the degree of

DOCTOR OF PHILOSOPHY

**Sponsoring Establishment: Department of Mechanical
and Production Engineering
Sheffield City Polytechnic
Sheffield, UK**

**Collaborating Establishment: Allied Steel and Wire Ltd
Castle Works
Cardiff
CF1 5XQ**

November 1988

ACKNOWLEDGEMENTS

The author gratefully acknowledges the invaluable suggestions and guidance given by Professor G R Symmons and Professor M S J Hashmi during the course of this work. Thanks are expressed to Dr R Crampton, whose suggestions were received with gratitude.

The technical assistance offered by Mr R Teasdale and his staff was much appreciated and in particular thanks go to Messrs R Sidebottom, R Tingle, R Wilkinson and M Jackson for their co-operation during the duration of this work.

The author acknowledges the assistance given by the Government of Pakistan for providing financial support towards this research and expresses his gratitude to the authorities of the Mehran University of Engineering and Technology, Jamshoro Sindh, Pakistan for granting leave, in order to complete this work.

Finally the support and encouragement of my wife and family deserve greater acknowledgement than words can express.

ABSTRACT

PLASTO-HYDRODYNAMIC DIE-LESS STRIP DRAWING

A H MEMON

A detailed investigation is carried out for a novel process of die-less strip drawing, in which conventional reduction dies have been replaced by a die-less reduction unit having a rectangular hole of stepped configuration. The smallest hole dimensions are larger than those of the incoming strip, thus eliminating direct metal to metal contact and hence the problem of die-friction and consequential die wear. The strip is plastically deformed by means of the combined effect of the hydrodynamic pressure and drag force generated in the unit due to the motion of the strip through a polymer melt.

An extensive experimental study has been undertaken, which showed that higher reductions were achieved at slower drawing speeds with gradual decrease in reduction at higher drawing speeds. The maximum reduction in area of the strip noted was about 12%. Various parameters were changed to examine their effects on the performance of the process.

Theoretical analyses have been developed considering Newtonian and non-Newtonian characteristics of the pressure medium. These analyses enable the predictions to be made of (the pressure distribution, within the reduction unit, on-set of plastic yielding of the strip material, shear and axial stresses, and the percentage reduction in strip size. The analyses incorporate critical shear stress limit of the polymer melt, the strain hardening and the strain rate sensitivity of the strip material.

The predicted results for the percentage reduction in strip size appear to under-estimate the experimental values at the slow drawing speed and over-estimate them at the higher drawing speed.

CONTENTS

	<u>Page</u>
Acknowledgements	(i)
Declaration	(ii)
Abstract	(iii)
Contents	(iv)
Index to Figures	(vii)
Index to Plates	(xvi)
Notations	(xvii)
<u>Chapter 1 : Introduction</u>	
1.1 The Drawing Process	1
1.2 Hydrodynamic Lubrication	4
1.3 Plasto-Hydrodynamic Die-Less Drawing	6
1.4 Present Work	8
<u>Chapter 2 : Design and Development of the Experimental Equipment</u>	
2.1 Description of the Existing Rig	11
2.2 Modification to the Existing Rig	11
2.3 Design of the Die-less Reduction Unit	12
2.4 Melt Chamber and Hopper	13
2.5 Instrumentation	13
2.5.1 Heater Bands	14
2.5.2 Temperature Controllers	14
2.5.3 Thermocouples	14
2.5.4 Pressure Transducers	14
2.5.5 Load Indicator	15
<u>Chapter 3 : Experimental Materials</u>	
3.1 Rheology of Polymer Melts	26
3.1.1 Introduction	26
3.1.2 Rheological Behaviour	26

	<u>Page</u>
3.1.2.1 Viscosity-Temperature Dependence	27
3.1.2.2 Viscosity-Pressure Dependence	29
3.1.2.3 Effect of Shear Rate on Viscosity	30
3.1.2.4 Flow Instabilities	31
3.2 Stress-Strain Characteristics of the Strip Material	32
 <u>Chapter 4 : Experimental Results</u>	
4.1 Experimental Procedure	42
4.2 Experimental Results	43
4.2.1 Percentage Reduction Versus Speed	44
4.2.2 Results of Pressures	87
4.2.3 Drawing Stress Versus Speed	107
4.2.4 Determination of the Deformation Profiles	128
 <u>Chapter 5 : Theoretical Analysis</u>	
5.1 Introduction	131
5.2 Analysis	131
5.3 Newtonian Solution	136
5.3.1 Assumed Deformation Profile	137
5.3.1.1 Determination of the Maximum Pressure Prior to Deformation	137
5.3.1.2 Determination of the Shear Stress in Sections A and B	138
5.3.1.3 Prediction of Yield Point	139
5.3.1.4 Hydrodynamic Pressure and Axial Stress in Deformation Zone	139
5.3.1.5 Prediction of Reduction in Step Size and Drawing Stress	147
5.3.2 Numerical Solution	150
5.4 Theoretical Results	156
5.4.1 Results from the Closed Form Analytical Solution	156
5.4.2 Results from Numerical Solution	166
 <u>Chapter 6 : Non-Newtonian Analysis</u>	
6.1 Introduction	193
6.2 Determination of the Maximum Pressure and the Shear Stress Prior to Deformation	193
6.3 Prediction of Yielding Point	201

	<u>Page</u>
6.4 Hydrodynamic Pressure and Axial Stress in Deformation Zone	201
6.5 Percentage Reduction in the Strip Size	203
6.6 Results from the Analysis	205
6.6.1 Theoretical Results of the Percentage Reduction	206
6.6.2 Theoretical Point of Yielding	222
6.6.3 Results for Pressure Distribution	226
6.6.4 Deformation Profiles	226
<u>Chapter 7 : Discussion</u>	
7.1 Introduction	232
7.2 Experimental Results	232
7.3 Theoretical Results	237
7.4 Comparison between Experimental and Theoretical Results	243
<u>Chapter 8 : Conclusions</u>	
8.1 Conclusions	253
8.2 Suggestions for Future Work	254
References	256
Appendix I Expression for b^*	AI.1
Appendix II Velocity in Deformation Zone	AII.1
Appendix III Listing of the Computer Programme for Newtonian Analysis	AIII.1
(a) Closed Form Analytical Solution	AIII.1
(b) Numerical Solution	AIII.5
Appendix IV Listing of the Computer Programme for Non-Newtonian Analysis	AIV.1
Appendix V Papers Published	AV.1

INDEX TO FIGURES

<u>Figure No</u>		<u>Page</u>
1	General Arrangement of Die-less Strip Drawing Bench	16
2	Die-less Reduction Unit (a) Cover Block (b) Two Blocks with Channels	19
3	Photograph of the Die-less Reduction Unit (a) Different Components of the Unit (b) Assembled View	20
4	Detail Drawing of Die-Less Reduction Unit	21
5	Flow Curves for Polyethylene (Alkathene WVG23)	33
6	Flow Curves for ELVAX650	34
7	Melt Viscosity at Constant Stress and Pressure as a Function of Temperature	35
8	Melt Viscosity at Constant Stress and Temperature as a Function of Pressure	36
9	Temperature/Pressure Equivalence for Constant Viscosity	37
10	Typical Curves of Apparent Shear Viscosity vs Shear Stress for Five Thermoplastics (at Atmospheric Pressure)	38
11	Typical Curves showing the Temperature Dependence of the Apparent Shear Viscosity of a Low Density Polyethylene (Alkathene XDG33, Atmospheric Pressure)	39
12	The Yield Characteristics of the Copper Strip (AR 7.98)	40
13	The Yield Characteristics of the Copper Strip (AR 12.01)	41
14	Effect of Gap h_3 on Percentage Reduction in (a) Thickness (b) Width for Strip of Aspect Ratio 7.98 with WVG23, 130°C	50
15	Effect of Gap h_3 on Percentage Reduction in (a) Thickness (b) Width for Strip of Aspect Ratio 7.98 with WVG23, 150°C	51
16	Effect of Gap h_3 on Percentage Reduction in (a) Thickness (b) Width for Strip of Aspect Ratio 7.98 with ELVAX650, 140°C	52
17	Effect of Gap h_3 on Percentage Reduction in (a) Thickness (b) Width for Strip of Aspect Ratio 7.98 with ELVAX650, 170°C	53

18	Effect of Gap h_3 on Percentage Reduction in (a) Thickness (b) Width for Strip of Aspect Ratio of 12.01 with WVG23, 130°C	54
19	Effect of Gap h_3 on Percentage Reduction in (a) Thickness (b) Width for Strip of Aspect Ratio of 12.01 with ELVAX650, 140°C	55
20	Effect of Gap h_3 on Percentage Reduction in Area for Strip of Aspect Ratio 7.98 with WVG23, 130°C	56
21	Effect of Gap h_3 on Percentage Reduction in Area for Strip of Aspect Ratio 7.98 with WVG23, 150°C	57
22	Effect of Gap h_3 on Percentage Reduction in Area for Strip of Aspect Ratio 7.98 with ELVAX650, 140°C	58
23	Effect of Gap h_3 on Percentage Reduction in Area for Strip of Aspect Ratio 12.01 with WVG23, 130°C	59
24	Effect of Gap h_3 on Percentage Reduction in Area for Strip of Aspect Ratio 12.01 with ELVAX650, 140°C	60
25	Effect of Gap Ratio on Percentage Reduction in (a) Thickness (b) Width for Strip of Aspect Ratio 7.98 with WVG23, 130°C	61
26	Effect of Gap Ratio on Percentage Reduction in (a) Thickness (b) Width for Strip of Aspect Ratio 7.98 with WVG23, 150°C	62
27	Effect of Gap Ratio on Percentage Reduction in (a) Thickness (b) Width for Strip of Aspect Ratio 7.98 with ELVAX650, 140°C	63
28	Effect of Gap Ratio on Percentage Reduction in (a) Thickness (b) Width for Strip of Aspect Ratio 7.98 with ELVAX650, 170°C	64
29	Effect of Gap Ratio on Percentage Reduction in (a) Thickness (b) Width for Strip of Aspect Ratio 12.01 with WVG23, 130°C	65
30	Effect of Gap Ratio on Percentage Reduction in (a) Thickness (b) Width for Strip of Aspect Ratio 12.01 with ELVAX650, 140°C	66

31	Effect of Gap Ratio on Percentage Reduction in Area for Strip of Aspect Ratio 7.98 with WVG23, 130°C	67
32	Effect of Gap Ratio on Percentage Reduction in Area for Strip of Aspect Ratio 7.98 with WVG23, 150°C	68
33	Effect of Gap Ratio on Percentage Reduction in Area for Strip of Aspect Ratio 7.98 with ELVAX650, 140°C	69
34	Effect of Gap Ratio on Percentage Reduction in Area for Strip of Aspect Ratio 7.98 with ELVAX650, 170°C	70
35	Effect of Gap Ratio on Percentage Reduction in Area for Strip of Aspect Ratio 12.01 with WVG23, 130°C	71
36	Effect of Gap Ratio on Percentage Reduction in Area for Strip of Aspect Ratio 12.01 with ELVAX650, 140°C	72
37	Effect of Length Ratio on Percentage Reduction in (a) Thickness (b) Width for Strip of Aspect Ratio 7.98 with WVG23, 130°C	73
38	Effect of Length Ratio on Percentage Reduction in (a) Thickness (b) Width for Strip of Aspect Ratio 7.98 with ELVAX650, 140°C	74
39	Effect of Length Ratio on Percentage Reduction in Area for Strip of Aspect Ratio 7.98 with WVG23, 130°C	75
40	Effect of Length Ratio on Percentage Reduction in Area for Strip of Aspect Ratio 7.98 with ELVAX650, 140°C	76
41	Effect of Polymer Melt Viscosity on Percentage Reduction in (a) Thickness (b) Width for Strip of Aspect Ratio 7.98 with WVG23	77
42	Effect of Polymer Melt Viscosity on Percentage Reduction in (a) Thickness (b) Width for Strip of Aspect Ratio 7.98 with ELVAX650	78
43	Effect of Polymer Melt Viscosity on Percentage Reduction in (a) Thickness (b) Width for Strip of Aspect Ratio 12.01 with WVG23	79
44	Effect of Polymer Melt Viscosity on Percentage Reduction in Area for Strip of Aspect Ratio 7.98 with WVG23	80

45	Effect of Polymer Melt Viscosity on Percentage Reduction in Area for Strip of Aspect Ratio 7.98 with ELVAX650	81
46	Effect of Polymer Melt Viscosity on Percentage Reduction in Area for Strip of Aspect Ratio 12.01 with WVG23	82
47	Effect of Aspect Ratio on Percentage Reduction in (a) Thickness (b) Width with WVG23, 130°C	83
48	Effect of Aspect Ratio on Percentage Reduction in (a) Thickness (b) Width with ELVAX650, 140°C	84
49	Effect of Aspect Ratio on Percentage Reduction in Area with WVG23, 130°C	85
50	Effect of Aspect Ratio on Percentage Reduction in Area with ELVAX650, 140°C	86
51	Effect of Gap h_3 on Pressure Near the Step in (a) Section A (P), (b) Section B (P*) for Strip of AR 7.98 with WVG23, 130°C	90
52	Effect of Gap h_3 on Pressure Near the Step in (a) Section A (P), (b) Section B (P*) for Strip of AR 7.98 with WVG23, 150°C	91
53	Effect of Gap h_3 on Pressure Near the Step in (a) Section A (P), (b) Section B (P*) for Strip of AR 7.98 with ELVAX650, 140°C	92
54	Effect of Gap h_3 on Pressure Near the Step in (a) Section A (P), (b) Section B (P*) for Strip of AR 7.98 with ELVAX650, 170°C	93
55	Effect of Gap Ratio on Pressure Near the Step in (a) Section A (P), (b) Section B (P*) for Strip of AR 7.98 with WVG23, 130°C	94
56	Effect of Gap Ratio on Pressure Near the Step in (a) Section A (P), (b) Section B (P*) for Strip of AR 7.98 with WVG23, 150°C	95
57	Effect of Gap Ratio on Pressure Near the Step in (a) Section A (P), (b) Section B (P*) for Strip of AR 7.98 with ELVAX650, 140°C	96
58	Effect of Gap Ratio on Pressure in (a) Section A (P), (b) Section B (P*) for Strip of AR 7.98 with ELVAX650, 170°C	97
59	Effect of Length Ratio on Pressure (P) near the Step in Section A for Strip of AR 7.98 with WVG23, 130°C	98

60	Pressure Distribution within the Unit with WVG23, 130°C	99
61	Pressure Distribution within the Unit with WVG23, 130°C	100
62	Pressure Distribution within the Unit with WVG23, 130°C	101
63	Pressure Distribution within the Unit with WVG23, 130°C	102
64	Pressure Distribution within the Unit with ELVAX650, 140°C	103
65	Pressure Distribution within the Unit with ELVAX650, 140°C	104
66	Pressure Distribution within the Unit with ELVAX650, 140°C	105
67	Pressure Distribution within the Unit with ELVAX650, 140°C	106
68	Effect of Gap h_3 on Drawing Stress for Strip of AR 7.98 with WVG23, 130°C	110
69	Effect of Gap h_3 on Drawing Stress for Strip of AR 7.98 with WVG23, 150°C	111
70	Effect of Gap h_3 on Drawing Stress for Strip of AR 7.98 with ELVAX650, 140°C	112
71	Effect of Gap h_3 on Drawing Stress for Strip of AR 7.98 with ELVAX650, 170°C	113
72	Effect of Gap h_3 on Drawing Stress for Strip of AR 12.01 with WVG23, 130°C	114
73	Effect of Gap h_3 on Drawing Stress for Strip of AR 12.01 with ELVAX650, 140°C	115
74	Effect of Gap Ratio on Drawing Stress for Strip of AR 7.98 with WVG23, 130°C	116
75	Effect of Gap Ratio on Drawing Stress for Strip of AR 7.98 with WVG23, 150°C	117
76	Effect of Gap Ratio on Drawing Stress for Strip of AR 7.98 with ELVAX650, 140°C	118
77	Effect of Gap Ratio on Drawing Stress for Strip of AR 7.98 with ELVAX650, 170°C	119

78	Effect of Gap Ratio on Drawing Stress for Strip of AR 12.01 with WVG23, 130°C	120
79	Effect of Gap Ratio on Drawing Stress for Strip of AR 12.01 with ELVAX650, 140°C	121
80	Effect of Length Ratio on Drawing Stress for Strip of AR 7.98 with WVG23, 130°C	122
81	Effect of Length Ratio on Drawing Stress for Strip of AR 7.98 with ELVAX650, 140°C	123
82	Effect of Polymer Melt Viscosity on Drawing Stress for Strip of AR 7.98 with WVG23	124
83	Effect of Polymer Melt Viscosity on Drawing Stress for Strip of AR 7.98 with ELVAX650	125
84	Effect of Polymer Melt Viscosity on Drawing Stress vs Drawing Speed for Strip of AR 12.01 with WVG23	126
85	Effect of Polymer Melt Viscosity on Drawing Stress for Strip of AR 12.01 with ELVAX650	127
86	Deformation Profiles with WVG23, 130°C	129
87	Deformation Profile with ELVAX650, 140°C	130
88	Schematic Diagram of the Process (a) Zones and Deformation Profile for Thickness (b) Deformation Profile for Width (c) Sections A and B and Directions of x, y, z	132
89	Stresses Acting on a Small Element	143
90	Theoretical Effect of Gap Ratio on Percentage Reduction in Thickness	158
91	Theoretical Effect of Length Ratio on Percentage Reduction in Thickness	159
92	Theoretical Effect of Initial Yield Stress on Percentage Reduction in Thickness	160
93	Theoretical Effect of Critical Shear Stress on Percentage Reduction in Thickness	161
94	Theoretical Effect of Gap Ratio on Drawing Stress	162
95	Theoretical Effect of Length Ratio on Drawing Stress	163
96	Theoretical Effect of Initial Yield Stress on Drawing Stress	164

97	Theoretical Effect of Critical Shear Stress on Drawing Stress	165
98	Theoretical Effect of Gap Ratio on Percentage Reduction in Thickness	169
99	Theoretical Effect of Gap Ratio on Yielding Point	170
100	Theoretical Effect of Length Ratio on Percentage Reduction in Thickness	171
101	Theoretical Effect of Initial Yield Stress on Percentage Reduction in Thickness	172
102	Theoretical Effect of Initial Yield Stress on Yielding Point	173
103	Theoretical Effect of Strain Hardening Constant on Percentage Reduction in Thickness	174
104	Theoretical Effect of Viscosity on Percentage Reduction in Thickness	175
105	Theoretical Effect of Viscosity on Yielding Point	176
106	Theoretical Effect of Critical Shear Stress on Percentage Reduction in Thickness	177
107	Theoretical Effect of Gap Ratio on Percentage Reduction in Area	178
108	Theoretical Effect of Length Ratio on Percentage Reduction in Area	179
109	Theoretical Effect of Initial Yield Stress on Percentage Reduction in Area	180
110	Theoretical Effect of Strain Hardening Constant on Percentage Reduction in Area	181
111	Theoretical Effect of Viscosity on Percentage Reduction in Area	182
112	Theoretical Effect of Critical Shear Stress on Percentage Reduction in Area	183
113	Theoretical Effect of Gap Ratio on Drawing Stress	184
114	Theoretical Effect of Length Ratio on Drawing Stress	185
115	Theoretical Effect of Viscosity on Drawing Stress	186
116	Theoretical Effect of Critical Shear Stress on Drawing Stress	187

117	Theoretical Effect of Gap Ratio on Pressure Distribution within the Unit	188
118	Theoretical Effect of Drawing Speed on Pressure Distribution within the Unit	189
119	Theoretical Effect of Viscosity on Pressure Distribution within the Unit	190
120	Theoretically Calculated Deformation Profiles for Different Gap Ratios	191
121	Theoretically Calculated Deformation Profiles for Different Speeds	192
122	Theoretical Effect of Gap Ratio on Percentage Reduction in Thickness	208
123	Theoretical Effect of Gap Ratio on Percentage Reduction in Area	209
124	Theoretical Effect of Length Ratio on Percentage Reduction in Thickness	210
125	Theoretical Effect of Length Ratio on Percentage Reduction in Area	211
126	Theoretical Effect of Initial Yield Stress on Percentage Reduction in Thickness	212
127	Theoretical Effect of Initial Yield Stress on Percentage Reduction in Area	213
128	Theoretical Effect of Strain Hardening Constant on Percentage Reduction in Thickness	214
129	Theoretical Effect of Strain Hardening Constant on Percentage Reduction in Area	215
130	Theoretical Effect of Viscosity on Percentage Reduction in Thickness	216
131	Theoretical Effect of Viscosity on Percentage Reduction in Area	217
132	Theoretical Effect of Non-Newtonian Factor on Percentage Reduction in Thickness	218
133	Theoretical Effect of Non-Newtonian Factor on Percentage Reduction in Area	219
134	Theoretical Effect of Critical Shear Stress on Percentage Reduction in Thickness	220

<u>Figure No</u>		<u>Page</u>
135	Theoretical Effect of Critical Shear Stress on Percentage Reduction in Area	221
136	Theoretical Effect of Gap Ratio on Yielding Point	223
137	Theoretical Effect of Initial Yield Stress on Yielding Point	224
138	Theoretical Effect of Viscosity on Yielding Point	225
139	Theoretical Effect of Gap Ratio on Pressure Distribution within the Unit	227
140	Theoretical Effect of Drawing Speed on Pressure Distribution within the Unit	228
141	Theoretical Effect of Viscosity on Pressure Distribution within the Unit	229
142	Theoretically Calculated Deformation Profiles for Different Gap Ratios	230
143	Theoretically Calculated Deformation Profiles for Different Drawing Speeds	231
144	Percentage Reduction in (a) Thickness (b) Width with Two Different Polymers	246
145	Comparison between Experimental Results (WVG23, 130°C) and Theoretical Percentage Reduction in Thickness	247
146	Comparison between Experimental Results (WVG23, 130°C) and Theoretical Percentage Reduction in Area	248
147	Comparison between Experimental Results (ELVAX650, 140°C) and Theoretical Percentage Reduction in Area	249
148	Comparison between Experimental Results (WVG23, 130°C) and Theoretical Pressure Distribution within the Unit	250
149	Comparison between Experimental (WVG23, 130°C) and Theoretical Deformation Profiles	251
150	Comparison between Experimental (ELVAX650, 140°C) and Theoretical Deformation Profiles	252

INDEX TO PLATES

<u>Plate No</u>		<u>Page</u>
1	General View of Dieless Strip Drawing Bench	17
2	Integral Part for Holding Strip Coil and Guiding the Strip into the Unit	18
3	Melt Chamber and Hopper	22
4	Temperature Controller and UV Recorder	23
5	Thermocouples and Pressure Transducers	24
6	Load Indicator	25

NOTATIONS

t	Thickness of the Strip
W	Width of the Strip
L	Length of the Unit
h	Gap between the Strip and Die-less Reduction Unit
V	Drawing Speed
P	Hydrodynamic Pressure
P'	Pressure Gradient
τ	Shear Stress
σ_x	Axial Stress
σ_d	Drawing Stress
x	Distance along the Unit
X_1	Yielding Point
s	Dynamic/Static Stress Ratio
Y_0	Initial Yield Stress
Y	Yield Stress of the Strip Material
K_0	Strain Hardening Constant
ϵ	Natural Strain
n	Strain Hardening Index
N	Strain Rate Sensitivity Constant
T_1	Strain Rate Sensitivity Index
μ	Viscosity of the Polymer Melt
K	Non-Newtonian Factor
$\dot{\gamma}$	Shear Rate
a	Area of the Strip
b, B	Factor determining Theoretical Deformation Profile for Thickness
b*, B*	Factor determining Theoretical Deformation Profile for Width

PRT Percentage Reduction in Thickness
PRW Percentage Reduction in Width
PRA Percentage Reduction in Area
Rh Gap Ratio, h_1/h_2
RL Length Ratio, L_1/L_2
AR Aspect Ratio, W_1/t_1

Suffixes

1 Inlet Zone in Section A
2 Exit Zone in Section A
3 Section B
i Deformation Zone
* Section B (Deformation Zone)
 $C_1 - C_{11}$ are Constants of Integration

$A_1 - A_9$
and
 $B_1 - B_6$
are Computation Variables

CHAPTER 1

INTRODUCTION

1.1 The Drawing Process

In the conventional cold drawing process, the reduction in area of wire, strip or tube is achieved by pulling the material through a shaped die. Normally, conical shaped dies are used for wire and tube and wedge shaped dies are used for strip drawing. The minimum size of the die is always smaller than the incoming material and the die acts primarily to reduce the material to a specific size.

In the drawing process, metal to metal contact takes place causing friction and ultimately reduction in the die life due to wear. To minimize wear, lubricants are used which are vitally important in the metal forming process. Effective lubrication results in a reduction of friction coefficient, with consequential reduction in the force and power requirements. Most metal deformation processes are performed predominantly with boundary lubrication. The film is extremely thin and the large pressures cause contact between a large number of asperities, hence friction always exists in conventional metal forming processes.

Several methods have been described in plane strain strip drawing to determine the friction coefficient and effect of lubrication. Fukui et al⁽¹⁾ developed an apparatus to measure the friction coefficient directly during the metal strip drawing process. They used parallel dies with a tapered plug and an average coefficient of friction was determined by measuring normal force and friction force. The aim was to study the effects of various factors such as the type of lubricant, strip material, drawing speed, surface

finish of the die and work material on the friction coefficient. Their work had shown that friction coefficient was dependent on the drawing speed and on the type of lubricant. It was found that in most cases an increase in speed caused a reduction in friction coefficient for lubricants of low viscosity or of inferior lubricity such as spindle oil. No general rule for the correlation between the kind of speed dependence or strip material had been established. The experimental results also showed that friction coefficient was primarily dependent on surface roughness. A decrease in friction coefficient was observed, with increasing roughness of strip surface, and with the dies of smoother surface.

Lancaster and Rowe⁽²⁾ conducted experimental work to study the influence of lubrication upon cold drawing using wedge shaped dies and a plug bar arrangement. Their work was divided into two parts. The first part related to the evaluation of a soft solid lubricant that could be passed through the die with the work material. They found that the film thickness depended upon the lubricant, surface finish of the specimen and the geometry of the dies. They concluded that with angles up to 10° the regime was one of thin film type, provided that the surfaces of the specimen were grit blasted. With a specimen of smooth surface finish the regime of lubrication was predominantly of boundary type. The quantity of the lubricant passing with the specimen was found to be strongly dependent on the die angle. The second part of their work presented a comparison of experimentally measured coefficient of friction and drawing stress with the existing drawing theories (3, 4, 5). Sheet drawing tests were carried out by Kudo et al⁽⁶⁾ to investigate cold forming friction and lubrication. They carried out experiments with aluminium and copper sheets at speeds ranging

from 0.2 to 3000 mm/s, using various lubricants, with an apparatus which enabled them to record separately the tangential and normal loads at the die surface. They presented experimental results showing the dependence of friction coefficient on reduction, speed and lubricant.

Wilson and Cazeault⁽⁷⁾ used a split die arrangement to measure friction at the workpiece-tooling interface in strip drawing. They investigated different combinations of lubricant, die-angle, reduction, speed and strip orientation to determine the influence of each factor on the frictional conditions. They found that the friction was strongly affected by the geometry of the process whereas the drawing speed and orientation of the strip had little effect on friction. Rao et al⁽⁸⁾ carried out experiments for the plane-strain strip drawing process using transparent sapphire dies. The aim of their work had been to gather a reference collection of experimental data covering parameters such as die angle, speed, back tension and interface friction variations. Transparent dies had been used so that the interface displacements could be observed directly and the relative velocities determined. The principal objective of velocity measurement was to provide boundary condition information at the tool interface and be used in theoretical models, to calculate interface friction in place of an assumed coefficient of friction. A numerical solution was presented⁽⁹⁾ and the predicted values were compared with experimental data of reference⁽⁸⁾.

To meet industrial demands of high speed drawing, researchers had concentrated their studies on the drawing of different metallic sections at high speeds. Parsons et al⁽¹⁰⁾ presented a paper

giving a feasibility report on high speed impact drawing. In their work they analysed the process theoretically considering the mechanics of the deformation of the bar and the dynamics of the process. A brief description of experimental results in bar drawing was presented.

Baxter⁽¹¹⁾ carried out work on high speed drawing of strip and tube. A major portion of his work related to the drawing of strip at high speed through wedge shaped dies. In his work he observed the presence of hydrodynamic lubrication at high speeds. He also developed an expression to evaluate the lubricant film thickness with the aim of investigating theoretically the presence of hydrodynamic lubrication during drawing.

Devenpeck and Rigo⁽¹²⁾ reported the development of a research apparatus which was basically a combination of a laboratory rolling mill and a specially designed die-block. The apparatus was used to perform high speed drawing tests of thin strip. This set up enabled them to carry out experimental studies in drawing long lengths (1.5 km) of thin strip at high speeds (0.5 to 6.1 m/s). They conducted tests with tin plated steel strip using two lubricant fluids in addition to the tap water and studied the effect of different parameters such as speed, cumulative length of strip, and reduction on process friction factor and wear.

1.2 Hydrodynamic Lubrication

The attendant die wear gave impetus to consideration of the possibility of maintaining full film lubrication, which, if perfectly realized would minimize the coefficient of friction and the tool wear. Therefore, attempts have been made to make use of hydrodynamic lubrication in the drawing process. Among the first

investigations in this respect was that carried out by Christopherson and Naylor⁽¹³⁾ in connection with wire drawing. A long close fitting pressure tube attached to the inlet of a conventional die was used. Oil was used for lubrication. As the wire was pulled through the tube and die, high pressures were generated in the lubricant by viscous action. Experimental results showed that hydrodynamic conditions were achieved under the designed conditions. A simplified analysis of the lubricant flow in the tube, assuming isothermal conditions, was presented. Their theoretical analysis for the inlet tube configuration was extended, together with considerations in deformation zone, by Tattersal⁽¹⁴⁾ and by Osterle and Dixon⁽¹⁵⁾.

Cheng⁽¹⁶⁾ presented a theory of plasto-hydrodynamic lubrication for rolling of strip taking into account thermal, plasticity and lubricant aspects. Bedi⁽¹⁷⁾ analysed wire drawing through a conical die assuming complete hydrodynamic lubrication enabling the calculation of hydrodynamic film thickness and viscous friction coefficient. Bloor et al⁽¹⁸⁾ produced a theoretical analysis for elasto-plasto-hydrodynamic lubrication for strip drawing through wedge shaped dies taking account of the elastic component in the strip at entry and exit to the die, and the pressure-viscosity characteristics of the lubricant. It was shown by comparing the magnitude of the predicted lubricant film thickness that hydrodynamic lubrication could be developed during the process. Based upon the same work reported in ref (18), Dowson et al⁽¹⁹⁾ presented an elasto-plasto-hydrodynamic lubrication analysis for wire drawing process.

Lancaster⁽²⁰⁾ conducted high speed drawing tests with the objective of determining the possibility of establishing hydrodynamic lubrication without the use of pressure tubes or compound dies. Tests with aluminium (hard and soft) and low carbon steel^{bars} were conducted at drawing speeds up to 30 m/s. Lanoline and polyglycols were used as lubricants. The experimental results indicated that speed alone was not sufficient to allow hydrodynamic films to be developed. It was observed that hydrodynamic films were possible but these depended on the properties of the material being drawn, the lubricant and the die angle. The conditions required to maintain full separation between the workpiece and the tool were discussed and specified by Avitzur⁽²¹⁾.

An experimental study with cold sheet drawing through wedge shaped dies was carried out by Kudo et al⁽²²⁾ to investigate plasto-hydrodynamic lubrication in metal forming processes. A thermal rigid-plasto-hydrodynamic analysis was developed to calculate the average coefficient of friction over the die surface, the lubricant film thickness and interface temperature. Theoretical analyses for hydrodynamic lubrication including thermal effects for rolling and drawing through conventional dies had been presented by Wilson and Mahdavian⁽²³⁾, Dow et al⁽²⁴⁾, Mahdavian and Wilson⁽²⁵⁾.

1.3 Plasto-hydrodynamic Die-less Drawing

To ensure stable hydrodynamic conditions the correct selection of the lubricant is particularly important. The viscosity characteristics of the lubricant should be such that they provide laminar lubricant flow in the pressure tube and at the same time, maintain the requisite adhesion of the lubricant to the work material.

Recently, investigations have been made towards finding alternative lubricants to those which are commonly in use. The use of a polymer melt during drawing was introduced by Symmons et al^(26, 27). Limited experiments were conducted to investigate the coating properties of polymer melt in wire drawing. Crampton⁽²⁸⁾ extended this work to study the lubrication ability of polymer melt for wire drawing process by changing parameters such as the polymer melt temperature, wire material and drawing speed. The apparatus used for the above works was basically similar to that used by Christopherson, except that polymer melt was used as the lubricating agent. Analytical solutions^(29, 30) were presented for the deformation process of wire taking into account, non-Newtonian characteristic of polymer melt, and the effect of strain hardening and strain rate sensitivity on wire material. On the basis of experimental evidence (ref 28) it was found that the deformation in the wire commenced in the inlet tube before it enters the die. Hence the die was of secondary importance and acted as a seal. It was postulated that the reduction in wire diameter could be achieved by using a polymer melt in conjunction with a tubular conical unit alone, the smallest bore size of which is greater than wire diameter. Furthermore, work carried out by Hashmi, Symmons and Parvinmehr⁽³¹⁻³³⁾ using a stepped bore reduction unit with smallest bore larger than the incoming wire in place of a conventional reduction die showed that a reduction in the wire diameter could be achieved. Thus a new concept in drawing was investigated and patented as 'Plasto-hydrodynamic Die-less Drawing'.

In this novel technique, the wire is pulled through a melt chamber filled with polymer melt and then through a stepped bore reduction

unit. The pulling action causes the gap between the wire and inner surface to be filled with polymer melt which in turn gives rise to drag force and hydrodynamic pressure. The combined effect of these two parameters becomes sufficient to cause permanent deformation in the wire. The salient feature of the new process was that as the smallest bore size was larger than the incoming wire, no metal to metal contact took place which, as a result, eliminated the problem of wear. Hashmi and Symmons⁽³⁴⁻³⁵⁾ presented analytical and numerical solutions for a solid continuum pulled through a conical orifice filled with a viscous fluid. A non-Newtonian analysis for plasto-hydrodynamic die-less wire drawing incorporating the limiting shear stress of polymer melt and the strain hardening and strain rate sensitivity of the wire material, was produced by Parvinmehr et al⁽³⁶⁾. Panwher et al⁽³⁷⁾ reported work carried out on the die-less tube sinking process and presented an analytical solution based upon Newtonian characteristics. Subsequently Panwher⁽³⁸⁾ analysed the system taking account of non-Newtonian characteristics of the polymer melt.

Furthermore, Symmons et al⁽³⁹⁻⁴¹⁾ presented analyses for the die-less wire drawing process using a viscosity-pressure and viscosity-temperature relationship of exponential form. Their aim was to examine individually the effect of pressure and temperature on polymer melt viscosity and consequently on the performance of the process.

1.4 Present Work

From the discussions in the foregoing section it is evident that much work has been done for the wire drawing process; for both the conventional die set-up and unconventional arrangement where experimental and theoretical results are available.

The literature for strip drawing reviewed in the previous section describes the following characteristics in general,

- (a) determination of friction coefficient and its dependence on the parameters of the process,
- (b) evaluation of the lubricant film thickness, to predict the presence of hydrodynamic lubrication,
- (c) all the investigations are related to the use of the conventional wedge shaped dies.

The aim of the present investigation is to apply the novel technique of die-less drawing reported in references (33, 38) to strip drawing with the objective of defining the process and to develop a theoretical model as a means for predicting the effects of different parameters involved in the process.

Initial experimental studies on the new system showed positive results. However, plane strain conditions were not observed, as the strip is reduced in both thickness and width. An extensive experimental study has been undertaken to investigate the effects of various parameters on the performance of the process.

The objectives of the present project are:

- (i) to study the effects of the geometry of the die-less reduction unit on pressure distribution, drawing stress and attainable reduction in strip size,
- (ii) to study effects of drawing speed and polymer melt temperature on the performance of process,
- (iii) to develop a mathematical model for the prediction of various parameters involved in the process such as pressure distribution, initiation of yielding, product size and the drawing stress,

- (iv) to examine the correlation between experimental and theoretical results,
- (v) to assess the feasibility of the process in comparison with the conventional process.

CHAPTER 2

DESIGN AND DEVELOPMENT OF THE EXPERIMENTAL EQUIPMENT

2.1 Description of the Existing Rig

The test apparatus was originally commissioned for tube sinking and was modified to facilitate the present work.

It is a chain type draw bench made by Marshal Richards Barco shown in Figure 1 and Plate 1. The maximum length that can be drawn is 8 ft (approx 2.4 m). A variable speed electric motor made by Crofts (11 KW/415 V/3 Phase/50 Cycles) with integral speed gear unit made by Ronald power transmission (GM6T ratio 47.08) drives the chain sprocket. The output speed of the unit being variable between 0.1 to 0.5 m/s.

The test rig consists of a dog clamp fitted with a spring loaded hook which can slide freely between rail guides and can be engaged or disengaged to the running chain by a lever. At the far end of the bench an emergency ramp is bolted which disengages the dog clamp from the chain. A strain gauge load cell with maximum capacity of 40 kN is also fitted and connected with a load indicator. The die-less reduction unit is bolted to the hinged die-plate which rests against the load cell block.

2.2 Modification to the Existing Rig

To accommodate the coil of strip and guide the undrawn strip properly into the reduction unit the following devices were added to the existing rig. An integral part (Plate 2) was designed and fabricated. It consists of a circular disk for the accommodating strip coil and a set of rollers to keep the strip centralized and guide it while being fed into the system.

2.3 Design of the Die-less Reduction Unit

It was extremely difficult to machine a stepped rectangular hole in a solid piece of material to accommodate the strip and therefore it became necessary to manufacture the unit in split form.

Again due to the stepped configuration it was not practicable to produce the required hole by using two blocks. Different methods were considered to get the required shape of the hole. Two methods were selected for the fabrication of the unit. In one method the unit had to be made into three blocks, see Figure 2, in which one part has the dimensions of the channel before the step while the other part has those after the step. The two blocks are clamped with bolts at the end and finally bolted to a third block having a projected portion for the provision of the step. The second method was to make two main blocks with housings to accommodate two separate inserts machined to the required geometrical configuration as shown in Figure 3.

As the pressure generated is of high magnitude, the major problem was one of sealing at the edge of mating parts in order to prevent any leakage during drawing. The latter design was selected (to make the units for conducting the experimental work) for ease of machining. This allowed variation in geometrical configuration easier by making modifications to the inserts only.

All the parts of the unit were made from steel (EN8), by milling and grinding operations. Initially the blocks were milled to rough size close to the final dimensions and finally ground precisely to the required dimensions with a tolerance of ± 0.002 mm. The inserts were made to a press fit in the housings and in the first instance copper seals were used between the inner mating

surfaces of the block and inserts to prevent leakage. Afterwards it was found that if the inserts were machined to a good press fit then it was not necessary to use the seals. Therefore for subsequent work, inserts were made to a press fit. This saved considerable time in producing a reduction unit by eliminating the process of machining V-grooves for copper seals. The two blocks were bolted together tightly. Provisions were made in the unit to fit five pressure transducers, two at the top face and three on one side to record the generated hydrodynamic pressure. Two holes were also drilled for inserting two thermocouples to monitor the temperature of the unit. The detailed drawing of the unit is given in Figure 4. A heater band was clamped to the unit to heat it to a pre-set temperature.

2.4 Melt Chamber and Hopper

To carry sufficient quantity of polymer melt for a full set of tests, a melt chamber and hopper was designed as shown in Plate 3. The hopper facilitated feeding of polymer granules into the melt chamber and served as a reservoir. Heater bands were used for heating the melt chamber and the hopper and the temperature was controlled thermostatically. The melt chamber was bolted to the entrance face of the unit.

2.5 Instrumentation

In order to determine the feasibility of the system and the correlation between theoretical and experimental results a number of equipments and devices were used to monitor, control and record various parameters during the drawing tests. These included heater bands, temperature controllers, thermocouples, pressure transducers, charge amplifiers, UV recorder and load indicator.

2.5.1 Heater Bands

Watlow ring type heater bands were used for heating the melt chamber and the hopper (Plate 3). The dimensional details are:

ID (mm)	Width (mm)	Volts	Watts
70	38	240	400

A pair of L-type heater bands was used for the Unit (Plate 3) with dimensional details as follows:

Width (mm)	Length (mm)	Volts	Watts
50	70	240	320

2.5.2 Temperature Controllers

An electronic On-Off temperature controller relay (type K) encased in a 48 x 48 DIN standard case, with a graduated scale marked 0-400°C was used to maintain the pre-set temperature. This unit is designed to be used with nickle-chrome/nickle-aluminium type K thermocouples to monitor temperature. A relay changeover contact within the unit operates at a pre-determined temperature previously set by a potentiometer knob mounted on the face of the unit. Two LEDs mounted in the unit indicated supply and relay status. The temperature controllers are shown in Plate 4.

2.5.3 Thermocouples

To monitor the temperature continuously, inconel sheathed mineral insulated, 1.5 mm O.D, thermocouples shown in Plate 5 were used. These thermocouples have an operating temperature range -200° to +1100°C with a response time of 0.3 sec.

2.5.4 Pressure Transducers

Commercially available high pressure Piezo-electric quartz transducers (Kistler type 6201 and 6203) were used to measure the

generated hydrodynamic pressure during the drawing tests. The operating capacity of these transducers is, maximum pressure of 5000 bar and a maximum temperature of 240°C. To prevent leakage of the polymer melt, metal rings were used while mounting the transducers on the unit. The arrangement of the transducers on the unit is shown in Figure 4 and Plate 5. The output from the pressure transducers was fed into ultra violet (UV) recorder via charge amplifiers, shown in Plate 4.

2.5.5 Load Indicator

The Elliot load indicator (type BCF/2), shown in Plate 6, was used to indicate the drawing load. It is an electronic instrument operating in conjunction with resistance strain gauge load cell. The installation forms a closed control loop incorporating a self balancing load to reference error signal system. It consists of a circular graduated scale, the load being indicated by a mechanical pointer. The movement of the pointer is linear and proportional to the changes in load applied to the load cell. The circular scale is graduated from 0-40 kN with a minimum scale of 0.2 kN.

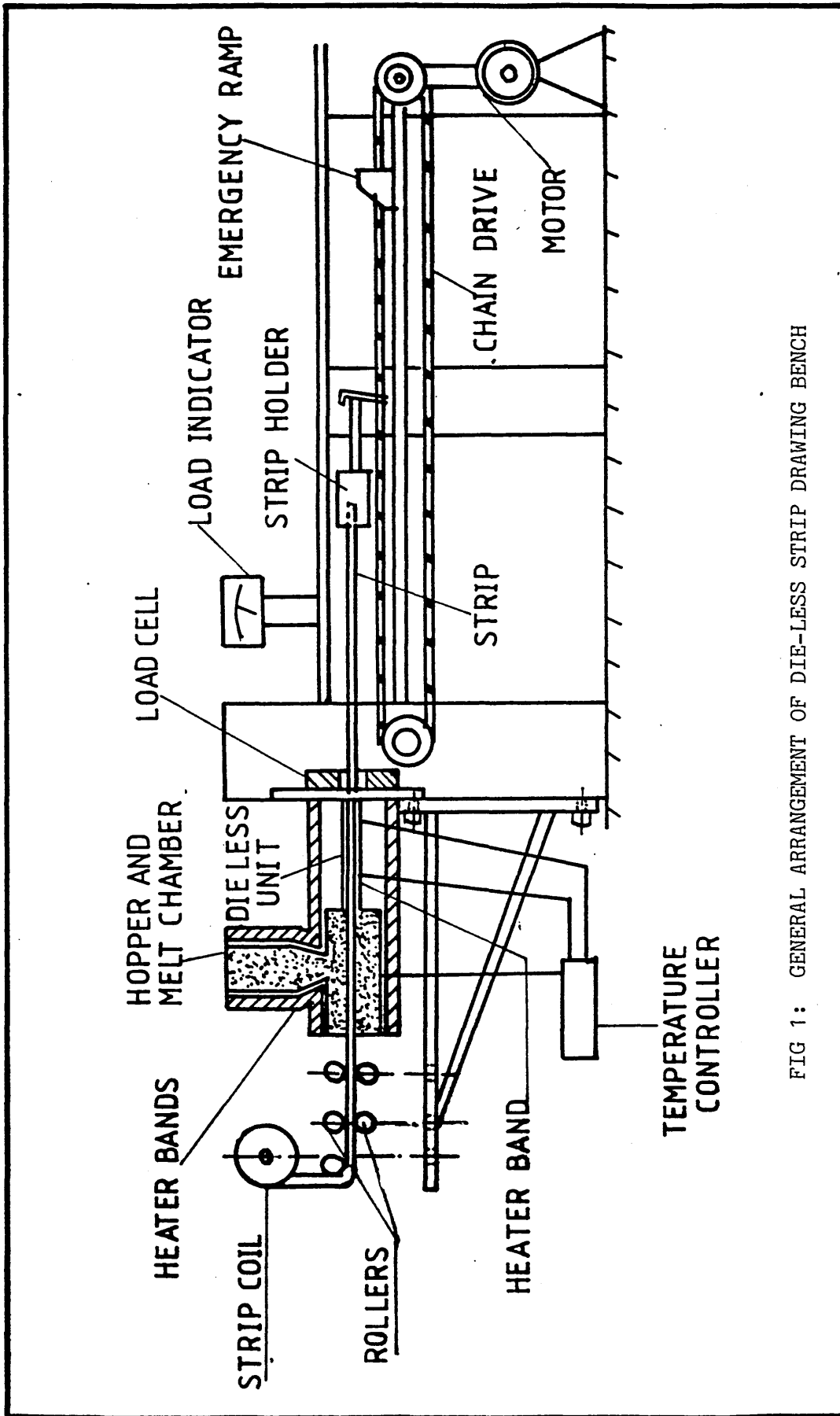


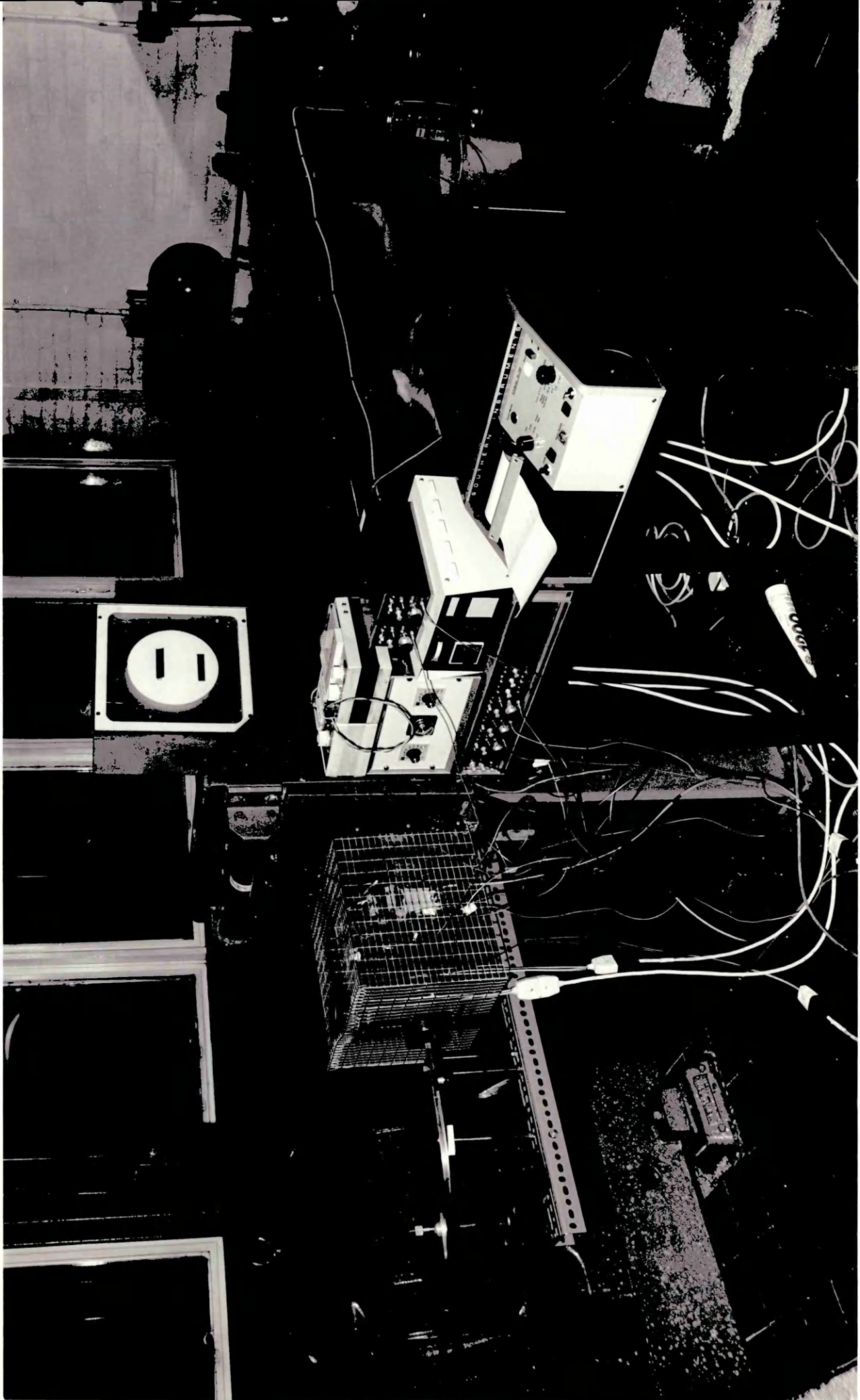
FIG 1: GENERAL ARRANGEMENT OF DIE-LESS STRIP DRAWING BENCH

GENERAL VIEW OF THE DRAW BENCH
AND
THE ARRANGEMENT OF THE DIE-LESS STRIP DRAWING EQUIPMENT

PLATE 1

THE ARRANGEMENT OF THE DIE-LESS STRIP DRAWING EQUIPMENT
AND
GENERAL VIEW OF THE DRAW BENCH

PLATE 1



STRIP COIL

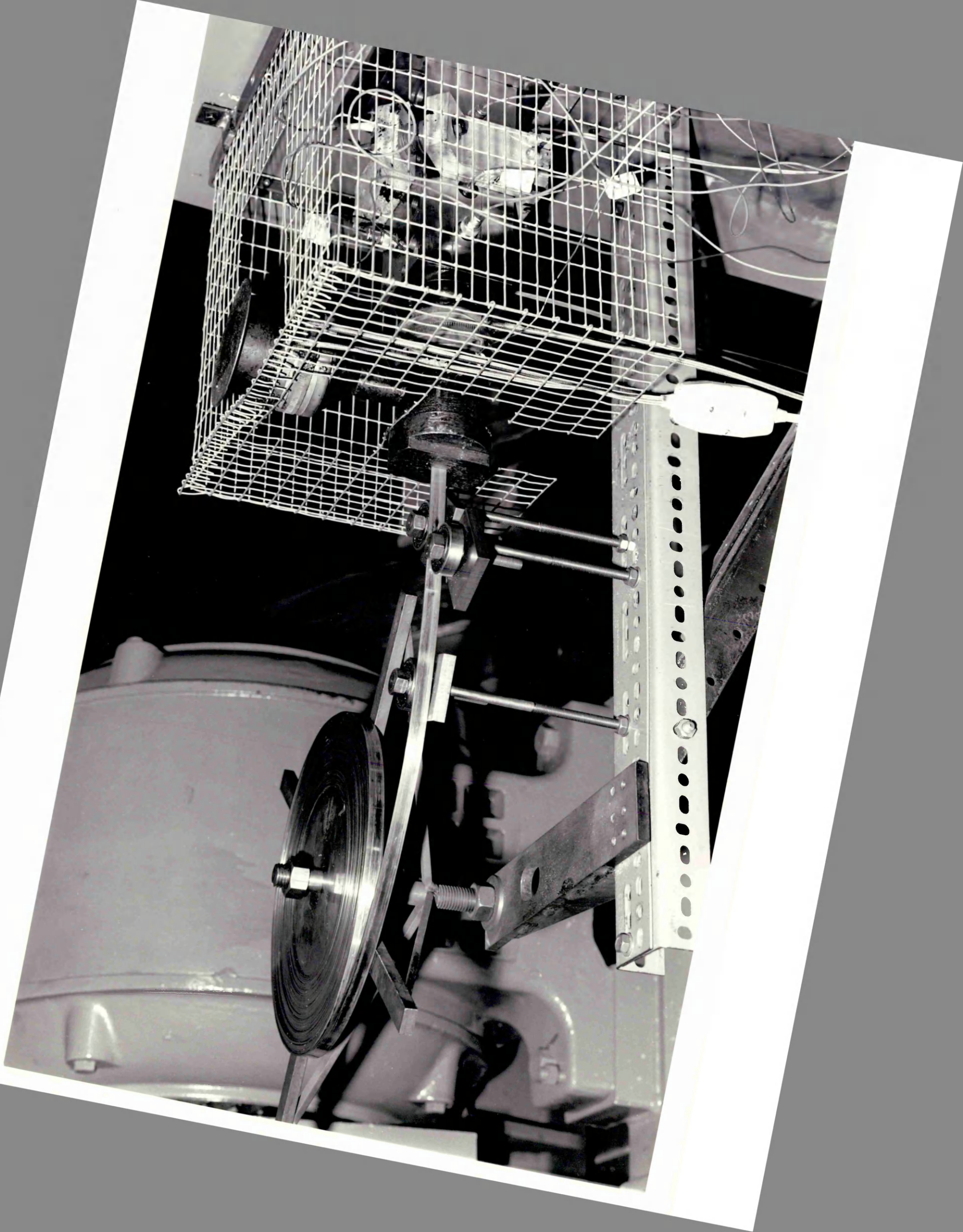
DISK

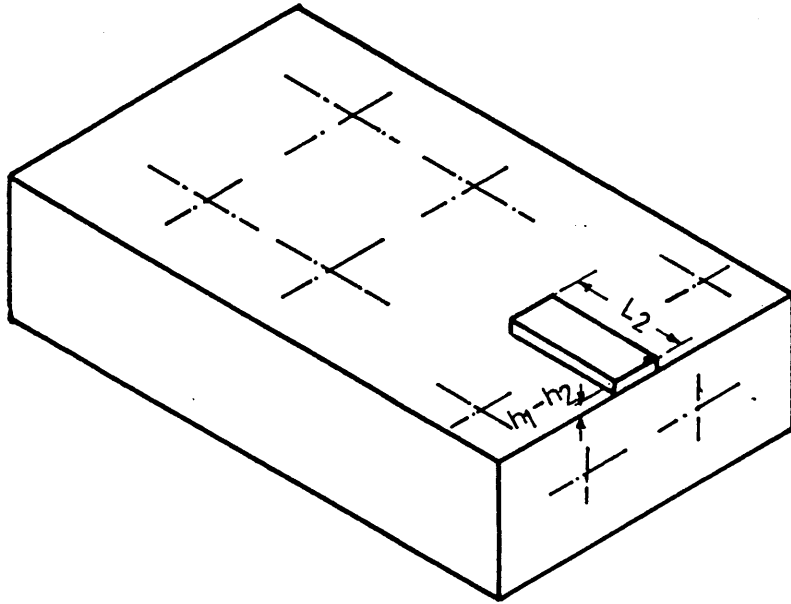
ROLLERS

BOGGER2

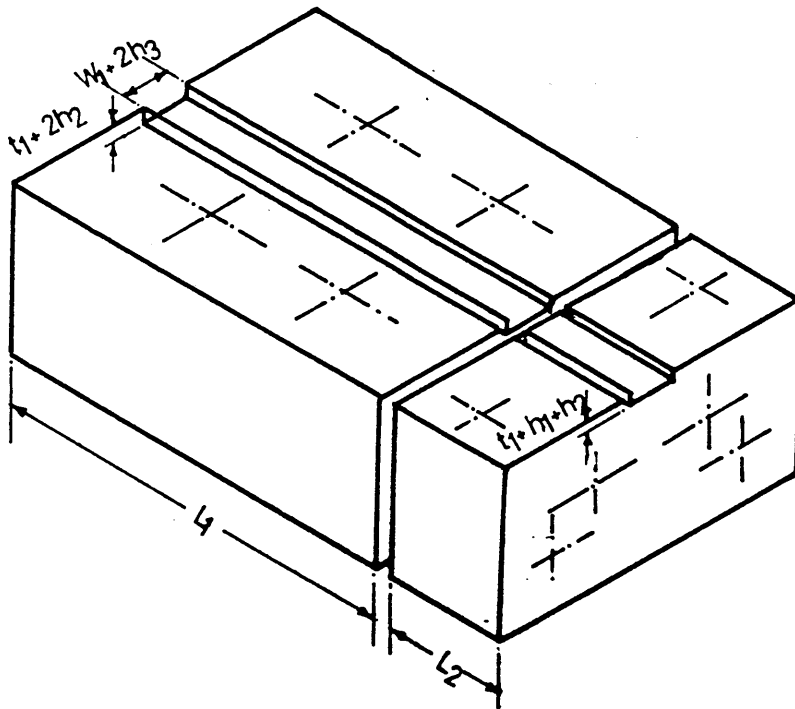
DISK

STRIP COIL





(a)

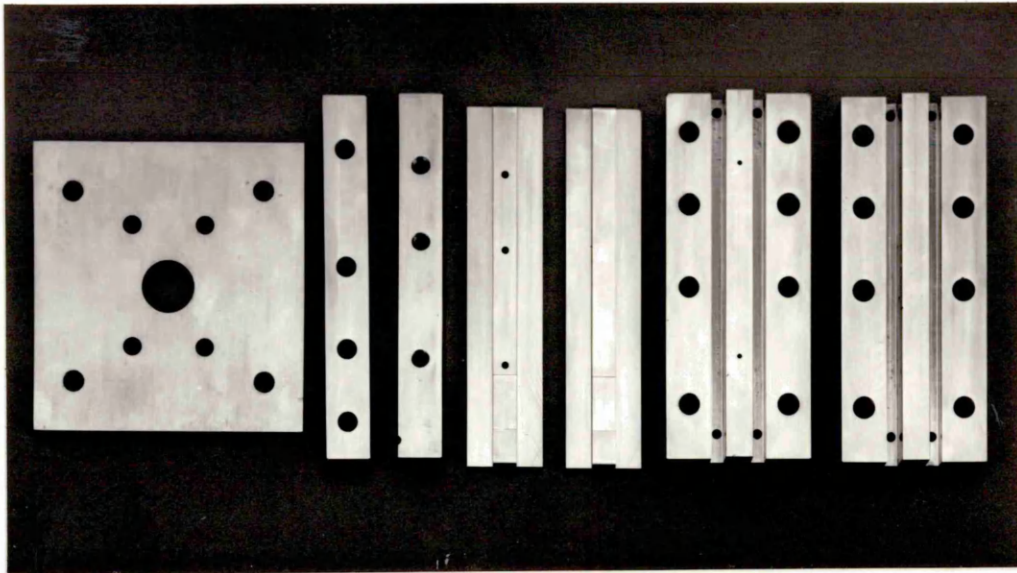


(b)

FIG 2: DIE-LESS REDUCTION UNIT

(a) COVER BLOCK

(b) TWO BLOCKS WITH CHANNELS



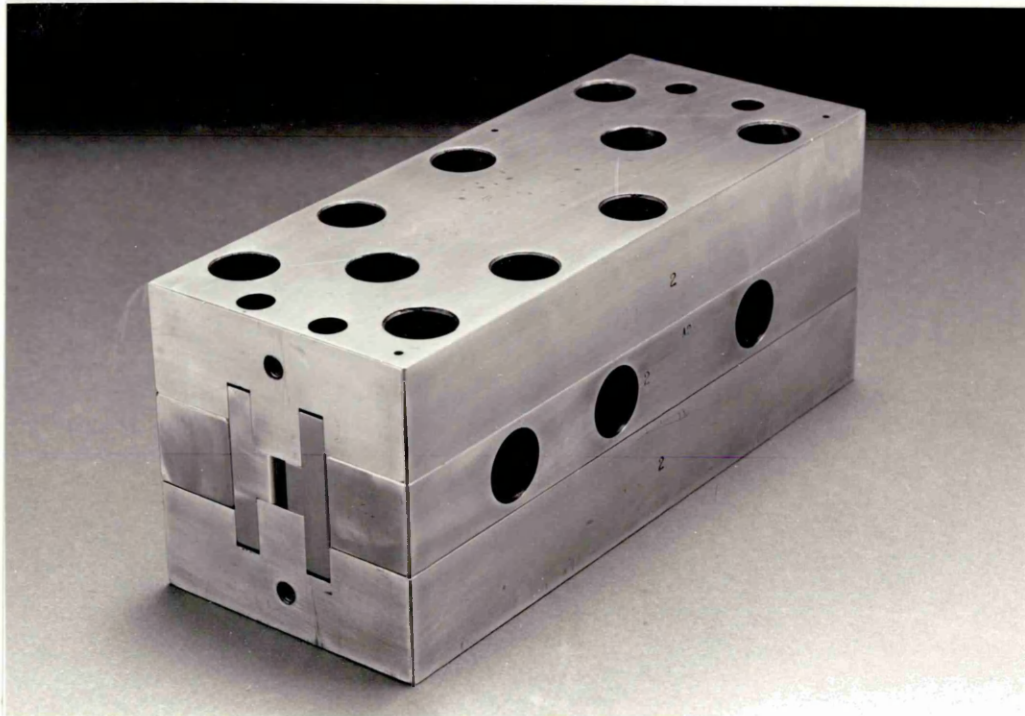
Plate

Spacers

Inserts

Main Blocks

(a)



(b)

FIG 3: PHOTOGRAPH OF THE DIE-LESS REDUCTION UNIT
(a) DIFFERENT COMPONENTS OF THE UNIT
(b) ASSEMBLED VIEW

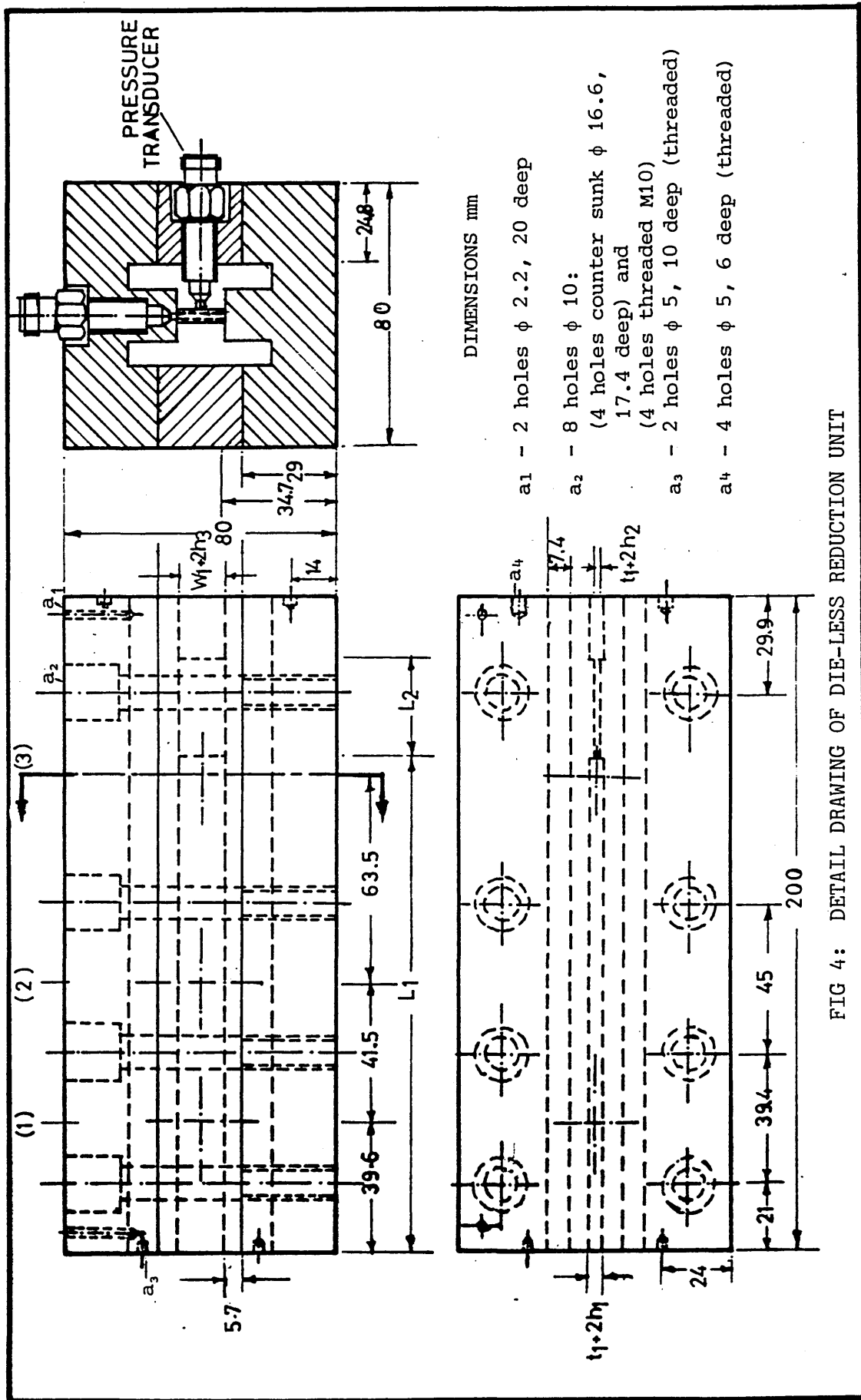
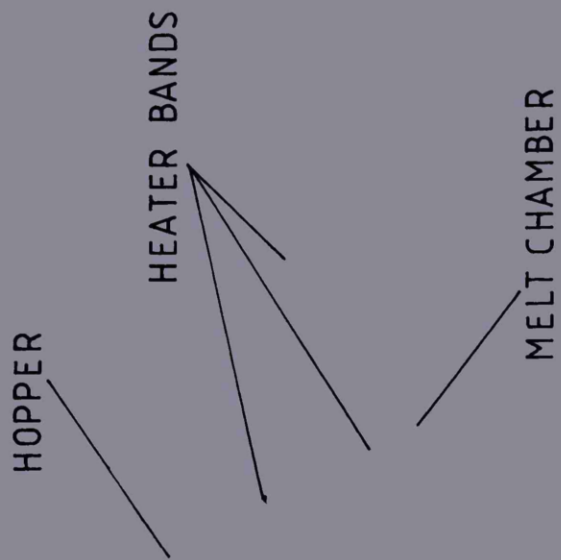


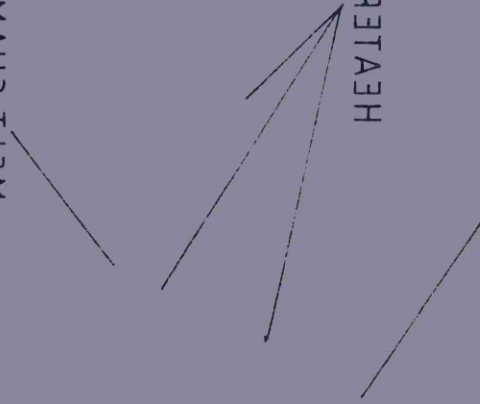
FIG 4: DETAIL DRAWING OF DIE-LESS REDUCTION UNIT

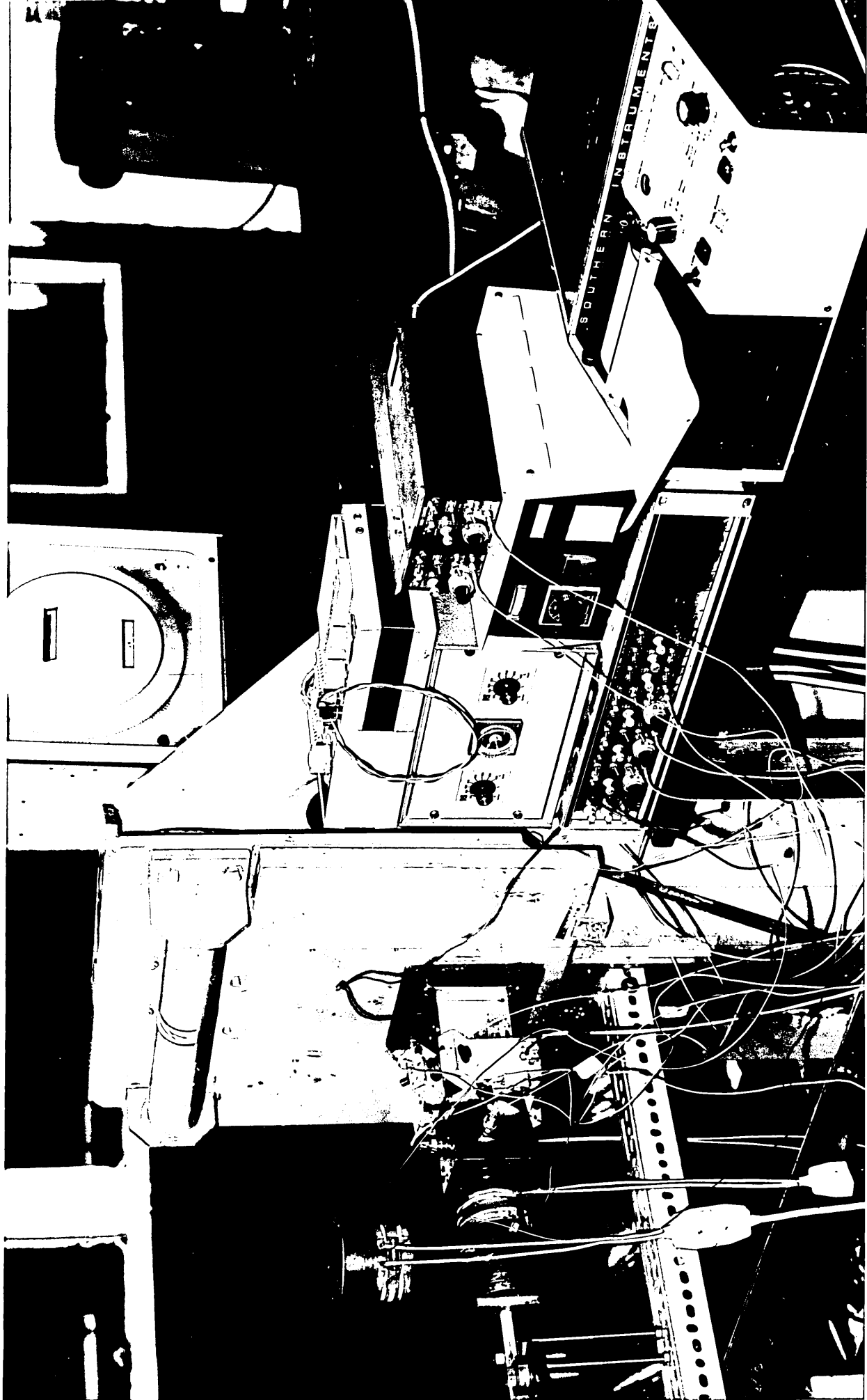


WEGT CHAMBER

HEATER BANDS

HOPPER





CHARGE AMPLIFIERS

ELECTRONIC
THERMOMETER



TEMPERATURE CONTROLLERS

UV RECORDER

CHARGE AMPLIFIERS

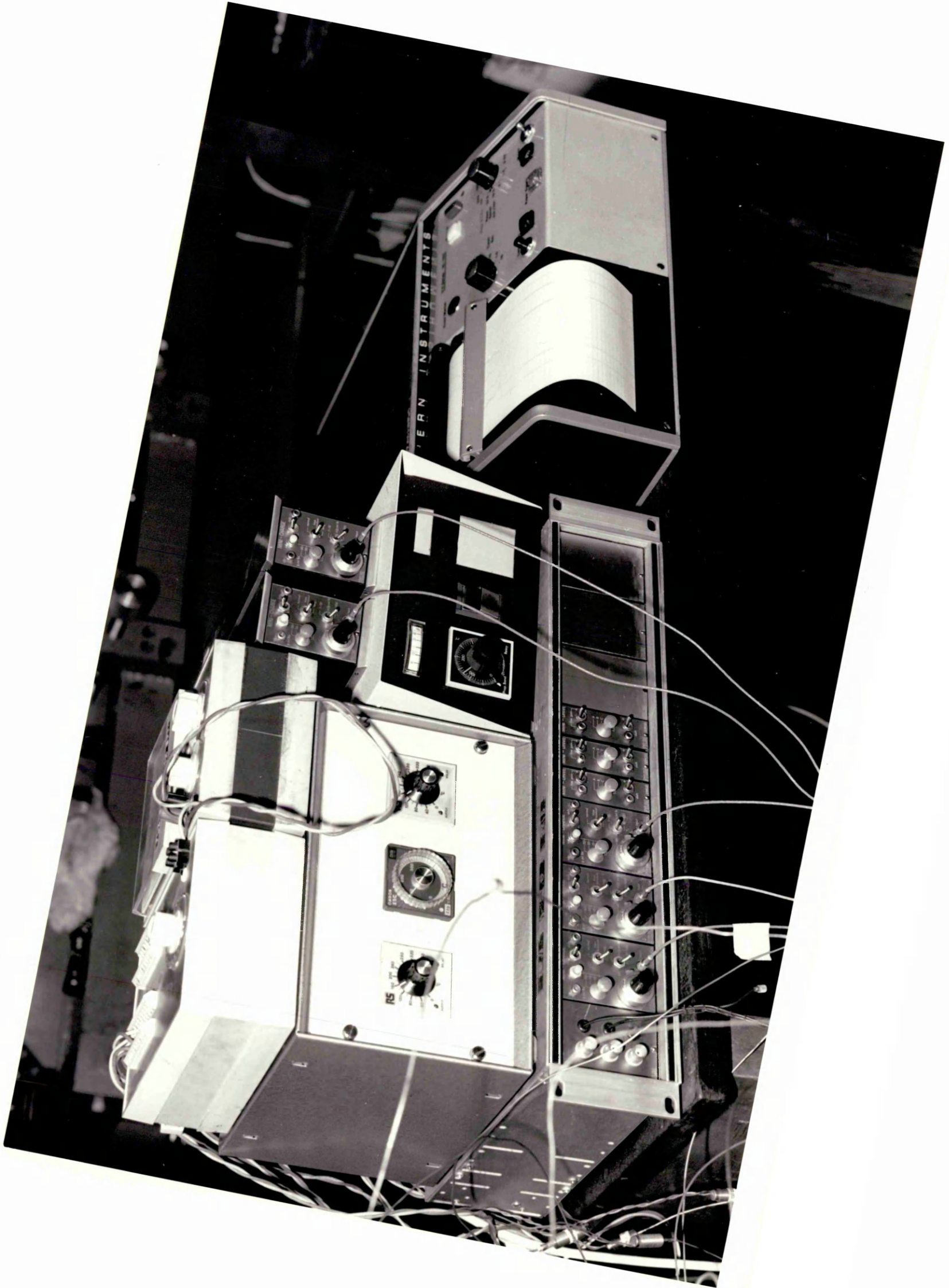
UV RECORDER

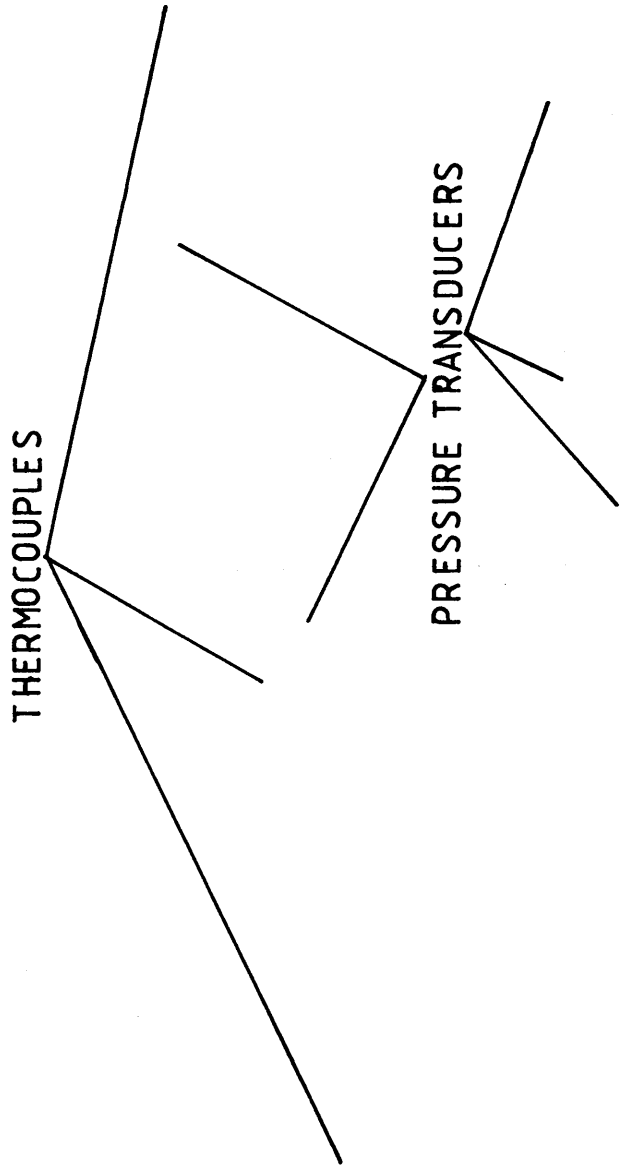
CHARGE AMPLIFIER

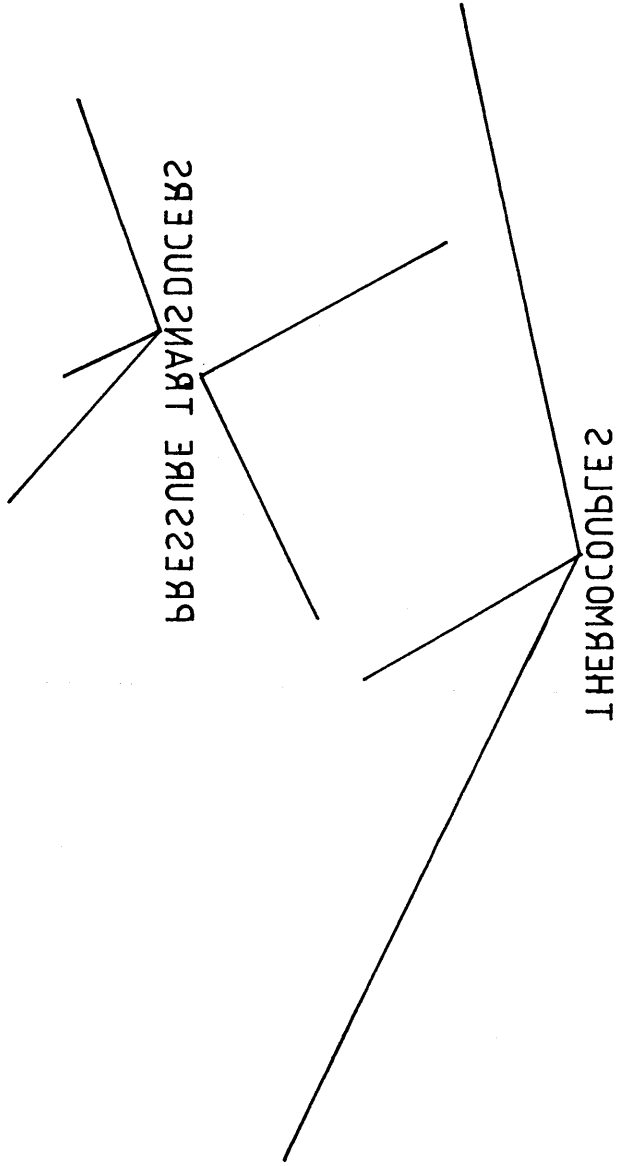
TEMPERATURE CONTROLLER

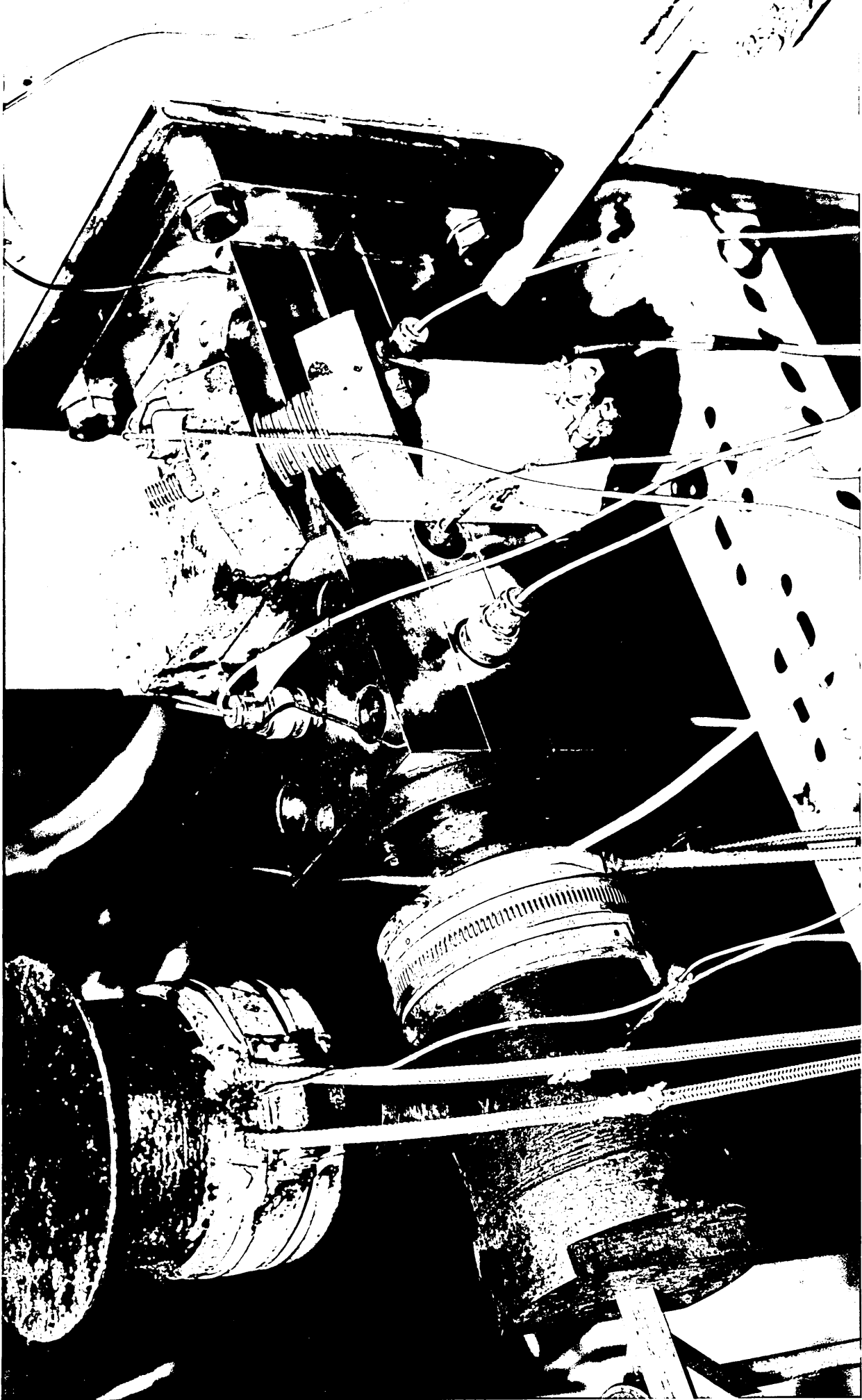
CHARGE AMPLIFIER

THERMOMETER
ELECTRONIC







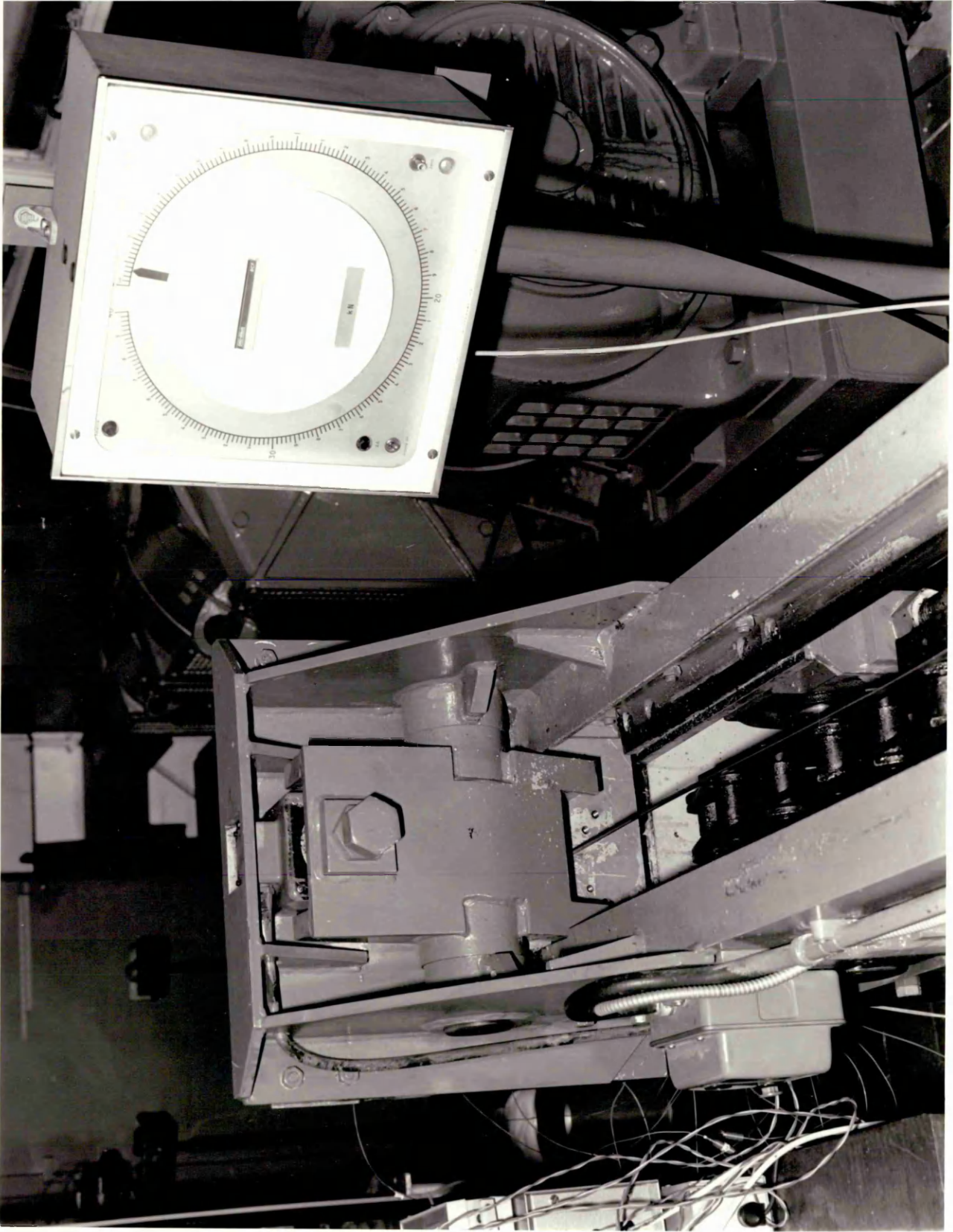


LOAD INDICATOR

LOAD CELL

ROTACIOM I DA0J

TOVD CEFF



EXPERIMENTAL MATERIALS

3.1 Rheology of Polymer Melts

3.1.1 Introduction

In this novel process molten polymer was used as the pressure medium. The polymers used in the present study were low density polyethylene (Alkathene WVG23) and ELVAX650. Limited experiments were conducted on a Devenport extrusion rheometer to determine the initial melt viscosity and other rheological characteristics related to the present set-up. Figures 5 and 6 show the results of rheological behaviour of the melt at different temperatures and shear rates.

The rheological results were found to conform to a cubic non-linear equation of the form

$$\tau + K\tau^3 = \mu\dot{\gamma}$$

where

τ = Shear stress

$\dot{\gamma}$ = Shear rate

K = Non-Newtonian factor

μ = Initial viscosity of polymer melt

3.1.2 Rheological Behaviour

Polymers consist of long molecules built up by successive linking of monomers (mostly made by chemical bond between carbon and hydrogen atoms) into chain or network structures. The small molecules are not bonded chemically but lie close together and forces that operate between these are known as Van-der-Waal's forces. Molecules of long chain polymers slide past each other

under a shear force above a glass transition temperature ie the material is capable of flowing and such materials are known as thermoplastics, whereas polymers with strong cross linked structures are generally known as thermosetting polymers.

The rheological behaviour of polymer melts and solutions is complex and there is no usable constitutive equation that describes quantitatively all the flow phenomenon involving polymer melts. Hence it is customary that only those equations which are related to the problem on hand are used for predicting the various flow aspects of polymers. It is generally agreed that viscosity has a dominant effect on the flow of any fluidic medium. Therefore it is important to determine the viscosity of the fluid and examine the parameters which influence the viscosity.

In the present study the polymers used are in the melt condition at certain temperatures, and at certain shear rates dependent upon the velocity of the strip. The factors affecting the viscosity of the polymers are temperature of polymer melt, pressure and induced stress and strains.

3.1.2.1 Viscosity-Temperature Dependence

The viscosity of a polymer melt is temperature dependent, being lower at higher temperatures, at a given stress level. Attempts have been made to obtain a fundamental explanation of the difference in temperature dependence of viscosity between different polymers. Several empirical treatments for developing master curves have also been published (42-44). These publications indicate that the temperature dependence of viscosity is purely a function of the melt temperature and the glass transition temperature of the polymer melt. For polymers far above the glass

transition temperature or melting point, the viscosity may be related by an Arrhenius equation of the form

$$\mu = k \exp \left(\frac{E}{RT} \right) \quad (3.1)$$

where

μ , is melt viscosity

k , at a given shear stress is constant characteristics of the polymer and its molecular weight

R , gas constant

The activation energy, E , is generally in the range between 2.09×10^7 to 2.09×10^8 joules/Kg mole (45).

William, Landell and Ferry⁽⁴⁶⁾ showed that viscosity, μ , of a polymer melt at a given temperature, T , may be related to its viscosity, μ_0 , at an arbitrary reference temperature, T_0 , and could be expressed by the universal WLF equation

$$\mu = \mu_0 \exp \left[\frac{-8.86 (T - T_0)}{101.6 + T - T_0} \right] \quad (3.2)$$

The WLF equation is applicable over the temperature range of $T_0 \pm 50^\circ$. An alternative equation of viscosity-temperature dependence is given by

$$\mu = \mu_{Tg} \exp \left[\frac{-17.44 (T - Tg)}{51.6 + T - Tg} \right] \quad (3.3)$$

where

Tg , is glass transition temperature of the polymer melt

μ_{Tg} , is the melt viscosity at temperature Tg .

In general, the WLF equation begins to fail as a valid representation of viscosity-temperature dependence in the temperature region $Tg + 100$, and in some high region the behaviour becomes Arrhenius in form.

Another empirical equation often used for melts (47) is

$$\mu = a e^{-bT} \quad (3.4)$$

where a and b are constants.

The data (48) indicating the temperature dependence of the melt viscosity at constant stress and pressure are presented in Figure 7. From Figure 7, it can be seen that viscosity of low density polyethylene decreases by a factor of 3 when increasing the temperature by 40°C. The melt viscosity temperature dependence resulting from Figure 7 could be expressed by,

$$\mu = \mu_0 e^{-\alpha T} \quad (3.5)$$

where

μ , is melt viscosity

μ_0 , is initial viscosity at a reference temperature

α , is constant for a given polymer and its value varies from 0.02 to 0.1.

3.1.2.2 Viscosity-Pressure Dependence

If the pressure is applied to the melt there is a time dependent decrease in volume which has the effect of producing a higher viscosity in the melt. The effect of hydrostatic pressure on the apparent viscosity is not as well understood as the effects of temperature and shear rate. Maxwell and Jung⁽⁴⁹⁾ studied the effect of hydrostatic pressure on melt viscosity of branched polyethylene and polystyrene at constant shearing stress. They conducted experiments between 0 to 24,000 Psi (165 MNm⁻²) and experimental results showed that the apparent viscosity of polyethylene increased 14-fold in this pressure range and that of polystyrene increased by 135-fold when the pressure was increased from atmospheric to 18000 Psi (124 MNm⁻²).

Westover⁽⁵⁰⁻⁵¹⁾ reported that the higher molecular weight polyethylene (low melt flow index) increases more in viscosity with pressure than do the lower molecular weight (high melt index) of the same density or density range. He measured apparent viscosity of several polymeric materials between atmospheric pressure and 25000 Psi (172 MNm⁻²), at fixed temperature and shear stress. He showed that the apparent viscosity of polyethylene increased by a factor of five when hydrostatic pressure was changed from 2000 psi to 25000 psi (13.8 to 172 MNm⁻²). It was noted that polypropylene responded in the same way as did the polyethylene. The viscosity of polystyrene increased over 100-fold as hydrostatic pressure was increased from 2000 to 25000 psi (13.8 to 172 MNm⁻²). Choi⁽⁵²⁾ determined that the apparent viscosity of polyethylene (9.95 gg/cc density and 0.4 melt index, at 190°C and 7.12 sec⁻¹) was increased nearly four fold as the average pressure in the barrel was raised from atmospheric to 24000 psi (165 MNm⁻²). Data (48) indicating the pressure dependence of melt viscosity at constant stress and temperature are presented in Figure 8.

The influence of the pressure on viscosity is quantitatively similar but opposite in sign to that of temperature. The suitable way of representing that dependence is to describe a temperature/pressure equivalence (48). Figure 9 shows the effect of an increase in pressure in terms of equivalent drop in temperature necessary to maintain constant viscosity.

3.1.2.3 Effect of Shear Rate on Viscosity

Polymer melt is non-Newtonian in behaviour and its viscosity is also affected by shear rate. The apparent viscosity decreases as the rate of shear increases. Figure 10 presents shear viscosity

data for five materials at their normal processing temperatures. Figure 11 demonstrates the variation in apparent viscosity with temperature and shear rates.

3.1.2.4 Flow Instabilities

When polymer melts are subjected to higher rates of shear a condition of slip occurs and several kinds of flow instability can develop. The magnitude of shear stress at which this flow instability occurs is called the critical shear stress. Different kinds of defects occur due to flow instabilities, two main defects are known as shark skin and melt fracture. The two defects are distinguishable by the characteristic ridge like structure running transversely to the flow direction in shark skin, whereas melt fracture gives helical or irregular patterns.

Several workers (53-59) have studied to elucidate the melt flow instabilities and there is general agreement on the following points:

- (i) instability sets in at a critical value of shear stress,
- (ii) critical shear stress has values in the region of 0.1 to 1.0 MN/m² for most polymers,
- (iii) critical shear stress does not vary widely with temperature,
- (iv) a discontinuity in the slope of viscosity-shear stress occurs,
- (v) the flow defects occur when non-Newtonian fluids were involved,
- (vi) the flow defects are often associated with die-entrance and surface finish.

3.2 Stress-Strain Characteristics of the Strip Material

Copper strip of two aspect ratios were used for the experimental work. The stress-strain characteristics of the strip material were determined by performing plane-strain compression tests, so that the data could be used in the theoretical analysis. The compression test specimens were lubricated during the test to minimize frictional effects. Figures 12 and 13 show the stress-strain curves of the materials tested. The stress-strain curves were fitted to take the form

$$y = y_0 + K_0 \varepsilon^n$$

where,

y_0 = initial yield stress

K_0 = strain hardening constant

ε = natural strain

n = strain hardening index

The values obtained for the experimental material are listed below:

Material I

$$W_1 = 12.7 \text{ mm} \quad t_1 = 1.59 \text{ mm}$$

$$y_0 = 75 \text{ MNm}^{-2} \quad K_0 = 600 \text{ MNm}^{-2} \quad n = 0.6$$

Material II

$$W_1 = 19.1 \text{ mm} \quad t_1 = 1.59 \text{ mm}$$

$$y_0 = 78 \text{ MNm}^{-2} \quad K_0 = 554 \text{ MNm}^{-2} \quad n = 0.54$$

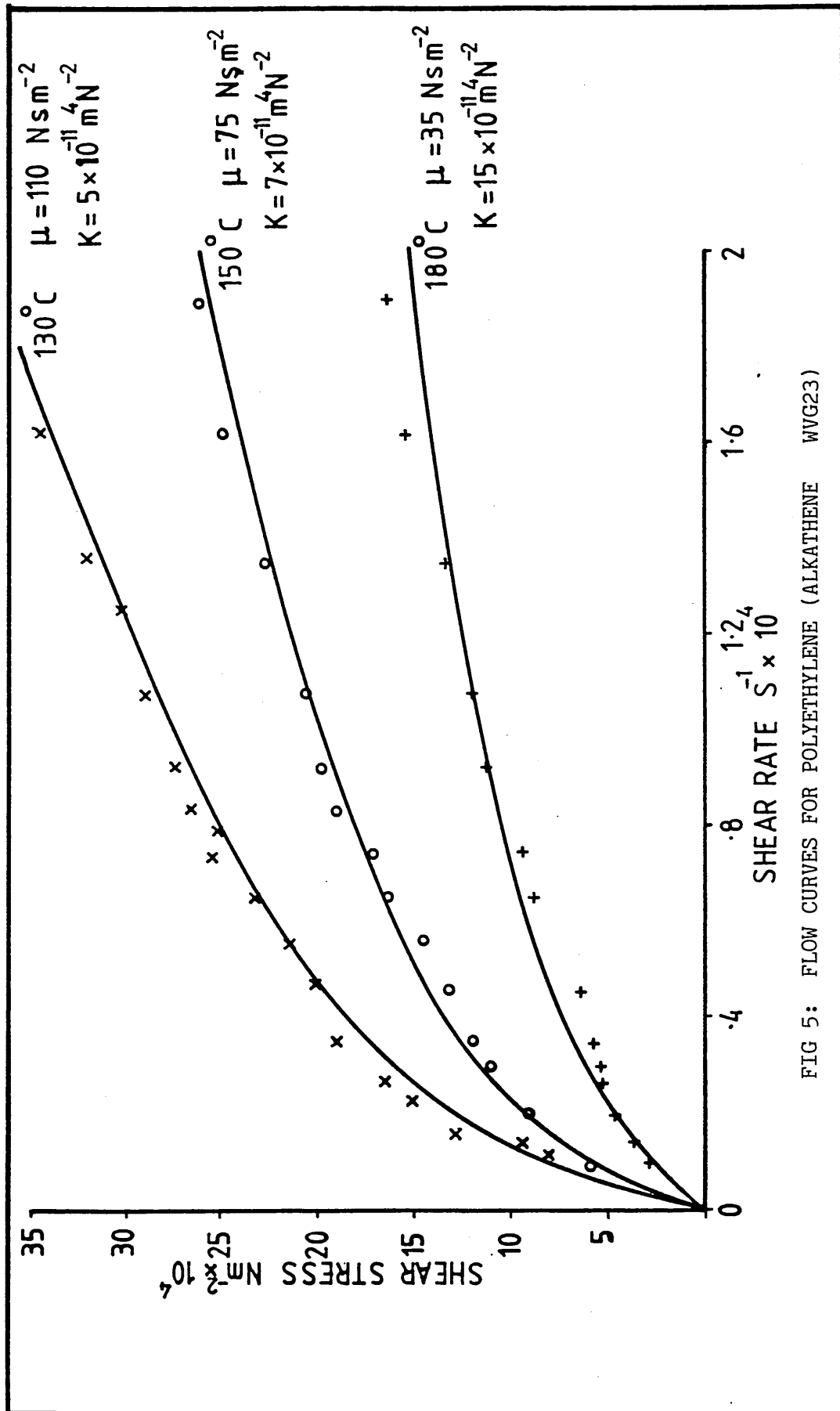


FIG 5: FLOW CURVES FOR POLYETHYLENE (ALKATHENE WVG23)

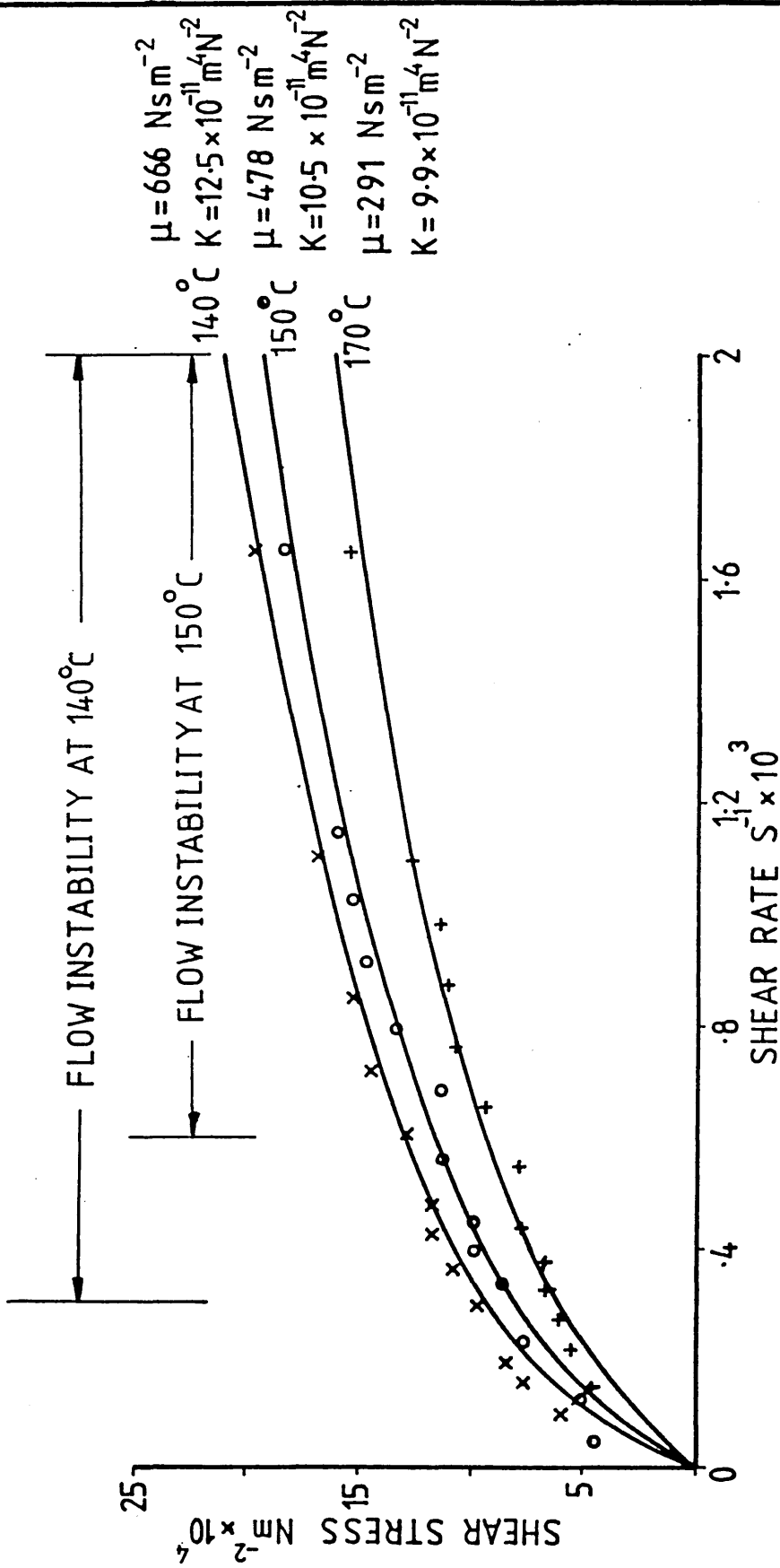


FIG 6: FLOW CURVES FOR ELVAX650

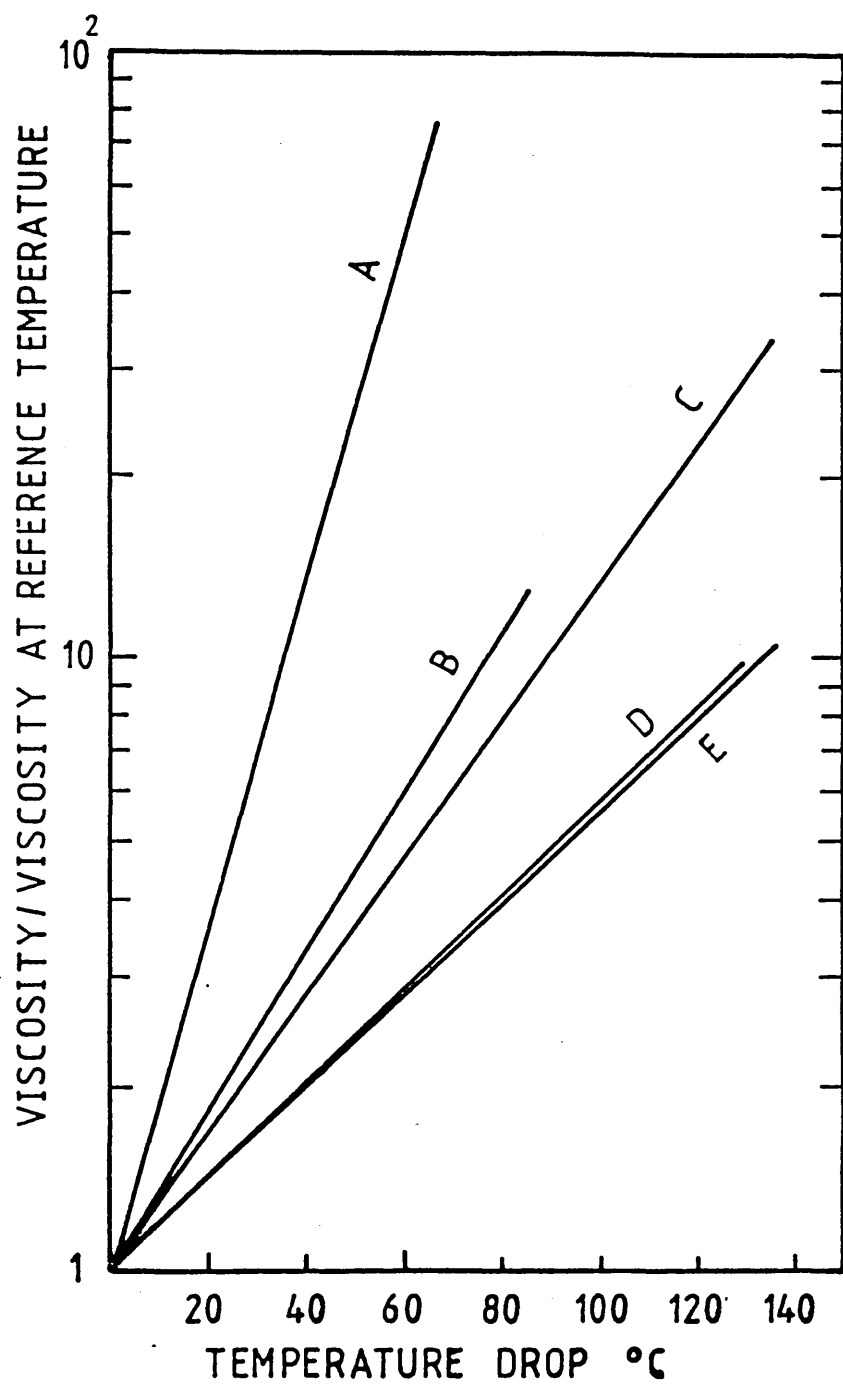


FIG 7: MELT VISCOSITY AT CONSTANT STRESS AND PRESSURE AS A FUNCTION OF TEMPERATURE (REFERENCE 48)
 A - ACRYLIC POLYMER; B - TYPE 6,6 NYLON
 C - LOW DENSITY POLYETHYLENE ; D - ACETAL COPOLYMER
 E - POLYPROPYLENE

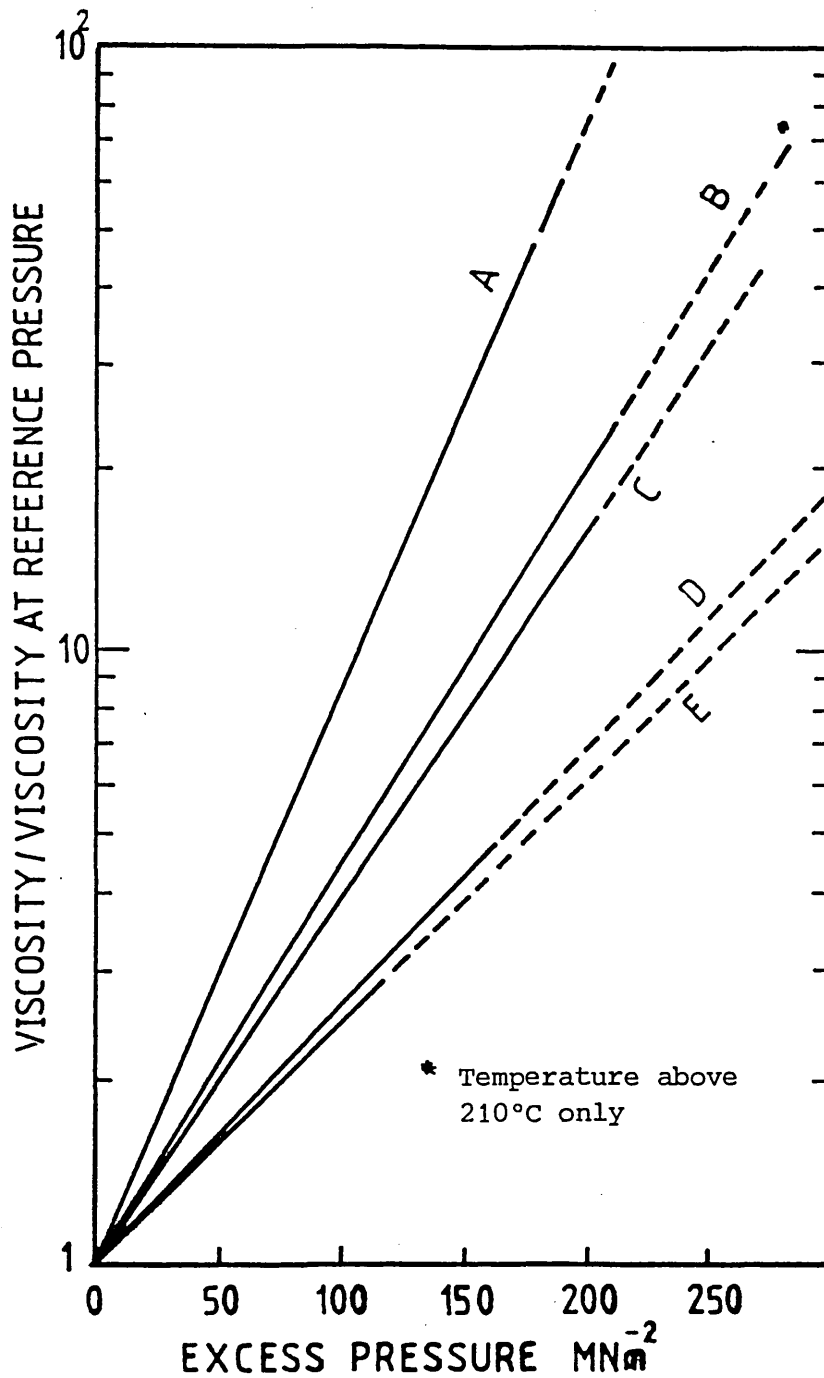


FIG 8: MELT VISCOSITY AT CONSTANT STRESS AND TEMPERATURE
AS A FUNCTION OF PRESSURE (REFERENCE 48)
A - ACRYLIC POLYMER; B - POLYPROPYLENE
C - LOW DENSITY POLYETHYLENE; D - TYPE 6,6 NYLON
E - ACETAL COPOLYMER

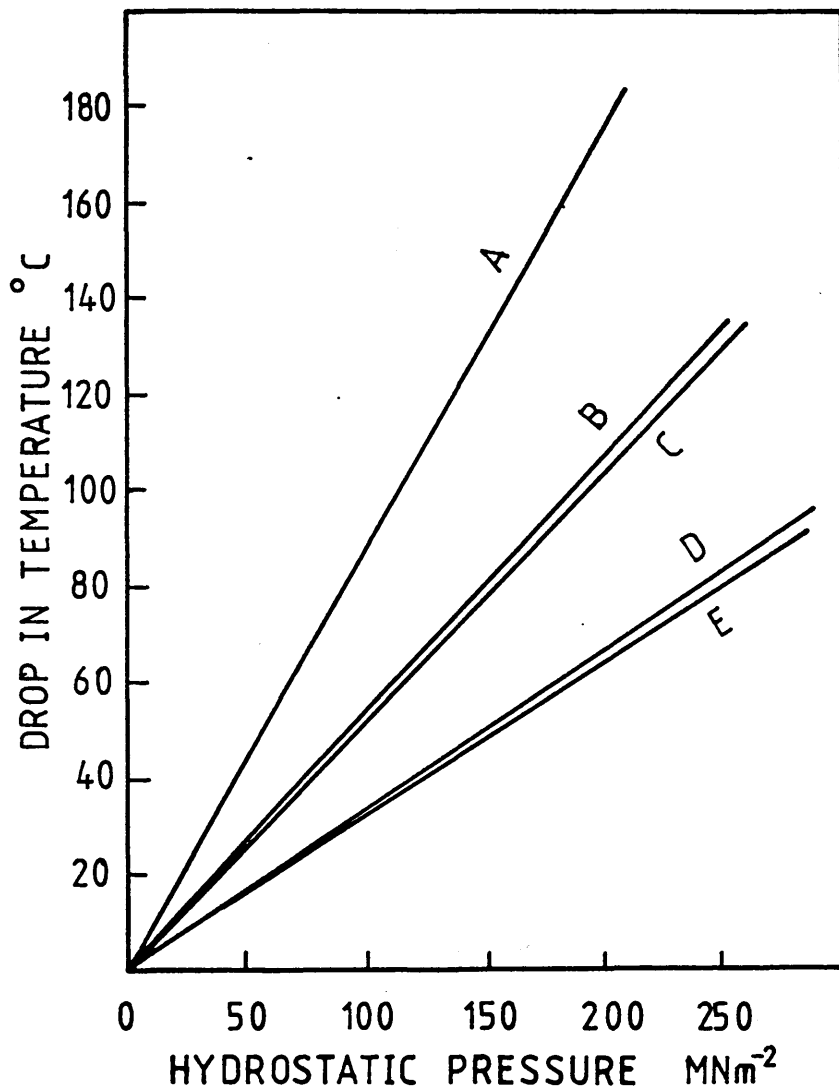


FIG 9: TEMPERATURE/PRESSURE EQUIVALENCE FOR CONSTANT VISCOSITY (REFERENCE 48)

- A - POLYPROPYLENE; B - LOW DENSITY POLYETHYLENE
 C - ACETAL COPOLYMER; D - ACRYLIC POLYMER
 E - TYPE 6,6 NYLON

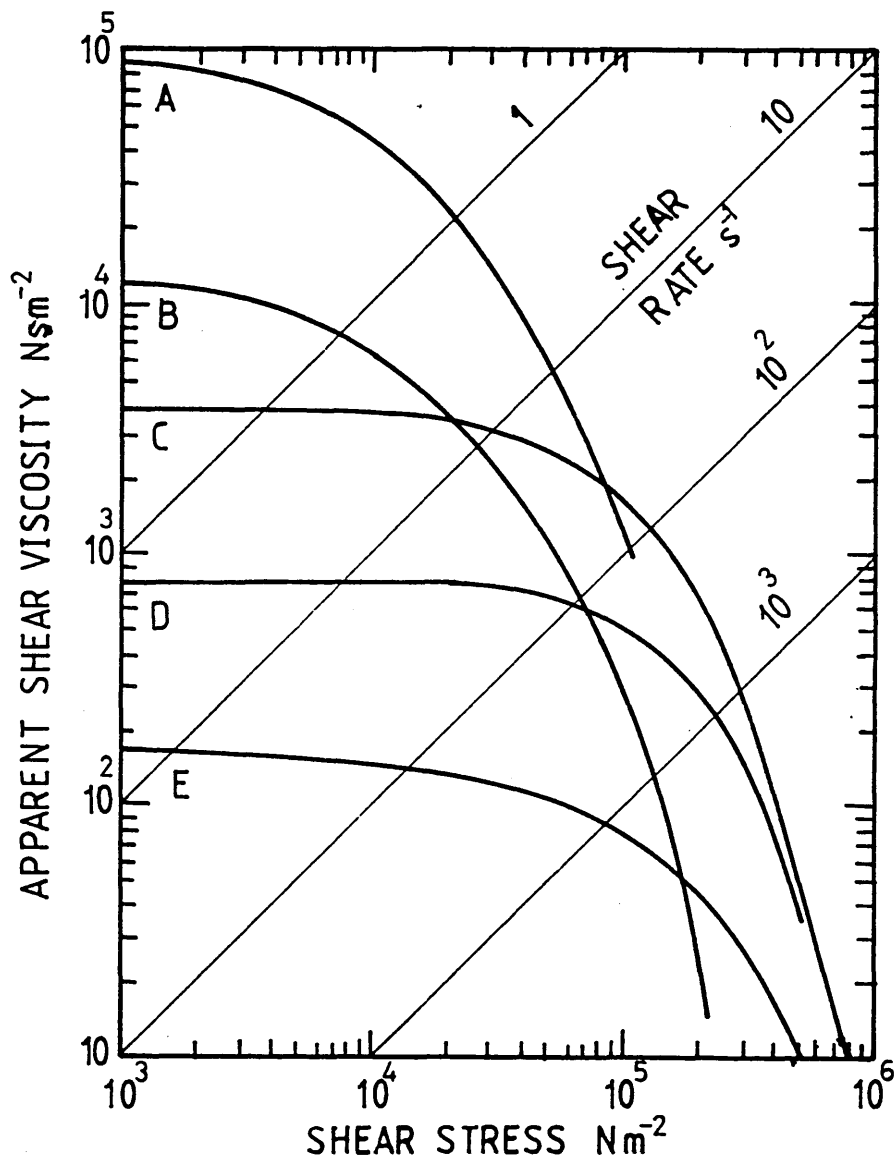


FIG 10: TYPICAL CURVES OF APPARENT SHEAR VISCOSITY VS SHEAR STRESS FOR FIVE THERMOPLASTICS (AT ATMOSPHERIC PRESSURE) (REFERENCE 48)

- A - LOW DENSITY POLYETHYLENE AT 170°C
- B - PROPYLENE/ETHYLENE COPOLYMER AT 230°C
- C - ACRYLIC AT 230°C
- D - ACETAL COPOLYMER AT 200°C
- E - NYLON AT 285°C

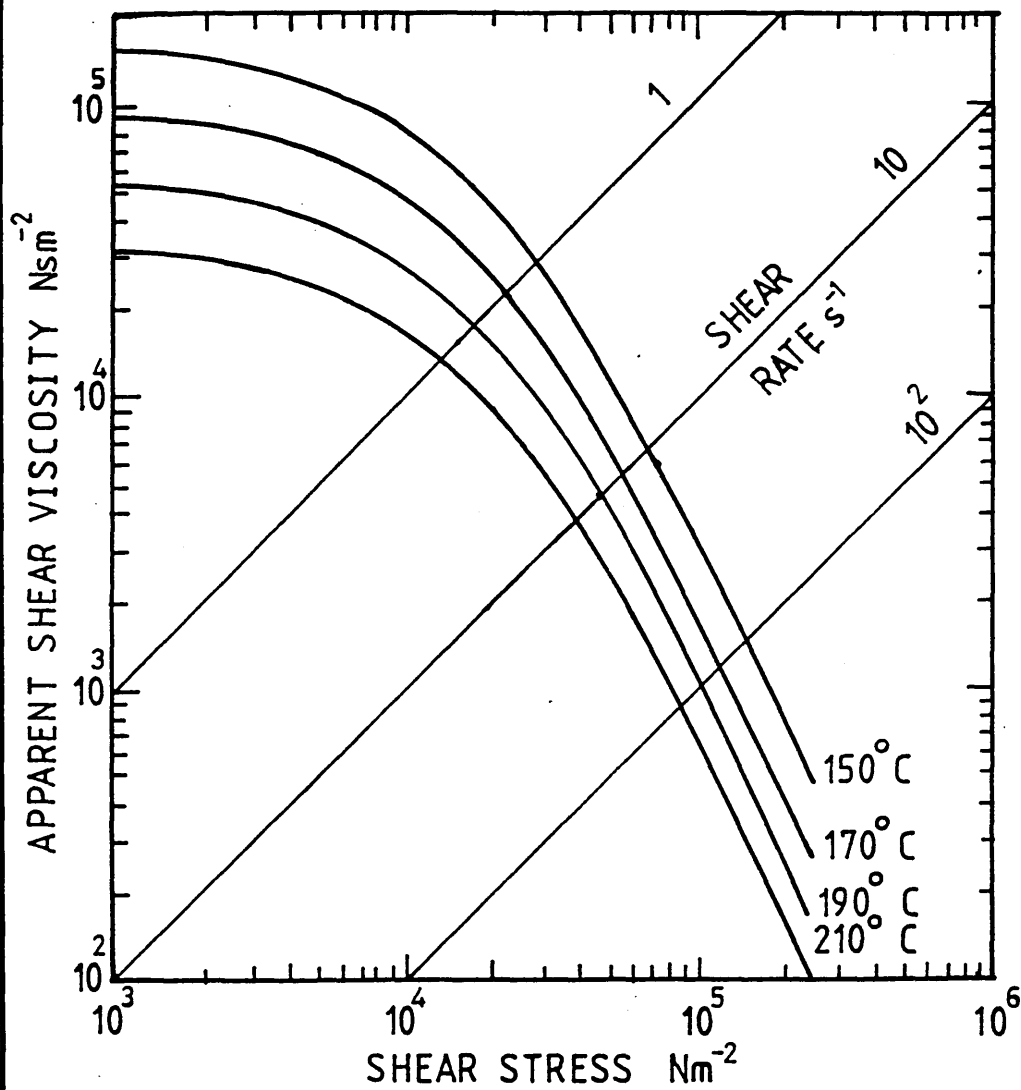


FIG 11: TYPICAL CURVES SHOWING THE TEMPERATURE DEPENDENCE OF THE APPARENT SHEAR VISCOSITY OF A LOW DENSITY POLYETHYLENE (ALKATHENE XDG33, ATMOSPHERIC PRESSURE) (REFERENCE 48)

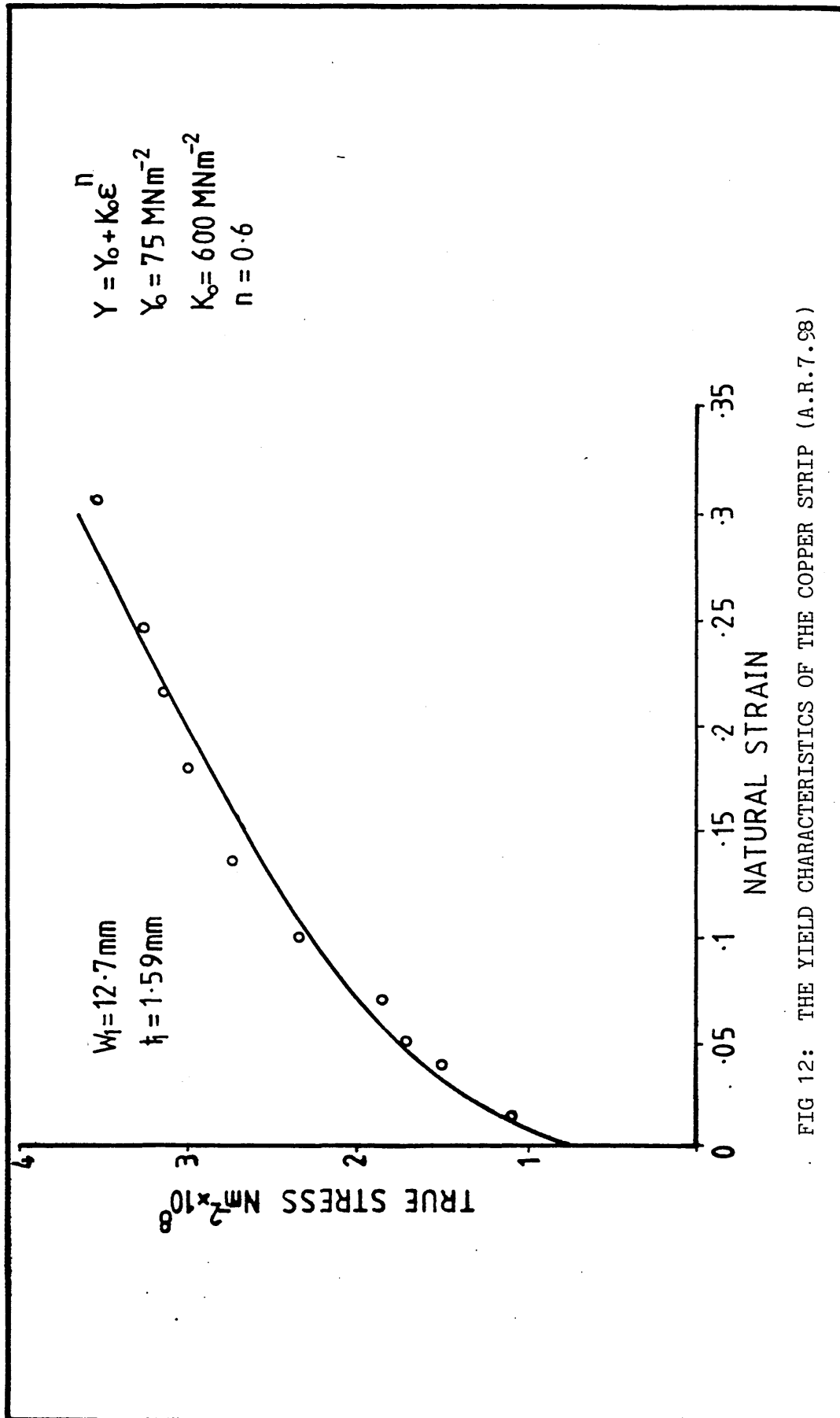


FIG 12: THE YIELD CHARACTERISTICS OF THE COPPER STRIP (A.R.7.98)

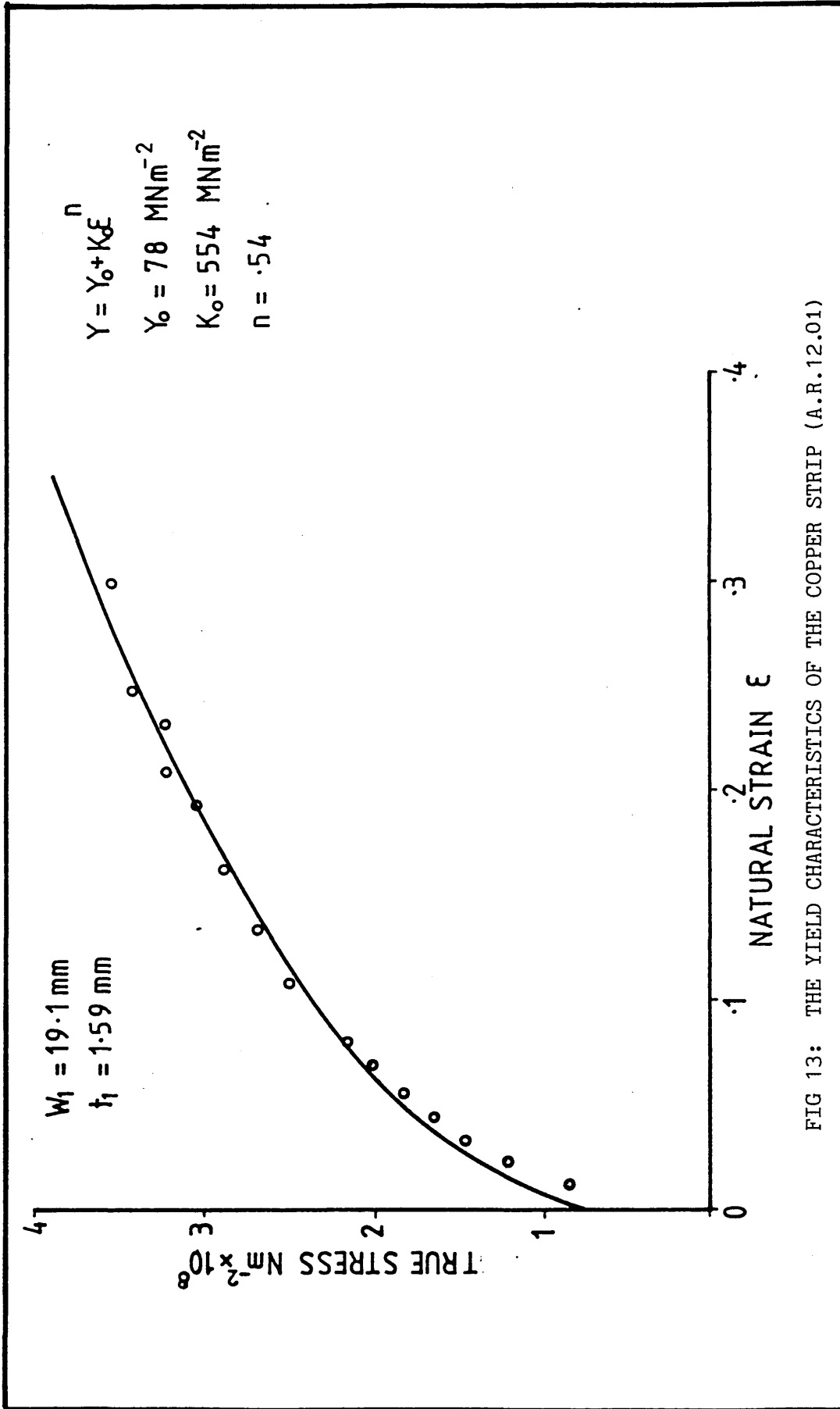


FIG 13: THE YIELD CHARACTERISTICS OF THE COPPER STRIP (A.R.12.01)

CHAPTER 4

EXPERIMENTAL RESULTS

4.1 Experimental Procedure

The experimental procedure involved passing of strip between guiding rollers and feeding a sufficient length through the melt chamber and the reduction unit to facilitate gripping by the dog clamp. The melt chamber and hopper were then filled with a quantity of polymer granules sufficient to carry out at least one set of tests. Five pressure transducers were mounted on the reduction unit, three for recording the pressure in Section A and the other two for Section B. The melt temperature was set on the temperature regulator and the heater bands were switched on. The equipment was left for 1½ hours to reach the steady state temperature condition. The temperature was monitored and controlled thermostatically. The motor was started and the required speed was obtained by adjusting the regulating knob, the other instrumentation was also switched on. The charge amplifiers for the pressure transducers were switched to the long time position and the paper drive on the UV recorder was set in motion before engaging the dog clamp to the running chain. While drawing the strip the drawing load was noted from the load indicator and when about 2m length of the strip was drawn the dog clamp was disengaged from the chain. The UV paper drive and charge amplifiers were switched back to their original position. The test number and drawing load were recorded on a data sheet, the same number was noted on the UV paper for subsequent collection and analysis. An identification tag was also placed on the drawn strip. The

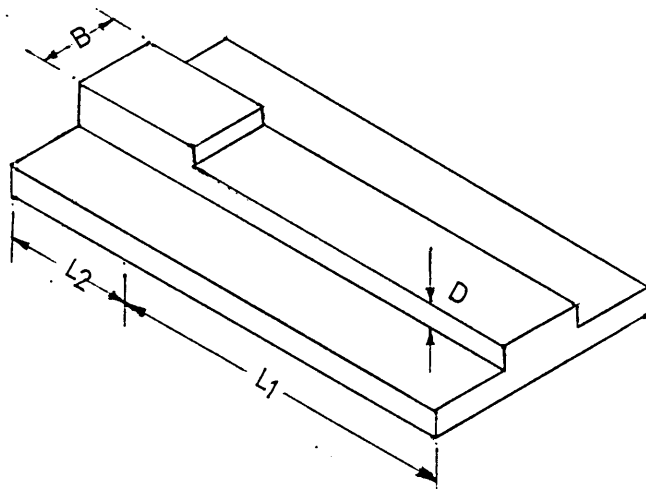
speed of the motor was then increased in suitable steps and the procedure was repeated for each increment. When analysing the experimental data the traces on the UV paper were measured and recorded on the data sheet. The drawn strip was measured for both thickness and width at three different positions after peeling off the coating, in order to calculate the reduction in strip size.

4.2 Experimental Results

Experiments were carried out systematically, by changing the geometry of the unit and melt temperature, at different drawing speeds varying between 0.1 and 0.5 m/s to investigate the effects of these factors on the process. The geometry of the unit was varied by altering,

- (a) width B of inserts to get the variation in gap h_3 in the Section B,
- (b) dimension D to get different values of gap h_1 and hence gap ratios h_1/h_2 ,
- (c) length L_1 to obtain different length ratios L_1/L_2 .

Two kinds of polymers, [low density polyethylene (Alkathene WVG23) and ELVAX650], and strip of two different widths (12.7mm and 19.1mm) were used to examine the effect of working fluid and aspect ratio respectively on the process parameters. The melt temperature was also varied to study the effect of melt viscosity. For every test the pressure, drawing load and the reduction in strip size were recorded. Dimensional details of the inserts of the die-less reduction unit used for the tests are shown in the schematic diagram shown below:



Schematic Diagram of the Insert

Dimensions of the units employed for tests were:

To examine the effect of gap h_3 ;

$$h_1 = 0.2\text{mm} \quad h_2 = 0.02\text{mm}$$

$$L_1 = 150\text{mm} \quad L_2 = 30\text{mm}$$

$$h_3 = 0.50, 0.22, 0.13 \text{ and } 0.04 \text{ mm}$$

To examine the effect of gap ratio h_1/h_2 ;

$$h_2 = 0.02\text{mm} \quad h_3 = 0.133\text{mm}$$

$$L_1 = 150\text{mm} \quad L_2 = 30\text{mm}$$

$$h_1 = 0.2, 0.3, 0.4 \text{ and } 0.5\text{mm}.$$

To study the effect of length ratio L_1/L_2 ;

$$h_1 = 0.3\text{mm} \quad h_2 = 0.02\text{mm}$$

$$h_3 = 0.133\text{mm} \quad L_2 = 30\text{mm}$$

$$L_1 = 130, 150 \text{ and } 169.5\text{mm}$$

The experimental results obtained are presented in this section in graphical form for convenience. A full discussion on these results is presented in Chapter 7.

4.2.1 Percentage Reduction Versus Speed

Figures 14 to 24 show the effect of gap h_3 on percentage reduction in thickness, width and area of the strip against the drawing speed.

Figures 14 and 15 give the percentage reduction in thickness and width of 12.7mm wide strip when WVG23 was used at temperatures 130°C and 150°C respectively. The reductions were found initially to increase up to a certain value of speed for both temperatures. Further increase in speed caused the reductions to decrease. This trend was found for all gaps. The maximum reductions of 7.4% in thickness and 4.6% in width were observed with a small gap of 0.04 mm at a speed of 0.2 m/s, which fall to 5.6% in thickness and 4.0% in width at a higher speed of 0.5 m/s at a melt temperature of 130°C. A marked difference was observed for measured percentage reductions in thickness at lower temperature, which showed no significant difference for the three gaps of 0.22 , 0.13 and 0.04 mm, at speeds up to 0.2 m/s. It is evident from the curves for the two gaps of 0.13 and 0.04 mm that the percentage reduction in thickness is not significantly different.

The results obtained using ELVAX650 at temperatures of 140°C and 170°C are presented in Figures 16 and 17. The general trends were found to be the same as in Figures 14 and 15. A noticeable difference was the level of reductions in width. This polymer produced higher percentage reductions in width (typically 5.5% in width and 6.3% in thickness at 0.3 m/s) as compared to those obtained using WVG23 (typically 4.26% in width and 6.4% in thickness at 0.3 m/s). A maximum reduction of 6.3% in thickness and 5.5% in width were observed, using gap $h_3 = 0.04$ mm, at speed of 0.3 m/s which decreased to 4.8 per cent in thickness and 4.8% in width at higher speed of 0.5 m/s. The effect of gap h_3 on percentage reduction in thickness at lower temperature was found to be similar to that observed with WVG23.

Figure 18 shows the reductions measured for the strip, 19.1mm wide, using WVG23 at 130°C. The results obtained with ELVAX650 at 140°C are presented in Figure 19. These results indicate the same trends as observed with narrow strip (Figures 14 to 17). It was noticed that when ELVAX650 was used the observed percentage reduction in width was approximately of the same magnitude for both gaps.

Figures 20 to 24 show the measured percentage reduction in area for the two strips with two polymers at various temperatures. These results show similar trends to those observed in Figures 14 to 19. A maximum reduction in area in excess of 11% was noted for the lower temperature of the polymer melt and gap of $h_3 = 0.04$ mm.

Figures 25 to 36 demonstrate the effect of the gap ratio h_1/h_2 on the observed percentage reductions in thickness, width and area of the strip with the two polymers at different melt temperatures.

Figures 25 and 26 show the results giving percentage reduction in thickness and width of the narrow strip with polymer WVG23 at melt temperatures of 130°C and 150°C respectively. It was observed that initially an increase in gap h_1 caused an increase in the reductions. The reductions were found to increase with speed and eventually reached a maximum at a certain speed. Further increase in speed caused the deformation of the strip to reduce. A maximum reduction in excess of 8% in thickness and 4% in width was measured with gap ratio of 15 at melt temperature of 130°C. The percentage reduction in width was found to be approximately of same magnitude beyond the speed of 0.35 m/s for all gap ratios.

The results obtained by using polymer ELVAX650 at temperatures of 140°C and 170°C are plotted in Figures 27 and 28 respectively. These results show similar behaviour to those given in Figures 25 and 26. It was also noted that with this polymer the resulting percentage reduction in width (typically 5.48% in width and 8.1% in thickness) was greater compared to that obtained with polymer WVG23 (typically 4.48% in width and 8.3% in thickness) for same gap ratio, a pattern which has been observed for the results with gap h_3 . Maximum reductions of 8.1% in thickness and 5.7% in width were attained with a gap ratio of 15 at melt temperature of 140°C.

Curves giving the percentage reduction in thickness and width for the strip, 19.1mm wide, with two polymers at different temperatures are shown in Figures 29 and 30. These figures show similar trends as observed with narrow strips. There was a marked difference between the percentage reduction in size achieved with the two sections of the strip. It was found that smaller percentage reductions were obtained when wider strips were used.

The measured percentage reduction in area for the two strips with two kinds of polymers at different melt temperatures are plotted in Figures 31 to 36. Maximum reduction in excess of 12% for the strip, 12.7mm wide, and in excess of 10% with wider strip was observed at a temperature of 130°C using a unit with the gap ratio of 15.

Figures 37 to 40 show the effect of length ratio on percentage reduction in the size of the strip against the drawing speed.

Figure 37 shows the curves for the results obtained by using three different length ratios with WVG23 at 130°C. It was observed that more reductions occurred when length ratio of 5 was used. At the speeds higher than 0.2 m/s, similar percentage reductions in thickness were measured for the two length ratios of 4.33 and 5.65. In addition, no significant difference in percentage reduction in width was observed beyond the speed of 0.4 m/s with all the length ratios.

Figure 38 shows the graphs for the results obtained with polymer ELVAX650 at 140°C, using the reduction units with three different length ratios. The trend of the results was found to be similar to Figure 37. It was noticed that similar percentage reductions were obtained with the two length ratios of 4.33 and 5.65 at slow drawing speeds up to 0.2 m/s. Higher percentage reductions were observed with length ratio of 5. The measured percentage reductions in width were found to be greater compared to those obtained with WVG23.

The effect of length ratio on the total percentage reduction in area for the two polymers is demonstrated in Figures 39 and 40. The general trends of the results were consistent to those observed in Figures 37 and 38.

Figures 41 to 46 present the effect of melt viscosity on the reductions in the strip size with the two polymers for the two strips.

Figure 41 shows the percentage reduction in thickness and width of 12.7mm wide strip, using WVG23 at 130°C, 150°C and 180°C with constant gap and length ratios. At all speeds larger reductions

were obtained at the lowest temperature of 130°C and as the temperature was increased the percentage reductions reduced by about 50% at higher temperature of 180°C.

Figure 42 shows the curves for percentage reduction in thickness and width of the strip 12.7mm wide, using ELVAX650 at temperatures of 140°C, 150°C and 170°C. Higher reductions in the strip size were observed at melt temperature of 140°C, and the percentage reductions were found to reduce by about 25% when the melt temperature was increased from 140°C to 170°C, at the drawing speeds greater than 0.25 m/s.

Similar graphs for 19.1mm wide strip using WVG23 as pressure medium at temperatures of 130°C, 150°C and 180°C are represented in Figure 43. Again higher percentage reductions were observed at low melt temperature, ie 130°C.

Figures 44 to 46 demonstrate the effect of viscosity on the percentage reduction in area for the two sections of the strip with the polymers WVG23 and ELVAX650.

Figures 47 to 50 illustrate the effect of aspect ratio on the percentage reduction in the strip size against the drawing speed. Figures 47 and 48 give the percentage reductions in the thickness and width of the strip with the polymers WVG23 at 130°C and ELVAX650 at 140°C respectively. The effect of the aspect ratio on percentage reduction in area is given by Figures 49 and 50 for the two polymers.

It was observed that maximum percentage reductions were obtained with the strip of small aspect ratio over the whole range of drawing speed.

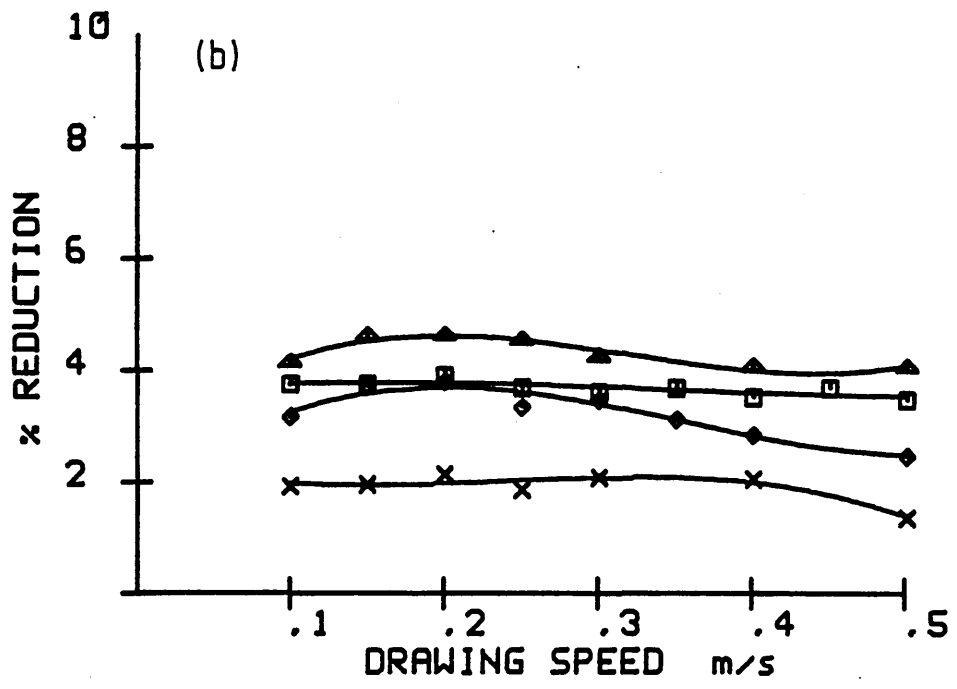
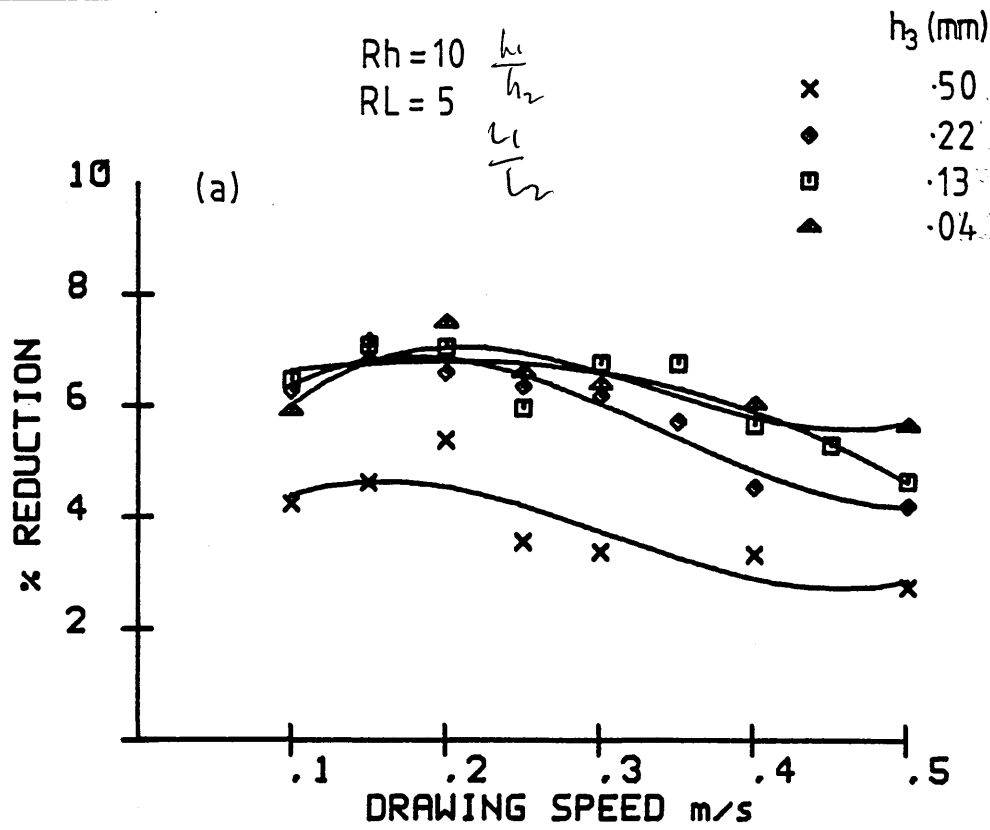
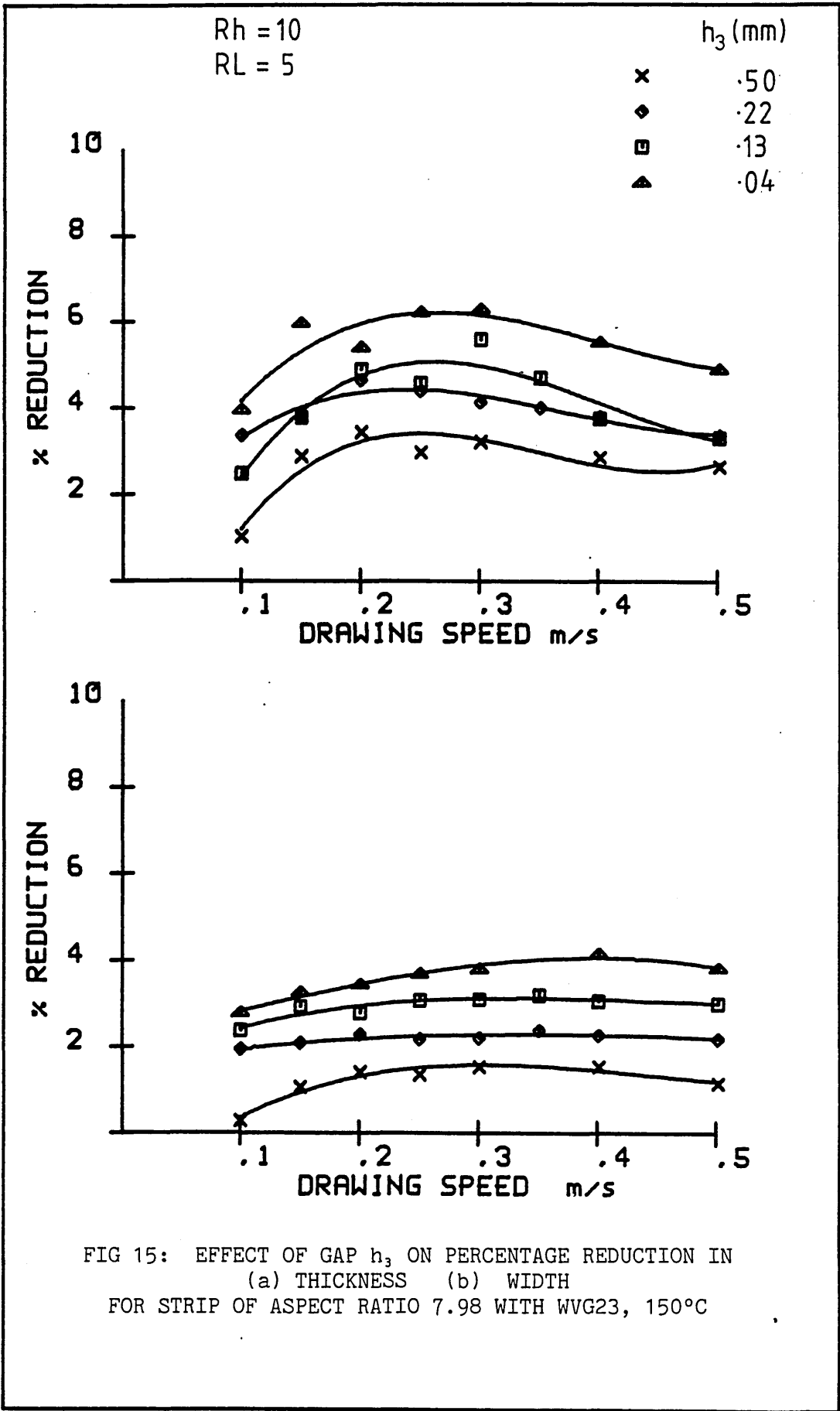


FIG 14: EFFECT OF GAP h_3 ON PERCENTAGE REDUCTION IN
 (a) THICKNESS (b) WIDTH
 FOR STRIP OF ASPECT RATIO 7.98 WITH WVG23, 130°C

$\frac{w_1}{t_1}$



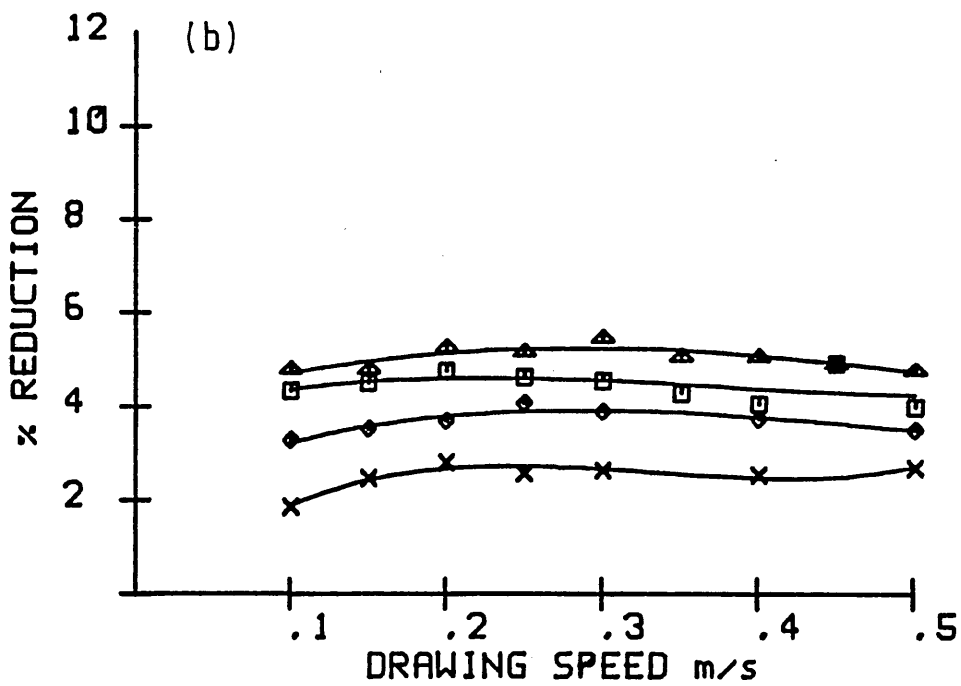
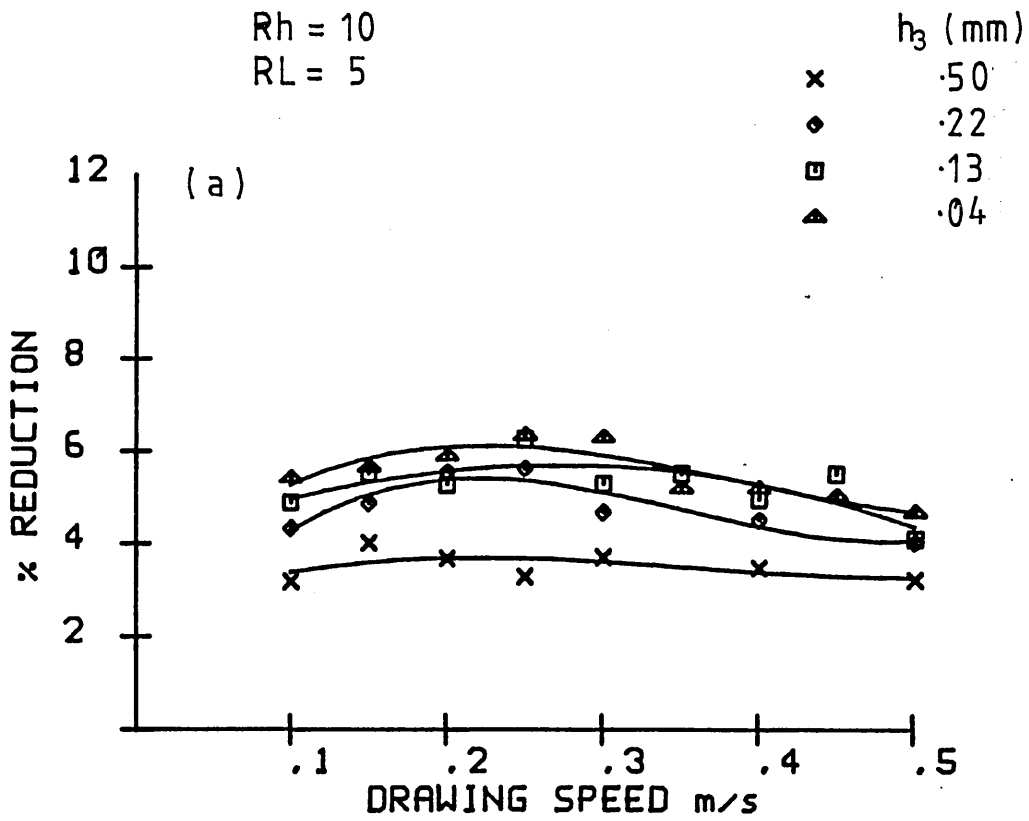


FIG 16: EFFECT OF GAP h_3 ON PERCENTAGE REDUCTION IN
 (a) THICKNESS (b) WIDTH
 FOR STRIP OF ASPECT RATIO 7.98 WITH ELVAX650, 140°C

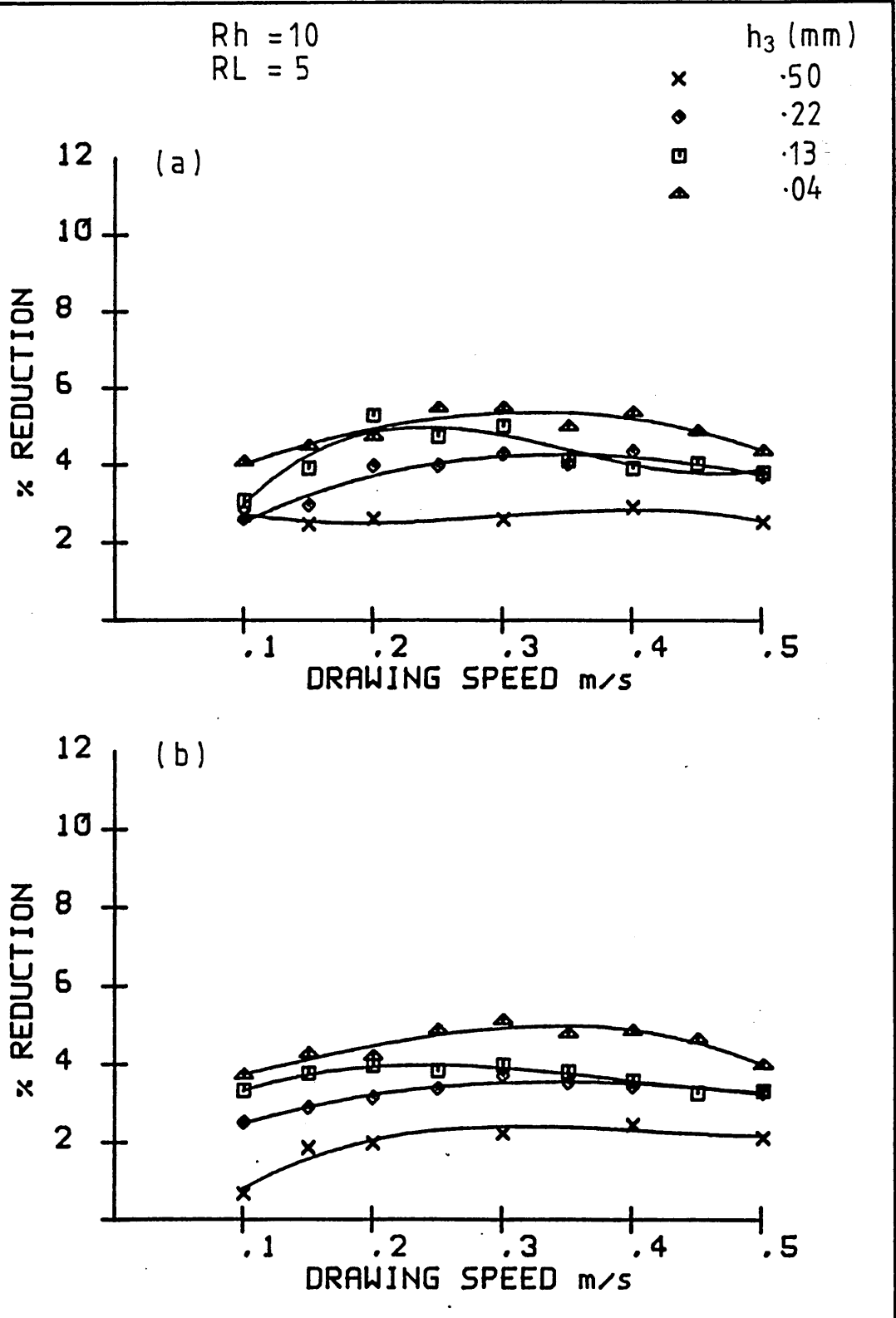


FIG 17: EFFECT OF GAP h_3 ON PERCENTAGE REDUCTION IN
 (a) THICKNESS (b) WIDTH
 FOR STRIP OF ASPECT RATIO 7.98 WITH ELVAX650, 170°C

Rh = 10
RL = 5

h_3 (mm)

x .22
♦ .13

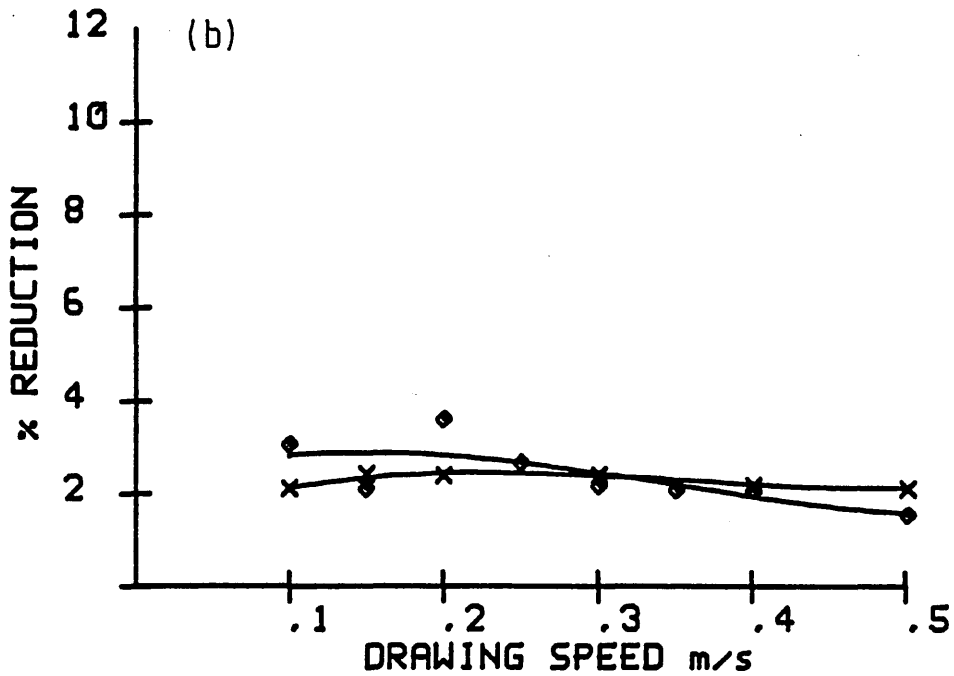
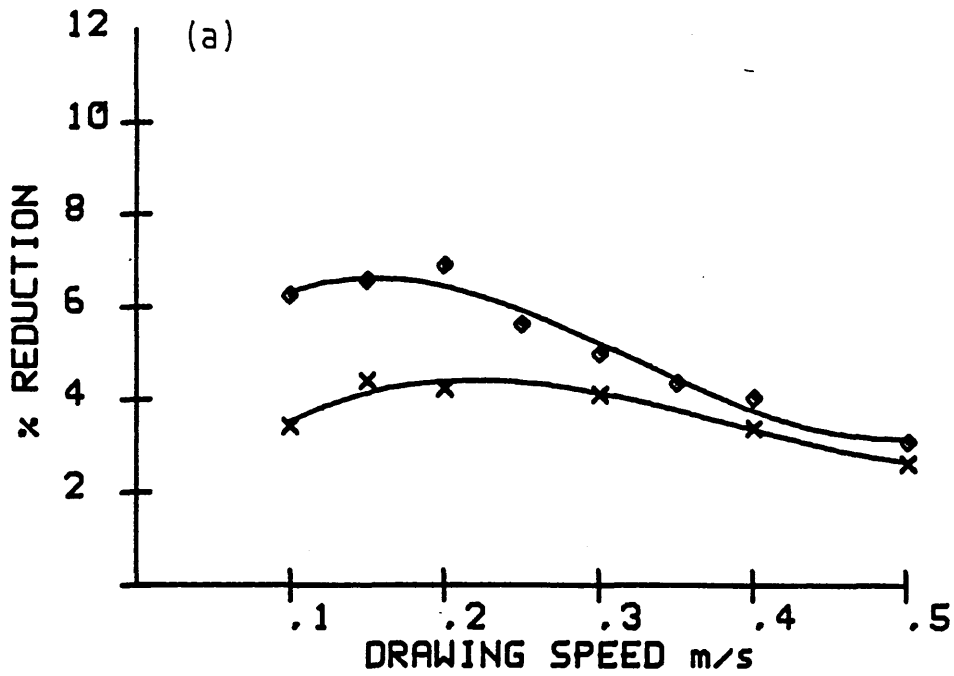


FIG 18: EFFECT OF GAP h_3 ON PERCENTAGE REDUCTION IN
(a) THICKNESS (b) WIDTH
FOR STRIP OF ASPECT RATIO OF 12.01 WITH WVG23, 130°C

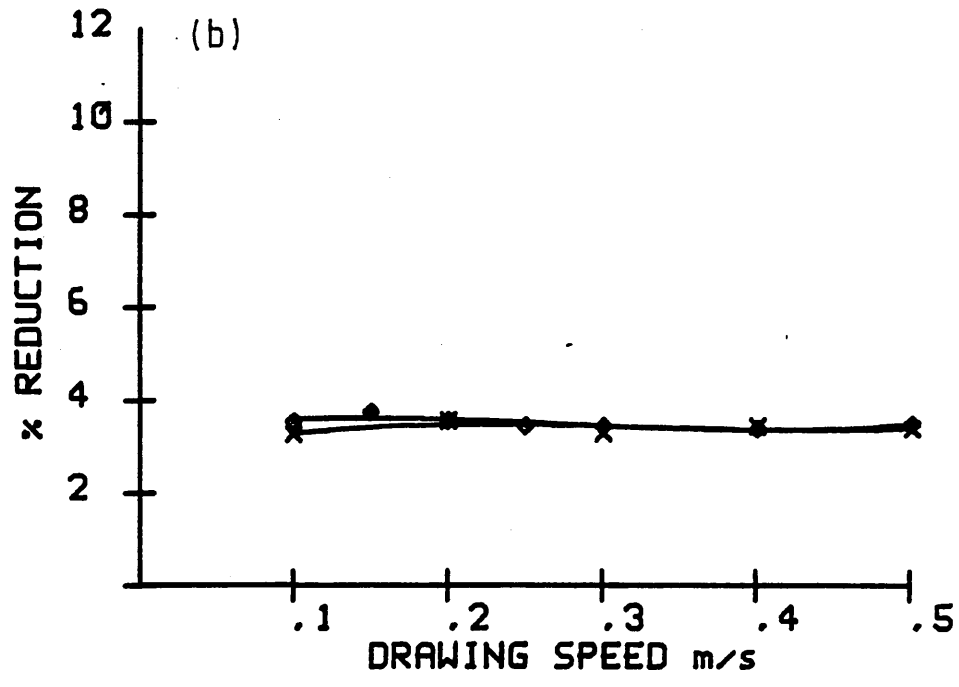
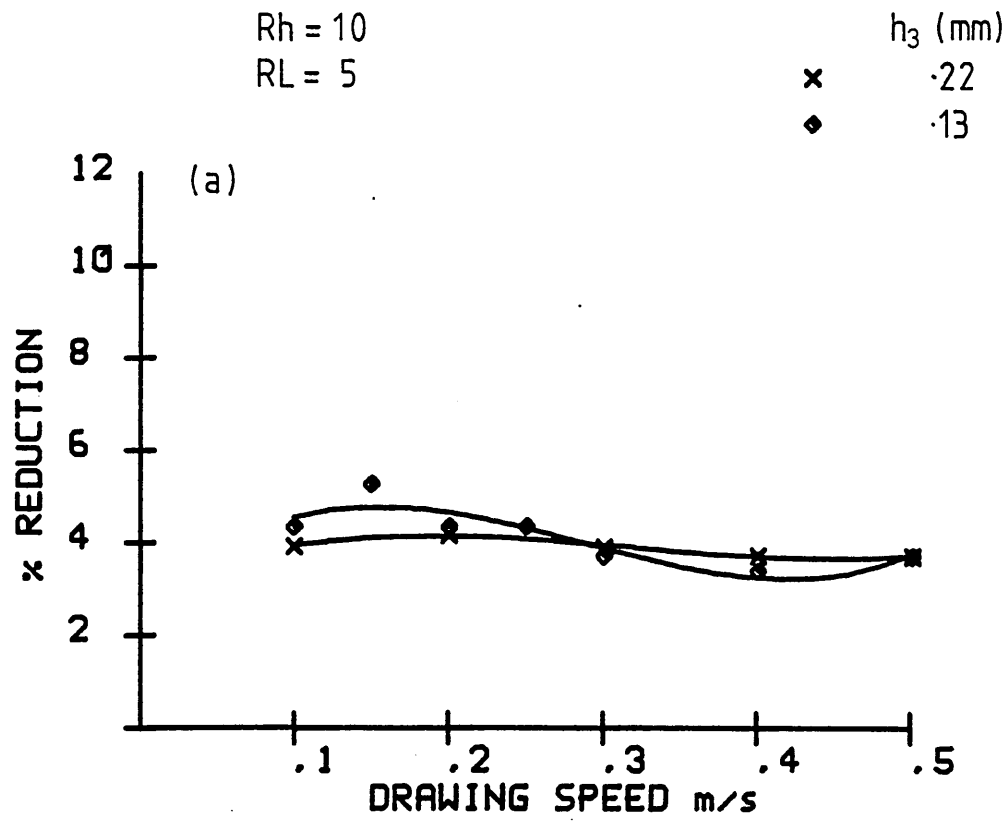


FIG 19: EFFECT OF GAP h_3 ON PERCENTAGE REDUCTION IN
 (a) THICKNESS (b) WIDTH
 FOR STRIP OF ASPECT RATIO 12.01 WITH ELVAX650, 140°C

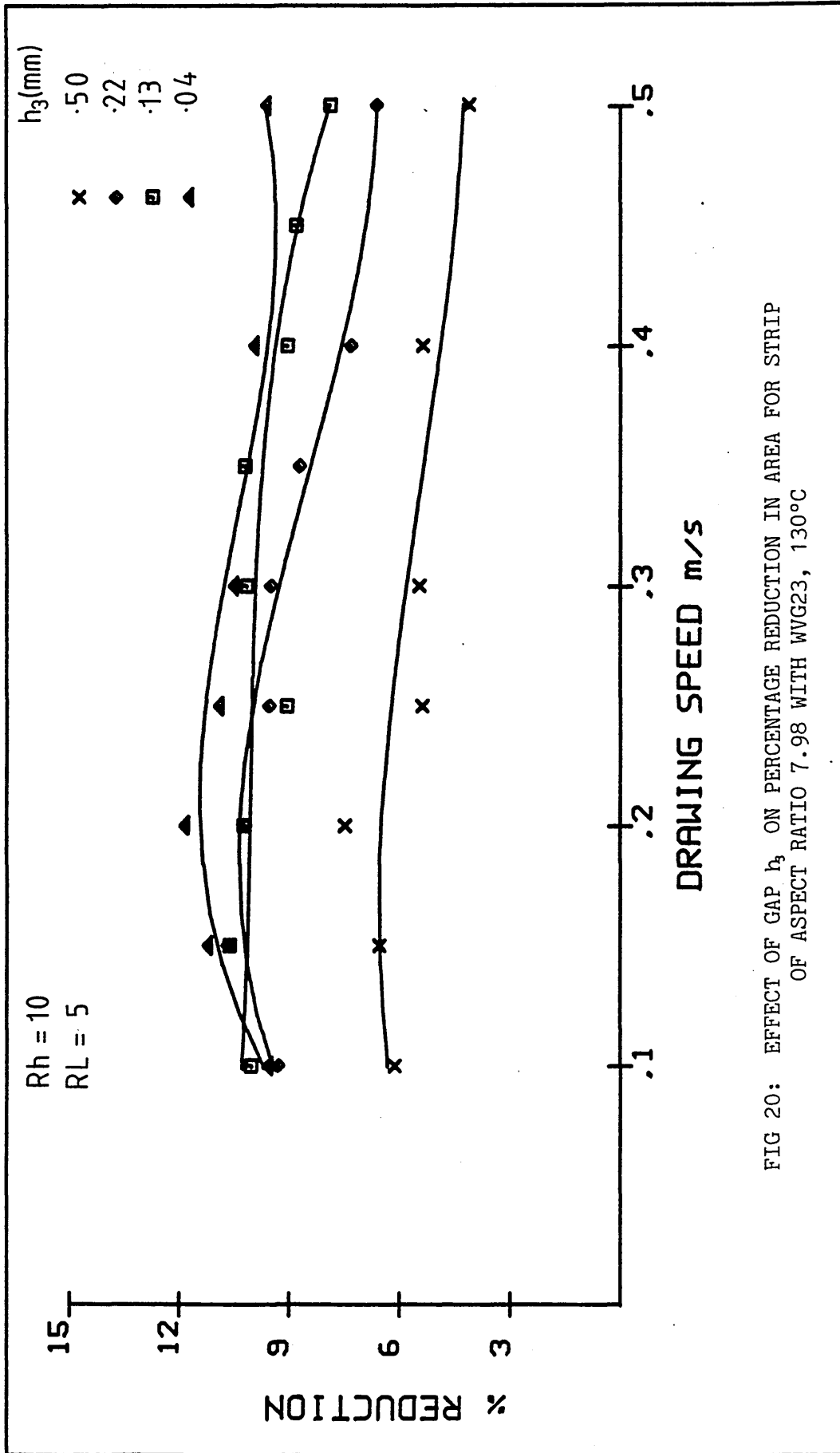


FIG 20: EFFECT OF GAP h_3 ON PERCENTAGE REDUCTION IN AREA FOR STRIP OF ASPECT RATIO 7.98 WITH WVG23, 130°C

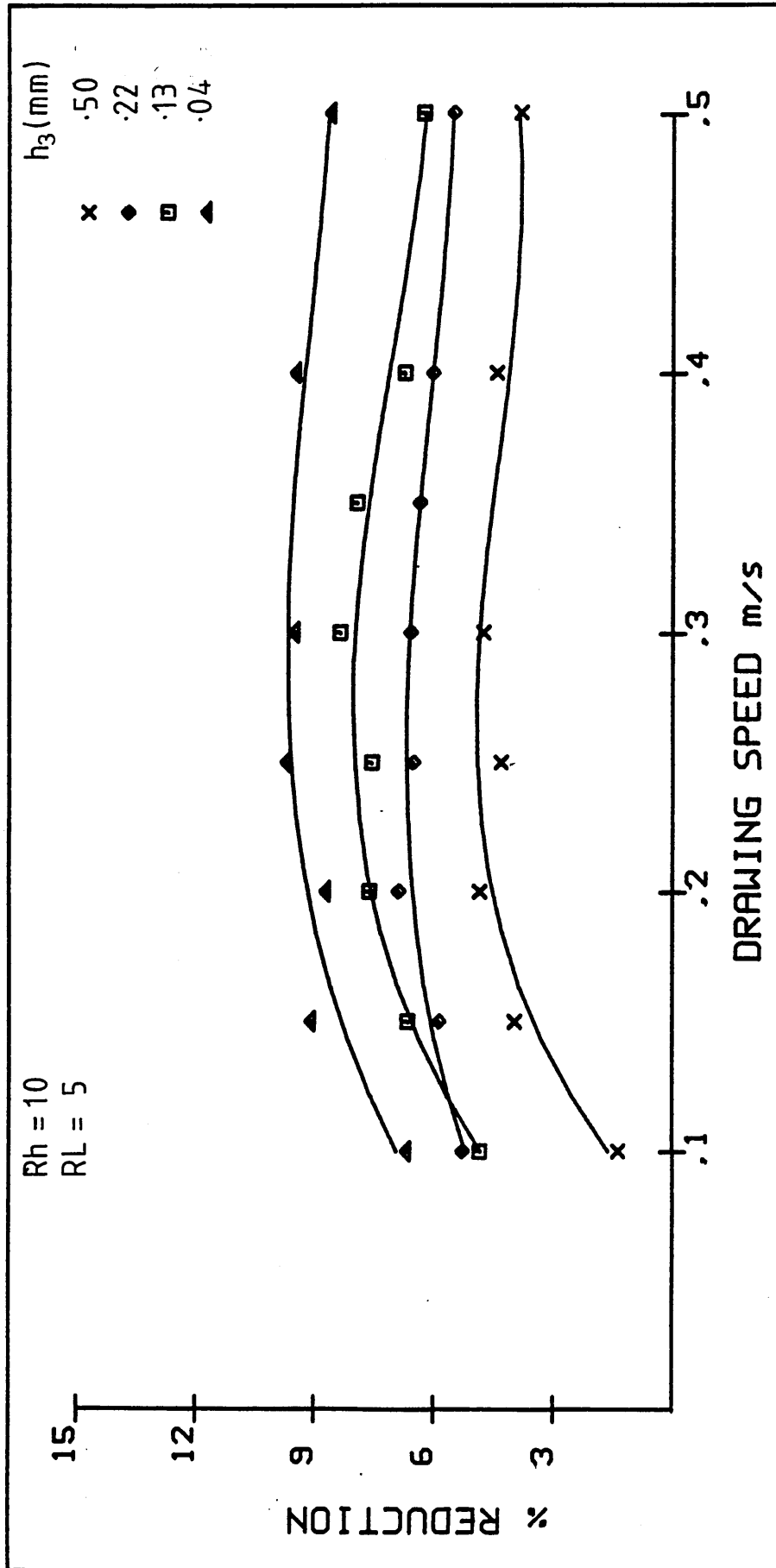


FIG 21: EFFECT OF GAP h_3 ON PERCENTAGE REDUCTION IN AREA FOR STRIP OF ASPECT RATIO 7.98 WITH WVG23, 150°C

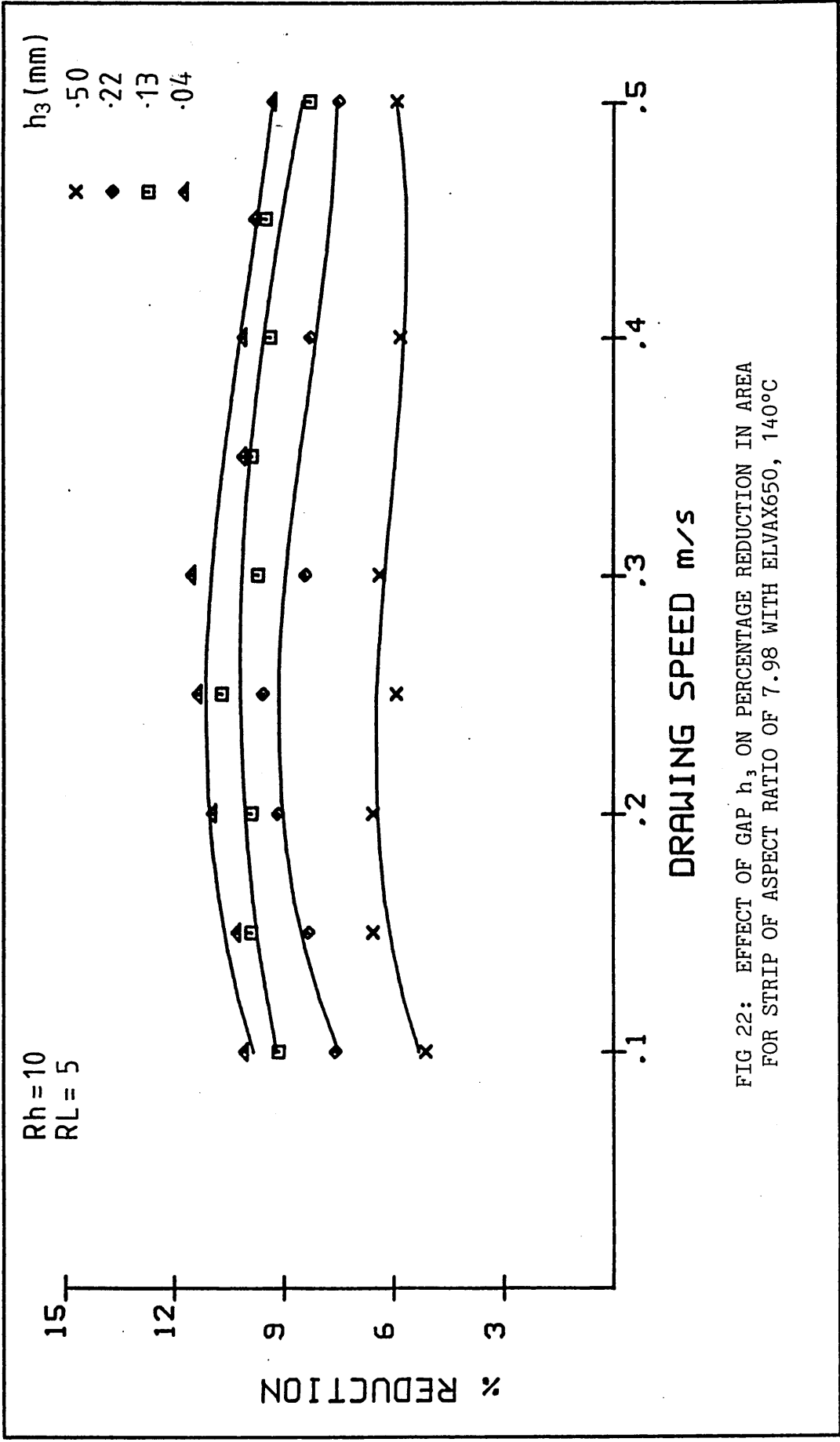


FIG 22: EFFECT OF GAP h₃ ON PERCENTAGE REDUCTION IN AREA FOR STRIP OF ASPECT RATIO OF 7.98 WITH ELVAX650, 140°C

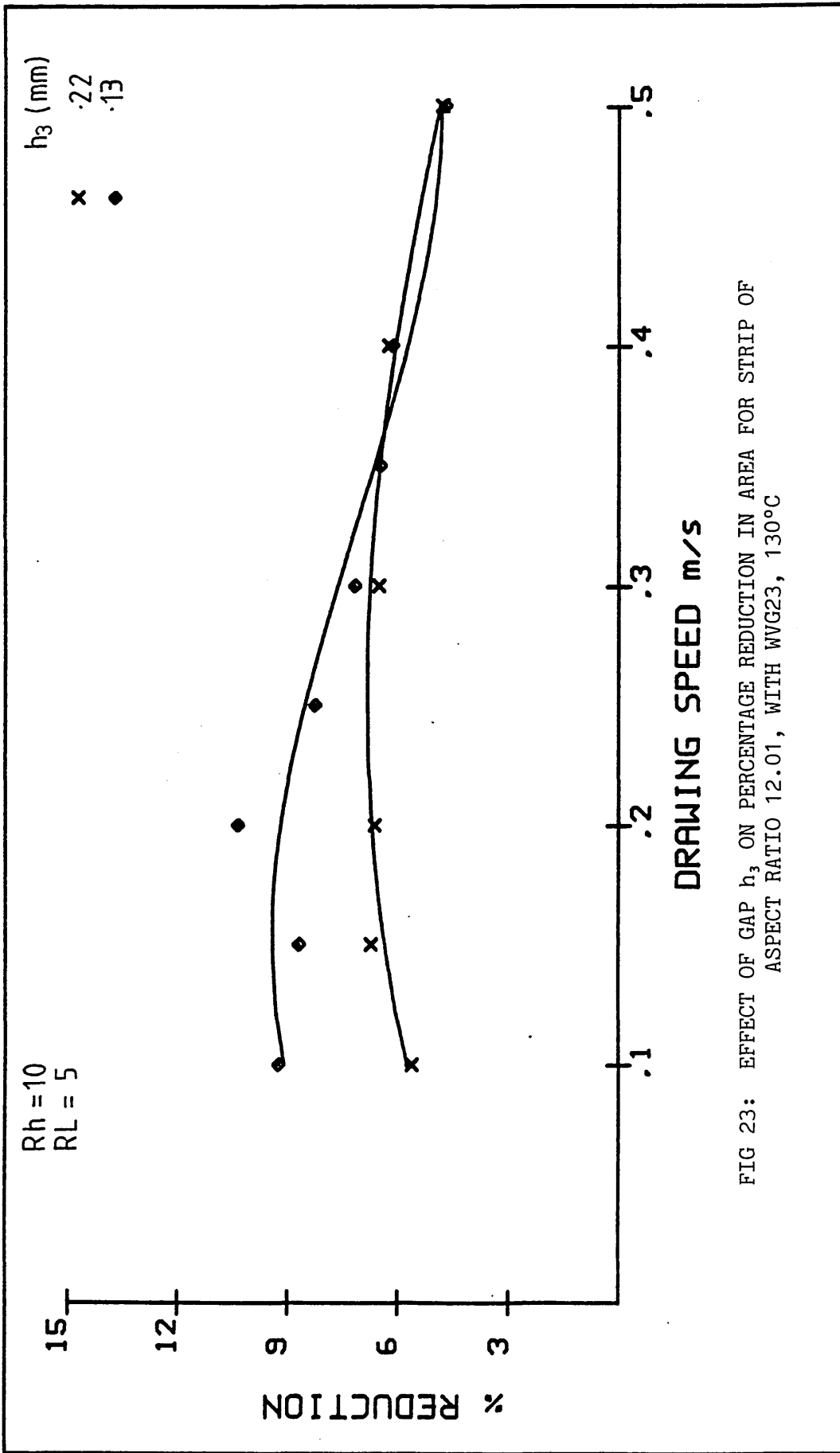


FIG 23: EFFECT OF GAP h₃ ON PERCENTAGE REDUCTION IN AREA FOR STRIP OF ASPECT RATIO 12.01, WITH WVG23, 130°C

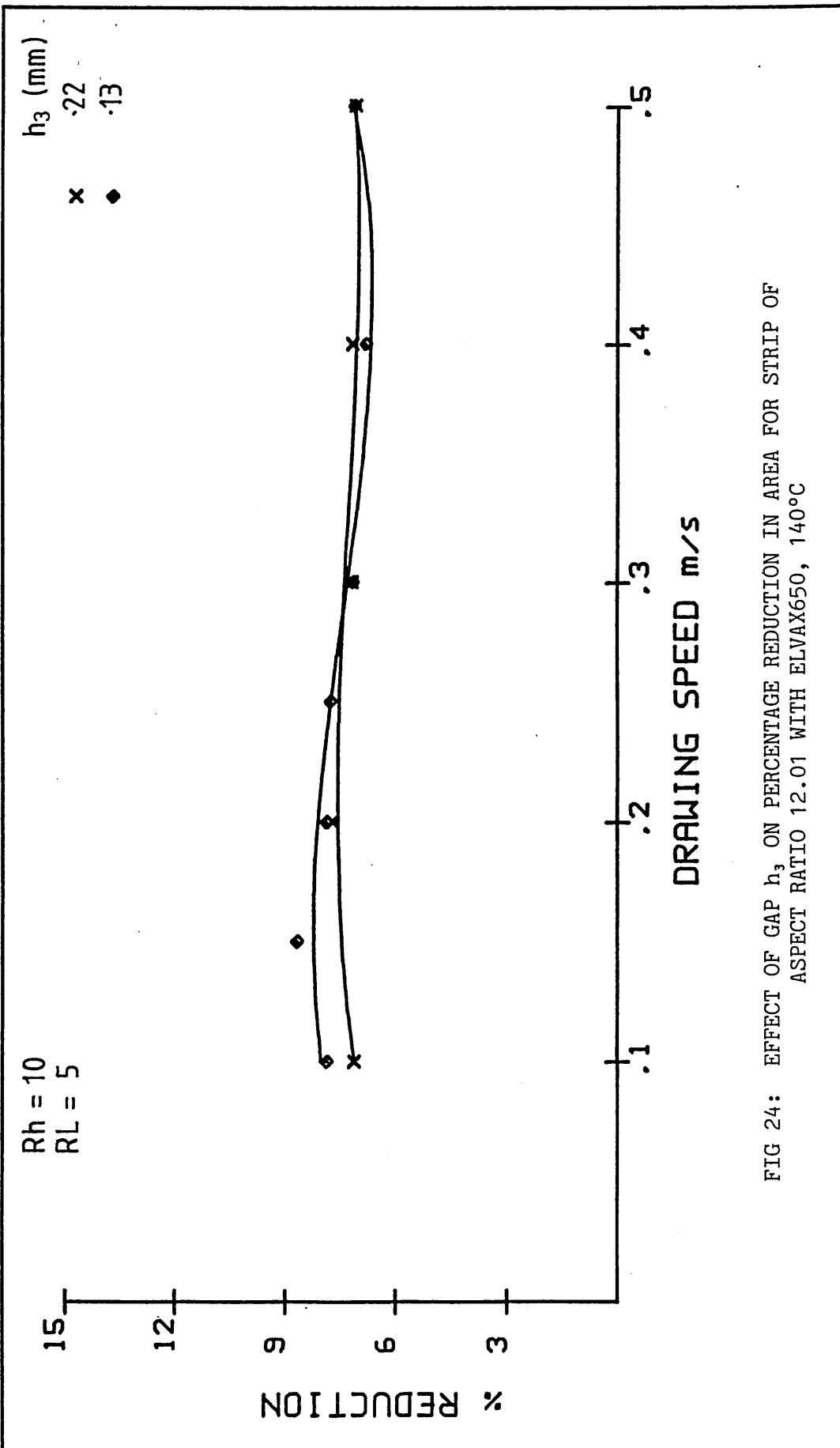


FIG 24: EFFECT OF GAP h_3 ON PERCENTAGE REDUCTION IN AREA FOR STRIP OF ASPECT RATIO 12.01 WITH ELVAX650, 140°C

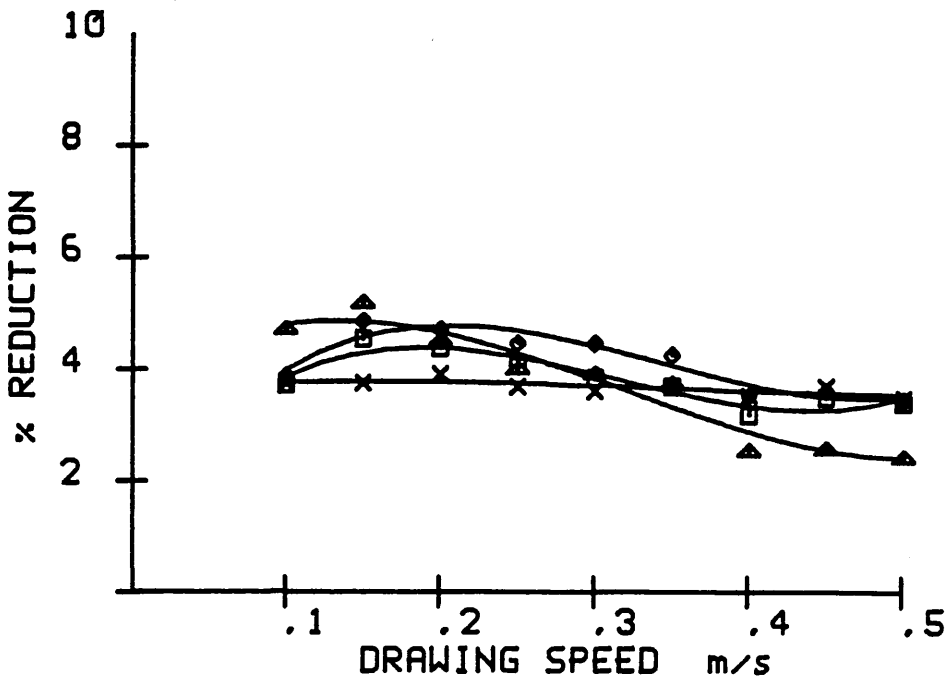
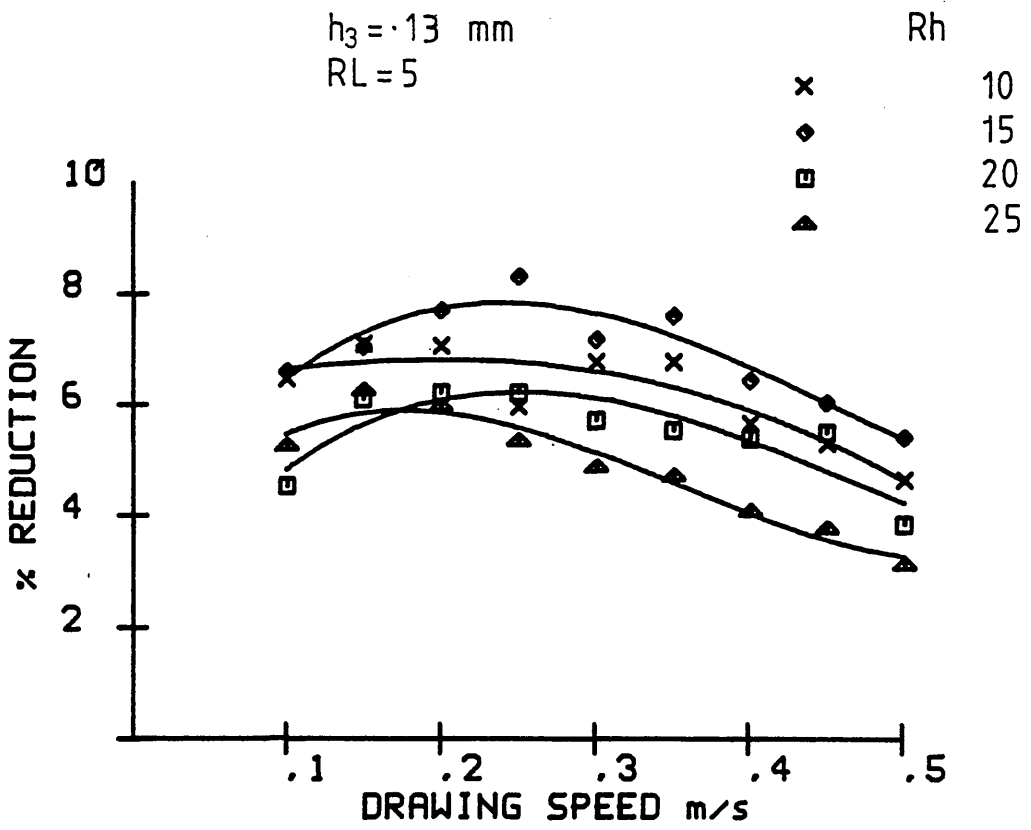
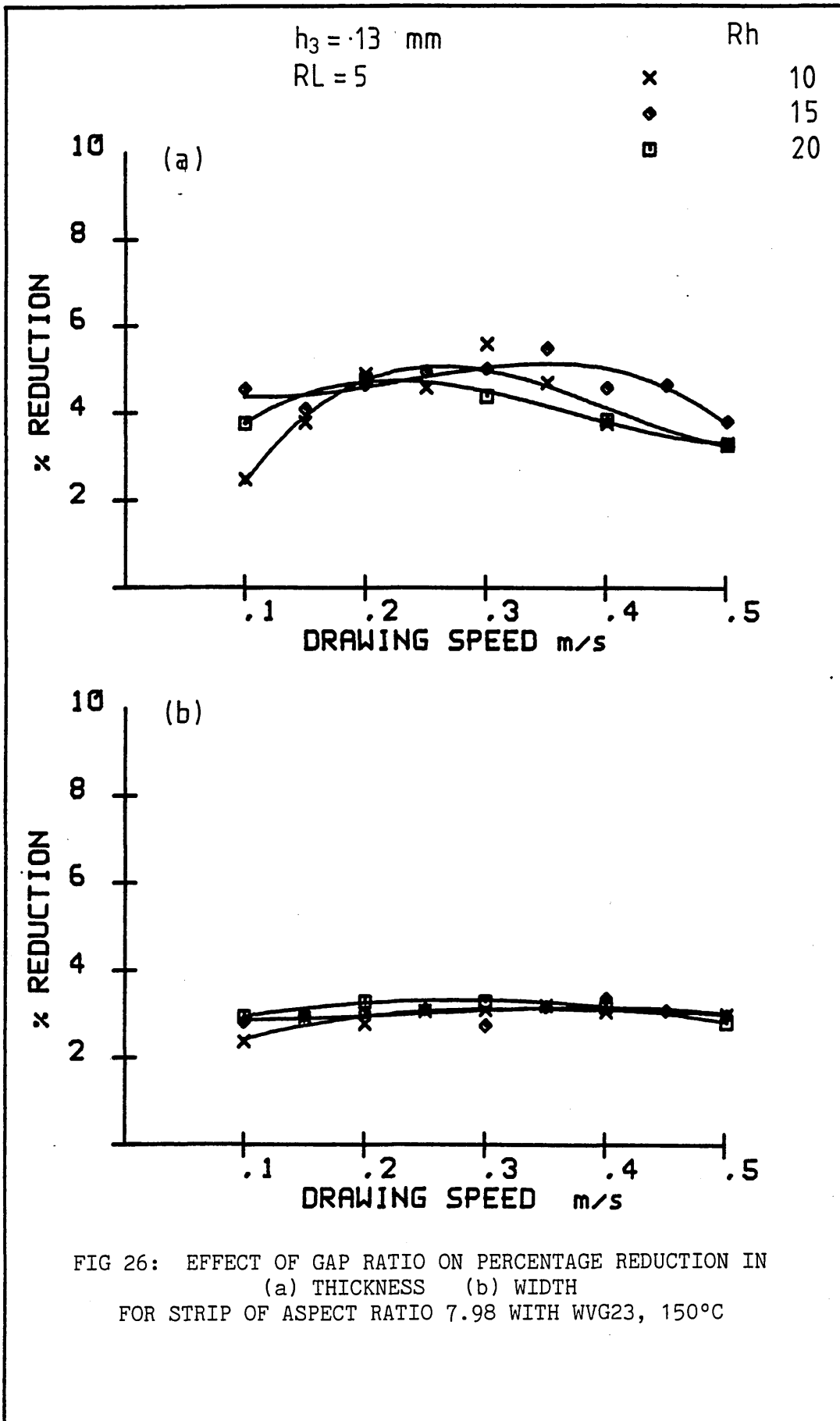


FIG 25: EFFECT OF GAP RATIO ON PERCENTAGE REDUCTION IN
 (a) THICKNESS (b) WIDTH
 FOR STRIP OF ASPECT RATIO 7.98 WITH WVG23, 130°C



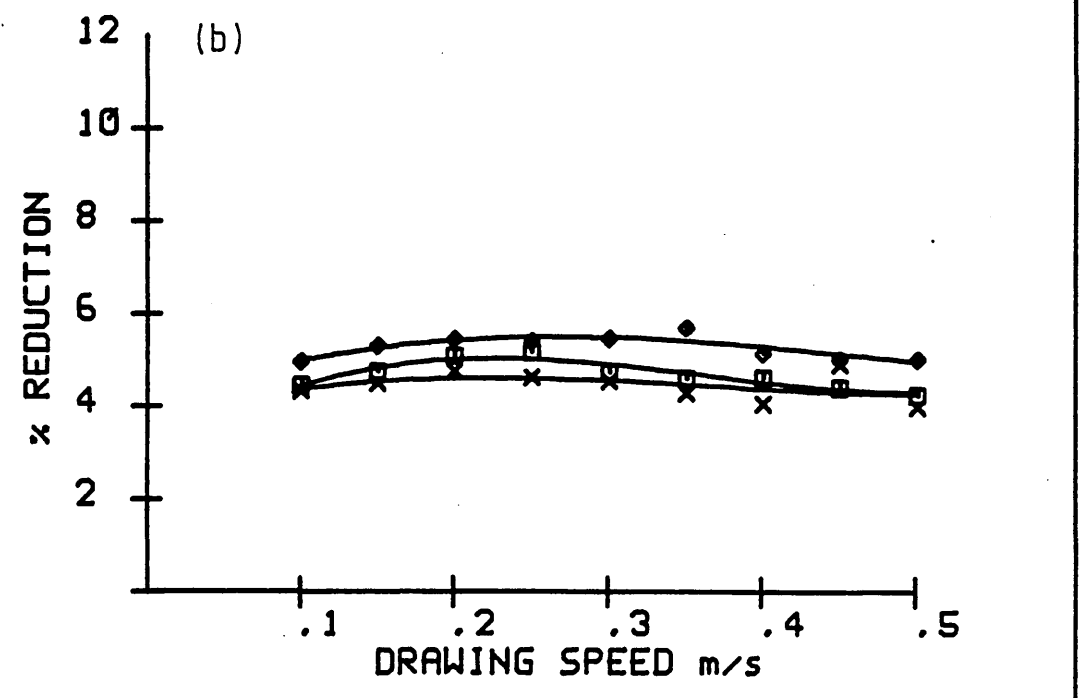
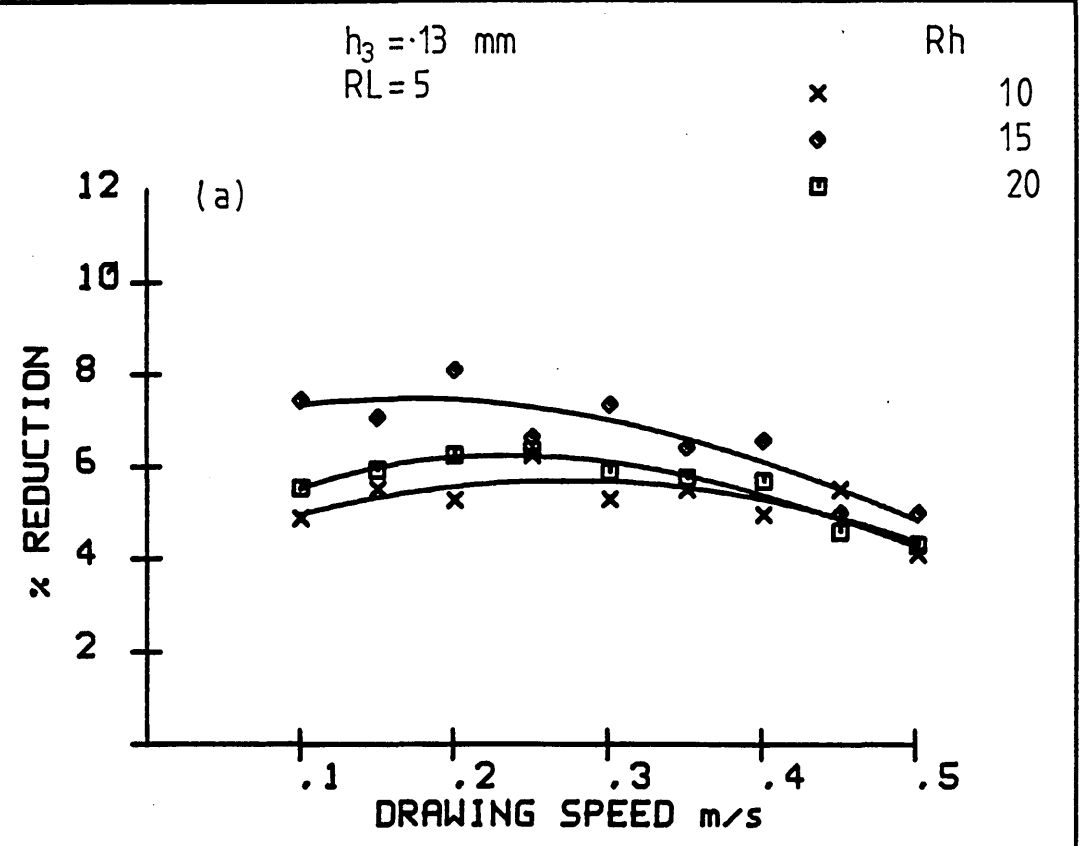


FIG 27: EFFECT OF GAP RATIO ON PERCENTAGE REDUCTION IN
 (a) THICKNESS (b) WIDTH
 FOR STRIP OF ASPECT RATIO 7.98 WITH ELVAX650, 140°C

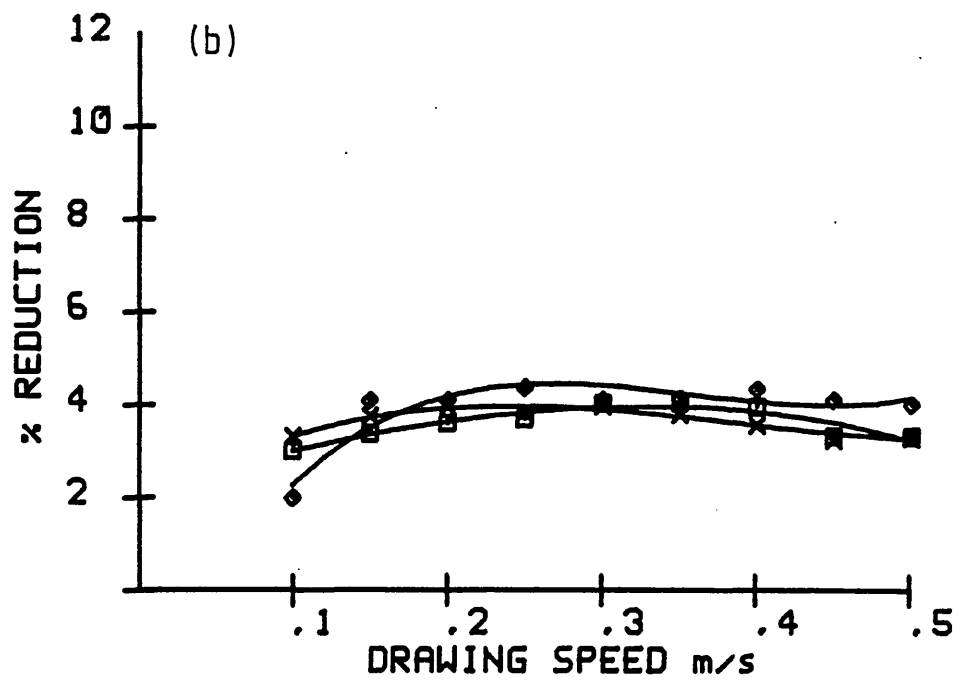
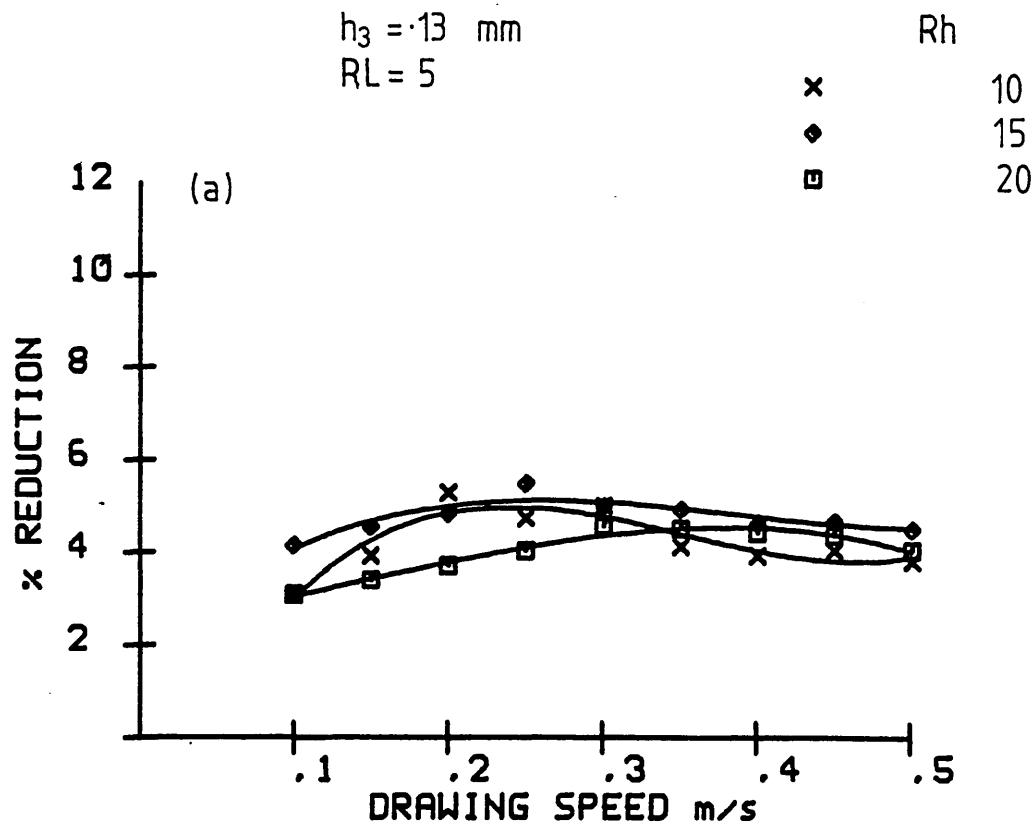


FIG 28: EFFECT OF GAP RATIO ON PERCENTAGE REDUCTION IN
 (a) THICKNESS (b) WIDTH
 FOR STRIP OF ASPECT RATIO 7.98 WITH ELVAX650, 170°C

$h_3 = .13$ mm
RL = 5

Rh

x 10
♦ 15

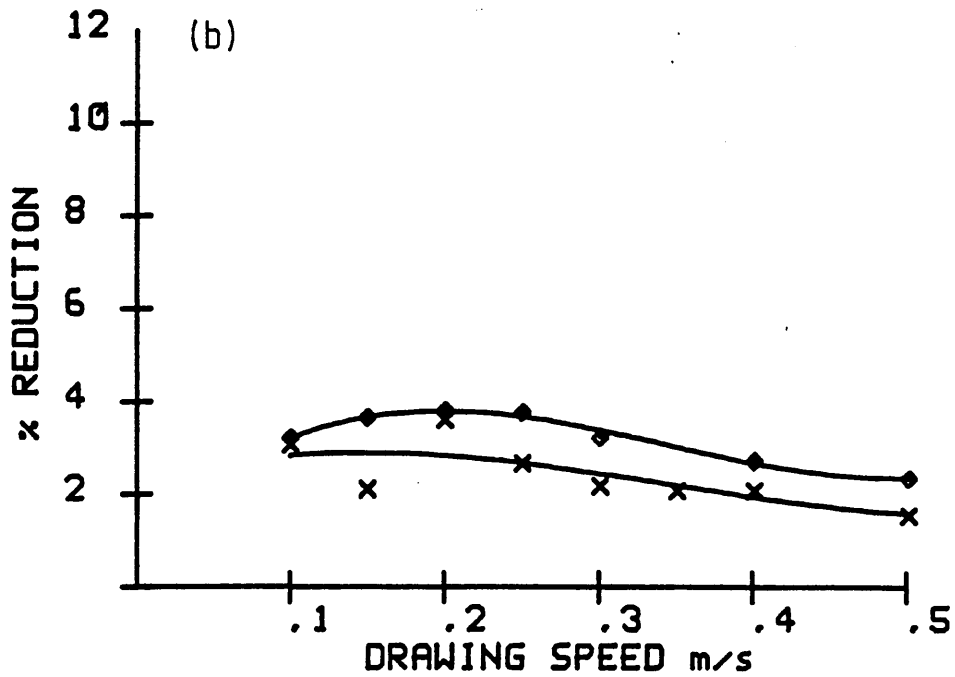
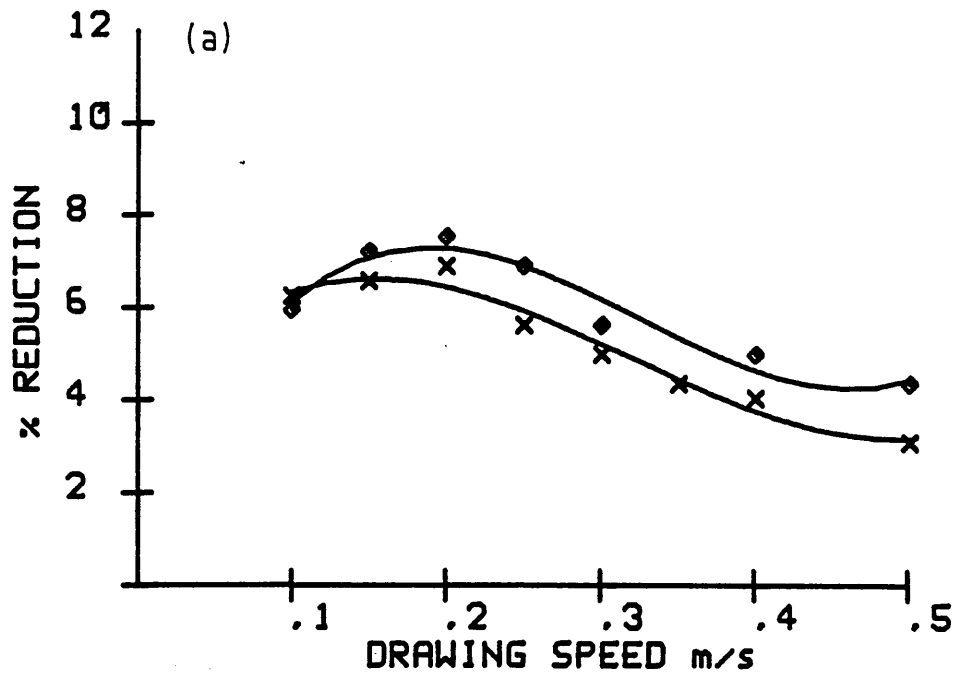


FIG 29: EFFECT OF GAP RATIO ON PERCENTAGE REDUCTION IN
(a) THICKNESS (b) WIDTH
FOR STRIP OF ASPECT RATIO 12.01 WITH WVG23, 130°C

$h_3 = .13$ mm

RL = 5

Rh

x 10

◊ 15

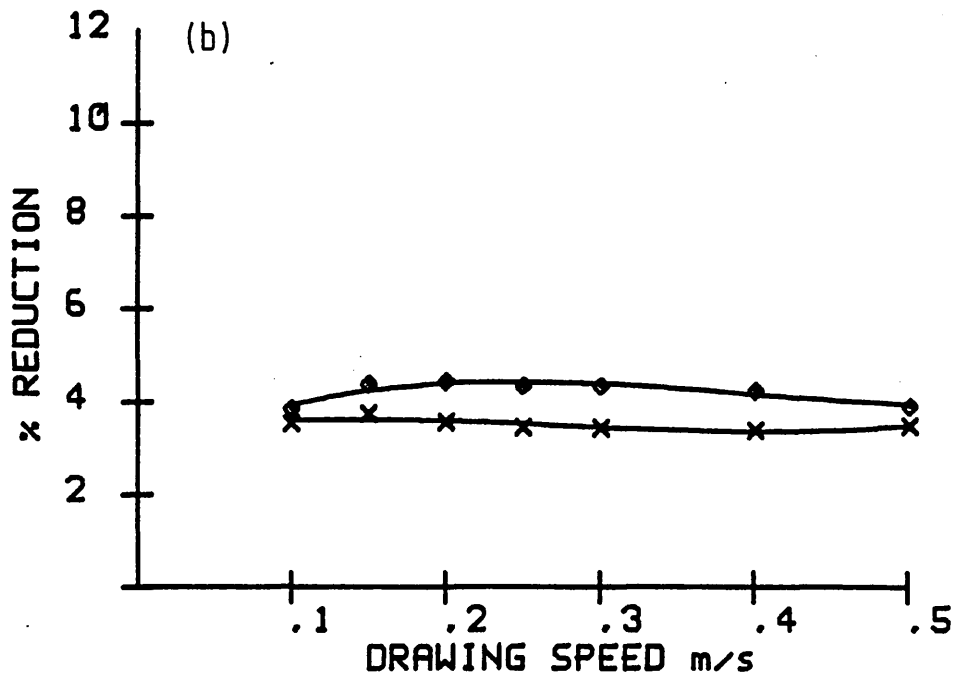
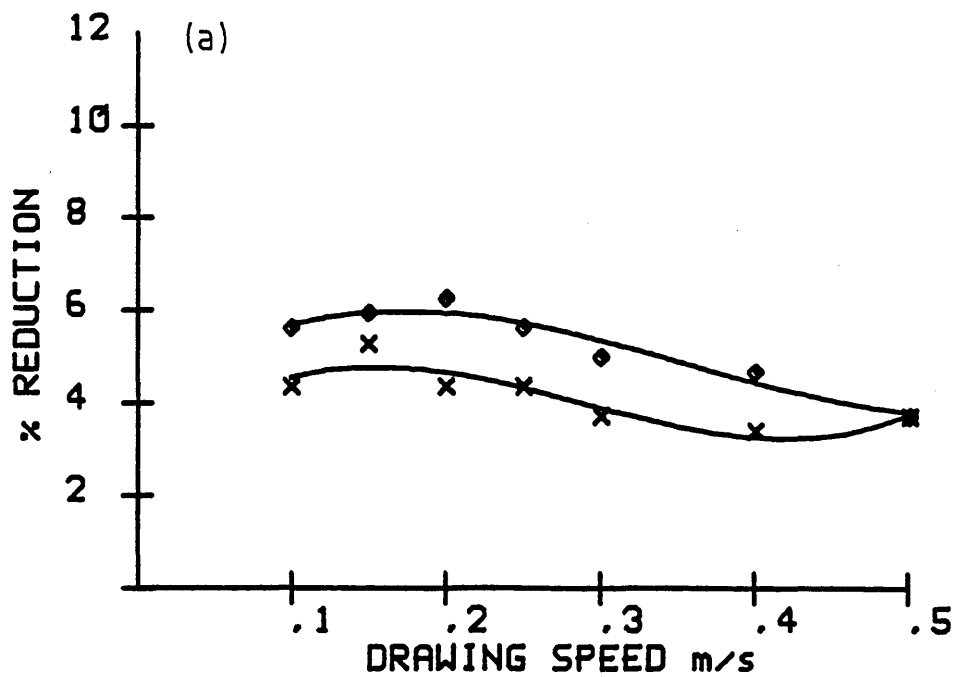


FIG 30: EFFECT OF GAP RATIO ON PERCENTAGE REDUCTION IN
(a) THICKNESS (b) WIDTH
FOR STRIP OF ASPECT RATIO 12.01 WITH ELVAX650, 140°C

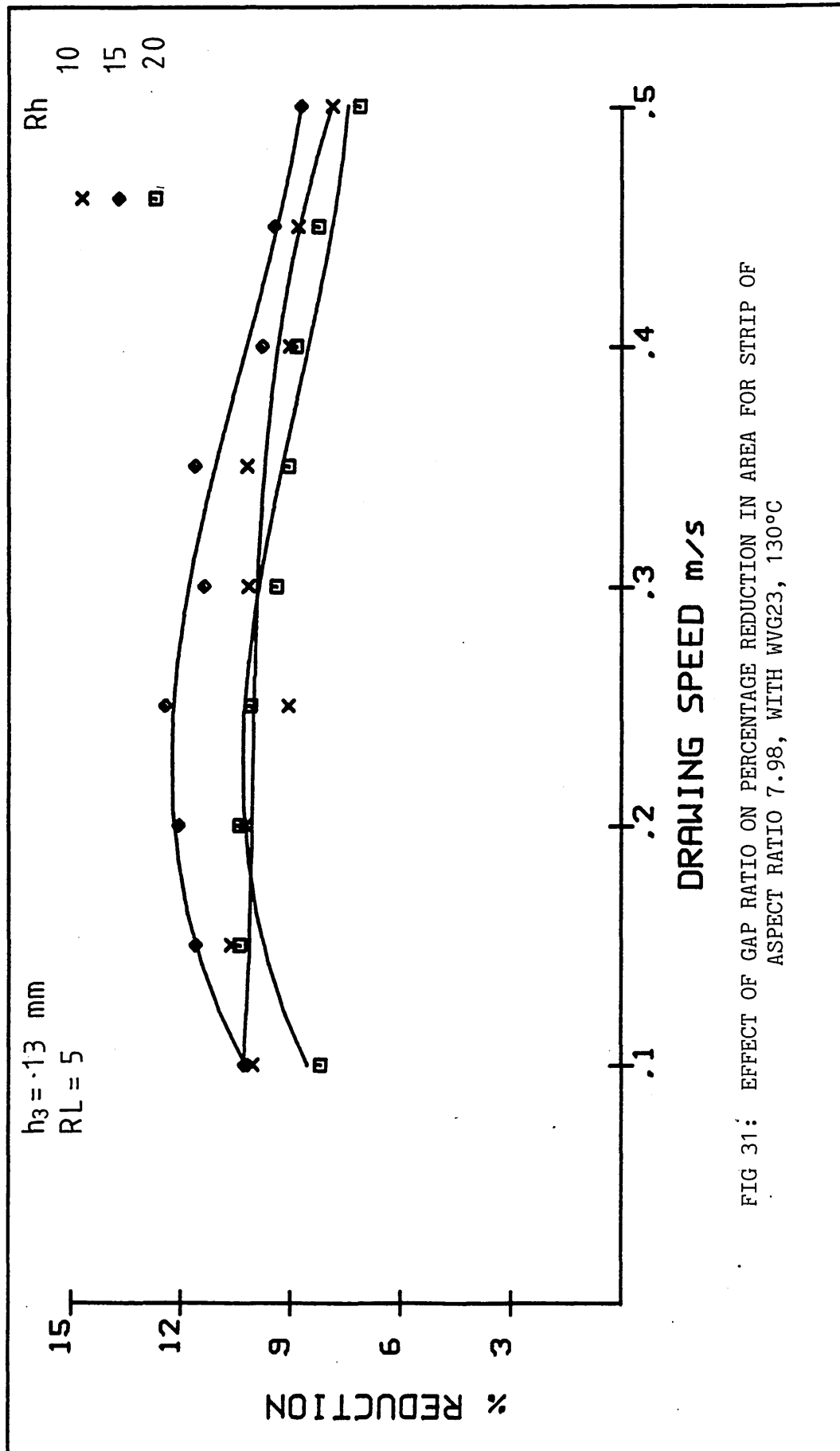


FIG 31: EFFECT OF GAP RATIO ON PERCENTAGE REDUCTION IN AREA FOR STRIP OF ASPECT RATIO 7.98, WITH WVG23, 130°C

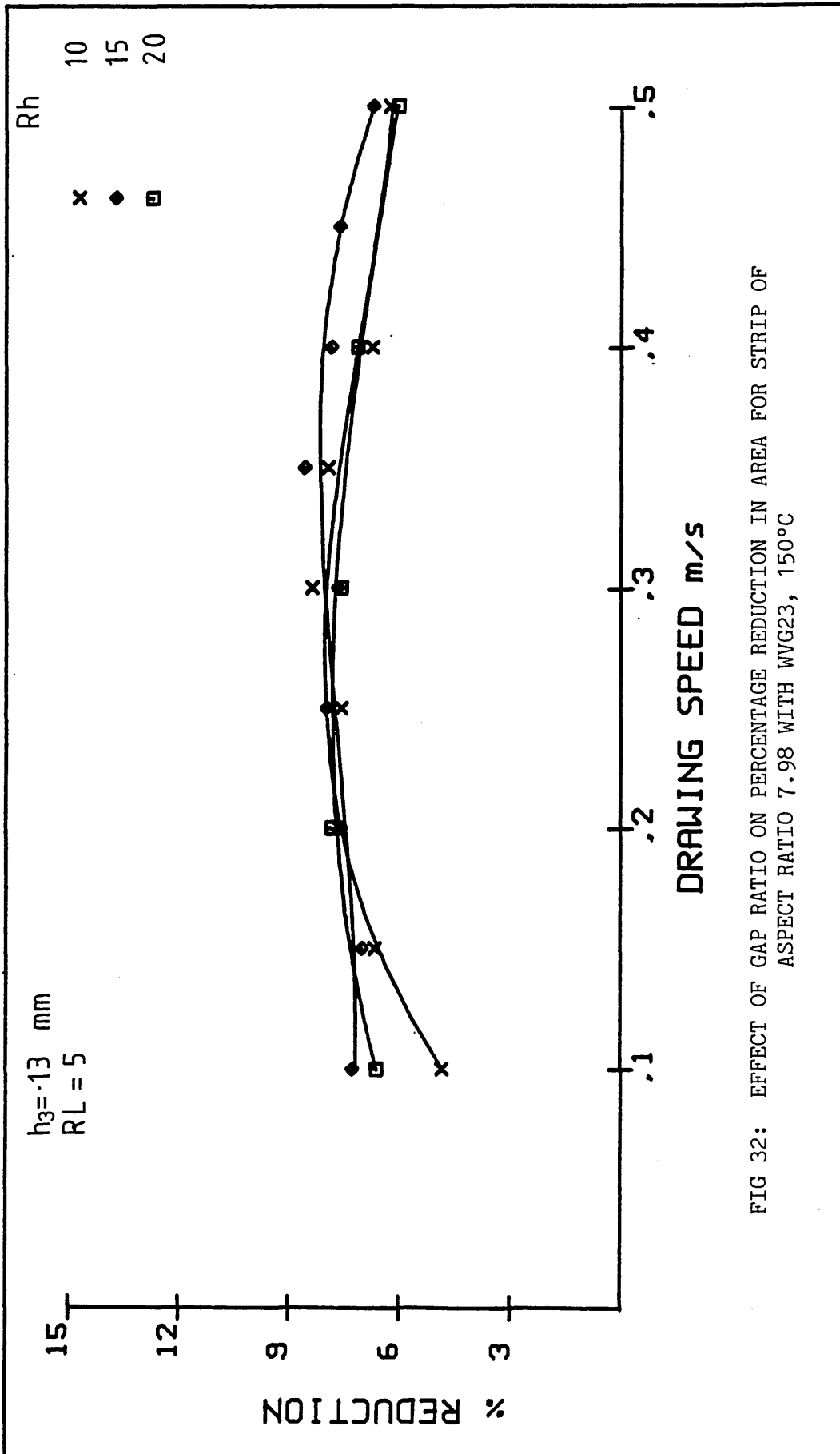


FIG 32: EFFECT OF GAP RATIO ON PERCENTAGE REDUCTION IN AREA FOR STRIP OF ASPECT RATIO 7.98 WITH WVG23, 150°C

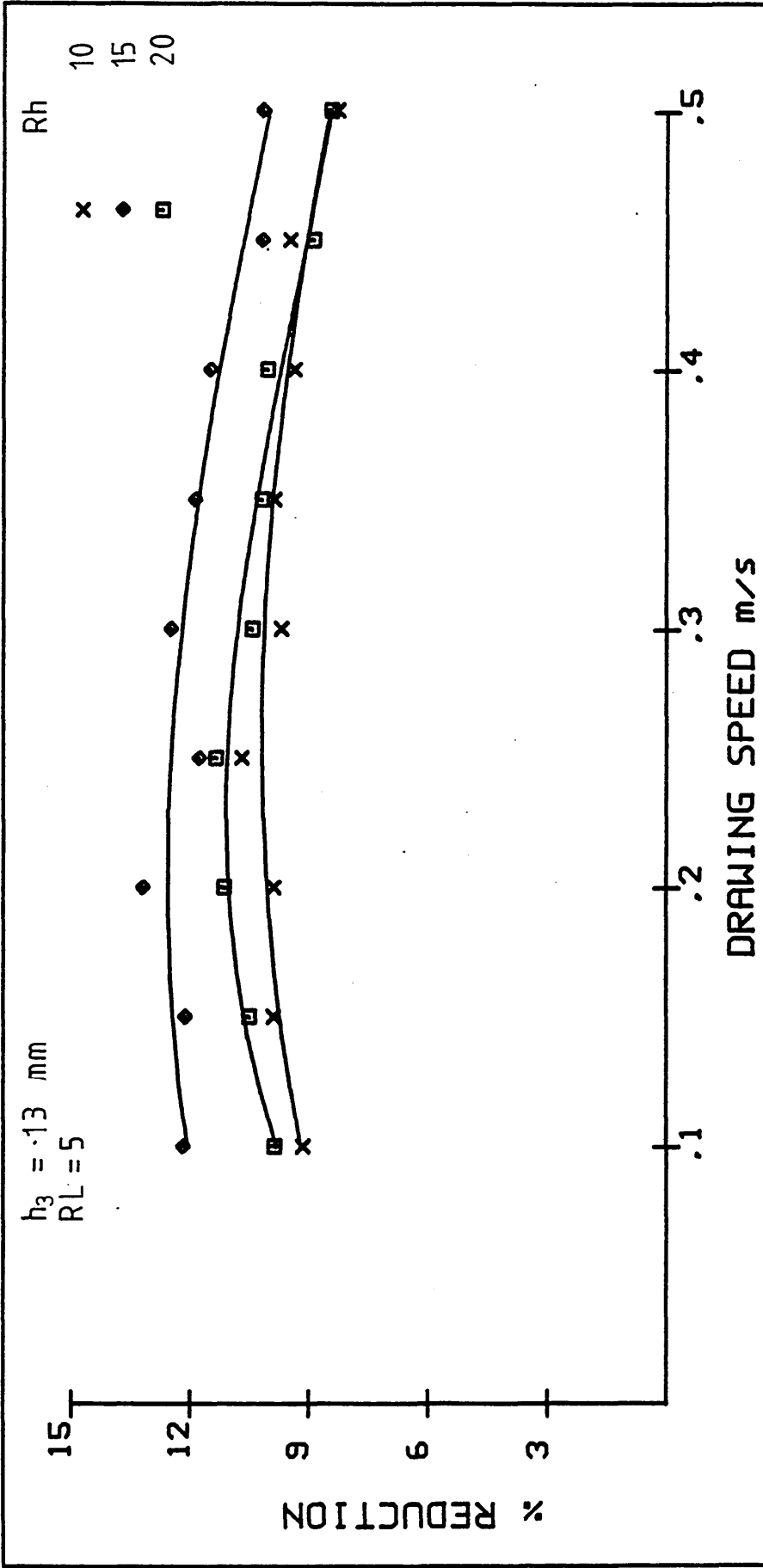


FIG 33: EFFECT OF GAP RATIO ON PERCENTAGE REDUCTION IN AREA FOR STRIP OF ASPECT RATIO 7.98, WITH ELVAX650, 140°C

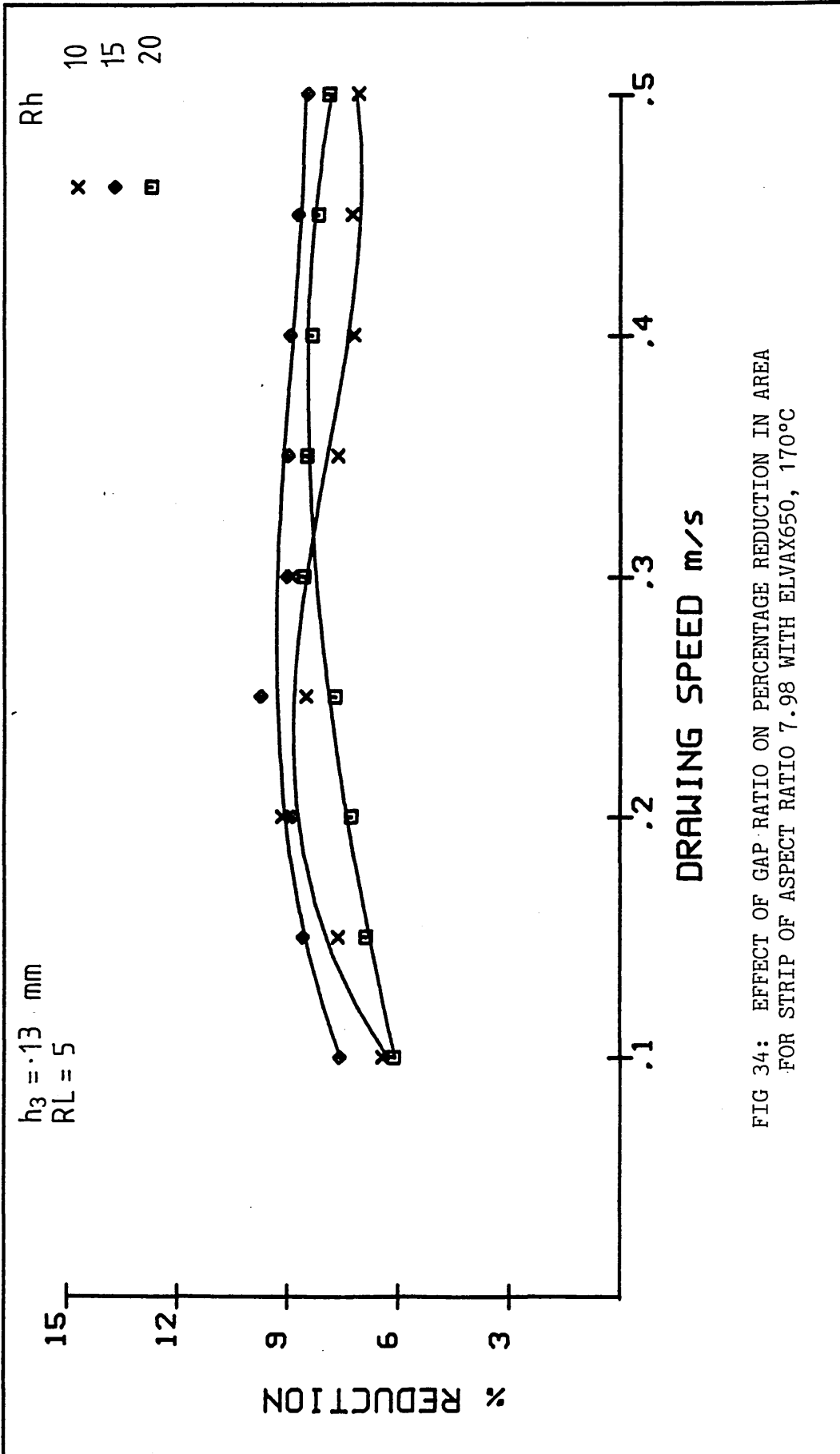


FIG 34: EFFECT OF GAP RATIO ON PERCENTAGE REDUCTION IN AREA
 FOR STRIP OF ASPECT RATIO 7.98 WITH ELVAX650, 170°C

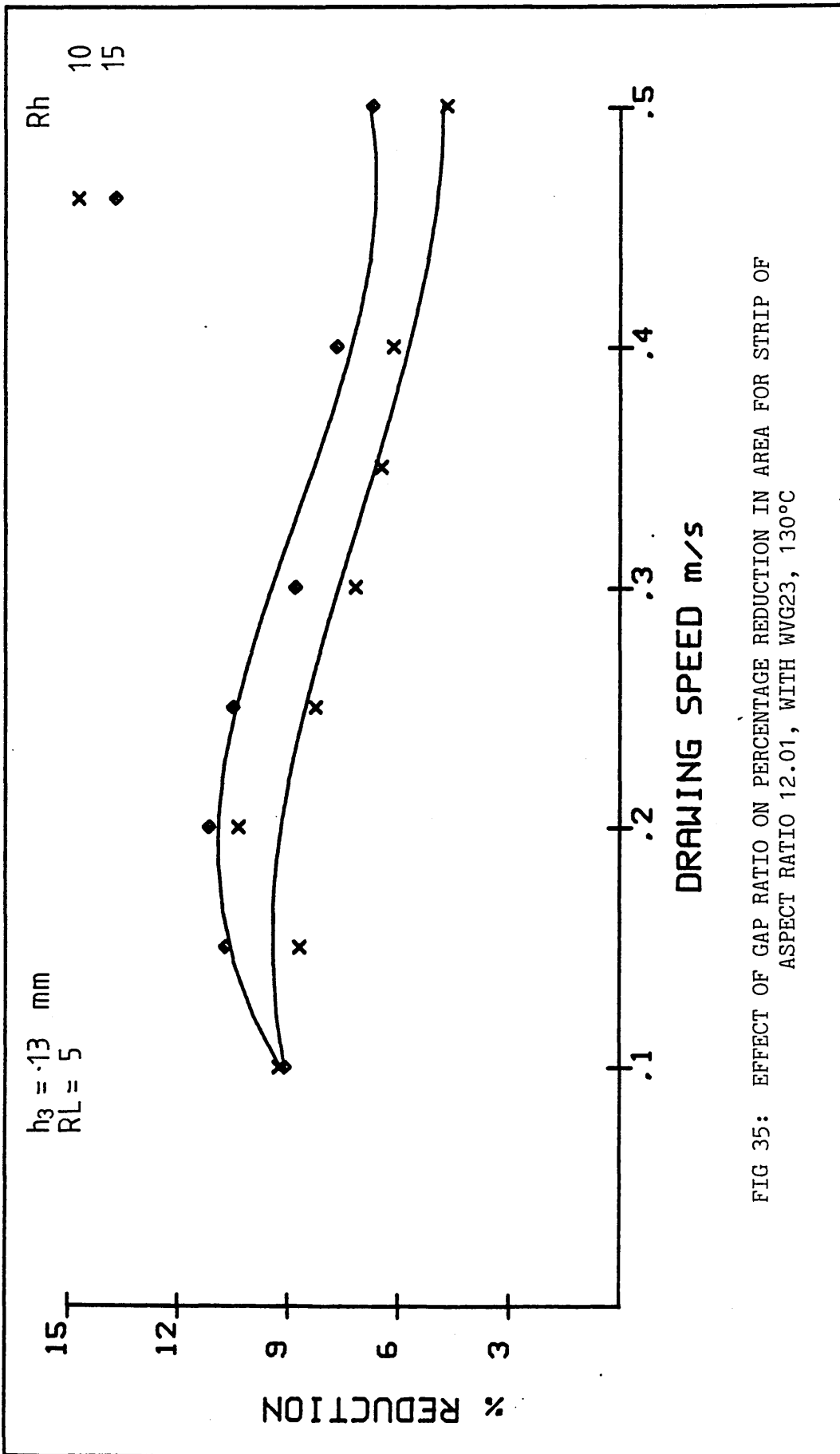


FIG 35: EFFECT OF GAP RATIO ON PERCENTAGE REDUCTION IN AREA FOR STRIP OF ASPECT RATIO 12.01, WITH WVG23, 130°C

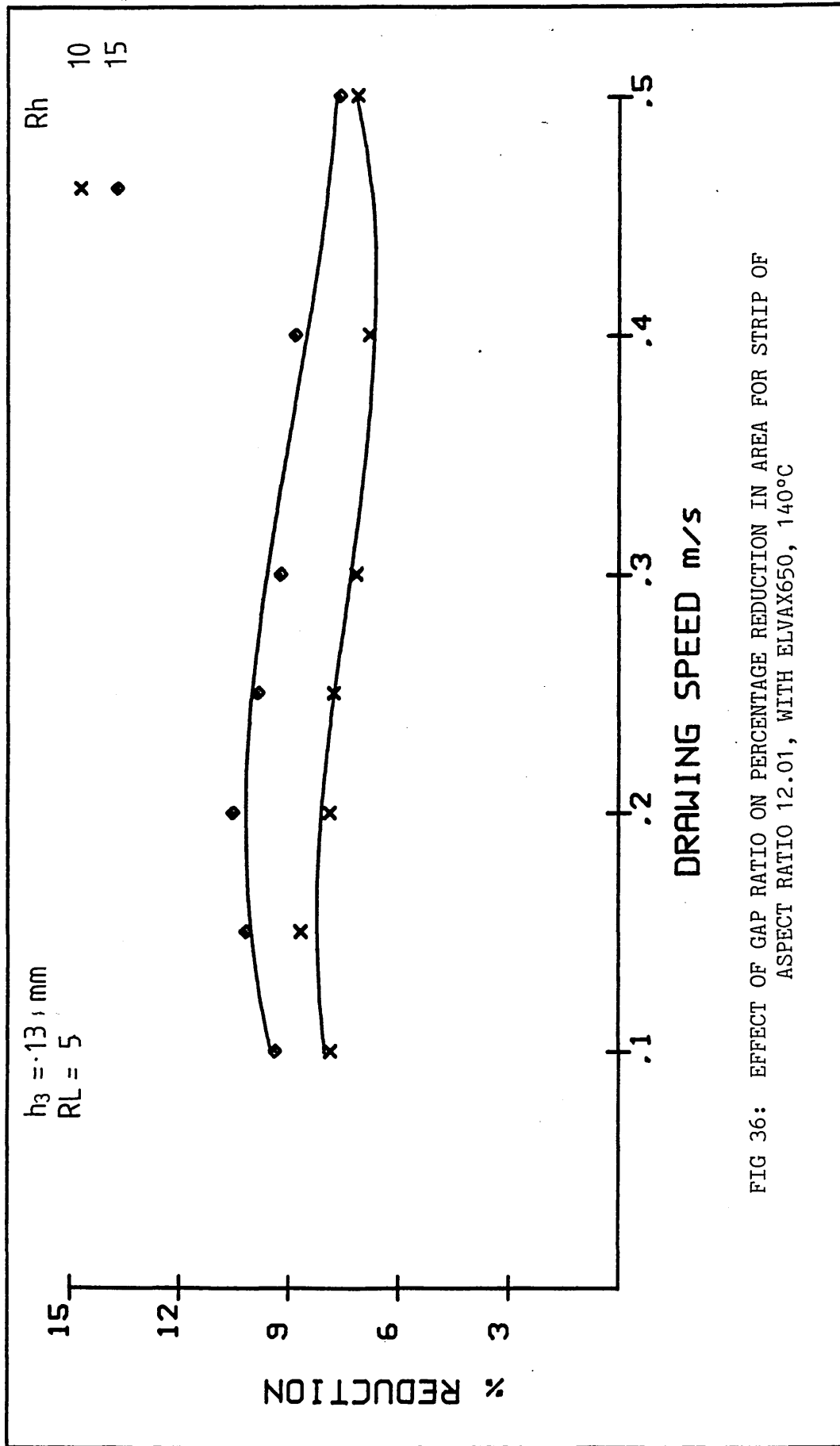
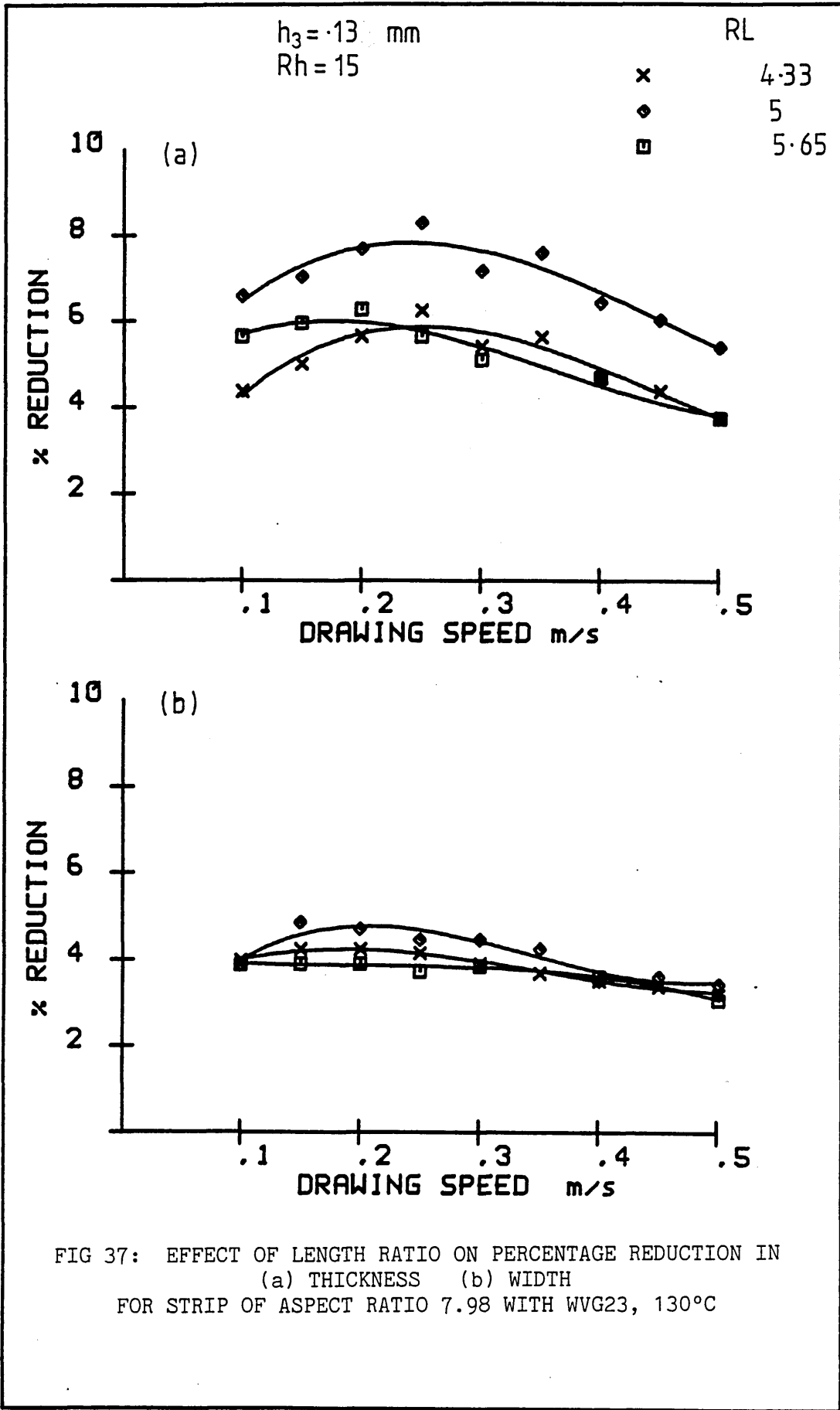


FIG 36: EFFECT OF GAP RATIO ON PERCENTAGE REDUCTION IN AREA FOR STRIP OF ASPECT RATIO 12.01, WITH ELVAX650, 140°C



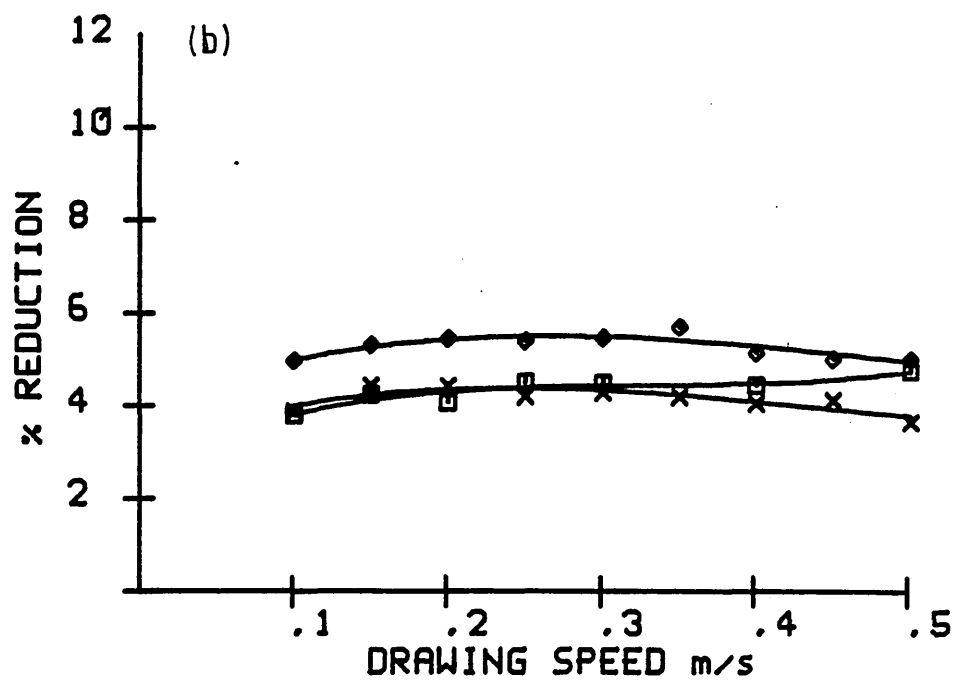
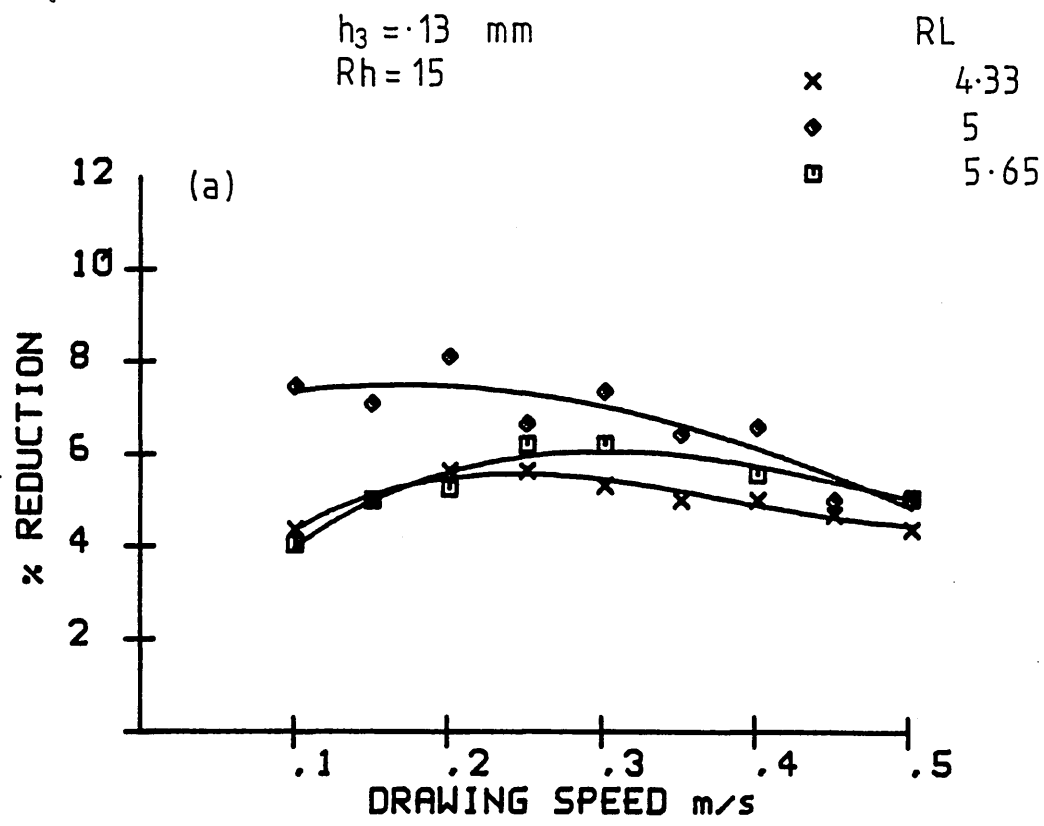


FIG 38: EFFECT OF LENGTH RATIO ON PERCENTAGE REDUCTION IN
 (a) THICKNESS (b) WIDTH
 FOR STRIP OF ASPECT RATIO 7.98, WITH ELVAX650, 140°C

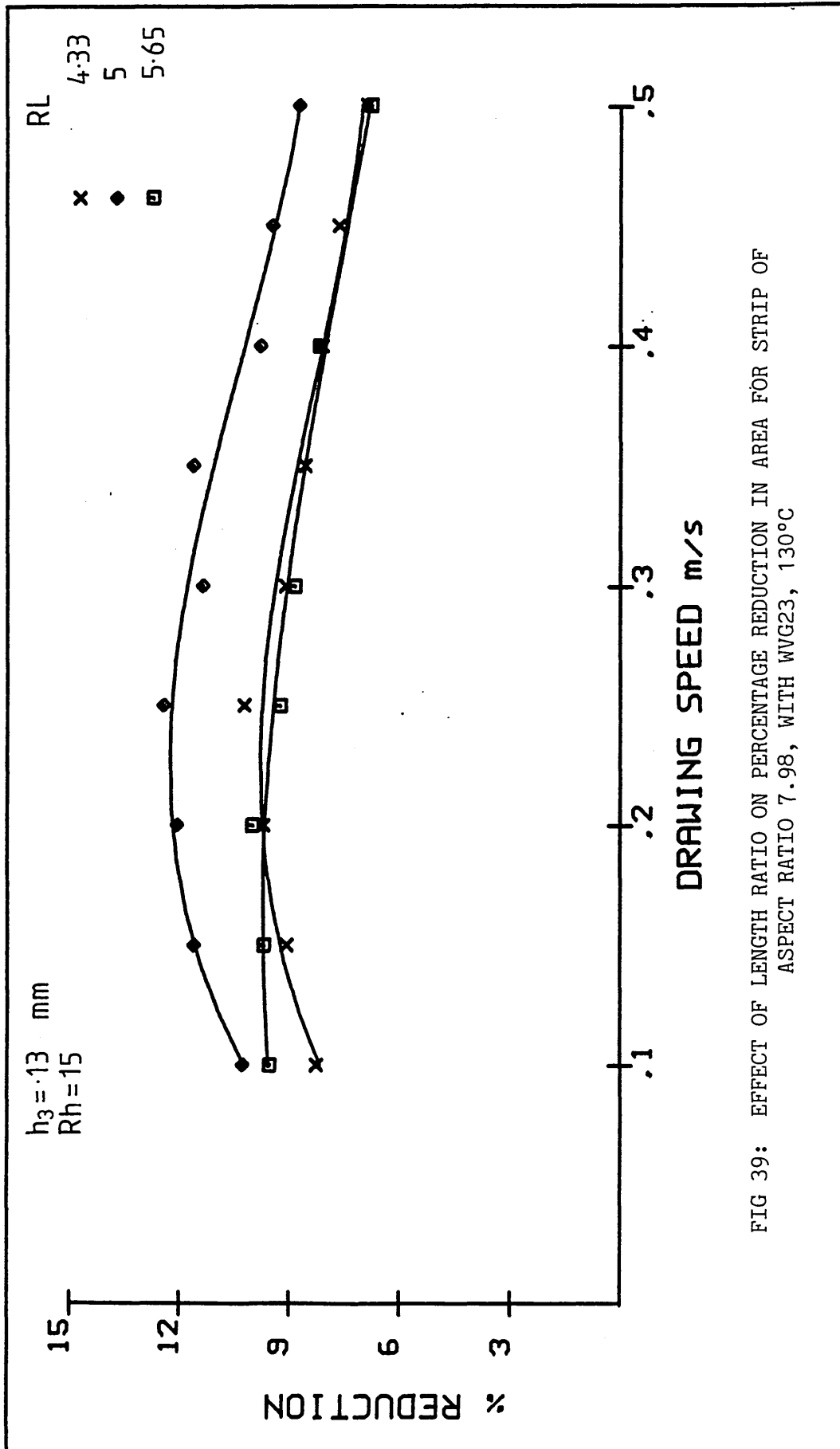


FIG 39: EFFECT OF LENGTH RATIO ON PERCENTAGE REDUCTION IN AREA FOR STRIP OF ASPECT RATIO 7.98, WITH WVG23, 130°C

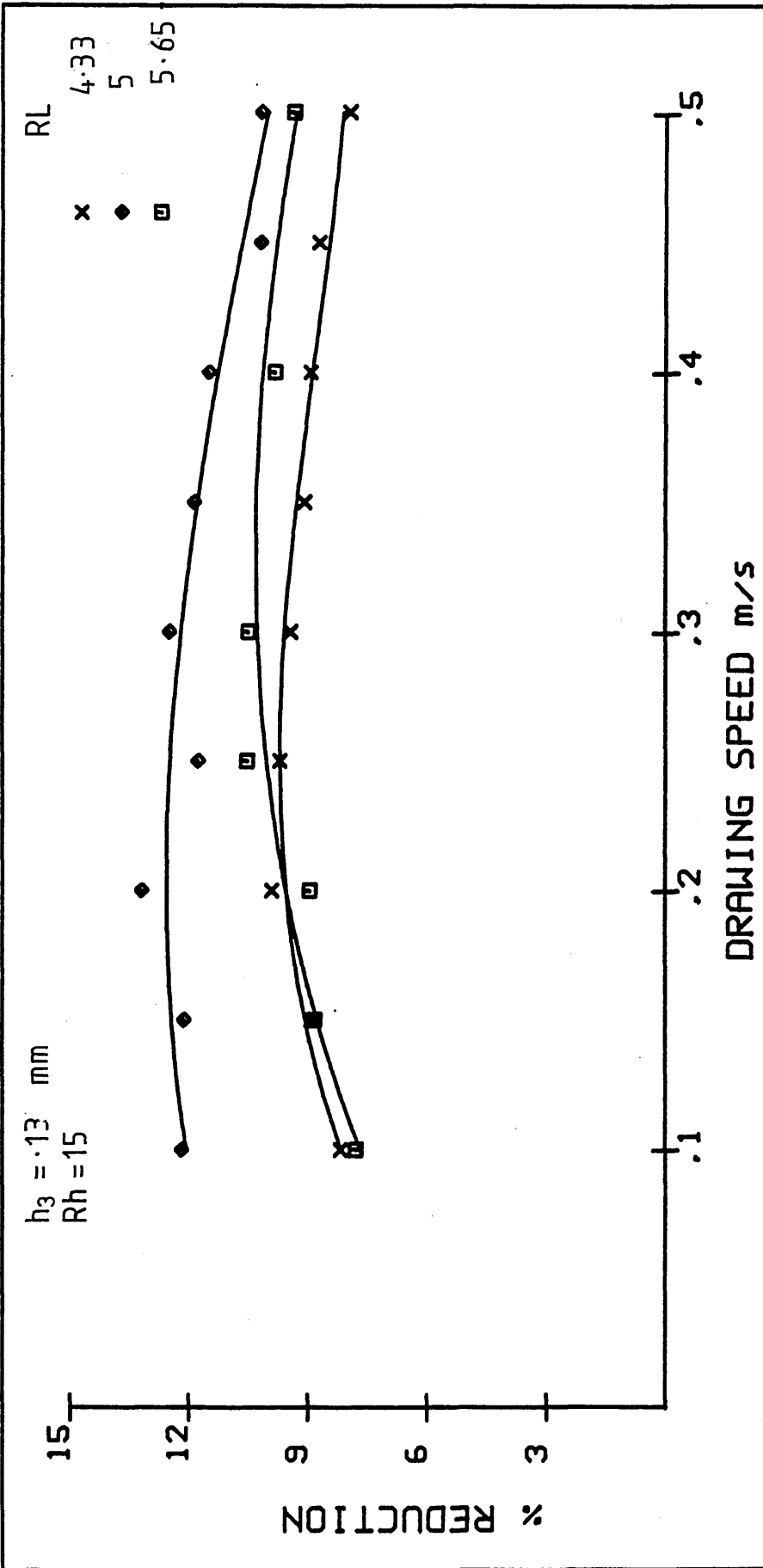
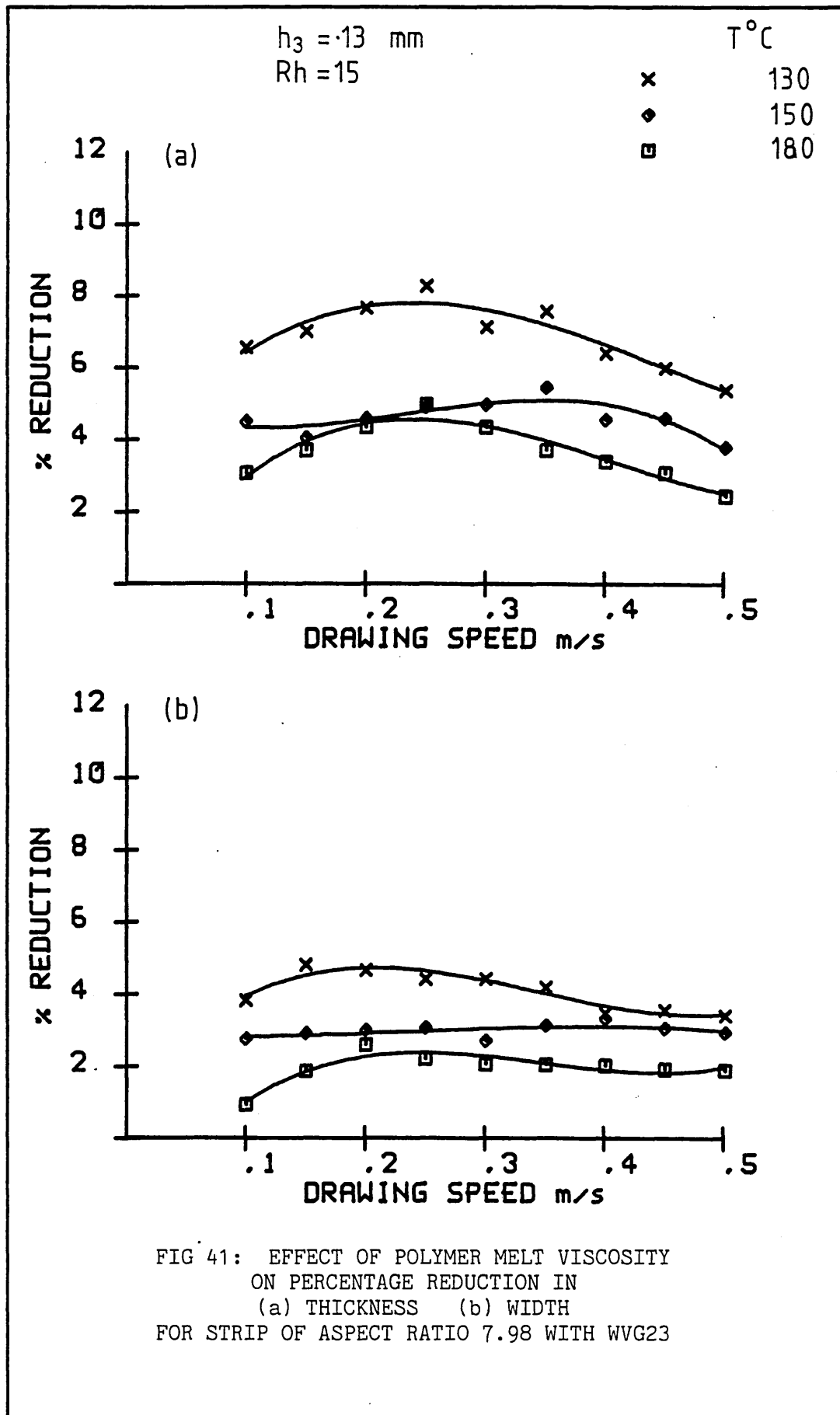


FIG 40: EFFECT OF LENGTH RATIO ON PERCENTAGE REDUCTION IN AREA FOR STRIP OF ASPECT RATIO 7.98, WITH ELVAX650, 140°C



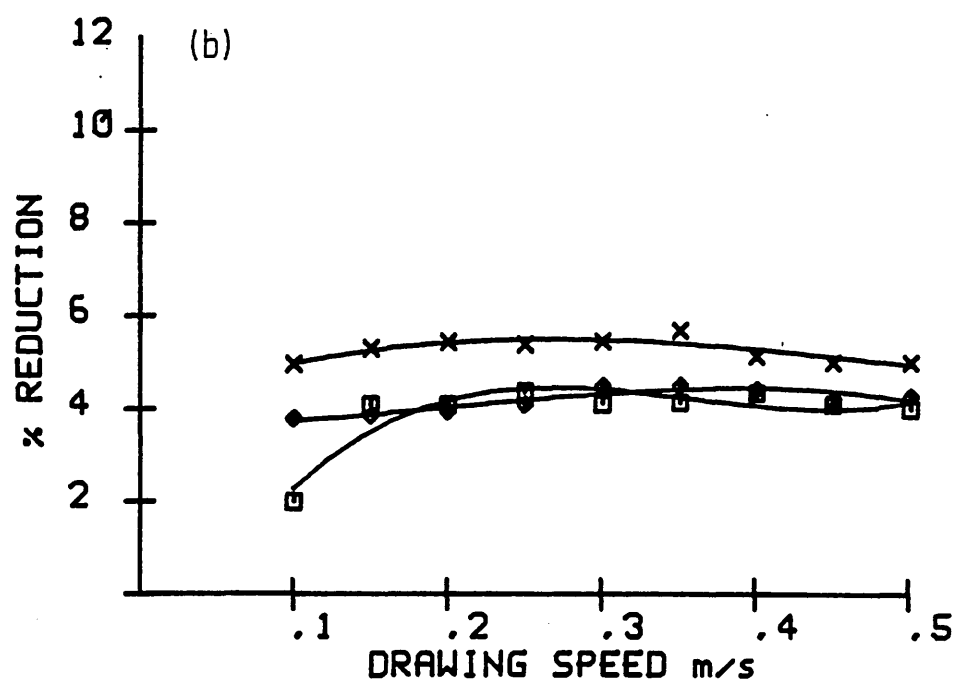
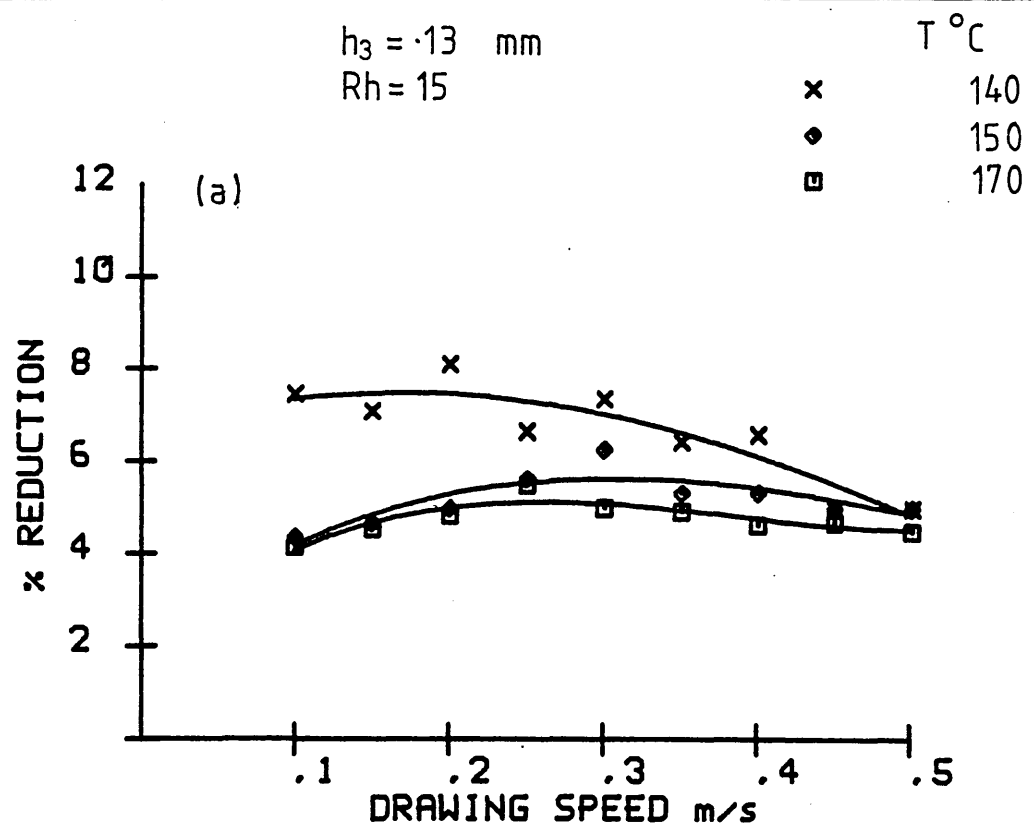


FIG 42: EFFECT OF POLYMER MELT VISCOSITY
 ON PERCENTAGE REDUCTION IN
 (a) THICKNESS (b) WIDTH
 FOR STRIP OF ASPECT RATIO 7.98 WITH ELVAX650

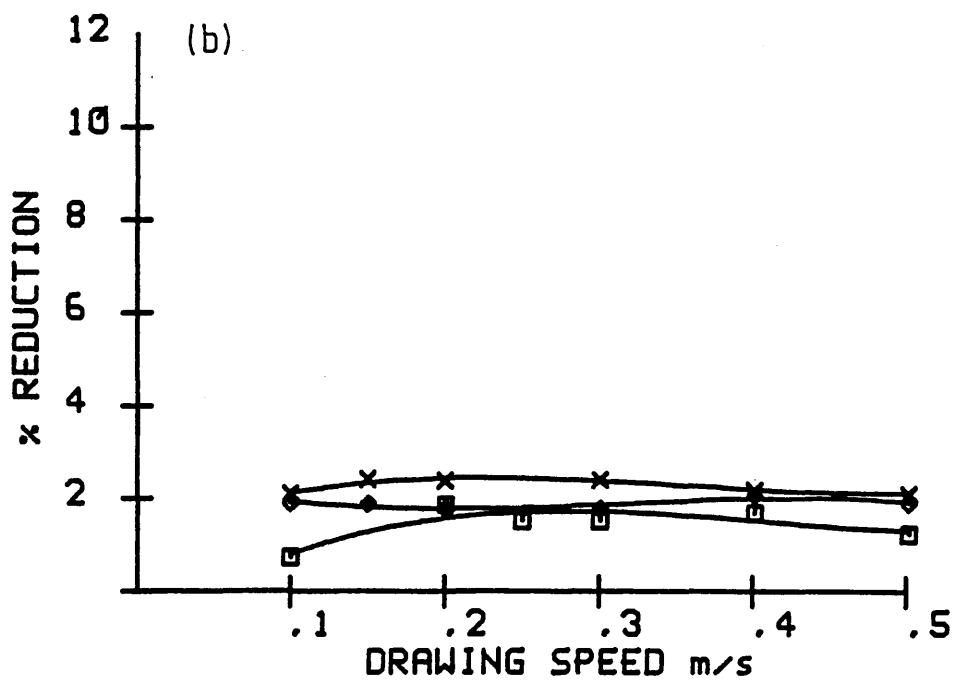
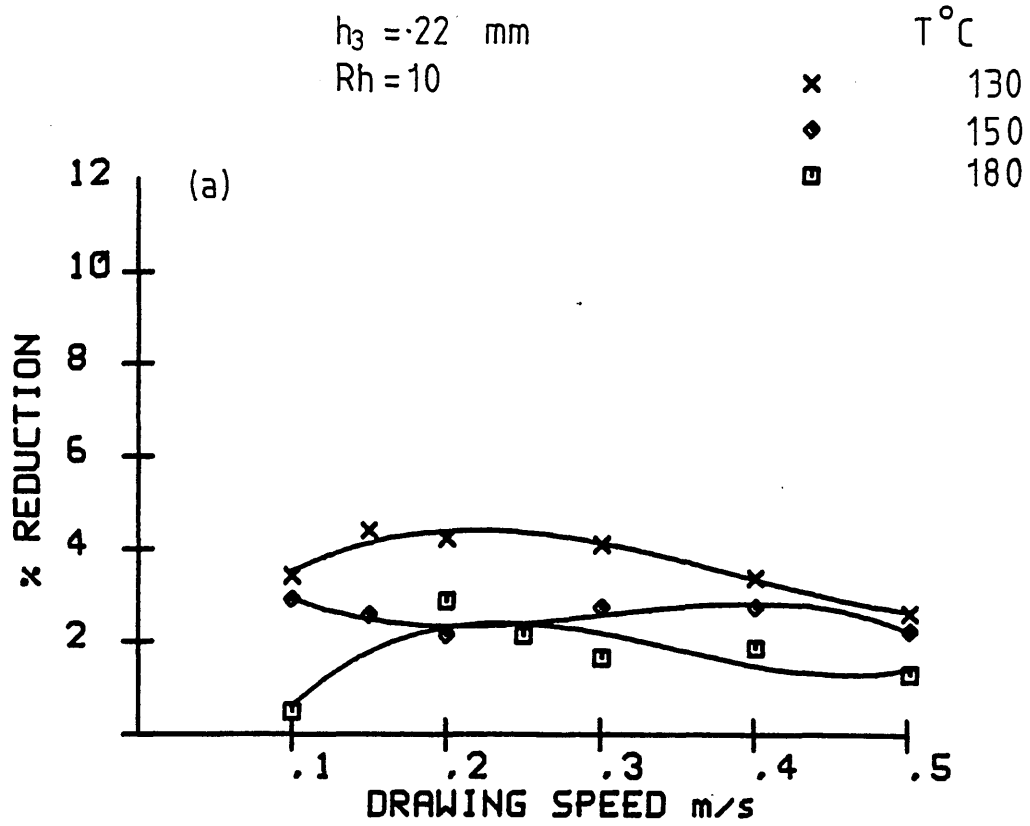


FIG 43: EFFECT OF POLYMER MELT VISCOSITY ON PERCENTAGE REDUCTION IN
 (a) THICKNESS (b) WIDTH
 FOR STRIP OF ASPECT RATIO 12.01 WITH WVG23

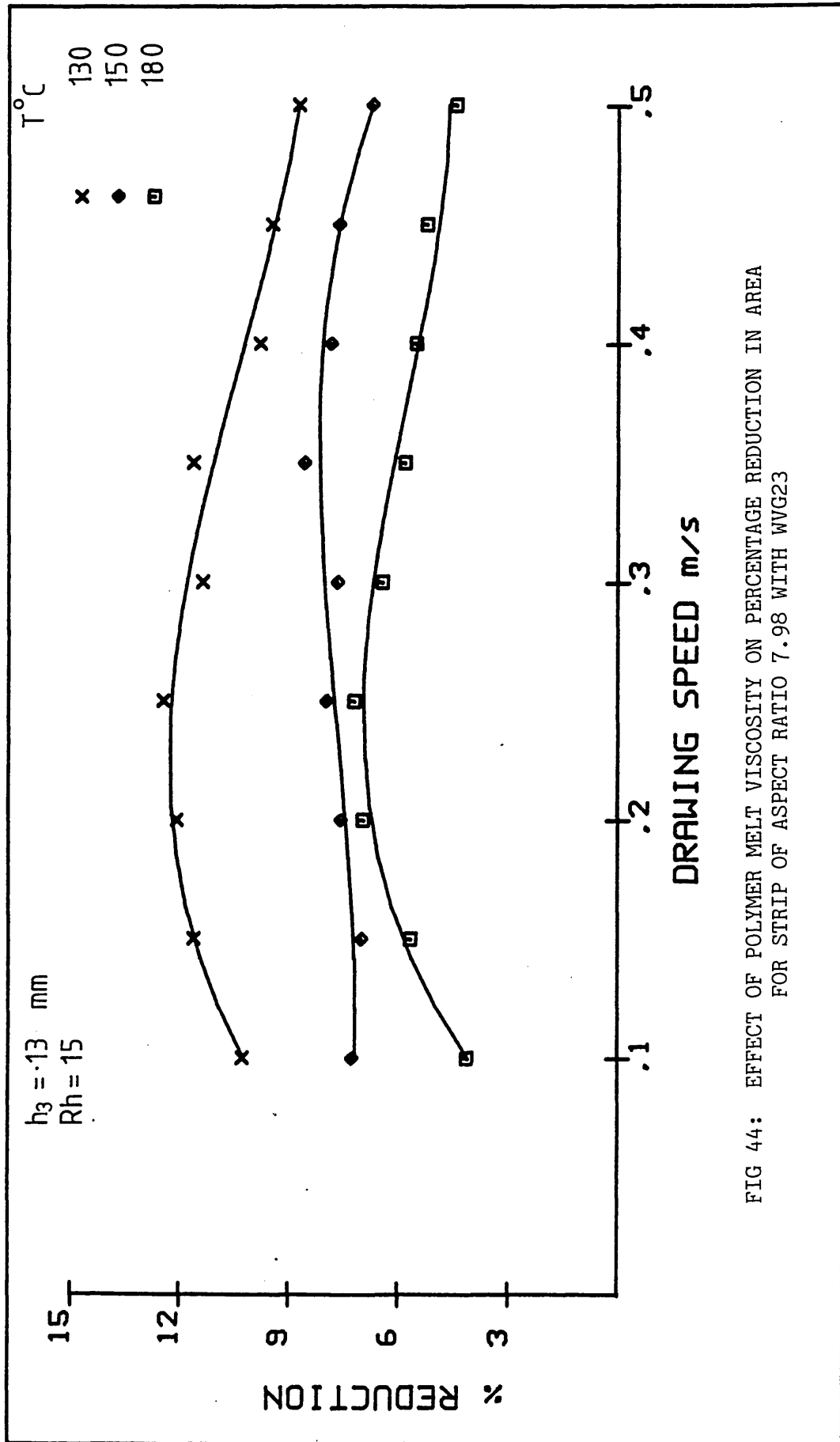


FIG 44: EFFECT OF POLYMER MELT VISCOSITY ON PERCENTAGE REDUCTION IN AREA FOR STRIP OF ASPECT RATIO 7.98 WITH WVG23

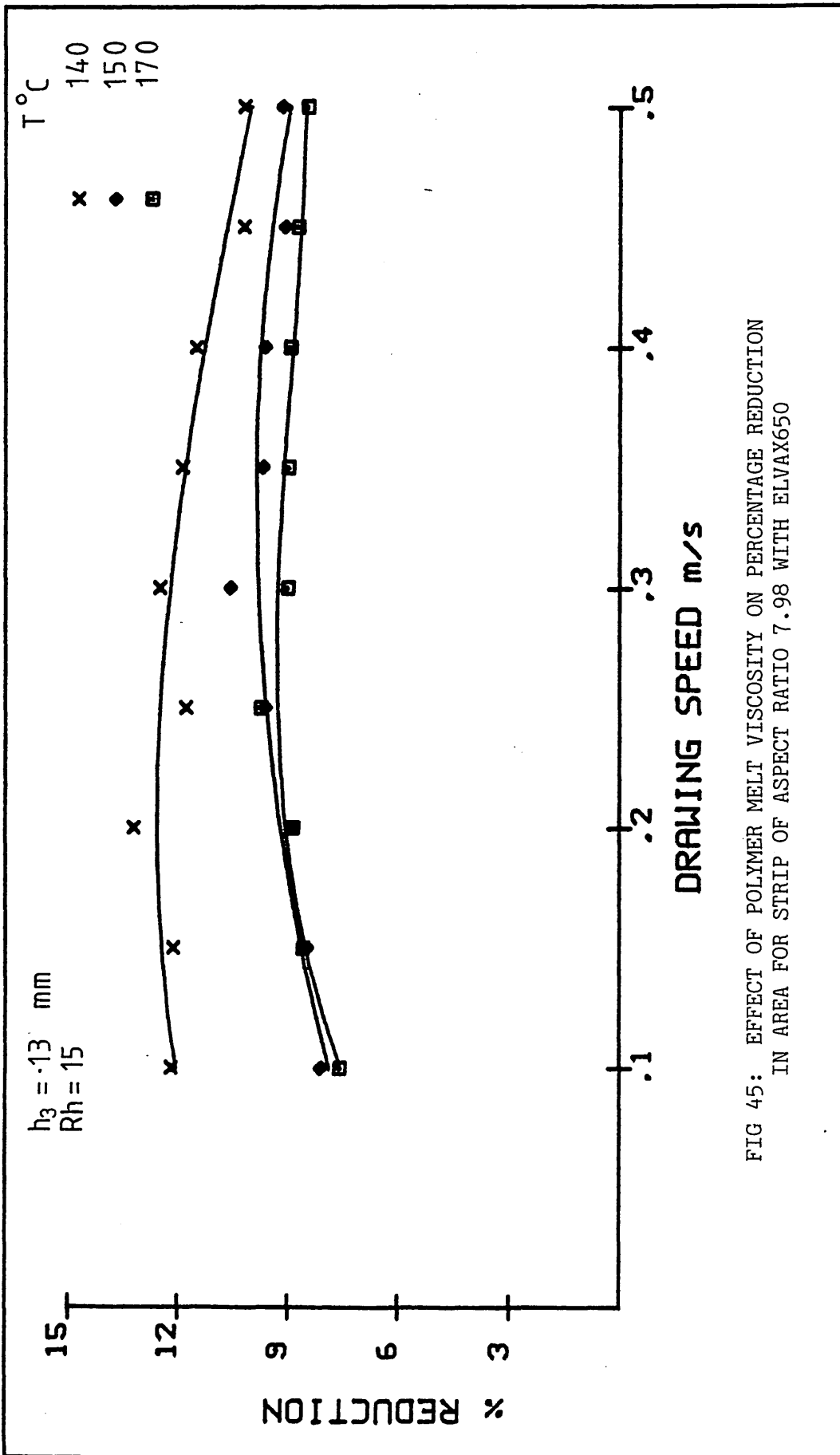


FIG 45: EFFECT OF POLYMER MELT VISCOSITY ON PERCENTAGE REDUCTION IN AREA FOR STRIP OF ASPECT RATIO 7.98 WITH ELVAX650

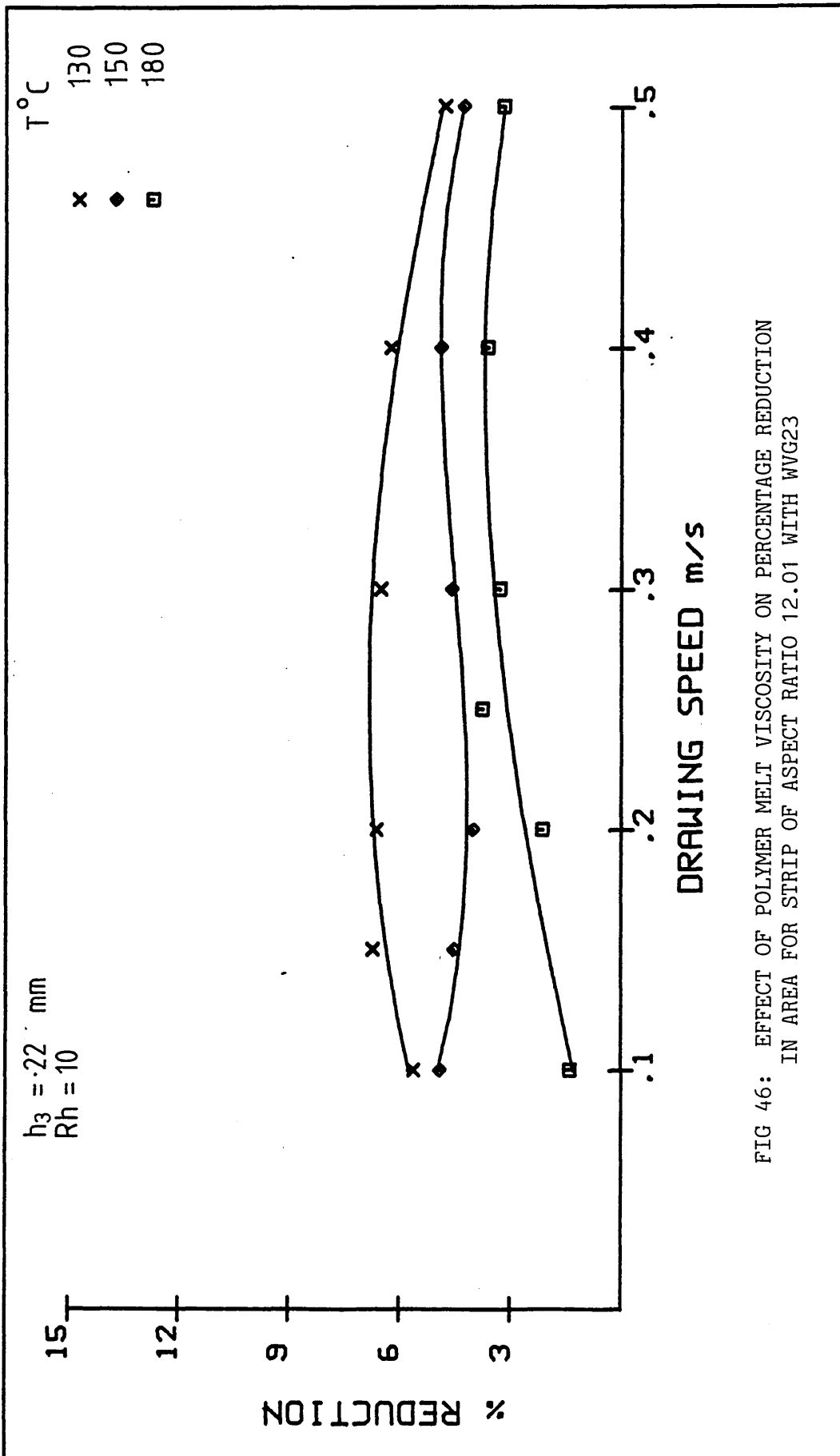


FIG 46: EFFECT OF POLYMER MELT VISCOSITY ON PERCENTAGE REDUCTION IN AREA FOR STRIP OF ASPECT RATIO 12.01 WITH WVG23

$h_3 = .13 \text{ mm}$
 $R_h = 15$

AR

x 7.98
 ♦ 12.01

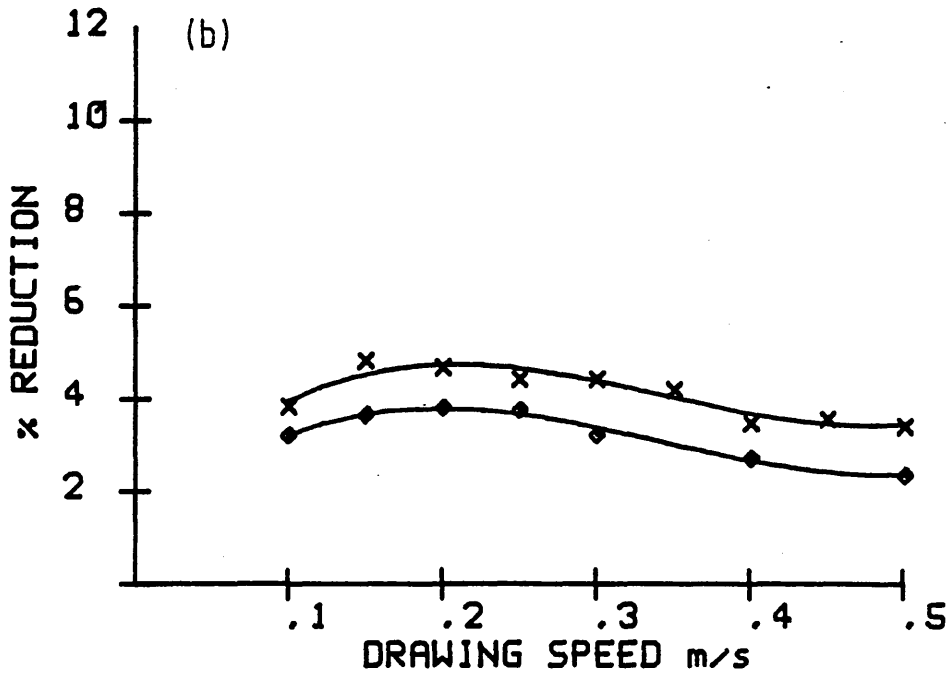
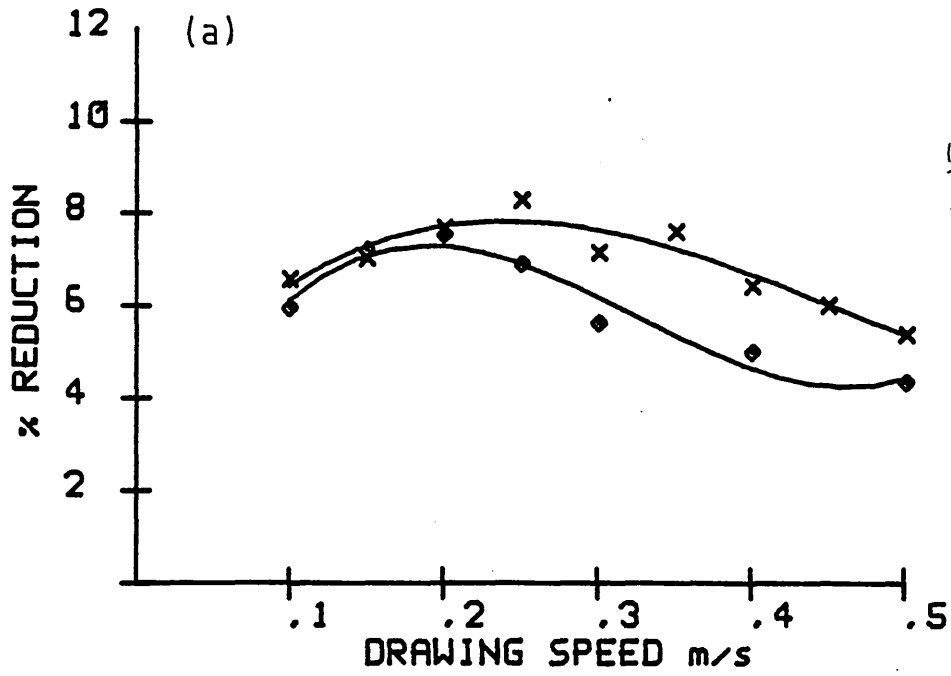


FIG 47: EFFECT OF ASPECT RATIO
 ON PERCENTAGE REDUCTION IN
 (a) THICKNESS (b) WIDTH
 WITH WVG23, 130°C

$h_3 = .13$ mm
 $R_h = 15$

AR

x 7.98
◊ 12.01

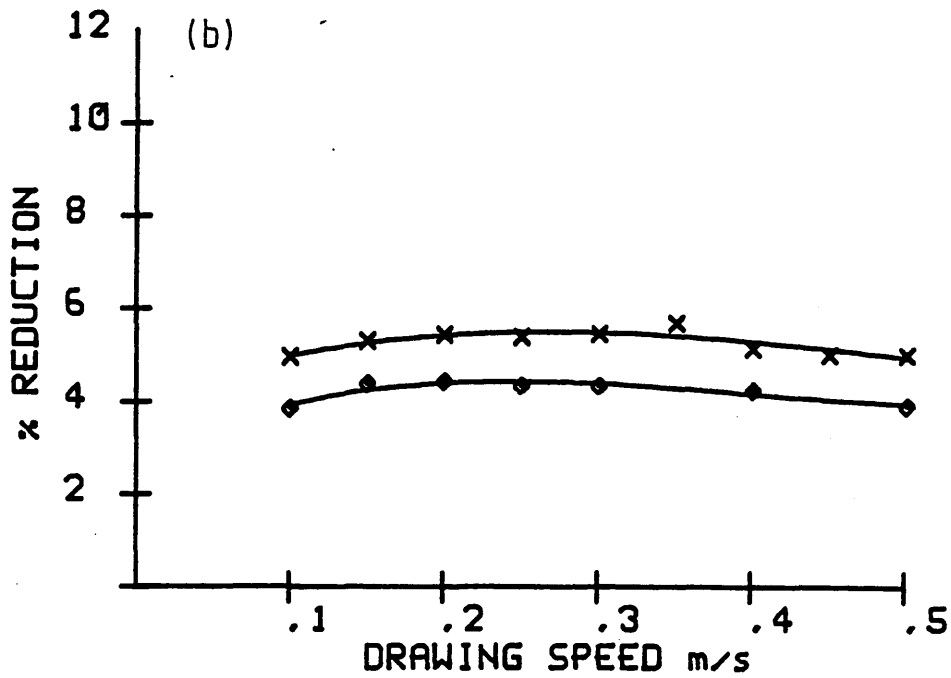
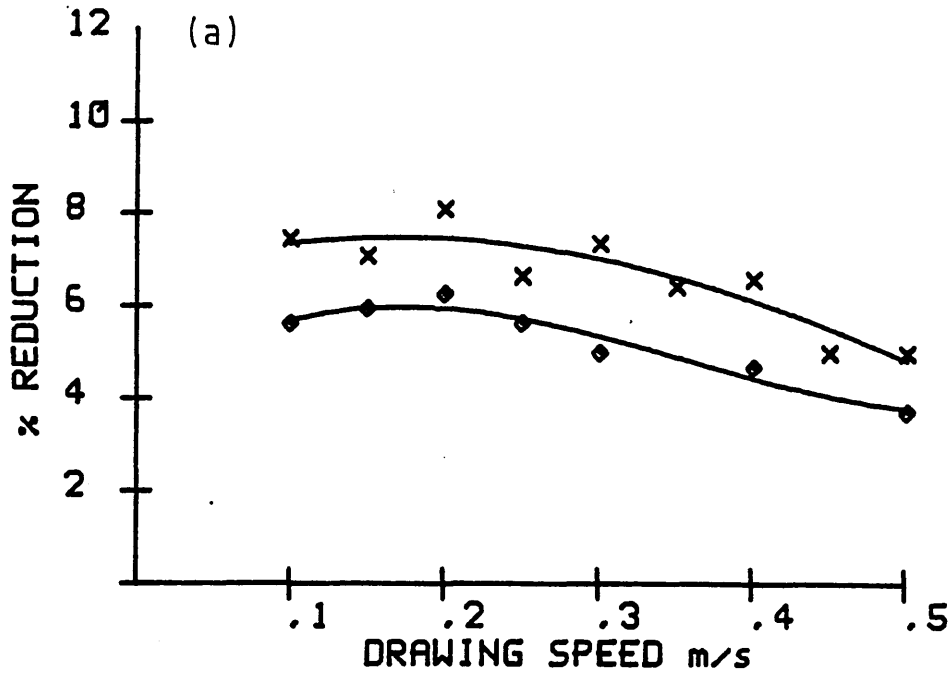


FIG 48: EFFECT OF ASPECT RATIO
ON PERCENTAGE REDUCTION IN
(a) THICKNESS (b) WIDTH
WITH ELVAX650, 140°C

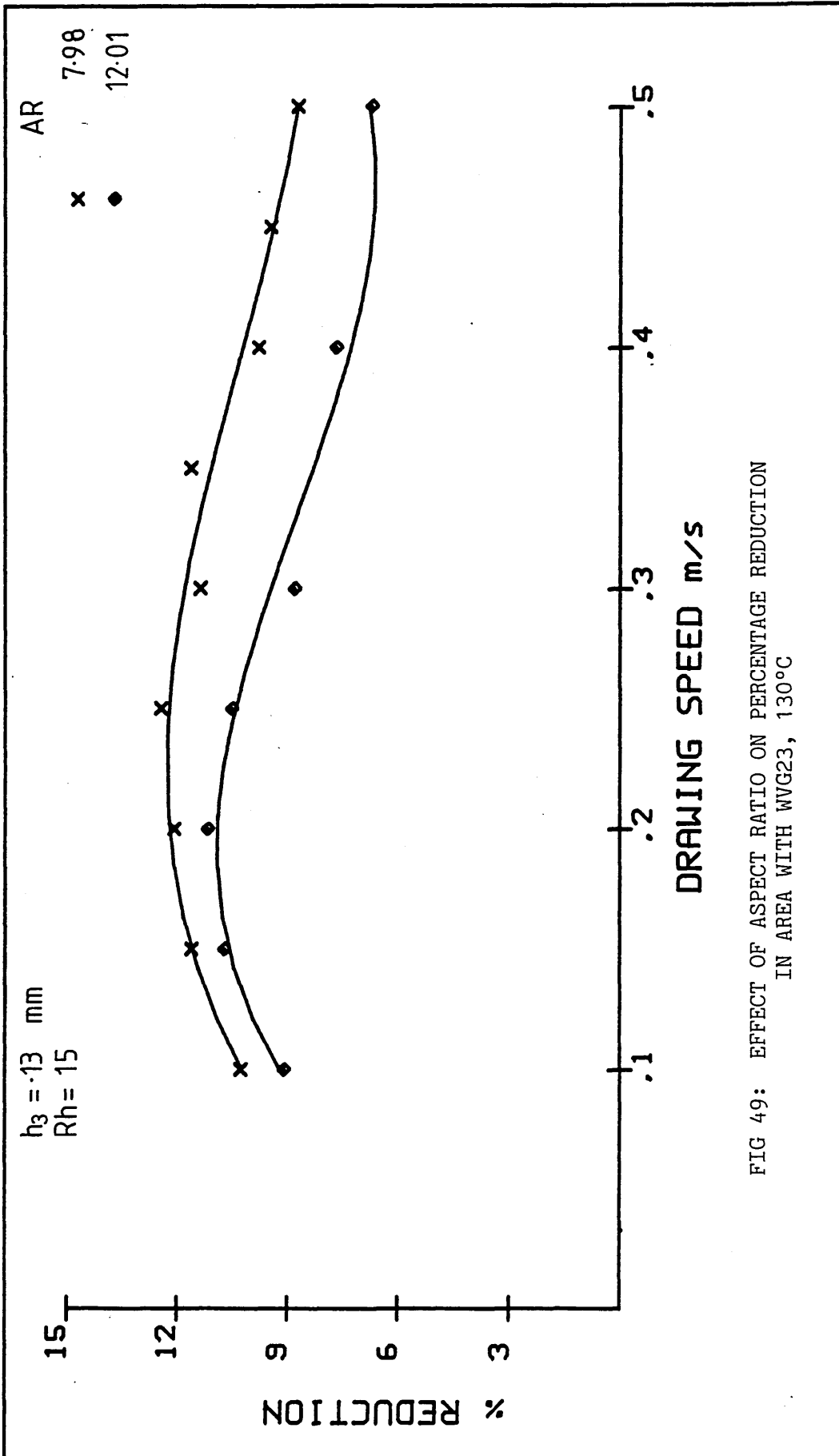


FIG 49: EFFECT OF ASPECT RATIO ON PERCENTAGE REDUCTION
 IN AREA WITH WVG23, 130°C

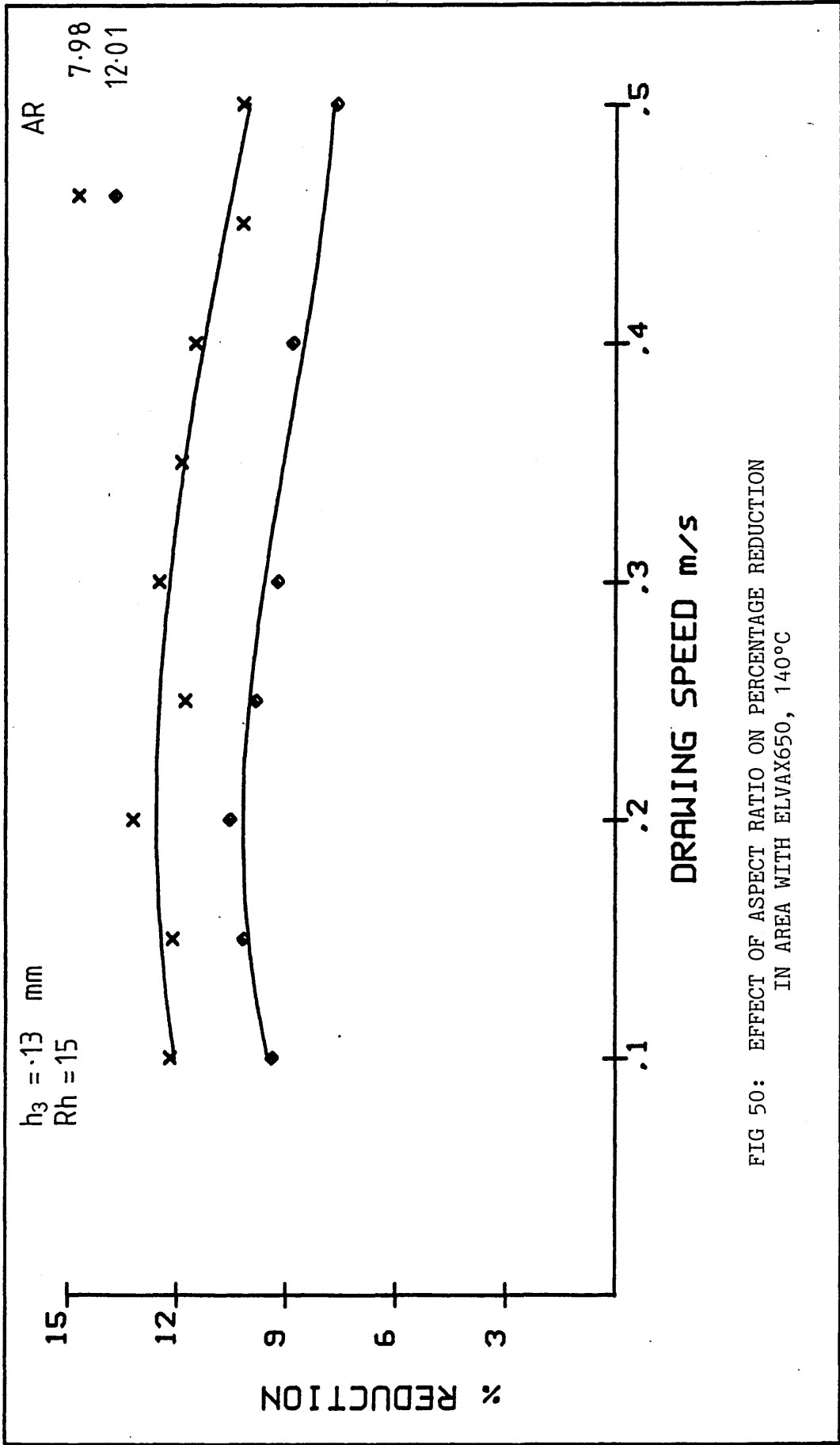


FIG 50: EFFECT OF ASPECT RATIO ON PERCENTAGE REDUCTION IN AREA WITH ELVAX650, 140°C

4.2.2 Results of Pressure

Hydrodynamic pressures were measured for the two sections A and B, by means of pressure transducers mounted on the reduction unit. The results are presented in two sections,

- (a) measured pressure near the step versus speed,
- (b) pressure profiles in the unit.

Numbers alongside the curves on each figure refer to the locations of the pressure transducers as shown in Figure 4.

(a) Pressure near the step versus speed

Figure 51 illustrates the variations in the measured hydrodynamic pressure near the step in two sections, for the drawing units having different values of gap h_3 , when WVG23 was used at temperature of 130°C as pressure medium. These results showed that pressures generated in the two sections followed the same trend. The pressures in Section B were noted to be slightly smaller compared to those in Section A. Higher pressures were recorded for smaller gap of 0.13 mm and 0.04 mm in the two sections (A and B) and the measured pressures were found to be approximately of same order with the two gaps.

Figure 52 shows the effect of gap h_3 on the pressure in two sections, when WVG23 was used at a melt temperature of 150°C. Measured pressures for Section B were found smaller compared to those for Section A. At higher gaps the differences were significant and the minimum pressure measured in Section B at speed of 0.5 m/s for the gap of 0.50 mm was found to be approximately 50% of the pressure measured in the Section A for the same gap and speed. Higher pressures were measured for the small gap of 0.04 mm, which were found to give similar trends to

those shown in Figure 51. No significant change was noticed in the measured pressures at speeds in excess of 0.3 m/s. The pressure was found to remain fairly constant at higher speeds when gaps of 0.04 , 0.13 and 0.22 mm were used.

Figures 53 and 54 show similar curves for the polymer ELVAX650 at temperatures of 140°C and 170°C respectively. The pressures measured with this polymer showed similar trends to those observed with WVG23. Higher pressures were recorded for smaller gap of 0.04 mm.

Figure 55 demonstrates the variations in the pressures against drawing speed using WVG23 at 130°C for different gap ratios. Pressures measured for Section B were found to be smaller compared to those measured for Section A. It was noticed that gap ratio has little effect on the pressure and the measured pressure was found to be fairly constant at higher drawing speeds.

The effect of gap ratio on the pressure variations using polymer WVG23 at temperature of 150°C is shown in Figure 56. At this temperature constant pressures were recorded at speeds in excess of 0.3 m/s in Section A. Pressures recorded for Section B, using higher gap ratios of 15 and 20 were found to be of the same magnitude.

Figure 57 shows the effect of gap ratio on the variations in the pressure versus speed using ELVAX650 at 140°C. It was noted that pressures of approximately the same magnitude were generated with higher gap ratios of 15 and 20, at all speeds in Section A and at speeds greater than 0.2 m/s in Section B.

Figure 58 gives the graphs for pressure variations with speed for different gap ratios, when polymer ELVAX650 was used at temperature of 170°C. The gap ratio was found to have a little effect at this temperature. The measured pressures were found to be approximately of the same magnitude for three gap ratios over the whole range of speed in Section A and at speeds greater than 0.2 m/s in Section B.

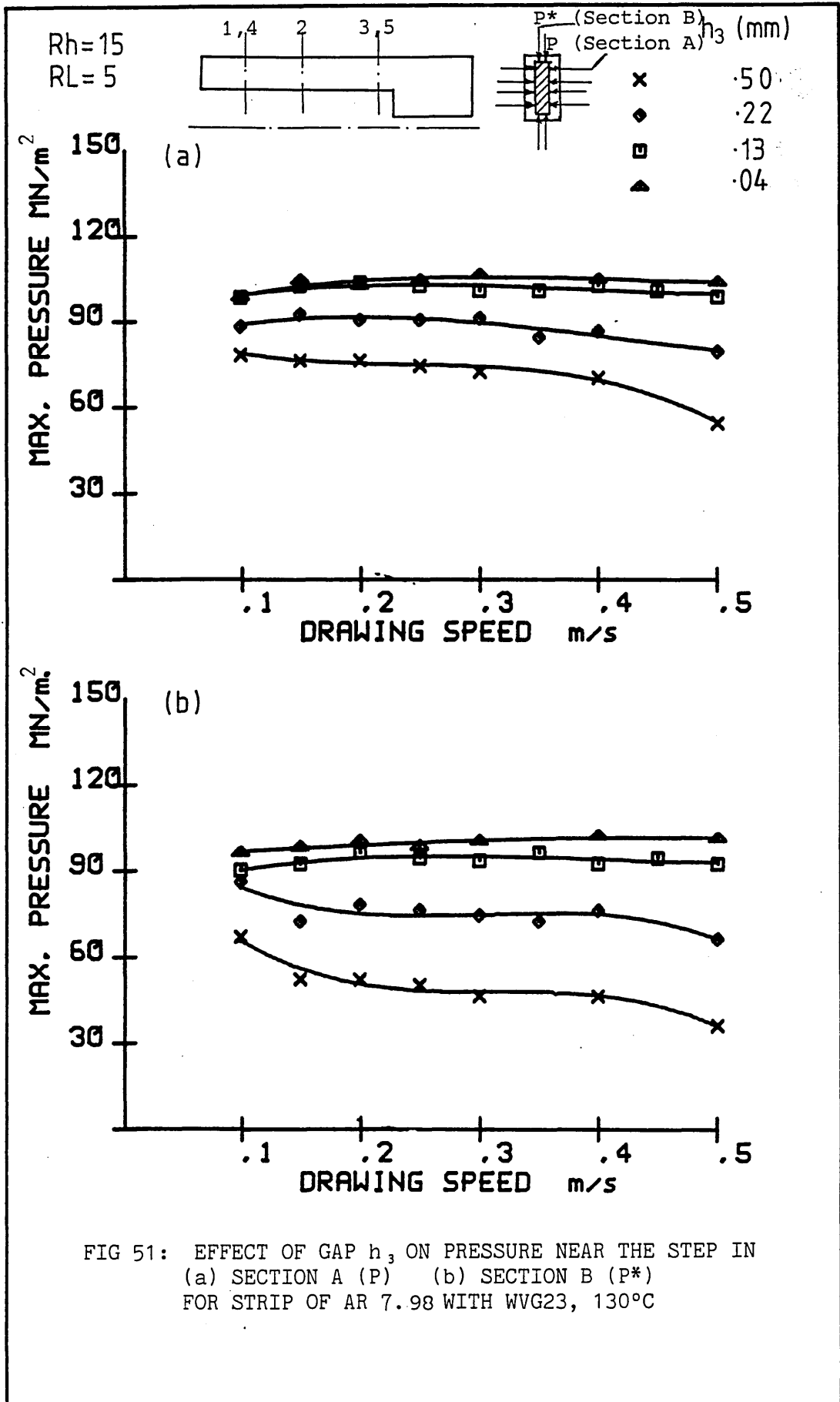
The effect of length ratio on the variation in pressure near the step when WVG23 at 130°C was used as pressure medium is shown in Figure 59. These results show that recorded pressures were of the same order at all the drawing speeds.

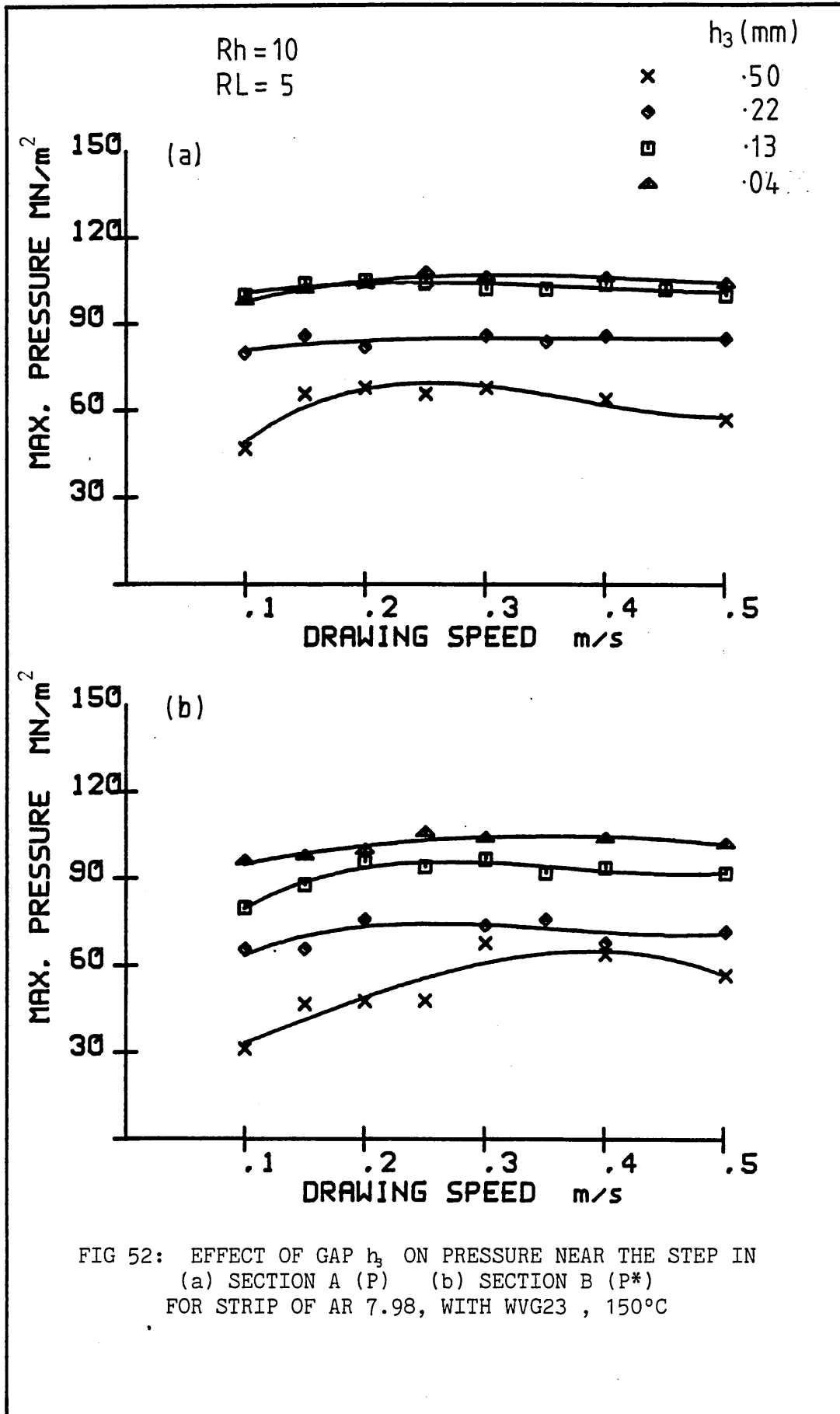
It was also observed that, generally the magnitude of the pressures measured near the step remained fairly constant for speeds higher than 0.3 m/s.

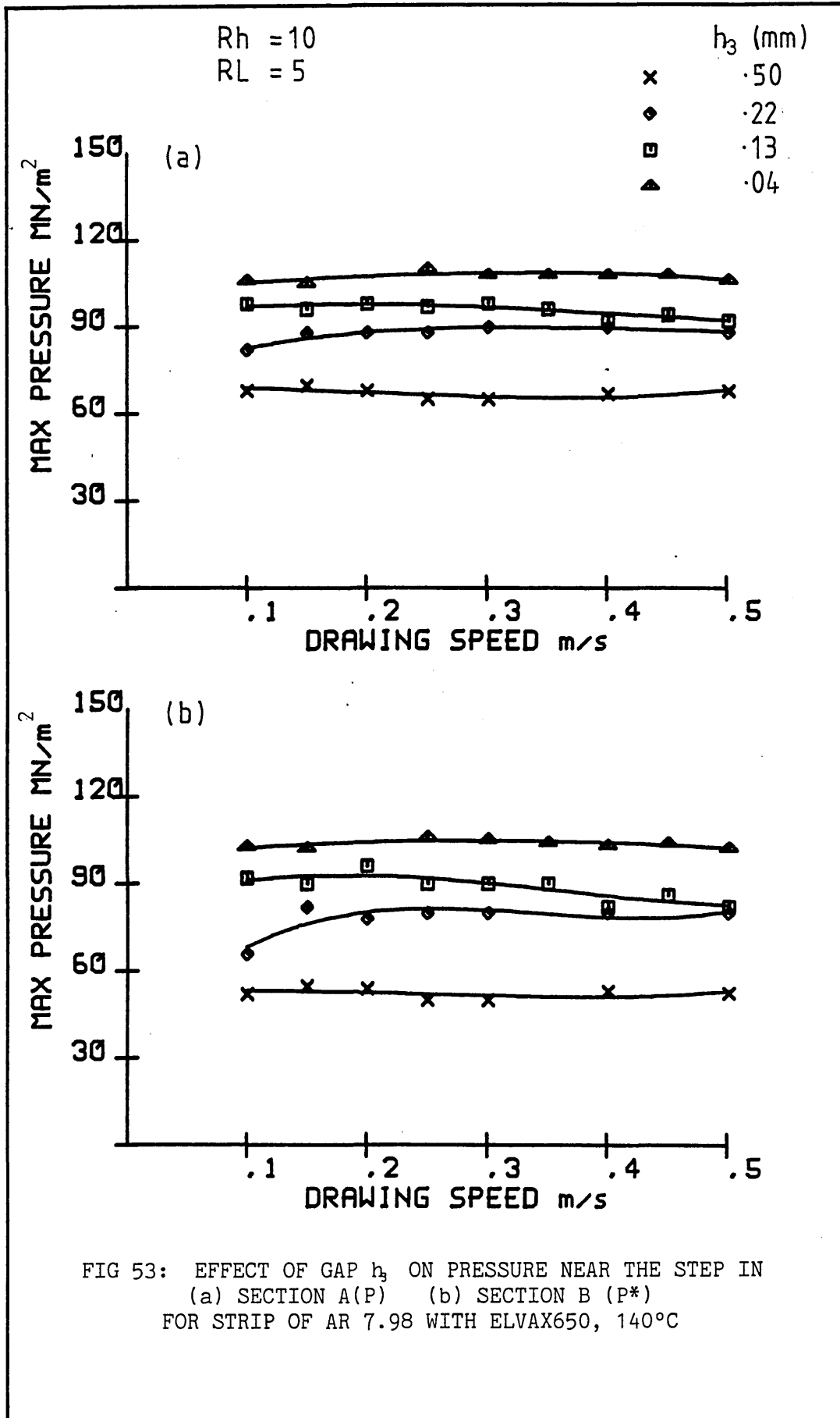
(b) Pressure Profiles in the Unit

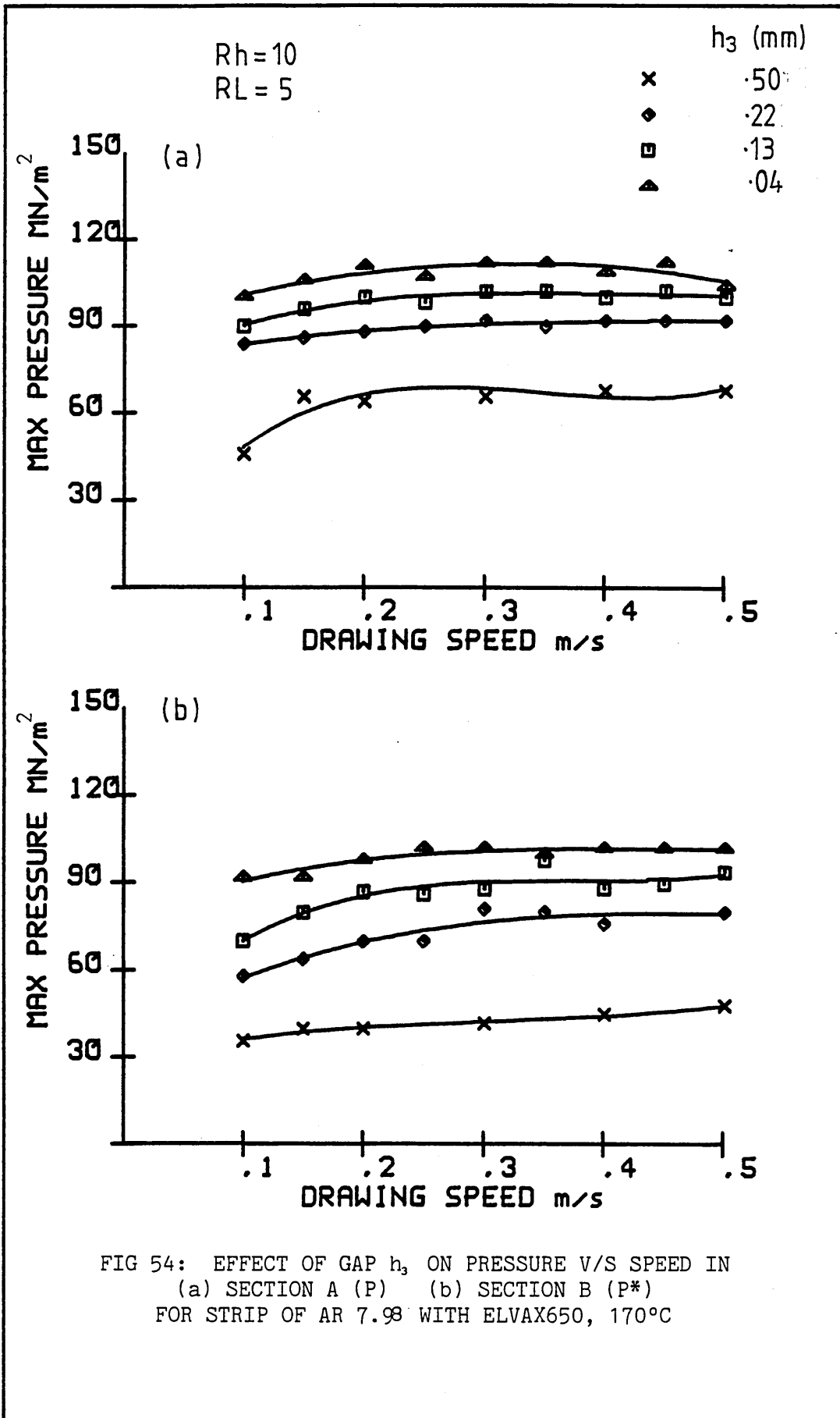
Figures 60-63 show the pressure profiles along the unit in Section A, at typical two drawing speeds demonstrating the effect of gap h_3 and h_1 when WVG23 at 130°C was used as the pressure medium. In all the cases measured pressures were found to increase from the entry point towards the step. The maximum pressure near the step was found to vary between 76-110 MNm⁻².

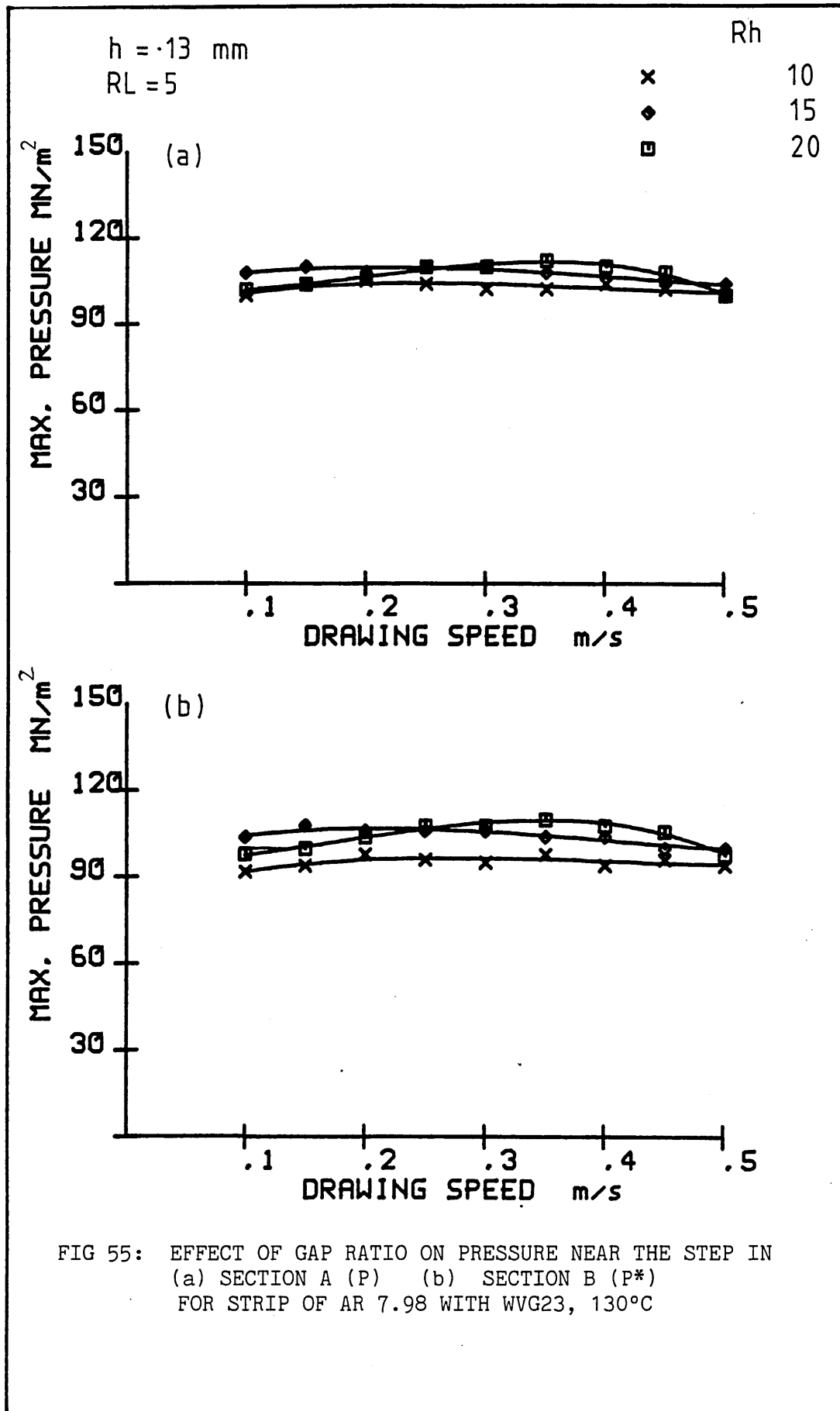
Figures 64-67 are the plots of profiles for Section A, determined by using polymer ELVAX650 at 140°C for two different drawing speeds. Similar trends were observed to those shown in Figures 60-63. The maximum readings were noted near the step in all cases and the magnitudes of the maximum pressure near the step were found to be between 65-110 MNm⁻².

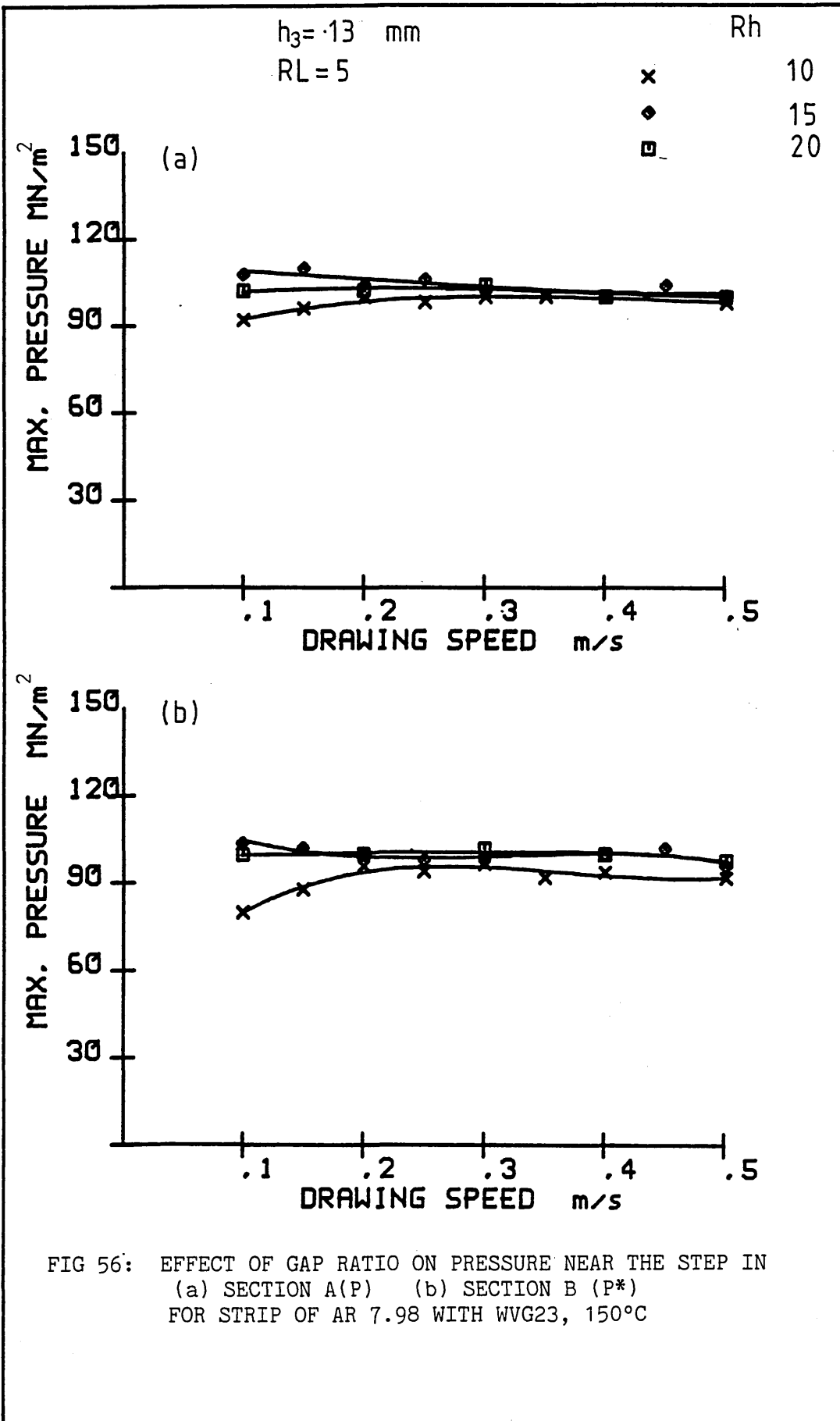


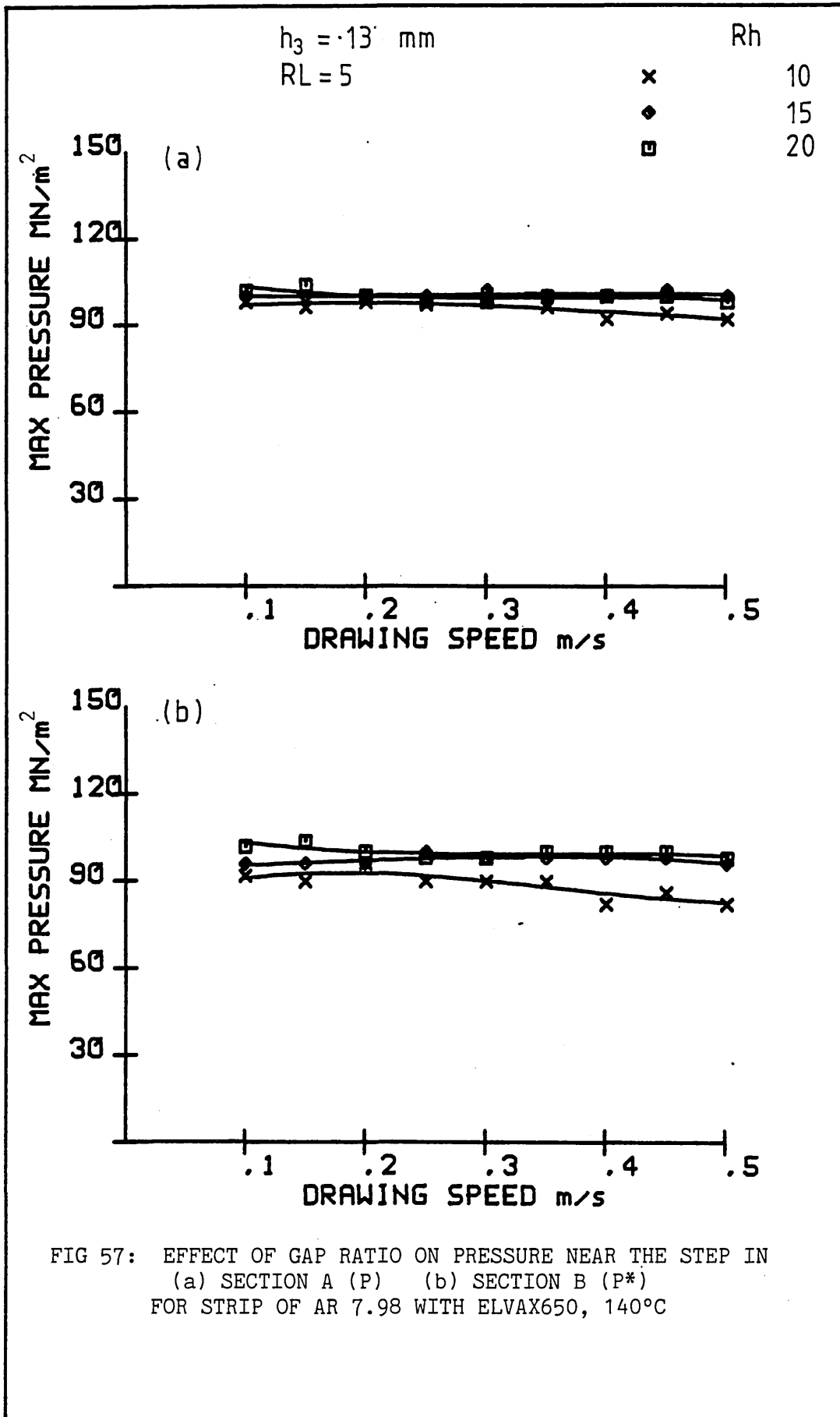












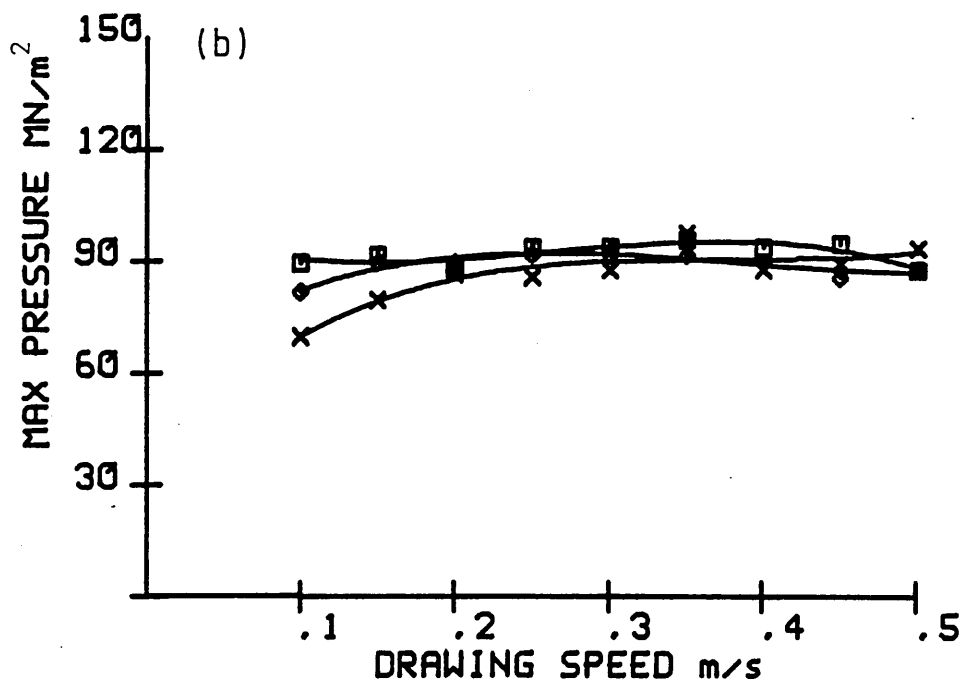
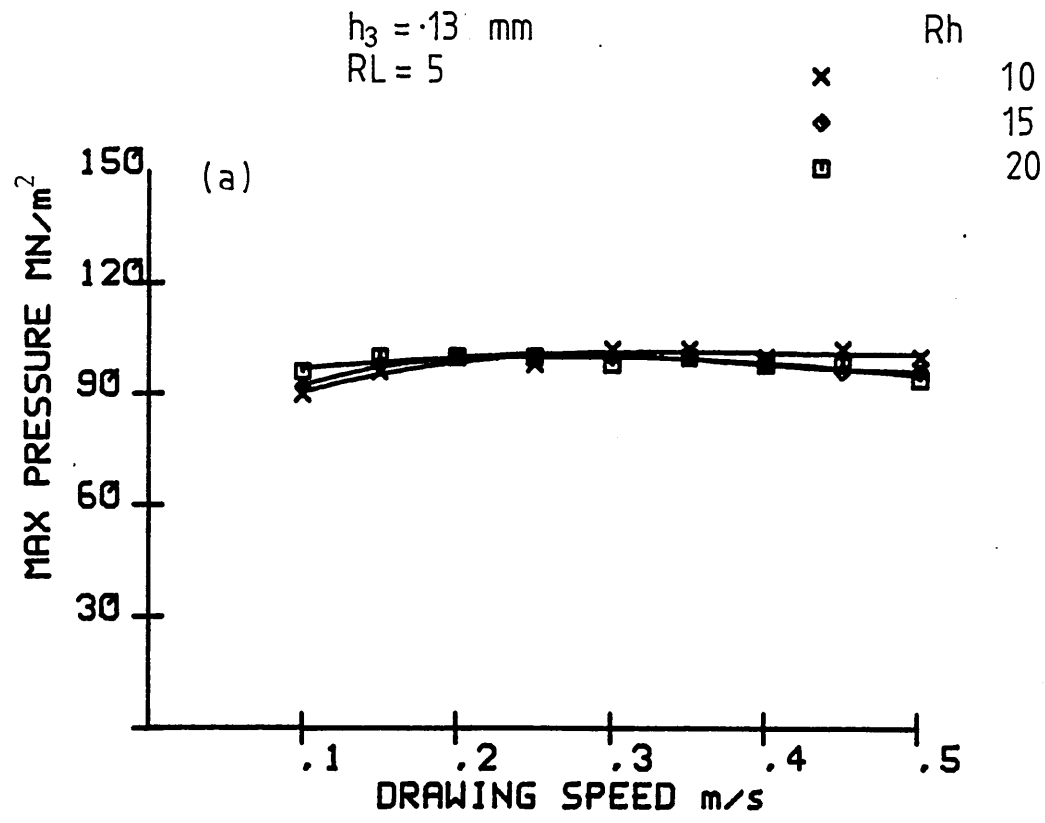


FIG 58: EFFECT OF GAP RATIO ON PRESSURE IN
 (a) SECTION A (P) (b) SECTION B (P*)
 FOR STRIP OF AR 7.98, WITH ELVAX650, 170°C

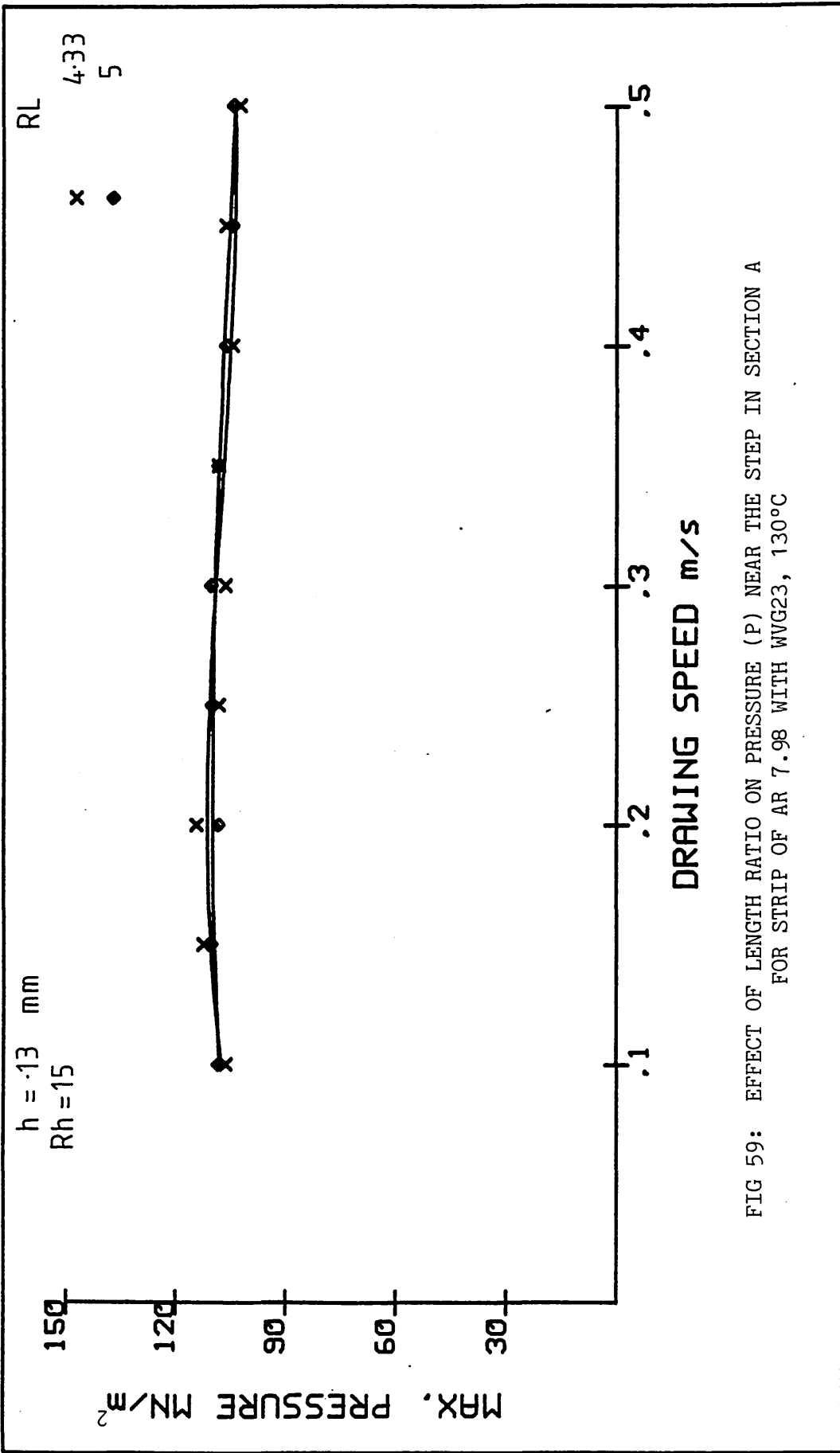


FIG 59: EFFECT OF LENGTH RATIO ON PRESSURE (P) NEAR THE STEP IN SECTION A FOR STRIP OF AR 7.98 WITH WVG23, 130°C

h_3
 ——— .04
 ——— .13
 - - - .50

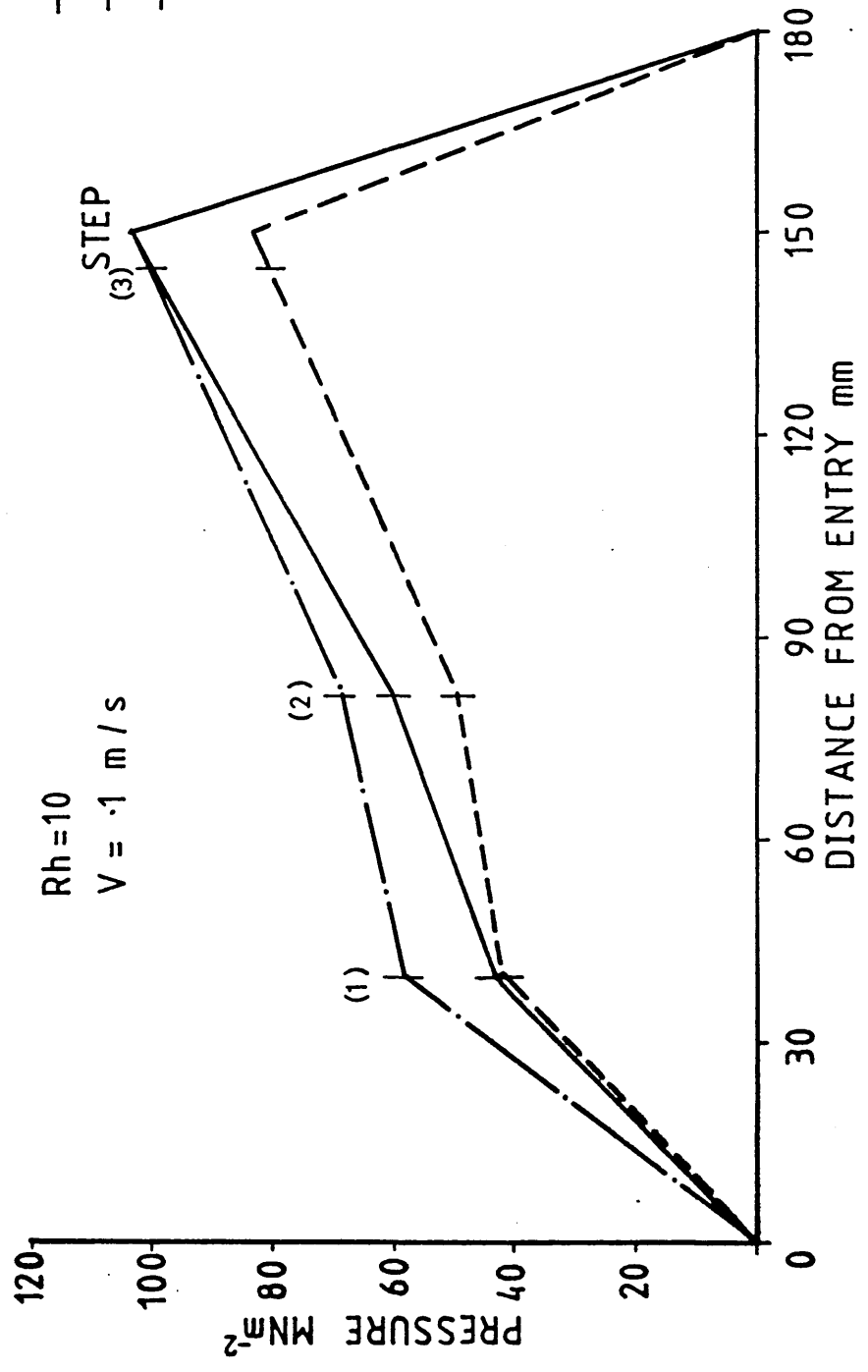


FIG 60: PRESSURE DISTRIBUTIONS WITHIN THE UNIT WITH WVG23, 130°C

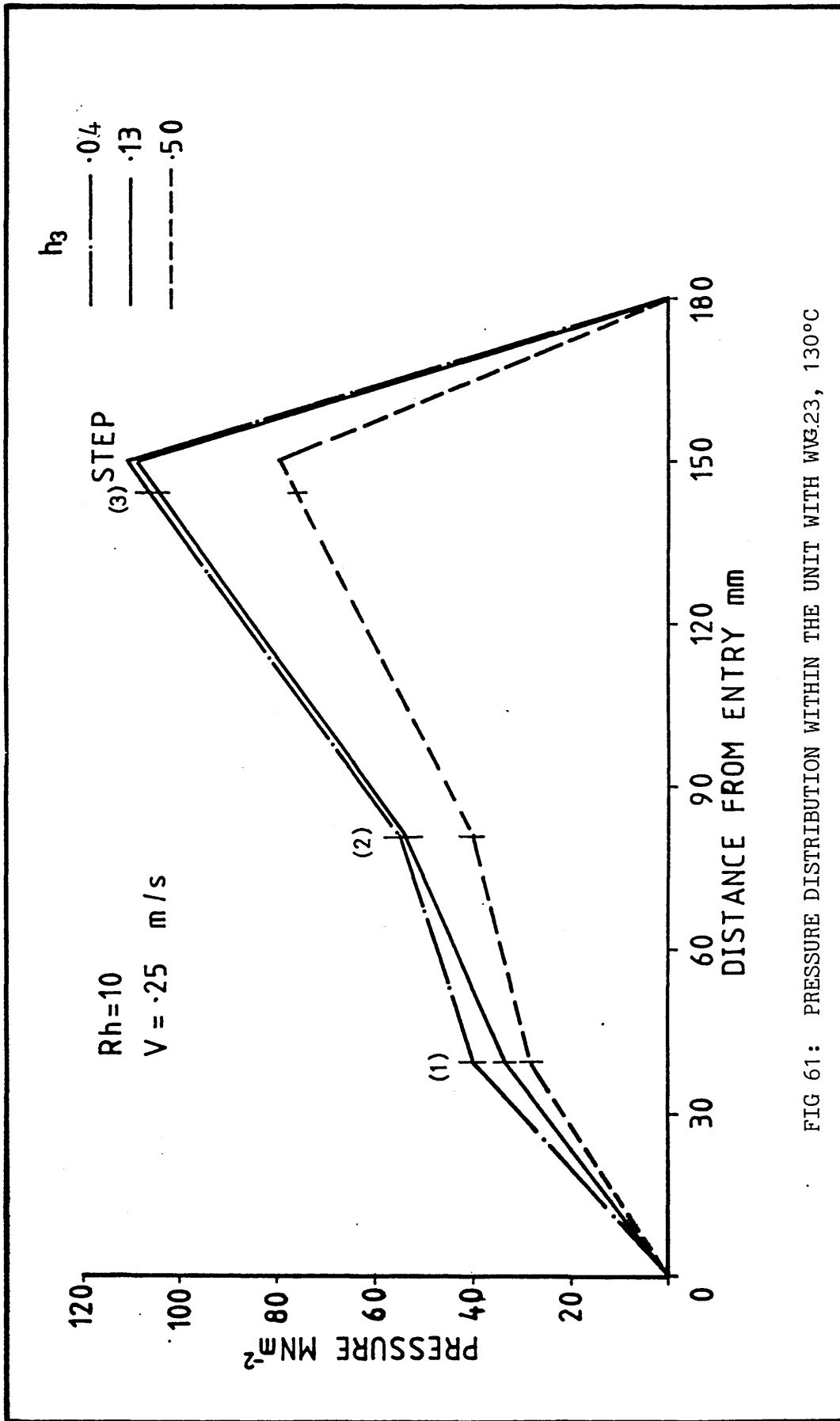


FIG 61: PRESSURE DISTRIBUTION WITHIN THE UNIT WITH WG23, 130°C

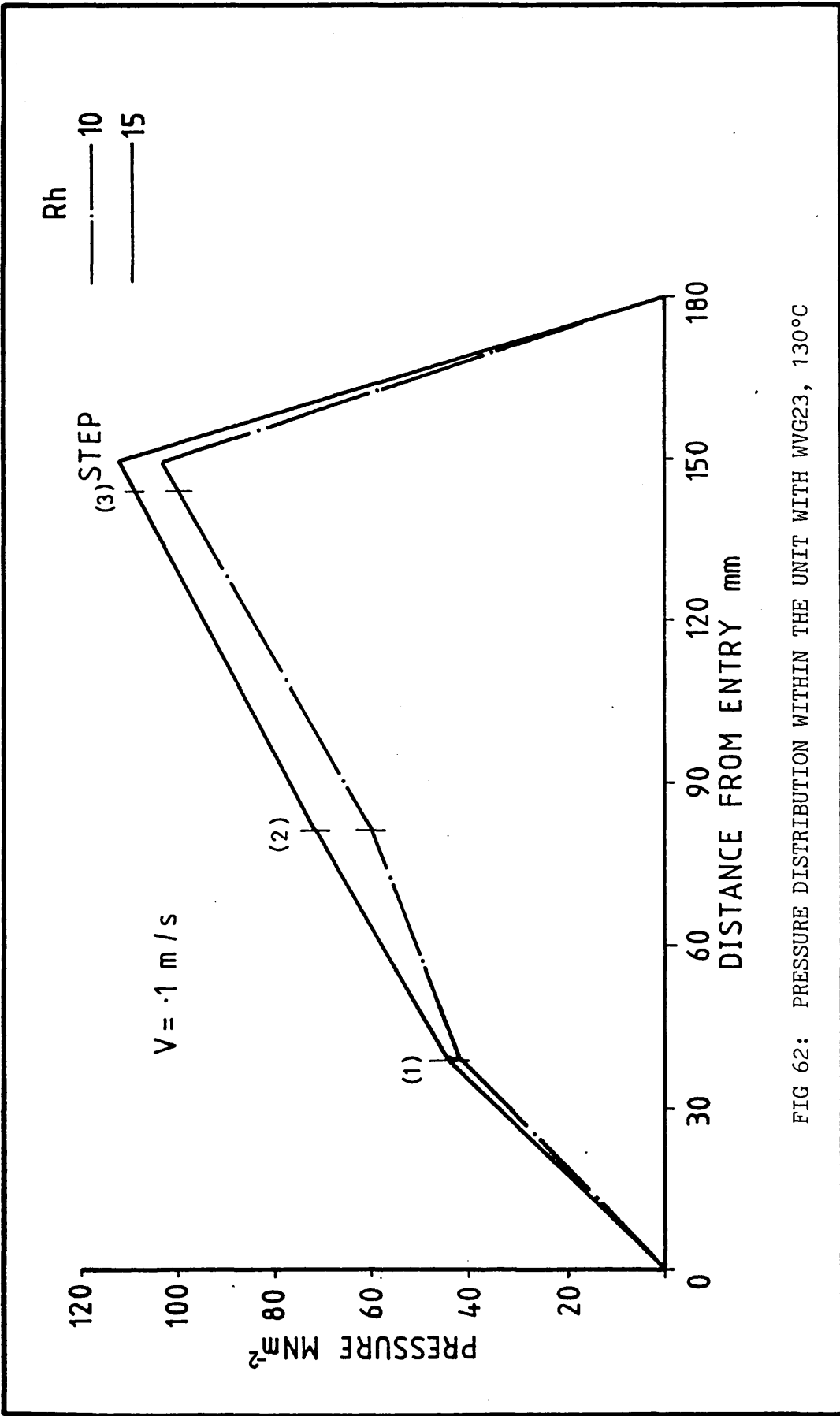


FIG 62: PRESSURE DISTRIBUTION WITHIN THE UNIT WITH WVG23, 130°C

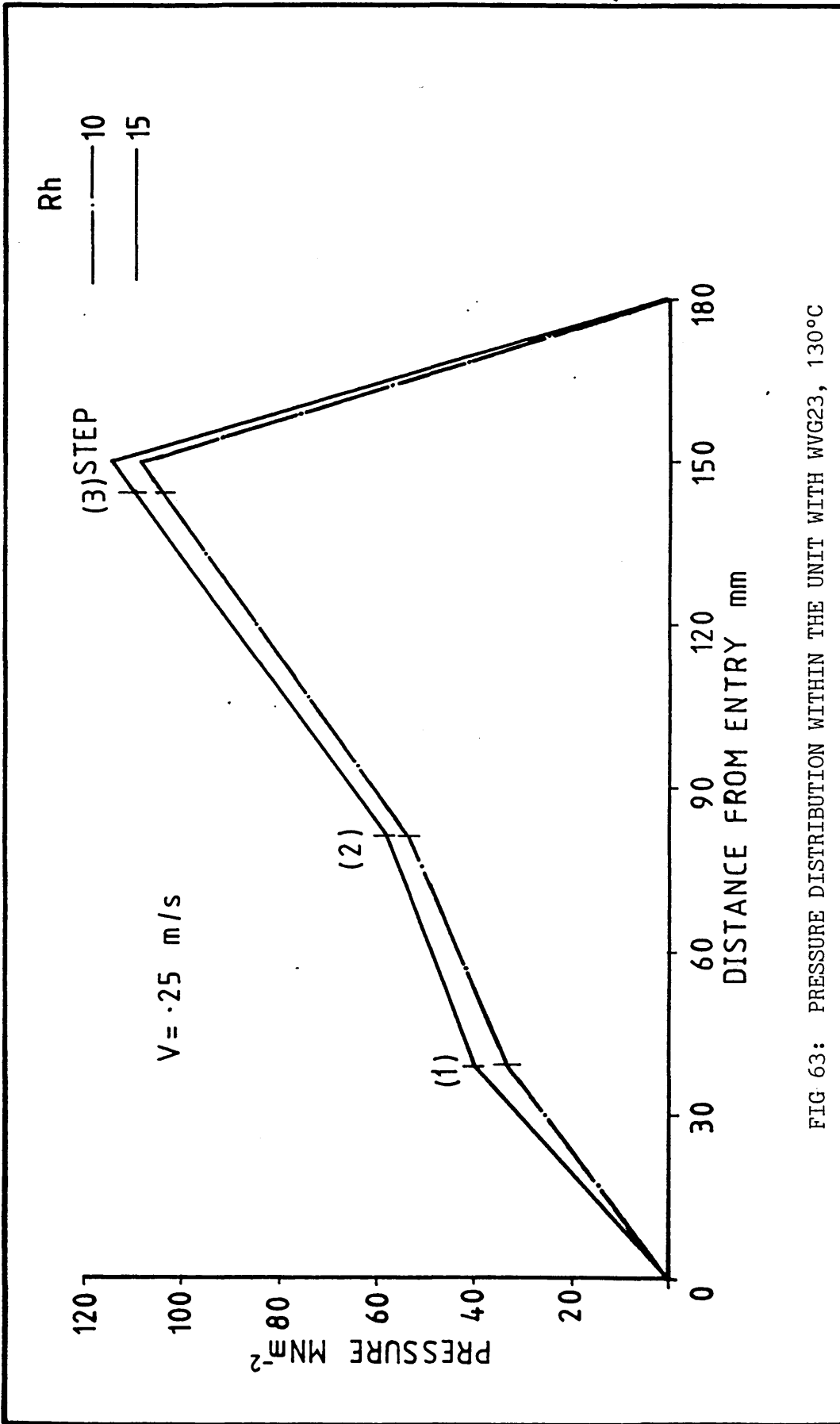


FIG 63: PRESSURE DISTRIBUTION WITHIN THE UNIT WITH WVG23, 130°C

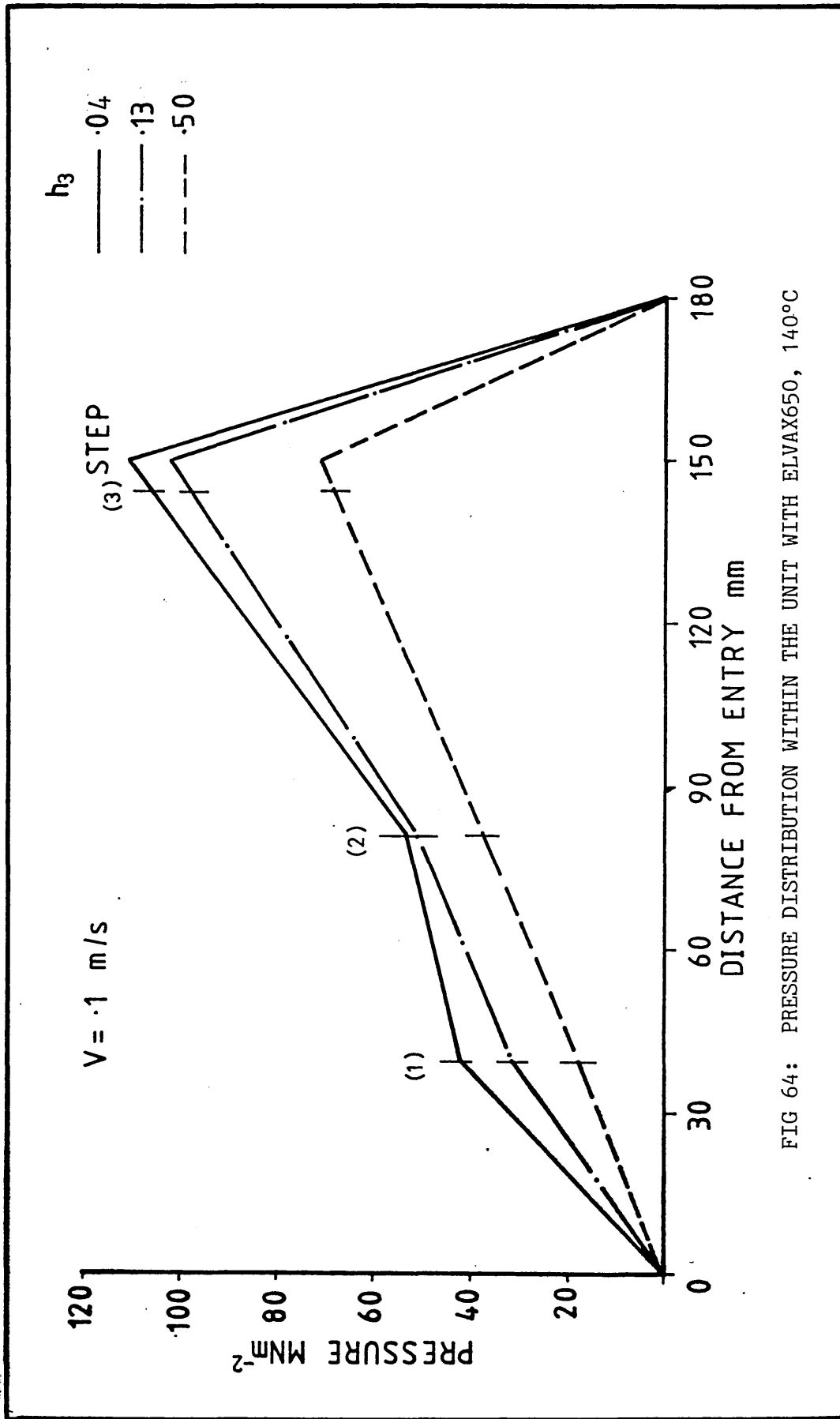


FIG 64: PRESSURE DISTRIBUTION WITHIN THE UNIT WITH ELVAX650, 140°C

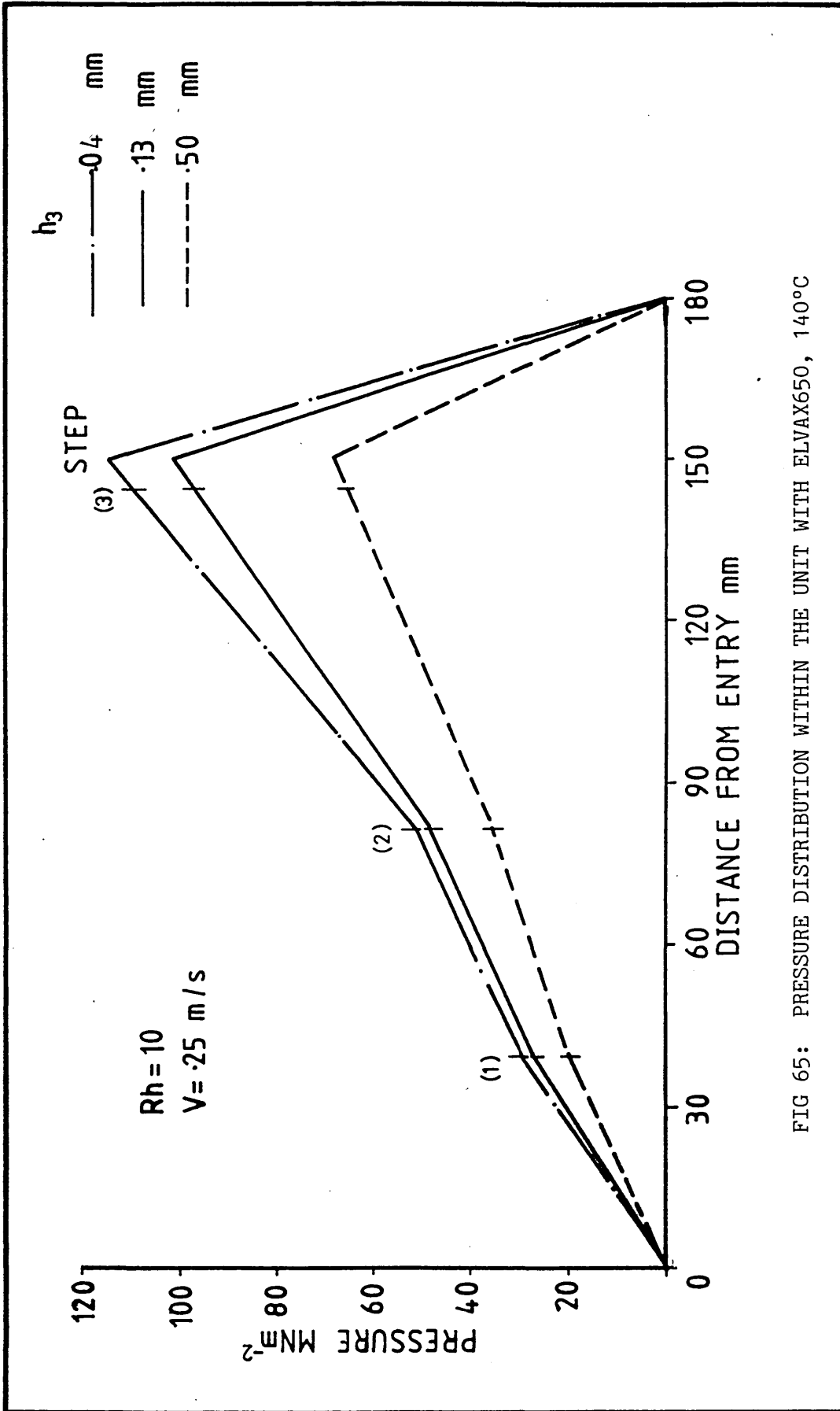


FIG 65: PRESSURE DISTRIBUTION WITHIN THE UNIT WITH ELVAX650, 140°C

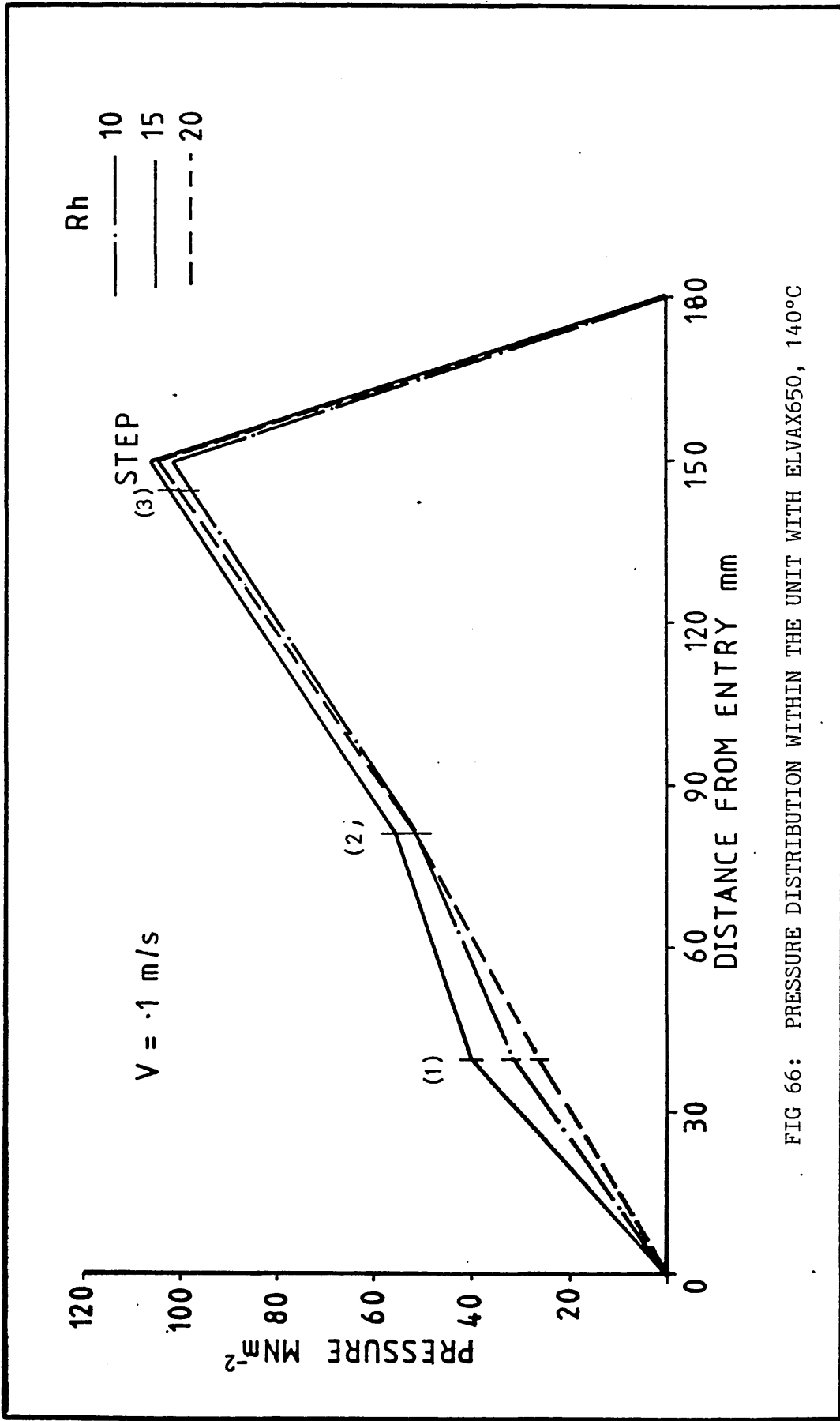


FIG 66: PRESSURE DISTRIBUTION WITHIN THE UNIT WITH ELVAX650, 140°C

Rh
 ——— 10
 ——— 15
 - - - 20

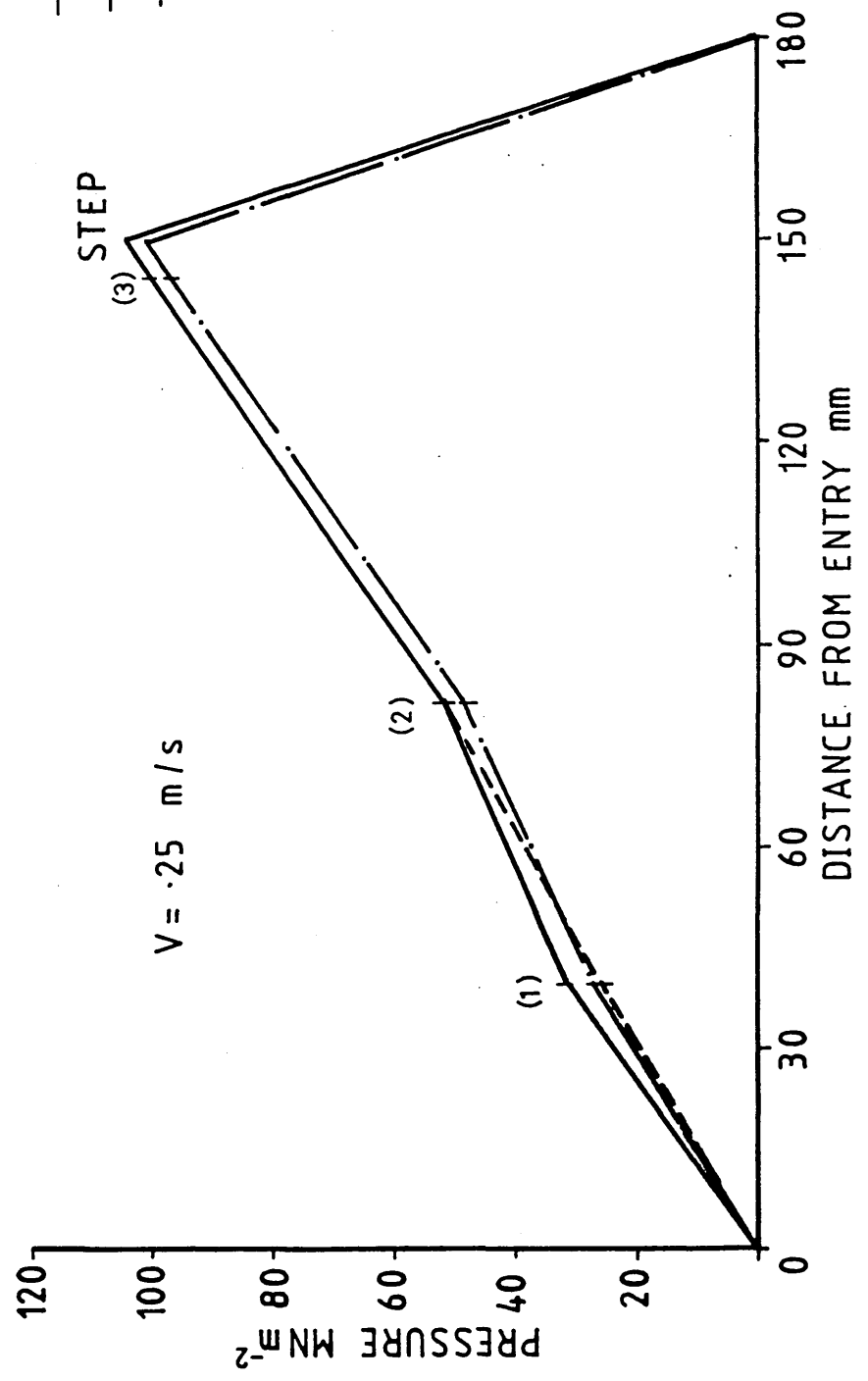


FIG 67: PRESSURE DISTRIBUTION WITHIN THE UNIT WITH ELVAX650, 140°C

4.2.3 Drawing Stress versus Speed

Drawing load was recorded from the load indicator connected to the strain gauge load cell. The results are presented in terms of drawing stress.

Figures 68 and 69 show the variations in drawing stress with speed using WVG23 at temperatures of 130°C and 150°C for the different values of gap h_3 . These results indicate an increase in drawing stress with an increase in drawing speed up to a certain speed and then a decrease for the further increases in drawing speed. Beyond the drawing speed of 0.3 m/s the magnitude of the drawing stress was determined to be similar with all of the gaps for the polymer temperature of 150°C. The maximum drawing stress (about 50 MNm⁻²) was noticed at a drawing speed of 0.2 m/s, at a temperature of 130°C and (about 23 MNm⁻²) at the speed of 0.25 m/s for the melt temperature of 150°C, when a gap of $h_3 = 0.04$ mm was used.

Figures 70 and 71 present the drawing stresses measured with ELVAX650 at temperatures of 140°C and 170°C. The general tendency of the curves was found to be similar to the results obtained with WVG23. With this polymer a maximum value of drawing stress (about 52 MNm⁻²) was noticed at a drawing speed of 0.4 m/s for a gap of $h_3 = 0.50$ mm and at speed of 0.3 m/s for the other three gaps (about 55-60 MNm⁻²), at temperature of 140°C. Drawing stresses measured for strip of larger width with the two polymers using reduction units of different values of gap h_3 are plotted in Figures 72 and 73. Higher drawing stresses were noted for gap of 0.13 mm.

Figures 74 and 75 show the variations in the drawing stresses for various gap ratios when WVG23 was used as pressure medium at

temperatures of 130°C and 150°C. It was observed that the drawing stresses of approximately the same order were produced with the gap ratios of 10 and 20 at temperatures of 130°C and with gap ratios of 15 and 20 at temperatures of 150°C. These results showed similar trends to those shown previously; higher drawing speeds produce lower drawing stresses. Maximum drawing stress (about 51 MNm⁻²) was noted at speed of 0.25 m/s and temperature of 130°C, for gap ratio of 15.

The effect of gap ratio on the drawing stresses using polymer ELVAX650 at temperatures of 140°C and 170°C is demonstrated by Figures 76 and 77. A noticeable difference was marked at melt temperature of 140°C when a gap ratio of 15 was used, and the drawing stresses were found to increase at higher speeds and maximum drawing stress (about 77 MNm⁻²) was noted at drawing speed of 0.5 m/s. The general trends were observed to be the same as those in Figures 74 and 75. Figures 78 and 79 present the results when strip of large aspect ratio was drawn. The drawing stresses produced by using WVG23 at temperature of 130°C are shown in Figure 78 and those produced by using ELVAX650 at 140°C are shown in Figure 79. The maximum drawing stresses were noted with a gap ratio of 15.

Figures 80 and 81 illustrate the effect of length ratio on drawing stresses using WVG23 at 130°C and ELVAX650 at 140°C respectively. It was found that general trends remained the same as were noticed previously. The maximum drawing stresses were observed for the length ratio of 5 with both polymers.

Figure 82 shows the variations in the drawing stress with speed for 12.7mm wide strip with WVG23 polymer at three different

temperatures (130°C, 150°C and 180°C). This figure shows that the minimum drawing stress was noted at lower viscosity ie at higher temperature. At the temperature of 130°C, generally higher drawing stresses were noted and as the temperature was increased the drawing stress was reduced by about 50% at melt temperature of 180°C for the same drawing speed.

The effect of viscosity on drawing stress for strip of small aspect ratio versus speed with ELVAX650 at melt temperatures of 140°C, 150°C and 170°C is demonstrated in Figure 83. Higher drawing stresses were observed at melt temperature of 140°C.

Figures 84 and 85 show the effect of viscosity on drawing stress for wider strip using WVG23 (130°C, 150°C and 180°C) and ELVAX650 (140°C, 150°C and 170°C) respectively. The higher drawing stresses were noted at the lower melt temperatures for each polymer. When polyethylene WVG23 was used it was observed that two temperatures (150°C and 180°C) have little effect on the drawing stress. Similarly ELVAX650 at temperature 140°C and 150°C showed no significant difference in drawing stress at speeds in excess of 0.3 m/s.

It was also observed that generally the drawing stresses produced by ELVAX650 were relatively of higher magnitudes to those when WVG23 was used as the pressure medium.

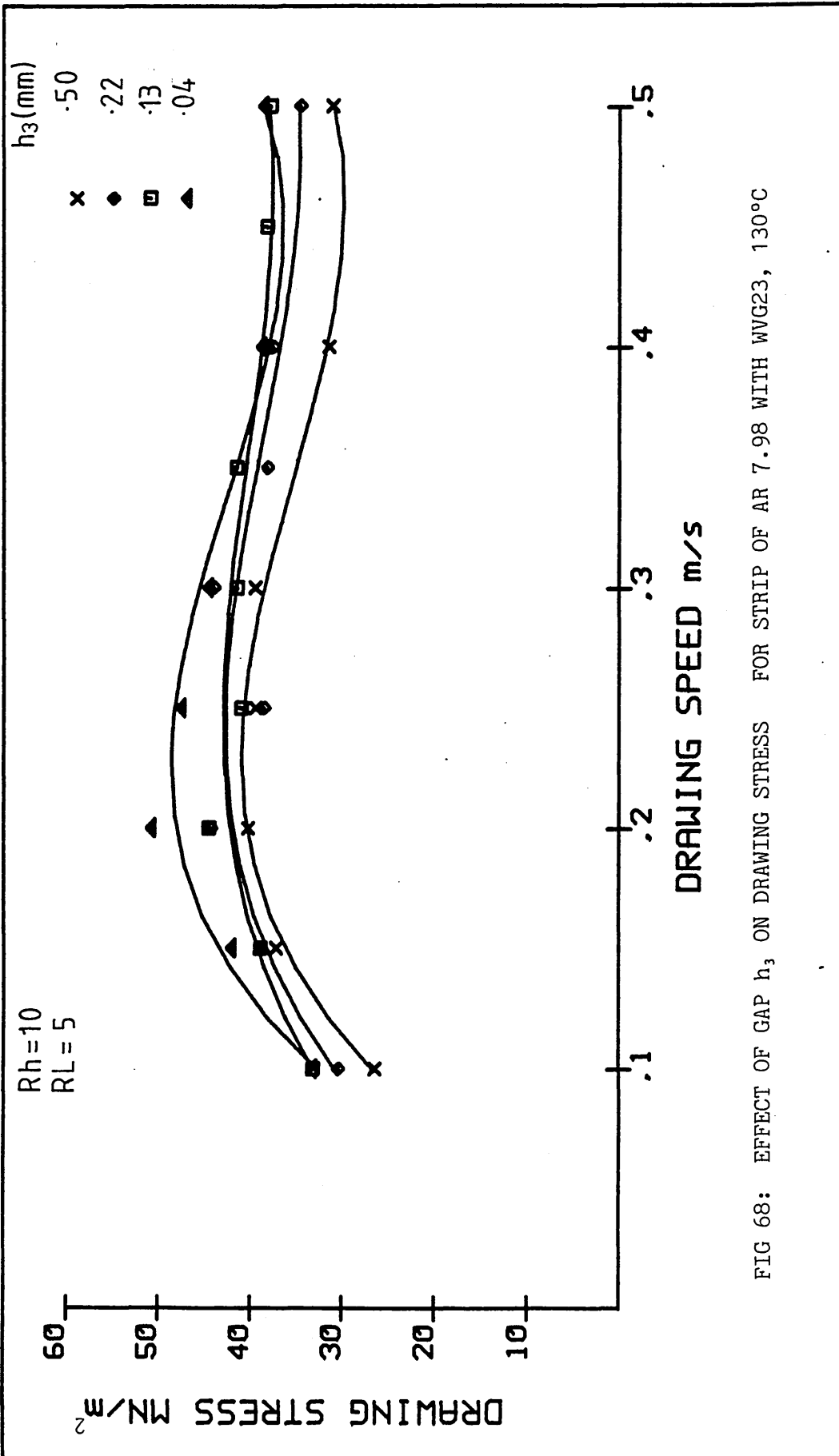


FIG 68: EFFECT OF GAP h_3 ON DRAWING STRESS FOR STRIP OF AR 7.98 WITH WVG23, 130°C

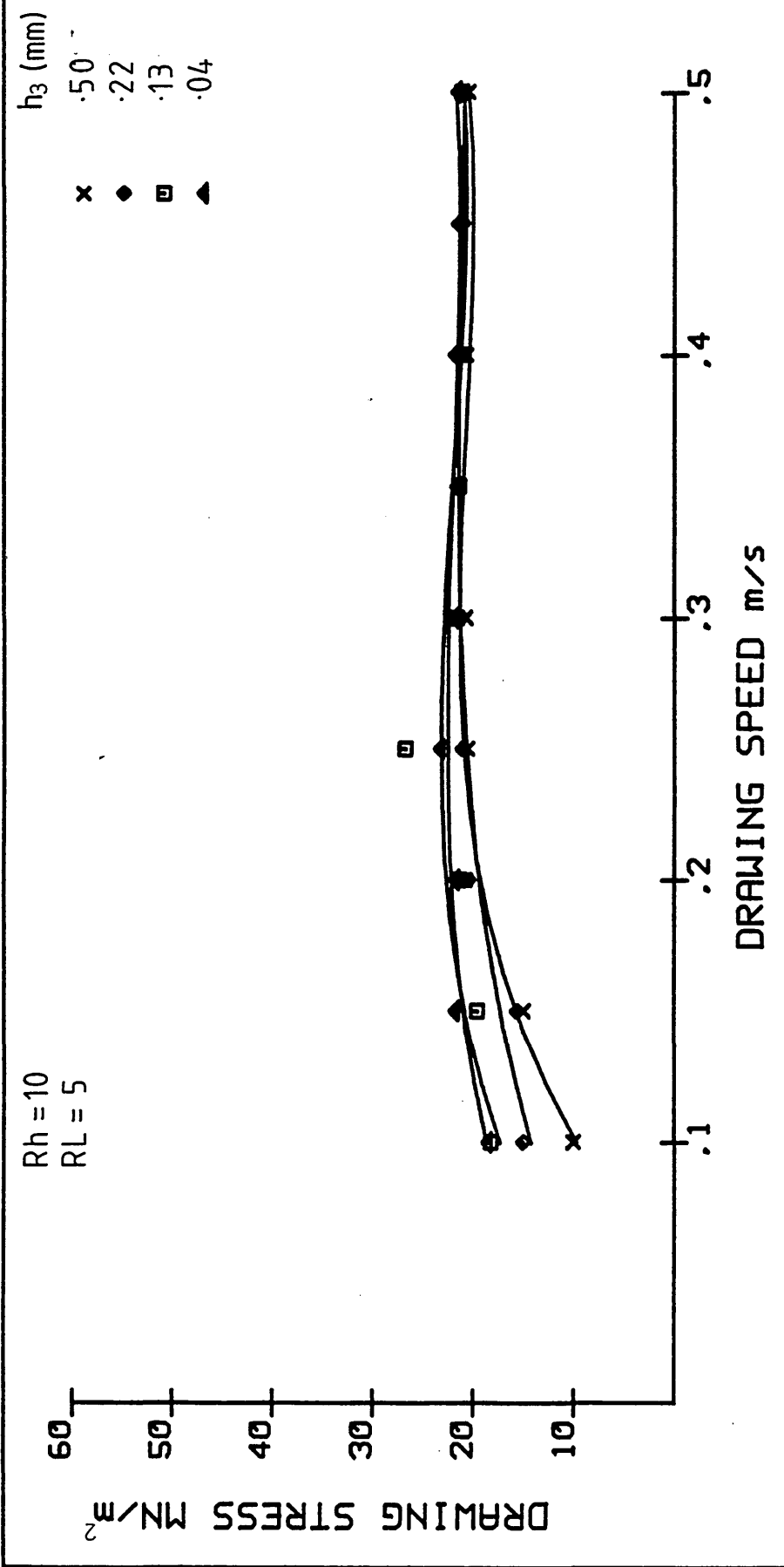


FIG 69: EFFECT OF GAP h_3 ON DRAWING STRESS FOR STRIP OF AR 7.98 WITH WVG23, 150°C

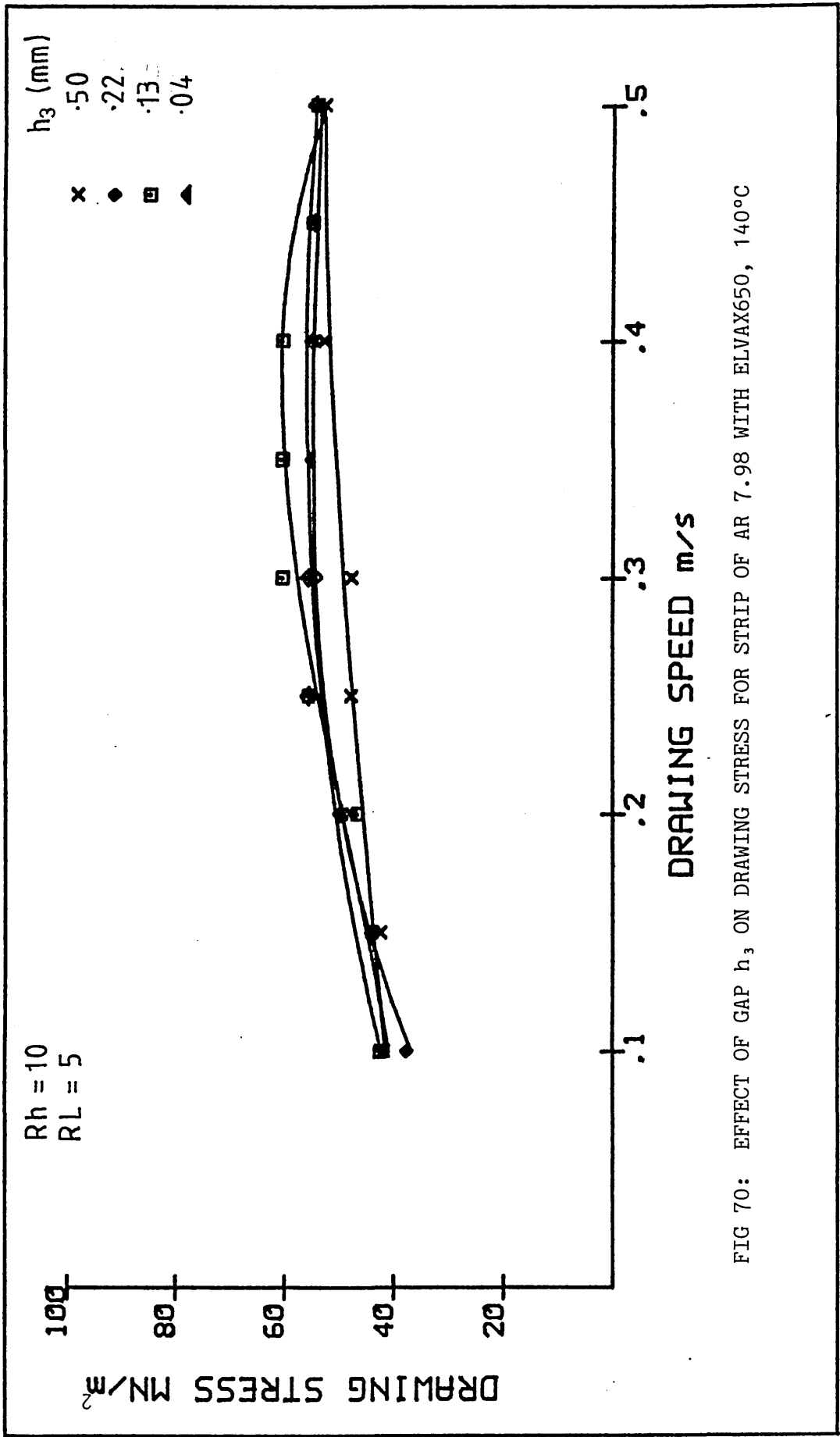


FIG 70: EFFECT OF GAP h_3 ON DRAWING STRESS FOR STRIP OF AR 7.98 WITH ELVAX650, 140°C

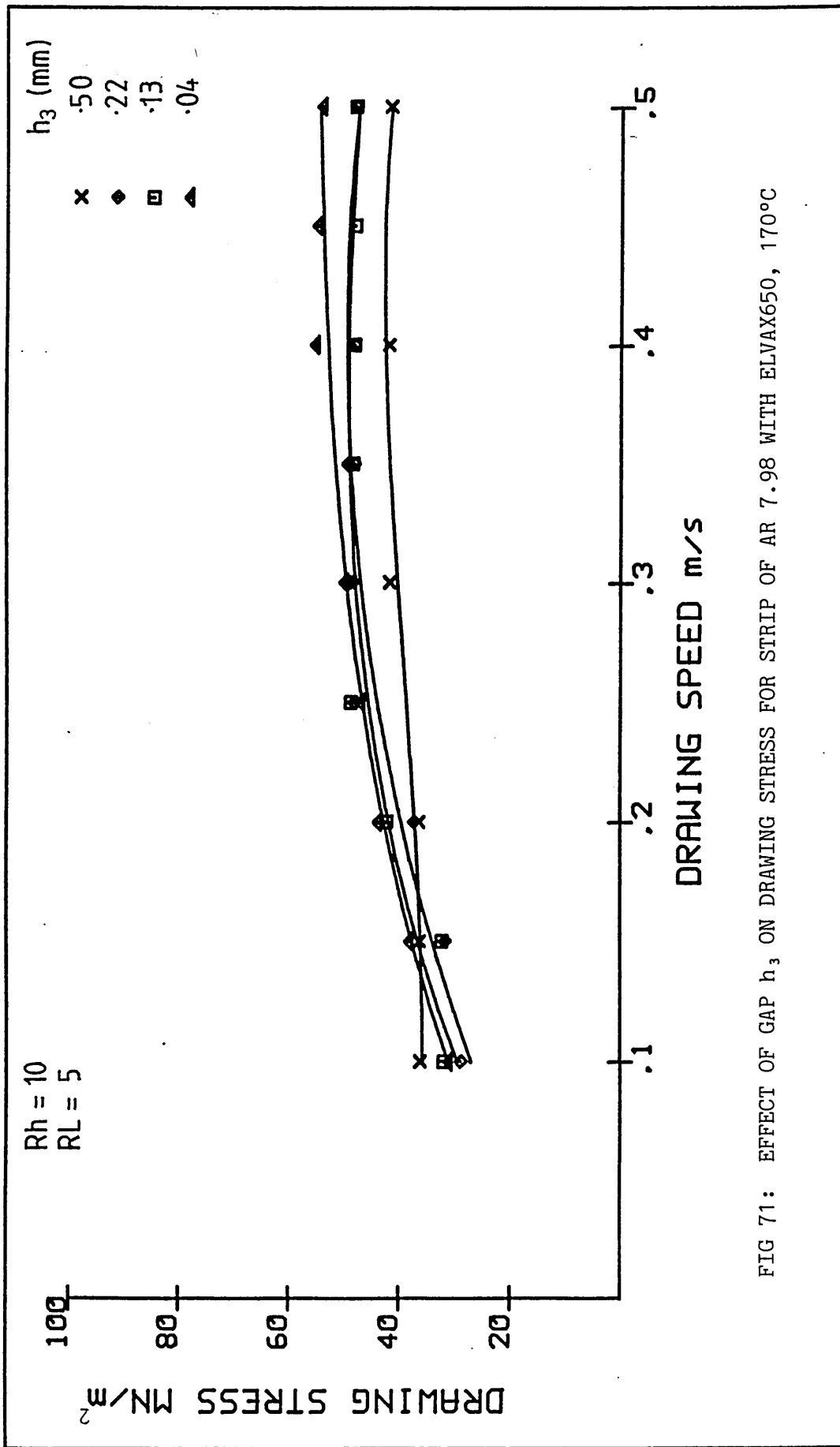


FIG 71: EFFECT OF GAP h_3 ON DRAWING STRESS FOR STRIP OF AR 7.98 WITH ELVAX650, 170°C

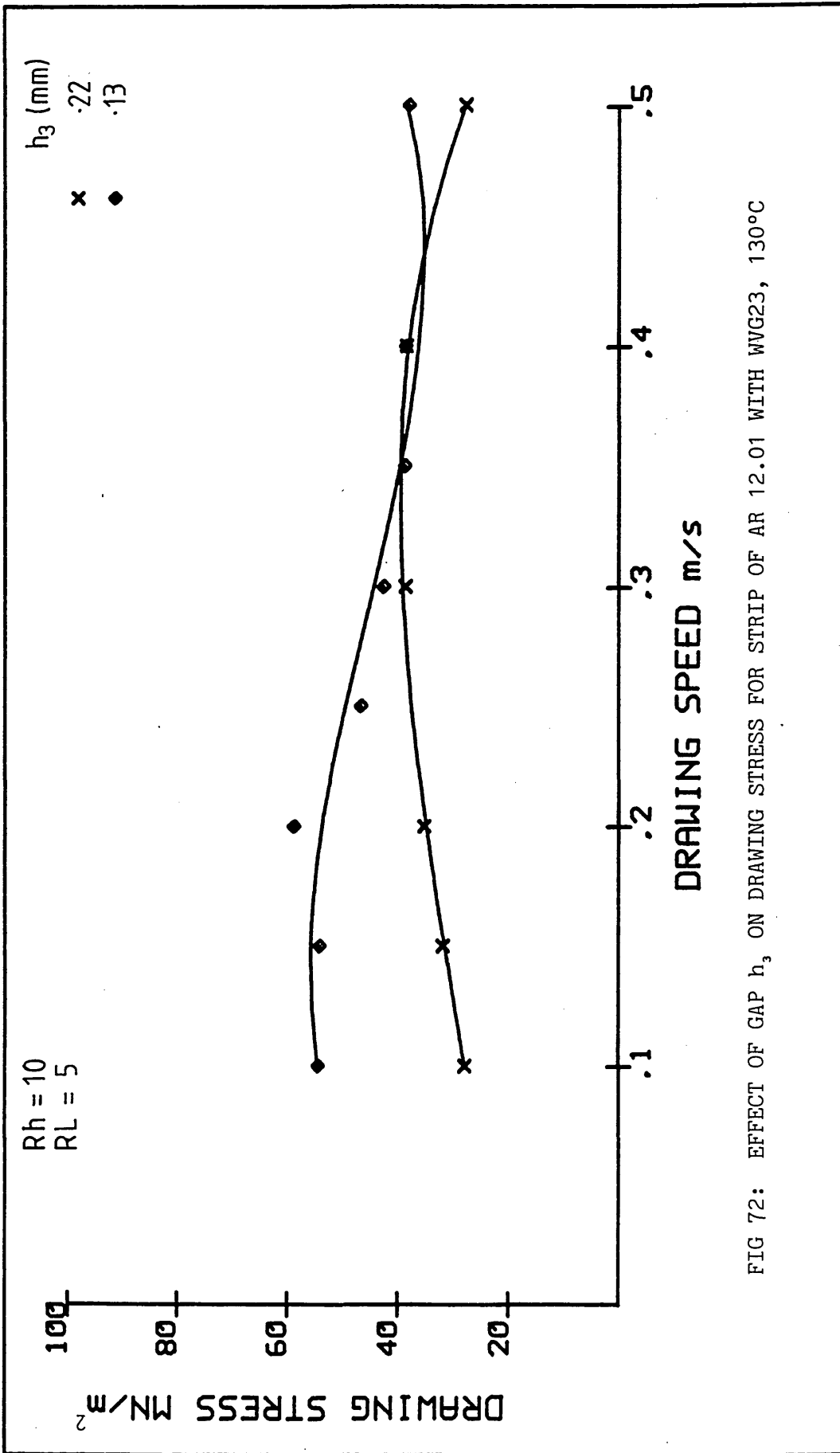


FIG 72: EFFECT OF GAP h_3 ON DRAWING STRESS FOR STRIP OF AR 12.01 WITH WVG23, 130°C

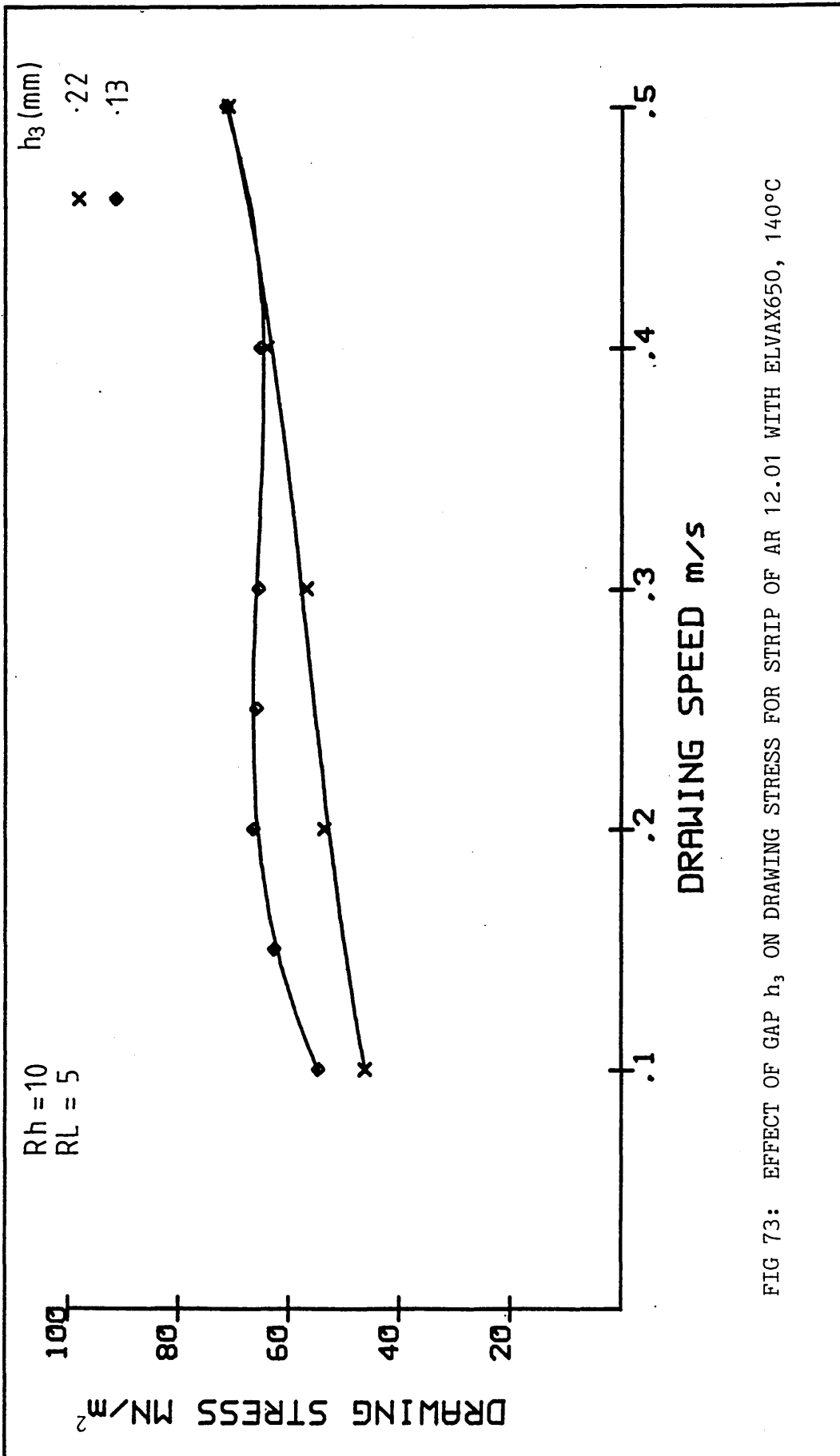


FIG 73: EFFECT OF GAP h_3 ON DRAWING STRESS FOR STRIP OF AR 12.01 WITH ELVAX650, 140°C

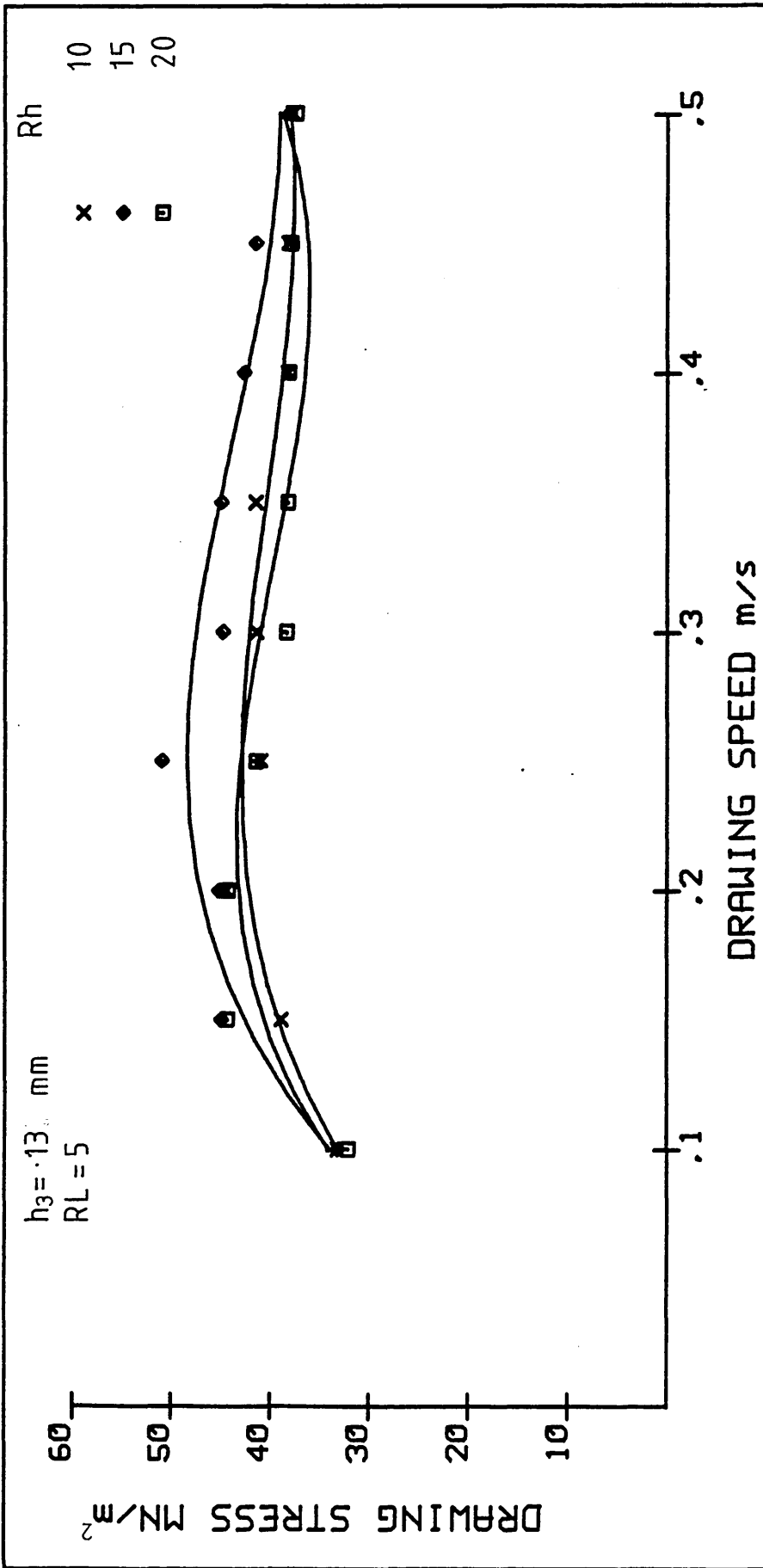


FIG 74: EFFECT OF GAP RATIO ON DRAWING STRESS FOR STRIP OF AR 7.98 WITH WVG23, 130°C

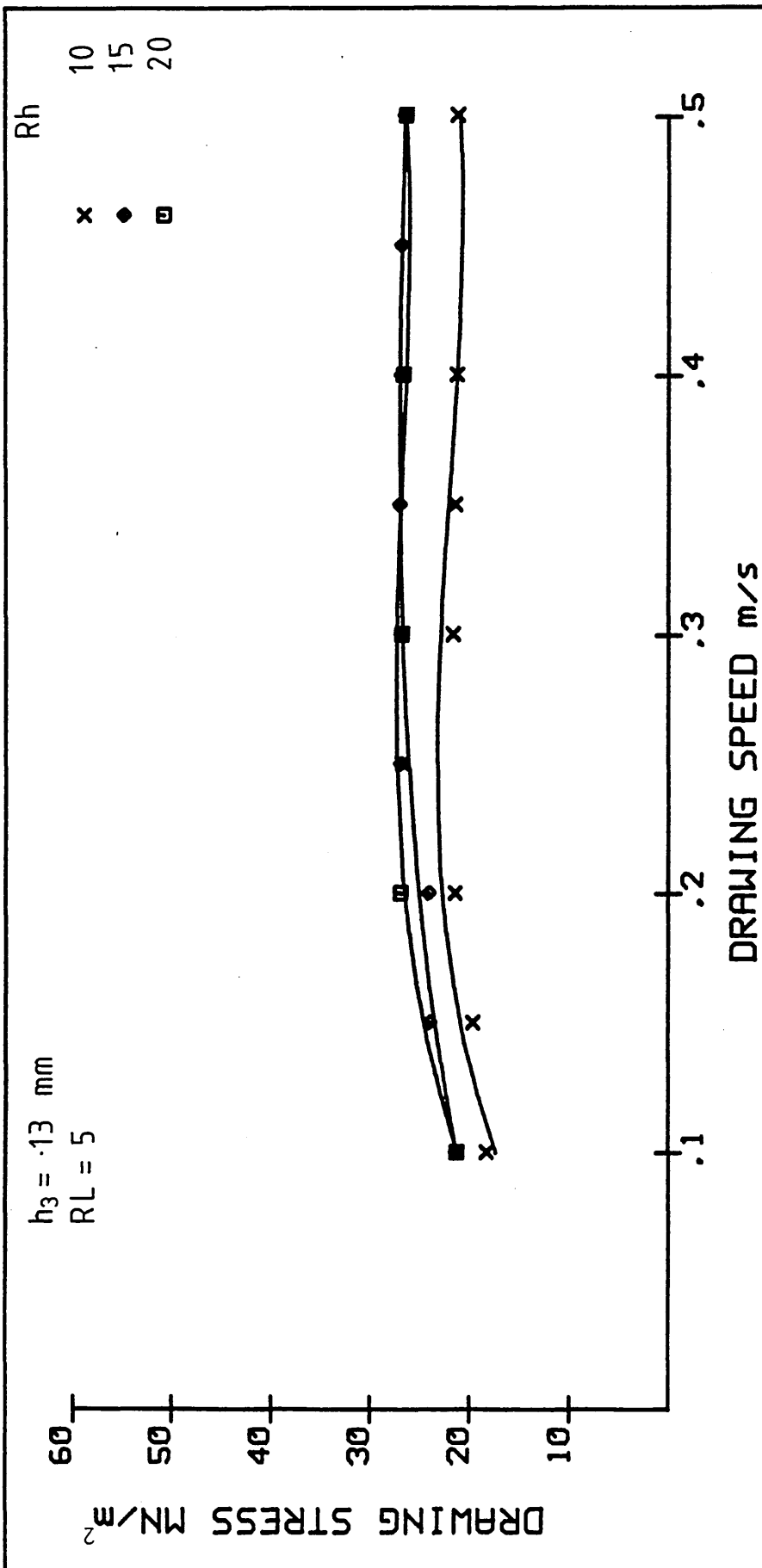


FIG 75: EFFECT OF GAP RATIO ON DRAWING STRESS FOR STRIP OF AR 7.98 WITH WVG23, 150°C

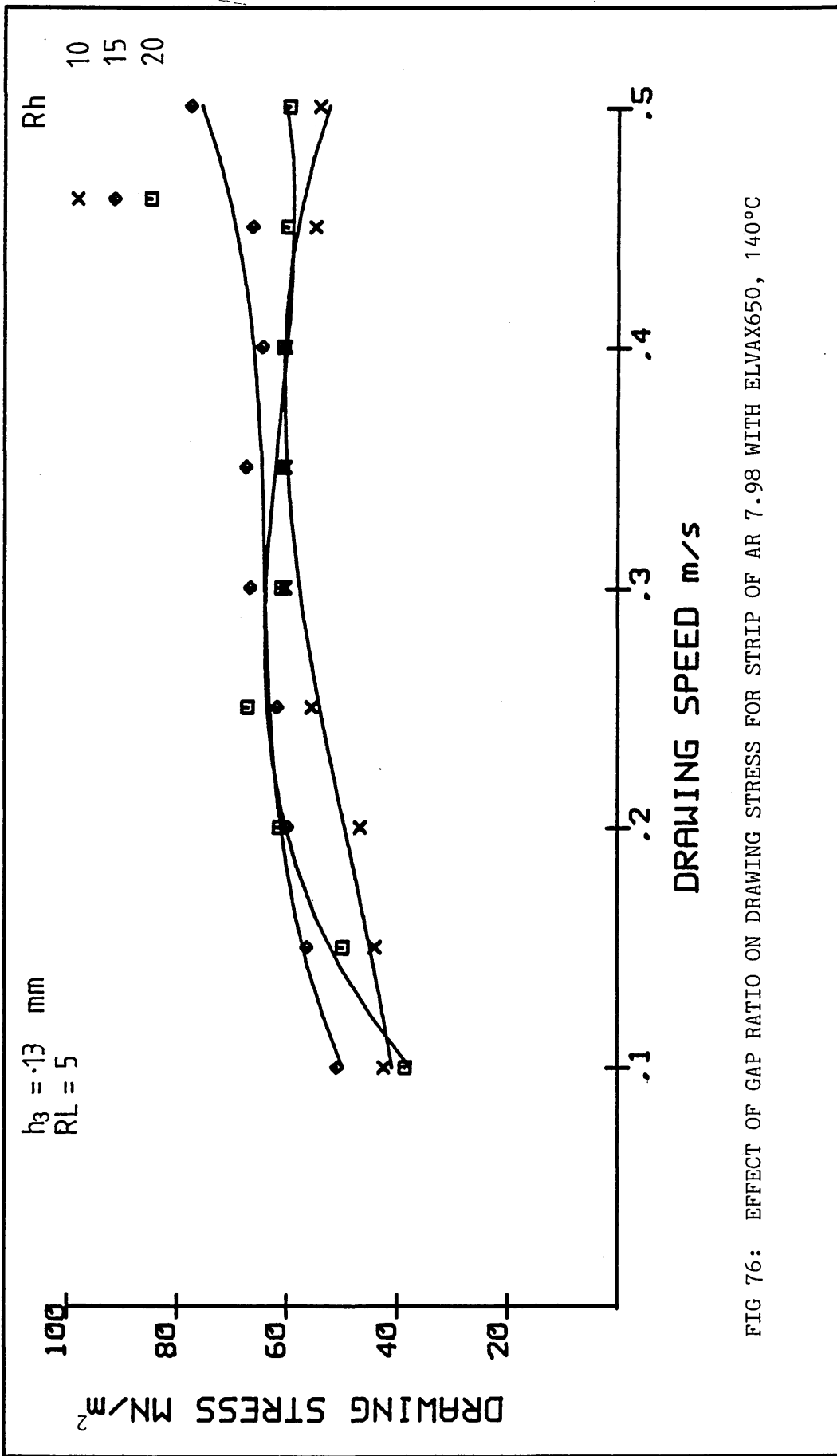


FIG 76: EFFECT OF GAP RATIO ON DRAWING STRESS FOR STRIP OF AR 7.98 WITH ELVAX650, 140°C

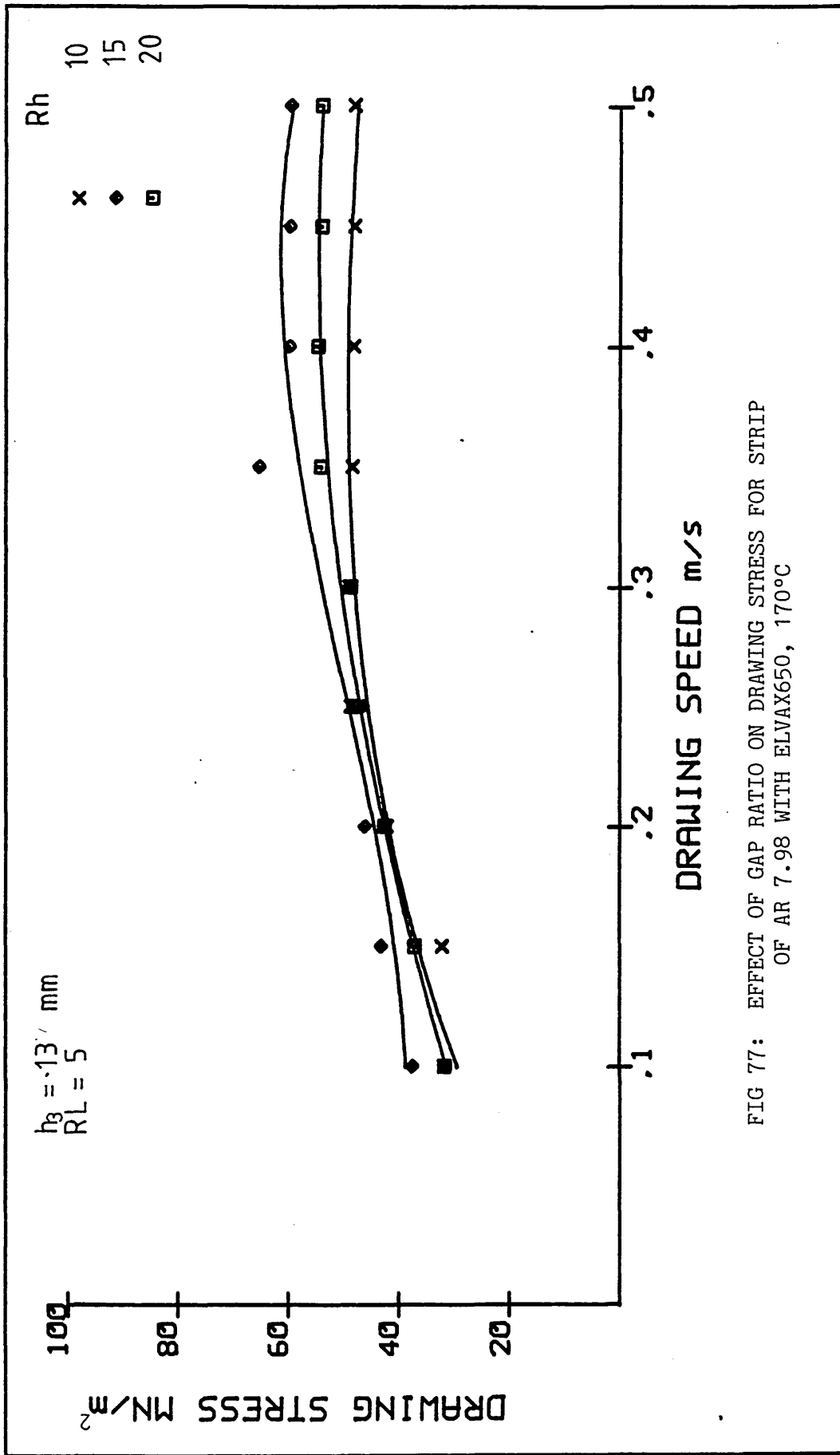


FIG 77: EFFECT OF GAP RATIO ON DRAWING STRESS FOR STRIP OF AR 7.98 WITH ELVAX650, 170°C

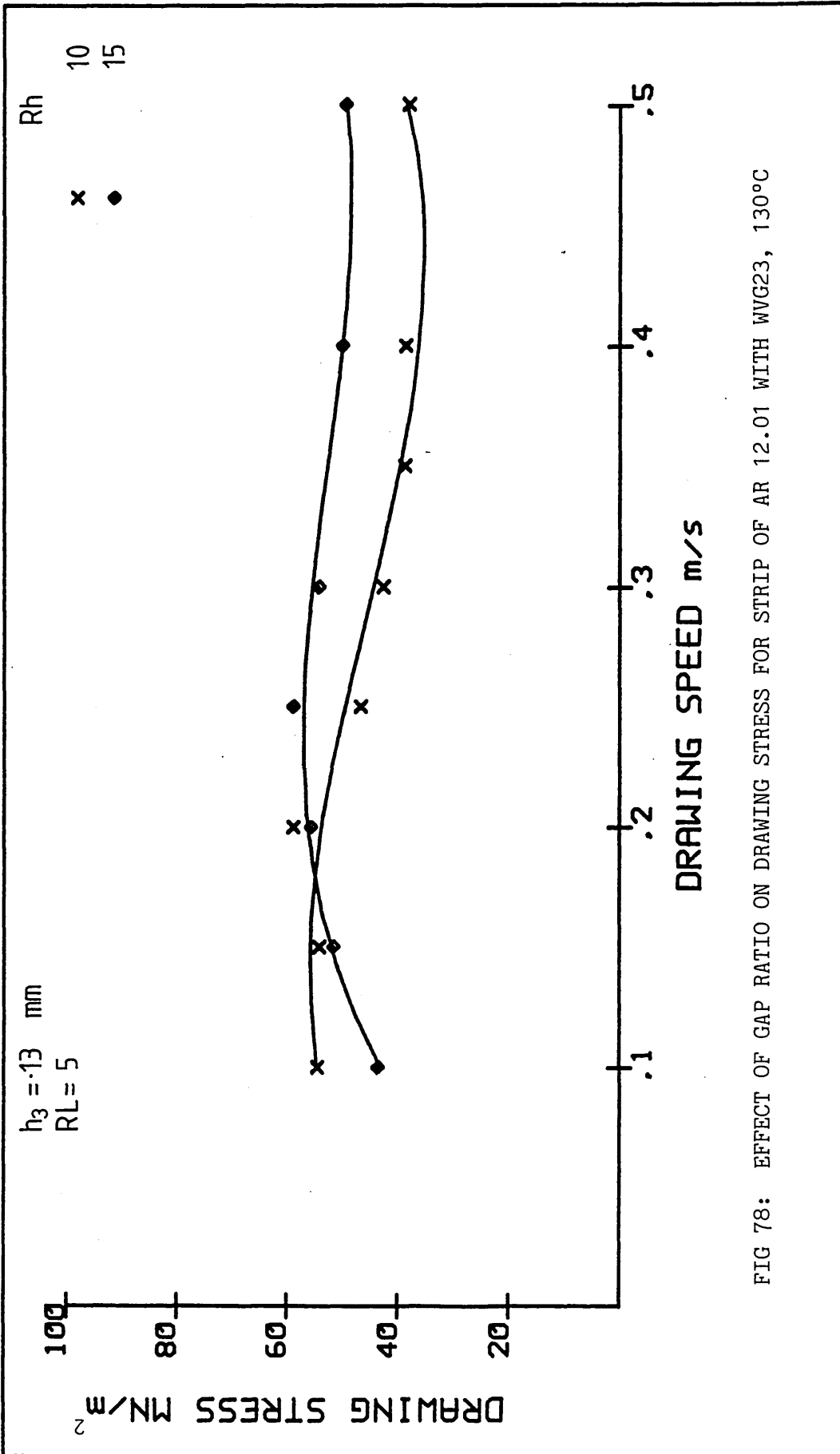


FIG 78: EFFECT OF GAP RATIO ON DRAWING STRESS FOR STRIP OF AR 12.01 WITH WVG23, 130°C

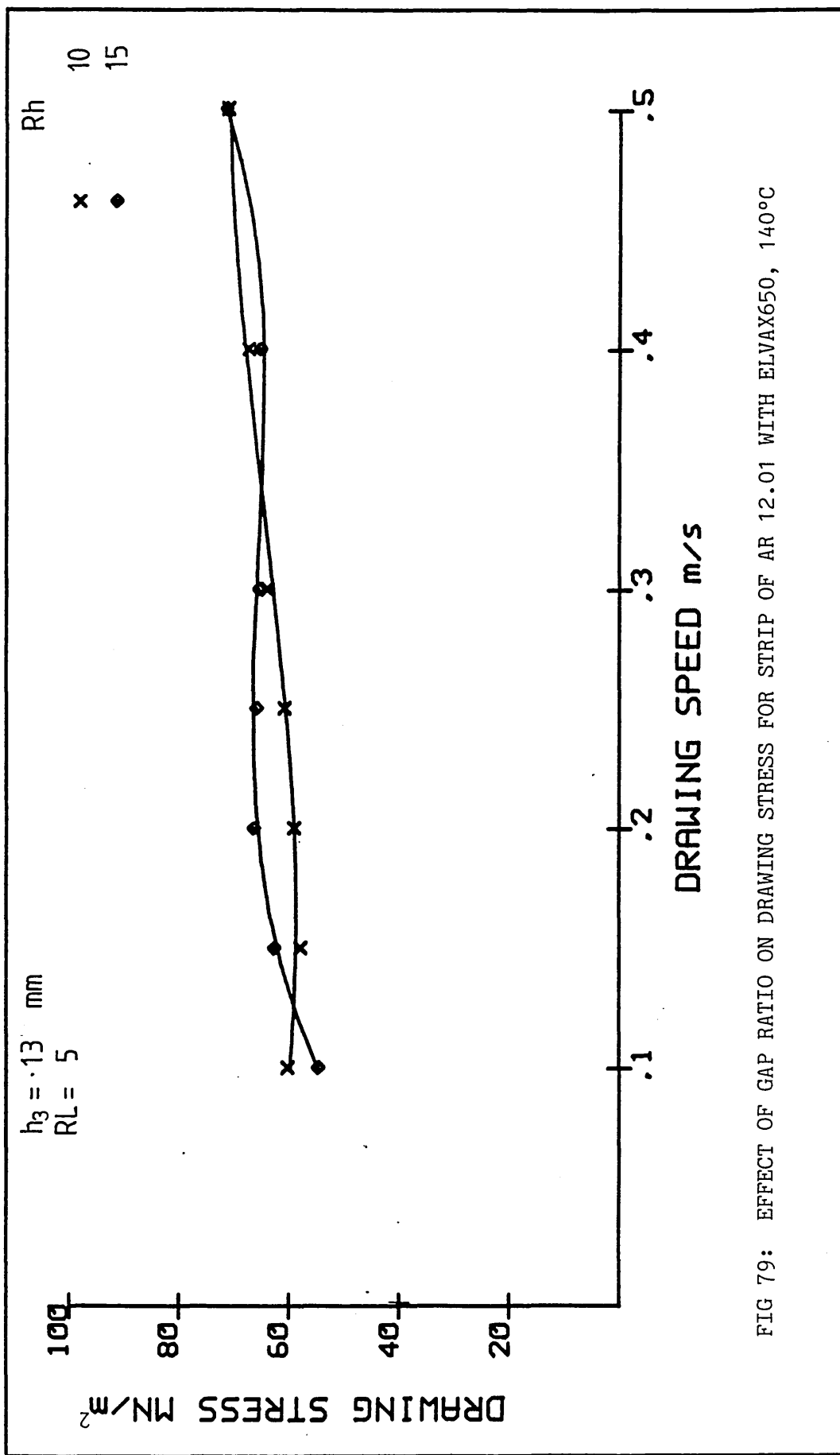


FIG 79: EFFECT OF GAP RATIO ON DRAWING STRESS FOR STRIP OF AR 12.01 WITH ELVAX650, 140°C

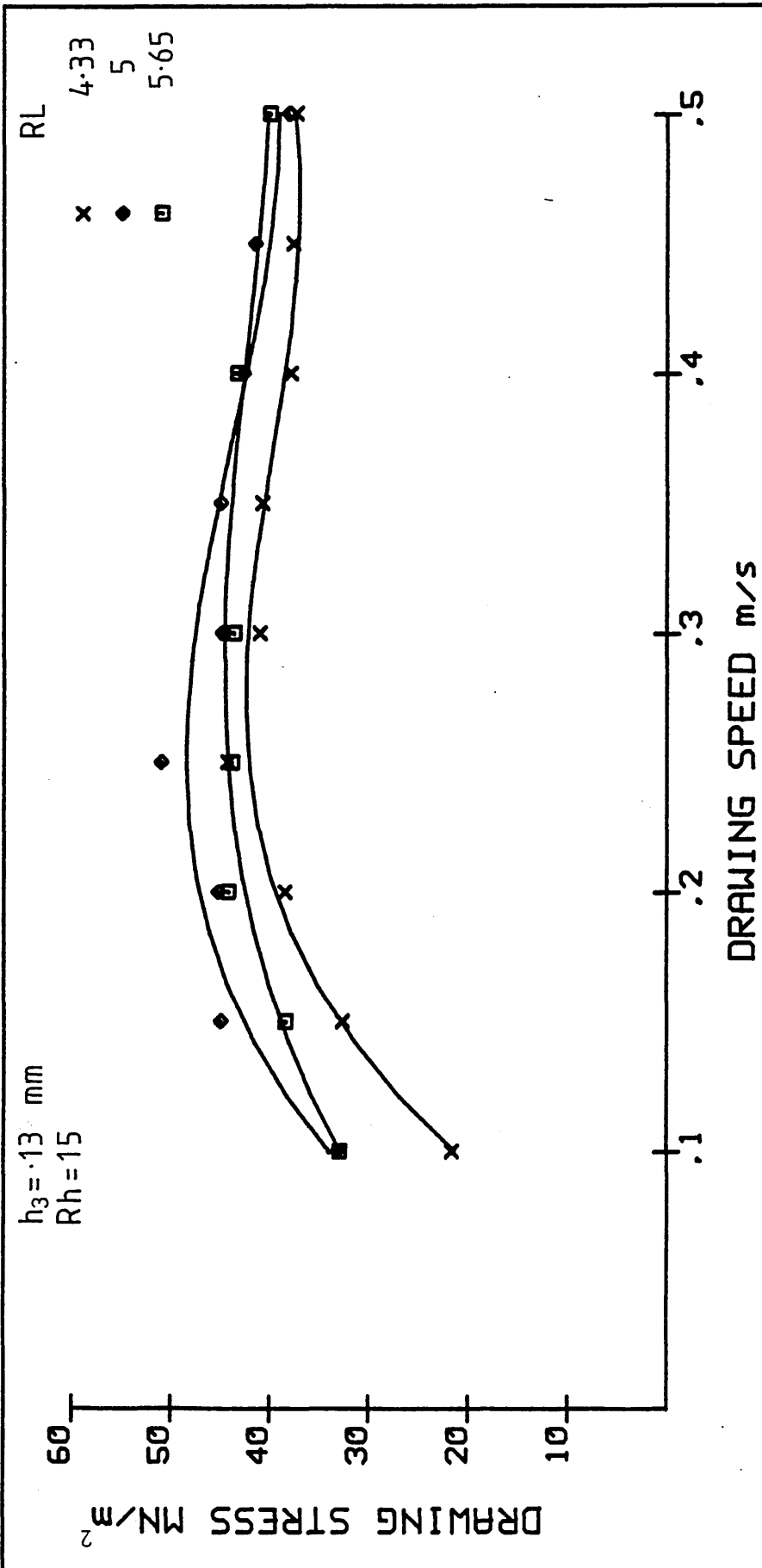


FIG 80: EFFECT OF LENGTH RATIO ON DRAWING STRESS FOR STRIP OF AR 7.98 WITH WVG23, 130°C

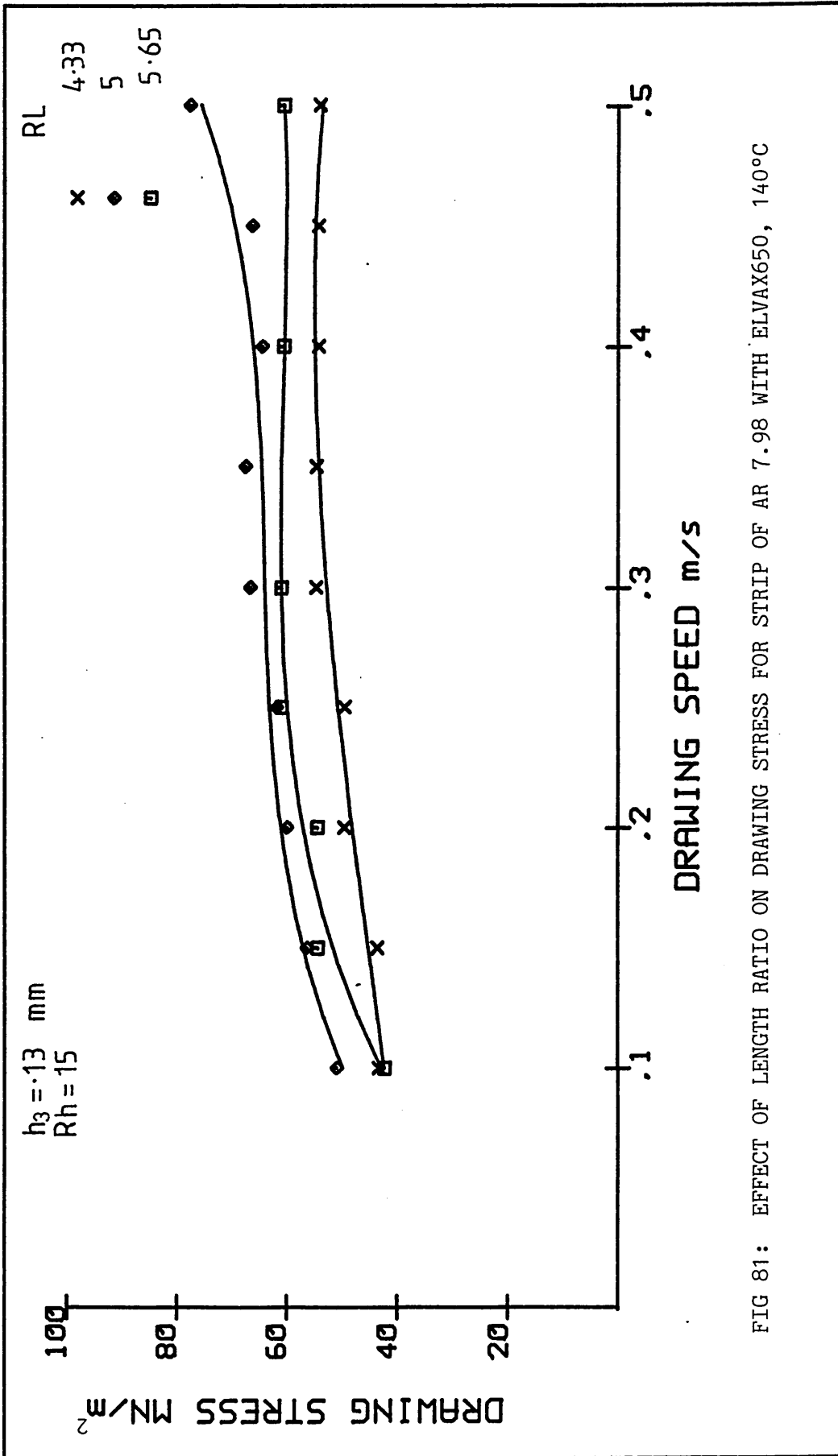


FIG 81: EFFECT OF LENGTH RATIO ON DRAWING STRESS FOR STRIP OF AR 7.98 WITH ELVAX650, 140°C

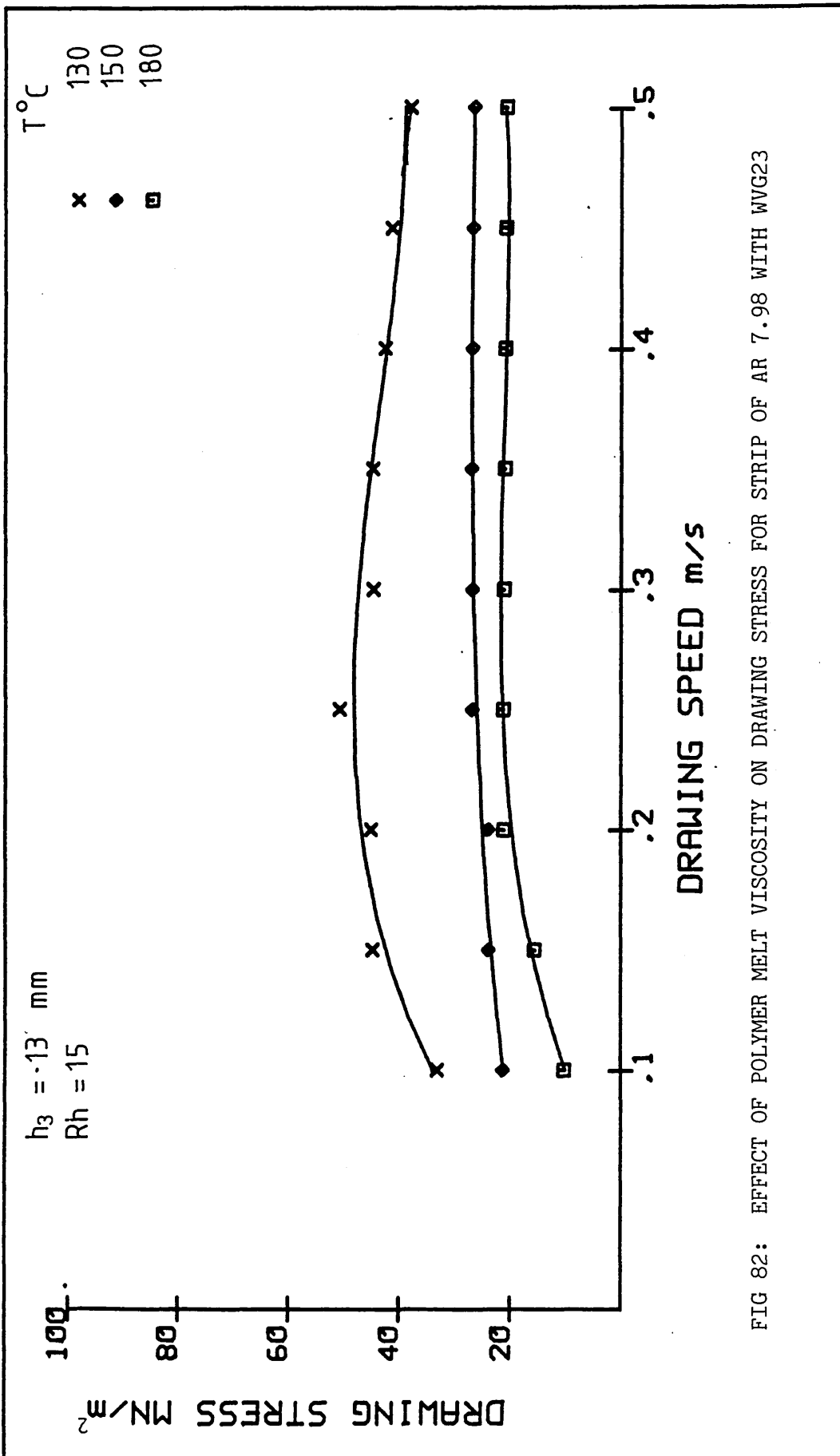


FIG 82: EFFECT OF POLYMER MELT VISCOSITY ON DRAWING STRESS FOR STRIP OF AR 7.98 WITH WVG23

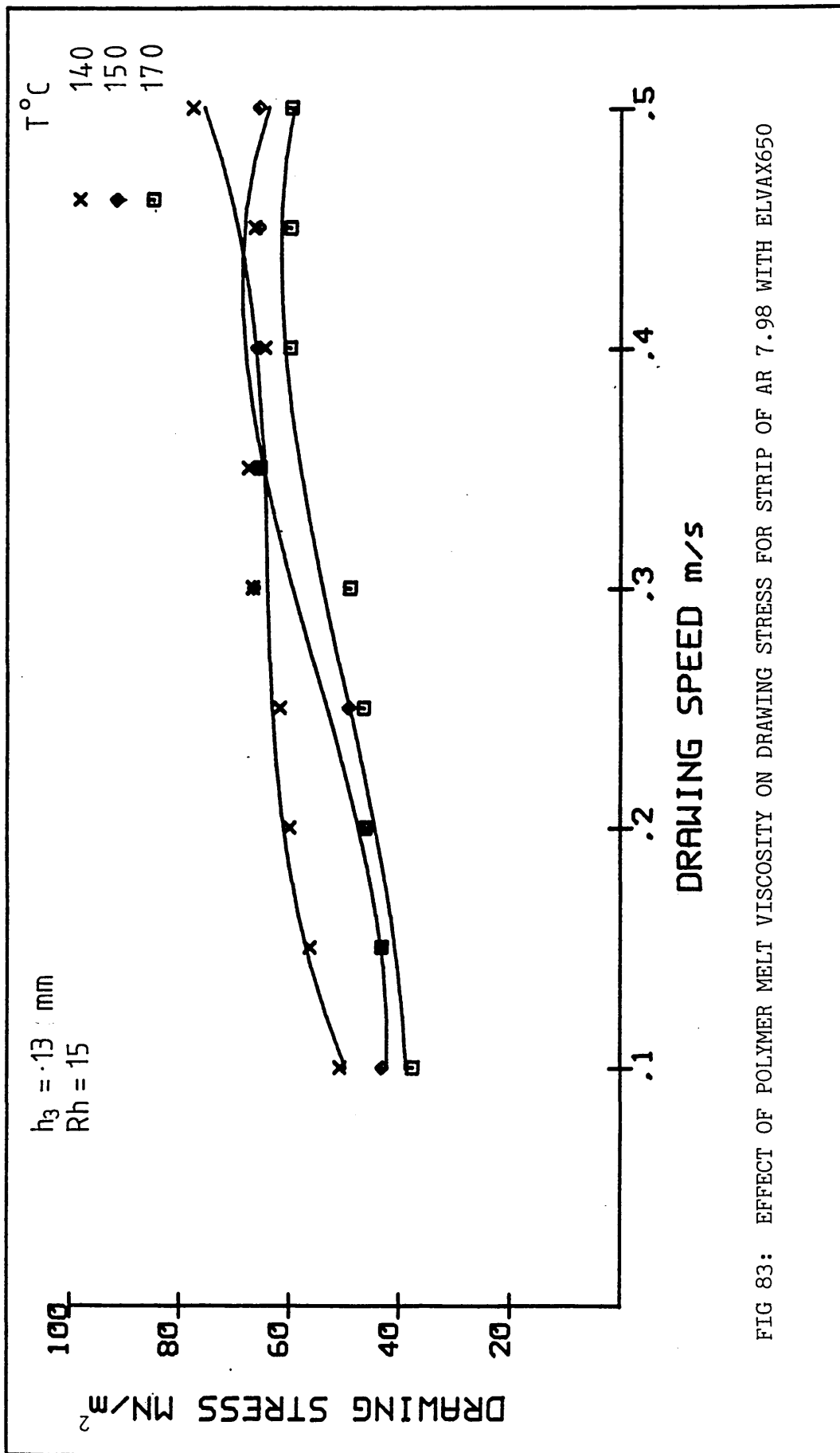


FIG 83: EFFECT OF POLYMER MELT VISCOSITY ON DRAWING STRESS FOR STRIP OF AR 7.98 WITH ELVAX650

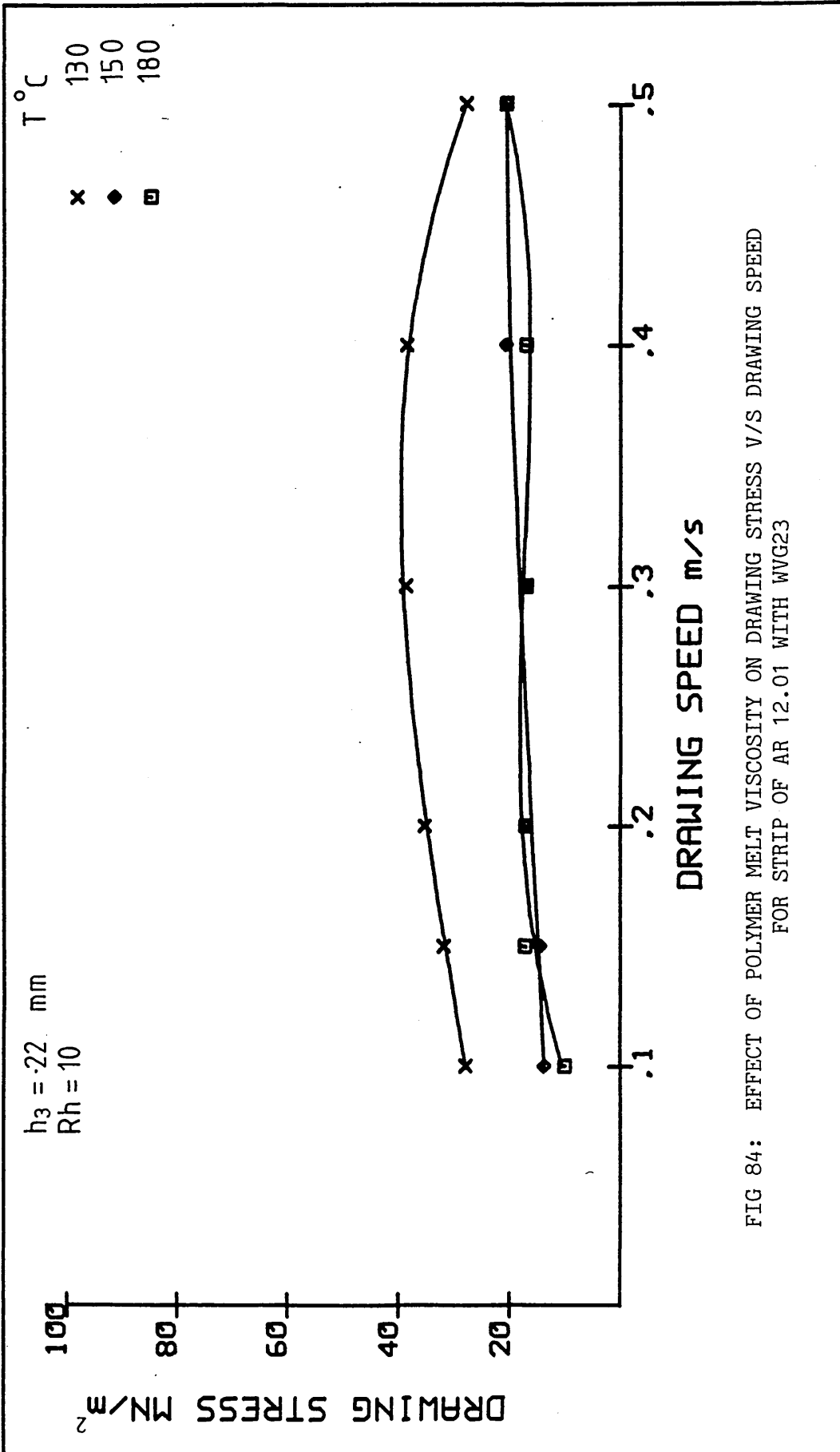


FIG 84: EFFECT OF POLYMER MELT VISCOSITY ON DRAWING STRESS V/S DRAWING SPEED FOR STRIP OF AR 12.01 WITH WVG23

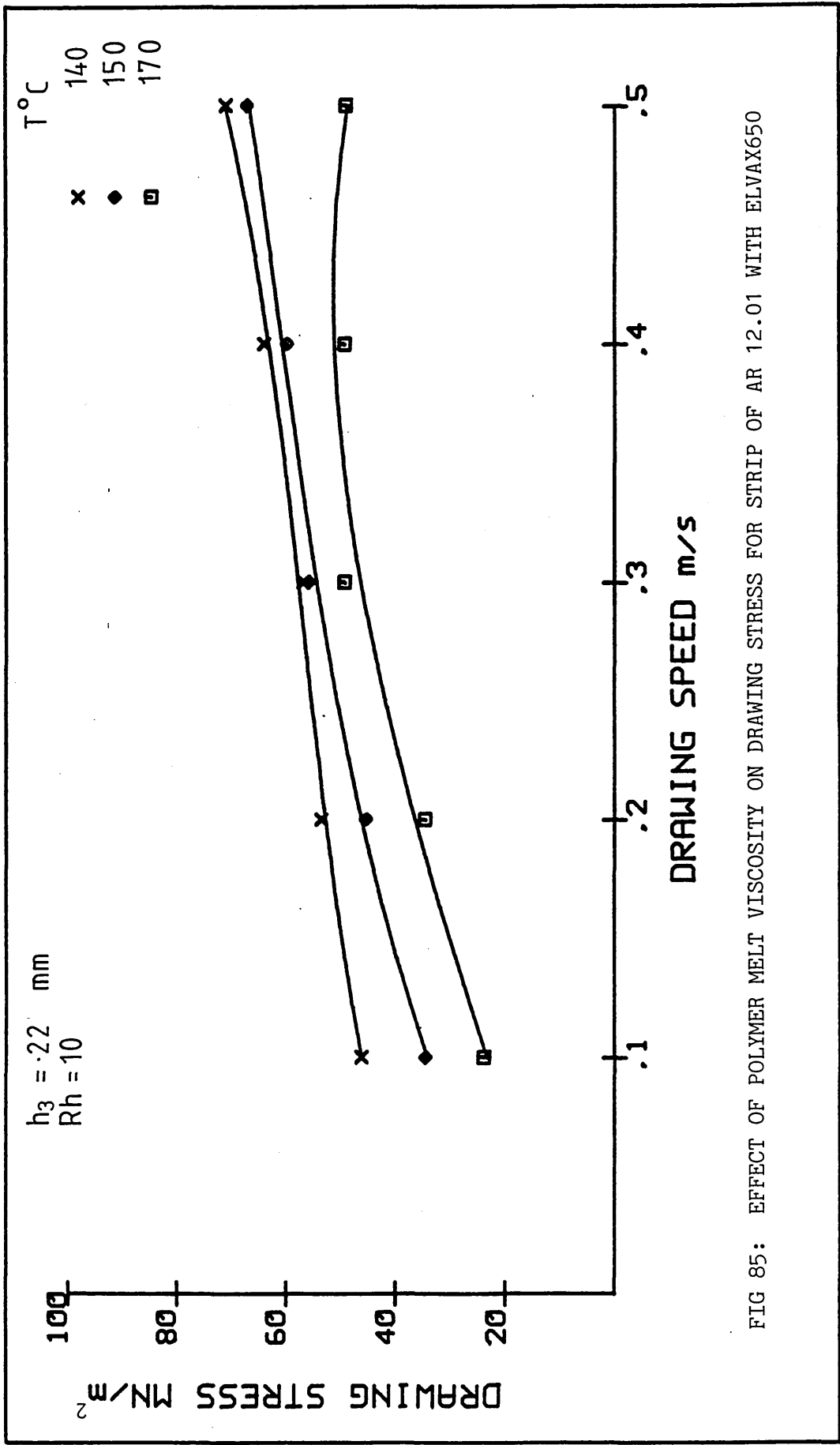


FIG 85: EFFECT OF POLYMER MELT VISCOSITY ON DRAWING STRESS FOR STRIP OF AR 12.01 WITH ELVAX650

4.2.4 Determination of the Deformation Profiles

The process was deliberately stopped, by disengaging the dog clamp while the strip was being drawn, to examine the deformation profiles of the strip undergoing the drawing process. The strip was marked at the inlet of the melt chamber and pulled out for investigations.

The thickness of the strip was measured at 5mm intervals with a point micrometer until a change in thickness was noticed. Then the thickness was measured at 2mm intervals. This test was repeated at different drawing speeds, using WVG23 at a temperature of 130°C and ELVAX650 at temperature of 140°C. Results are shown in Figures 86 and 87, which clearly exhibit the shapes of the effective die profiles formed in the unit.

Figure 86 shows three deformation profiles for strip drawn at three different speeds, using WVG23 at 130°C as pressure medium. The yielding point of the material was found to be at about 120mm from the entry point at a drawing speed of 0.2 m/s. The position of yielding at drawing speed of 0.1 m/s and 0.3 m/s was found to be at 125mm from the entry point.

The deformation profile using ELVAX650 at a temperature of 140°C and at a drawing speed of 0.3 m/s is shown in Figure 87. The deformation was found to commence at 90mm from the entry point.

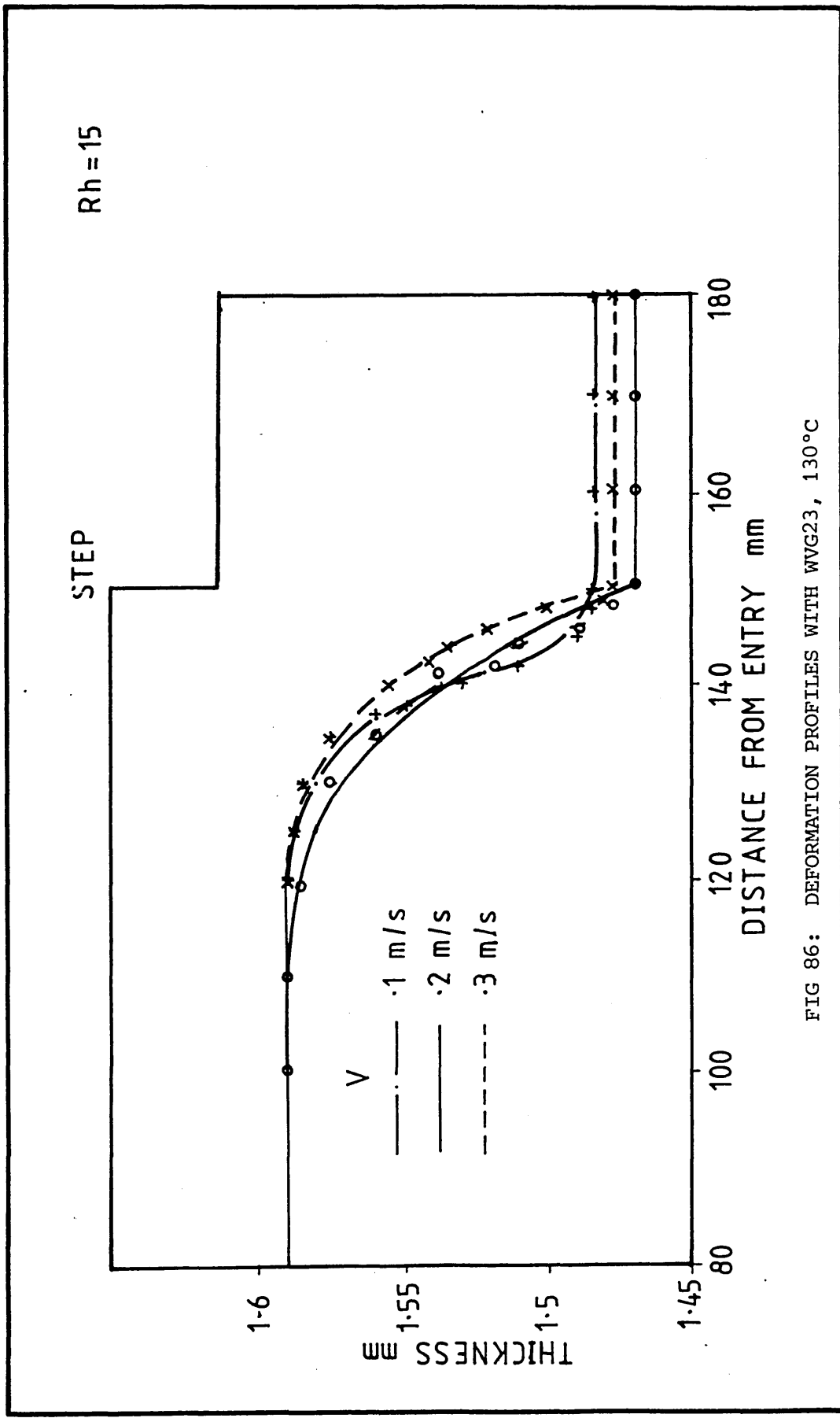


FIG 86: DEFORMATION PROFILES WITH WVG23, 130°C

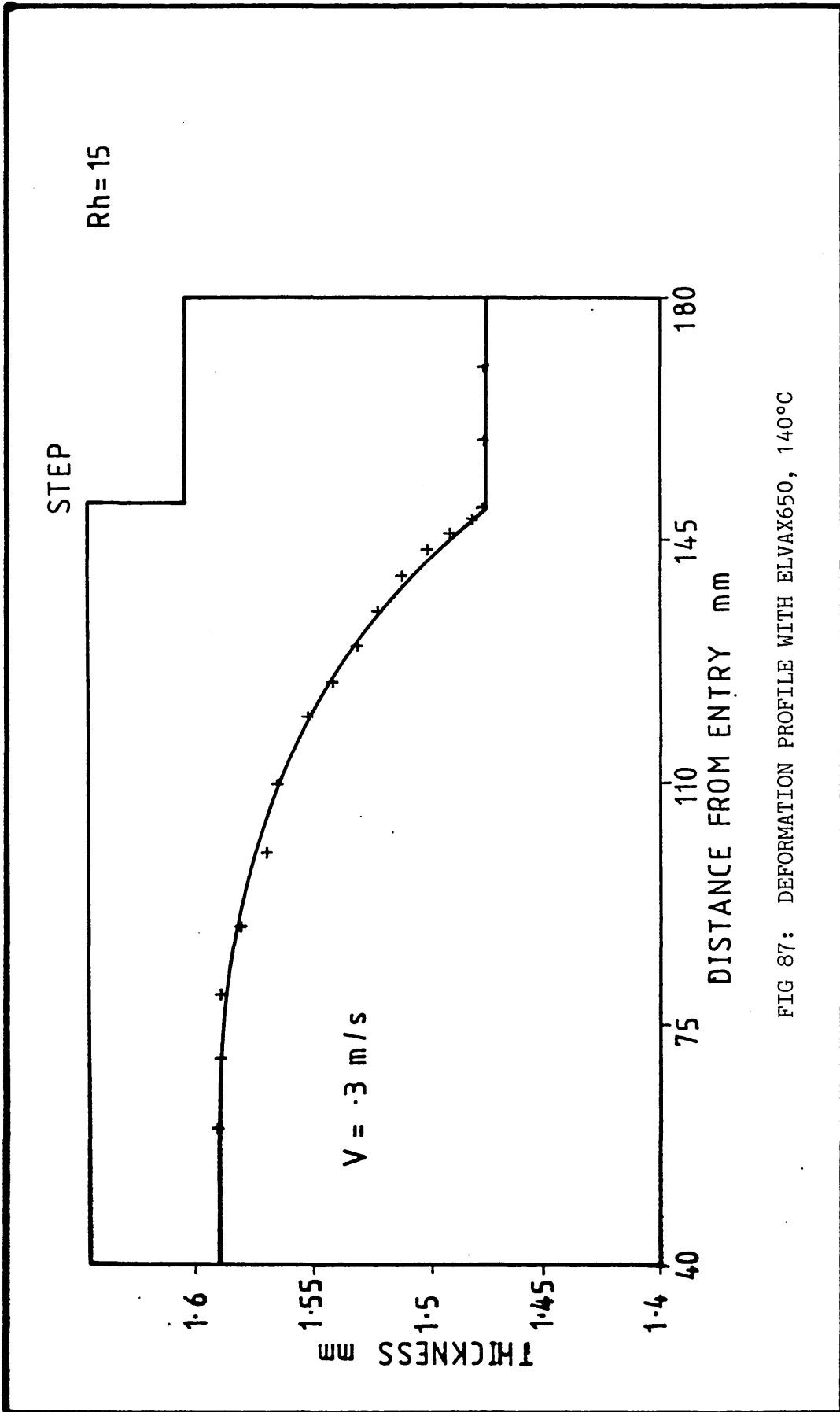


FIG 87: DEFORMATION PROFILE WITH ELVAX650, 140°C

5.1 Introduction

Several mathematical models have been presented for plane-strain strip drawing as reviewed in Chapter 1, with the objectives of determining the friction coefficient, evaluating drawing stress and the drawing limit. Theoretical and experimental treatments have also been carried out to observe the effectiveness of different lubricants and calculation of film thickness during the deformation process so as to predict the presence of hydrodynamic lubrication. All these works were related to the use of conventional reduction dies. Theoretical solutions for a new plasto-hydrodynamic die-less drawing process were presented (reference 31 to 41) for a circular cross-section workpiece.

In the present study a theoretical analysis has been conducted for die-less drawing of narrow strips of rectangular cross-section. The analysis is aimed at understanding the mechanics of the process and to establish the expressions for determining the various parameters involved in the process.

5.2 Analysis

The schematic diagram of the process is shown in Figure 88. The process can be divided into three zones shown in Figure 88a. The three zones are named as the inlet, deformation and exit zones.

Inlet zone; this zone extends from the entry point to the point where deformation commences. In this zone the material is assumed to be rigid and the polymer melt is dragged into the space between

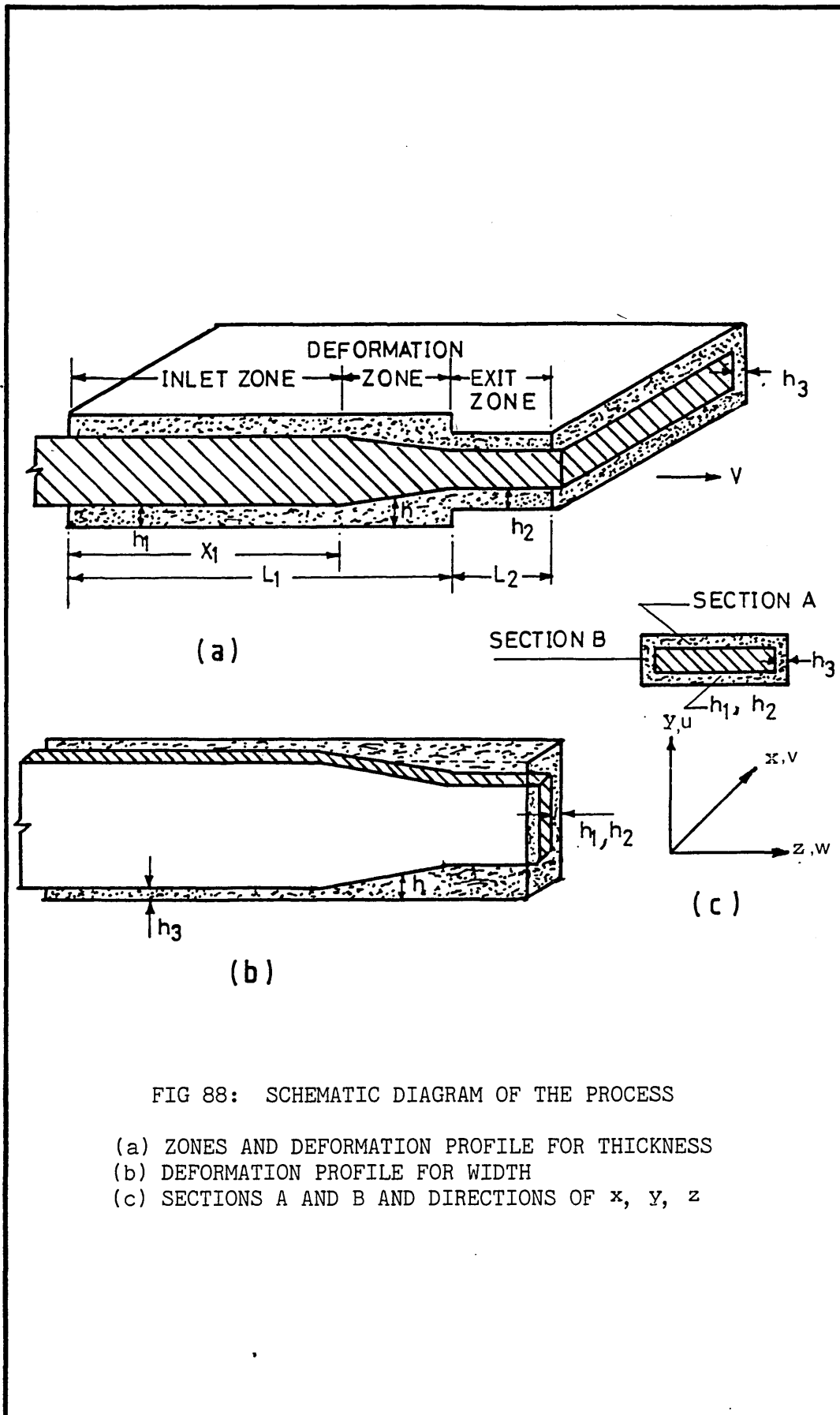


FIG 88: SCHEMATIC DIAGRAM OF THE PROCESS

- (a) ZONES AND DEFORMATION PROFILE FOR THICKNESS
- (b) DEFORMATION PROFILE FOR WIDTH
- (c) SECTIONS A AND B AND DIRECTIONS OF x, y, z

the workpiece and the unit causing the generation of hydrodynamic pressure.

Deformation zone; where the workpiece deforms plastically. This zone extends from the point of yielding to the step where the deformation is assumed to cease.

Exit zone; this zone extends from the step to the exit point. In this zone the material again becomes rigid and the pressure falls to zero.

Figure 88c depicts a section of the process considered instantaneously in a plane. In order to establish a relationship for determining the hydrodynamic pressure, the considered section is subdivided into sections 'A' and 'B'. Initially each section is analysed individually and then integrated to form the final equations for the determination of various parameters.

For an incompressible fluid flow, ignoring the inertia forces, Navier-Stokes equations are,

$$\begin{aligned}
 0 &= -\frac{\partial p}{\partial x} + \mu \left(\frac{\partial^2 v}{\partial x^2} + \frac{\partial^2 v}{\partial y^2} + \frac{\partial^2 v}{\partial z^2} \right) &) \\
 0 &= -\frac{\partial p}{\partial y} + \mu \left(\frac{\partial^2 u}{\partial x^2} + \frac{\partial^2 u}{\partial y^2} + \frac{\partial^2 u}{\partial z^2} \right) &) \\
 0 &= -\frac{\partial p}{\partial z} + \mu \left(\frac{\partial^2 w}{\partial x^2} + \frac{\partial^2 w}{\partial y^2} + \frac{\partial^2 w}{\partial z^2} \right) &)
 \end{aligned} \tag{5.1}$$

And the continuity equation is given by,

$$\frac{\partial v}{\partial x} + \frac{\partial u}{\partial y} + \frac{\partial w}{\partial z} = 0 \tag{5.2}$$

Section A

Considering a small element of the fluid, according to the geometrical configuration and given notations,

x , is the direction of flow,

y, the direction normal to the flow and to the width face of the strip

(z, direction is large compared to the distance 'h₁', between the two surfaces (ie surface of the strip and the unit wall).

For this configuration, in the steady state,

$$\frac{\partial}{\partial z} = 0, w = 0, u = 0, v = v(y)$$

and the continuity equation (5.2) becomes,

$$\frac{\partial v}{\partial x} = 0 \quad (5.3)$$

From equation (5.3) it is obvious that the velocity component is independent of x. And the equations (5.1) reduce to

$$\mu \frac{\partial p}{\partial x} = \mu \frac{\partial^2 v}{\partial y^2} \quad (5.4)$$

$$\frac{\partial p}{\partial y} = 0 \quad (5.5)$$

$$\frac{\partial p}{\partial z} = 0 \quad (5.6)$$

For a Newtonian fluid the expression for shear stress is,

$$\tau = \mu \frac{\partial v}{\partial y} \quad (5.7)$$

Combining equations (5.4) and (5.7),

$$\left(\frac{\partial p}{\partial x} \right) = \left(\frac{\partial \tau}{\partial y} \right) \quad (5.8)$$

Section B

In this section,

x, is the direction of flow,

z, is the direction normal to the flow and to the thickness face of the strip,

y, distance is large compared to the distance h₃.

In a similar way as for the Section A, it can be shown that in this section we obtain

$$\frac{\partial p}{\partial x} = \mu \frac{\partial^2 v}{\partial z^2} \quad (5.9)$$

$$\tau = \mu \frac{\partial v}{\partial z} \quad (5.10)$$

$$\left(\frac{\partial p}{\partial x}\right) = \left(\frac{\partial \tau}{\partial z}\right) \quad (5.11)$$

From the equations derived for Sections A and B, it can be observed that in the present situation, one dimensional fluid flow can be considered. Therefore the Reynold's equation given below can be used as the basis for deriving the various expressions.

$$\frac{\partial}{\partial x} \left(\frac{h^3}{\mu} \frac{\partial p}{\partial x} \right) = \frac{\partial}{\partial x} (6Vh) \quad (5.12)$$

Now referring to the geometrical configuration of the system, it is obvious that in Section A, the gap h_1 is varying in x direction, ie there is a converging fluid flow, which causes the generation of the hydrodynamic pressure in this section. In Section B the gap, h_3 , remains constant all along the length hence, initially, no pressure is generated in this section. But once the pressure is generated in Section A and if we consider the taken section instantaneously in a plane, a hydrostatic condition can be assumed and therefore the generated pressure will be acting equally on all the sides of the strip. For determination of different parameters in the analysis, the pressure and pressure gradient in Section A has been considered the same for Section B.

In general the following assumptions were made,

- (i) The dominant flow of polymer melt is laminar and axial.
- (ii) The pressure is generated in x direction and along the width face of the strip in Section A.

- (iii) The pressure acts equally in both sections.
- (iv) Deformation occurs before the step and no deformation takes place after the step.
- (v) Edge effects are negligible.

For a better understanding of the mechanics of the process and formulation of the equations relating different parameters of the process, the analysis is carried out in five parts;

- 1 Determination of the maximum pressure in the inlet section of the unit if no deformation of the strip takes place.
- 2 Prediction of the shear stress prior to deformation.
- 3 Prediction of the yielding point.
- 4 Hydrodynamic pressure and the axial stress in the deformation zone.
- 5 Prediction of the percentage reduction in strip size and drawing stress.

As a first attempt, a model has been developed based on the assumption that the pressure medium is a Newtonian fluid, and is presented in the next section. An analysis incorporating non-Newtonian characteristics of the polymer melt will be presented in Chapter 6.

5.3 Newtonian Solution

In the formulation of different expressions, the following assumptions were made in addition to those described in section 5.2;

- (i) The polymer melt behaves like a Newtonian fluid.
- (ii) Isothermal conditions exist.

The analysis has been carried out in two modes;

- (a) using an assumed deformation profile,
- (b) numerical solution.

It is well understood that after a certain value of shear stress, slip occurs at the interface of the polymer melt and the surface of the strip and has been discussed in Chapter 3. This property of polymer melt flow is also introduced in the present mathematical model.

5.3.1 Assumed Deformation Profile

5.3.1.1 Determination of the Maximum Pressure Prior to Deformation

For Section A, integrating equation (5.4) w.r.t. y

$$v = \frac{1}{2\mu} \left(\frac{\partial P}{\partial x} \right) y^2 + C_1 y + C_2 \quad (5.13)$$

where v is the velocity at any point in the flow, and C_1 and C_2 are constants of integration.

Inlet Zone

Applying boundary conditions that

$$\text{at } y = 0, v = V$$

$$\text{and at } y = h_1, v = 0$$

the values of constants C_1 and C_2 can be evaluated which on substitution equation (5.13) will give an expression for the velocity distribution in the inlet zone.

$$v = \frac{1}{2\mu} \left(\frac{\partial P}{\partial x_1} \right) (y^2 - h_1 y) + V \left(1 - \frac{y}{h_1} \right) \quad (5.14)$$

The fluid flow in the inlet zone is given by,

$$Q_1 = \int_0^{h_1} v \, dy \quad (5.15)$$

Substituting for v from equation (5.14) into equation (5.15) and integrating gives;

$$Q_1 = - \frac{h_1^3}{12\mu} \left(\frac{\partial P}{\partial x} \right)_1 + \frac{V h_1}{2} \quad (5.16)$$

Similarly, the flow rate Q_2 in the exit zone in Section A is given by,

$$Q_2 = \frac{h_2^3}{12\mu} \left(\frac{\partial p}{\partial x} \right)_2 + \frac{Vh_2}{2} \quad (5.17)$$

Now steady state flow of fluid gives,

$$\frac{\partial}{\partial x}(Q_1) = \frac{\partial}{\partial x}(Q_2) = 0$$

In a stepped configuration the maximum pressure is at the step.

Let P_m be the maximum pressure at step when no deformation takes place, and it can be shown that;

$$\left(\frac{\partial p}{\partial x} \right)_1 = \frac{P_m}{L_1} \quad (5.18)$$

$$\left(\frac{\partial p}{\partial x_2} \right) = - \frac{P_m}{L_2} \quad (5.19)$$

For continuity of flow;

$$Q_1 = Q_2 \quad (5.20)$$

Substituting the respective values from equations (5.16), (5.17), (5.18) and (5.19), simplification of equation (5.20) will give;

$$P_m = \frac{6\mu V(h_1 - h_2)}{(h_1^3/L_1 + h_2^3/L_2)} \quad (5.21)$$

5.3.1.2 Determination of the Shear Stresses in Sections A and B

Shear stress at the surface of the strip along the width face in Section A for inlet zone is given by,

$$\tau_1 = \mu \left. \frac{\partial v}{\partial y} \right|_{y=0}$$

substituting the value of $\frac{\partial v}{\partial y}$ from equation (5.14), and for $\frac{\partial p}{\partial x}$ from

equation (5.18), shear stress in Section A for inlet zone is given by;

$$\tau_1 = - \frac{h_1}{2} \left(\frac{P_m}{L_1} \right) - \frac{\mu V}{h_1} \quad (5.22)$$

Similarly shear stress τ_2 in Section A for exit zone will be given by;

$$\tau_2 = \frac{h_2}{2} \left(\frac{P_m}{L_2} \right) - \frac{\mu V}{h_2} \quad (5.23)$$

With the assumption that the pressure gradient in Section B will be the same as in Section A, the equation for determining shear stress in Section B will be;

$$\tau_3 = -\frac{h_3}{2} \left(\frac{Pm}{L_1} \right) - \frac{\mu V}{h_3} \quad (5.24)$$

5.3.1.3 Prediction of Yield Point

The principal stresses acting on the strip are;

$$\sigma_1 = \sigma_{x_1}, \quad \sigma_2 = -P_1, \quad \sigma_3 = -P_3$$

But $P_3 = P_1$,

$$\sigma_2 = \sigma_3 = -P_1$$

Substituting the values of principal stresses, Von-Mises yield criteria gives,

$$P_1 + \sigma_{x_1} = Y_0 \quad (5.25)$$

Suppose yielding starts at a point, X_1 distance from the entry of the unit. The equilibrium of the forces in X-direction at this point gives;

$$\begin{aligned} \sigma_{x_1} W_1 t_1 &= 2\tau_1 W_1 X_1 + 2\tau_3 t_1 X_1, \\ \sigma_{x_1} &= \frac{2\tau_1 X_1}{t_1} + \frac{2\tau_3 X_1}{W_1} \end{aligned} \quad (5.26)$$

Also $\frac{P_1}{X_1} = \frac{Pm}{L_1}$

$$P_1 = \frac{Pm}{L_1} X_1 \quad (5.27)$$

Substituting values from equation (5.26) and (5.27) into equation (5.25) and simplifying;

$$X_1 = \frac{Y_0}{\left(\frac{Pm}{L_1} + \frac{2\tau_1}{t_1} + \frac{2\tau_3}{W_1} \right)} \quad (5.28)$$

5.3.1.4 Hydrodynamic Pressure and Axial Stress in Deformation Zone

Assuming deformation takes place linearly, so that film thickness 'h' and 'h*' at any point in the deformation zone, in Section A and Section B respectively, is given by;

$$h_i = h_1 + bx \quad (5.29)$$

$$h_i^* = h_3 + b^*x \quad (5.30)$$

And the deformation profile may be described by;

$$t_i = t_1 - 2bx \quad (5.31)$$

$$W_i = W_1 - 2b^*x \quad (5.32)$$

where b and b^* are constants and give the slope of the deformation line with x , in Section A and Section B respectively.

Applying the boundary conditions;

$$\rightarrow \text{at } y = 0, v_i = V,$$

$$\rightarrow \text{and } y = h_i, v_i = 0.$$

The expression for determining the velocity of fluid flow in the deformation zone, from equation (5.13), is given by;

$$v_i = \frac{1}{2\mu} \left(\frac{\partial p}{\partial x} \right)_i (y^2 - h_i y) + V \left(1 - \frac{y}{h_i} \right) \quad (5.33)$$

The flow of polymer melt in the deformation zone, in Section A, will be given by;

$$Q_i = \int_0^{h_i} v_i dy$$

$$Q_i = - \frac{h_i^3}{12\mu} \left(\frac{\partial p}{\partial x} \right)_i + \frac{V h_i}{2} \quad (5.34)$$

Applying the steady state flow condition,

$$\frac{\partial}{\partial x} (Q_i) = 0 \text{ gives,}$$

$$\frac{\partial}{\partial x} \left[h_i^3 \left(\frac{\partial p}{\partial x} \right)_i \right] = \frac{\partial h_i}{\partial x} (6\mu V) \quad (5.35)$$

Referring to Figure 88a;

$$\frac{\partial h_i}{\partial x} = b$$

$$\frac{\partial}{\partial x} \left[\left(\frac{\partial p}{\partial x} \right)_i h_i^3 \right] = 6\mu V b \quad (5.36)$$

Integrating the above equation w.r.t.x

$$\left(\frac{\partial p}{\partial x} \right)_i h_i^3 = 6\mu V b x + C_3$$

Applying the boundary condition,

$$\text{At } x = 0, h_i = h_1 \text{ and } \left(\frac{\partial p}{\partial x}\right)_i = \frac{Pm}{L_1}$$

Value of constant C_3 can be determined which on resubstitution gives;

$$\left(\frac{\partial p}{\partial x}\right)_i = \frac{6\mu Vbx}{(h_1 + bx)^3} + \frac{Pm h_1^3}{L_1(h_1 + bx)^3} \quad (5.37)$$

Equation (5.37) gives the pressure distribution in the deformation zone in Section A.

Using partial fractions and integrating equation (5.37),

$$P_i = 6\mu V \left[\frac{h_1}{2b(h_1 + bx)^2} - \frac{1}{b(h_1 + bx)} \right] - \frac{h_1^3 Pm}{L_1} \left[\frac{1}{2b(h_1 + bx)^2} \right] + C_4 \quad (5.38)$$

Where C_4 is constant of integration and can be determined by applying boundary conditions,

At the point where deformation starts,

$$x = 0, \quad P_i = P_1 \quad \text{gives,}$$

$$C_4 = \frac{Pm}{L_1} X_1 + \frac{Pm}{L_1} \left(\frac{h_1}{2b}\right) + \frac{3\mu V}{bh_1}$$

Substituting for C_4 into equation (5.38) gives,

$$P_i = \frac{6\mu V}{b} \left[\frac{h_1}{2(h_1 + bx)^2} - \frac{1}{(h_1 + bx)} + \frac{1}{2h_1} \right] + \frac{Pm}{L_1} \left[X_1 + \frac{h_1}{2b} - \frac{h_1^3}{2b(h_1 + bx)^2} \right] \quad (5.39)$$

Equation (5.39) is an expression for determining the hydrodynamic pressure in Section A along the x direction.

If h_1 is replaced by h_i , equation (5.22) will give an expression for calculating shear stress in the deformation zone for Section A ie,

$$\tau_i = -\frac{h_i}{2} \left(\frac{\partial P}{\partial x}\right)_i - \frac{\mu V}{h_i} \quad (5.40)$$

Substituting the value of $\left(\frac{\partial P}{\partial x}\right)_i$ from equation (5.37) into equation

(5.40) gives,

$$\tau_i = - \frac{\mu V}{(h_1 + bx)^2} [4bx + h_1 + \frac{Pm h_1^3}{2\mu V L_1}] \quad (5.41)$$

Now with the assumption that the pressure gradient in Section B will remain the same as in Section A, it can be shown that the shear stress in Section B in the deformation zone is given by,

$$\tau_i^* = - \frac{(h_3 + b^*x)}{2} \left[\frac{6\mu Vbx}{(h_1 + bx)^3} + \frac{Pm}{L_1} \frac{h_1^3}{(h_1 + bx)^3} \right] - \frac{\mu V}{(h_3 + b^*x)} \quad (5.42)$$

Referring to Figure 89, the equilibrium of forces in the x direction gives,

$$\begin{aligned} \sigma_{x_i} W_i t_i &= (\sigma_{x_i} + d\sigma_{x_i})(W_i + dW_i)(t_i + dt_i) + 2P_i \sin\theta \frac{dt_i}{2\sin\theta} \\ W_i + 2\tau_i \cos\theta \frac{dt_i}{2\sin\theta} W_i + 2P_i^* \sin\beta \frac{dW_i}{2\sin\beta} t_i + 2\tau_i^* \cos\beta \frac{dW_i}{2\sin\beta} t_i \end{aligned}$$

Ignoring terms containing two or more than two smaller quantities simplifying the above equation we obtain,

$$d\sigma_{x_i} = - \frac{dt_i}{t_i} (P_i + \sigma_{x_i}) - \frac{dW_i}{W_i} (P_i^* + \sigma_{x_i}) - \tau_i \cot\theta \frac{dt_i}{t_i} - \tau_i^* \cot\beta \frac{dW_i}{W_i} \quad (5.43)$$

Referring to Figures 89b and 89c, and using equations (5.31) and (5.32),

$$\cot\theta = - \frac{1}{b} \quad (5.44)$$

$$\cot\beta = - \frac{1}{b^*} \quad (5.45)$$

Using the assumption that $P_i^* = P_i$ and applying Levy-Mises flow rule it can be shown that (Appendix I),

$$\frac{dW_i}{W_i} = \frac{dt_i}{t_i} \quad (5.46)$$

$$\text{and } b^* = mb \quad (5.47)$$

where m is constant and equal to the ratio of initial width to the initial thickness ie $m = W_1/t_1$

Now substituting for P_i^* and $\frac{dW_i}{W_i}$ into equation (5.43) and applying

Von-Mises yield criteria that

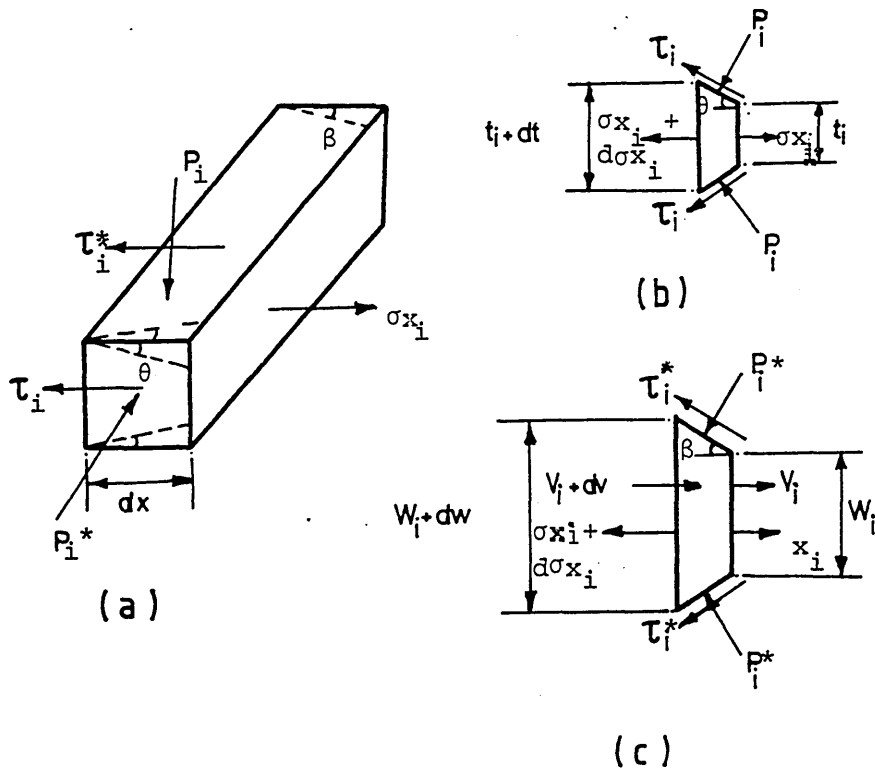


FIG 89: STRESSES ACTING ON A SMALL ELEMENT

$P_i + \sigma x_i = Y_i$ we get,

$$d\sigma x_i = -\frac{dt_i}{t_i} [2Y_i + \tau_i \cot\theta + \tau_i^* \cot\beta] \quad (5.48)$$

Substituting values of $\cot\theta$ and $\cot\beta$ from equations (5.44 and 5.45) respectively, equation (5.48) can be reduced to;

$$d\sigma x_i = \frac{2b dx}{(t_1 - 2bx)} [2Y_i - \frac{\tau_i}{b} - \frac{\tau_i^*}{b^*}] \quad (5.49)$$

Equation (5.49) is the governing equation to evaluate the axial stress in the deformation zone.

Assuming the material property to be rigid non-linearly strain-hardening expressed by,

$$Y_i = Y_o + K_o \epsilon^n$$

where,

$$\epsilon = \ln\left(\frac{a_1}{a_i}\right)$$

or $\epsilon = 2\ln\left(\frac{t_1}{t_i}\right)$ [using equations A5 and A7, see Appendix I]

$$\therefore Y_i = Y_o + 2^n K_o \left\{ \ln\left(\frac{t_1}{t_i}\right) \right\}^n \quad (5.50)$$

Substituting values from equations (5.41), (5.42) and (5.50) into equation (5.49) we get,

$$d\sigma x_i = \frac{2b dx}{t_1 - 2bx} \left[2 \left\{ Y_o + 2^n K_o \left\{ \ln\left(\frac{t_1}{t_i}\right) \right\}^n \right\} - \frac{1}{b} \left\{ -\frac{\mu V}{(h_1 + bx)^2} \right. \right. \\ \left. \left. (4bx + h_1 + \frac{Pm h_1^3}{2\mu V L_1}) \right\} - \frac{1}{b^*} \left\{ \left(-\frac{(h_3 + b^* x)}{2} \right) \times \left(\frac{6\mu V b x}{(h_1 + bx)^3} + \right. \right. \right. \\ \left. \left. \left. \frac{Pm h_1^3}{L_1 (h_1 + bx)^3} \right) - \frac{\mu V}{(h_3 + b^* x)} \right\} \right]$$

Simplifying the above equation we get,

$$d\sigma x_i = A_1 \left\{ \frac{bx dx}{(t_1 - 2bx)(h_1 + bx)^2} \right\} + A_2 \left\{ \frac{dx}{(t_1 - 2bx)(h_1 + bx)^2} \right\} \\ + A_3 \left\{ \frac{dx}{(t_1 - 2bx)(h_1 + bx)^2} \right\} + A_4 \left\{ \frac{bx dx}{(t_1 - 2bx)(h_1 + bx)^3} \right\} \\ + A_5 \left\{ \frac{b^2 x^2 dx}{(t_1 - 2bx)(h_1 + bx)^3} \right\} + A_6 \left\{ \frac{dx}{(t_1 - 2bx)(h_1 + bx)^3} \right\} +$$

$$\begin{aligned}
& A_7 \left\{ \frac{bx \, dx}{(t_1 - 2bx)(h_1 + bx)^3} \right\} + A_8 \left\{ \frac{dx}{(t_1 - 2bx)(h_3 + b^*x)} \right\} \\
& + A_9 \left\{ \frac{dx}{(t_1 - 2bx)} \right\} + 2^{n+2} bKo \left[\frac{\left\{ \ln \frac{t_1}{(t_1 - 2bx)} \right\}^n}{(t_1 - 2bx)} dx \right] \quad (5.51)
\end{aligned}$$

where,

$$\begin{aligned}
A_1 &= 8\mu V & A_2 &= 2\mu V h_1 \\
A_3 &= \frac{Pmh_1^3}{L_1} & A_4 &= \frac{6\mu V b h_3}{b^*} \\
A_5 &= 6\mu V & A_6 &= \frac{Pmh_1^3 h_3 b}{b^* L_1} \\
A_7 &= \frac{Pmh_1^3}{L_1} & A_8 &= \frac{2\mu V b}{b^*} \\
A_9 &= 4bY_0
\end{aligned}$$

Using partial fractions, equation (5.51) gives;

$$\begin{aligned}
d_{ox} x_i &= A_1 \left\{ \frac{2t_1}{(t_1 + 2h_1)^2(t_1 - 2bx)} + \frac{t_1}{(t_1 + 2h_1)^2(h_1 + bx)} \right. \\
&- \left. \frac{h_1}{(t_1 + 2h_1)(h_1 + bx)^2} \right\} dx + (A_2 + A_3) \left\{ \frac{4}{(t_1 + 2h_1)^2(t_1 - 2bx)} \right. \\
&+ \left. \frac{2}{(t_1 + 2h_1)^2(h_1 + bx)} + \frac{1}{(t_1 + 2h_1)(h_1 + bx)^2} \right\} dx \\
&+ (A_4 + A_7) \left\{ \frac{4t_1}{(t_1 + 2h_1)^3(t_1 - 2bx)} + \frac{2t_1}{(t_1 + 2h_1)^3(h_1 + bx)} \right. \\
&+ \left. \frac{t_1}{(t_1 + 2h_1)^2(h_1 + bx)^2} - \frac{h_1}{(t_1 + 2h_1)(h_1 + bx)^3} \right\} dx \\
&+ A_5 \left\{ \frac{2t_1^2}{(t_1 + 2h_1)^3(t_1 - 2bx)} + \frac{t_1^2}{(t_1 + 2h_1)^3(h_1 + bx)} \right. \\
&- \left. \frac{2h_1(t_1 + h_1)}{(t_1 + 2h_1)^2(h_1 + bx)^2} + \frac{h_1^2}{(t_1 + 2h_1)(h_1 + bx)^3} \right\} dx \\
&+ A_6 \left\{ \frac{8}{(t_1 + 2h_1)^3(t_1 - 2bx)} + \frac{4}{(t_1 + 2h_1)^3(h_1 + bx)} \right. \\
&+ \left. \frac{2}{(t_1 + 2h_1)^2(h_1 + bx)^2} + \frac{1}{(t_1 + 2h_1)(h_1 + bx)^3} \right\} dx \\
&+ A_8 \left\{ \frac{2b}{(b^*t_1 + 2bh_3)(t_1 - 2bx)} + \frac{b^*}{(b^*t_1 + 2bh_3)(h_3 + b^*x)} \right\} dx \\
&+ A_9 \left\{ \frac{1}{(t_1 - 2bx)} \right\} dx + 2^{n+2} bKo \left[\frac{\left\{ \ln \frac{t_1}{(t_1 - 2bx)} \right\}^n}{(t_1 - 2bx)} \right] dx
\end{aligned}$$

Simplification of the above equation gives,

$$\begin{aligned} d\alpha_i = & B_1 \left\{ \frac{dx}{(t_1 - 2bx)} \right\} + B_2 \left\{ \frac{dx}{(h_1 + bx)} \right\} + B_3 \left\{ \frac{dx}{(h_1 + bx)^2} \right\} \\ & + B_4 \left\{ \frac{dx}{(h_1 + bx)^3} \right\} + B_5 \left\{ \frac{dx}{(h_3 + b^*x)} \right\} + B_6 \left[\frac{\left\{ \ln \frac{t_1}{(t_1 - 2bx)} \right\}^n}{(t_1 - 2bx)} \right] dx \end{aligned} \quad (5.52)$$

where,

$$\begin{aligned} B_1 = & \frac{2t_1A_1 + 4(A_2 + A_3)}{(t_1 + 2h_1)^2} + \frac{4t_1(A_4 + A_7) + 2t_1^2A_5 + 8A_6}{(t_1 + 2h_1)^3} \\ & + \frac{2bA_8}{b^*t_1 + 2bh_3} + A_9 \\ B_2 = & \frac{t_1A_1 + 2(A_2 + A_3)}{(t_1 + 2h_1)^2} + \frac{2t_1(A_4 + A_7) + t_1^2A_5 + 4A_6}{(t_1 + 2h_1)^3} \\ B_3 = & \frac{A_2 + A_3 - A_1h_1}{(t_1 + 2h_1)} + \frac{t_1(A_4 + A_7) - 2A_5h_1(t_1 + h_1) + 2A_6}{(t_1 + 2h_1)^2} \\ B_4 = & \frac{A_6 + A_5h_1^2 - (A_4 + A_7)h_1}{(t_1 + 2h_1)} \\ B_5 = & \frac{b^*A_8}{(b^*t_1 + 2bh_3)} \\ B_6 = & 2^{n+2} bK_0 \end{aligned}$$

Integrating equation (5.52) w.r.t.x

$$\begin{aligned} \alpha_i = & - \frac{B_1}{2b} \ln(t_1 - 2bx) + \frac{B_2}{b} \ln(h_1 + bx) - \frac{B_3}{b(h_1 + bx)} \\ & - \frac{B_4}{2b(h_1 + bx)^2} + \frac{B_5}{b^*} \ln(h_3 + b^*x) \\ & + \frac{B_6}{2b(n+1)} \left\{ \ln \left(\frac{t_1}{t_1 - 2bx} \right) \right\}^{n+1} + C_5 \end{aligned} \quad (5.53)$$

Where C_5 is the constant of integration and can be determined by applying the boundary condition that at the point where deformation starts,

$$x = 0, \quad \alpha_i = \alpha_1$$

$$C_5 = \frac{B_1}{2b} \ln t_1 - \frac{B_2}{b} \ln h_1 + \frac{B_3}{bh_1} + \frac{B_4}{2bh_1^2} - \frac{B_5}{b^*} \ln h_3 + \alpha_1$$

Substituting the value of C_5 into equation (5.53), we obtain;

$$\begin{aligned}
\sigma x_i &= \frac{B_1}{2b} \ln\left(\frac{t_1}{t_1 - 2bx}\right) + \frac{B_2}{b} \ln\left(\frac{h_1 + bx}{h_1}\right) + \frac{B_3}{b} \left(\frac{1}{h_1} - \frac{1}{h_1 + bx}\right) \\
&+ \frac{B_4}{2b} \left[\frac{1}{h_1^2} - \frac{1}{(h_1 + bx)^2}\right] + \frac{B_5}{b^*} \ln\left(\frac{h_3 + b^*x}{h_3}\right) \\
&+ \frac{B_6}{2b(n+1)} \left[\ln\left(\frac{t_1}{t_1 - 2bx}\right)\right]^{n+1} + \sigma x_1
\end{aligned} \tag{5.54}$$

5.3.1.5 Prediction of Reduction in Strip Size and Drawing Stress

Again using the Von-Mises yield criteria, the deformation will continue when the equation,

$$P_i + \sigma x_i = Y_i = Y_o + K_o \epsilon^n \tag{5.55}$$

is satisfied.

It is assumed that the deformation ceases at $x = L_1 - X_1$, the values of P_i and σx_i are substituted into equation (5.55) from equations (5.39) and (5.54) respectively. The parameter 'b' is the only unknown parameter for a given drawing speed and the geometry of the unit. Equation (5.55) may be iterated to establish the value of b. Once this value is established, the percentage reduction in strip size at any point for $X_1 < x < L_1$ is given by,

$$\begin{aligned}
\text{PRT} &= \left(1 - \frac{t_i}{t_1}\right) \times 100 \quad) \\
& \quad) \\
& \quad) \\
\text{PRW} &= \left(1 - \frac{W_i}{W_1}\right) \times 100 \quad) \\
& \quad) \\
& \quad) \\
\text{PRA} &= \left(1 - \frac{W_i t_i}{W_1 t_1}\right) \times 100 \quad) \\
& \quad)
\end{aligned} \tag{5.56}$$

And drawing stress is given by

$$\sigma d = \sigma x_i + \sigma x_2$$

where,

$$\sigma x_2 = \frac{2\tau_4 L_2}{t_i} + \frac{2\tau_5 L_2}{W_i} \tag{5.57}$$

$$\tau_4 = \frac{P_i h_4}{2L_2} - \frac{\mu V}{h_4}$$

$$\tau_5 = \frac{P_i h_5}{2L_2} - \frac{\mu V}{h_5}$$

and $h_4 = h_i - h_1 + h_2$, $h_5 = h_i^*$

Condition of Slip

As already described, at a certain value of shear stress, slip will occur at the interface of the polymer melt and the strip surface. When this condition occurs, then it is assumed that the pressure gradient, ie the value of maximum pressure prior to deformation at that particular speed, will remain constant for all values of speed beyond that particular value. Also the shear stress in both sections will remain constant during deformation.

With these assumptions the expressions for shear stress and pressure remain the same as derived in the previous section.

These are listed below;

$$\tau_1 = - \frac{h_1 P_m}{2L_1} - \frac{\mu V_c}{h_1} \quad (5.58)$$

$$\tau_3 = - \frac{h_1 P_m}{2L_1} - \frac{\mu V_c}{h_3} \quad (5.59)$$

$$P_i = \frac{6\mu V}{b} \left[\frac{h_1}{2(h_1 + bx)^2} - \frac{1}{(h_1 + bx)} + \frac{1}{2h_1} \right] + \frac{P_m}{L_1} \left[X_1 + \frac{h_1}{2b} - \frac{h_1^3}{2b(h_1 + bx)^2} \right] \quad (5.41)$$

Where V_c is the speed at which shear stress reaches its critical value.

The basic equation for axial stress in the deformation zone is given by equation (5.49) and replacing τ_i and τ_i^* by τ_c and τ_c^* .

$$d\sigma_{x_i} = \frac{2bdx}{(t_1 - 2bx)} \left[2Y_i - \frac{\tau_c}{b} - \frac{\tau_c^*}{b^*} \right] \quad (5.60)$$

Substituting for Y_i and integrating equation (5.60)

$$\sigma_{x_i} = - 2Y_o \ln(t_1 - 2bx) + \frac{2^{n+1} K_o}{(n+1)} \left\{ \ln\left(\frac{t_1}{t_1 - 2bx}\right) \right\}^{n+1} + \frac{\tau_c \ln(t_1 - 2bx)}{b} + \frac{\tau_c^* \ln(t_1 - 2bx)}{b^*} + C_6 \quad (5.61)$$

Applying the boundary condition that the at point where deformation starts

$$x = 0, \sigma x_i = \sigma x_1,$$

Value of constant C_6 can be determined which on back substitution gives,

$$\begin{aligned} \sigma x_i = & 2Y_0 \ln\left(\frac{t_1}{t_1 - 2bx}\right) + \frac{2^{n+1}K_0}{n+1} \left\{ \ln\left(\frac{t_1}{t_1 - 2bx}\right) \right\}^{n+1} \\ & + \frac{\tau_c}{b} \ln\left(\frac{t_1 - 2bx}{t_1}\right) + \frac{\tau_c^*}{b^*} \ln\left(\frac{t_1 - 2bx}{t_1}\right) + \sigma x_1 \end{aligned} \quad (5.62)$$

The equations for reduction in strip size, drawing stress and the solution procedure are the same as for the previous section. The speed at which slip will take place was determined when shear stress τ_1 in Section A reached critical value τ_c and the corresponding value of τ_3 was assumed to be the critical shear stress τ_c^* in Section B.

5.3.2 Numerical Solution

The rate of straining also affects the level of yield stress of the material. To incorporate this effect into the analysis and because of the mathematical complexity, the governing equations in the deformation zone have been solved using finite difference techniques. The equations before deformation takes place will be the same as derived in Section 5.3.1.

Consider two points in the deformation zone at a distance Δx apart, (see Figure 89), assuming that deformation between these two points takes place linearly so that,

$$\frac{dt}{dx} = \text{constant} = B \quad (5.1A)$$

$$\text{and} \quad \frac{dW}{dx} = \text{constant} = B^* \quad (5.2A)$$

Expressing equations (5.1A) and (5.2A) in finite difference form we get,

$$\begin{aligned} \frac{t_{i-1} - t_i}{x_i - x_{i-1}} &= B \\ t_{i-1} - t_i &= B\Delta x \\ t_i &= t_{i-1} - B\Delta x \end{aligned} \quad (5.3A)$$

Similarly

$$W_i = W_{i-1} - B^*\Delta x \quad (5.4A)$$

And

$$dh = \frac{1}{2} dt \quad (5.5A)$$

$$dh^* = \frac{1}{2} dW \quad (5.6A)$$

Writing equations (5.5A) and (5.6A) in finite difference form and simplifying gives,

$$h_i = h_{i-1} + \frac{1}{2} B\Delta x \quad (5.7A)$$

$$h_i^* = h_{i-1}^* + \frac{1}{2} B^* \Delta x \quad (5.8A)$$

The change in the area of strip will also cause the velocity to change in the deformation zone hence this was also considered.

By considering the continuity of flow of metal, it can be shown that the current velocity is given by (Appendix II),

$$V_i = V_{i-1} \left(\frac{W_{i-1} t_{i-1}}{W_i t_i} \right) \quad (5.9A)$$

Substituting $P_i^* = P_i$ and applying Von-Mises yield criteria

$$P_i + \sigma x_i = Y_i,$$

Equation (5.43) can be written in the form;

$$d\sigma x_i = - \frac{dt_i}{t_i} Y_i - \frac{dW_i}{W_i} Y_i - \tau_i \cot \theta \frac{dt_i}{t_i} - \tau_i^* \cot \beta \frac{dW_i}{W_i} \quad (5.10A)$$

Referring to figures 89b and 89c,

$$\cot \theta = \frac{2dx}{dt_i} \quad (5.11A)$$

$$\cot \beta = \frac{2dx}{dW_i} \quad (5.12A)$$

Substituting values from equations (5.11A) and (5.12A) into equation (5.10A) will give,

$$d\sigma x_i = - \frac{dt_i}{t_i} Y_i - \frac{dW_i}{W_i} Y_i - \frac{2\tau_i dx}{t_i} - \frac{2\tau_i^* dx}{W_i} \quad (5.13A)$$

The above equation in the difference form gives,

$$\begin{aligned} \sigma x_{i-1} - \sigma x_i &= - \left(\frac{t_{i-1} - t_i}{t_i} + \frac{W_{i-1} - W_i}{W_i} \right) Y_i - \frac{2\tau_i \Delta x}{t_i} - \frac{2\tau_i^* \Delta x}{W_i} \\ \sigma x_i &= \left(\frac{t_{i-1}}{t_i} + \frac{W_{i-1}}{W_i} - 2 \right) Y_i + \frac{2\tau_i \Delta x}{t_i} + \frac{2\tau_i^* \Delta x}{W_i} + \sigma x_{i-1} \end{aligned} \quad (5.14A)$$

Equation (5.14A) is the equation for determining the axial stress in the deformation zone. This equation is also the function of shear stresses acting on the strip which can be determined by using equations (5.22) and (5.24) and can be written in finite difference form as,

$$\tau_i = -\frac{h_i}{2} \left(\frac{\partial P}{\partial x} \right)_i - \frac{\mu V_i}{h_i} \quad (5.15A)$$

$$\tau_i^* = -\frac{h_i^*}{2} \left(\frac{\partial P}{\partial x} \right)_i - \frac{\mu V_i}{h_i^*} \quad (5.16A)$$

The flow of polymer melt in the deformation zone can be given by equation (5.34) which when written in finite difference notations gives,

$$Q_i = -\frac{h_i^3}{12\mu} \left(\frac{\partial P}{\partial x} \right)_i + \frac{V_i h_i}{2} \quad (5.17A)$$

Now, for continuity of flow,

$$Q_i = Q_1 \quad (5.18A)$$

Substituting for Q_i and Q_1 from equations (5.17A) and (5.16) into equation (5.18A) and simplifying,

$$\left(\frac{\partial P}{\partial x} \right)_i = \frac{1}{h_i^3} \left[\frac{P_m h_1^3}{L_1} + 6\mu(V_i h_i - V h_1) \right] \quad (5.19A)$$

Now
$$\left(\frac{\partial P}{\partial x} \right)_i = \frac{P_i - P_{i-1}}{\Delta x}$$

$$P_i = \left(\frac{\partial P}{\partial x} \right)_i \Delta x + P_{i-1} \quad (5.20A)$$

P_i is the hydrodynamic pressure at any point in the deformation zone.

The stress strain relationship of the strip material is given by,

$$Y_i = Y_0 + K_0 \varepsilon^n \quad (5.21A)$$

where

$$\varepsilon = \ln\left(\frac{a_1}{a_i}\right) = \ln\left(\frac{W_1 t_1}{W_i t_i}\right)$$

Substituting for ε into equation (5.21A) and writing in difference notations

$$Y_i = Y_0 + K_0 \left[\ln\left(\frac{W_1 t_1}{W_i t_i}\right) \right]^n \quad (5.22A)$$

Now the strain rate at a point in the deformation zone is defined by

$$\dot{\epsilon} = \frac{d\epsilon}{dt'}$$

where t' denotes time

$$\text{Now } d\epsilon = \frac{da}{a}$$

$$\therefore \dot{\epsilon} = -\frac{da}{a} \cdot \frac{1}{dt'} \quad (5.23A)$$

For practical evaluation it is necessary to assume a mean value of strain rate

$$\bar{\epsilon}_m = \frac{1}{x} \int_0^x \dot{\epsilon} dx$$

where x is the distance along the axis of draw measured from the entry.

The mean strain rate over a small distance may be defined by

$$\bar{\epsilon}_m = \frac{1}{x_i - x_{i-1}} \int_{a_{i-1}}^{a_i} \dot{\epsilon} dx \quad (5.24A)$$

where,

$$\text{at } x = x_{i-1}, \quad a = a_{i-1};$$

$$\text{and at } x = x_i, \quad a = a_i$$

Replacing the value of $\dot{\epsilon}$ from equation (5.23A), equation (5.24A)

gives,

$$\bar{\epsilon}_m = \frac{1}{\Delta x} \int_{a_{i-1}}^{a_i} -\frac{da}{a} \frac{dx}{dt'}$$

$$\text{But } \frac{dx}{dt'} = v_i$$

$$\therefore \bar{\epsilon}_m = -\frac{v_i}{\Delta x} \int_{a_{i-1}}^{a_i} \frac{da}{a}$$

$$\bar{\epsilon}_m = \frac{v_i}{\Delta x} \ln\left(\frac{a_{i-1}}{a_i}\right) \quad (5.25A)$$

A flow rule of the form

$$s = \frac{Y_d}{Y_s} = 1 + \left(\frac{\bar{\epsilon}_m}{N}\right)^{\frac{1}{T_1}}$$

where,

Y_d = dynamic yield stress of the material

Y_s = static yield stress of the material

N and T_1 are constants

has been proposed by Hashmi⁽⁶⁰⁾. In finite difference notation the above equation takes the form,

$$s_i = 1 + \left(\frac{\dot{\epsilon}m}{N}\right)^{\frac{1}{T_1}}$$

Combining this with equation (5.22A) gives;

$$Y_i = s_i [Y_0 + K_0 \left\{ \ln \left(\frac{W_i t_i}{W_1 t_1} \right) \right\}^n] \quad (5.26A)$$

The yield criteria is given by,

$$\begin{aligned} P_i + \alpha x_i &= Y_i \\ \text{or } P_i + \alpha x_i - Y_i &= 0 \end{aligned} \quad (5.27A)$$

Solution Procedure

At any point in the deformation zone, the value of t_i , h_i , B^* , W_i , h_i^* can be determined from equations (5.3A), (5.7A), (5.47), (5.4A) and (5.8A) for an arbitrary value of B and a step size of Δx . Using equation (5.9A) the value of V_i can be calculated. By substituting V_i , h_i and h_i^* into equations (5.19A), (5.15A) and (5.16A) the values of $\left(\frac{\partial P}{\partial x}\right)_i$, τ_i and τ_i^* can be calculated and Y_i can be estimated from equation (5.26A). Then τ_i , τ_i^* , t_i , W_i and Y_i may be substituted into equation (5.14A) to determine αx_i .

Having calculated αx_i , P_i and Y_i the value of B may be iterated until equation (5.27A) is satisfied. This procedure may be repeated in suitable steps of Δx from the position of yield of the strip inside the reduction unit where $i = X_1$, up to where $i = L_1 - X_1$. It is assumed that deformation ceases at the step, therefore

at the step when equation (5.27A) is satisfied, the final dimensions of the strip are $t = t_i$ and $W = W_i$.

Condition of Slip

In a similar way as was described in Section 5.3.1, it was assumed that when τ_1 reaches the critical value a condition of slip is observed. The speed at which this condition takes place is known as the critical speed. Thereafter it is assumed that τ_i, τ_i^* are equal to τ_1 and τ_3 respectively and P_i remains constant for further increases in the speed. With these assumptions, the equations derived in the previous section were solved following the same procedure described earlier to evaluate the various parameters.

5.4 Theoretical Results

The theoretical results were calculated from the equations derived in the previous section. The data below are the standard parameters which were used to solve the equations and were varied to show their effect on the performance of the process.

Dimensions of the Reduction Unit:

Inlet length,	$L_1 = 150\text{mm}$	
Exit length,	$L_2 = 30\text{mm}$	
Inlet gap,	$h_1 = 0.3\text{mm}$)
Exit gap,	$h_2 = 0.02\text{mm}$) Section A
Inlet and Exit gap,	$h_3 = 0.13\text{mm}$) Section B

Data for Copper Strip:

Initial thickness,	$t_1 = 1.59\text{mm}$
Initial width,	$W_1 = 12.7\text{mm}$
Initial yield stress,	$Y_0 = 75 \text{ MNm}^{-2}$
Strain hardening constant,	$K_0 = 600 \text{ MNm}^{-2}$
Strain hardening index,	$n = 0.6$
Strain rate sensitivity constant,	$N = 55 \times 10^3$
Strain rate sensitivity index,	$T_1 = 3.8$

Data for Polymer Melt:

Initial Viscosity,	$\mu = 110 \text{ Nsm}^{-2}$
Critical shear stress,	$\tau_c = 0.28 \text{ MNm}^{-2}$

5.4.1 Results from Closed Form Analytical Solution

Figures 90-97 show the effects of gap ratio, length ratio, material yield stress and critical shear stress on the percentage reduction and drawing stress. These results were produced by using the equations developed assuming a linear deformation profile.

The effect of gap ratio resulting from changed values of h_1 is demonstrated in Figure 90. This figure suggests that by using smaller gap ratios higher reductions should be achieved.

The effect of length ratio is shown in Figure 91. These graphs indicate that the inlet length has a direct effect on the predicted results, by increasing the inlet length, greater reductions should be obtained.

Figure 92 demonstrates the effect of initial yield stress on the percentage reduction when plotted against drawing speed. It is evident, as expected, that more reduction should be obtained for the material of low yield point value.

Figure 93 shows the effect of critical shear stress, this figure demonstrates that critical shear stress alters the speed at which slip will take place. For higher critical shear stresses, larger reductions are predicted.

Figures 94-97 represent the variations in the drawing stress for the different set-ups. These figures show similar trends and are consistent with the results observed in Figures 90-93.

The results obtained by this analysis indicate an increase in the reduction with increase in speed, even though a condition of slip was introduced into the analysis. The critical shear stress limit only changes the rate of reduction which is low compared with the rate before the condition of slip is detected.

$h_2 = \text{const.} = .02 \text{ mm}$

Rh
— 10
— 15
- - - 20

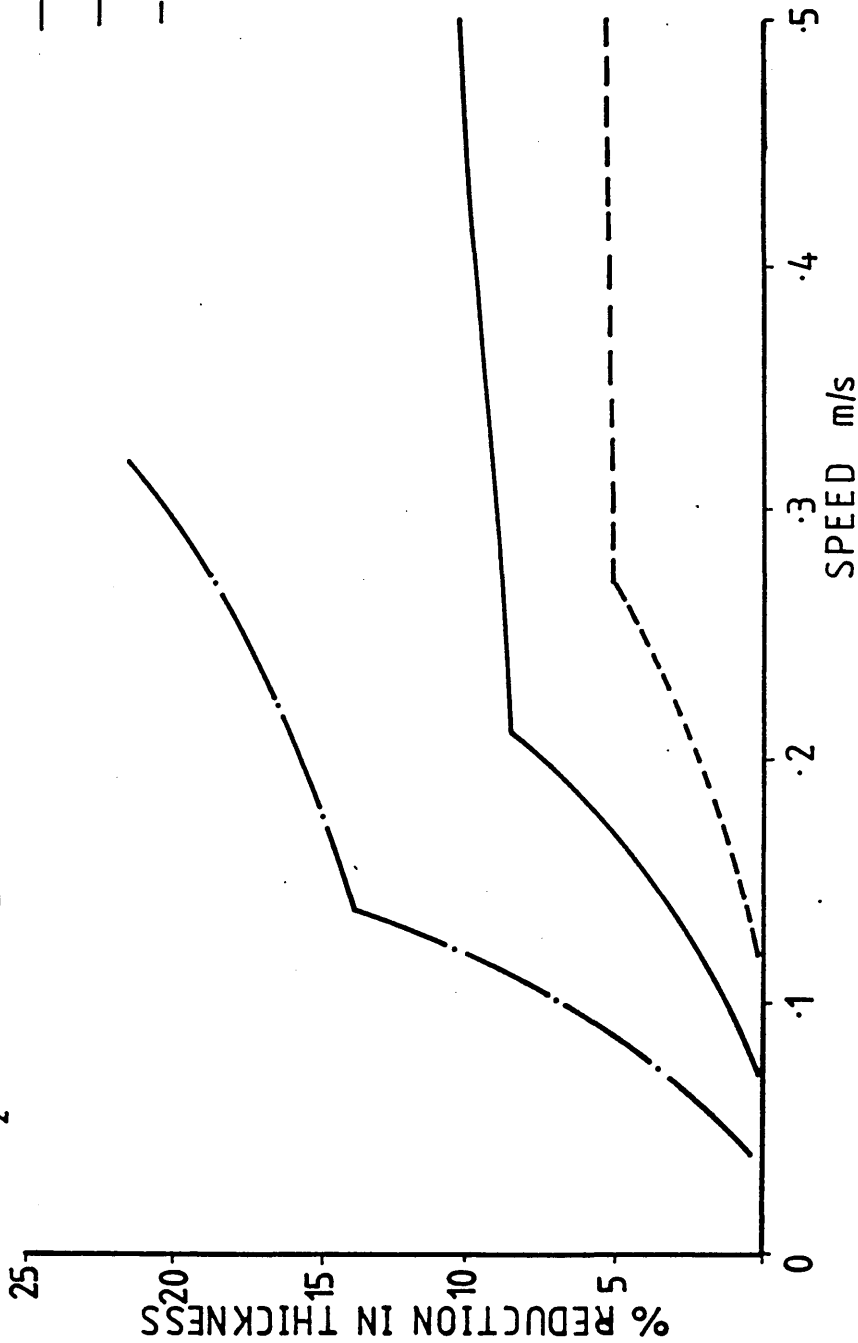


FIG 90: THEORETICAL EFFECT OF GAP RATIO ON PERCENTAGE REDUCTION IN THICKNESS

RL
 --- 5.65
 — 5
 - - - 4.33

$L_2 = \text{const.} = 30 \text{ mm}$

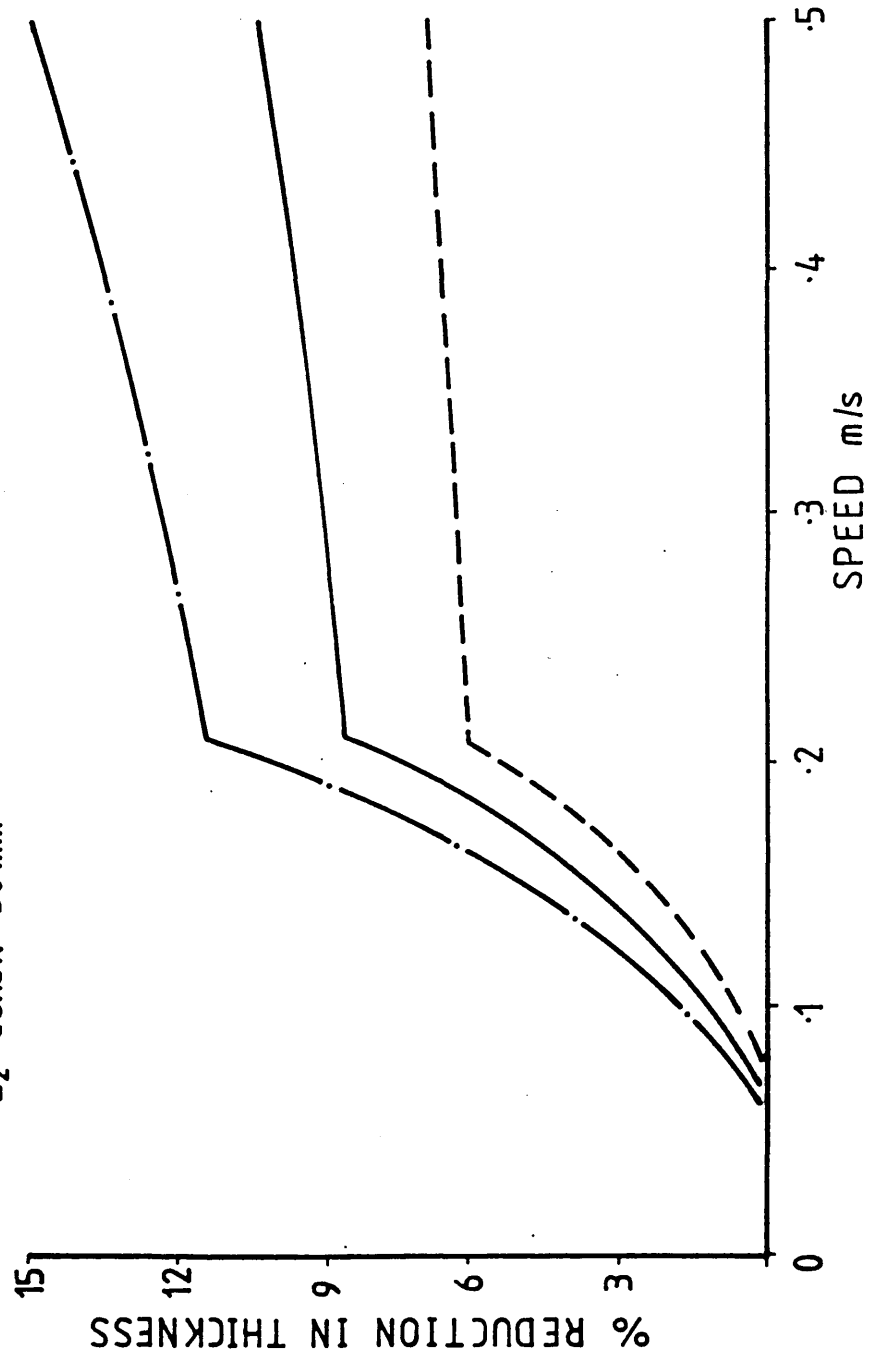


FIG 91: THEORETICAL EFFECT OF LENGTH RATIO ON PERCENTAGE REDUCTION IN THICKNESS

Y_0
 —·— 50 MNm⁻²
 — 75 MNm⁻²
 - - - 100 MNm⁻²

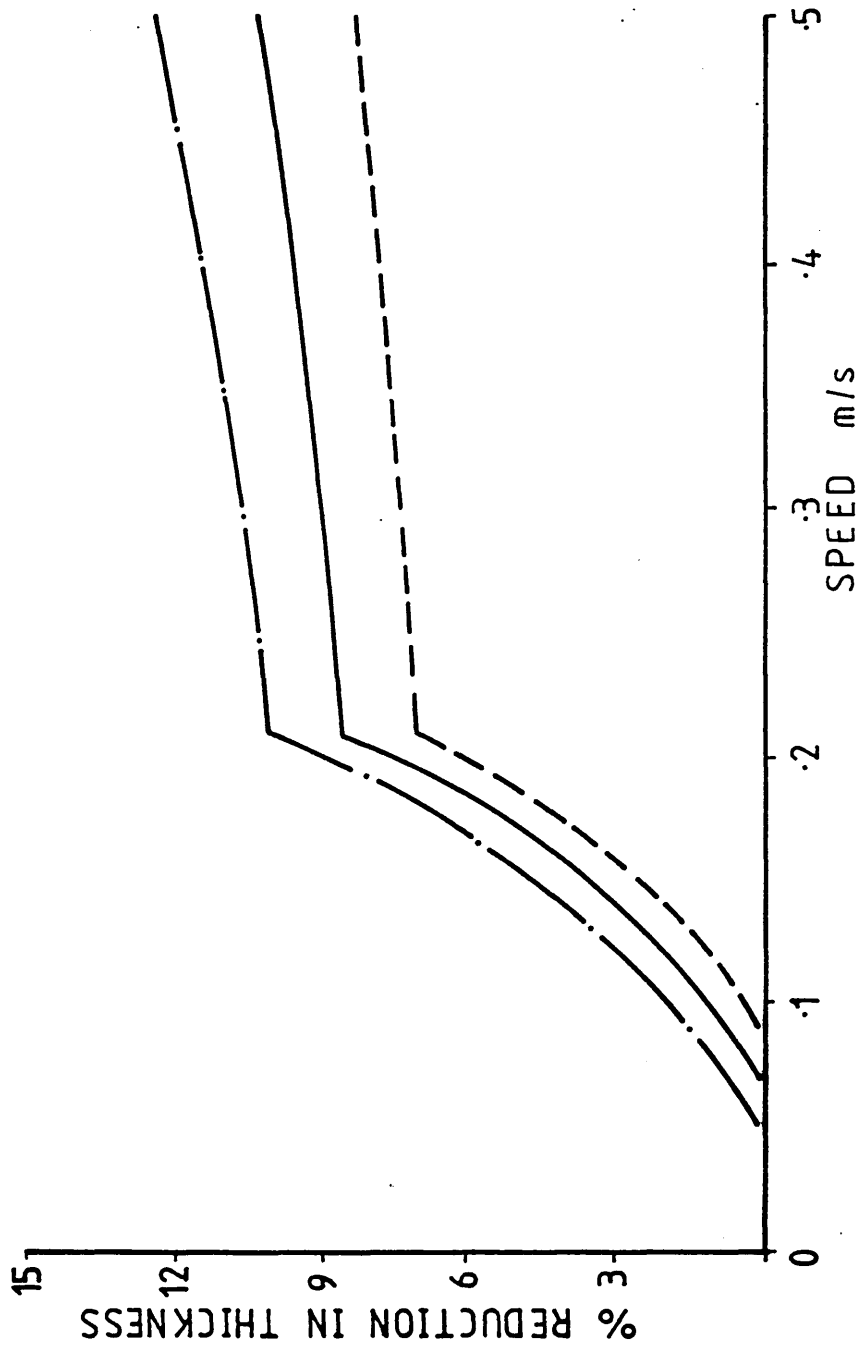


FIG 92: THEORETICAL EFFECT OF INITIAL YIELD STRESS ON PERCENTAGE REDUCTION IN THICKNESS

τ_c
 --- .22 MNm⁻²
 -.-. .25 MNm⁻²
 — .28 MNm⁻²

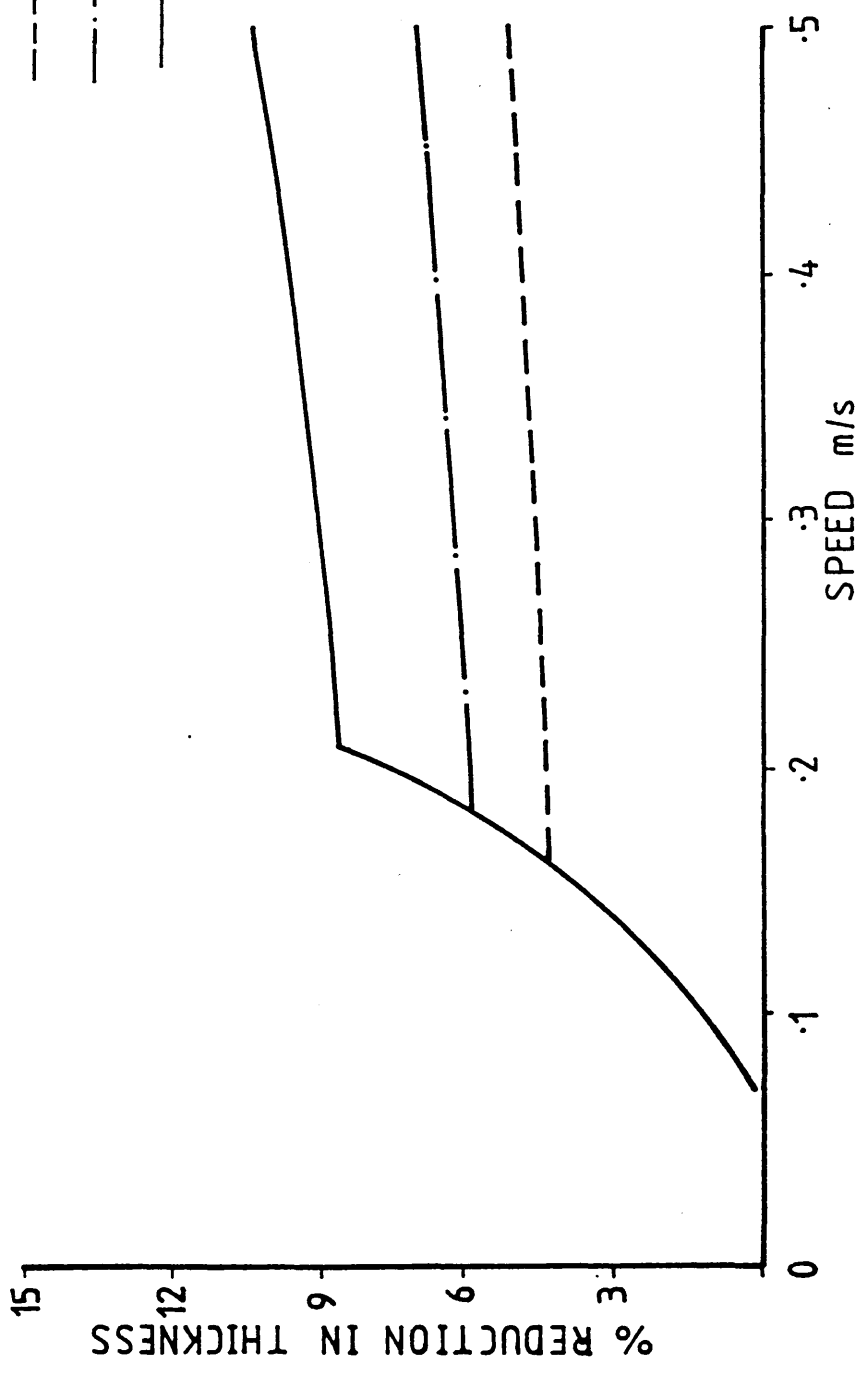


FIG 93: THEORETICAL EFFECT OF CRITICAL SHEAR STRESS ON PERCENTAGE REDUCTION IN THICKNESS

$h_2 = \text{const.} = .02 \text{ mm}$

Rh
— · — 10
— 15
- - - 20

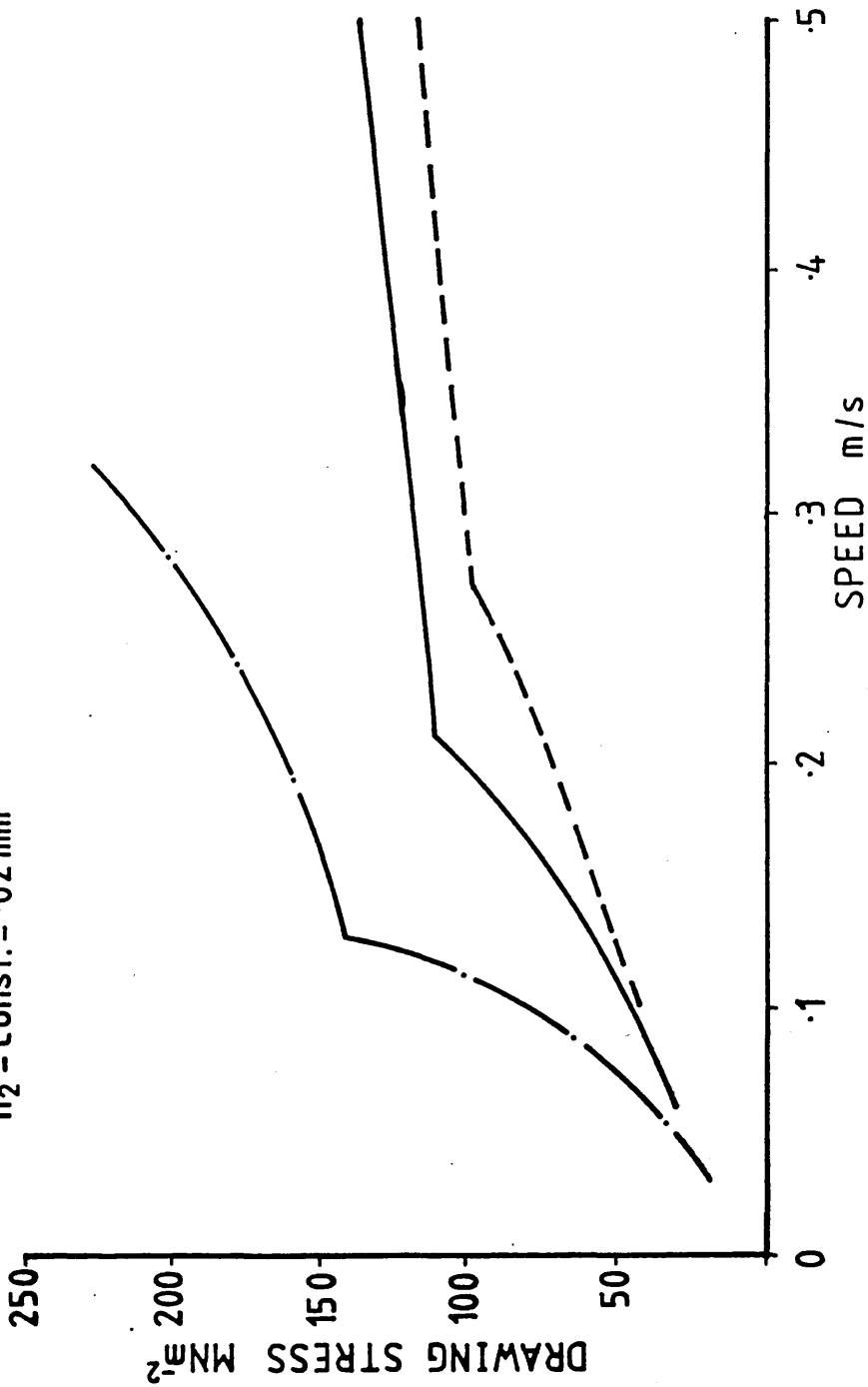


FIG 94: THEORETICAL EFFECT OF GAP RATIO ON DRAWING STRESS

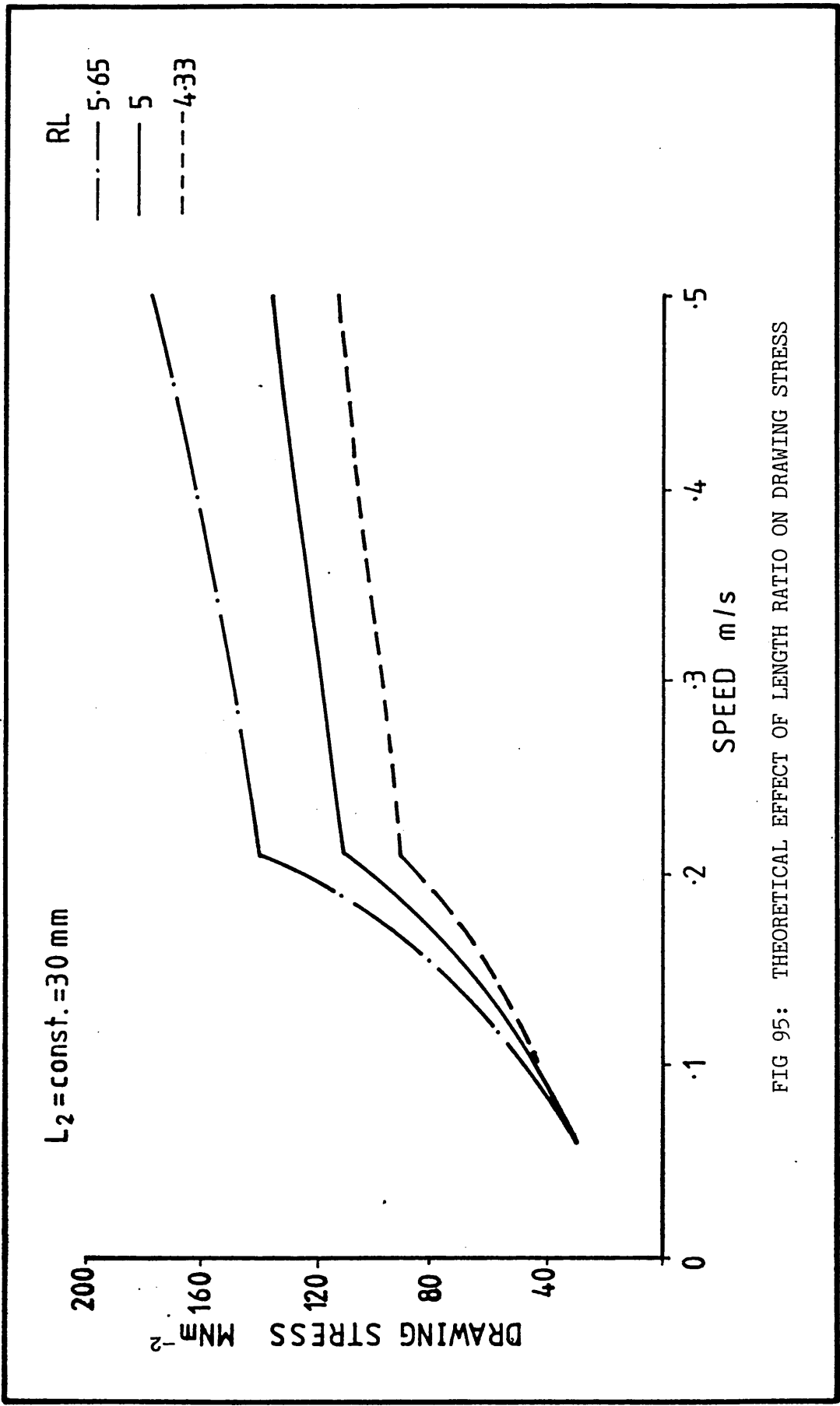


FIG 95: THEORETICAL EFFECT OF LENGTH RATIO ON DRAWING STRESS

Y_0
 — 50 MNm^{-2}
 — 75 MNm^{-2}
 - - - 100 MNm^{-2}

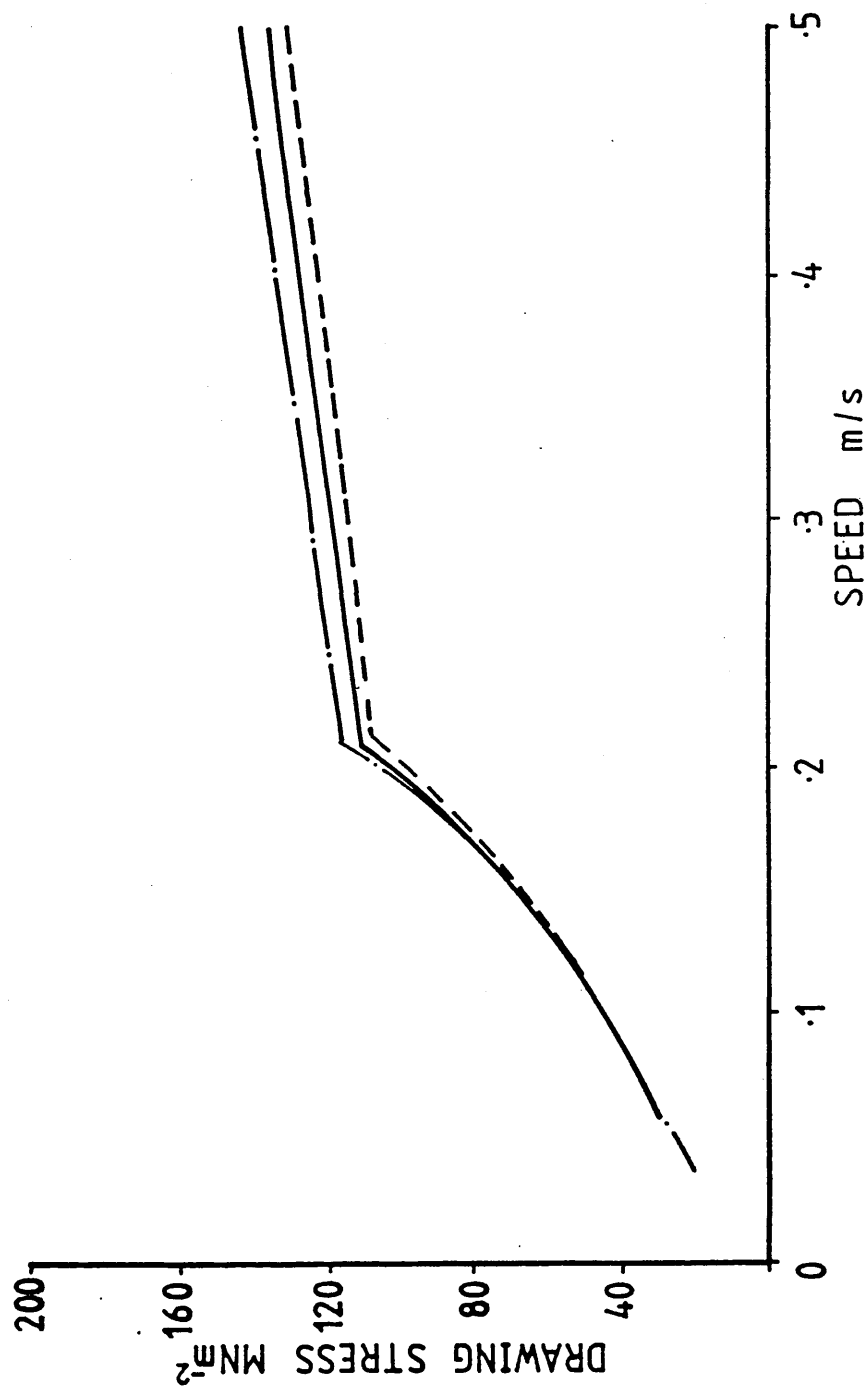


FIG 96: THEORETICAL EFFECT OF INITIAL YIELD STRESS ON DRAWING STRESS

τ_c
 .22 MNm⁻²
 .25 MNm⁻²
 .28 MNm⁻²

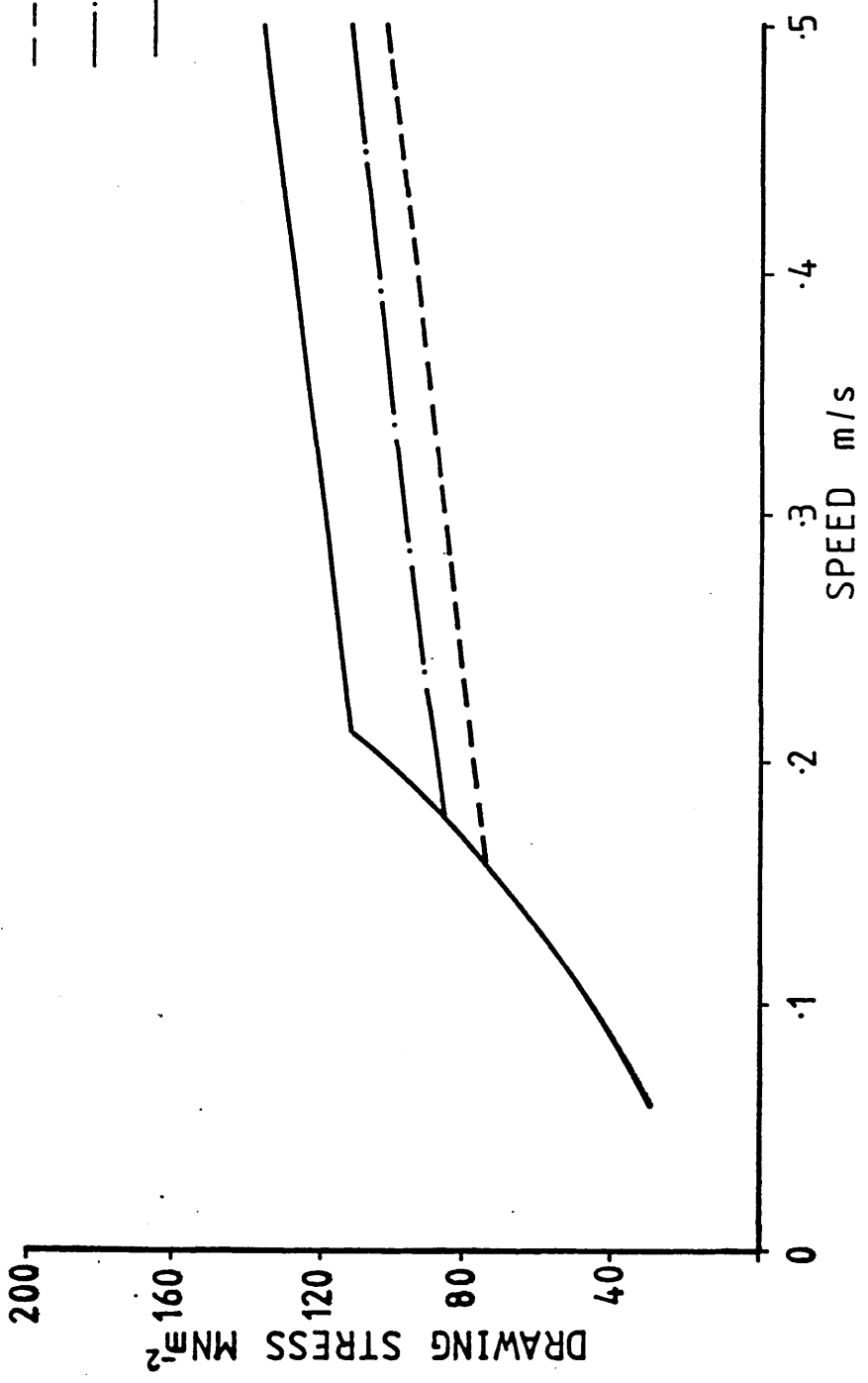


FIG 97: THEORETICAL EFFECT OF CRITICAL SHEAR STRESS ON DRAWING STRESS

5.4.2 Results from Numerical Solution

This analysis produced results which are in better agreement with experimental results in comparison with those predicted on the basis of an assumed linear deformation profile. The results were predicted by using the equations derived in Section 5.3.2.

The effect of the gap ratio on percentage reduction in thickness and yielding point of the strip with drawing speed is shown in Figures 98 and 99. These figures suggest that for a lower gap ratio (ie gap h_1), the deformation starts further away from the step, for a given drawing speed and a greater reduction should be obtained. A maximum reduction in thickness of about 16% was predicted for the gap ratio of 10.

Figure 100 shows the effect of length ratio on percentage reduction in thickness when plotted against the drawing speed. This figure suggests that more reductions should be obtained for the same drawing speed by using longer inlet lengths. With a length ratio of 5.65 a maximum percentage reduction in thickness of about 12% was predicted.

The effect of material yield stress on the percentage reduction in thickness and yield point is presented in Figures 101 and 102. These graphs indicate that for a material of low yield stress more reductions should be achieved for the same drawing speed. This is also evident from the point of initiation of yielding which indicates a larger deformation zone for low yield stress (see Figure 102).

Figure 103 demonstrates the effect of strain hardening constant on percentage reduction in thickness versus drawing speed. This

figure shows that the lower value of strain hardening constant causes greater reduction.

The effect of melt viscosity on the percentage reduction in thickness and yield point is shown in Figures 104 and 105. These graphs show that higher viscosities cause the larger deformations before slip occurs. However it is interesting to note that results predicted for $\mu = 110 \text{ Nsm}^{-2}$ are greater after slip takes place. This may be because of the distance X_1 which remains constant after slip (see Figure 105), and the fact that for higher viscosity slip is predicted to occur at a relatively slower speed.

Figure 106 shows the effect of critical shear stress on the percentage reduction in thickness when plotted against the drawing speed. This figure indicates that the value of critical shear stress changes the value of drawing speed for the condition of slip to occur. For a lower value of critical shear stress the slip condition is predicted at a relatively low speed and hence smaller reductions are predicted.

The effects of different parameters on the reduction in area versus drawing speed are shown in Figures 107-112.

Figures 113 to 116 demonstrate the variations in drawing stress when plotted against the drawing speed for different operating conditions. These figures show similar trends and are consistent with the predicted results for reduction in area.

The distribution of the pressure along the reduction unit was calculated for different conditions and is presented in Figures 117 to 119. The graphs indicate that the pressure increases

linearly only up to the point of yielding. The predicted pressures are of a magnitude sufficient to cause plastic deformation in combination with the induced axial stress.

The deformation profiles calculated theoretically for different gap ratios and drawing speeds are presented in Figures 120 and 121. A specific deformation profile was predicted for each case.

Rh
 — 10
 — 15
 - - 20

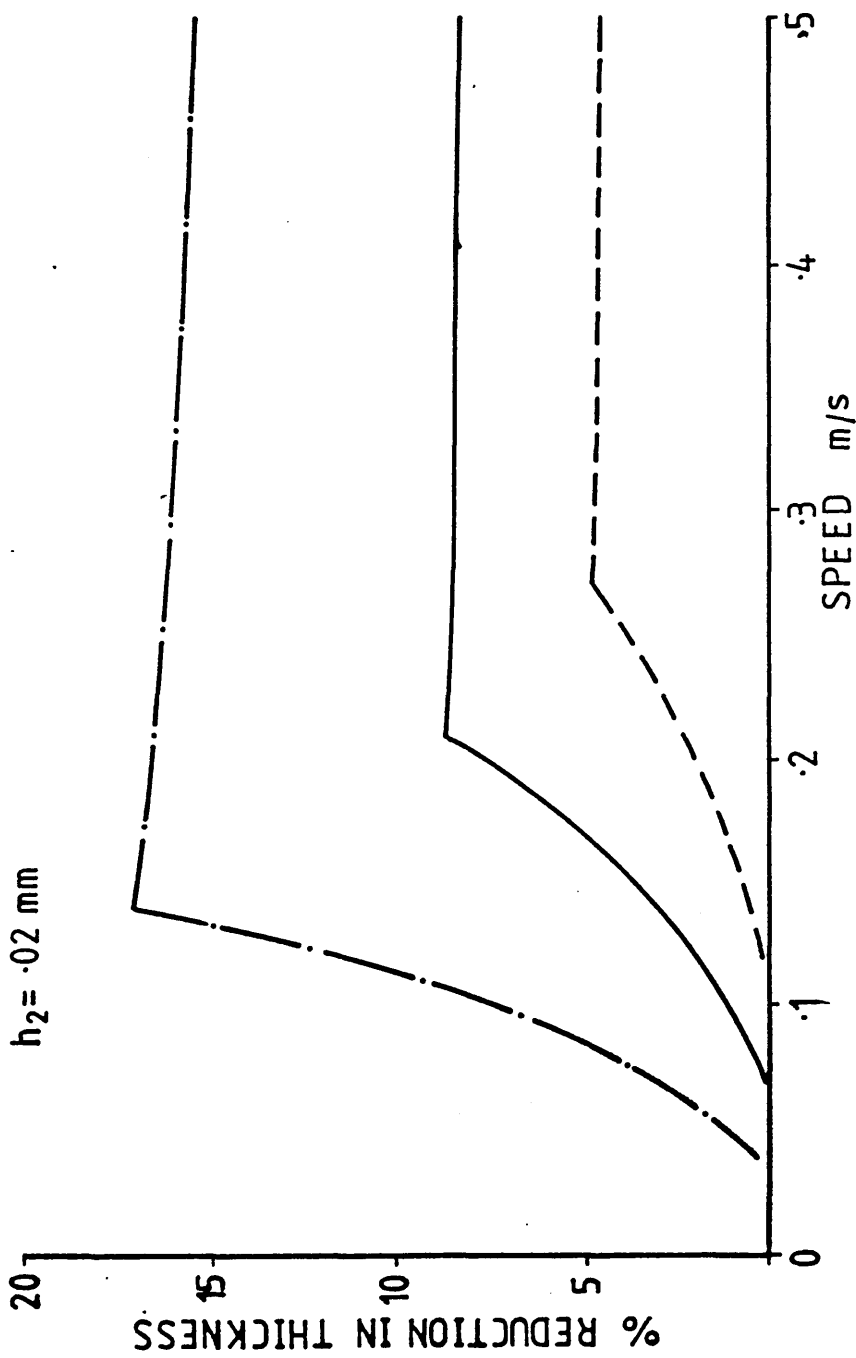


FIG 98: THEORETICAL EFFECT OF GAP RATIO ON PERCENTAGE REDUCTION IN THICKNESS

Rh
 ——— 10
 ——— 15
 - - - 20

$h_2 = \text{const.} = .02 \text{ mm}$

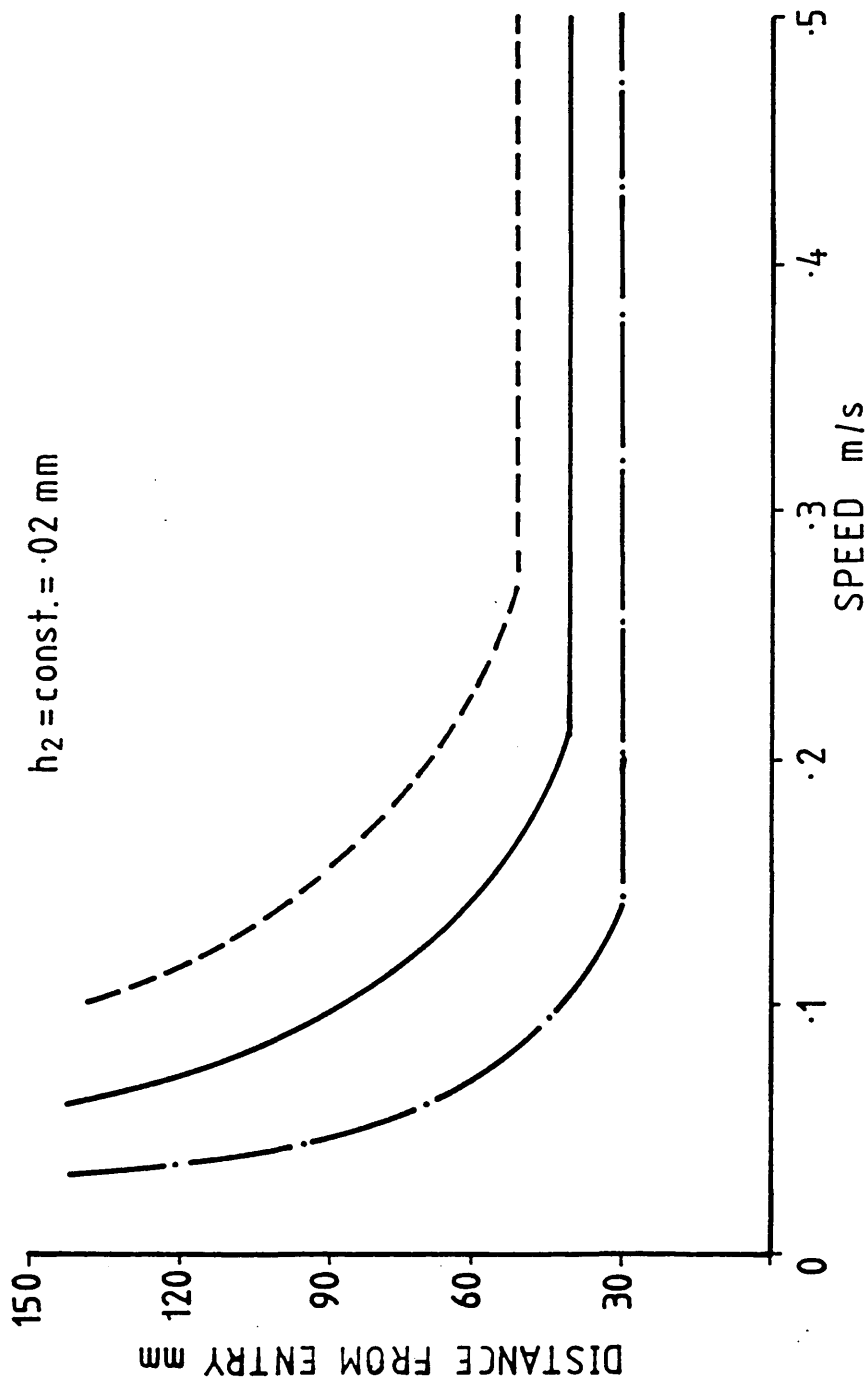


FIG 99: THEORETICAL EFFECT OF GAP RATIO ON YIELDING POINT

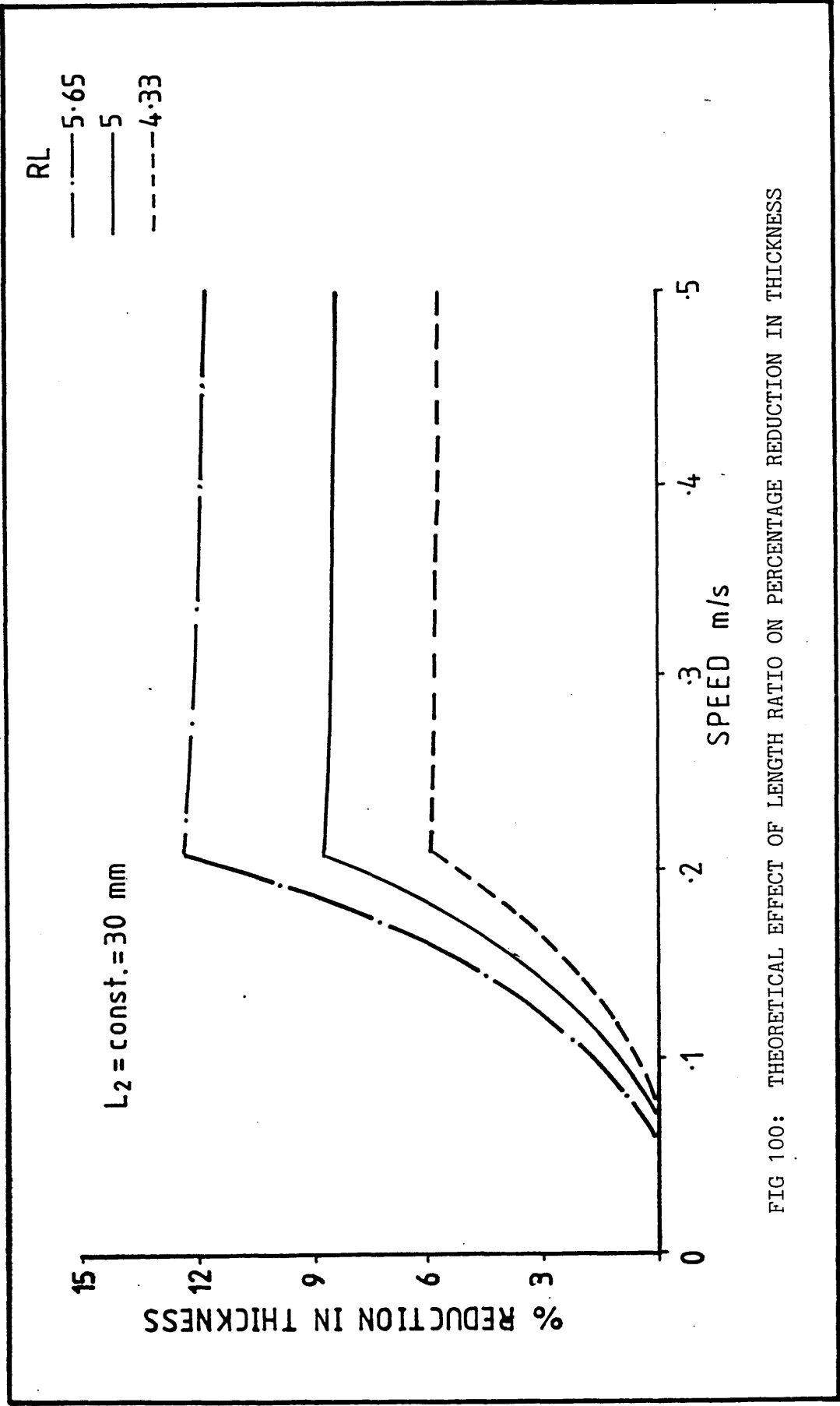


FIG 100: THEORETICAL EFFECT OF LENGTH RATIO ON PERCENTAGE REDUCTION IN THICKNESS

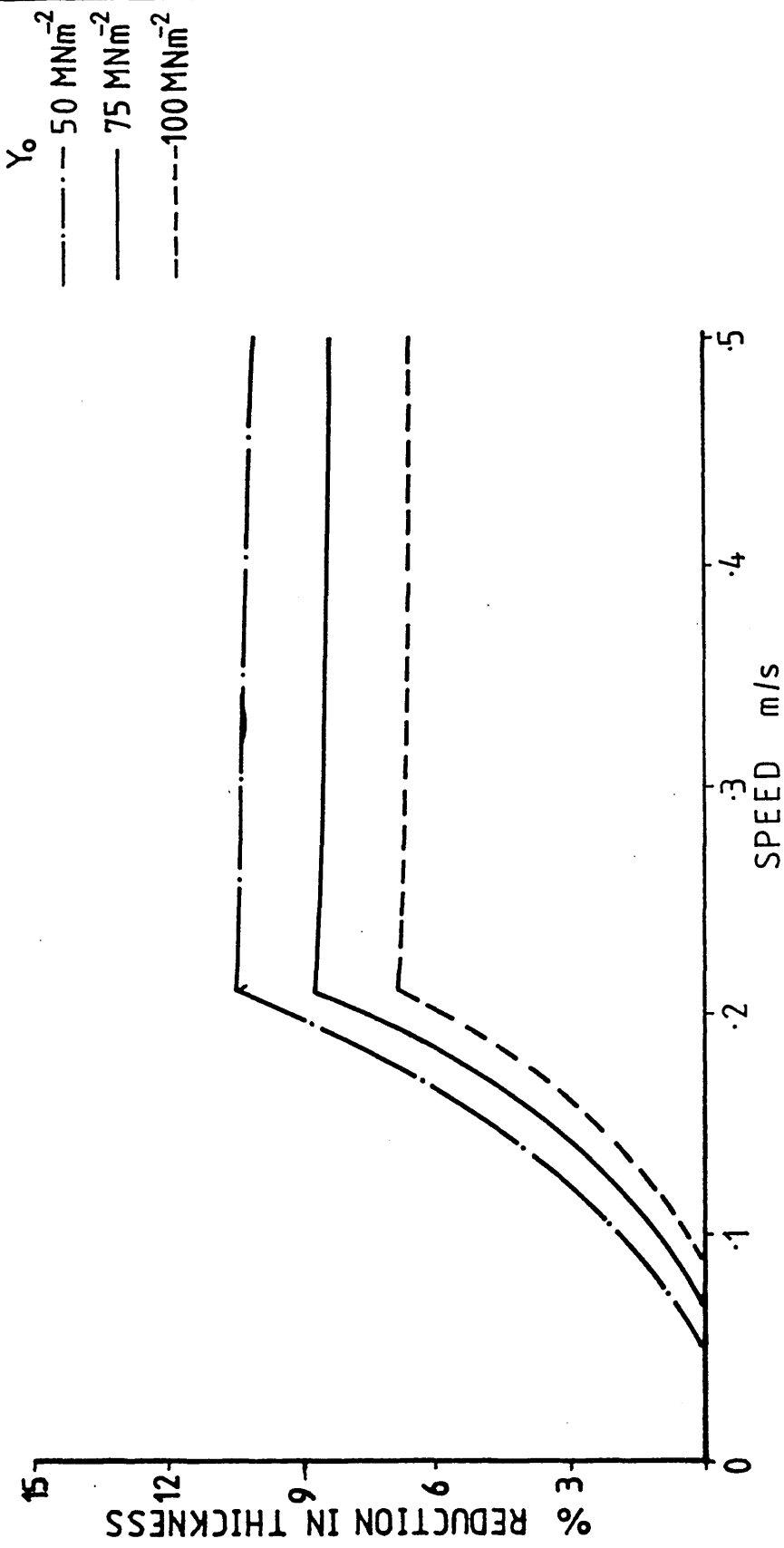


FIG 101: THEORETICAL EFFECT OF INITIAL YIELD STRESS ON PERCENTAGE REDUCTION IN THICKNESS

Y_0
 — 50 MNm^{-2}
 — 75 MNm^{-2}
 - - - 100 MNm^{-2}

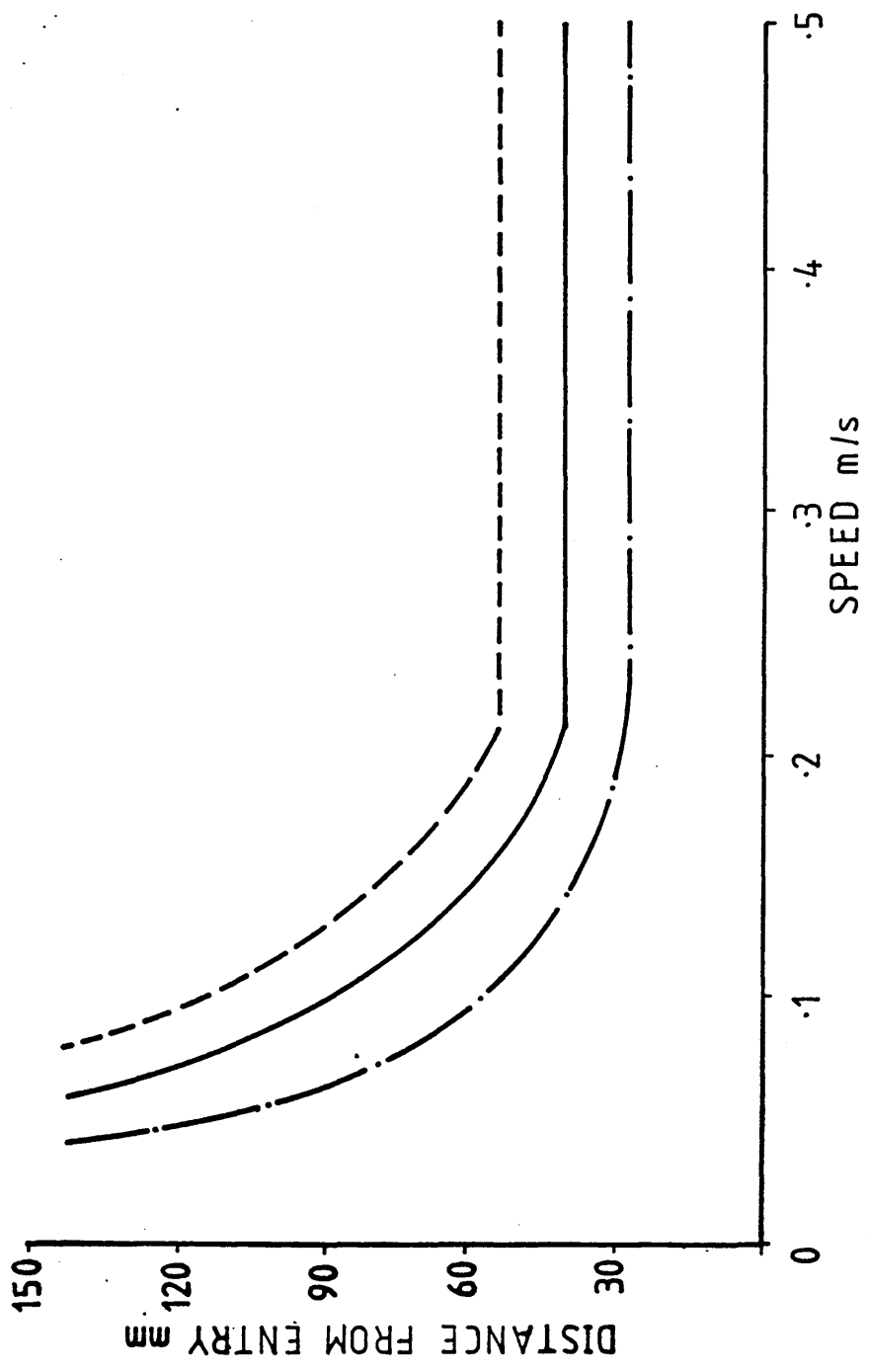


FIG 102: THEORETICAL EFFECT OF INITIAL YIELD STRESS ON YIELDING POINT

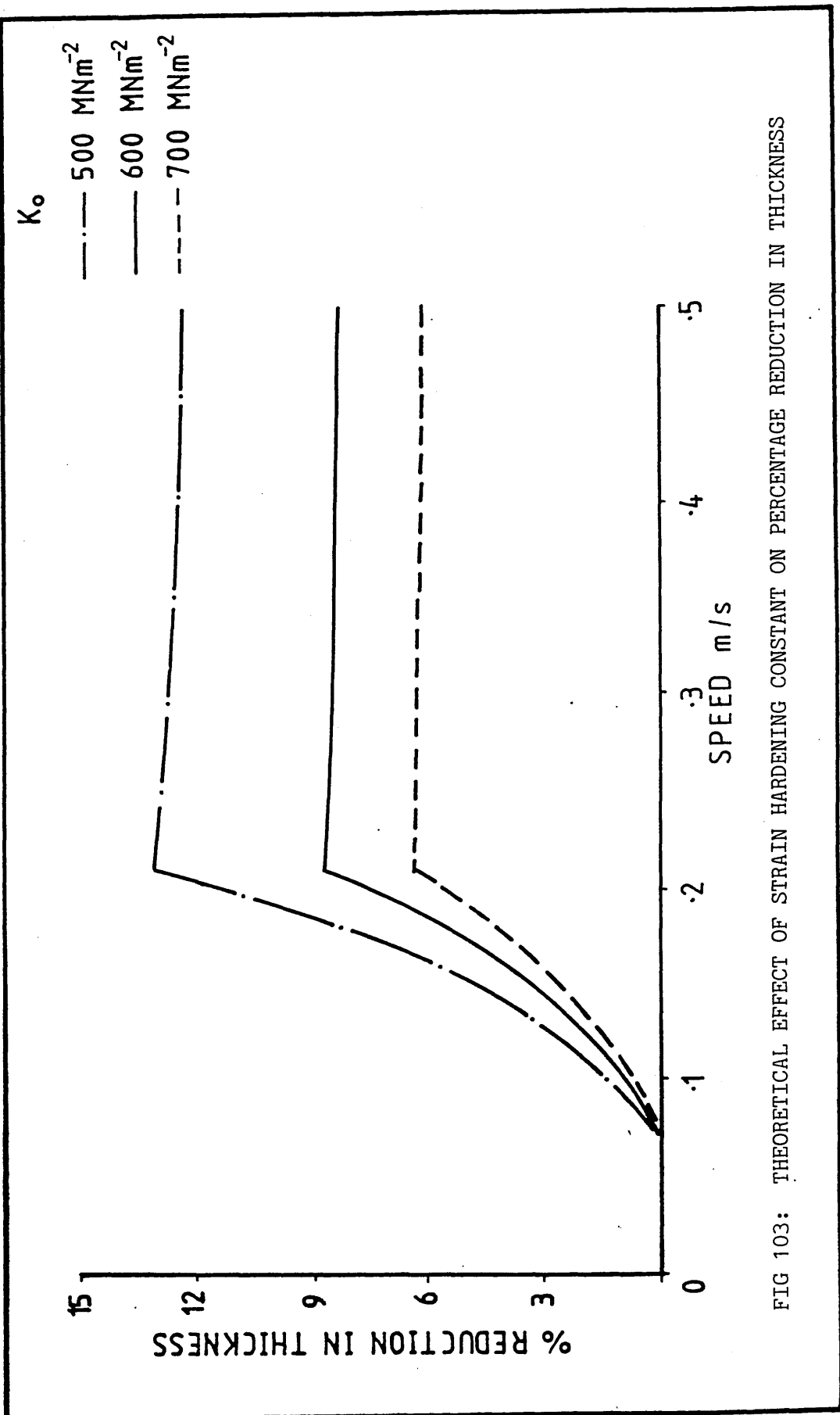


FIG 103: THEORETICAL EFFECT OF STRAIN HARDENING CONSTANT ON PERCENTAGE REDUCTION IN THICKNESS

μ
 --- 75 Ns m^{-2}
 — 110 Ns m^{-2}
 - · - 140 Ns m^{-2}

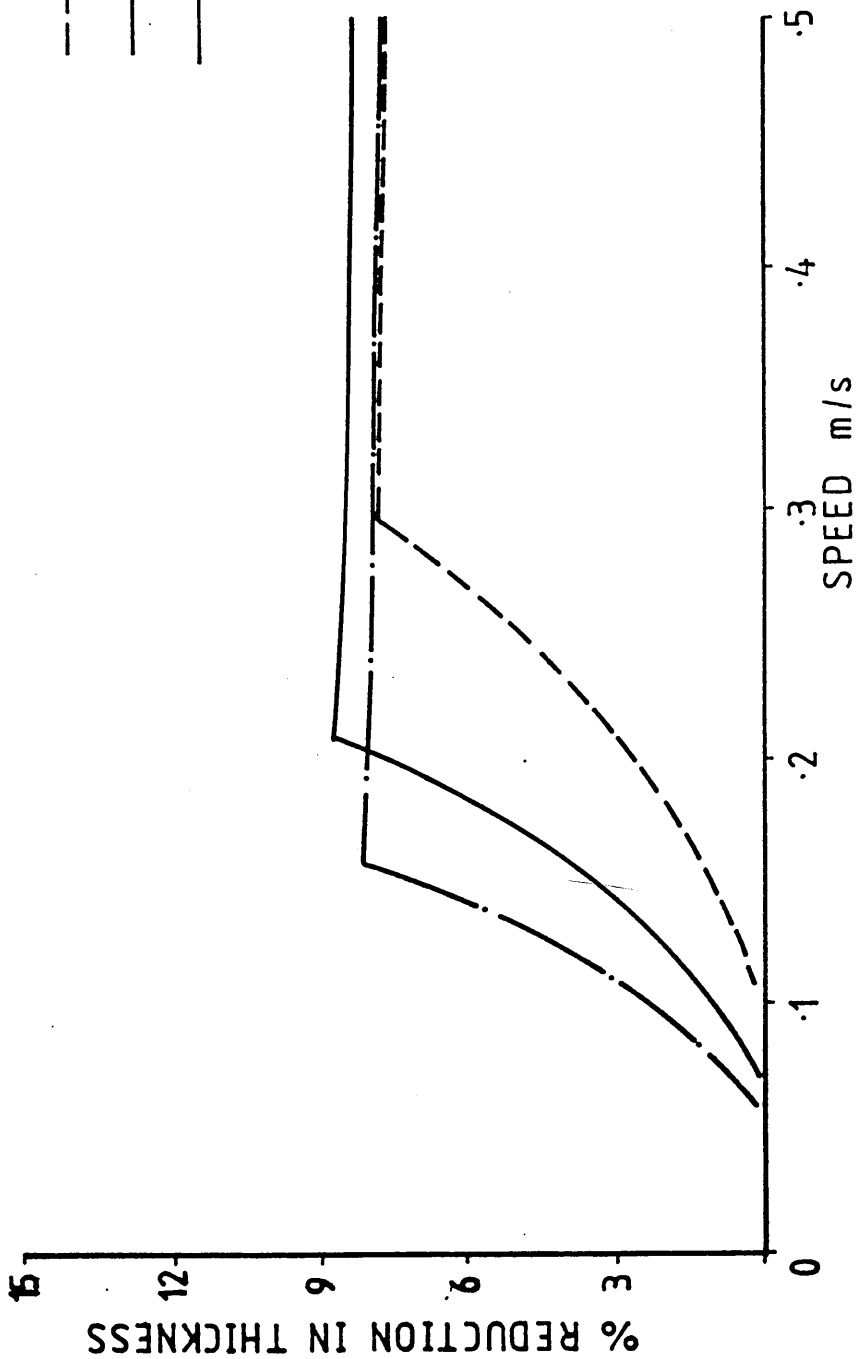


FIG 104: THEORETICAL EFFECT OF VISCOSITY ON PERCENTAGE REDUCTION IN THICKNESS

μ
 --- 75 Ns m^{-2}
 — 110 Ns m^{-2}
 - · - 140 Ns m^{-2}

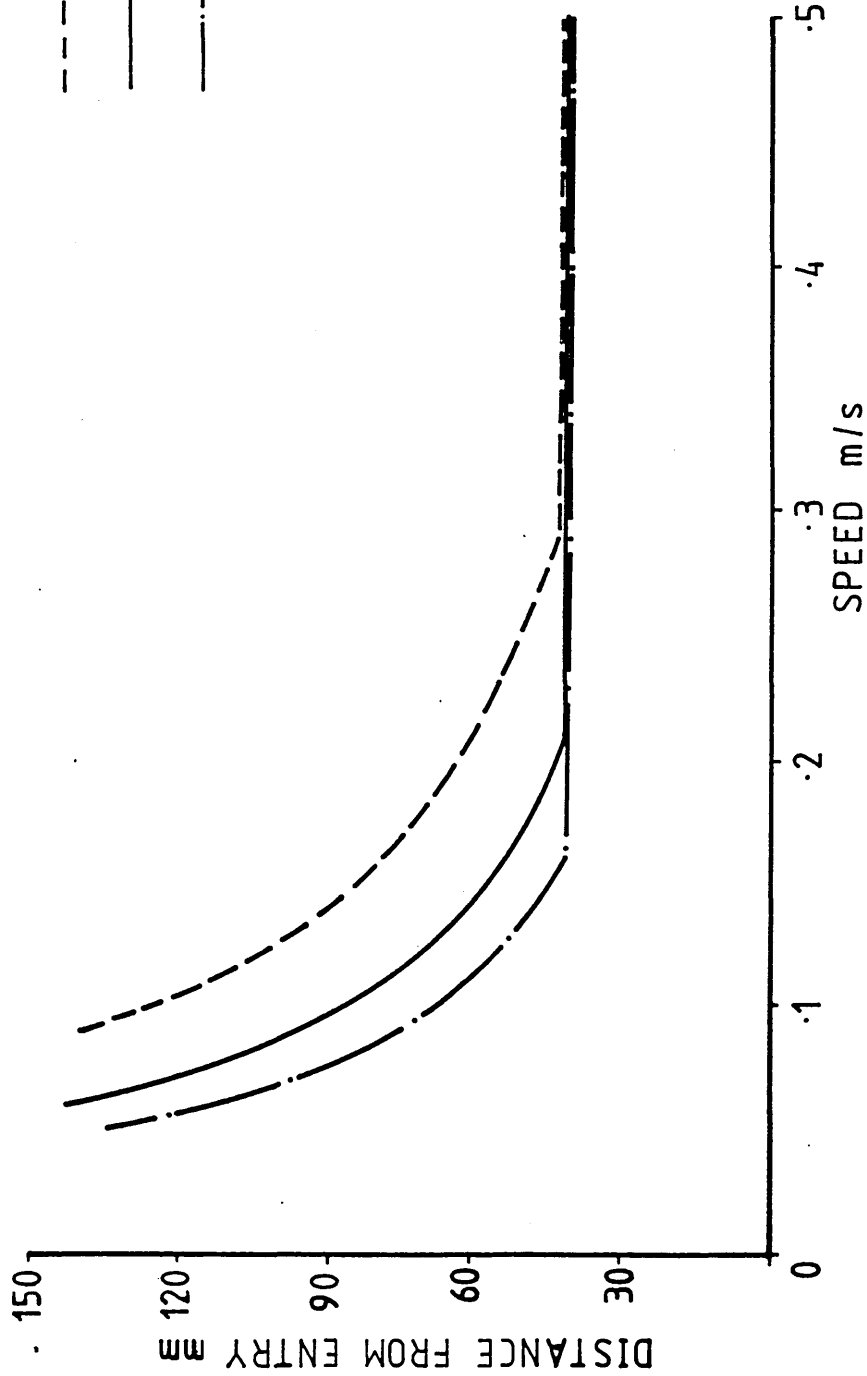


FIG 105: THEORETICAL EFFECT OF VISCOSITY ON YIELDING POINT

τ_c
 .22 MNm⁻²
 .25 MNm⁻²
 .28 MNm⁻²

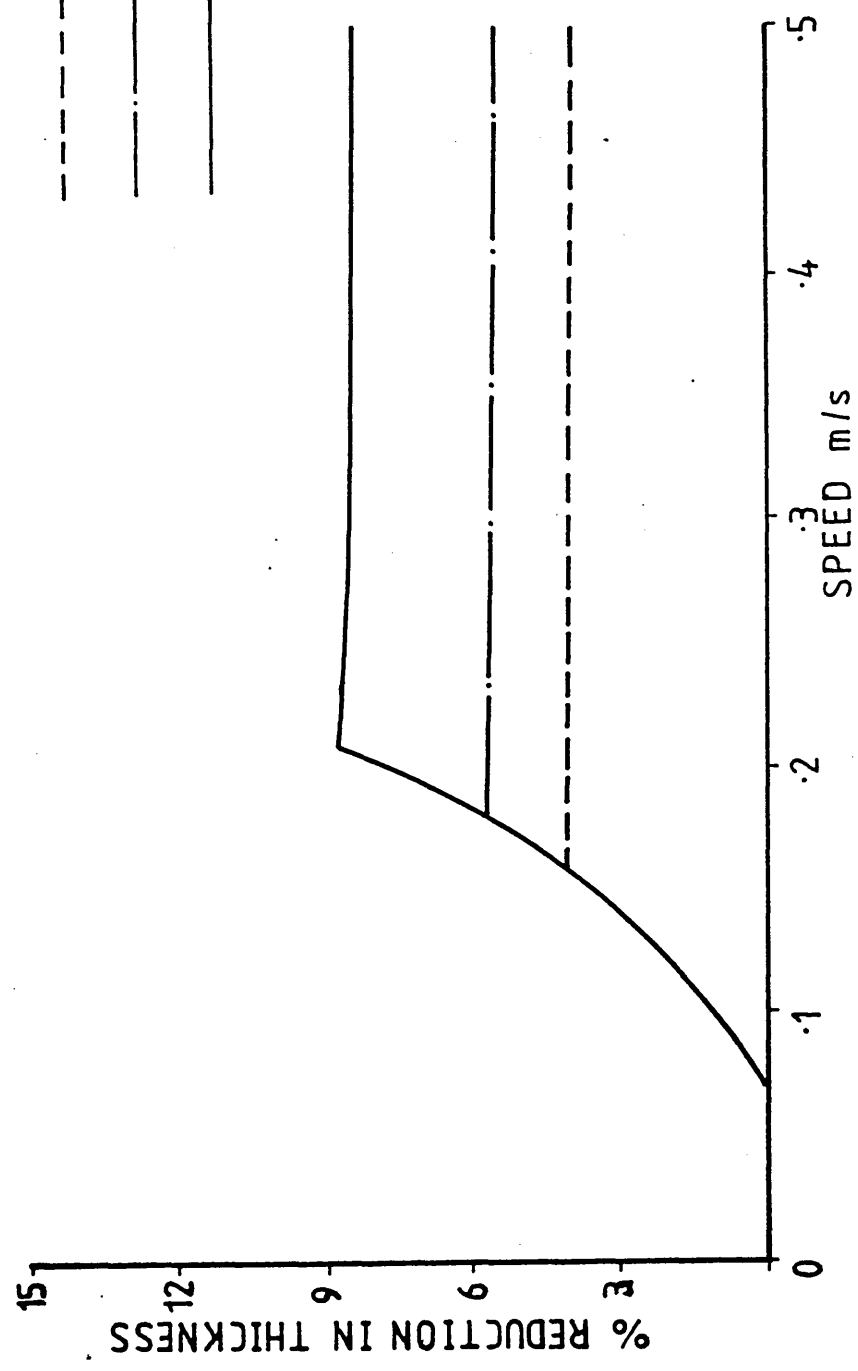


FIG 106: THEORETICAL EFFECT OF CRITICAL SHEAR STRESS ON PERCENTAGE REDUCTION IN THICKNESS

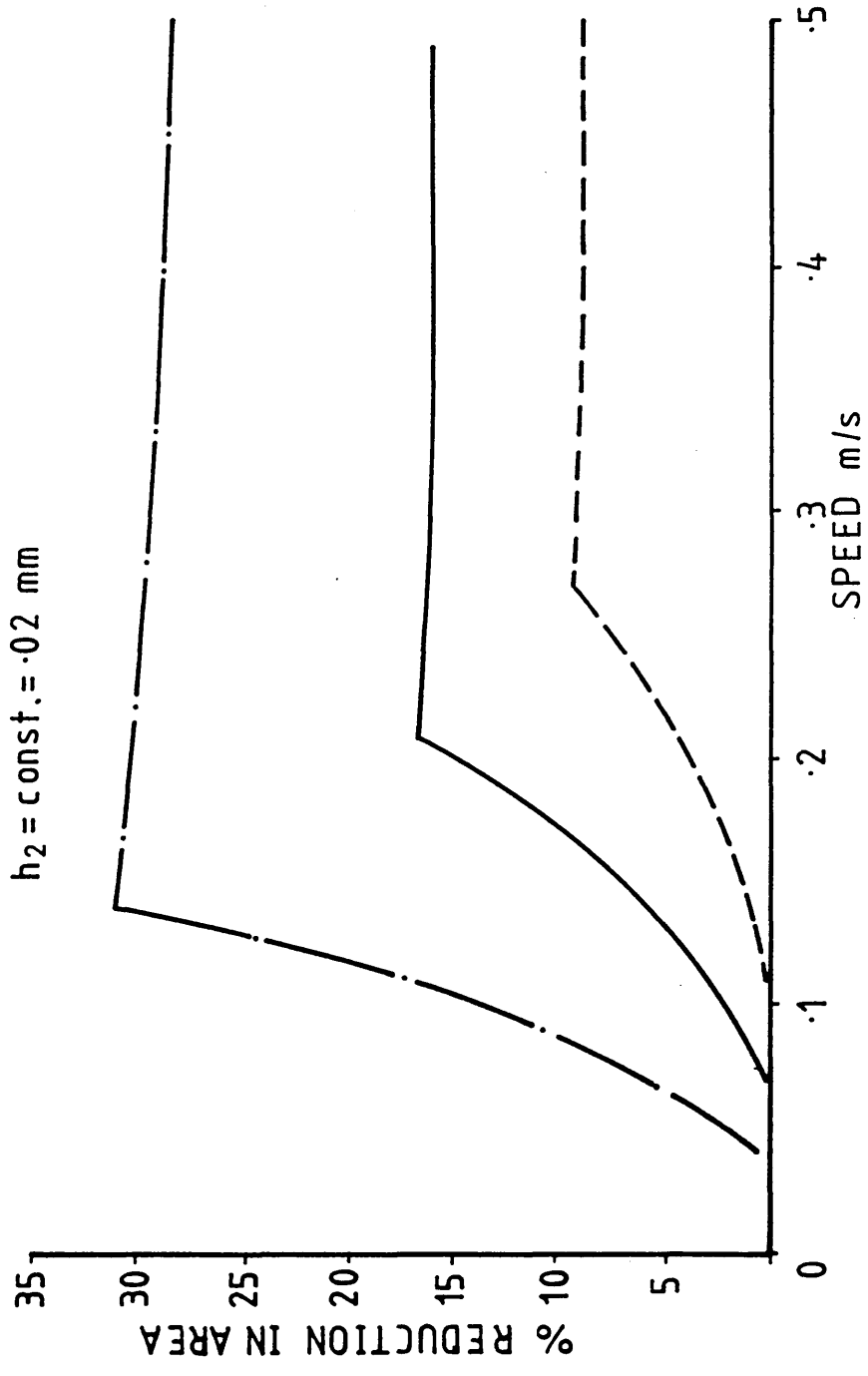


FIG 107: THEORETICAL EFFECT OF GAP RATIO ON PERCENTAGE REDUCTION IN AREA

RL
 --- 5.65
 --- 5
 --- 4.33

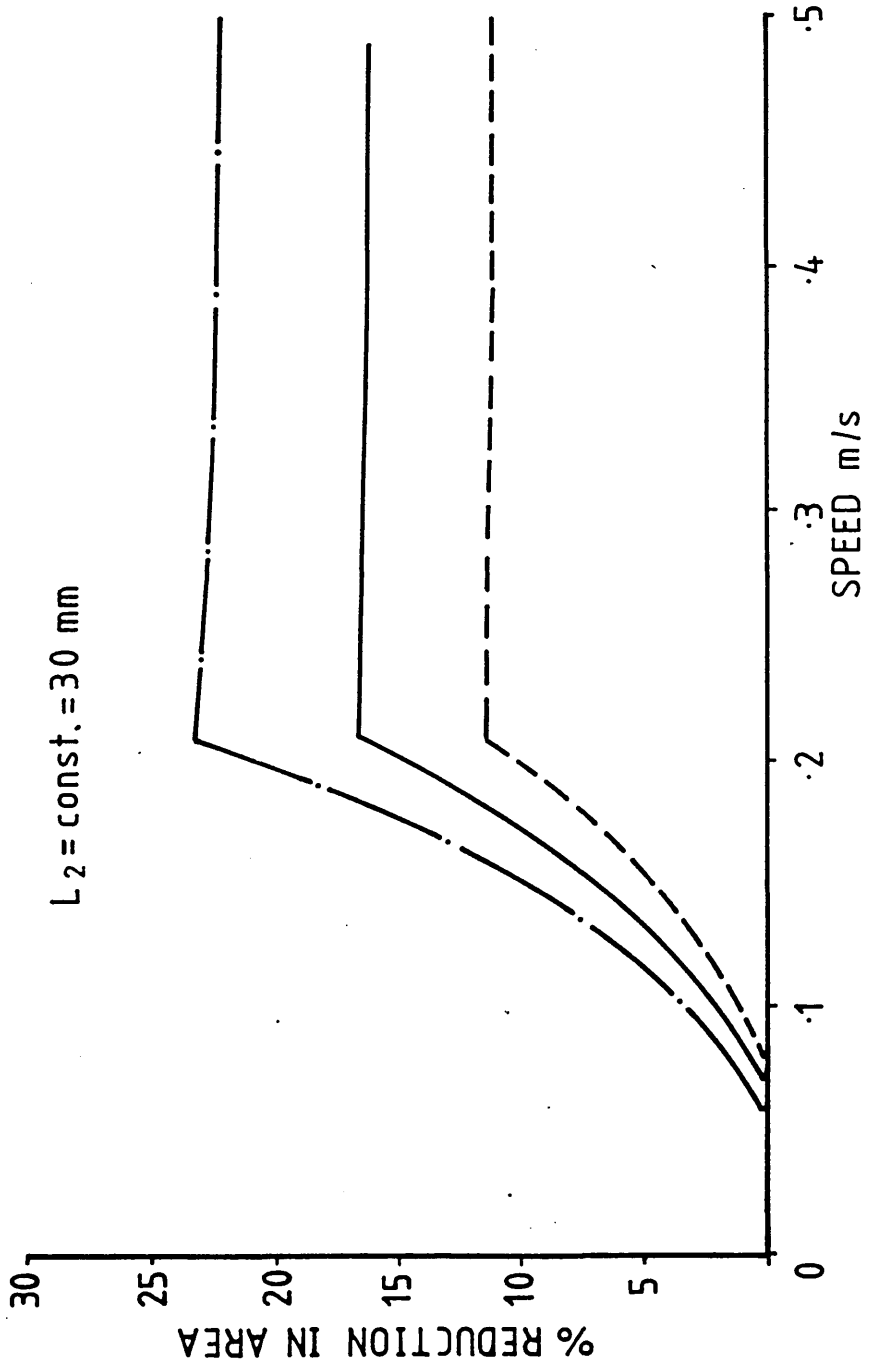


FIG 108: THEORETICAL EFFECT OF LENGTH RATIO ON PERCENTAGE REDUCTION IN AREA

Y_0 — 50 MNm^{-2}
 — 75 MNm^{-2}
 - - - 100 MNm^{-2}

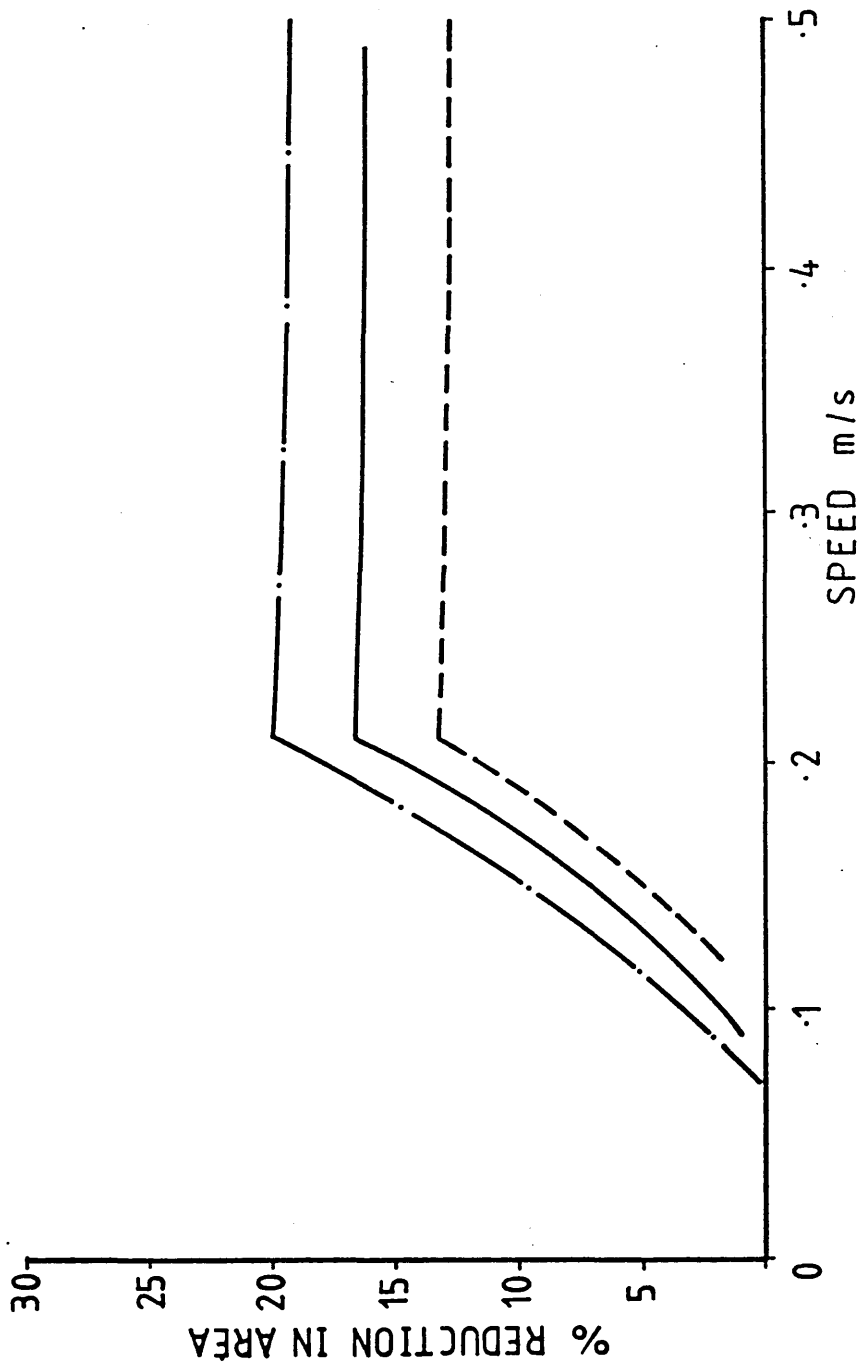


FIG 109: THEORETICAL EFFECT OF INITIAL YIELD STRESS ON PERCENTAGE REDUCTION IN AREA

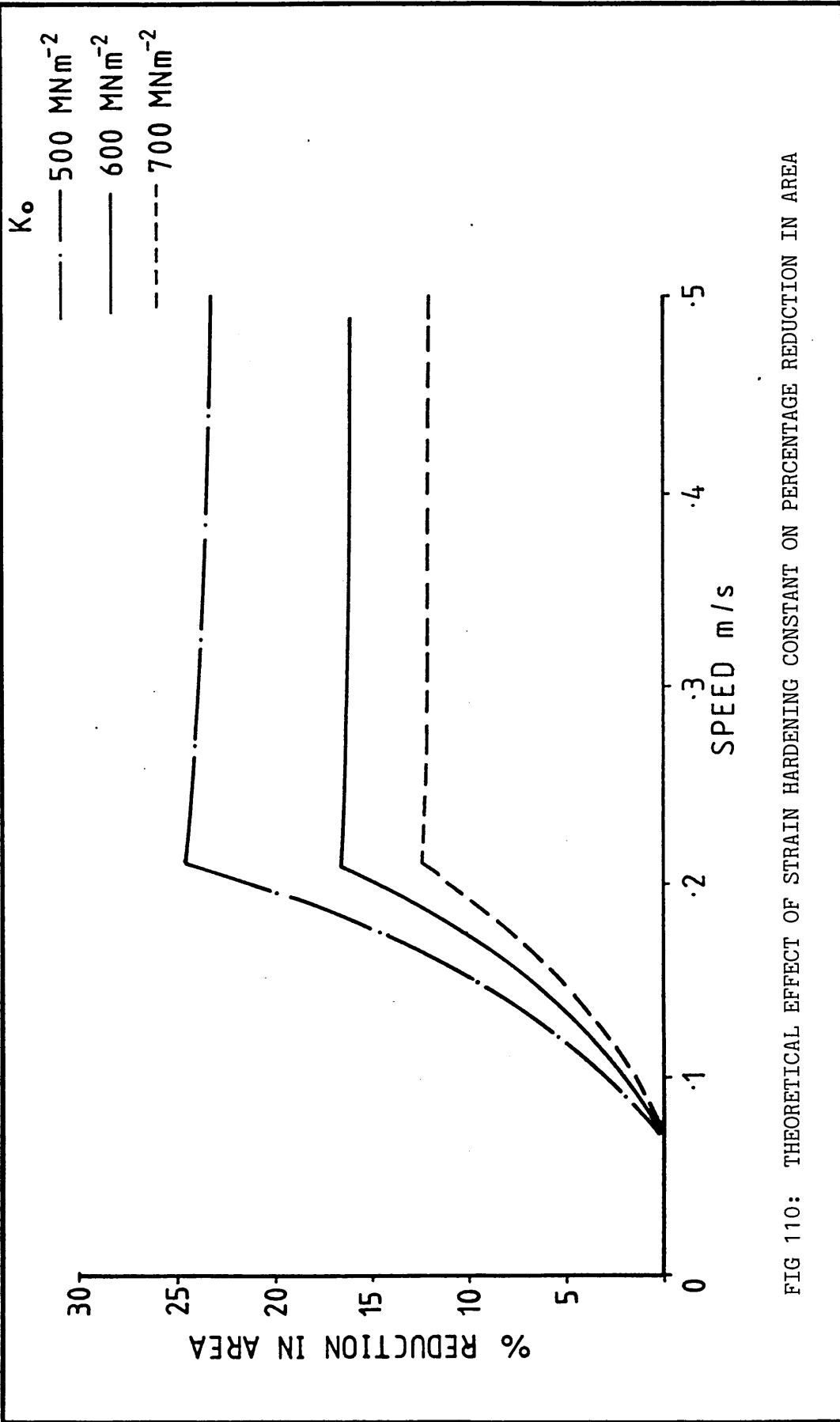


FIG 110: THEORETICAL EFFECT OF STRAIN HARDENING CONSTANT ON PERCENTAGE REDUCTION IN AREA

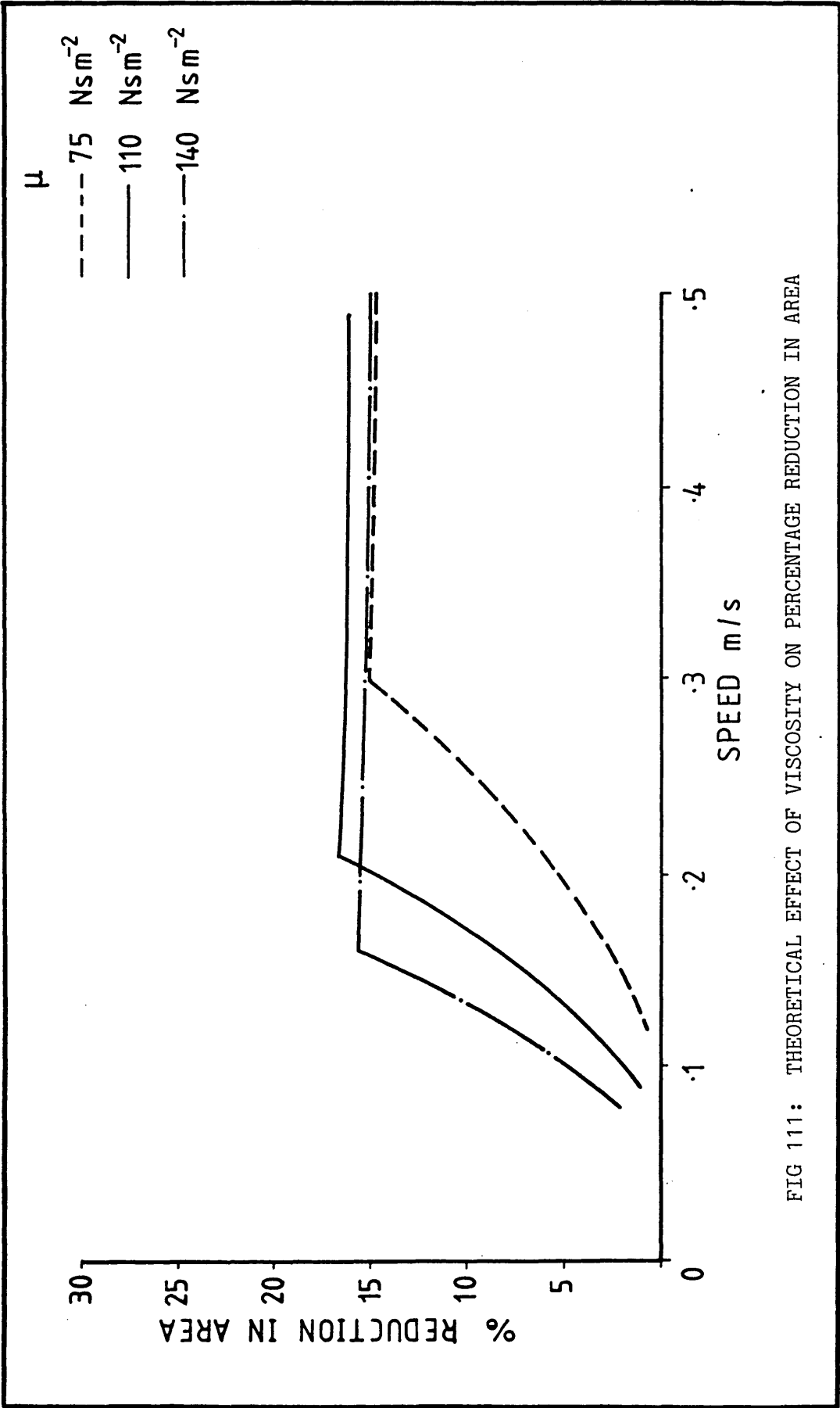


FIG 111: THEORETICAL EFFECT OF VISCOSITY ON PERCENTAGE REDUCTION IN AREA

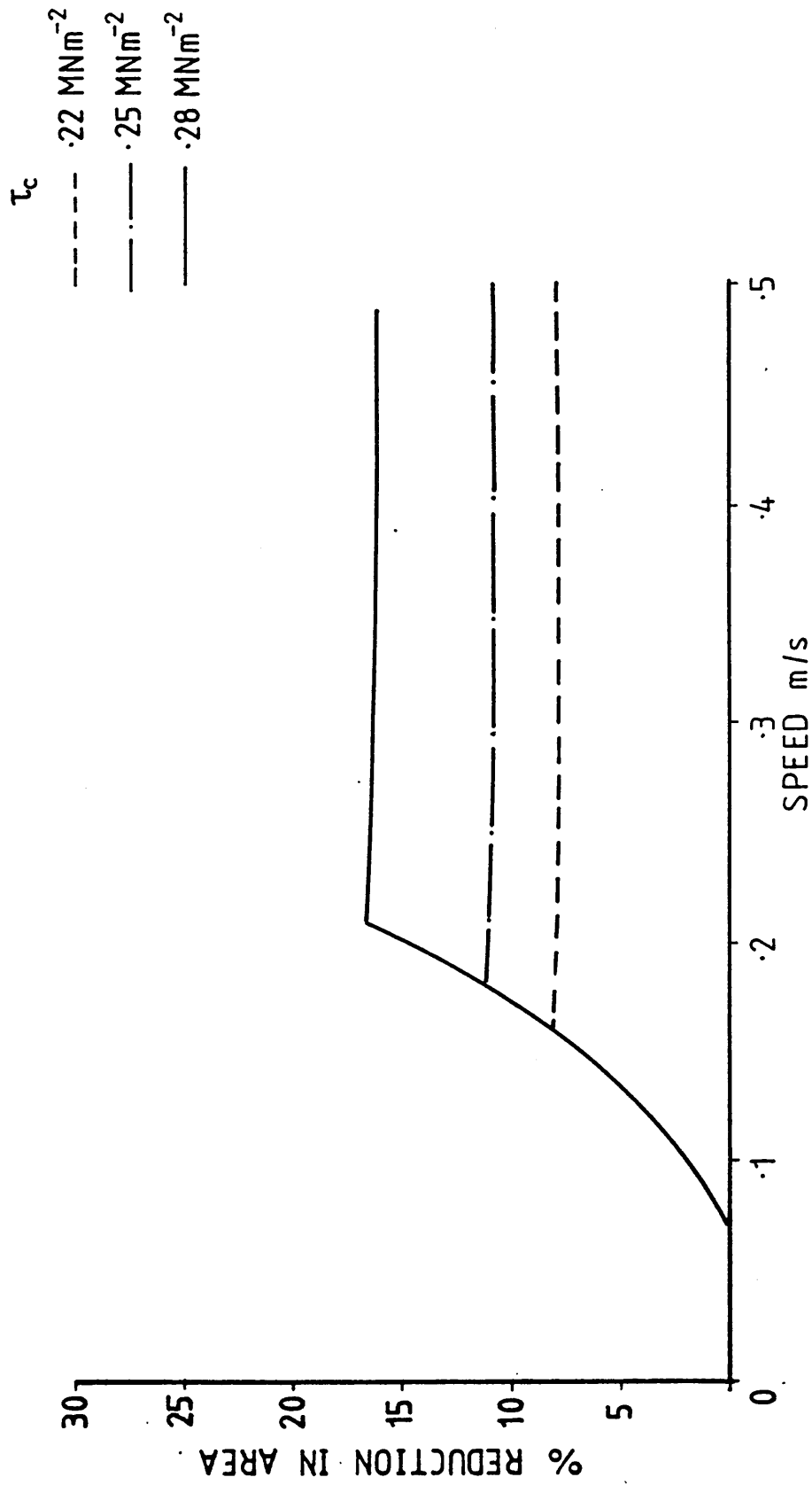


FIG 112: THEORETICAL EFFECT OF CRITICAL SHEAR STRESS ON PERCENTAGE REDUCTION IN AREA

$h_2 = \text{const.} = .02 \text{ mm}$

Rh
— · — 10
— 15
- - - 20

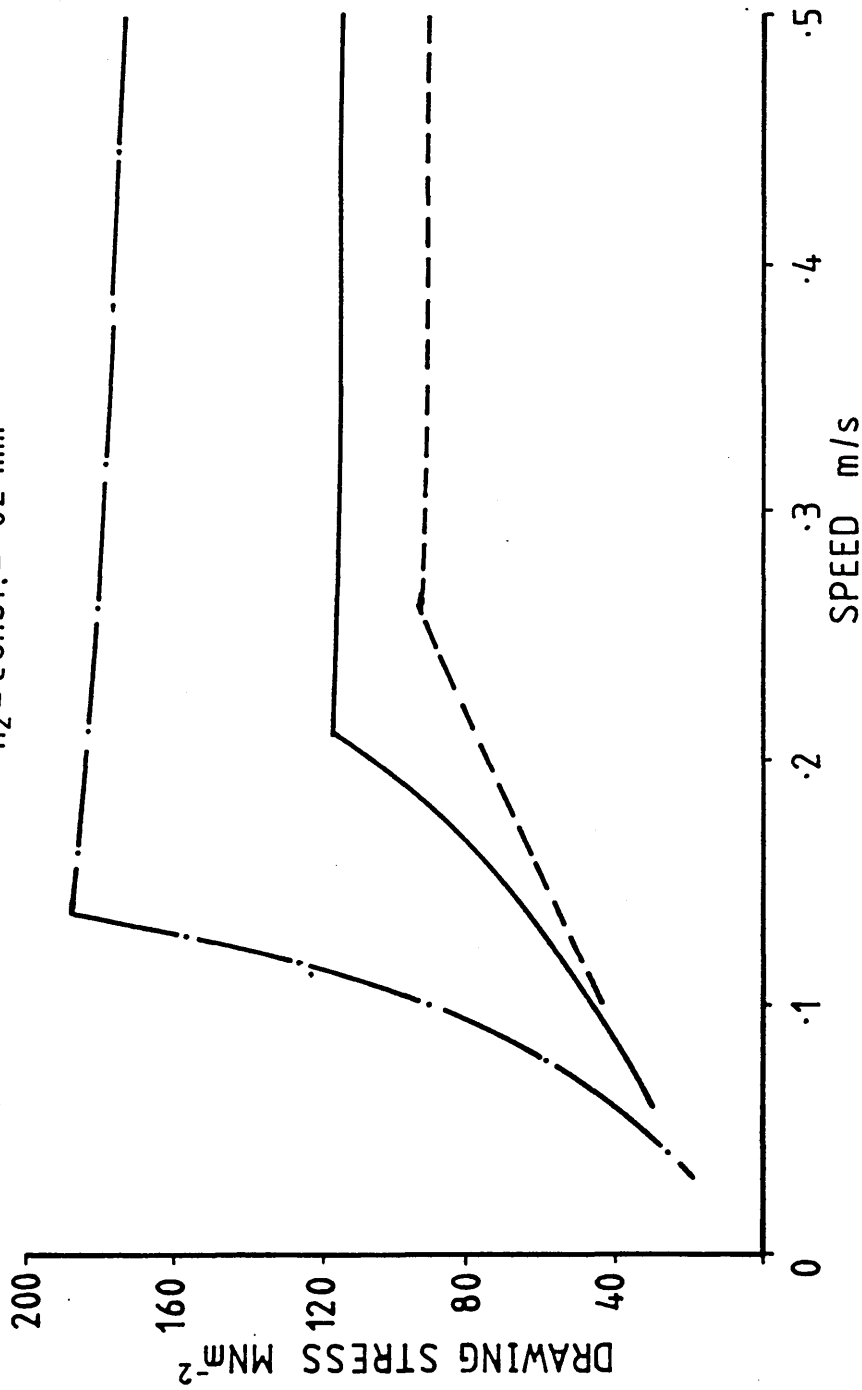


FIG 113: THEORETICAL EFFECT OF GAP RATIO ON DRAWING STRESS

$L_2 = \text{const.} = 30 \text{ mm}$

RL
— 5.65
— 5
- - - 4.33

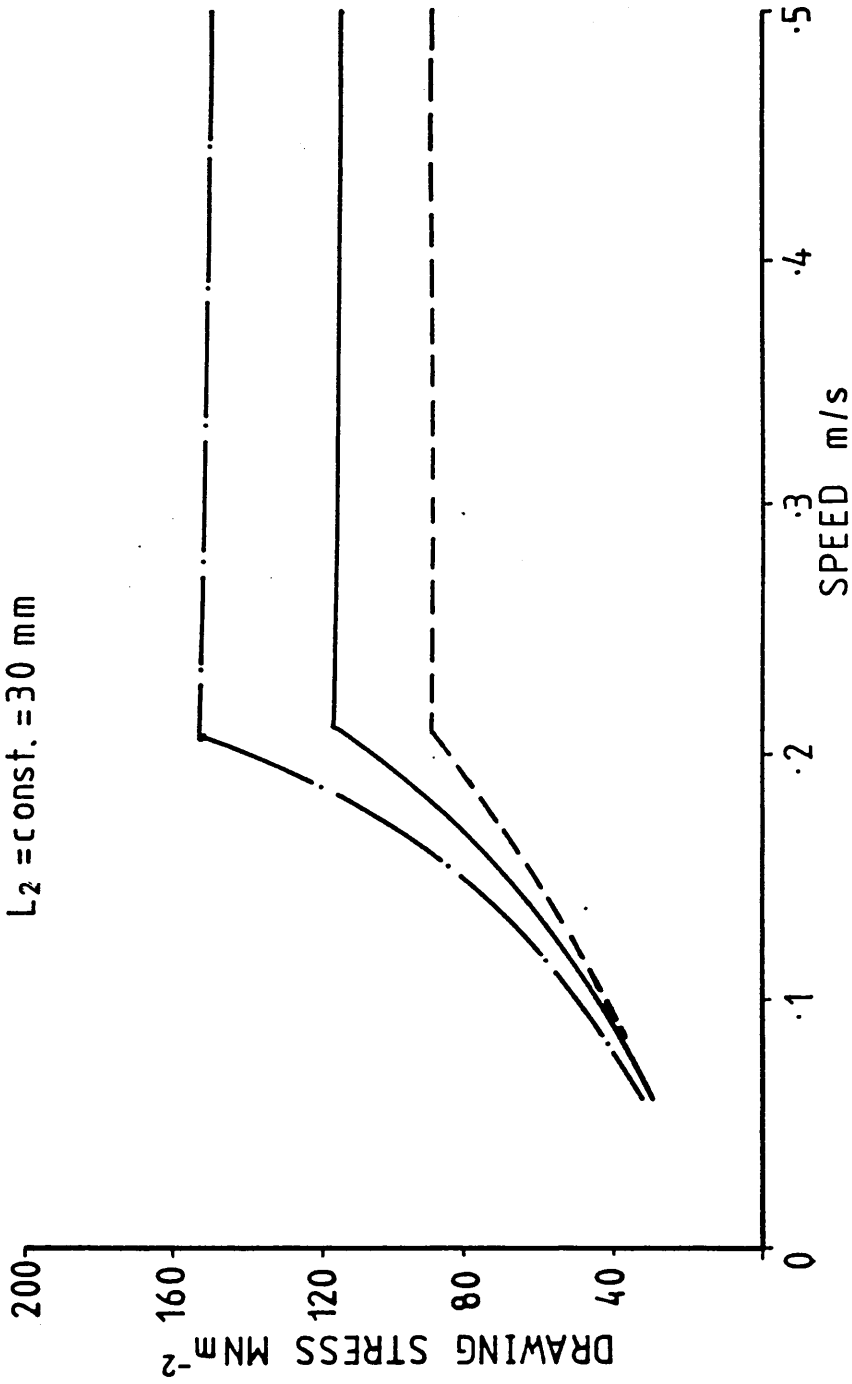


FIG 114: THEORETICAL EFFECT OF LENGTH RATIO ON DRAWING STRESS

μ
 --- 75 Nsm^{-2}
 — 110 Nsm^{-2}
 - · - 140 Nsm^{-2}

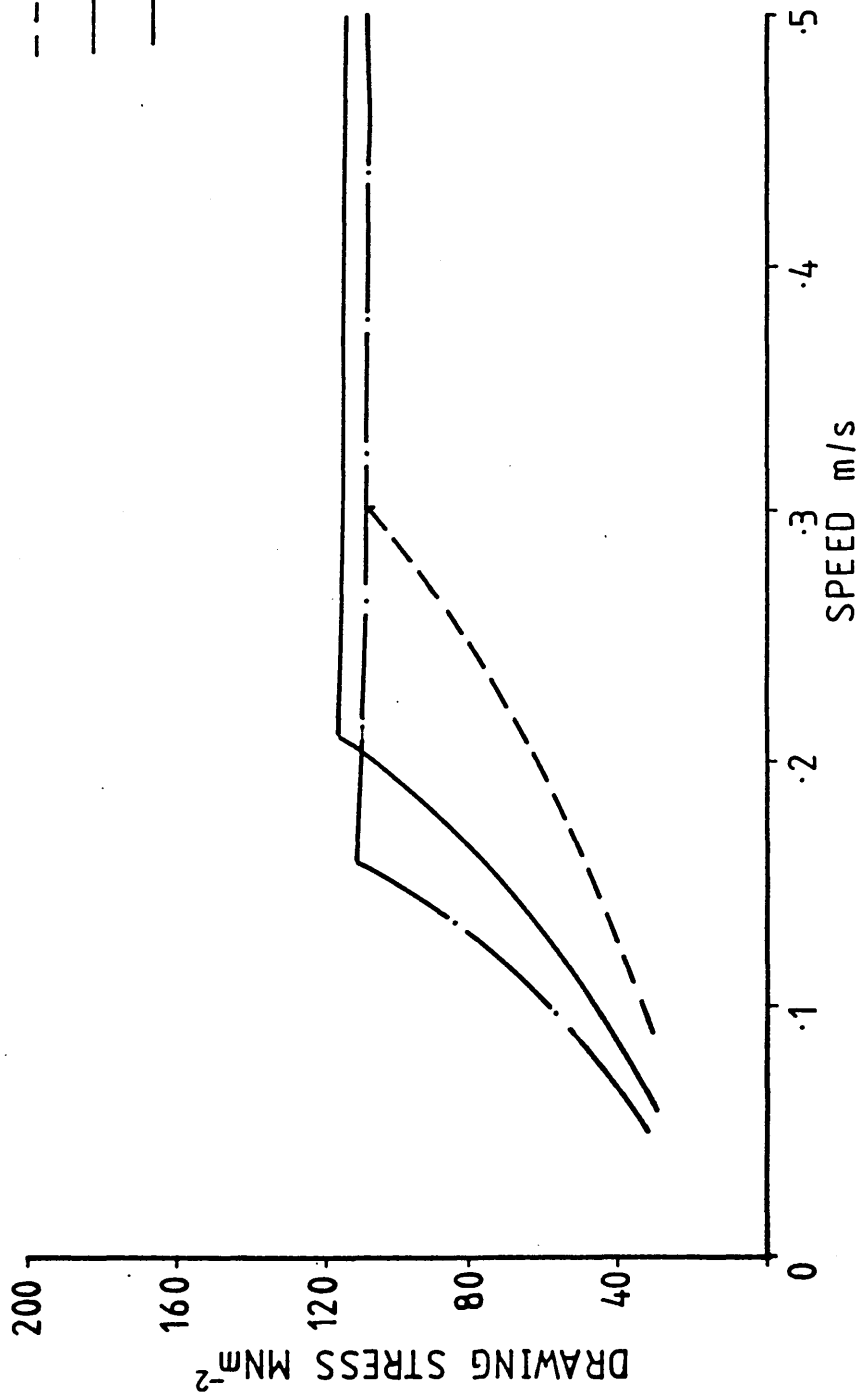


FIG 115: THEORETICAL EFFECT OF VISCOSITY ON DRAWING STRESS

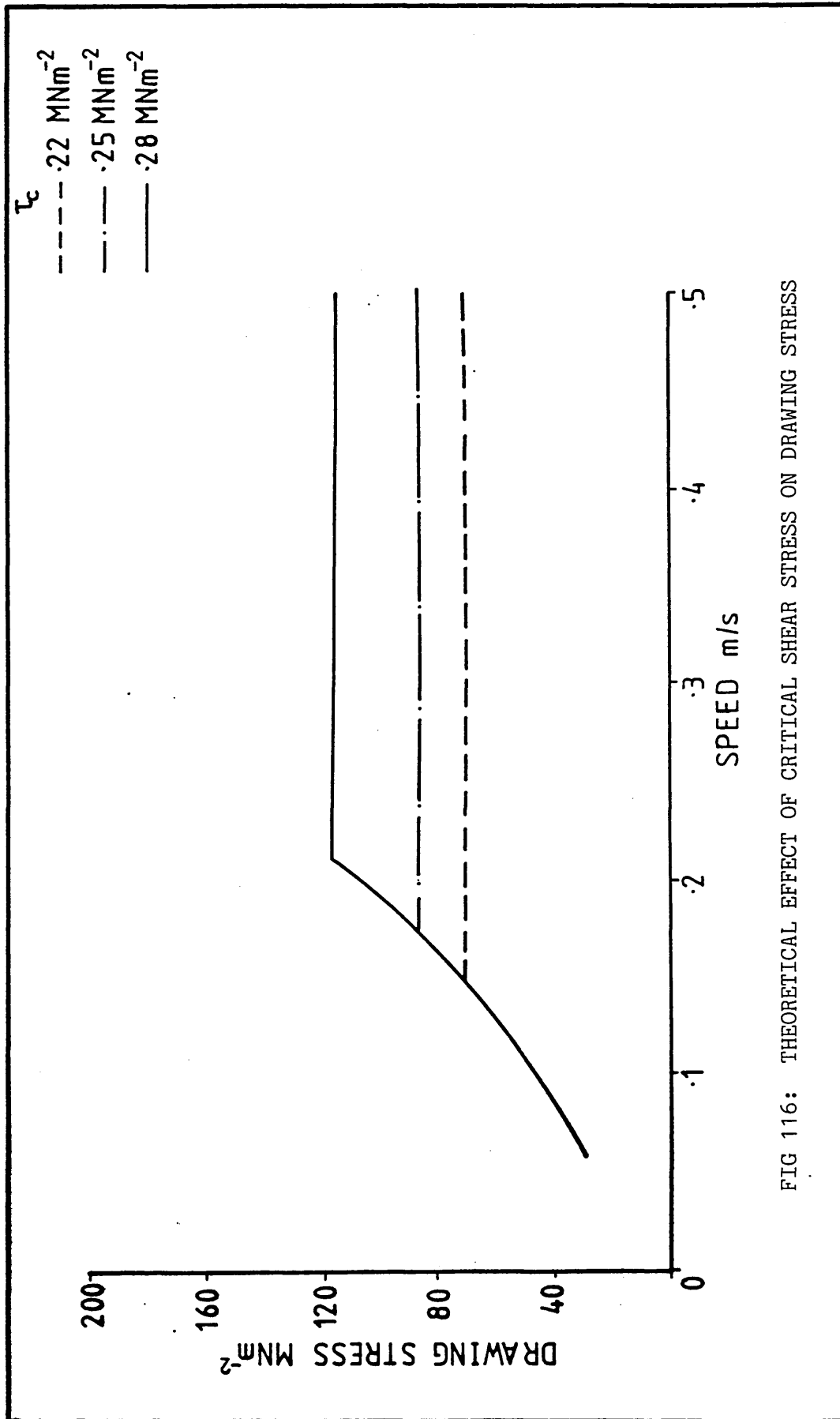


FIG 116: THEORETICAL EFFECT OF CRITICAL SHEAR STRESS ON DRAWING STRESS

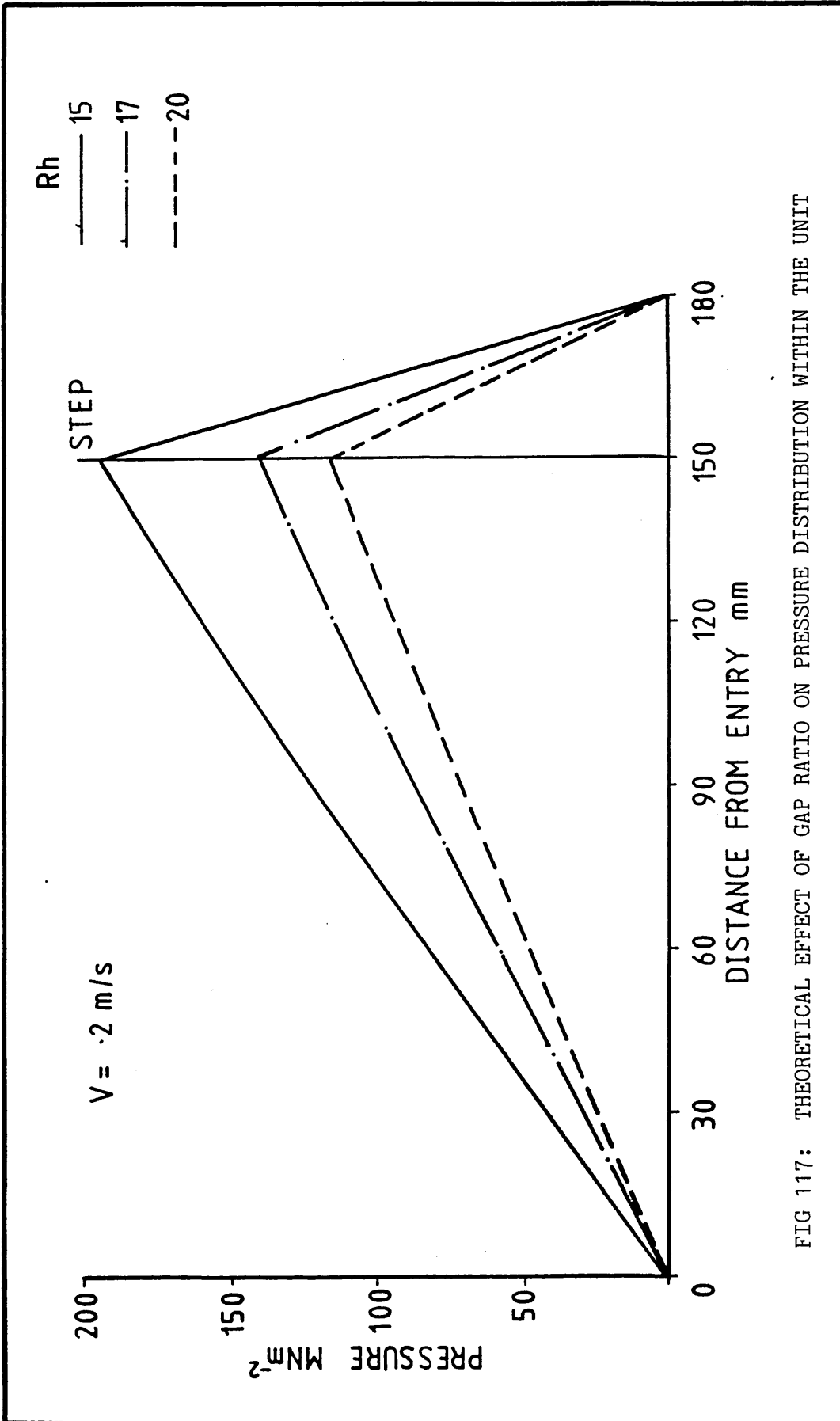


FIG 117: THEORETICAL EFFECT OF GAP RATIO ON PRESSURE DISTRIBUTION WITHIN THE UNIT

V
 --- .15 m/s
 — .2 m/s

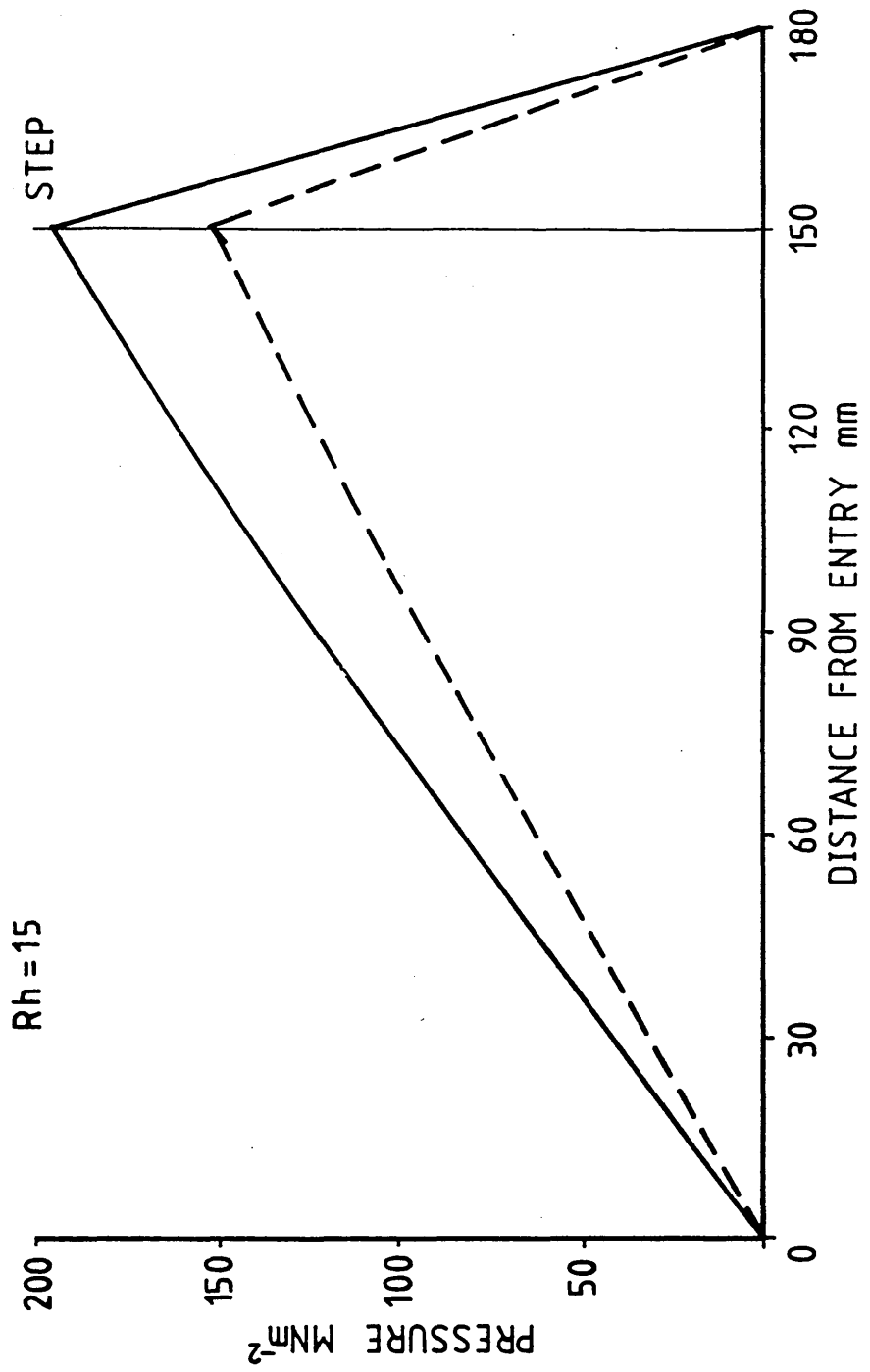


FIG 118: THEORETICAL EFFECT OF DRAWING SPEED ON PRESSURE DISTRIBUTION WITHIN THE UNIT

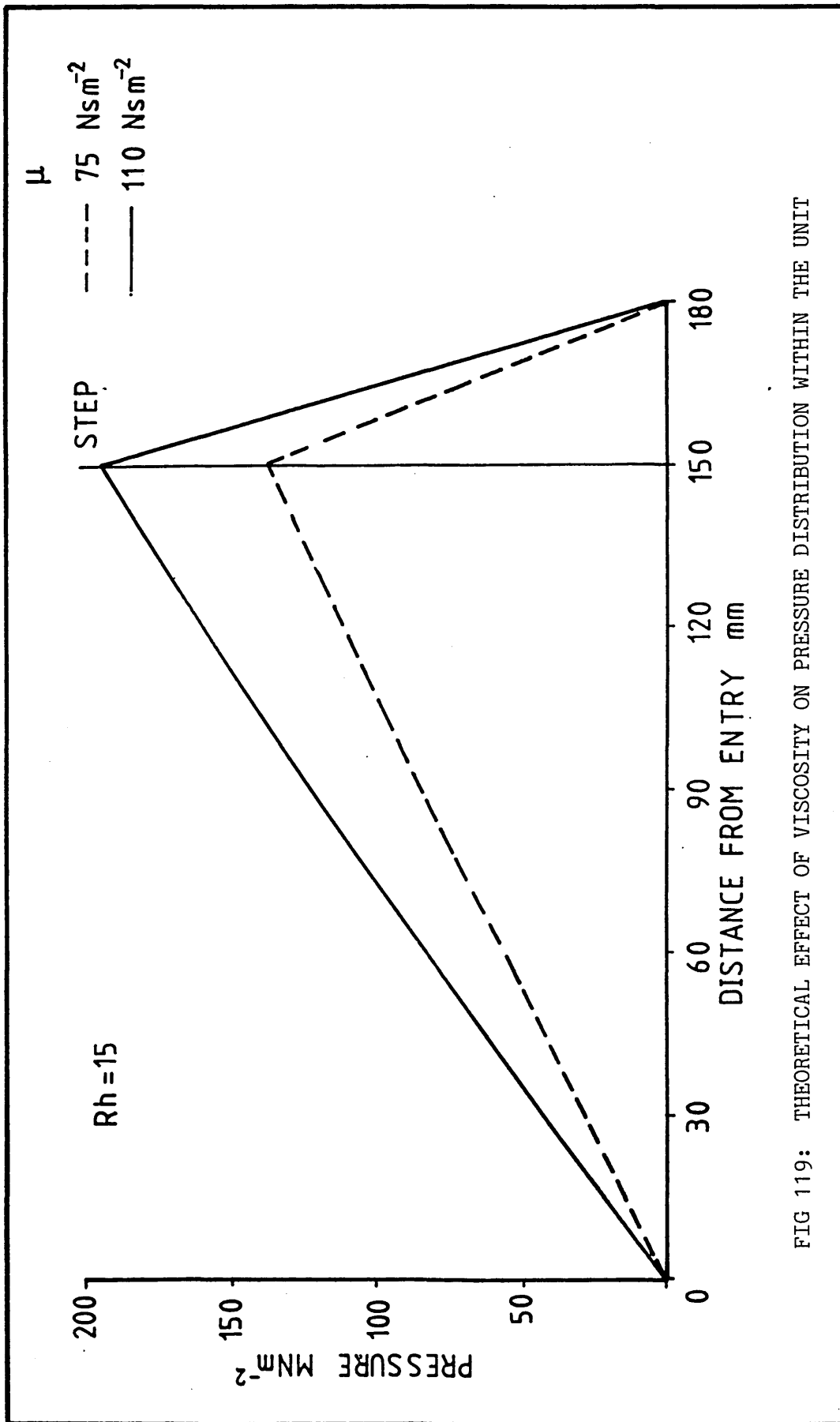


FIG 119: THEORETICAL EFFECT OF VISCOSITY ON PRESSURE DISTRIBUTION WITHIN THE UNIT

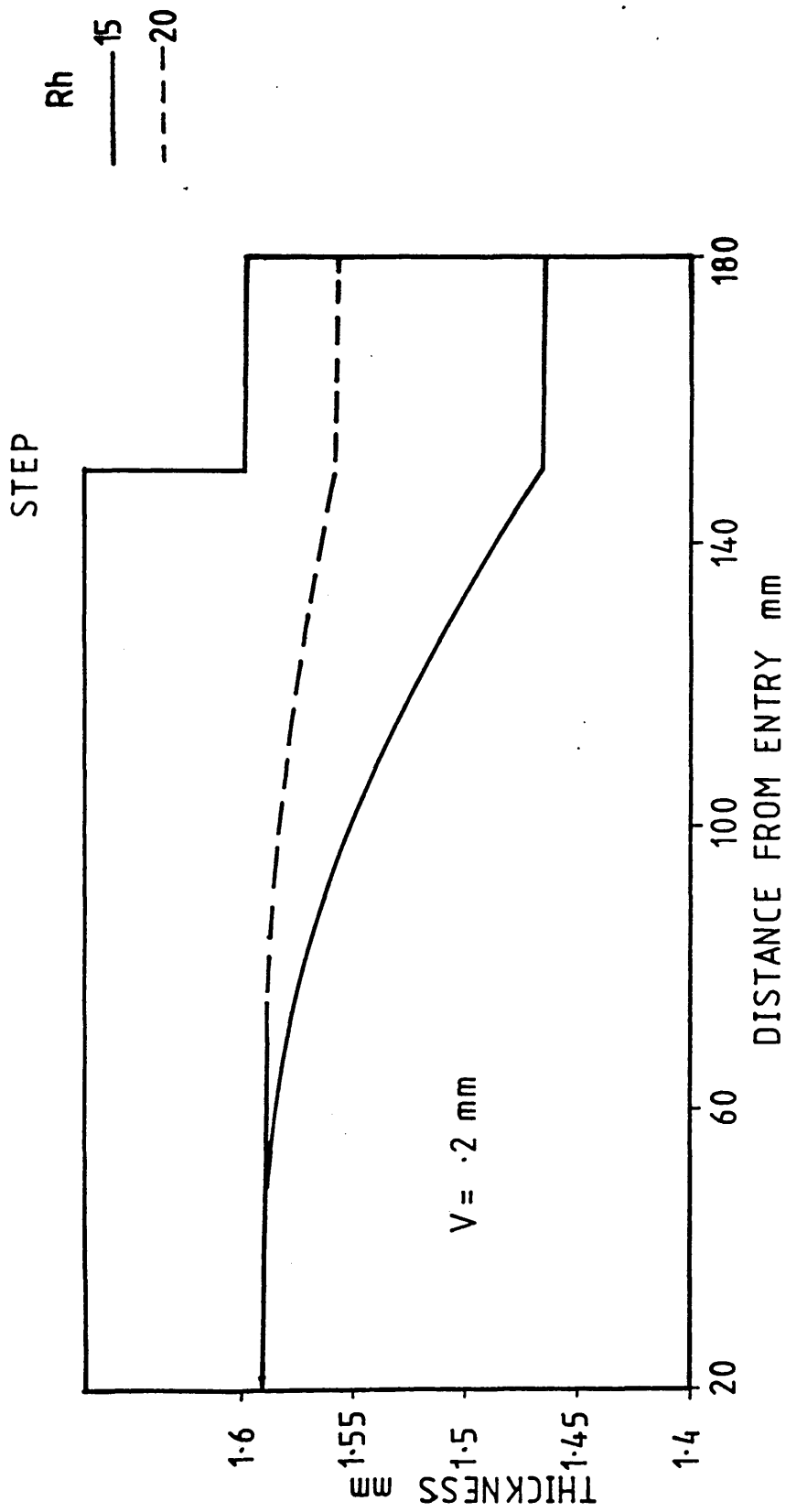


FIG 120: THEORETICALLY CALCULATED DEFORMATION PROFILES FOR DIFFERENT GAP RATIOS

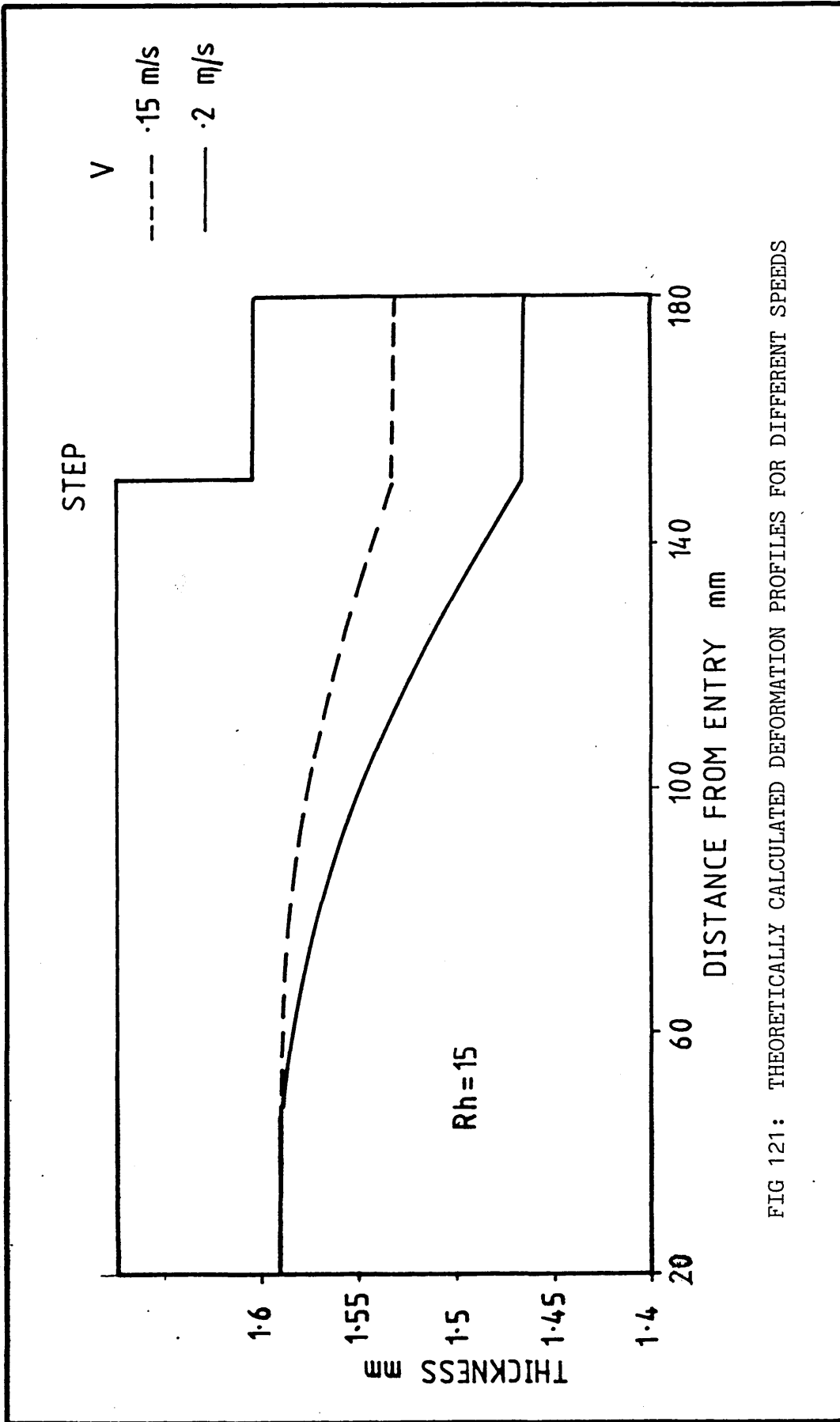


FIG 121: THEORETICALLY CALCULATED DEFORMATION PROFILES FOR DIFFERENT SPEEDS

CHAPTER 6

NON-NEWTONIAN ANALYSIS

6.1 Introduction

In the present work, polymers are used as a pressure medium. These are non-Newtonian in behaviour and their rheological behaviour is dependent upon many factors as discussed in Chapter 3. An analysis assuming a Newtonian fluid has been developed in Chapter 5. In this chapter a theoretical analysis of the process is presented, utilising a non-linear empirical expression relating shear stress and rate of shear. The relationship was suggested by Rabinowitsch (61) for a non-Newtonian, shear thinning viscous fluid flow and is given in the form;

$$\tau + K\tau^3 = \mu \frac{\partial v}{\partial y} \quad (6.1)$$

The analysis has been carried out incorporating the condition of slip at the interface of the polymer melt and the strip, thus giving a limiting shear stress. The strain hardening and strain rate sensitivity of the strip material has also been included in the analysis. The assumptions described in Section (5.2) have been used to establish the different equations.

6.2 Determination of the Maximum Pressure and the Shear Stress Prior to Deformation

The relationship between the pressure and shear stress in the inlet zone for Section A is given by the equilibrium of forces;

$$\left(\frac{\partial P}{\partial x}\right) = \left(\frac{\partial \tau}{\partial y}\right)$$

Integrating w.r.t.y

$$\tau = \left(\frac{\partial P}{\partial x}\right)y + C_7$$

Applying the boundary condition that at $y = 0$,

$$\tau = \tau_1$$

$$C_7 = \tau_1$$

$$\tau = P_1' y + \tau_1 \quad (6.2)$$

where P_1' is pressure gradient.

Substituting the value of τ from equation (6.2) into equation (6.1) gives,

$$P_1' y + \tau_1 + K(P_1' y + \tau_1)^3 = \mu \left(\frac{\partial v}{\partial y} \right)$$

$$\mu \left(\frac{\partial v}{\partial y} \right) = P_1' y + \tau_1 + K(P_1'^3 y^3 + 3P_1'^2 \tau_1 y^2 + 3P_1' \tau_1^2 y + \tau_1^3)$$

Integrating the above equation w.r.t. y , noting that μ and P_1' remain constant through the thickness of the film,

$$\mu v = \frac{P_1' y^2}{2} + \tau_1 y + K \left(\frac{P_1'^3 y^4}{4} + \frac{3P_1'^2 \tau_1 y^3}{3} + \frac{3P_1' \tau_1^2 y^2}{2} + \tau_1^3 y \right) + C_8$$

$$v = \frac{P_1' y^2}{2\mu} + \frac{\tau_1 y}{\mu} + \frac{K}{\mu} \left(\frac{P_1'^3 y^4}{4} + P_1'^2 \tau_1 y^3 + \frac{3P_1' \tau_1^2 y^2}{2} + \tau_1^3 y \right) + C_9$$

Condition of No Slip

Applying the boundary conditions that

$$\text{At } y = 0, v = V; \quad y = h_1, v = 0;$$

$$v = \frac{P_1' y^2}{2\mu} + \frac{\tau_1 y}{\mu} + \frac{K}{\mu} \left(\frac{1}{4} P_1'^3 y^4 + P_1'^2 \tau_1 y^3 + \frac{3}{2} P_1' \tau_1^2 y^2 + \tau_1^3 y \right) + V \quad (6.3)$$

$$\therefore \frac{1}{2} P_1' h_1^2 + \tau_1 h_1 + K \left(\frac{1}{4} P_1'^3 h_1^4 + P_1'^2 \tau_1 h_1^3 + \frac{3}{2} P_1' \tau_1^2 h_1^2 + \tau_1^3 h_1 \right)$$

$$+ \mu V = 0$$

$$\text{or } \frac{1}{2K} P_1' h_1 + \frac{\tau_1}{K} + \left(\frac{1}{4} P_1'^3 h_1^3 + P_1'^2 \tau_1 h_1^2 + \frac{3}{2} P_1' \tau_1^2 h_1 + \tau_1^3 \right) + \frac{\mu V}{K h_1} = 0$$

$$\text{or } \tau_1^3 + \left(\frac{3}{2} P_1' h_1 \right) \tau_1^2 + \left(\frac{1}{K} + P_1'^2 h_1^2 \right) \tau_1 + \left(\frac{1}{2K} P_1' h_1 + \frac{1}{4} P_1'^3 h_1^3 + \frac{\mu V}{K h_1} \right) = 0$$

$$\text{Let } J_1 = \frac{3}{2} P_1' h_1$$

$$J_2 = \frac{1}{K} + P_1'^2 h_1^2$$

$$J_3 = \frac{1}{2K} P_1' h_1 + \frac{1}{4} P_1'^3 h_1^3 + \frac{\mu V}{K h_1}$$

Therefore

$$\tau_1^3 + J_1\tau_1^2 + J_2\tau_1 + J_3 = 0 \quad (6.4)$$

If the transformation

$$\tau_1 = \phi_1 - \frac{J_1}{3}$$

is introduced in equation (6.4)

$$\left(\phi_1 - \frac{J_1}{3}\right)^3 + J_1\left(\phi_1 - \frac{J_1}{3}\right)^2 + J_2\left(\phi_1 - \frac{J_1}{3}\right) + J_3 = 0$$

Simplification of the above equation gives

$$\phi_1^3 + \left(J_2 - \frac{J_1^2}{3}\right)\phi_1 + \left(J_3 + \frac{2J_1^3}{27} - \frac{J_1J_2}{3}\right) = 0 \quad (6.5)$$

Substituting values of J_1 , J_2 , and J_3 into equation (6.5),

$$\phi_1^3 + \left(\frac{1}{K} + \frac{1}{4}P_1^2h_1^2\right)\phi_1 + \frac{\mu V}{Kh_1} = 0$$

Define

$$D_1 = \frac{1}{K} + \frac{1}{4}P_1^2h_1^2$$

$$D_2 = \frac{\mu V}{Kh_1}$$

$$\therefore \phi_1^3 + D_1\phi_1 + D_2 = 0 \quad (6.6)$$

Equation (6.6) is a cubic equation, which has been solved by using Cardan's formula⁽⁶²⁾ and the real root is given by;

$$\phi_1 = \left[-\frac{D_2}{2} + \left(\frac{D_2^2}{4} + \frac{D_1^3}{27}\right)^{\frac{1}{2}}\right]^{\frac{1}{3}} + \left[-\frac{D_2}{2} - \left(\frac{D_2^2}{4} + \frac{D_1^3}{27}\right)^{\frac{1}{2}}\right]^{\frac{1}{3}}$$

Substituting values of D_1 , D_2 , ϕ_1 and J_1 we get,

$$\tau_1 + \frac{P_1h_1}{2} = \left[-\frac{\mu V}{2Kh_1} + \left\{\frac{\mu^2V^2}{4K^2h_1^2} + \frac{1}{27}\left(\frac{1}{K} + \frac{1}{4}P_1^2h_1^2\right)^3\right\}^{\frac{1}{2}}\right]^{\frac{1}{3}} +$$

$$\left[-\frac{\mu V}{2Kh_1} - \left\{\frac{\mu^2V^2}{4K^2h_1^2} + \frac{1}{27}\left(\frac{1}{K} + \frac{1}{4}P_1^2h_1^2\right)^3\right\}^{\frac{1}{2}}\right]^{\frac{1}{3}}$$

$$\therefore \tau_1 = \left[-\frac{\mu V}{2Kh_1} + \left\{\frac{\mu^2V^2}{4K^2h_1^2} + \frac{1}{27}\left(\frac{1}{K} + \frac{1}{4}P_1^2h_1^2\right)^3\right\}^{\frac{1}{2}}\right]^{\frac{1}{3}} +$$

$$\left[-\frac{\mu V}{2Kh_1} - \left\{\frac{\mu^2V^2}{4K^2h_1^2} + \frac{1}{27}\left(\frac{1}{K} + \frac{1}{4}P_1^2h_1^2\right)^3\right\}^{\frac{1}{2}}\right]^{\frac{1}{3}} - \frac{1}{2}P_1h_1 \quad (6.7)$$

Equation (6.7) enables the shear stress in the inlet zone in Section A to be calculated for the condition when P_1' is defined.

The flow of polymer melt in the inlet zone is given by,

$$Q_1 = \int_0^{h_1} v \, dy$$

Substituting the value of v from equation (6.3)

$$Q_1 = \int_0^{h_1} \left[\frac{P_1' y^2}{2\mu} + \frac{\tau_1 y}{\mu} + \frac{K}{\mu} \left(\frac{1}{4} P_1'^3 y^4 + P_1'^2 y^3 \tau_1 + \frac{3}{2} P_1' \tau_1^2 y^2 + \tau_1^3 y \right) + v \right] dy$$

Integrating,

$$Q_1 = \frac{P_1' h_1^3}{6\mu} + \frac{\tau_1 h_1^2}{2\mu} + \frac{K}{\mu} \left(\frac{1}{20} P_1'^3 h_1^5 + \frac{1}{4} P_1'^2 h_1^4 \tau_1 + \frac{1}{2} P_1' \tau_1^2 h_1^3 + \frac{1}{2} \tau_1^3 h_1^2 \right) + v h_1 \quad (6.8)$$

Now from steady state flow we have

$$\left(\frac{\partial P}{\partial x} \right)_1 = P_1' = \text{Constant}$$

For a stepped configuration the pressure has its maximum value at the step

$$\left(\frac{\partial P}{\partial x} \right)_1 = P_1' = \frac{P_m}{L_1} \quad (6.9)$$

Where P_m is maximum pressure at the step which is still to be determined.

Now, for the exit zone in Section A,

$$\left(\frac{\partial P}{\partial x} \right) = - \left(\frac{\partial \tau}{\partial y} \right)$$

Integrating,

$$\tau = - P_2' y + \tau_2 \quad (6.10)$$

Where τ_2 is the shear stress at the surface of the strip at $y = 0$.

Substituting the value of τ from equation (6.10) into equation (6.1),

$$\mu \left(\frac{dv}{dy} \right) = - P_2' y + \tau_2 + K \left(- P_2'^3 y^3 + \tau_2^3 + 3 P_2'^2 y^2 \tau_2 - 3 \tau_2^2 P_2' y \right)$$

Integrating,

$$v = - \frac{P_2' y^2}{2\mu} + \frac{\tau_2 y}{\mu} + \frac{K}{\mu} \left(- \frac{1}{4} P_2'^3 y^4 + \tau_2^3 y + P_2'^2 y^3 \tau_2 - \frac{3}{2} P_2' \tau_2^2 y^2 \right) + C_{10}$$

Applying the boundary conditions that

At $y = 0$, $v = V$ and at $y = h_2$, $v = 0$

$$v = -\frac{P_2' y^2}{2\mu} + \frac{\tau_2 y}{\mu} + \frac{K}{\mu} \left(-\frac{1}{4} P_2'^3 y^4 + \tau_2^3 y + P_2'^2 y^3 \tau_2 - \frac{3}{2} P_2' y^2 \tau_2^2 \right) + V \quad (6.11)$$

And $\tau_2^3 + \left(-\frac{3}{2} P_2' h_2 \right) \tau_2^2 + \left(\frac{1}{K} + P_2'^2 h_2^2 \right) \tau_2 + \left(\frac{\mu V}{K h_2} - \frac{1}{4} P_2'^3 h_2^3 - \frac{P_2' h_2}{2K} \right)$

= 0

Let

$$J_1' = -\frac{3}{2} P_2' h_2$$

$$J_2' = \frac{1}{K} + P_2'^2 h_2^2$$

$$J_3' = \frac{\mu V}{K h_2} - \frac{1}{4} P_2'^3 h_2^3 - \frac{P_2' h_2}{2K}$$

$\therefore \tau_2^3 + J_1' \tau_2^2 + J_2' \tau_2 + J_3' = 0$

Again introducing transformation

$$\tau_2 = \phi_2 - \frac{J_1'}{3} \quad \text{gives,}$$

$$\phi_2^3 + D_1' \phi_2 + D_2' = 0 \quad (6.13)$$

where

$$D_1' = \frac{1}{K} + \frac{1}{4} P_2'^2 h_2^2$$

and $D_2' = \frac{\mu V}{K h_2}$

Equation (6.13) can be solved in a similar way to equation (6.6),

the real root being given by,

$$\phi_2 = \left[-\frac{D_2'}{2} + \left(\frac{D_2'^2}{4} + \frac{D_1'^3}{27} \right)^{\frac{1}{2}} \right]^{\frac{1}{3}} + \left[-\frac{D_2'}{2} - \left(\frac{D_2'^2}{4} + \frac{D_1'^3}{27} \right)^{\frac{1}{2}} \right]^{\frac{1}{3}}$$

Substituting values of ϕ_2 , D_1' , D_2' and J_1' we get,

$$\tau_2 = \left[-\frac{\mu V}{2K h_2} + \left\{ \frac{\mu^2 V^2}{4K^2 h_2^2} + \frac{1}{27} \left(\frac{1}{K} + \frac{1}{4} P_2'^2 h_2^2 \right)^3 \right\}^{\frac{1}{2}} \right]^{\frac{1}{3}} + \left[-\frac{\mu V}{2K h_2} - \left\{ \frac{\mu^2 V^2}{4K^2 h_2^2} + \frac{1}{27} \left(\frac{1}{K} + \frac{1}{4} P_2'^2 h_2^2 \right)^3 \right\}^{\frac{1}{2}} \right]^{\frac{1}{3}} + \frac{P_2' h_2}{2} \quad (6.14)$$

Equation (6.14) gives the shear stress on the surface of strip in the exit zone. The flow of polymer melt in the exit zone for Section A is,

$$Q_2 = \int_0^{h_2} v \, dy$$

Substituting the value of v from equation (6.11) integration gives

$$Q_2 = -\frac{P_2' h_2^3}{6\mu} + \frac{\tau_2 h_2^2}{2\mu} + \frac{K}{\mu} \left(-\frac{1}{20} P_2'^3 h_2^5 + \frac{1}{2} \tau_2^3 h_2^2 + \frac{1}{4} P_2'^2 h_2^4 \tau_2 - \frac{1}{2} P_2' h_2^3 \tau_2^2 \right) + V h_2 \quad (6.15)$$

Again for steady state flow

$$P_2' = \left(\frac{\partial P}{\partial x} \right)_2 = \text{Constant}$$

or
$$P_2' = \frac{Pm}{L_2} \quad (6.16)$$

Using the relationship given by equation (5.11), here we assume that

$$\left(\frac{\partial P}{\partial x} \right)_3 = \left(\frac{\partial P}{\partial x} \right)_1$$

$$\therefore \left(\frac{\partial \tau}{\partial z} \right) = \left(\frac{\partial P}{\partial x} \right)_1$$

Integrating w.r.t. z and applying the boundary condition that at

$$z = 0, \tau = \tau_3;$$

$$\tau = P_1' z + \tau_3 \quad (6.17)$$

Substitution of the equation (6.17) into equation (6.1) gives,

$$\mu \left(\frac{\partial v}{\partial z} \right) = P_1' z + \tau_3 + K (P_1'^3 z^3 + 3P_1'^2 z^2 \tau_3 + 3P_1' z \tau_3^2 + \tau_3^3)$$

Integrating,

$$v = \frac{P_1' z^2}{2\mu} + \frac{\tau_3 z}{\mu} + \frac{K}{\mu} \left(\frac{P_1'^3 z^4}{4} + P_1'^2 z^3 \tau_3 + \frac{3}{2} P_1' z^2 \tau_3^2 + \tau_3^3 z \right) + C_{11}$$

Applying boundary condition, at $z = 0, v = V$

$$v = \frac{P_1' z^2}{2\mu} + \frac{\tau_3 z}{\mu} + \frac{K}{\mu} \left(\frac{P_1'^3 z^4}{4} + P_1'^2 z^3 \tau_3 + \frac{3}{2} P_1' z^2 \tau_3^2 + \tau_3^3 z \right) + V \quad (6.18)$$

and applying boundary condition that at $z = h_3, v = 0$

$$\frac{P_1' h_3^2}{2\mu} + \frac{\tau_3 h_3}{\mu} + \frac{K}{\mu} \left(\frac{1}{4} P_1'^3 h_3^4 + P_1'^2 h_3^3 \tau_3 + \frac{3}{2} P_1' h_3^2 \tau_3^2 + \tau_3^3 h_3 \right) + V = 0$$

which on simplification gives

$$\tau_3^3 + J_1'' \tau_3^2 + J_2'' \tau_3 + J_3'' = 0 \quad (6.19)$$

where

$$J_1'' = \frac{3}{2} P_1' h_3$$

$$J_2'' = \frac{1}{K} + P_1'^2 h_3^2$$

$$J_3'' = \frac{1}{2K} P_1' h_3 + \frac{1}{4} P_1'^3 h_3^3 + \frac{\mu V}{K h_3}$$

Using the transformation

$$\tau_3 = \phi_3 - \frac{J_1''}{3}$$

equation (6.19) can be simplified and is given in the form,

$$\phi_3^3 + D_1'' \phi_3 + D_2'' = 0 \quad (6.20)$$

where

$$D_1'' = \frac{1}{K} + \frac{1}{4} P_1'^2 h_3^2$$

$$D_2'' = \frac{\mu V}{K h_3}$$

Equation (6.20) can be solved in a similar way to equation (6.6),

and the real root is given by,

$$\phi_3 = \left[-\frac{D_2''}{2} + \left(\frac{D_2''^2}{4} + \frac{D_1''^3}{27} \right)^{\frac{1}{2}} \right]^{\frac{1}{3}} + \left[-\frac{D_2''}{2} - \left(\frac{D_2''^2}{4} + \frac{D_1''^3}{27} \right)^{\frac{1}{2}} \right]^{\frac{1}{3}}$$

Substituting for D_1'' , D_2'' , ϕ_3 and J_1''

$$\tau_3 = \left[-\frac{\mu V}{2K h_3} + \left\{ \frac{\mu^2 V^2}{4K^2 h_3^2} + \frac{1}{27} \left(\frac{1}{K} + \frac{1}{4} P_1'^2 h_3^2 \right)^3 \right\}^{\frac{1}{2}} \right]^{\frac{1}{3}} + \left[-\frac{\mu V}{2K h_3} - \left\{ \frac{\mu^2 V^2}{4K^2 h_3^2} + \frac{1}{27} \left(\frac{1}{K} + \frac{1}{4} P_1'^2 h_3^2 \right)^3 \right\}^{\frac{1}{2}} \right]^{\frac{1}{3}} - \frac{P_1' h_3}{2} \quad (6.21)$$

Equation (6.21) is an expression to determine the shear stress on the surface of the strip in Section B.

For continuity of flow

$$Q_1 = Q_2$$

or $Q_1 - Q_2 = 0$ (6.22)

Now, equations (6.9), (6.7), (6.8), (6.16), (6.14) and (6.15) can be solved simultaneously using an iteration method for a numerical value of P_m until equation (6.22) is satisfied.

Hence the maximum pressure, shear stress and flow rate can be determined in the inlet zone before deformation for Section A. Substituting respective values into equation (6.21), the shear stress for Section B can be calculated.

6.3 Prediction of Yielding Point

The equation for evaluating the value of a point X_1 from the entry where the plastic deformation will commence, will be the same as determined in Section (5.3.1.3). Here the equation is given for reference;

$$X_1 = \frac{Y_0}{\frac{2\tau_1}{t_1} + \frac{2\tau_3}{W_1} + \frac{P_m}{L_1}} \quad (6.23)$$

6.4 Hydrodynamic Pressure and Axial Stress in the Deformation Zone

To simplify the mathematical operation, finite difference techniques, as described in Section (5.3.2) have been used to establish the governing equations in the deformation zone.

The equations for thickness, width, film thickness and the velocity in the deformation zone will be the same as derived in Section (5.3.2) and are listed below,

$$t_i = t_{i-1} - B\Delta x \quad (6.24)$$

$$W_i = W_{i-1} - B^*\Delta x \quad (6.25)$$

$$h_i = h_{i-1} + \frac{1}{2}B\Delta x \quad (6.26)$$

$$h^*_i = h_{i-1} + \frac{1}{2}B^*\Delta x \quad (6.27)$$

$$V_i = (V_{i-1}) \left(\frac{W_{i-1} t_{i-1}}{W_i t_i} \right) \quad (6.28)$$

The equations (6.7) and (6.8) give shear stress and flow rate in the inlet zone for Section A, which can be rewritten in finite difference form to determine the flow rate and shear stress in the deformation zone.

Therefore,

$$\tau_i = \left[-\frac{\mu V_i}{2Kh_i} + \left\{ \frac{\mu^2 V_i^2}{4K^2 h_i^2} + \frac{1}{27} \left(\frac{1}{K} + \frac{1}{4P_i} (2h_i^2)^3 \right)^{\frac{1}{2}} \right\}^{\frac{1}{3}} \right] + \left[-\frac{\mu V_i}{2Kh_i} - \left\{ \frac{\mu^2 V_i^2}{4K^2 h_i^2} + \frac{1}{27} \left(\frac{1}{K} + \frac{1}{4P_i} (2h_i^2)^3 \right)^{\frac{1}{2}} \right\}^{\frac{1}{3}} - \frac{1}{2P_i} h_i \right] \quad (6.29)$$

$$Q_i = \frac{P_i' h_i^3}{6\mu} + \frac{\tau_i h_i^2}{2\mu} + \frac{K}{\mu} \left(\frac{1}{20} P_i' h_i^5 + \frac{1}{4} P_i' h_i^4 \tau_i + \frac{1}{2} P_i' \tau_i h_i^3 + \frac{1}{2} \tau_i h_i^3 \right) + V_i h_i \quad (6.30)$$

For the continuity of flow,

$$Q_i = Q_1$$

$$Q_i - Q_1 = 0 \quad (6.31)$$

The initial viscosity μ and the non-Newtonian factor K were determined experimentally to conform to the equation (6.1). In the present analysis it has been assumed that the initial viscosity μ remains constant during the process. Substituting values of Q_1 and Q_i from equations (6.8) and (6.30) respectively, equation (6.31) can be iterated for an assumed value of B and a suitable interval to evaluate the value of P_i' .

Now,

$$P_i' = \frac{P_i - P_{i-1}}{\Delta x}$$

$$P_i = P_{i-1} + P_i' \Delta x \quad (6.32)$$

Equation (6.32) gives the hydrodynamic pressure at any point in the deformation zone.

Rewriting equation (6.21), the shear stress in Section B can be determined, ie,

$$\tau_i^* = \left[-\frac{\mu V_i}{2K h_i^*} + \left\{ \frac{\mu^2 V_i^2}{4K^2 h_i^{*2}} + \frac{1}{27} \left(\frac{1}{K} + \frac{1}{4} P_i' h_i^{*2} \right)^3 \right\}^{\frac{1}{2}} \right]^{\frac{1}{3}} + \left[-\frac{\mu V_i}{2K h_i^*} - \left\{ \frac{\mu^2 V_i^2}{4K^2 h_i^{*2}} + \frac{1}{27} \left(\frac{1}{K} + \frac{1}{4} P_i' h_i^{*2} \right)^3 \right\}^{\frac{1}{2}} \right]^{\frac{1}{3}} - \frac{1}{2} P_i' h_i^* \quad (6.33)$$

The expression for evaluating parameter b^* has been established in Appendix I and can be rewritten in the form,

$$B^* = mB \quad (6.34)$$

where

$$m = \frac{W_1}{t_1}$$

Axial Stress

The governing differential equation in the deformation zone using Von-Mises yield criteria is given by equation (5.13A),

ie,

$$d\sigma_x = - \frac{dt}{t} y_i - \frac{dW}{W} y_i - \frac{2\tau dx}{t} - \frac{2\tau^* dx}{W} \quad (6.35)$$

The above equation can be rewritten in finite difference form and on simplification it gives,

$$\sigma_x = \left(\frac{t_{i-1}}{t_i} + \frac{W_{i-1}}{W_i} - 2 \right) y_i + \frac{2\tau_i \Delta x}{t_i} + \frac{2\tau_i^* \Delta x}{W_i} + \sigma_{x_{i-1}} \quad (6.36)$$

The stress-strain relationship taking into account the effects of strain hardening and strain rate sensitivity is given by equation (5.26A), ie

$$y_i = s_i \left[y_0 + K_0 \left\{ \ln \left(\frac{W_i t_i}{W_1 t_1} \right) \right\}^n \right] \quad (6.37)$$

where,

$$s_i = 1 + \left(\frac{\dot{\epsilon}_{mi}}{N} \right)^{\frac{1}{T_1}}$$

$$\dot{\epsilon}_{mi} = \frac{V_i}{\Delta x} \ln \left(\frac{a_{i-1}}{a_i} \right)$$

N and T_1 are constants.

6.5 Percentage Reduction in the Strip Size

Substituting the pertinent values, equations (6.32) and (6.36) together with equation (6.37) can be iterated to evaluate the values of constants B and hence B* until equation $\sigma_x + P_i = Y_i$ is satisfied. Once parameters B and B* are determined then the percentage reduction in the strip size can be calculated by,

$$\begin{aligned} \text{PRT} &= \left(1 - \frac{t_i}{t_1} \right) \times 100 &) \\ & &) \\ & &) \\ \text{PRW} &= \left(1 - \frac{W_i}{W_1} \right) \times 100 &) \\ & &) \\ & &) \\ \text{PRA} &= \left(1 - \frac{W_i t_i}{W_1 t_1} \right) \times 100 &) \\ & &) \end{aligned} \quad (6.38)$$

Condition of Slip

It has been generally agreed that flow instabilities take place in a polymer melt flow when shear stress reaches a critical value which varies from 0.1 to 1 MNm⁻² for different polymers. In the present work a polymer melt was used as the pressure medium and therefore this characteristic should be included in the analysis. It was assumed that as the shear stress τ_1 in the inlet zone reaches a value of 0.22 MNm⁻², the condition of slip occurs at the interface of the strip and the polymer melt. The speed at which this happens is known as the critical speed.

Now, applying boundary conditions, the flow rate when slip occurs will be given by;

$$Q_s = \frac{P_1 h_1^3}{6\mu} + \frac{\tau_c h_1^2}{2\mu} + \frac{K}{\mu} \left(\frac{1}{20} P_1 h_1^5 + \frac{1}{4} P_1 h_1^4 \tau_c + \frac{1}{2} P_1 h_1^3 \tau_c^2 + \frac{1}{2} \tau_c^3 h_1^2 \right) + V_s h_1 \quad (6.39)$$

where Q_s is the flow rate of molten polymer when slip occurs and V_s is the velocity at which slip occurs.

Equation (6.39) shows that when slip occurs, the flow of polymer remains constant and subsequently the pressure and shear stress will also remain constant. The corresponding value of τ_3 is considered as the critical shear stress for Section B. Therefore, it was assumed that thereafter, for any increase in speed after the critical value, the pressure and shear stress will remain constant.

The equations regarding the other parameters involved in process will remain the same as derived in the previous section.

The solution procedure remains the same as is described in Section (5.3.2), except using the related equations derived in this section.

6.6 Results from the Analysis

The following data was used as the standard set for the physical parameters involved in the process, to calculate the different quantities by using the equations derived in the previous section. The values of different parameters were then varied to investigate the respective effects on the process. The results predicted by this analysis were found to be in closer agreement to those observed experimentally, in comparison with the Newtonian analysis.

Dimensions of Reduction Unit:

Inlet gap,	$h_1 = 0.3\text{mm}$)	
)	Section A
Exit gap,	$h_2 = 0.02\text{mm}$)	
Inlet/Exit gap,	$h_3 = 0.13\text{ mm}$)	Section B
Inlet length,	$L_1 = 150\text{mm}$		
Exit length,	$L_2 = 30\text{mm}$		

Data for Copper Strip:

Initial thickness,	$t_1 = 1.59\text{mm}$
Initial width,	$W_1 = 12.7\text{mm}$
Initial yield stress,	$Y_0 = 75\text{ MNm}^{-2}$
Strain hardening constant,	$K_0 = 600\text{ MNm}^{-2}$
Strain hardening index,	$n = 0.6$
Strain rate sensitivity constant,	$N = 55 \times 10^3$
Strain rate sensitivity index,	$T_1 = 3.8$

Data for Polymer Melt:

Initial viscosity, $\mu = 110 \text{ Nsm}^{-2}$

Non-Newtonian factor, $K = 5 \times 10^{-11} \text{ m}^4/\text{N}^2$

Critical shear stress, $\tau_c = 0.22 \text{ MN/m}^2$

6.6.1 Theoretical Results of Percentage Reduction

Figures 122 and 123 show the effect of gap ratio on the percentage reduction in thickness and the area of the strip. The different values of gap ratios were obtained by changing the inlet gap, h_1 , where gap h_2 was kept constant during the calculations. As the gap ratio was decreased an increase in the reduction was predicted. These figures suggest that by using a lower gap ratio, higher reductions should be achieved.

The different values of inlet length L_1 , were considered keeping L_2 constant. Results for different length ratios were obtained and are presented in Figures 124 and 125. These figures show a direct effect of the length ratio on the predicted reductions in thickness and area of the strip. Higher length ratio produces relatively greater reduction.

The effect of initial yield stress on the percentage reduction in strip size is demonstrated in Figures 126 and 127. These results indicate that more permanent deformation will take place for a material with a lower value of yield stress. A maximum reduction in area of about 20% should be achieved by using a material with initial yield stress equal to 50 MNm^{-2} .

Figures 128 and 129 show the theoretical effect of the strain hardening constant on the deformation in strip size versus speed. Similar trends were observed as shown in Figure 126 and 127.

Figures 130 and 131 demonstrate the effect of the polymer melt viscosity on the percentage reduction in thickness and area of the strip. These results show that higher reductions should be achieved at slow drawing speed by using more viscous fluid. At higher drawing speeds no significant difference is indicated and similar reductions are predicted for different values of viscosity. This is perhaps the critical shear stress which reaches its critical value at a relatively slow speed for higher viscosity causing the predicted reduction to be of the same level.

The curves in Figures 132 and 133 show the theoretical effect of non-Newtonian factor K , on the percentage reductions. For lower values of factor K , higher reductions are predicted for slow speed. At higher drawing speeds in excess of 0.35 m/s there is no significant difference in the predicted results.

Figures 134 and 135 show the effect of changing the critical shear stress for slip. It is demonstrated that an increase in the limiting shear stress, causes an increase in drawing speed at which slip would occur. Hence the higher the critical shear stress, the higher are the percentage reductions in strip size predicted.

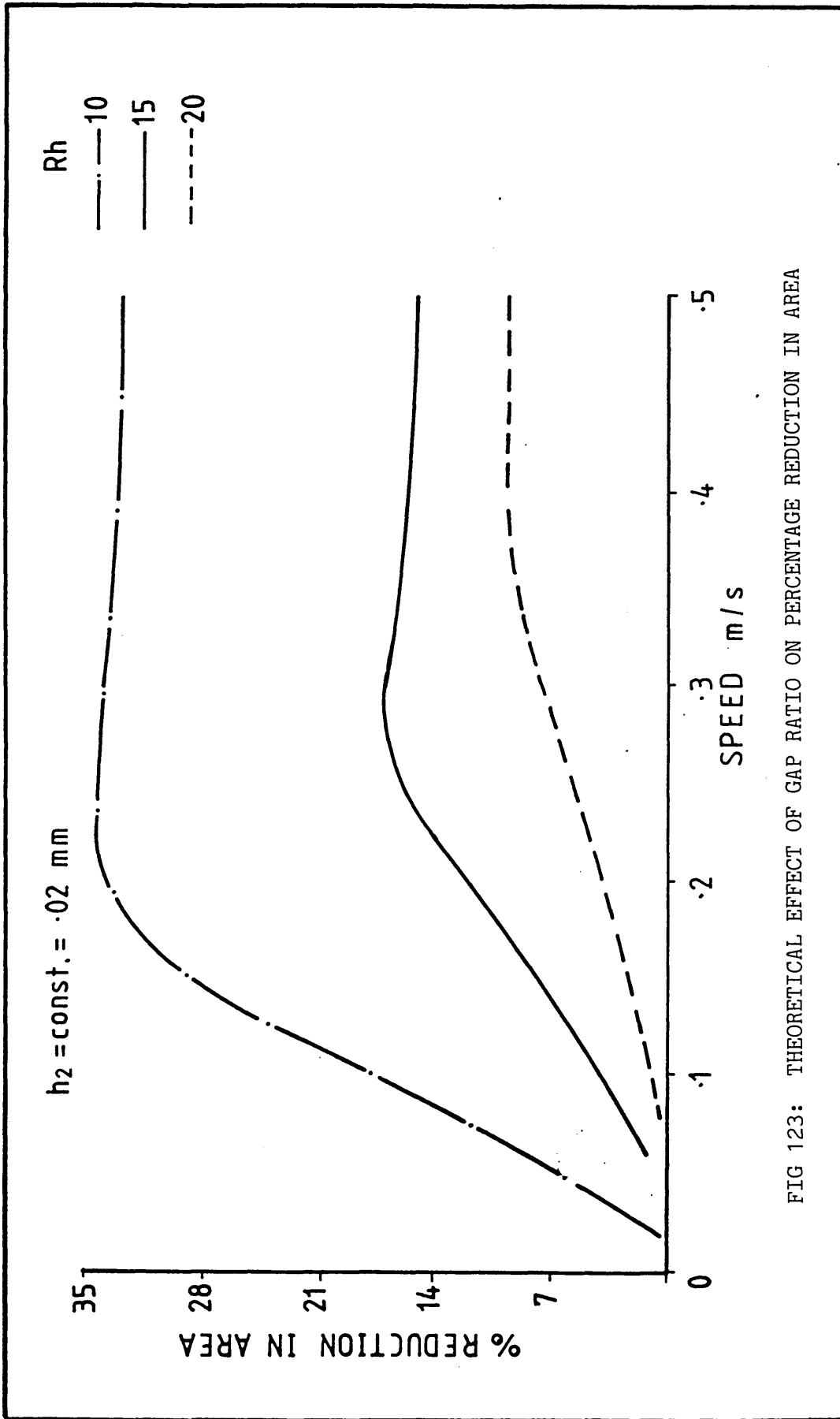


FIG 123: THEORETICAL EFFECT OF GAP RATIO ON PERCENTAGE REDUCTION IN AREA

RL
 ——— 5.65
 ——— 5
 - - - 4.33

$L_2 = \text{const.} = 30 \text{ mm}$

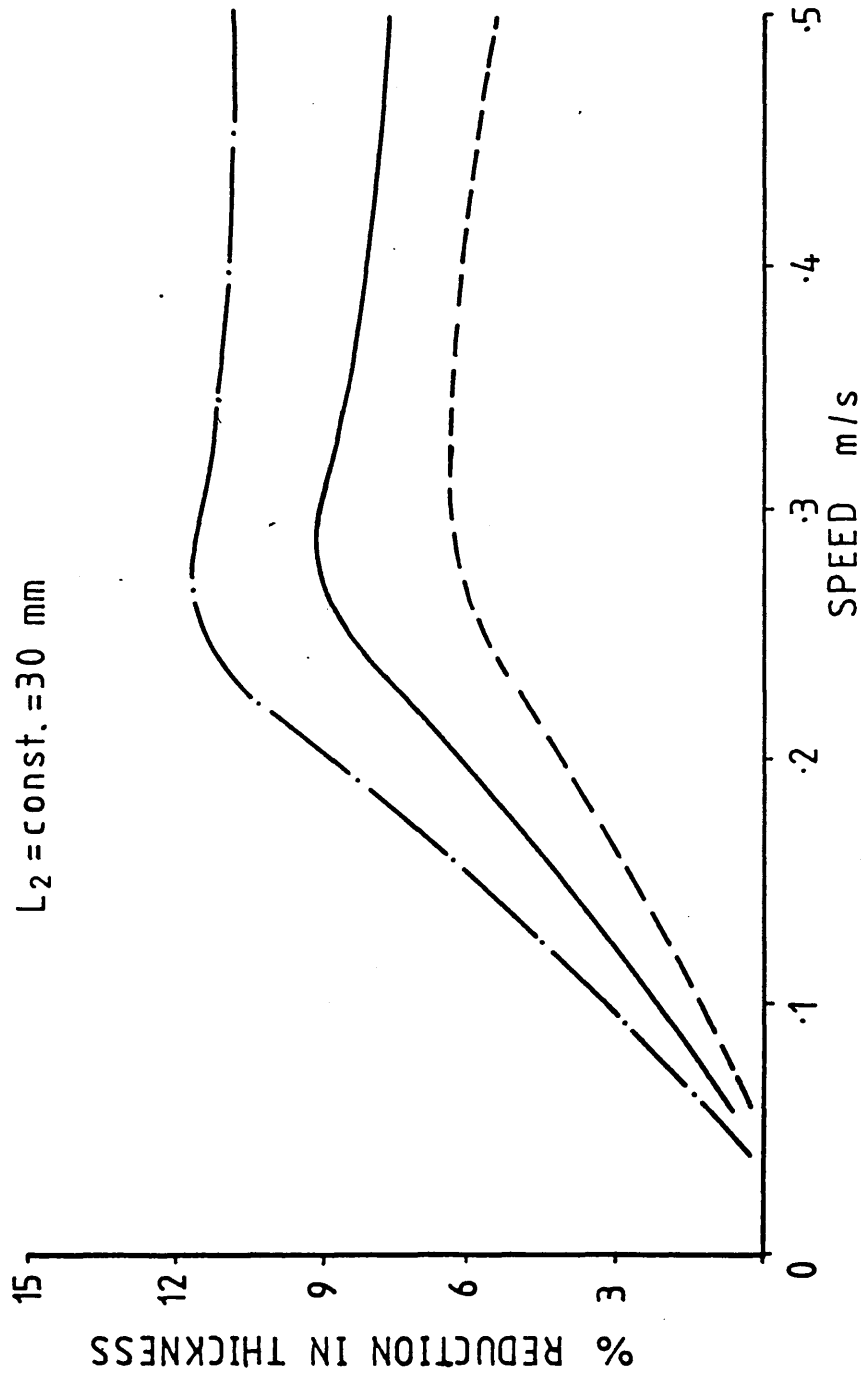


FIG 124: THEORETICAL EFFECT OF LENGTH RATIO ON PERCENTAGE REDUCTION IN THICKNESS

RL
 — 5.65
 — 5
 - - - 4.33

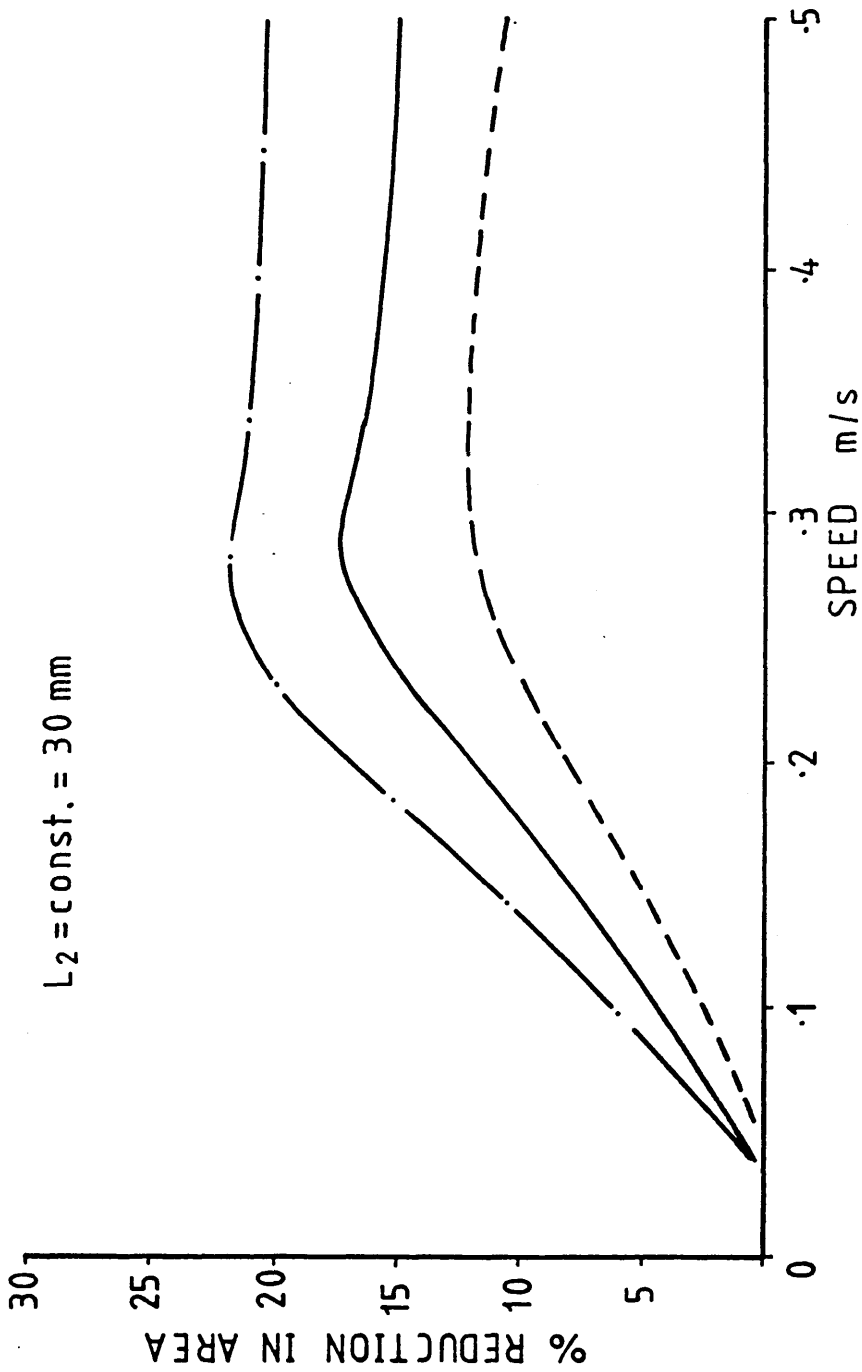


FIG 125: THEORETICAL EFFECT OF LENGTH RATIO ON PERCENTAGE REDUCTION IN AREA

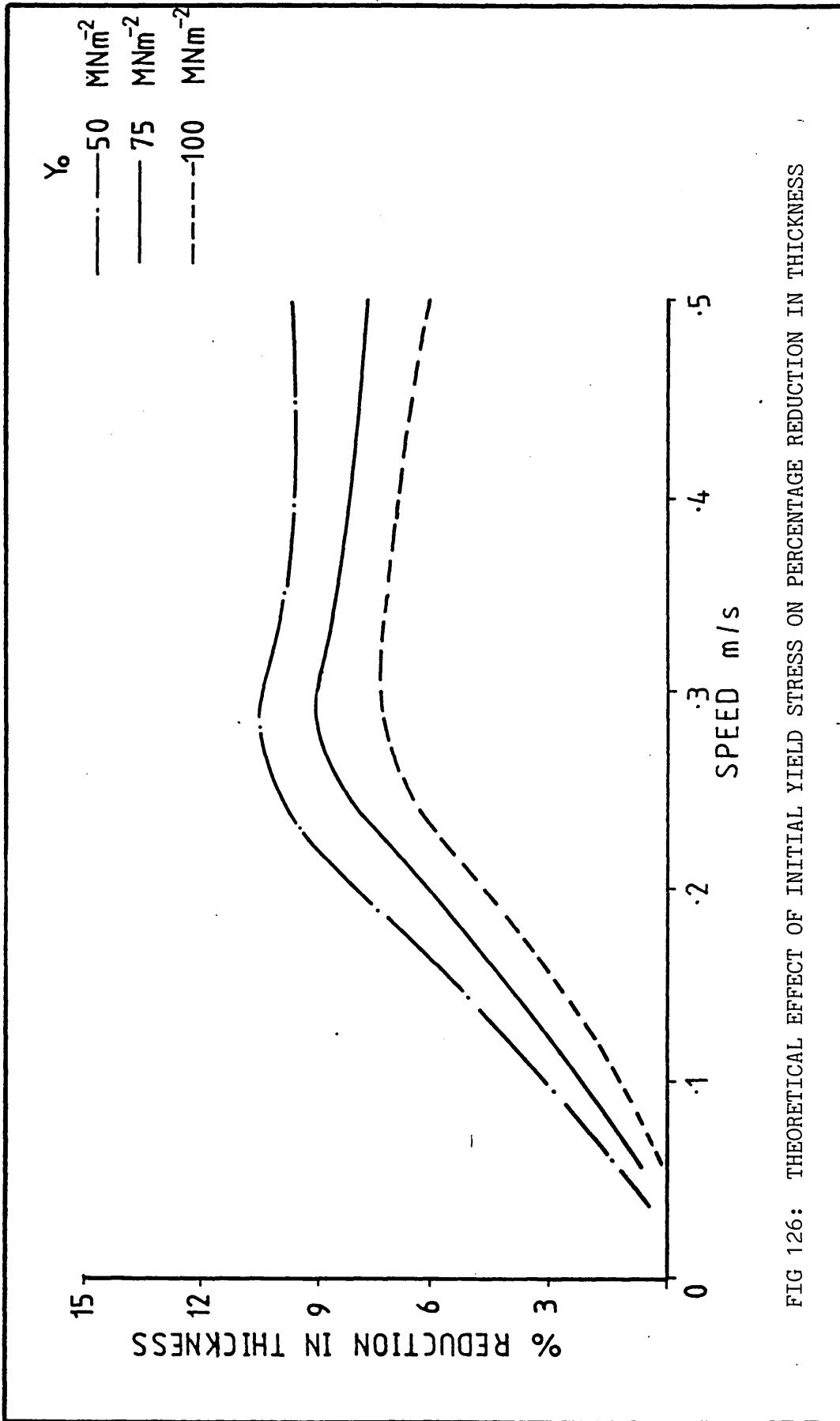


FIG 126: THEORETICAL EFFECT OF INITIAL YIELD STRESS ON PERCENTAGE REDUCTION IN THICKNESS

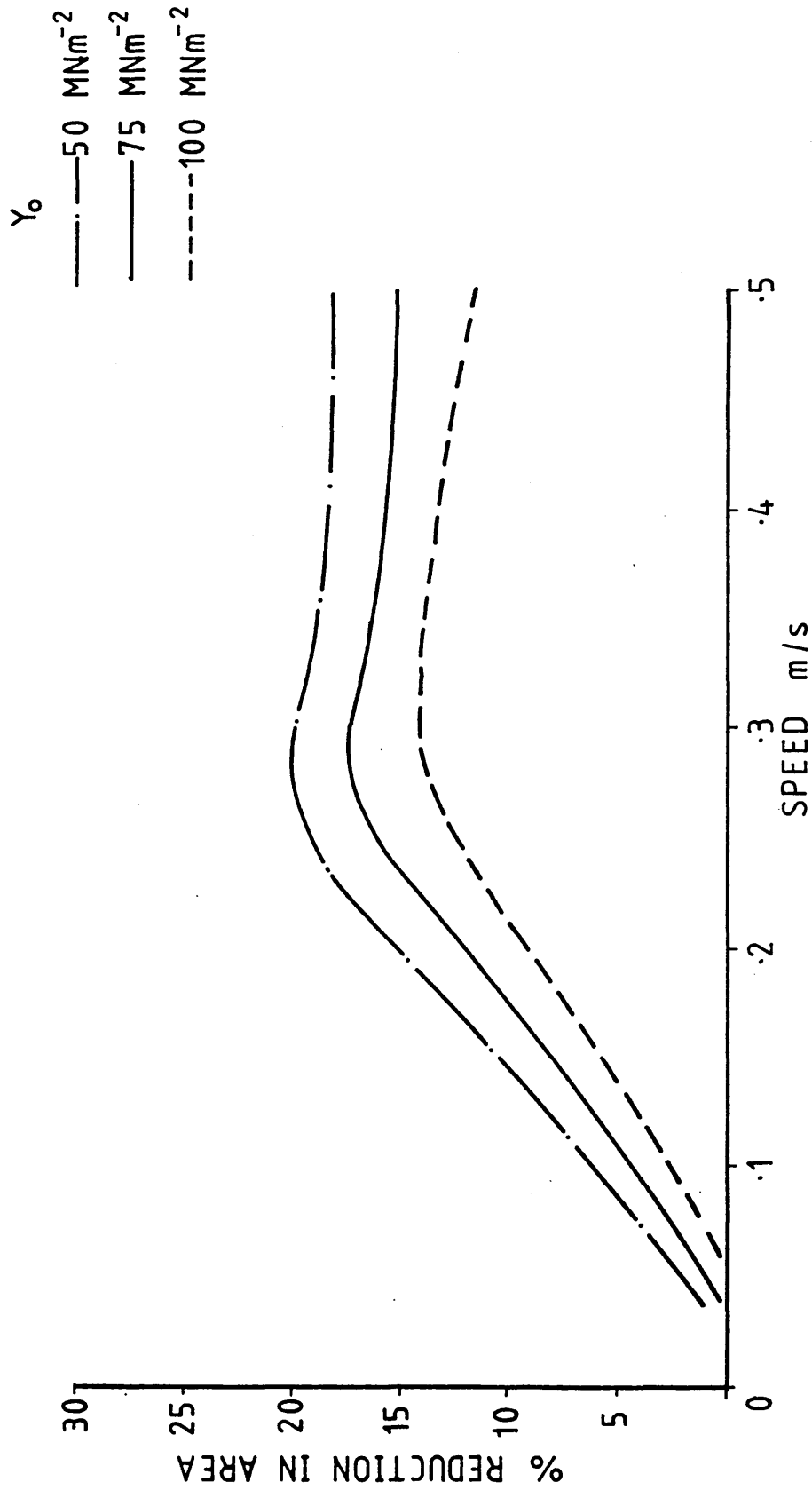


FIG 127: THEORETICAL EFFECT OF INITIAL YIELD STRESS ON PERCENTAGE REDUCTION IN AREA

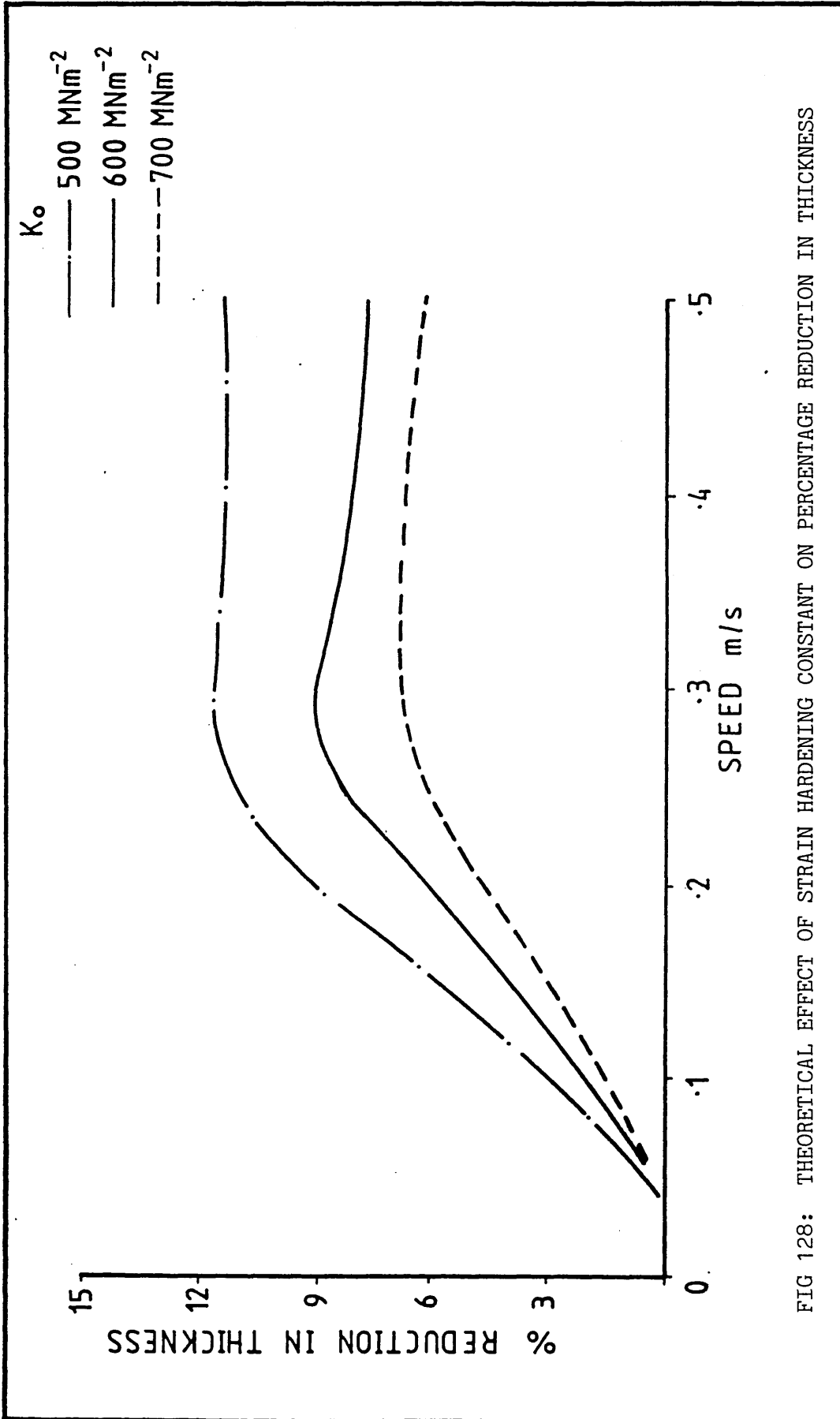


FIG 128: THEORETICAL EFFECT OF STRAIN HARDENING CONSTANT ON PERCENTAGE REDUCTION IN THICKNESS

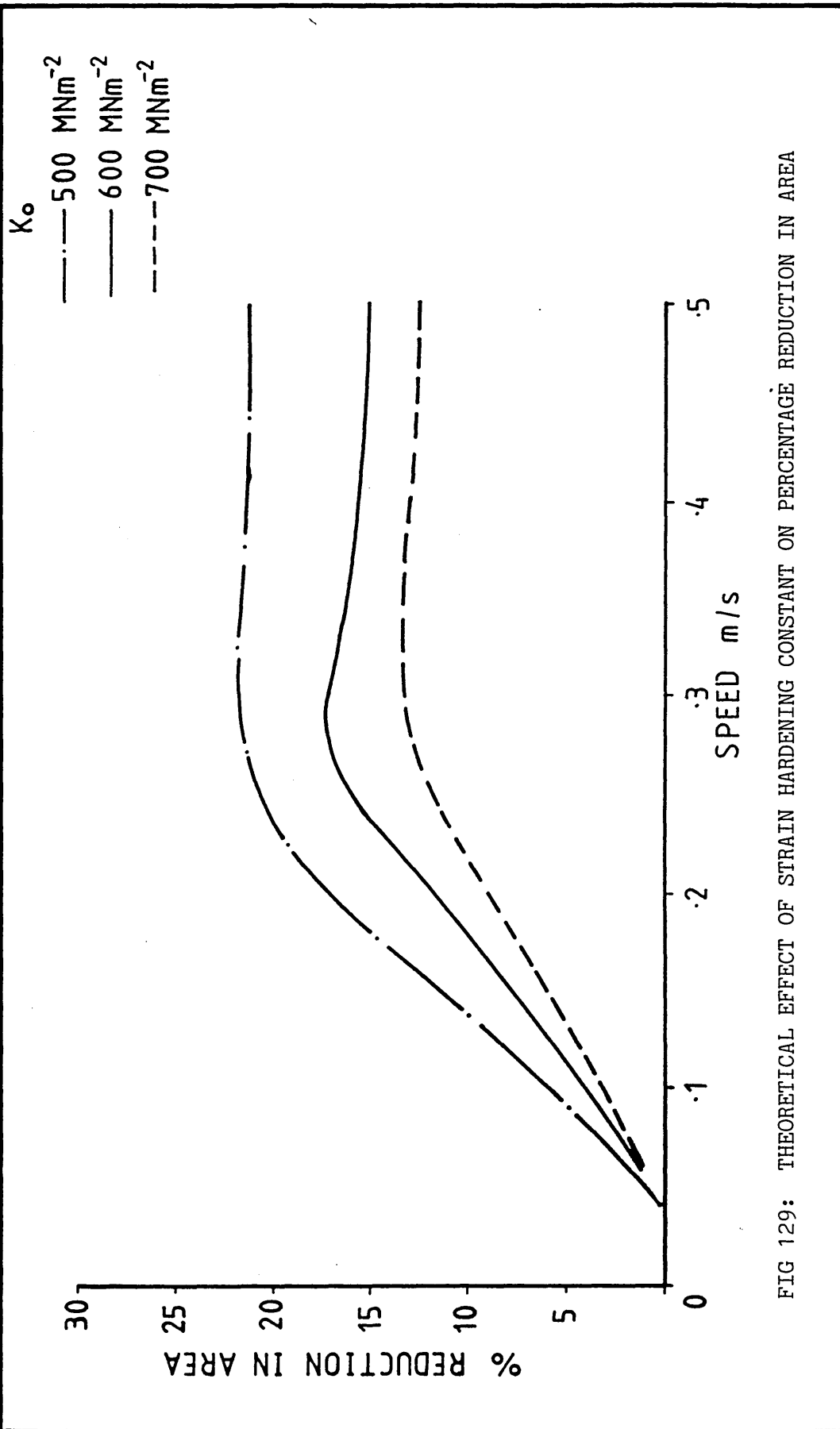


FIG 129: THEORETICAL EFFECT OF STRAIN HARDENING CONSTANT ON PERCENTAGE REDUCTION IN AREA

μ
 --- 75 Nsm^{-2}
 — 110 Nsm^{-2}
 - · - 140 Nsm^{-2}

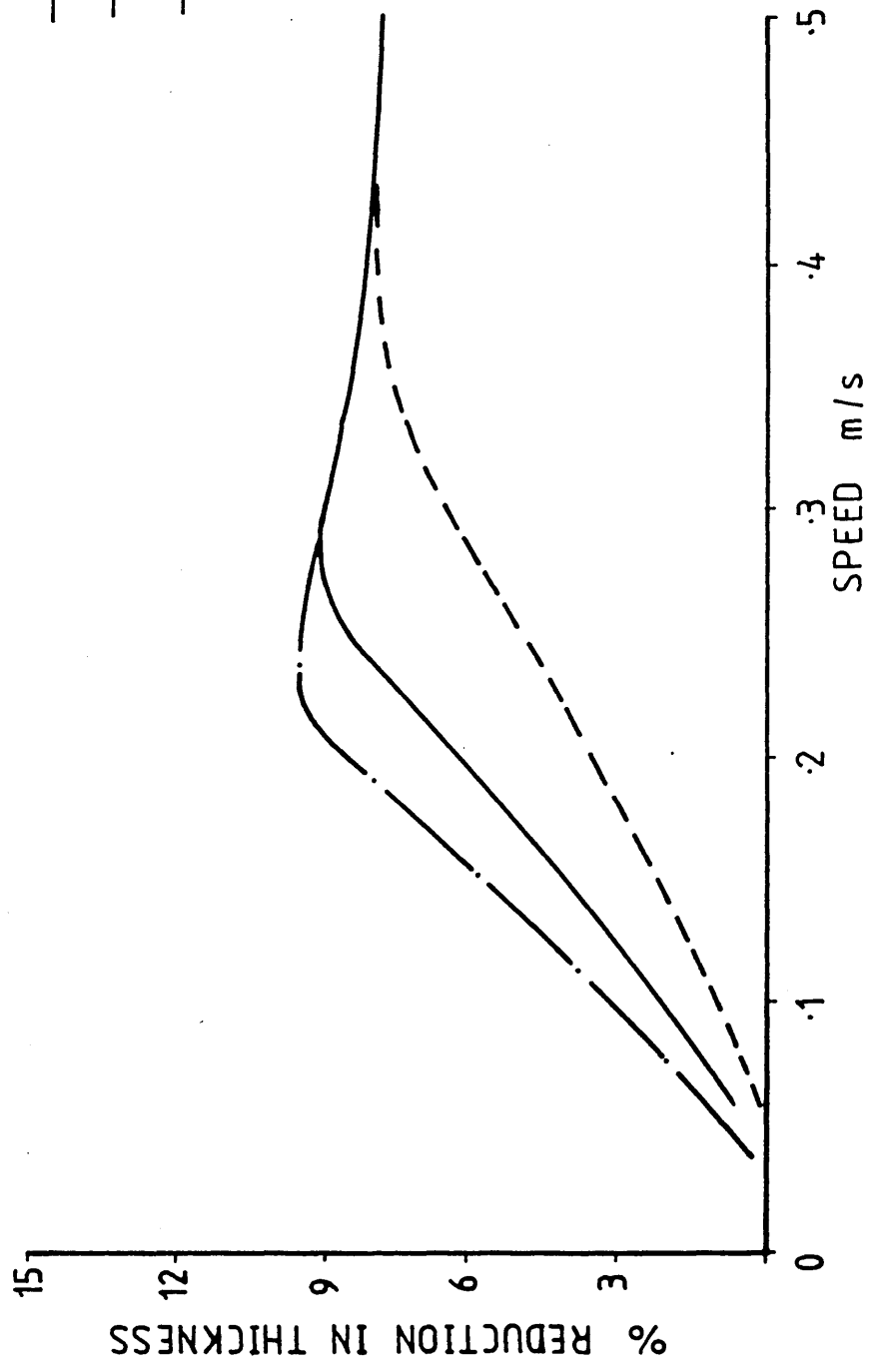


FIG 130: THEORETICAL EFFECT OF VISCOSITY ON PERCENTAGE REDUCTION IN THICKNESS

μ
 --- 75 Ns m^{-2}
 — 110 Ns m^{-2}
 - · - 140 Ns m^{-2}

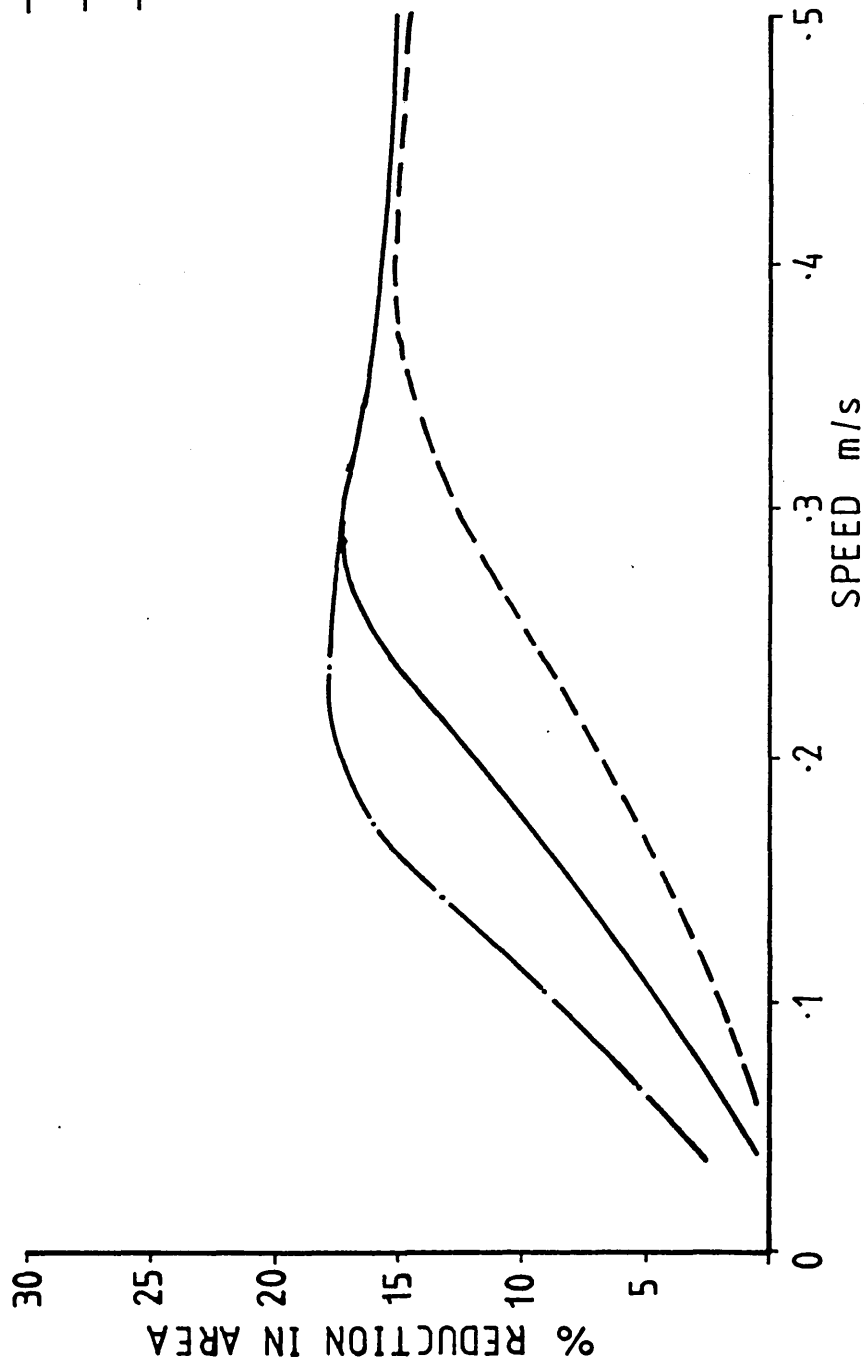


FIG 131: THEORETICAL EFFECT OF VISCOSITY ON PERCENTAGE REDUCTION IN AREA

k
 —·—·— $4 \times 10^{-11} \text{ m}^4 \text{ N}^{-2}$
 ——— $5 \times 10^{-11} \text{ m}^4 \text{ N}^{-2}$
 - - - $8 \times 10^{-11} \text{ m}^4 \text{ N}^{-2}$

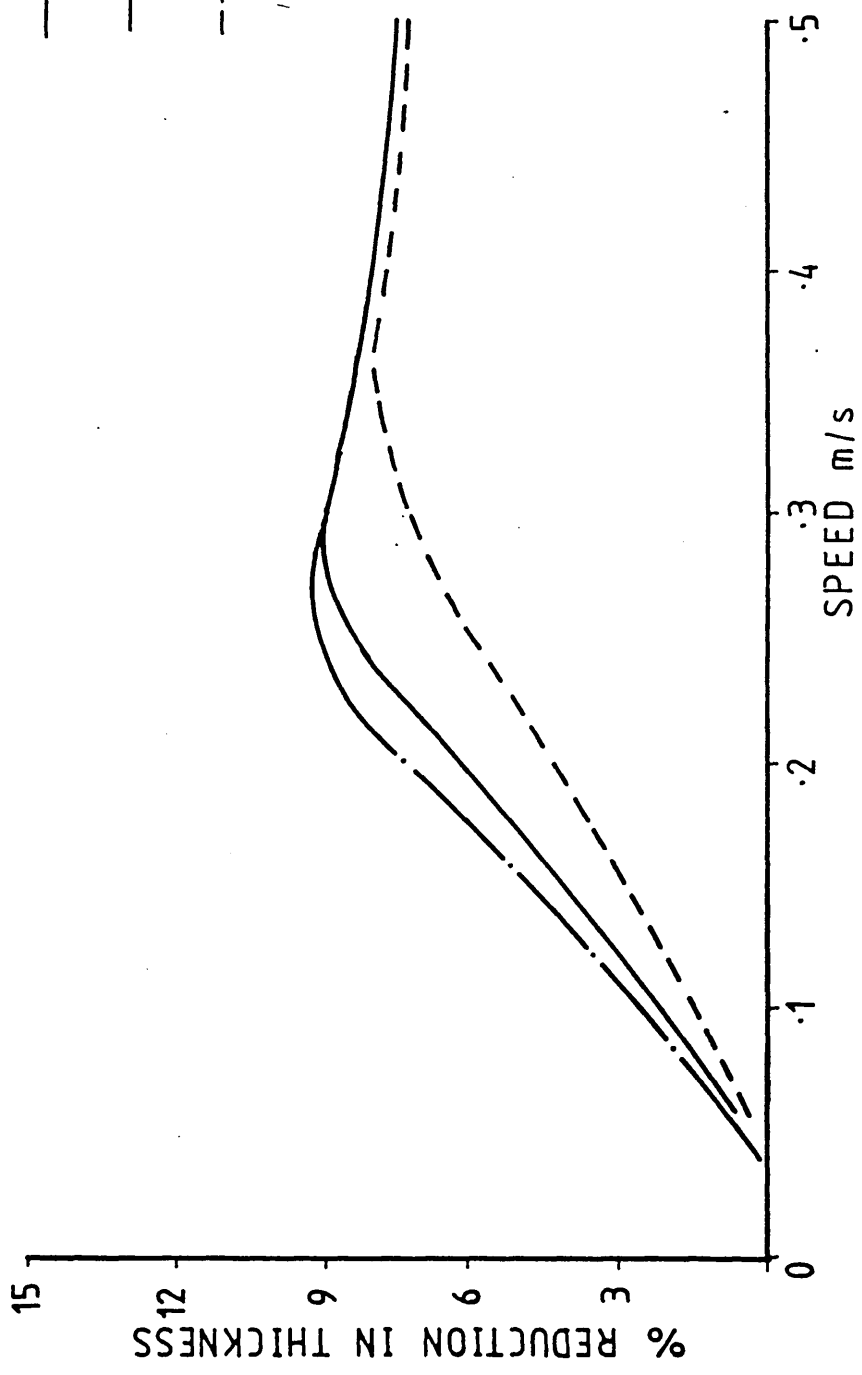


FIG 132: THEORETICAL EFFECT OF NON-NEWTONIAN FACTOR ON PERCENTAGE REDUCTION IN THICKNESS

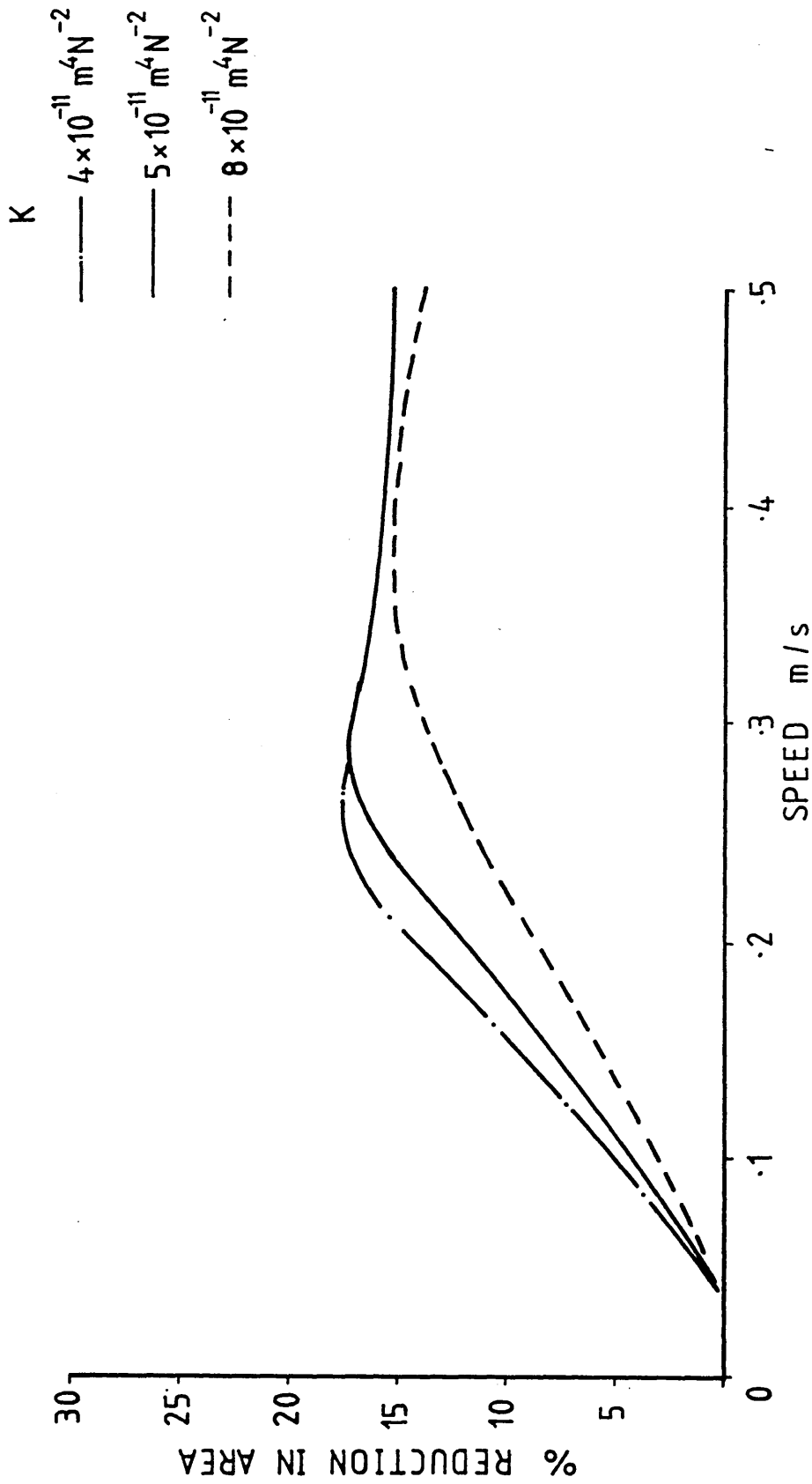


FIG 133: THEORETICAL EFFECT OF NON-NEWTONIAN FACTOR ON PERCENTAGE REDUCTION IN AREA

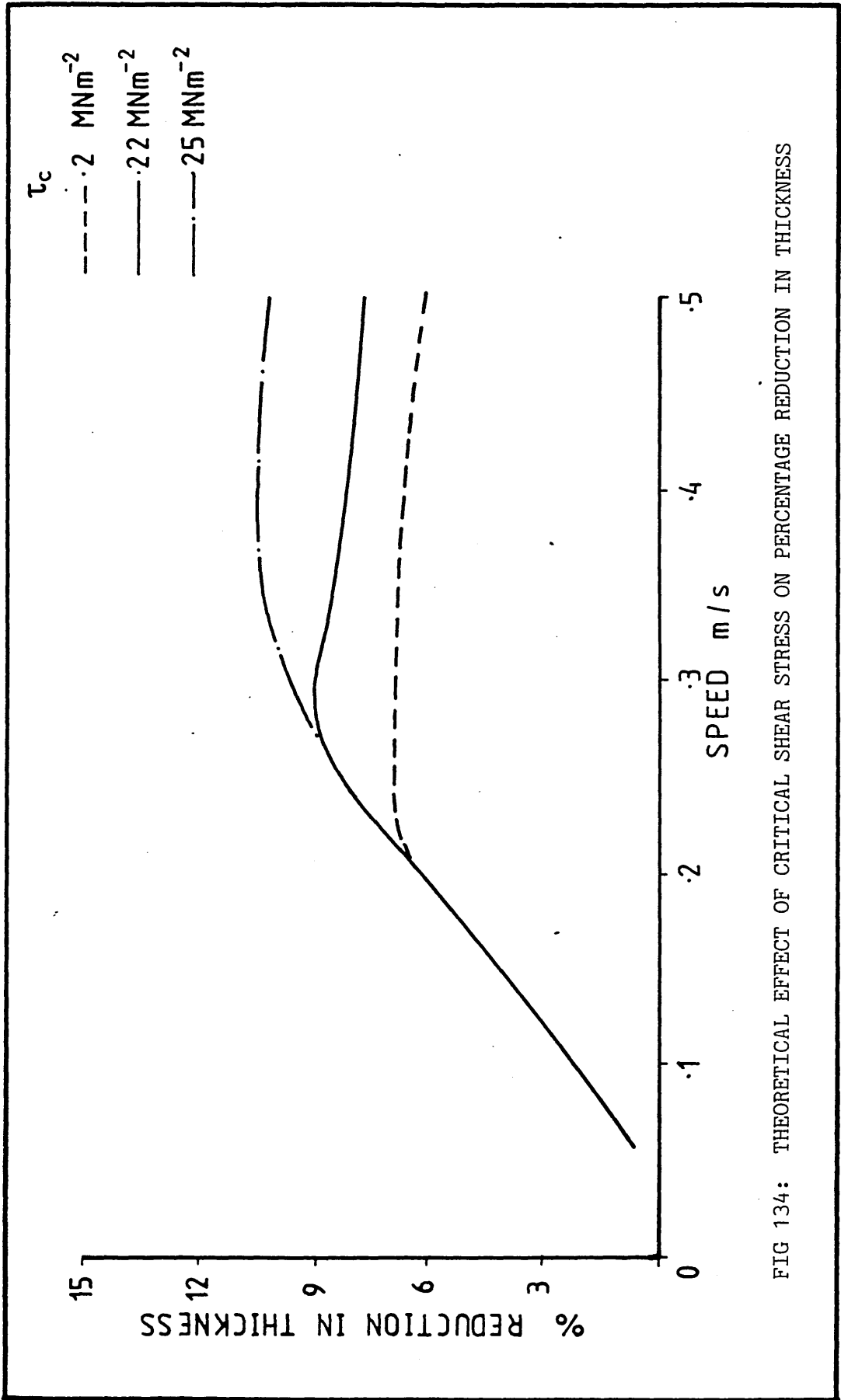


FIG 134: THEORETICAL EFFECT OF CRITICAL SHEAR STRESS ON PERCENTAGE REDUCTION IN THICKNESS

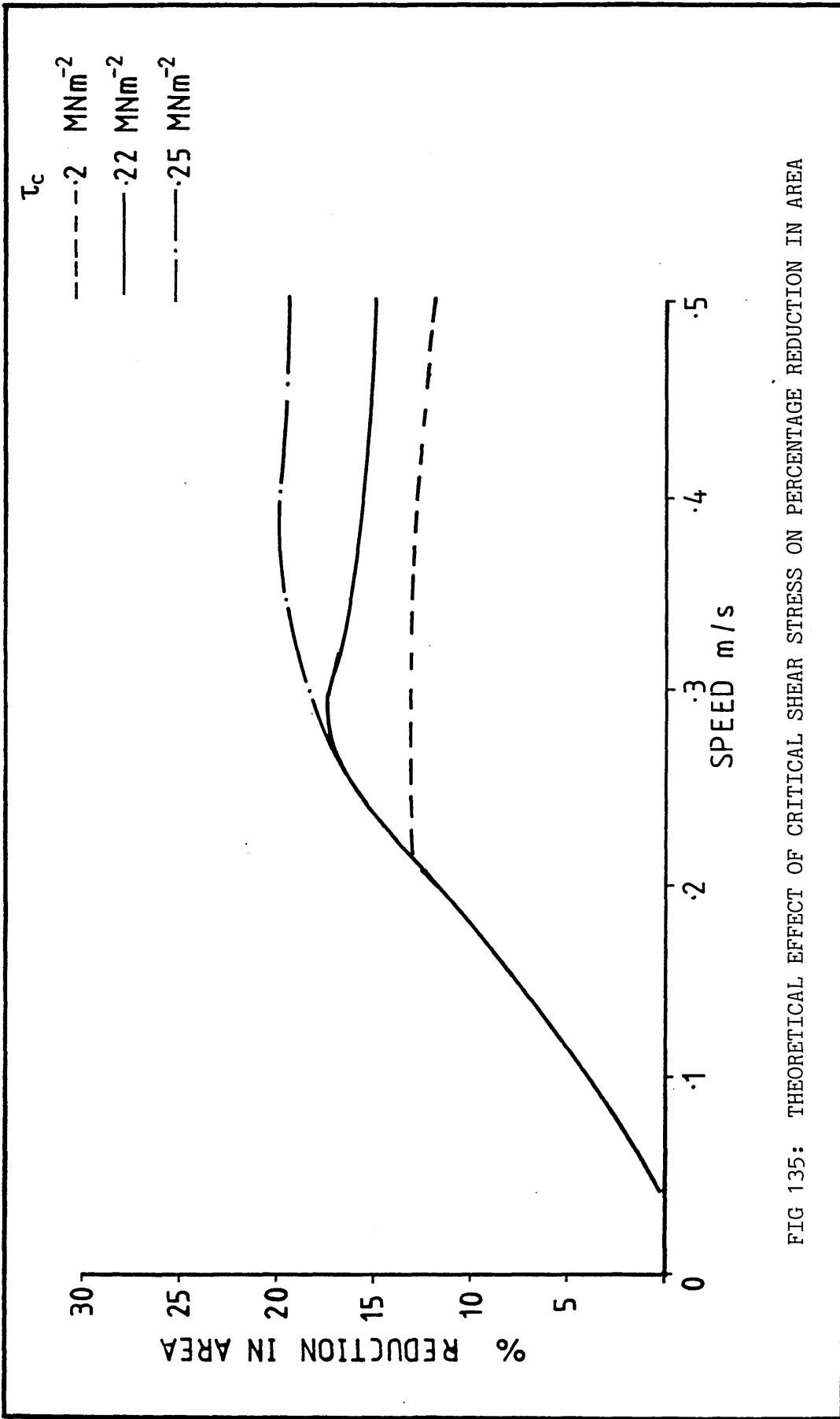


FIG 135: THEORETICAL EFFECT OF CRITICAL SHEAR STRESS ON PERCENTAGE REDUCTION IN AREA

6.6.2 Theoretical Point of Yielding

The effect of variations in different parameters on the position at which the strip yields plastically is presented in Figures 136 to 138.

Figure 136 represents the effect of the change in gap ratio. The smaller gap ratio, the lower the speed at which yielding starts. This figure also shows that as the gap ratio is decreased, the length of deformation zone is increased. Therefore, greater percentage reductions were predicted. It is also noticed that the point of yielding remains constant at higher drawing speeds after the critical shear stress limit is reached.

The effect of initial yield stress on the point of yielding is shown in Figure 137. With the increase in yield stress the position of the yielding from the entry is also increased, reducing the deformation zone.

Figure 138 demonstrates the effect of melt viscosity on the position at which yielding will start. These results indicate that the distance at which yielding occurs remains constant at the speeds in excess of 0.4 m/s. An increase in viscosity causes the deformation to start at slower speeds.

Rh
 ——— 10
 ——— 15
 - - - 20

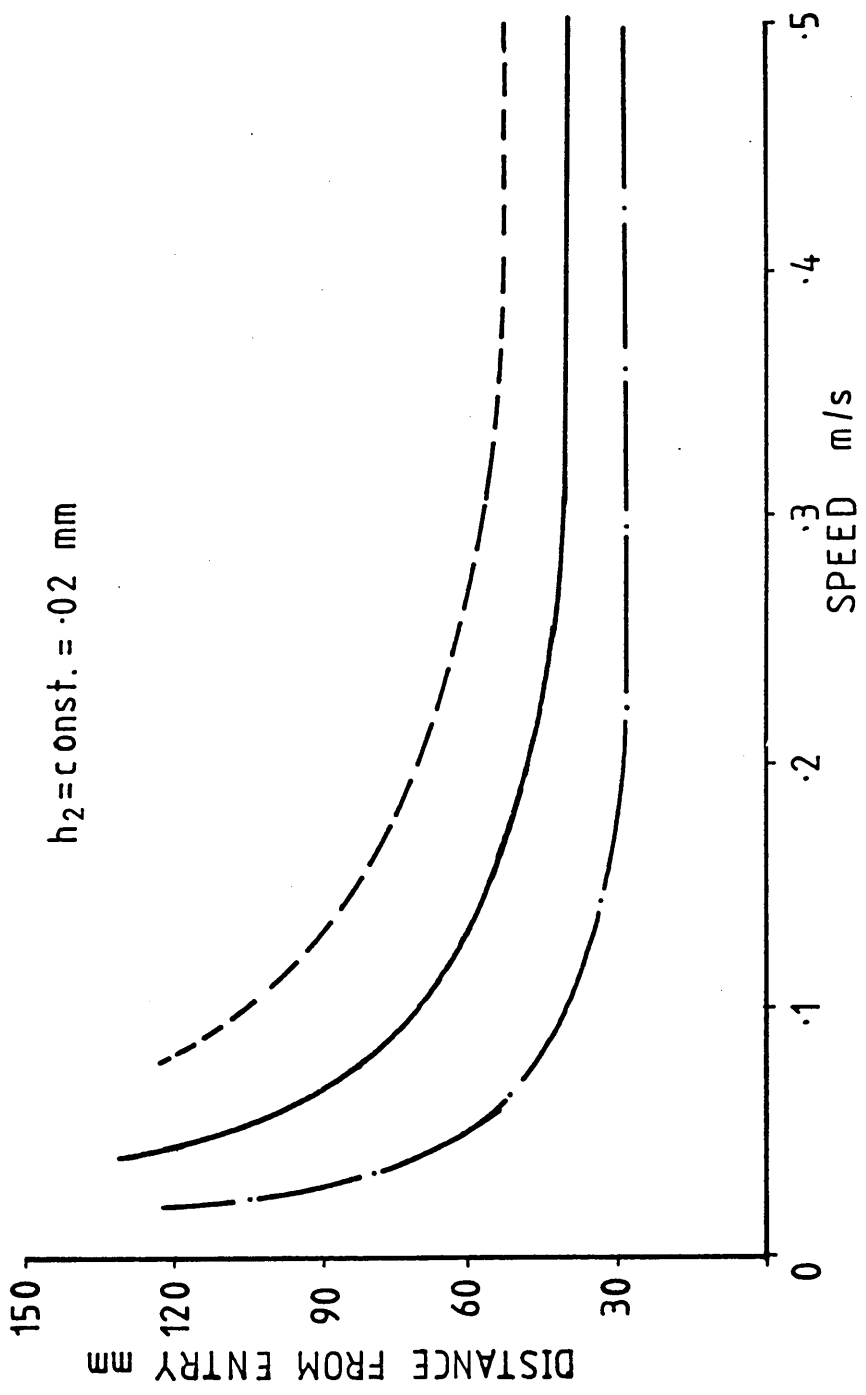


FIG 136: THEORETICAL EFFECT OF GAP RATIO ON YIELDING POINT

Y_0
 - - - 50 MNm⁻²
 ——— 75 MNm⁻²
 - - - 100 MNm⁻²

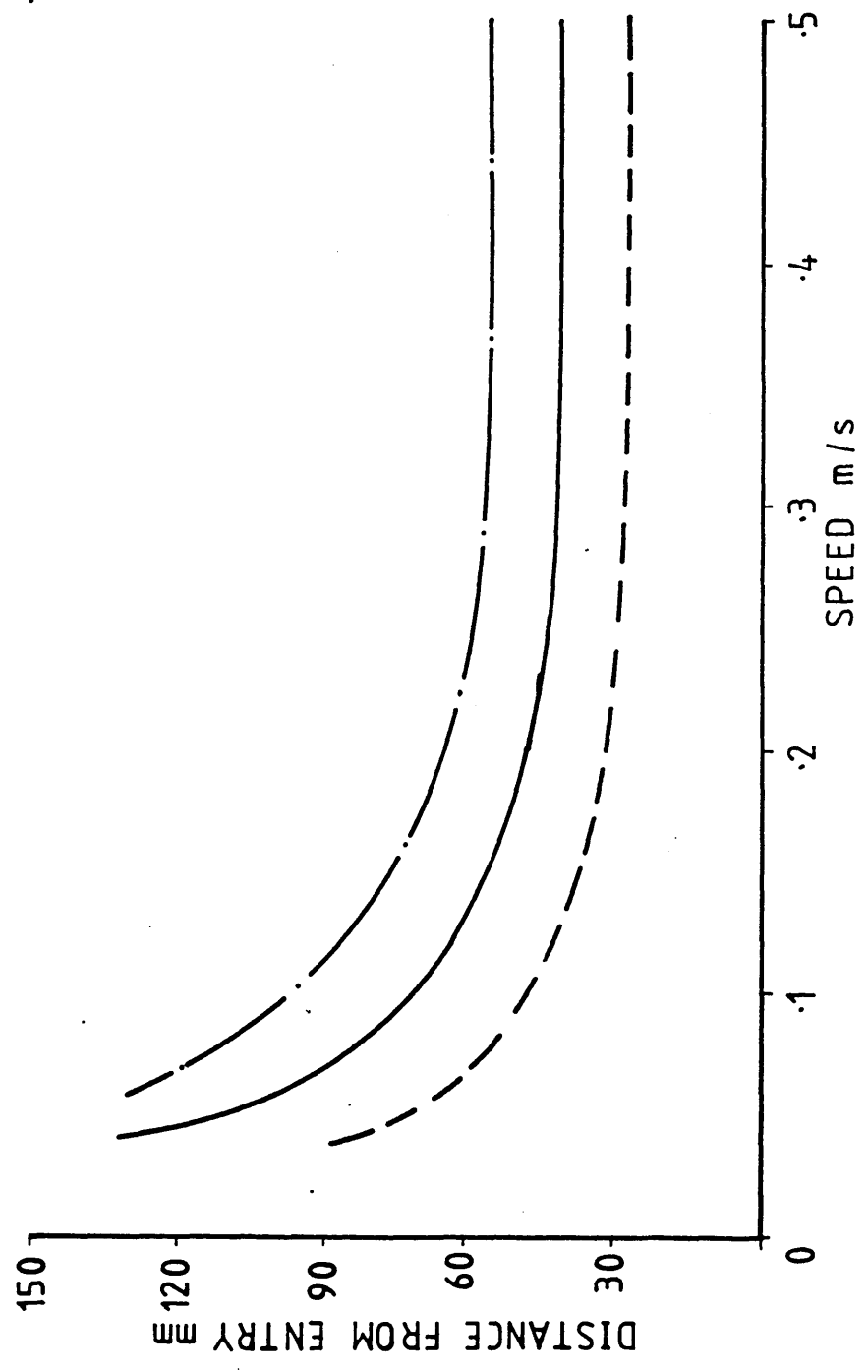


FIG 137: THEORETICAL EFFECT OF INITIAL YIELD STRESS ON YIELDING POINT

μ
 --- 75 Ns m^{-2}
 — 110 Ns m^{-2}
 -·- 140 Ns m^{-2}

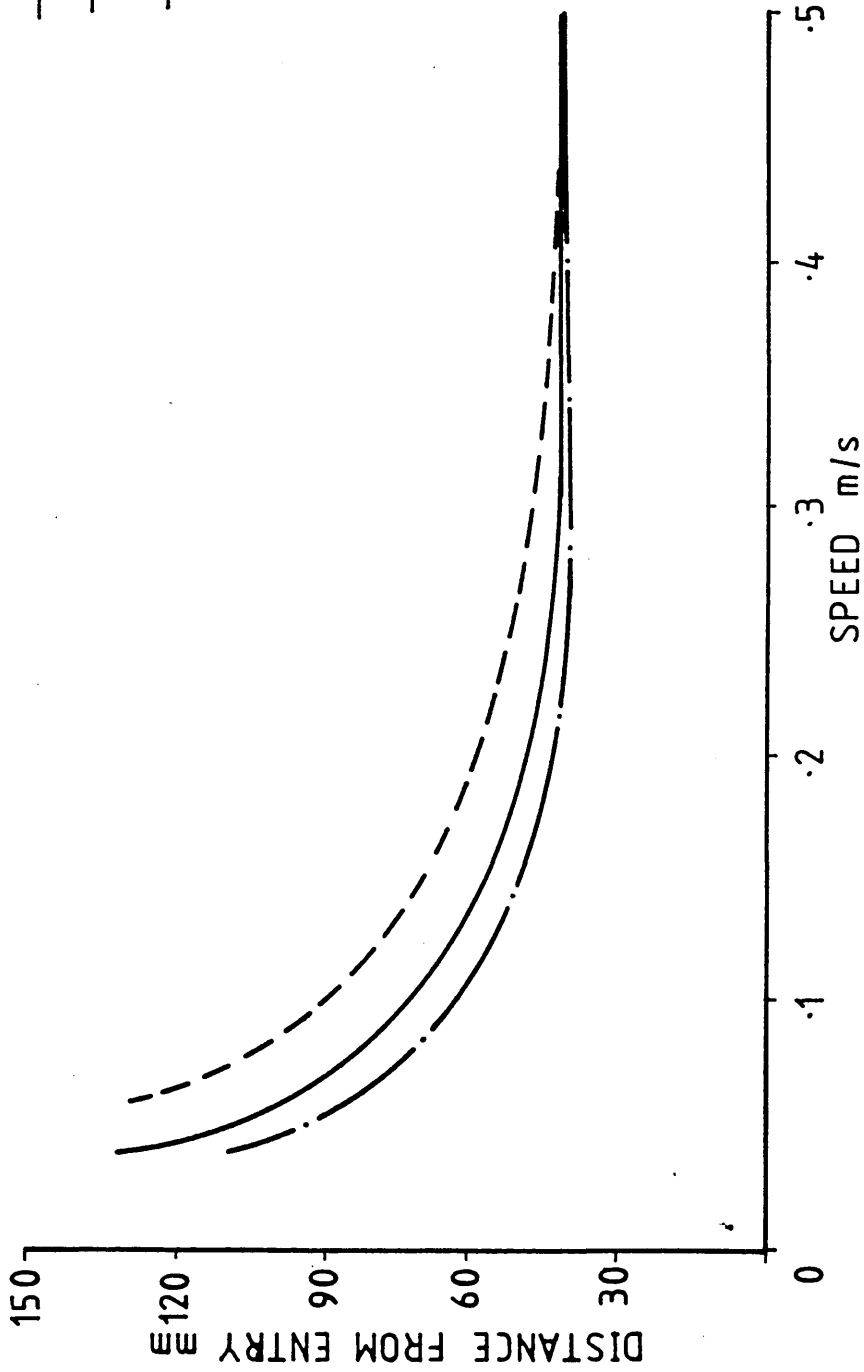


FIG 138: THEORETICAL EFFECT OF VISCOSITY ON YIELDING POINT

6.6.3 Results for Pressure Distribution

The variation in the predicted pressures along the length of the unit are presented in this Section. Figure 139 shows the pressure distribution versus drawing speed for different gap ratios at a constant drawing speed of 0.2 m/s.

The effect of drawing speed on the distribution of the pressure along the unit is demonstrated in Figure 140. The influence of viscosity on the pressure distribution is shown in Figure 141.

It is evident from these graphs that in every case the maximum pressure is at the step. The general trends of the results are identical to those observed in the case of Newtonian analysis.

6.6.4 Deformation Profiles

The deformation profiles for different gap ratios for the same drawing speed were calculated and are presented in Figure 142.

Figure 143 shows the effect of drawing speed on the theoretical deformation profile.

These figures indicate that a specific deformation profile was predicted for each case.

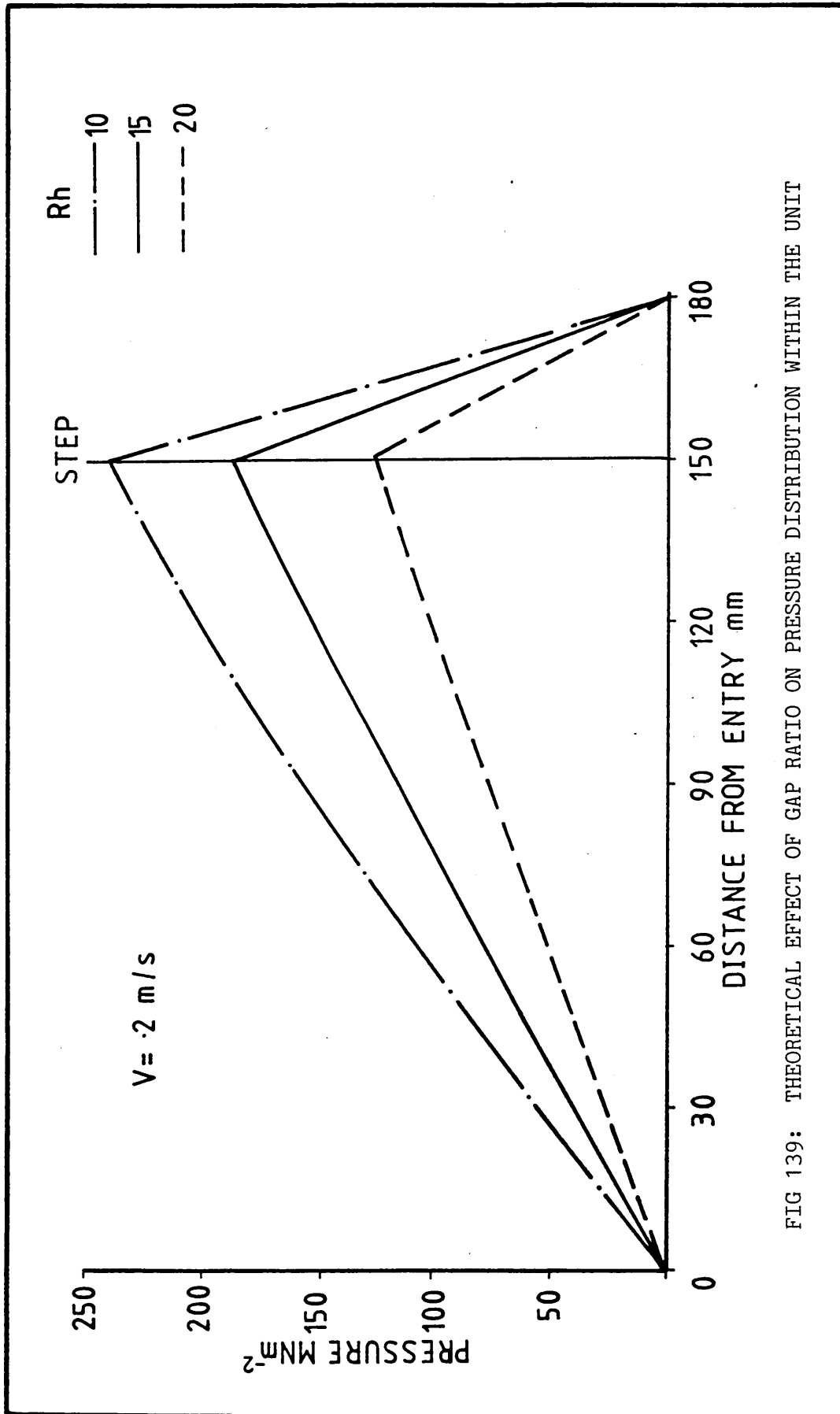


FIG 139: THEORETICAL EFFECT OF GAP RATIO ON PRESSURE DISTRIBUTION WITHIN THE UNIT

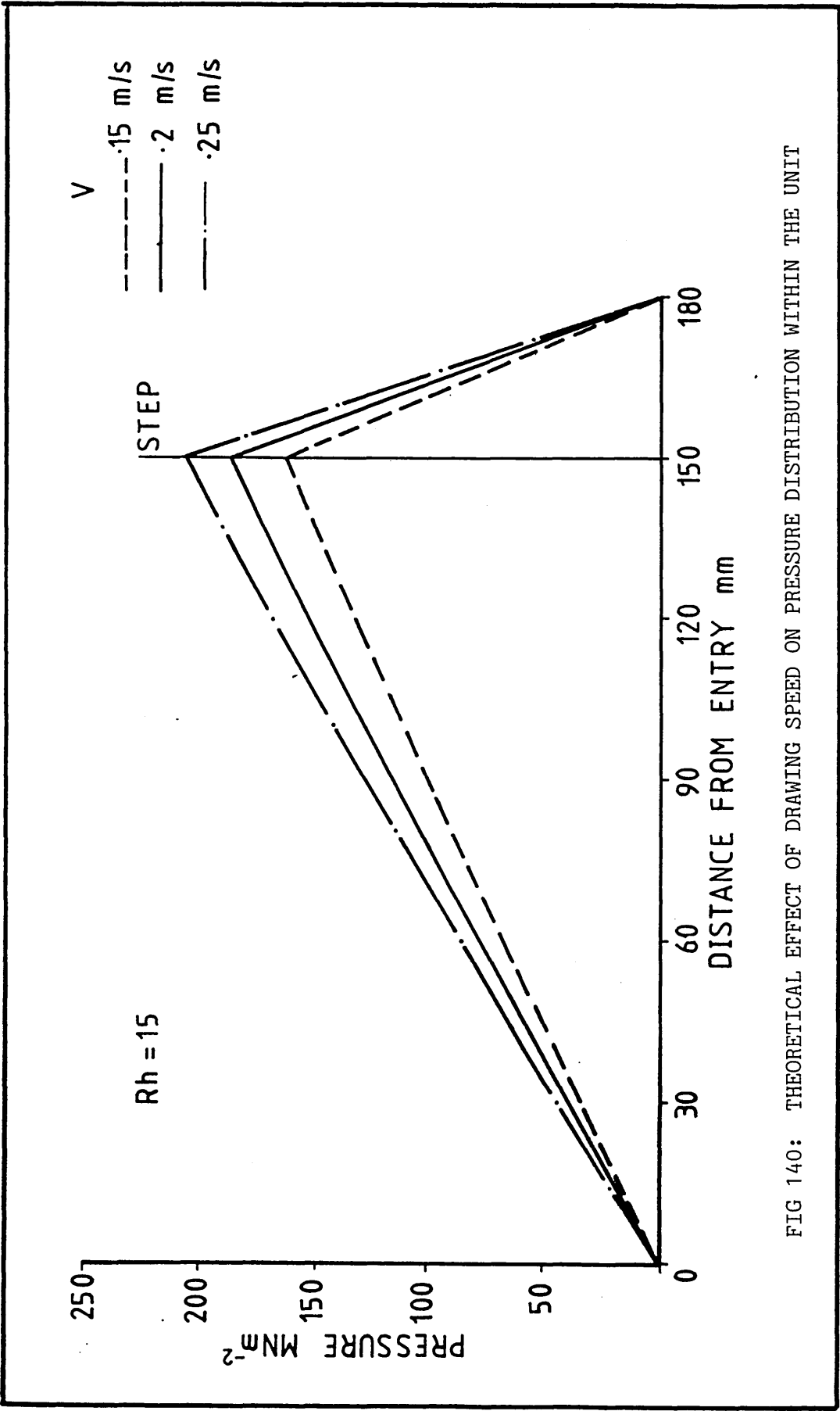


FIG 140: THEORETICAL EFFECT OF DRAWING SPEED ON PRESSURE DISTRIBUTION WITHIN THE UNIT

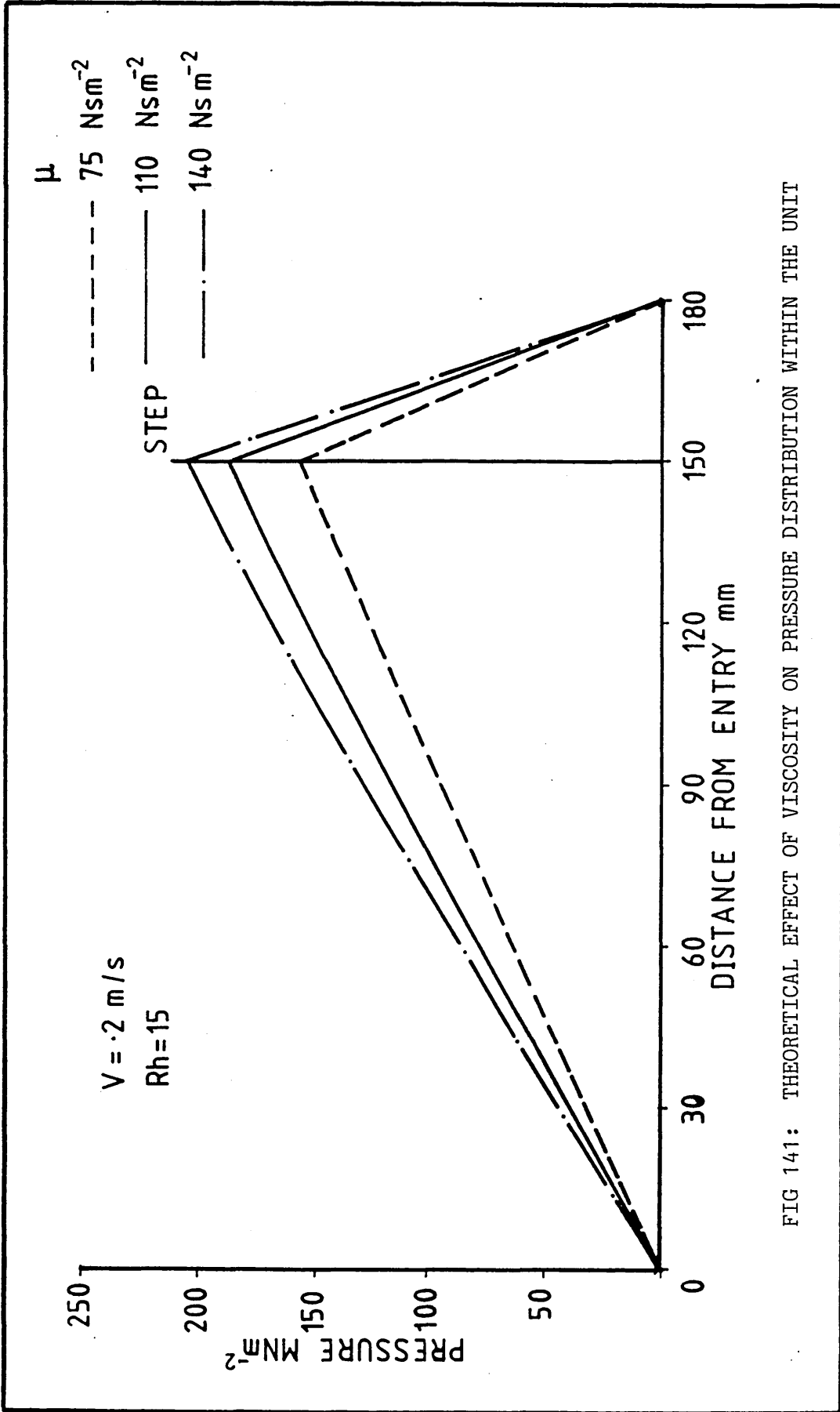


FIG 141: THEORETICAL EFFECT OF VISCOSITY ON PRESSURE DISTRIBUTION WITHIN THE UNIT

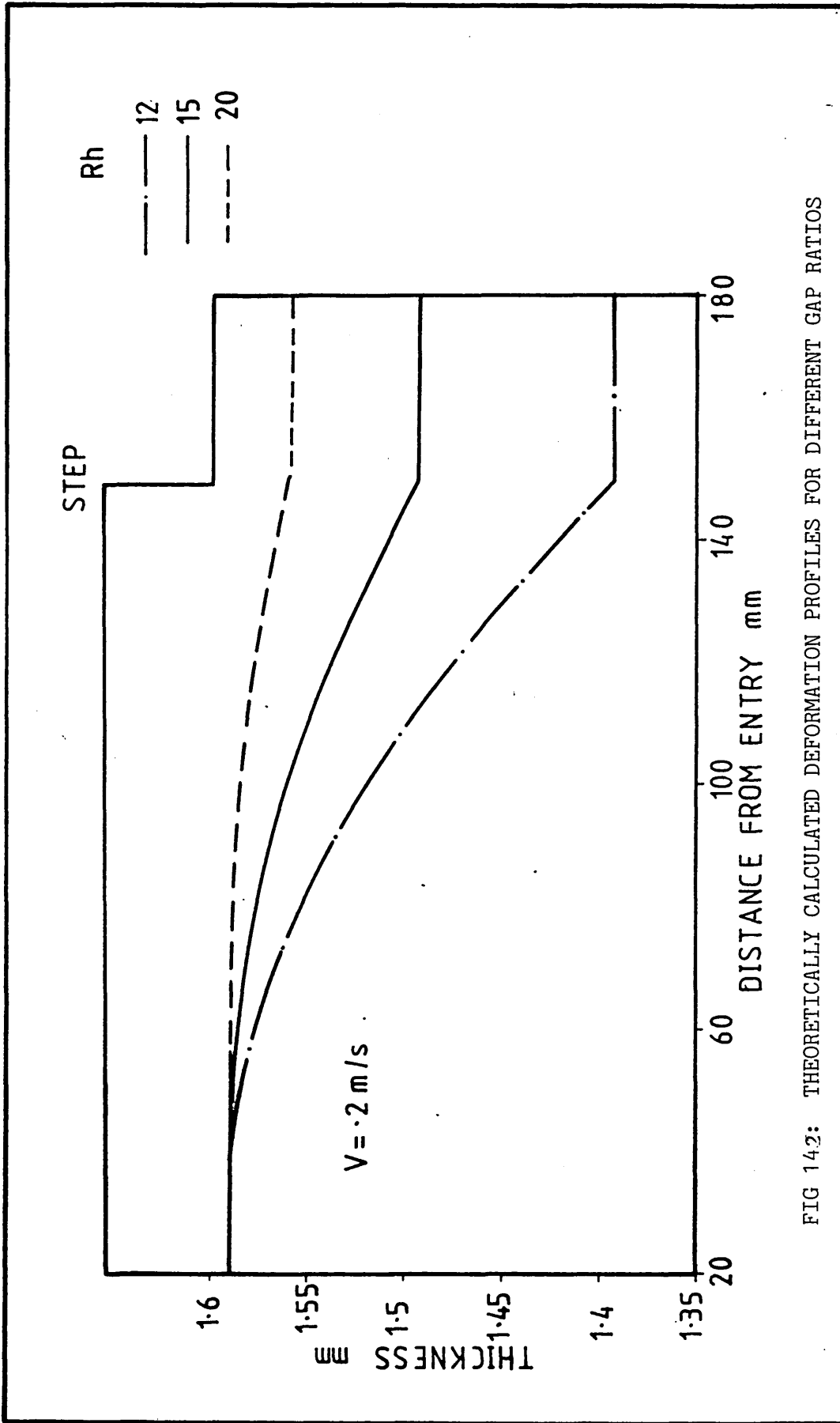


FIG 14.2: THEORETICALLY CALCULATED DEFORMATION PROFILES FOR DIFFERENT GAP RATIOS

V
 --- .15 m/s
 — .2 m/s
 -·- .25 m/s

STEP

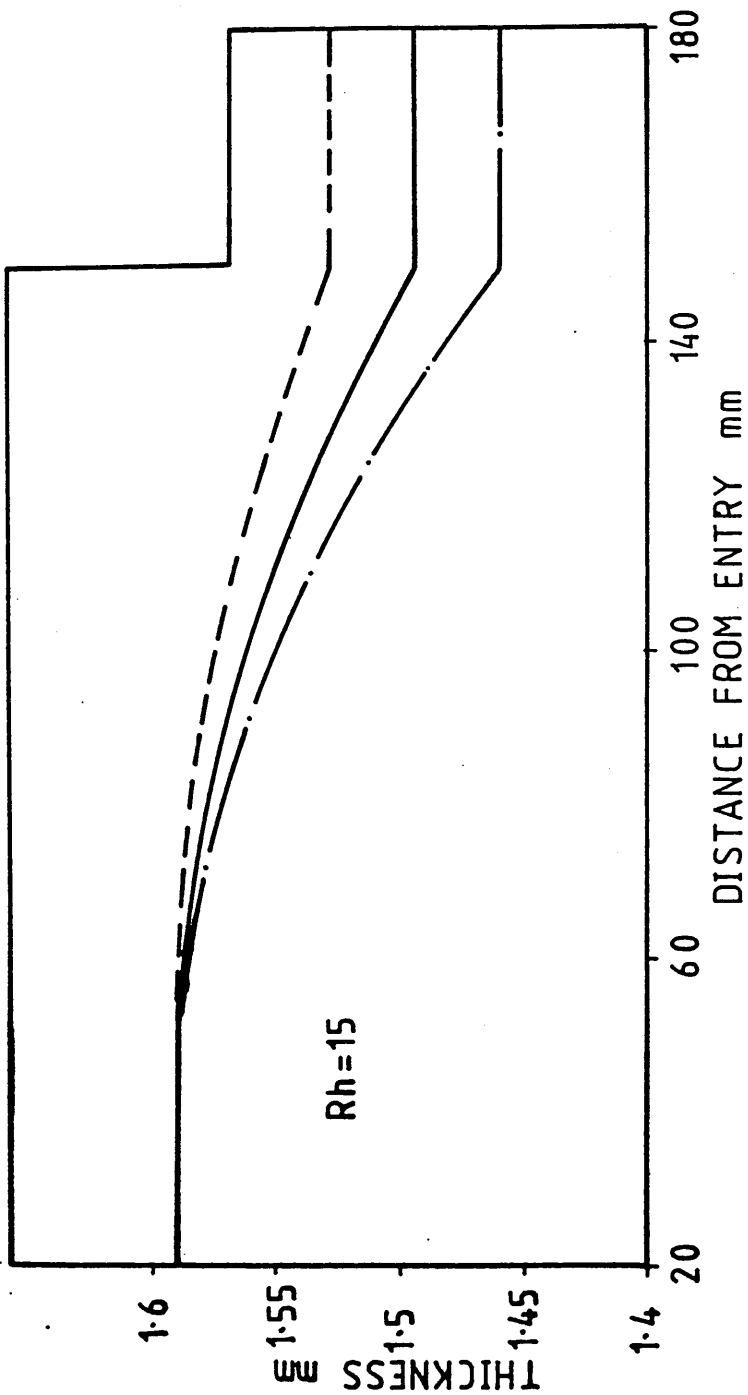


FIG 143: THEORETICALLY CALCULATED DEFORMATION PROFILES FOR DIFFERENT DRAWING SPEEDS

CHAPTER 7

DISCUSSION

7.1 Introduction

In the present work the application of a new die-less drawing process to draw narrow strips is studied. In this process the conventional reduction die has been replaced by a unit with a stepped rectangular hole and a polymer melt has been used to generate hydrodynamic pressure within the unit. To investigate the performance of the process, an extensive experimental and theoretical programme of study was undertaken, which produced a considerable amount of data. This chapter aims to highlight the salient points observed experimentally and theoretically and thereby carry out the comparison of the results.

7.2 Experimental Results

In order to elucidate the effect of various factors on the process, the experimental programme was conducted by varying important physical parameters such as geometry of the die-less reduction unit, polymer type, melt temperature and strip size. To get different geometrical configurations of the die-less reduction unit, the variables h_3 (gap in Section B), h_1 (inlet gap in Section A), and L_1 (inlet length in Section A) were varied, and the variables h_2 , L_2 (exit gap and length) were kept constant during the programme of tests. The drawing speed was also varied to observe its effect on the process.

The strip was drawn at different drawing speeds in the range of 0.1 m/s to 0.5 m/s and the drawing speed was found to have a dominant effect on the effectiveness of the process in terms of

reduction in thickness/width. It was observed that initially, reduction in the strip size increased with increase in drawing speed, but after a certain critical drawing speed further increase in speed caused a decrease in the reductions. This can be attributed to the rheological behaviour of the polymer melt. The polymer melt is non-Newtonian in behaviour and it may have influenced the performance in two ways. Firstly the viscosity of the melt is dependent on the shear stress and shear rate and decreases with an increase in shear stress (see Fig 10) and secondly flow instabilities, particularly slip (Chapter 3), which takes place at higher shear stresses in the range of 0.1-1.0 MNm⁻² (ref 53-59). Slip is thought to be the cause of the less promising performance at high speeds. With increase in the drawing speed shear stress is increased and as the critical value of shear stress is surpassed slip occurs at the polymer-strip interface. This is also evident from the results representing the measured pressures near the step and will be discussed later on.

Figures 14 to 24 show the effect of the gap h_3 , on the percentage reduction in thickness and width of the strip. These results emphasize that gap h_3 affects predominantly the reduction in width. An increase in the gap h_3 causes less reductions in the width. Referring to the basic equation of shear stress (see equation 24), it is obvious from this equation that an increase in gap h_3 will cause a decrease in shear stress and hence in axial stress which would be responsible for lower reductions at higher values of gap h_3 .

The results demonstrating the effect of gap ratio h_1/h_2 on the percentage reductions in the strip size, using two polymers is

presented in Figures 25 to 36. These results are obtained by changing the gap h_1 , and show that the gap h_1 has a significant effect on the percentage reduction in the thickness/width. It is evident that for given values of h_2 and h_3 , h_1 has an optimum value. For magnitudes of h_1 smaller or greater than this optimum value the reduction in thickness/width decrease. This may be explained in terms of pressures generated due to the geometry of the unit. A decrease in the inlet gap may cause a decrease in the flow rate resulting in lower pressures and hence lower reductions. This trend was confirmed when no deformation was observed by using a gap, h_1 , equal to 0.1 mm. On the other hand it should be noted that larger gap h_1 will cause lower shear stress (see equation 22) and hence axial stress which changes the magnitude of plastic deformations.

All these graphs showing the effect of the two gaps, ie gap h_3 and gap h_1 , indicate that both the gaps have a significant effect on the reductions in the strip size. Therefore optimum values are present for which the performance would be maximum.

The effect of length ratio is illustrated in Figures 37 and 38, these results were obtained by varying inlet length L_1 . Similar trends were observed as with gap ratio. It is evident that there is an optimum value of length L_1 and for the values of L_1 higher or lower than this the reduction in strip size decreases.

Figures 41 and 42 demonstrate the effect on the percentage reduction in strip for three different temperatures with the two polymers. Clearly, an increase in melt temperature will decrease the viscosity of the polymer melt, therefore higher reductions were obtained at lower temperatures.

Pressure transducers were mounted on the unit and located at different points along the length of the unit. The generated pressures were recorded on a UV recorder for each increment of the speed. Figures 51 to 59 illustrate the measured pressures near the step and Figures 60 to 67 show the pressure distribution along the unit. These results indicate that the maximum pressure occurs at a point near the step and after a certain critical speed, its magnitude remains fairly constant (irrespective of speed). This gives evidence of the fact that slip takes place during the drawing process.

The drawing load was monitored from the load indicator, shown in Plate No 6. The observed results represented in terms of drawing stresses are shown in Figures 68 to 85. These results show similar trends and are consistent with the results obtained for the reductions in area of the strip (see Figures 20 to 24, 31 to 36 and 39 to 40). It is noticed that the drawing stresses measured with the polymer ELVAX650 are of higher magnitudes compared to those recorded for WVG23. This trend may be explained by the fact that ELVAX650 was low melt flow index (MFI8) and hence more viscous causing an increase in the drawing load and in the reduction in area.

It was observed that the percentage reduction in width (typically 4.56% when corresponding percentage reduction in thickness was 5.34%) obtained with ELVAX650 was relatively higher compared to the percentage reduction in width (typically 3.2% when corresponding percentage reduction in thickness was 5.5%) achieved with WVG23. This could be attributed to the rheological characteristics of the polymer melt. ELVAX650 being of low MFI was more

viscous than WVG23, hence higher stresses produced in Section B with ELVAX650 might have caused greater reductions. This can also be observed by referring to Figure 144.

7.3 Theoretical Results

Two mathematical models have been developed which enabled the prediction of various results such as pressure distribution before and after the onset of yielding, shear and axial stresses, and the deformation profile of the strip. In the formulation of governing equations, various assumptions were made to simplify the mathematical treatment. The validity of these assumptions is discussed as follows:

- (i) Flow is laminar - This seems a reasonable assumption as the film thickness is small, the viscosity is high and the drawing speeds are low.
- (ii) Isothermal conditions exist - This may have introduced some errors in the results since viscosity is sensitive to the temperature change.
- (iii) Polymer slip occurs at the strip-polymer interface - The values of critical shear stress τ_c , used in the analysis were 0.28 MNm^{-2} in Newtonian analysis and 0.22 MNm^{-2} in non-Newtonian analysis. These values were selected as being within the range normally encountered ($0.1 - 1.0 \text{ MNm}^{-2}$, ref 53 to 59). It must be remembered that the data available was not for the polymers used in the present work and did not correlate to the pressures and shear stresses experienced in the present set-up. Hence the value of τ_c chosen for the analysis was only an approximation. In order to calculate the flow of polymer melt after slip occurs it was assumed that the polymer melt could not accommodate further increase in pressure when slip occurs and that a constant flow rate would prevail irrespective of the

drawing speed. These assumptions allowed the results to be calculated easily after slip occurred.

- (iv) The empirical equation proposed by Rabinowitsch for the flow of non-Newtonian fluids in the form,

$$\tau + K\tau^3 = \mu \frac{\partial v}{\partial y}$$

is used in the non-Newtonian analysis to predict the pressure and the shear stress in the unit within the no slip range. The non-Newtonian factor K and initial viscosity μ of the melt were both determined experimentally by curve fitting the above equation over the results obtained from the flow characteristics of the polymer melt (see Chapter 3). It must be noted that the above equation relates the viscosity with shear stress only, but this is also dependent upon many other factors. This might have resulted in some discrepancies.

- (v) Initial viscosity of polymer melt remains constant in the above Rabinowitsch equation, it is known that pressure increases the viscosity and the temperature rise has quantitatively the opposite effect, ie an increase in temperature causes a decrease in viscosity. During the process heat is generated in two ways, (a) shear flow and (b) plastic deformation of the material. Unless this is dissipated through the unit wall, it will result in an increase in the average melt temperature and hence reduction in the melt viscosity. On the other hand, the pressures generated are of high magnitude, which will result in an increase in the viscosity. Since initial viscosity was assumed to remain constant during the process, this might have caused some discrepancies in the

results. Although, some degree of cancelling effect would be present.

The predicted results in strip size showed that:

- (i) in the case of Newtonian analysis (closed form analytical solution), the reduction in strip size always increases with the drawing speed,
- (ii) in the case of Newtonian (numerical) and non-Newtonian analysis two zones were observed;
 - (a) at slower speeds the percentage reduction in area increased as the drawing speed was increased,
 - (b) after slip is predicted to occur, the percentage reduction in area reduced for further increase in the drawing speed.

As different parameters were varied, various trends were noticed from the results which are enumerated as below:

- (i) Increase in h_1 , decreased the percentage reduction in area and also altered the critical speed, ie by increasing gap h_1 slip was predicted to occur at higher speeds.
- (ii) Increase in inlet length, increased the percentage reductions.
- (iii) Increase in initial yield stress, decreased the percentage reductions. Increase in strain hardening constant has the same effect.
- (iv) Increase in viscosity, increased the percentage reduction in area before slip. It also decreased the critical speed at which slip would occur.
- (v) Increase in non-Newtonian factor K, decreased the percentage reduction before slip and increased the critical speed.

Some of the above results were expected and others became more apparent as the results were studied.

The predicted results seem to be very sensitive to inlet gap, h_1 . These are presented in Figures 122 to 123. With a small gap of $h_1 = 0.2$ mm the predicted results of reductions are of higher magnitude and slip was predicted to take place at slow speeds. When a gap of $h_1 = 0.4$ mm was used, slip was predicted at higher speeds and small deformations were predicted (maximum about 5%), since lower pressures were calculated.

The length ratio was found to have a direct effect on the deformations. Large inlet length caused greater deformations, since higher pressures were calculated.

Increases in yield stress and strain hardening constant caused lower reductions as expected. These factors simply change the level of flow stress. The higher the flow stress, lower are the reductions predicted. It was found that these factors (Y_0 , K_0) have a little effect on the critical drawing speed.

Slip was found to occur at slow speeds for higher value of the initial viscosity and larger reductions were predicted in strip size before the slip. It is of interest to note that the initial viscosity has no significant effect on the calculated percentage reductions at high speed (see Figures 130 and 131). It is thought to be the consequence of the fact that, when the condition of slip is predicted the shear stress and pressures are assumed to remain constant, which also causes the calculated deformation zone to remain constant for further increment in drawing speed, resulting in the predicted reductions to reduce gradually.

The reduction in the non-Newtonian factor was expected to increase the deformation as the fluid became more Newtonian. Similar trends were observed to those obtained for viscosity, after slip occurs.

Predicted results for the onset of yielding of the strip material produced another set of results. It may be noted that critical drawing speed is more distinguishable in the case of Newtonian analysis (Figures 99, 102 and 105) compared to the results obtained with the non-Newtonian analysis (Figures 136 to 138). The following observations were made from the results.

- 1 Increase in initial gap h_1 , increases the undeformed length of the strip. Initial yield stress had a similar effect.
- 2 Increase in viscosity, lengthens the deformation zone.
- 3 After slip, the predicted value of point X_1 , is constant for further increments in the speed.

These results could be justified by referring to the equation for determining the distance X_1 . This equation suggests that distance X_1 is directly proportional to the initial yield stress and inversely proportional to the pressure and shear stress. Therefore an increase in yield stress simply increases the undeformed zone. Similarly, any parameter which causes the prediction of higher pressures and shear stress in the unit will move the position of X_1 nearer to the entry point, thus increasing the deformation zone.

The pressure distribution in the unit demonstrating the effect of initial gap and viscosity are shown in Figures 117, 119, 139 and

141. These figures show that higher pressures were predicted for small value of h_1 and higher value of viscosity, hence confirming the effect of these parameters (h_1, μ) on the predicted percentage reductions, as higher percentage reductions were predicted with a decrease in gap h_1 and increase in viscosity.

7.4 Comparison between Experimental and Theoretical Results

Experimental and theoretical results were discussed in the foregoing sections. Some discrepancies were apparent between these results. In this section, it is aimed to discuss the possible causes of their occurrence.

Figures 145 to 147 show the typical experimental results of percentage reduction in thickness and area obtained with WVG23 at 130°C and ELVAX650 at 140°C for 12.7 mm wide strip. Theoretical results are calculated by using equations derived in two mathematical models and are plotted on the same graph for comparison. The dimensions of the unit and magnitudes of other variables were kept the same as those in the experiments. It is evident that the predictions from the closed form Newtonian analysis differ from experimental results both in trend and magnitude. Newtonian (numerical solution) and non-Newtonian analyses under-estimate the percentage reductions at slower speed and at higher speeds, for which the critical shear stress became applicable, the theoretical results over-estimate the experimental ones. However, the theoretical trends are similar to those of the experimental results. Possible explanations for these discrepancies may be as follows:

- 1 Non-Newtonian characteristics of the polymer melt and the difficulty in ascertaining the different parameters defining the rheology of the polymer melt. In the present analysis a relationship relating shear stress and viscosity for non-Newtonian fluid flow is used, whereas other influencing factors such as the dependence of viscosity upon pressure and temperature have been ignored. Also the analyses do not take account of any variations from the

isothermal and laminar flow conditions during the process.

It is thought that errors could have arisen from the absence of these factors.

2 The prediction of the slip to commence was based upon the value of critical shear stress τ_c , which was chosen from the available data. Variations in the value of τ_c was examined theoretically (Figures 134 and 135). These results demonstrate that critical shear stress not only alters the critical speed but also changes the predicted results after slip. The polymers used in references 53 to 59 were not exactly the same as those used in the present work, hence this might have caused errors.

3 It has been demonstrated that the performance of the process is very sensitive to the geometry of the unit particularly to the inlet gap h_1 . Any variation in this parameter would cause variations in the predicted results. The parameter h_1 was determined by measuring the thickness of the strip and width of the rectangular hole. Therefore an error may have occurred in determining this parameter, considering the errors in measuring and allowing for manufacturing tolerances. Hence this is also thought to be a probable cause.

Typical experimentally measured and theoretically calculated pressures are shown in Figure 148. Theoretical results from both analyses appear to overestimate the experimental results in each case. The predicted maximum pressure (at the step) is about twice the measured maximum pressure (near the step). However, the trends of experimentally measured pressures and theoretically calculated pressures are very similar.

Also for comparison purposes, the measured and predicted deformation profiles are shown in Figures 148 to 149. In the case of the polymer polyethylene WVG23 the yield occurred near to the step and the deformation took place in a much steeper manner than that predicted theoretically (see Figure 148). A good correlation was observed between theoretical and experimental deformation profiles when polymer ELVAX650 (see Figure 149) was used.

Also discrepancies between the theoretical and experimental results were observed in the variation in measured and predicted reductions in width. The present analyses predict the same percentage reductions in both thickness and width, but the measured percentage reduction in width were always found to be smaller compared to those in thickness (except in some cases at higher speed with ELVAX650). Possible reasons for this discrepancy are thought to be;

- (i) anisotropy of the strip material,
- (ii) rheological behaviour of the polymer melt. This is more apparent from the results obtained with ELVAX650 (see Figure 144).

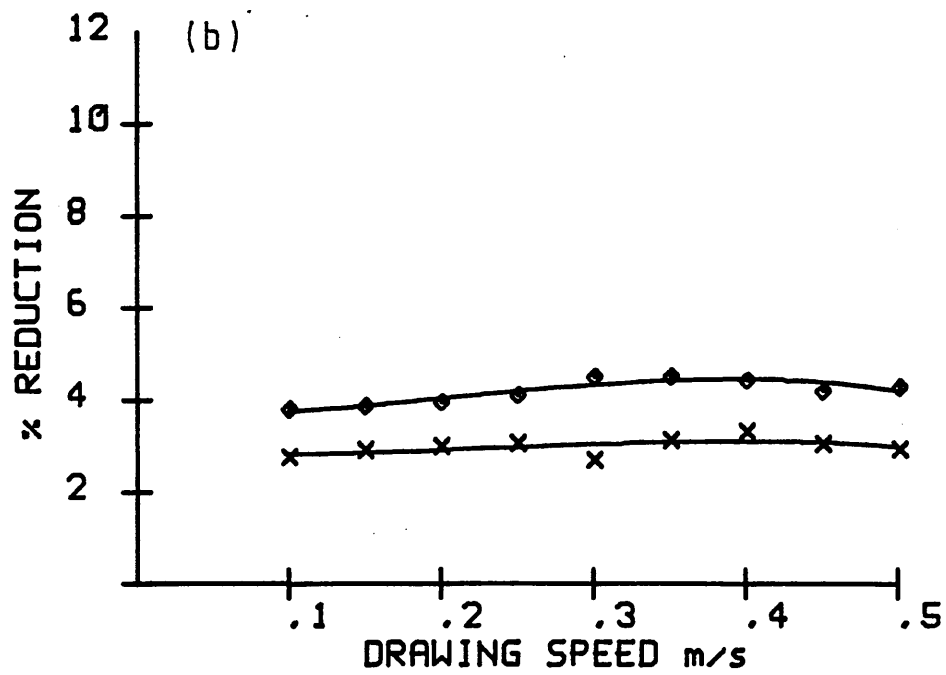
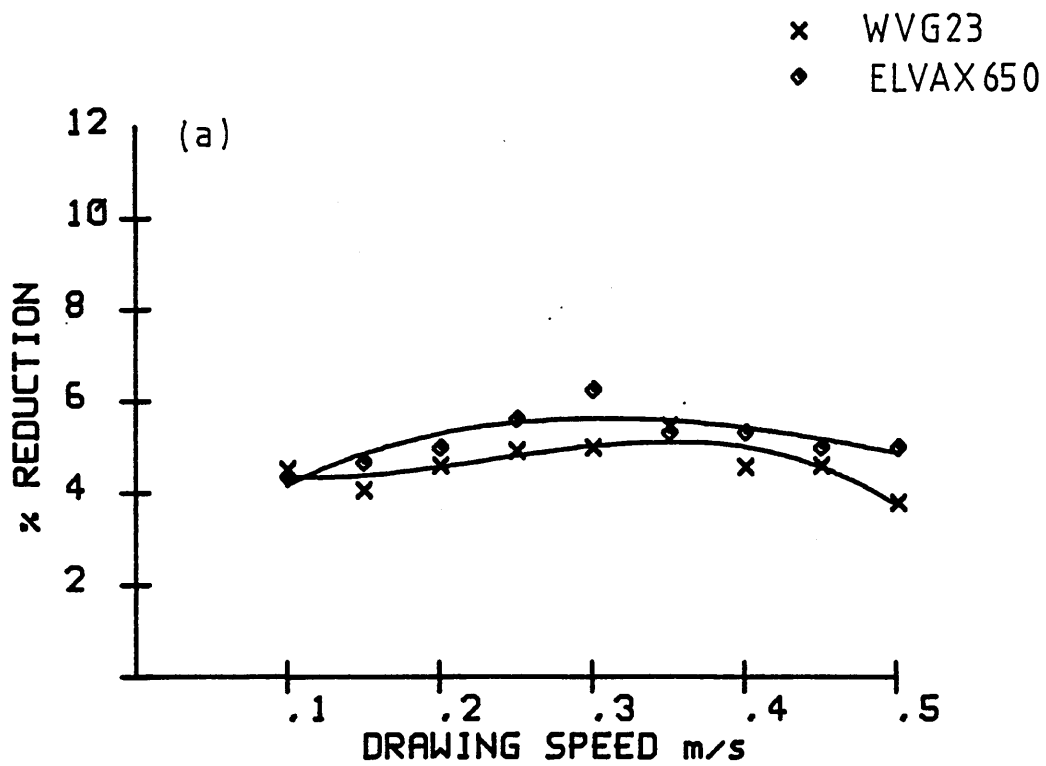


FIG 144: PERCENTAGE REDUCTION IN
 (a) THICKNESS (b) WIDTH
 WITH TWO DIFFERENT POLYMERS

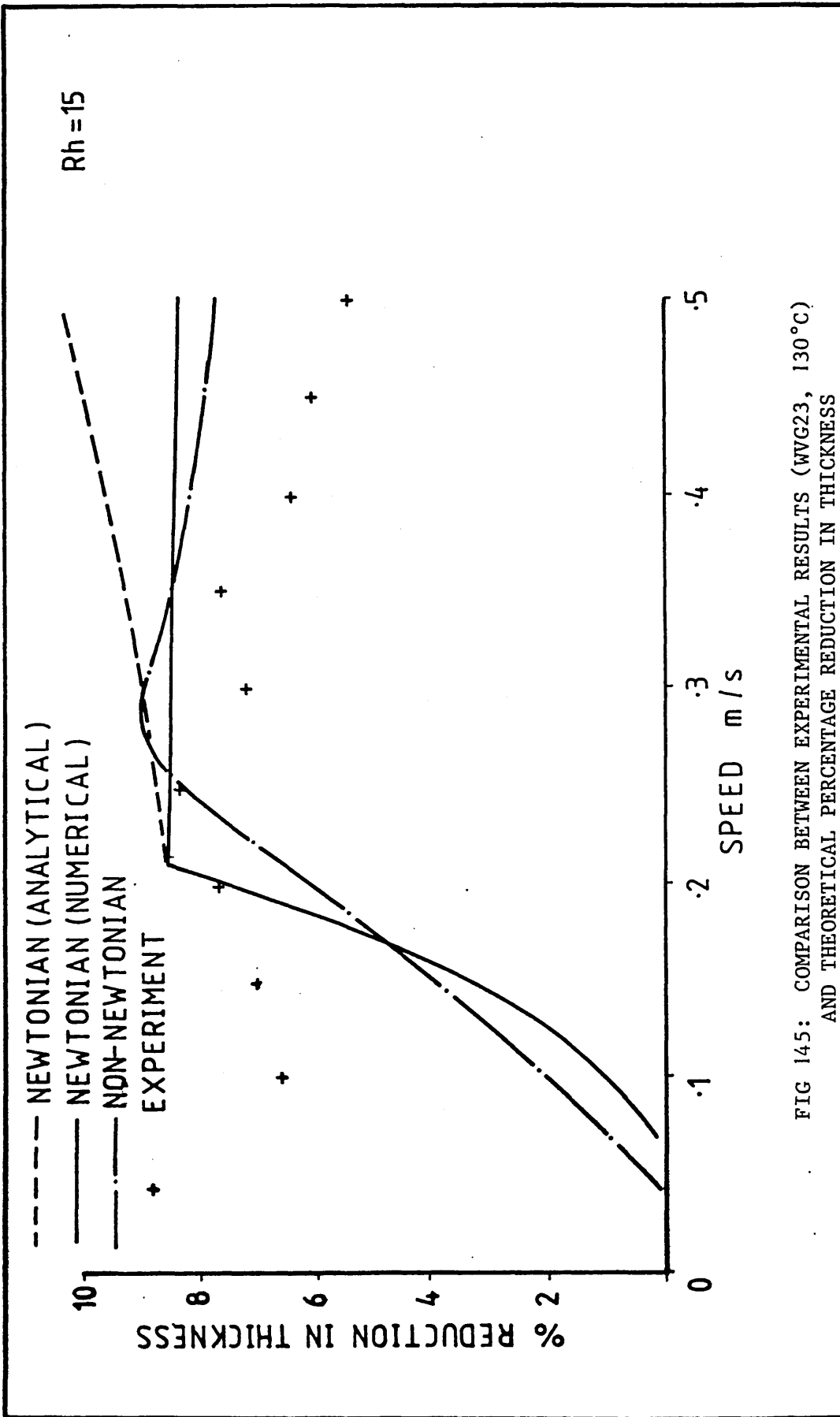


FIG 145: COMPARISON BETWEEN EXPERIMENTAL RESULTS (WVG23, 130 °C) AND THEORETICAL PERCENTAGE REDUCTION IN THICKNESS

Rh = 15

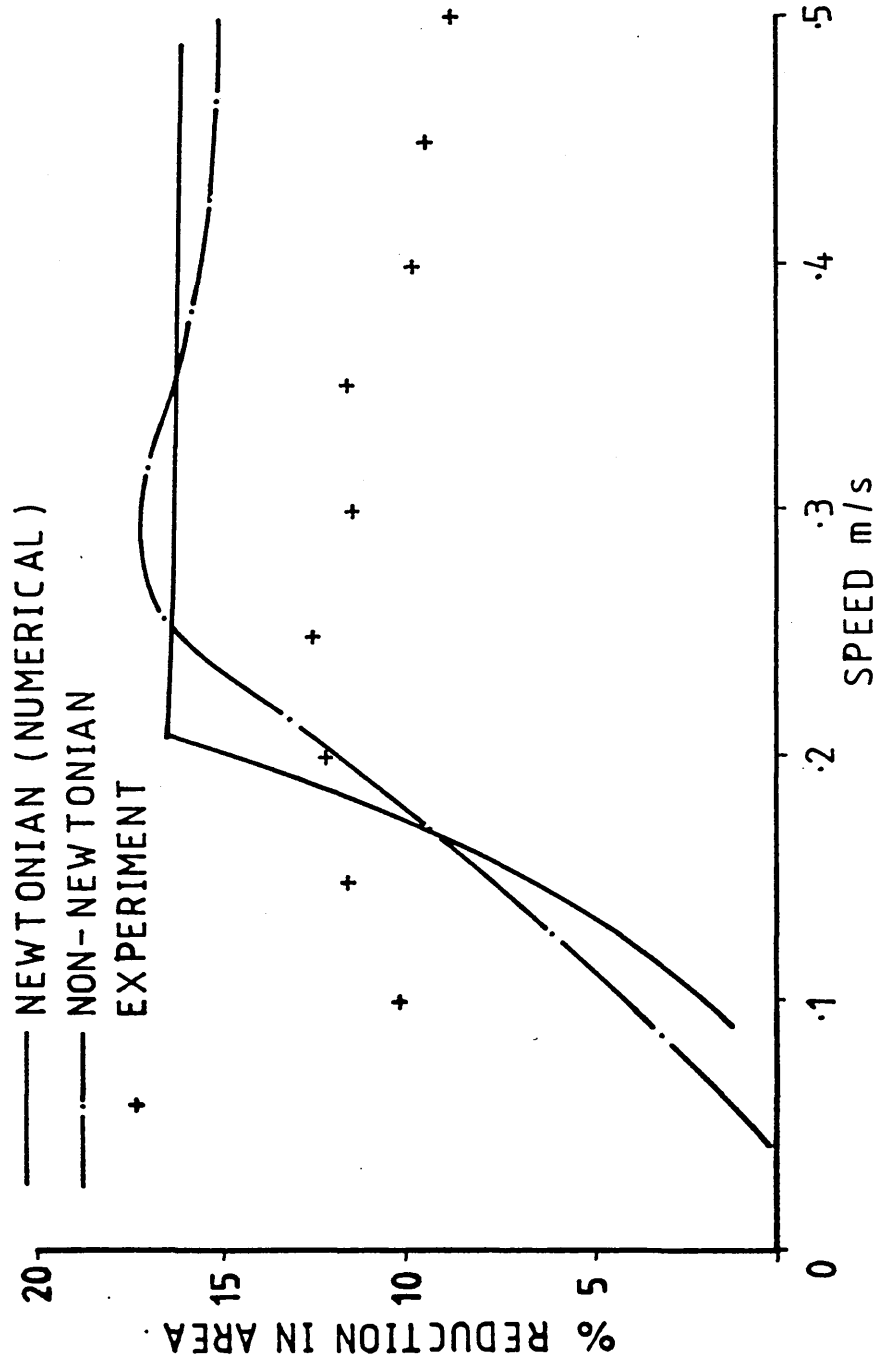


FIG 146: COMPARISON BETWEEN EXPERIMENTAL RESULTS (WVG23, 130°C) AND THEORETICAL PERCENTAGE REDUCTION IN AREA

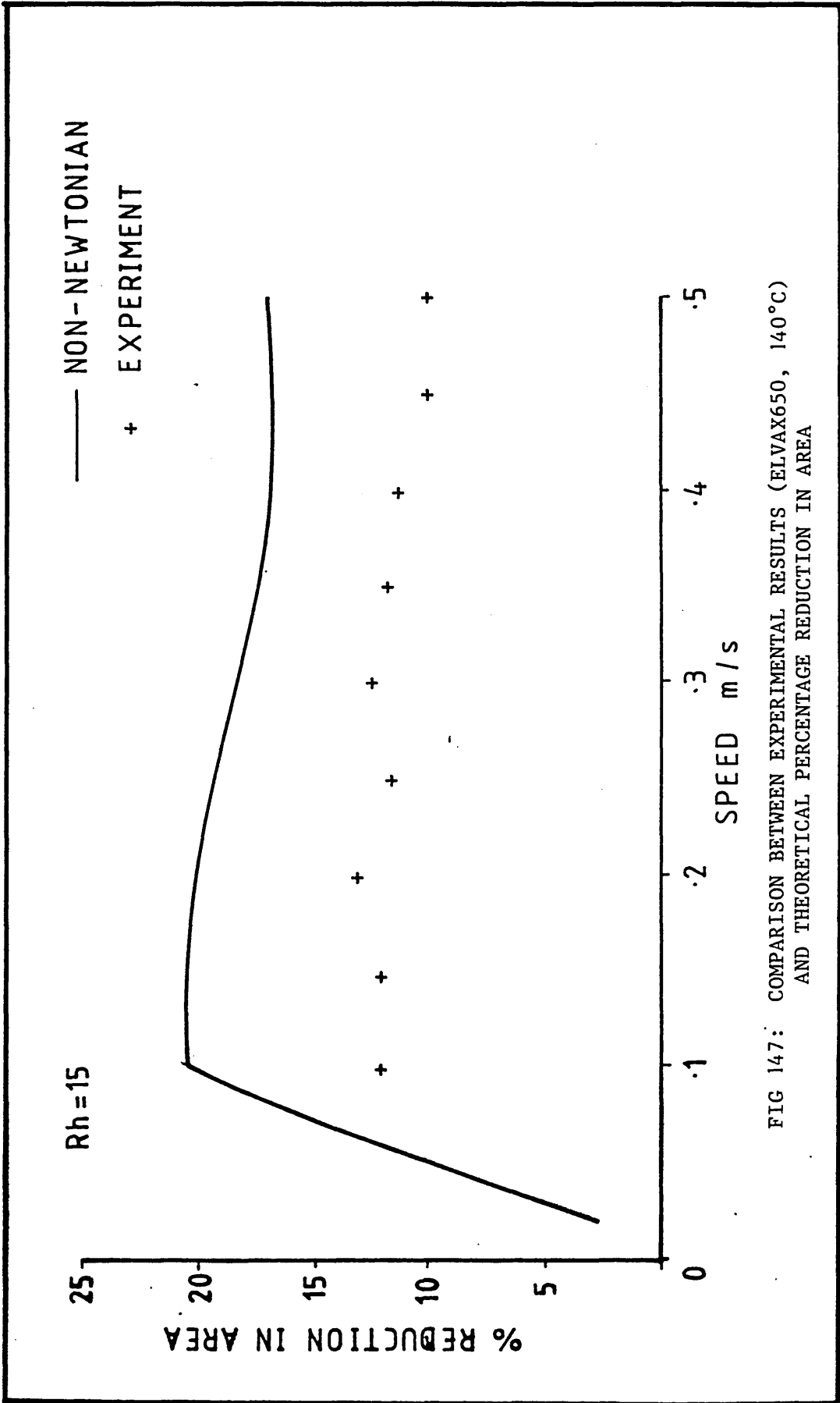


FIG 147: COMPARISON BETWEEN EXPERIMENTAL RESULTS (ELVAX650, 140°C) AND THEORETICAL PERCENTAGE REDUCTION IN AREA

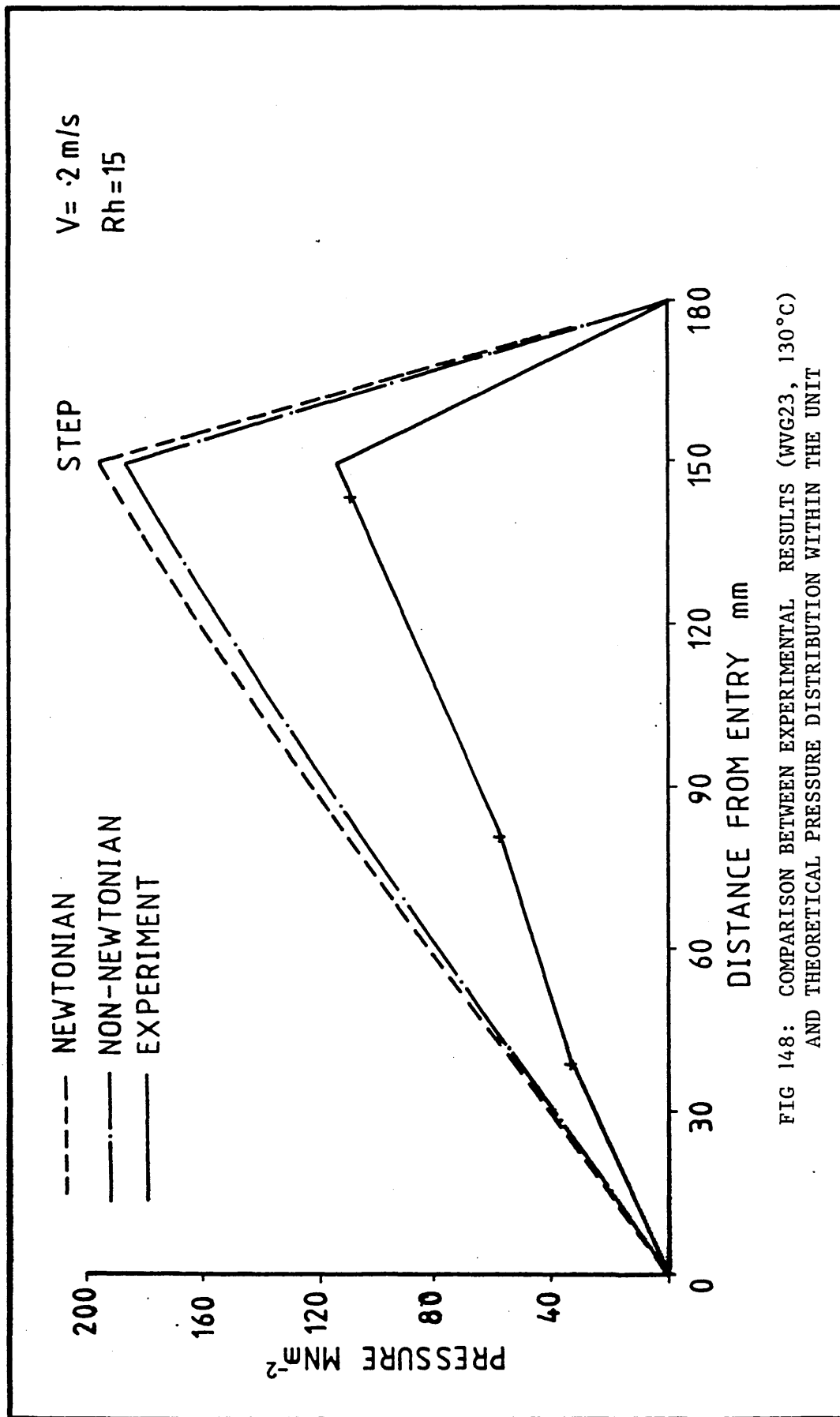


FIG 148: COMPARISON BETWEEN EXPERIMENTAL RESULTS (WVG23, 130°C)
 AND THEORETICAL PRESSURE DISTRIBUTION WITHIN THE UNIT

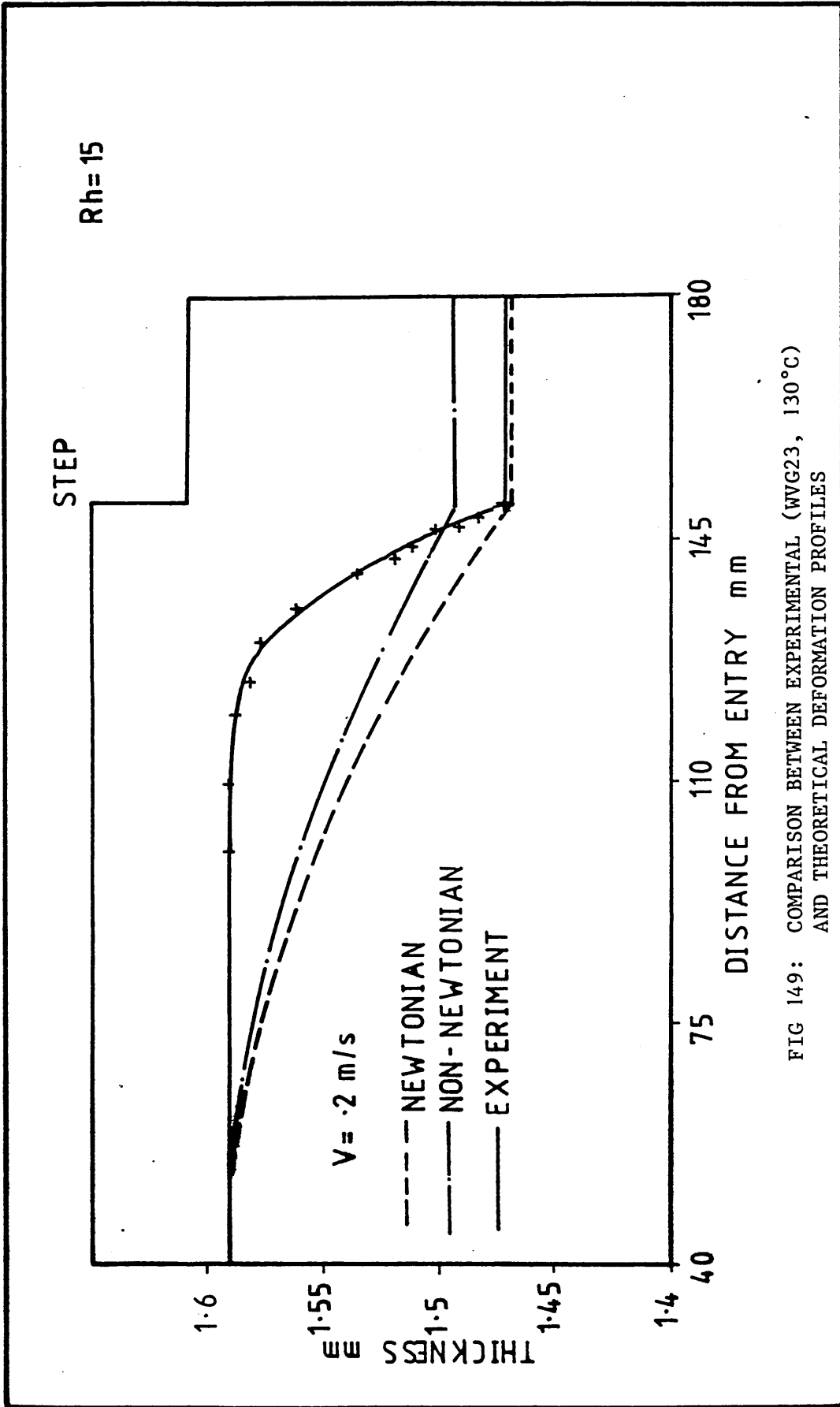


FIG 149: COMPARISON BETWEEN EXPERIMENTAL (WVG23, 130°C) AND THEORETICAL DEFORMATION PROFILES

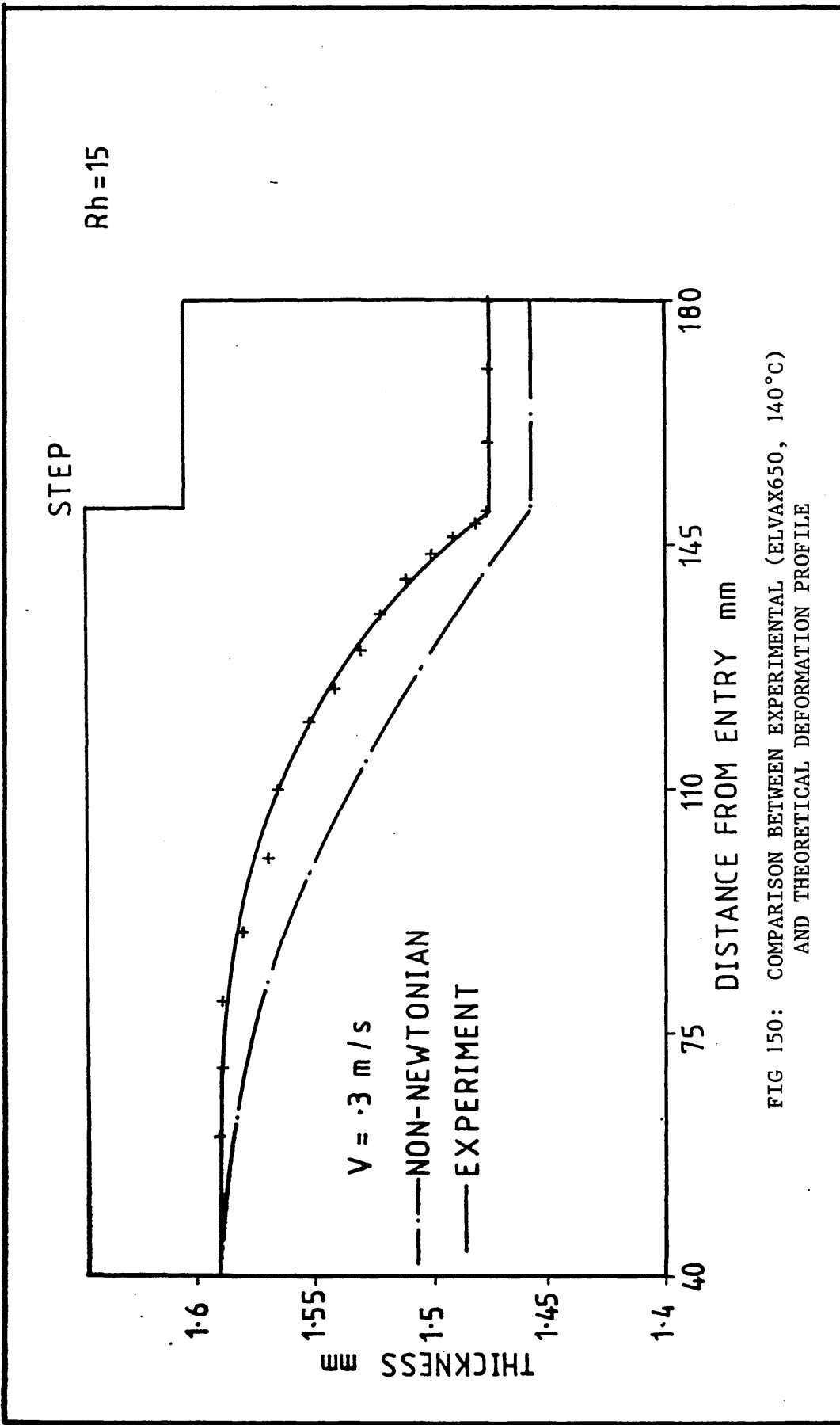


FIG 150: COMPARISON BETWEEN EXPERIMENTAL (ELVAX650, 140°C) AND THEORETICAL DEFORMATION PROFILE

CHAPTER 8

CONCLUSIONS

8.1 Conclusions

A novel process of die-less drawing of narrow strips has been developed. In this unique process, no conventional reduction dies are used. The reductions in strip size are obtained by using a die-less unit with a stepped rectangular hole and a polymer melt as the pressure medium. Sizes of the holes are such that the smallest hole is larger than the cross-section of the incoming strip, preventing direct metal to metal contact, hence overcoming friction and the tool wear encountered in conventional drawing processes. Deformations are caused due to the combined effect of hydrodynamic pressure and induced axial stresses developed by the converging flow of polymer melt (a viscous fluid). Extensive experimental work was conducted to investigate the application of the process. Experimental results showed that a reduction in area of the strip in excess of 12% could be achieved in a single pass by this novel technique. These results also show that the strip is deformed in both thickness and width directions. The magnitudes of the reduction in the two dimensions are significantly dependent upon the polymer type, the geometry of the die-less reduction unit and the drawing speed.

Mathematical models have been developed considering Newtonian and non-Newtonian characteristics of the polymer melt. The results from these models show reasonable correlation in trends but underestimate the percentage reduction at slower speeds and overestimate the percentage reductions at higher speeds when compared to the observed experimental results. However, these models help the understanding of the mechanics of the process.

8.2 Suggestions for Future Work

The technique of die-less drawing investigated in the present study showed that it could be applied to strip drawing. However, certain practical restrictions were noted. The strip was deformed in both thickness and width; the observed reductions were not of the same level. Another limitation observed was the fact that the lower reductions were obtained at higher speeds. Furthermore, discrepancies are also apparent between experimental and theoretical results (even after considering non-Newtonian characteristics of polymer melt flow). Further work could be undertaken both experimentally and theoretically to enhance the understanding of the process.

Experimentally:

In this process, the reduction in the strip size is caused due to viscous flow of the polymer melt through a unit with a stepped hole, and the obtained results are very much dependent upon the type of the polymer. The results indicated that the performance of the process was improved by using ELVAX650 (low MFI, high viscosity). The geometry of the unit has also a significant effect on the obtained results. Therefore in order to explore the viability of the process, further work should be carried out not only using the various polymers of different melt flow index but also on units of different geometry. For example a unit with steps in both sections (A and B).

Theoretically:

In the theoretical analysis the process has been assumed to be isothermal and possible effects of the heat generated due to the mechanical work and viscous shear friction and pressure

generated within the unit has been ignored. It has been demonstrated (Chapter 3) that the viscosity is very much dependent upon the temperature and pressure. An attempt has been made to include the viscosity-temperature dependence in the analysis. The results (Appendix V) clearly show the influence of this parameter on the predicted results.

Since the apparent viscosity of a polymer melt is a function of temperature and pressure, these two factors should be incorporated into the analysis. This should improve the theoretical results.

REFERENCES

- 1 FUKUI S, OHI T, KUDO H, TAKILA I AND SEINO J, 'Some aspects of friction in metal strip drawing', Int J Mech Sci, Vol 4, pp 297-312, 1962.
- 2 LANCASTER P R, ROWE G W, 'Experimental study of the influence of lubrication upon cold drawing under approximately plane-strain conditions at low speeds', Proc Instn Mech Engrs, Vol 178, Pt 1, No 3, pp 69-88, 1963-1964.
- 3 GREEN A P AND HILL R, 'Calculations of influence of friction and die geometry in sheet drawing', J Mech Phys Solids 1, 31, 1952.
- 4 HOFFMAN O AND SACHS G, 'Introduction to the theory of plasticity for engineers', McGraw-Hill, New York and London, 1953.
- 5 GREEN A P, 'Plane strain theories of drawing', Proc Instn Mech Engrs, London, 174, No 31, pp 847-864, 1960.
- 6 KUDO H, TANAKA S, IMAMURA K AND SUZUKI K, 'Investigation of cold forming friction and lubrication with a sheet drawing test', Annals of CIRP, Vol 25/1, pp 179-184, 1976.
- 7 WILSON W R D AND CAZEAULT P, 'Measurement of frictional conditions in lubricated strip drawing', NARMAC - IV, pp 165-171, 1976.
- 8 RAO R S, DEVENPECK M L, WRIGHT P K, APPLEBY E J, LU C Y AND RICHMOND O, 'New strip drawing experiments using transparent sapphire dies', Int J Mech Sci, Vol 27, No 11/12, pp 725-740, 1985.
- 9 APPLEBY E J, LU C Y, RAO R S, DEVENPECK M L, WRIGHT P K AND RICHMOND O, 'Strip drawing : A theoretical-experimental comparison', Int J Mech Sci, Vol 26, No 5, pp 351-362, 1984.
- 10 PARSONS B, TAYLOR R AND COLE B N, 'High speed drawing of metals : A first report', Proc Instn Mech Engrs, Vol 180, Pt 31, pp 230-240, 1965-66.
- 11 BAXTER R S, 'High speed drawing of metals', PhD Thesis, University of Leeds, 1968.
- 12 DEVENPECK M L AND RIGO J H, 'Research apparatus for simulating high speed drawing of thin strip', Procs 7th North American Manufacturing Research Conf, Univ of Michigan, pp 81-88, 1979.
- 13 CHRISTOPHERSON D G AND NAYLOR H, 'Promotion of fluid lubrication in wire drawing', Proc Inst Mech Engrs 169, pp 643-653, 1955.
- 14 TATTERSALL G H, 'Hydrodynamic lubrication in wire drawing', J Mech Engng Sci 3, No 4, p 378, 1961.
- 15 OSTERLE J F AND DIXSON J R, 'Viscous lubrication in wire drawing', ASLE transactions 5, pp 233-241, 1962.
- 16 CHENG H S, 'Plasto-hydrodynamic lubrication', Proc Symp Friction & Lubrication in Metal Processing, New York, pp 69-89, 1966.

- 17 BEDI D S, 'A hydrodynamic model for wire drawing', The Int Jr Prod Res, Vol 6, No 4, pp 329-343, 1968.
- 18 BLOOR S M, DOWSON D AND PARSONS B, 'An elasto-plasto-hydrodynamic lubrication analysis of the plane strain drawing process', Jr Mech Eng Sc, Vol 12, No 3, pp 178-190, 1970.
- 19 DOWSON D, PARSONS B AND LIDGITT P J, 'An elasto-plasto-hydrodynamic lubrication analysis of the wire drawing process', Inst Mech Engrs, C 16, pp 97-106, 1972.
- 20 LANCASTER P R, 'A study of lubrication in the high speed drawing process', Wire Industry, pp 294-297, 1972.
- 21 AVITZUR B, 'The application of hydrodynamic lubrication in wire drawing and extrusion', Wire Journal, pp 74-79, 1976.
- 22 KUDO H, TSUBOUCHI M, TAKADHA H AND OKAMURA K, 'An investigation into plasto-hydrodynamic lubrication with a cold sheet drawing test', Annals of CIRP, Vol 31/1, pp 175-180, 1982.
- 23 WILSON W R D AND MAHDAVIAN S M, 'A Thermal Reynolds equation and its application in the analysis of plasto-hydrodynamic inlet zones', Transactions of the ASME, pp 572-578, 1974.
- 24 DOW T A, KANNEL J W AND BUPARA S S, 'A hydrodynamic lubrication theory for strip rolling including thermal effects', Transactions of the ASME, pp 4-13, 1975.
- 25 MAHDAVIAN S M AND WILSON W R D, 'Lubricant flow in a plasto-hydrodynamic work zone', Transactions of the ASME, pp 16-21, 1976.
- 26 THOMPSON P J AND SYMMONS G R, 'A plasto-hydrodynamic analysis of the lubricating and coating of wire using a polymer melt during drawing', Proc Inst Mech Engr 13, 191, 1977.
- 27 SYMMONS G R, STEVENS A J AND THOMPSON P J, 'Hydrodynamic lubrication and coating of wire using a polymer melt during the drawing operation', Wire Industry, pp 469-473, 1978.
- 28 CRAMPTON R, 'Hydrodynamic lubrication and coating of wire using a polymer melt during drawing process', PhD Thesis, Sheffield City Polytechnic, 1980.
- 29 CRAMPTON R, SYMMONS G R AND HASHMI M S J, 'A non-Newtonian plasto-hydrodynamic analysis of the lubrication and coating of wire using a polymer melt during drawing', Int Symp Metal Working Lubrication, San Francisco, USA, p 107, 1980.
- 30 HASHMI M S J, CRAMPTON R AND SYMMONS G R, 'Effects of strain hardening and strain rate sensitivity of the wire material during drawing under non-Newtonian lubrication conditions', Int J Mach Tool Des Res, Vol 21, No 1, pp 71-86, 1981.
- 31 HASHMI M S J, SYMMONS G R AND PARVINMEHR H, 'A novel technique of wire drawing', Jr Mech Eng Sci (C) I Mech E, Vol 24, No 1, pp 1-4, 1982.

- 32 SYMMONS G R, HASHMI M S J AND PARVINMEHR H, 'Plasto-hydrodynamic die-less wire drawing : Theoretical treatment and experimental results', Proc Int Conf on developments in drawing of metals, Metal Society, London, pp 54-61, 1983.
- 33 PARVINMEHR H, 'Optimisation of plasto-hydrodynamic system of wire drawing using polymer melts', PhD Thesis, Sheffield City Polytechnic, 1983.
- 34 HASHMI M S J AND SYMMONS G R, 'A mathematical model for the drawing of a solid continuum through Newtonian fluid filled tubular orifice', Proc 4th Int Conf on Mathematical Modelling, Zurich, 1983.
- 35 HASHMI M S J AND SYMMONS G R, 'A numerical solution for the plasto-hydrodynamic drawing of a rigid non-linearly strain hardening continuum through a conical orifice, 2nd Int Conf on Numerical Methods for Non-linear Problems, Spain, 1984.
- 36 PARVINMEHR H, SYMMONS G R AND HASHMI M S J, 'A non-Newtonian plasto-hydrodynamic analysis of die-less wire drawing process using a stepped bore unit', Int Jr Mech Sci, Vol 29, No 4, pp 239-257, 1987.
- 37 PANWHAR M I, CRAMPTON R AND HASHMI M S J, 'Die-less tube sinking : A plasto-hydrodynamic analysis based on Newtonian fluid characteristics', Proc of 5th Polytechnic Symp on Manufacturing Engineering, Brighton Polytechnic, 1986.
- 38 PANWHER M I, 'A novel technique for tube sinking, PhD Thesis, Sheffield City Polytechnic, 1986.
- 39 SYMMONS G R, HASHMI M S J AND XIE Y D, 'The optimisation of a plasto-hydrodynamic wire drawing process', IASTED Conference, Paris, June 1987.
- 40 XIE Y, 'Modelling and control of die-less wire drawing, PhD Thesis, Sheffield City Polytechnic, 1987.
- 41 SYMMONS G R, XIE Y AND HASHMI M S J, 'Thermal effect on a plasto-hydrodynamic wire drawing process using a polymer melt', Xth Int Con on Rheology, Sydney, Australia, August 1988.
- 42 COGSWELL F N, 'Polymer melt rheology', George Goodman Ltd, London, 1981.
- 43 MENDELSON R A, 'Prediction of melt viscosity flow curves at various temperatures for some olefine polymers and copolymers', Polymer Engineering and Science, 8 (3), pp 235-240, 1968.
- 44 MENDELSON R A, 'A generalised melt viscosity-temperature dependance for styrene and acrylonitrite based polymers', Polymer Engineering and Science, 16 (10), pp 690-696, 1976.
- 45 NIELSEN L E, 'Polymer Rheology', Marcel Dekker Inc, New York and Basel, p 31, 1977.

- 46 WILLIAM M L, LANDEL R F AND FERRY J D, 'The temperature dependance of relaxation mechanisms in amorphus polymers and other glass forming liquids', Journal of American Chemical Society, 77, pp 3701-3707, 1955.
- 47 BRYDSON J A, 'Flow properties of polymer melts', George Goodwin Ltd, 1981.
- 48 OGORKIEWICZ R M, 'Thermoplastics, properties and design', A collective work by ICI Plastic Division, 1974.
- 49 MAXWELL B AND JUNG A, 'Hydrostatic pressure on polymer melt viscosity', Modern Plastic, pp 174-182, Nov 1957.
- 50 WESTOVER R F, 'Effect of hydrostatic pressure on polyethylene melt rheology', SPE Technical Papers, 6, pp 80-1 to 80-4, 1960.
- 51 WESTOVER R F, 'Effect of hydrostatic pressure on polyethylene melt rheology', SPE Transactions, pp 14-20, Jan 1961.
- 52 CHOI S Y, 'Determination of melt viscosity as a function of hydrostatic pressure in an extrusion rheometer', Jr of Poly Sc, Part A-2, Vol 6, pp 2043-2049, 1968.
- 53 BENBOW J J AND LAMB P, 'New aspects of melt fracture', SPE Transactions, pp 7017, Jan 1963.
- 54 TORDELLA J P, J Appl Phys, 27, p 454, 1957.
- 55 TORDELLA J P, Trans Soc Rheology, 1, p 203, 1957.
- 56 TORDELLA J P, 'Unstable flow of molten polymers : A second site of melt fracture', Jr Appl Poly Sci, Vol 7, pp 215-229, 1963.
- 57 WESTOVER R F, 'The significance of slip in polymer melt flow', Polymer Engineering and Science, pp 83-89, 1966.
- 58 HAN C D AND LAMONATE R R, 'A study of polymer melt flow instabilities in extrusion', Polymer Engineering and Science, Vol 11, No 5, Sept 1971.
- 59 METZNER A B, 'Fracture of non-Newtonian fluids at high shear stresses', Industrial and Engg Chem, Vol 50, No 10, pp 1577-1581, 1958.
- 60 HASHMI M S J, 'Strain rate sensitivity of commercially pure copper at room temperature and strain rate of up to 10^6 per second', Sheffield City Polytechnic Technical Report No SCP/MPE/R10, Oct 1978.
- 61 RABINOWITSCH B, 'Uber Die Viskostat Und Elastizitat Von Solen', Z Phys Chem, A 145, p 141, 1929.
- 62 REKTERYS K, 'Survey of applicable mathematics', Illiffe Publications, pp 77-79, 1969.

APPENDIX I

Expression for b*

According to Levy-Mises flow rule

$$\frac{d\epsilon_1}{\sigma'_1} = \frac{d\epsilon_2}{\sigma'_2} = \frac{d\epsilon_3}{\sigma'_3} = d\lambda \quad (A1)$$

where

$$\sigma'_1 = \sigma_1 - \sigma_m, \sigma'_2 = \sigma_2 - \sigma_m \text{ and } \sigma'_3 = \sigma_3 - \sigma_m$$

$$\text{where } \sigma_m = \frac{\sigma_1 + \sigma_2 + \sigma_3}{3}$$

$$\text{Now } \sigma_1 = \sigma_x, \sigma_2 = -P \text{ and } \sigma_3 = -P^*$$

$$d\epsilon_1 = d\epsilon_t, d\epsilon_2 = d\epsilon_t \text{ and } d\epsilon_3 = d\epsilon_w$$

$$\therefore \sigma'_1 = \sigma_x - \sigma_m, \sigma'_2 = -P - \sigma_m, \sigma'_3 = -P^* - \sigma_m$$

\therefore Equation (A1) gives

$$\frac{d\epsilon_t}{-P - \sigma_m} = \frac{d\epsilon_w}{-P^* - \sigma_m}$$

Assuming $P^* = P$

$$\text{Hence } d\epsilon_t = d\epsilon_w$$

$$\therefore \frac{dt_i}{t_i} = \frac{dW_i}{W_i} \quad (A2)$$

$$\text{Now } t_i = t_1 - 2bx$$

$$\text{or } dx = -\frac{dt_i}{2b} \quad (A3)$$

$$\text{and } W_i = W_1 - 2b^*x$$

$$\text{or } dx = -\frac{dW_i}{2b^*} \quad (A4)$$

Comparing equations (A3) and (A4)

$$\frac{dW_i}{dt_i} = \frac{b^*}{b}$$

$$b^* = b \frac{dW_i}{dt_i}$$

Substituting for $\frac{dW_i}{dt_i}$ from equation (A2)

$$b^* = b \frac{W_i}{t_i} \quad (A5)$$

$$\therefore b^* = \frac{b(W_1 - 2b^*x)}{(t_1 - 2bx)} \quad (A6)$$

Simplifying equation (A6) gives,

$$b^* = b \frac{W_1}{t_1} \quad (A7)$$

or $b^* = mb \quad (A8)$

where m is constant and equal to the ratio of the initial width to the initial thickness.

$$\frac{W_1}{t_1} = m$$

$$b^* = mb$$

Velocity in Deformation Zone

The continuity of flow of metal gives

$$(V_i + dV)(t_i + dt)(W_i + dW) = V_i t_i W_i \quad (A1)$$

Equation (A1) on simplifying and dividing by $V_i t_i W_i$ gives,

$$\begin{aligned} \frac{dt}{t_i} + \frac{dV}{V_i} + \frac{dVdt}{V_i t_i} + \frac{dW}{W_i} + \frac{dt dW}{t_i W_i} + \frac{dV dW}{V_i W_i} + \frac{dV dt dW}{V_i t_i W_i} &= 0 \\ \frac{dV}{V_i} \left[1 + \frac{dt}{t_i} + \frac{dW}{W_i} + \frac{dt dW}{t_i W_i} \right] &= - \frac{dt}{t_i} - \frac{dW}{W_i} - \frac{dt dW}{t_i W_i} \\ \frac{dV}{V_i} \left[\frac{t_i W_i + W_i dt + t_i dW + dt dW}{t_i W_i} \right] &= - \left[\frac{W_i dt + t_i dW + dt dW}{t_i W_i} \right] \\ \frac{dV}{V_i} [t_i W_i + W_i dt + t_i dW + dt dW] &= - [W_i dt + t_i dW + dt dW] \end{aligned}$$

Writing in finite difference form we obtain

$$\begin{aligned} \left(\frac{V_{i-1} - V_i}{V_i} \right) [t_i W_i + W_i (t_{i-1} - t_i) + t_i (W_{i-1} - W_i) + (t_{i-1} - t_i) \\ (W_{i-1} - W_i)] &= - [W_i (t_{i-1} - t_i) + t_i (W_{i-1} - W_i) + (t_{i-1} - t_i) \\ (W_{i-1} - W_i)] \quad (A2) \end{aligned}$$

On simplification equation (A2) gives

$$\begin{aligned} \left[\frac{V_{i-1}}{V_i} - 1 \right] [W_{i-1} t_{i-1}] &= - [W_{i-1} t_{i-1} - W_i t_i] \\ \frac{V_{i-1}}{V_i} - 1 &= \frac{W_i t_i - W_{i-1} t_{i-1}}{W_{i-1} t_{i-1}} \\ \frac{V_{i-1}}{V_i} - 1 &= \frac{W_i t_i}{W_{i-1} t_{i-1}} - 1 \\ V_i &= V_{i-1} \left(\frac{W_{i-1} t_{i-1}}{W_i t_i} \right) \quad (A3) \end{aligned}$$

LISTING OF THE COMPUTER PROGRAMME FOR NEWTONIAN,
A CLOSED FORM ANALYTICAL SOLUTION

```
DIMENSION V(500),X(500),E(500)
REAL L1,L2
5 WRITE(6,10)
10 FORMAT(2X,'THIS PROGRAMME CALCULATES THEORETICAL',2X,/,
11X,'REDUCTION IN AREA OF STRIP USING NEWTONIAN SOLUTION',2X,
11X/,1X,'AND THREE DIMENSIONAL DEFORMATION')
WRITE(6,15)
15 FORMAT(2X,'INPUT H1,H2,H3 IN METERS.')
READ(5,*)H1,H2,H3
WRITE(6,20)
20 FORMAT(2X,'INPUT INITIAL LENGTH L1,FINAL LENGTH L2,INITIAL VISCOS:
ITY VS')
READ(5,*)L1,L2,VS
WRITE(6,25)
25 FORMAT(2X,'YIELD STRESS Y1,STRAIN HARDENING CONSTANT K,INDEX N')
READ(5,*)Y1,A,F
WRITE(6,30)
30 FORMAT(2X,'INITIAL THICKNESS T1,WIDTH W1,CRITICAL SHEAR STRESS TCA
L)
READ(5,*)T1,W1,TCA
V(1)=0.00
G=W1/T1
DO 245 I=2,50
V(I)=V(I-1)+0.01
WRITE(6,35)
35 FORMAT(1X,'*****')
WRITE(6,40)V(I),H1,H2,H3,L1,L2,VS
40 FORMAT(2X,'V=' ,2X,F8.5,2X,'H1=' ,E8.2,2X,'H2=' ,E8.2,2X,'H3=' ,E8.2,
1X,'L1=' ,E8.2,2X,'L2=' ,E8.2,2X,'VS=' ,E8.2)
PM=(6*VS*V(I)*(H1-H2))/(((H1**3)/L1)+((H2**3)/L2))
TC1=-((PM*H1)/(2*L1))-(VS*V(I)/H1)
TC2=+((PM*H2)/(2*L2))-(VS*V(I)/H2)
TC3=-((PM*H3)/(2*L1))-(VS*V(I)/H3)
X1=(Y1)/((2*ABS(TC1)/T1)+(2*ABS(TC3)/W1)+(PM/L1))
IF (X1.GT.L1) GOTO 235
P1=(PM*X1)/L1
S1=(2*ABS(TC1)*X1/T1)+(2*ABS(TC3)*X1/W1)
WRITE(6,50) PM,TC1,X1,P1,S1
50 FORMAT(2X,'PM=' ,F12.2,2X,'TC1=' ,F10.2,2X,'X1=' ,F8.5,2X,'P1=' ,
1F12.2,2X,'S1=' ,F12.3)
IF (ABS(TC1).GE.TCA) GOTO 250
REP=INT(X1*1000)-1
N=L1*1000-REP
X(1)=0.0
STEP=1E-03
REM=1.E+03
REM3=1E-05
B=0.0
K=0.0
60 B=B+STEP
BB=G*B
K=K+1
X(J)=L1-X1
H=H1+B*X(J)
HH=H3+BB*X(J)
```

```

T=T1-(2*B*X(J))
W=W1-(2*BB*X(J))
IF(T.LT.STEP) GOTO 130
IF(W.LT.STEP) GOTO 130
T2=T1+2*H1
W2=W1+2*H3
5 F1=F+1
Y=Y1+A*((2*ALOG(T1/T))*F)
PS=(6*VS*V(I)/B)*((H1/(2*(H**2)))-(1/(H))+(1/(2*H1)))+(PM/L1)*
I(X1+(H1/(2*B))-((H1**3)/(2*B*(H**2))))
TC=-((VS*V(I)/H**2)*((4*B*X(J))+((PM*H1**3)/(2*VS*V(I)*L1))+H1)
TCC=-((HH/2)*(((6*VS*V(I)*B*X(J))/(H**3))+((PM*(H1**3))/(L1*(H**3)
1))))-(VS*V(I)/HH)
T3=T2**2
T4=T2**3
T5=ALOG(T1/T)
H5=ALOG(H/H1)
A1=9*VS*V(I)
A2=(A1/4)*H1
A3=PM*(H1**3)/L1
A4=(3*A1/4)*(B*H3/BB)
A5=3*A1/4
A6=A3*H3*B/BB
A7=A3
A8=(A1/4)*(B/BB)
C1=((T1*A1)+(2*(A2+A3)))/T3
C2=((2*T1*(A4+A7))+((T1**2)*A5)+(4*A6))/T4
C3=(BB*T1)+(2*B*H3)
B1=(2*C1)+(2*C2)+(2*B*A8/C3)+(4*B*Y1)
B2=C1+C2
B3=((A2+A3-(H1*A1))/T2)+((T1*(A4+A7)-(2*H1*(T1+H1)*A5)+(2*A6))/T3)
B4=(A6+((H1**2)*A5)-(H1*(A4+A7)))/T2
B5=BB*A8/C3
B6=(2*(F1+1))*B*A
SD=(1/B)*(((B1/2)*T5)+(B2*H5)+((B3/1)*((1/H1)-(1/H)))+(B4/2)*(((1
L/H1)**2)-((1/H)**2)))+(B5/BB)*ALOG(HH/H3))+((B6/(2*B*F1))*(T
15**F1))+S1
YM=PS+SD
RES=YM-Y
E(K)=ABS(RES)
RES2=E(K)-E(K-1)
IF(ABS(RES2).LE.REM3) GOTO 90
IF(ABS(RES).LE.REM) GOTO 90
IF(RES)80,90,60
0 B=B-STEP
STEP=STEP/10
GOTO 60
H4=H-H1+H2
FRT=((2*B*X(J))/T1)*100
PRW=(1-(W/W1))*100
FRA=(1-((W*T)/(W1*T1)))*100
TC4=((H4*PS)/(2*L2))-((VS*V(I)/H4)
TC21=((HH*PS)/(2*L2))-((VS*V(I)/HH)
S2=((2*ABS(TC4)*L2)/(T))+((2*ABS(TC21)*L2)/(W))
SD1=SD+S2

```

```

WRITE(6,91)PRT,T,SD1,W,PRW,FRA
91 FORMAT(2X,'PRT=',F8.5,1X,'Z',2X,'T=',F8.5,2X,'SD1=',F15.2,2X,'W=
1',F8.5,2X,'PRW=',F8.5,1X,'Z',2X,'FRA=',F8.5,1X,'Z')
GOTO 245
30 WRITE(6,140)
40 FORMAT(2X,'STRIP BREAKS AT THIS SPEED')
GOTO 370
110 WRITE(6,220)
20 FORMAT(2X,'-----')
1-----')
GOTO 245
135 WRITE(6,240)
140 FORMAT(2X,'X1 IS .GT. L1')
145 CONTINUE
GOTO 370
50 WRITE(6,260)
60 FORMAT(2X,'----- CONDITION OF SLIP DETECTED -----')
DO 360 II=1,60
V(II)=V(I)
X(I)=0.0
B10=0.0
K=0.0
STEP1=1E-03
REM1=1E05
F1=1+F
X(J)=L1-X1
70 B10=B10+STEP1
K=K+1
BB1=G*B10
T=TI-(2*B10*X(J))
W=W1-(2*BB1*X(J))
IF(T.LT.0) GOTO 130
IF(W.LT.0) GOTO 130
Y=Y1+A*((2*ALOG(T1/T))**F)
H=H1+B10*X(J)
HH=H3+BB1*X(J)
T5=ALOG(T1/T)
T6=ALOG(T/T1)
PS=(6*VS*V(II)/B10)*((H1/(2*(H**2)))-(1/(H))+(1/(2*H1)))+(PM/L1)*(
LX1+(H1/(2*B10))-((H1**3)/(2*B10*(H**2))))
SD=(2*Y1*T5)+(((2**F1)*A/F1)*(T5**F1))+((TC1/B10)*T6)+((TC3/BB1)*
LT6)+S1
YM=PS+SD
RES1=YM-Y
E(K)=ABS(RES1)
RES4=E(K)-E(K-1)
IF(ABS(RES4).LE.REM3) GOTO 310
IF(ABS(RES1).LE.REM1) GOTO 310.
IF(RES1)300,310,270
90 B10=B10-STEP1
STEP1=STEP1/10
GOTO 270
310 H41=H-H1+H2
TC21=((P5*H41)/2*L2)-(VS*V(II)/H41)
TC31=((P5*HH)/2*L2)-(VS*V(II)/HH)

```

```

S22=((2*ABS(TC21)*L2)/(T))+((2*ABS(TC31)*L2)/(W))
SD2=SD+S22
PRW=(1-(W/W1))*100
PRT=(1-(T/T1))*100
PRA=(1-((W*T)/(W1*T1)))*100
WRITE(6,341)V(II)
341 FORMAT(2X,'V=',F8.4)
WRITE(6,346)PRT,PRW,PRA
346 FORMAT(2X,'PRT=',F8.4,1X,'Z',2X,'PRW=',F8.4,1X,'Z',2X,'PRA=',F8.4,
1X,'Z')
WRITE(6,348)PS,SD,SD2
348 FORMAT(2X,'PS=',F10.0,2X,'S=',F10.0,2X,'SD=',F10.0)
347 WRITE(6,350)
350 FORMAT(2X,'*****
*****')
V(I)=V(II)+0.01
IF(V(I).GE.0.51) GOTO370
360 CONTINUE
370 WRITE(6,380)
380 FORMAT(2X,'TO RUN THIS PROGRAMME AGAIN TYPE 1,/,
12X,'OTHERWISE TYPE 0.')
READ(5,*)CC
IF(CC.EQ.1)GOTO 5
STOP
END

```

```

DIMENSION V(500),P(500),T(500),E(1000),E1(1000),S(500),PS(500)
DIMENSION H(500),TCC(500),TC(500),Y(1000),X(500),W(500),HH(500)
REAL L1,L2
5 WRITE(6,10)
10 FORMAT(2X,'THIS PROGRAMME CALCULATES THEORETICAL' ,//,2X,
1' REDUCTION IN THICKNESS AND WIDTH OF STRIP USING NUMERICAL SOLUTIO
IN' ,//,2X,' ASSUMING NEWTONIAN BEHAVIOR OF POLYMER MELT')
WRITE(6,15)
15 FORMAT(2X,'INPUT UNIT DIMENSIONS H1,H2,H3,L1,L2 IN METERS')
READ(5,*)H1,H2,H3,L1,L2
WRITE(6,20)
20 FORMAT(2X,'INPUT INITIAL THICKNESS T1 AND WIDTH W1')
READ(5,*)T1,W1
WRITE(6,25)
25 FORMAT(2X,'INPUT INITIAL YIELD STRESS Y0, STRAIN HARDENING CONSTANT
IA, STRAIN HARDENING INDEX F')
READ(5,*)Y0,A,F
WRITE(6,26)
26 FORMAT(2X,'INPUT STRAIN RATE SENSITIVITY CONSTANTS SRC ,SCR')
READ(5,*)SRC,SCR
WRITE(6,30)
30 FORMAT(2X,'INPUT INITIAL VISCOSITY OF POLYMER MELT VS0 AND SHEAR S
TRESS TCA')
READ(5,*)VS,TCA
READ(5,*)DD
VEL=0.00
35 DO 100 I=1,50
VEL=VEL+0.01
PM=6*VS*VEL*((H1-H2)/(((H1**3)/L1)+((H2**3)/L2)))
TC1=-(VS*VEL/H1)-(PM*H1/(2*L1))
TC2=-(VS*VEL/H2)+(PM*H2/(2*L2))
TC3=-(VS*VEL/H3)-(PM*H3/(2*L1))
X1=Y0/((PM/L1)+(2*ABS(TC1)/T1)+(2*ABS(TC3)/W1))
P1=(PM*X1)/L1
WRITE(6,40)
40 FORMAT(1H0,'*****
I*****')
WRITE(6,45)H1,H2,H3,L1,L2,A,VS
45 FORMAT(2X,'H1=',F6.5,2X,'H2=',F6.5,2X,'H3=',F6.5,2X,'L1=',F8.6,2X,
1'L2=',F8.6,'A=',F10.0,2X,'VS=',F6.2)
WRITE(6,50)PM,VEL,TC1,X1,P1
50 FORMAT(2X,'PM=',F12.2,'VEL=',F4.2,2X,'TC1=',F10.2,2X,'X1=',F8.5,2X
1', 'P1=',F12.2)
IF (X1.GT.L1) GOTO 100
REP=INT(X1*1000)-1
N=L1*1000-REP
P(1)=P1
S(1)=(2*ABS(TC1)*X1/T1)+(2*ABS(TC3)*X1/W1)
PS(1)=P(1)+S(1)
Y(1)=Y0
T(1)=T1
W(1)=W1
H(1)=H1
HH(1)=H3
X(1)=X1

```

```

TC(1)=TC1
TCC(1)=TC3
V(1)=VEL
DX=0.001
DO 93 J=2,N,1
STEP=1E-03
REM=1E-03
B=0.0
K=0.0
55 B=B+STEP
K=K+1
BB=B*W1/T1
X(J)=X(J-1)+DX
T(J)=T(J-1)-(B*DX)
W(J)=W(J-1)-(BB*DX)
H(J)=H(J-1)+(0.5*B*DX)
HH(J)=HH(J-1)+(0.5*BB*DX)
IF(T(J).LT.0) GOTO 150
IF(W(J).LT.0) GOTO 150
V(J)=V(J-1)*W(J-1)*T(J-1)/(W(J)*T(J))
DP=(PM*(H1**3)/(L1*(H(J)**3)))+6*VS*((V(J)*H(J)-VEL*H1)
1/(H(J)**3))
TC(J)=-((DP*H(J)/2)-(VS*V(J)/H(J))
P(J)=DP*DX+P(J-1)
PF=P(J)
TCC(J)=-((DP*HH(J)/2)-(VS*V(J)/HH(J))
F1=1+(((V(J)*ALOG((W(J-1)*T(J-1))/(W(J)*T(J)))/DX)/SRC)**(1/SCR))
Y(J)=F1*(Y0+A*((ALOG((W1*T1)/(W(J)*T(J))))**F))
S(J)=(((T(J-1)/T(J))+((W(J-1)/W(J))-2)*Y(J))+(2*ABS(TC(J))*DX/T(J))
1+(2*ABS(TCC(J))*DX/W(J))+S(J-1)
SS=S(J)
PS(J)=P(J)+S(J)
RES=PS(J)-Y(J)
E(K)=ABS(RES)
RES1=E(K)-E(K-1)
IF(ABS(RES).LE.1E05) GOTO 65
IF(ABS(RES1).LE.REM) GOTO 63
IF(RES) 60, 65,55
60 B=B-STEP
STEP=STEP/10
GOTO 53
65 PRT=(1-(T(J)/T1))*100
PRW=(1-(W(J)/W1))*100
PRA=(1-(W(J)*T(J))/(W1*T1))*100
H4=H(J)-H1+H2
TC4=((P(J)*H4)/(2*L2))-VS*V(J)/H4
TC5=((P(J)*HH(J))/(2*L2))-VS*V(J)/HH(J)
S2=(2*ABS(TC4)*L2/T(J))+2*ABS(TC5)*L2/W(J)
SD=S(J)+S2
IF(DI.EQ.1) GOTO95
70 WRITE(6,75)B,PF,Y(J),X(J),T(J),SS
75 FORMAT(2X,'B=',F6.9,2X,'P=',F12.2,2X,'Y=',F12.2,2X,'X=',F8.5,2X
1,'T=',F9.6,2X,'S=',F12.2)
80 WRITE(6,85)PRT,PRW,PRA,V(J),SD
85 FORMAT(2X,'PRT=',F8.5,1X,'X',2X,'PRW=',F8.5,1X,'X',2X,'PRA=',F8.5,

```

```

12X,'VD=' ,F4.2,2X,'SD=' ,F16.2)
WRITE(6,90)
90 FORMAT(2X,'.....
i.....')
95 CONTINUE
IF(ABS(TC1).GE.TCA) GOTO 110
IF(DD.NE.1) GOTO 100
WRITE(6,96)PRT,PRW,PRA,PF,SS,SD
96 FORMAT(2X,'PRT=' ,F8.5,1X,'Z' ,2X,'PRW=' ,F8.5,1X,'Z' ,2X,'PRA=' ,F8.5,
11X,'Z' ,2X,'PS=' ,F12.2,2X,'S=' ,F12.2,2X,'SD=' ,F12.2)
100 CONTINUE
GOTO 180
110 WRITE(6,115)
115 FORMAT(2X,'$$$$$$$$$$$$$ CONDITION OF SLIP WAS DETECTED $$$$$$$$$$$$
i$$')
DO170 J=1,60
VEL=VEL
DO 145 J=2,N,1
V(1)=VEL
STEP=1E-03
REML=1E-03
R=0.0
KI=0.0
120 B=B+STEP
KI=KI+1
BB=B*W1/T1
X(J)=X(J-1)+DX
T(J)=T(J-1)-(B*DX)
W(J)=W(J-1)-(BB*DX)
HH(J)=HH(J-1)+0.5*BB*DX
IF(T(J).LT.0) GOTO 130
IF(W(J).LT.0) GOTO 130
H(J)=H(J-1)+0.5*B*DX
V(J)=V(J-1)*W(J-1)*T(J-1)/(W(J)*T(J))
PF=P(J)
F1=1+(((V(J)*ALOG((W(J-1)*T(J-1))/(W(J)*T(J)))/DX)/SRC)**(1/SCR))
Y(J)=F1*(Y0+A*((ALOG((W1*T1)/(W(J)*T(J))))**F))
S(J)=(((T(J-1)/T(J))+((W(J-1)/W(J))-2)*Y(J))+(2*ABS(TC1)*DX/T(J))
i+(2*ABS(TC3)*DX/W(J))+S(J-1)
SS=S(J)
PS(J)=P(J)+S(J)
RES2=PS(J)-Y(J)
E1(K1)=ABS(RES2)
RES3=E1(K1)-E1(K-1)
IF(ABS(RES2).LE.1E05) GOTO 130
IF(ABS(RES3).LE.REML) GOTO 130
IF(RES2)125,130,120
125 B=B-STEP
STEP=STEP/10
GOTO 120
130 PRT=(1-(T(J)/T1))*100
PRW=(1-(W(J)/W1))*100
PRA=(1-(W(J)*T(J))/(W1*T1))*100
S2=(2*ABS(TC1)*L2/T(J))+(2*ABS(TC3)*L2/W(J))
SD=S2+S(J)

```

```

IF(DO.EQ.1) GOTO 145
WRITE(6,131)X(J)
131 FORMAT(2X,'X=',F6.4)
135 WRITE(6,140)PRT,PRW,PRA,VEL,PF,SS,SD
140 FORMAT(2X,'PRT=',F8.6,2X,'PRW=',F8.6,2X,'PRA=',F8.6,2X,'VEL=',F6.4
1,2X,'PS=',F12.2,2X,'S=',F12.2,2X,'SD=',F12.2)
145 CONTINUE
IF(DO.NE.1) GOTO 180
WRITE(6,146)VEL
146 FORMAT(2X,'VEL=',F6.4)
WRITE(6,147)PRT,PRW,PRA,PF,SS,SD
147 FORMAT(2X,'PRT=',F8.4,1X,'X',2X,'PRW=',F8.4,1X,'X',2X,'PRA=',F8.4,
12X,'PS=',F12.2,2X,'S=',F12.2,2X,'SD=',F12.2)
VEL=VEL+0.01
IF(VEL.GT.0.55) GOTO 180
GOTO 170
150 WRITE(6,160)V(J)
160 FORMAT(2X,'STRIP BREAKS AT THIS SPEED',2X,'V=',2X,F9.5)
GOTO 180
170 CONTINUE
180 WRITE(6,190)
190 FORMAT(2X,'TO RUN THIS PROGRAMME AGAIN TYPE 1,/,
12X,'OTHER WISE TYPE 0.')
READ(5,*)CC
IF(CC.EQ.1)GOTO 5
STOP
END

```

LISTING OF THE COMPUTER PROGRAMME FOR
NON-NEWTONIAN ANALYSIS

```
DIMENSION V(200),E1(2000),P(2000),S(2000),E10(2000)
DIMENSION Y(2000),PS(2000),T(1500),H(1500),X(1500)
DIMENSION HH(1500),W(1500)
DOUBLE PRECISION POIS1,QUET1,T11,T12,PHY1
DOUBLE PRECISION POIS2,QUET2,T21,T22,PHY2
DOUBLE PRECISION POIS3,QUET3,T31,T32,PHY3
DOUBLE PRECISION POIS4,QUET4,T41,T42,PHY4
DOUBLE PRECISION POIS5,QUET5,T51,T52,PHY5
REAL L1,L2
5 WRITE(6,10)
10 FORMAT(2X,'THIS PROGRAMME CALCULATES THEORETICAL ',/,2X,
1'PERCENTAGE REDUCTION IN AREA OF STRIP',/,2X,
1'USING STEPPED REDUCTION UNIT ASSUMING NON-NEWTONIAN BEHAVIOUR
10F POLYMER MELT')
WRITE(6,20)
20 FORMAT(2X,'INPUT L1,L2,H1,H2,H3 IN METERS')
READ(5,*)L1,L2,H1,H2,H3
WRITE(6,30)
30 FORMAT(2X,'INPUT INITIAL YIELD Y0,STRAIN HARDENING CONSTANT K,
1STRAIN HARDENING INDEX N')
READ(5,*)Y0,A,F
WRITE(6,40)
40 FORMAT(2X,'INPUT INITIAL THICKNESS T1,WIDTH W1')
READ(5,*)T1,W1
WRITE(6,50)
50 FORMAT(2X,'INPUT INITIAL VISCOSITY VSO ,SHEAR STRESS CONSTANT K1,
12X,CRITICAL SHEAR STRESS TCA')
READ(5,*)VIS,PC,TCA
WRITE(6,60)
60 FORMAT(2X,'INPUT STRAIN RATE SENSITIVITY CONSTANT N AND T')
READ(5,*)SR,SC
WRITE(6,70)
70 FORMAT(2X,'TO INCLUDE STRAIN RATE SENSITIVITY TYPE 1,/,
12X,'OTHERWISE TYPE 0')
READ(5,*)AA
WRITE(6,90)L1,L2,H1,H2,H3,Y0,A,F
90 FORMAT(2X,'L1=',F8.4,2X,'L2=',F8.4,2X,'H1=',F8.5,2X,'H2=',F8.5,
12X,'H3=',F8.5,2X,'Y0=',F12.2,2X,'K=',F12.2,2X,'N=',F4.2)
WRITE(6,95)VIS,PC,TCA,SR,SC
95 FORMAT(2X,'VIS=',F6.2,2X,'K1=',F14.12,2X,'TCA=',F10.2,2X,
1'SR=',F8.2,2X,'SRC=',F4.2)
READ(5,*)DD
VEL=0.00
100 DO 290 I=1,50
VEL=VEL+0.02
PM=0.0
STEP1=1E06
REM1=1E-08
110 PM=PM+STEP1
DP1=PM/L1
POIS1=(4+(PC*(DP1**2)*(H1**2)))/(12*PC)
QUET1=(VIS*VEL)/(2*PC*H1)
T11=-QUET1+(DSQRT((QUET1**2)+(POIS1**3)))
T12=+QUET1+(DSQRT((QUET1**2)+(POIS1**3)))
PHY1=(T11**(1/3))-(T12**(1/3))
```

```

TC1=PHY1-(DP1*H1/2)
Q1=((DP1*(H1**3))/(6*VIS))+((TC1*(H1**2))/(2*VIS))+ (VEL*H1)+(PC/VI
1S)*(((DP1**3)*(H1**5))/20)+((DP1**2)*(H1**4)*TC1/4)+(DP1*(H1**3)*
1(TC1**2)/2)+((TC1**3)*(H1**2)/2))
DP2=FM/L2
FOIS2=(4+(PC*(DP2**2)*(H2**2)))/(12*PC)
QUET2=(VIS*VEL)/(2*PC*H2)
T21=-QUET2+(DSQRT((QUET2**2)+(FOIS2**3)))
T22=+QUET2+(DSQRT((QUET2**2)+(FOIS2**3)))
PHY2=(T21**(1/3))-(T22**(1/3))
TC2=PHY2+(DP2*H2/2)
Q2=-((DP2*(H2**3))/(6*VIS))+((TC2*(H2**2))/(2*VIS))+ (VEL*H2)+(PC/V
1IS)*(-(DP2**3)*(H2**5)/20)+((H2**2)*(TC2**3)/2)+((DP2**2)*(H2**
14)*TC2/4)-(DP2*(H2**3)*(TC2**2)/2))
RES1=Q1-Q2
IF(ABS(RES1).LE.REM1) GOTO 130
IF(RES1) 120,130,110
120 PM=PM-STEP1
STEP1=STEP1/10
GOTO 110
130 WRITE(6,140)
140 FORMAT(1X,'*****')
1*****')
FOIS3=(4+(PC*(DP1**2)*(H3**2)))/(PC*12)
QUET3=(VIS*VEL)/(2*PC*H3)
T31=-QUET3+(DSQRT((QUET3**2)+(FOIS3**3)))
T32=-QUET3-(DSQRT((QUET3**2)+(FOIS3**3)))
PHY3=(T31**(1/3))+(T32**(1/3))
TC3=PHY3-(DP1*H3/2)
X1=Y0/((2*ABS(TC1)/T1)+(2*ABS(TC3)/W1)+(FM/L1))
WRITE(6,150)PM,TC1,VIS,X1,VEL,TC3
150 FORMAT(2X,'PM=',F12.2,2X,'TC1=',F10.0,2X,'VIS=',F6.2,2X,'X1=',
1F8.5,2X,'VEL=',F4.2,2X,'TC3=',F10.2)
IF(X1.GT.L1) GOTO 100
REP=(INT(X1*1000.0)-1)
N=L1*1000.0-REP
P(1)=FM*X1/L1
S(1)=(2*ABS(TC1)*X1/T1)+(2*ABS(TC3)*X1/W1)
Y(1)=Y0
PS(1)=P(1)+S(1)
T(1)=T1
H(1)=H1
X(1)=X1
HH(1)=H3
V(1)=VEL
W(1)=W1
DX=0.001
DO 230 J=2,N
STEP4=1E-03
REM4=1E-05
B=0.0
K=0.0
160 B=B+STEP4
BB=(W1/T1)*B
K=K+1

```

```

X(J)=X(J-1)+DX
T(J)=T(J-1)-(B*DX)
W(J)=W(J-1)-(BB*DX)
IF(T(J).LT.0) GOTO 300
IF(W(J).LT.0) GOTO 300
H(J)=H(J-1)+(0.5*B*DX)
HH(J)=HH(J-1)+0.5*BB*DX
V(J)=V(J-1)*((W(J-1)*T(J-1))/(W(J)*T(J)))
DP=0.0
REM3=1E-08
STEP3=1E08
170 DP=DP+STEP3
POIS4=(4+((DP**2)*(H(J)**2)*PC))/(12*PC)
QUET4=(VIS*V(J))/(2*PC*H(J))
T41=-QUET4+(DSQRT((QUET4**2)+(POIS4**3)))
T42=-QUET4-(DSQRT((QUET4**2)+(POIS4**3)))
PHY4=(T41**(1/3))+(T42**(1/3))
TC=PHY4-(DP*H(J)*0.5)
RES2=((DP*(H(J)**3))/(6*VIS))+((TC*(H(J)**2))/(2*VIS))+(PC/VIS)*((
1((DP**3)*(H(J)**5))/20)+((H(J)**2)*(TC**3)/2)+((DP**2)*(H(J)**4)*
1TC/4)+(DP*(H(J)**3)*(TC**2)/2))+V(J)*H(J))-R1
IF(ABS(RES2).LT.REM3) GOTO 190
IF(RES2)180,190,170
180 DP=DP-STEP3
STEP3=STEP3/10
GOTO 170
190 F(J)=DP*DX+F(J-1)
POIS5=(4+((DP**2)*(HH(J)**2)*PC))/(12*PC)
QUET5=(VIS*V(J))/(2*PC*HH(J))
T51=-QUET5+(DSQRT((QUET5**2)+(POIS5**3)))
T52=-QUET5-(DSQRT((QUET5**2)+(POIS5**3)))
PHYS=(T51**(1/3))+(T52**(1/3))
TCC=PHYS-(DP*HH(J)*0.5)
SRS=0.0
IF(AA.NE.1)GOTO 200
MSR=V(J)*(ALOG((W(J-1)*T(J-1))/(W(J)*T(J))))/DX
SRS=(MSR/SR)**(1/SC)
200 Y(J)=(1+SRS)*(Y0+A*(ALOG((W1*T1)/(W(J)*T(J))))**F)
S(J)=(Y(J)*((T(J-1)/T(J))+(W(J-1)/W(J))-2))+2*ABS(TC)*DX/T(J)+(2
1*ABS(TCC)*DX/W(J))+S(J-1)
PS(J)=P(J)+S(J)
RES3=PS(J)-Y(J)
E1(K)=ABS(RES3)
RES4=E1(K)-E1(K-1)
IF(ABS(RES3).LT.1E05) GOTO 215
IF(ABS(RES4).LE.REM4) GOTO 215
IF(RES3)210,215,160
210 B=B-STEP4
STEP4=STEP4/10
GOTO 160
215 PRT=(1-(T(J)/T1))*100
PRW=(1-(W(J)/W1))*100
PRA=(1-((W(J)*T(J))/(W1*T1)))*100
H4=H(J)-H1+H2
PF=P(J)

```

```

SS=S(J)
216 IF(DD.EQ.1) GOTO 230
240 WRITE(6,250)P(J),S(J),PS(J),Y(J),X(J),T(J),W(J)
250 FORMAT(2X,'P=',F12.2,2X,'S=',F12.2,2X,'P+S=',F12.0,2X,'Y=',F12.2,2
1X,'X=',F6.4,2X,'T=',F8.5,2X,'W=',F8.5)
WRITE(6,270)PRT,PRW,PRA,V(J)
270 FORMAT(2X,'PRT=',F8.5,1X,'Z',2X,'PRW=',F8.5,1X,'Z',2X,'PRA=',F8.5,
12X,'VD=',F6.4)
WRITE(6,280)
280 FORMAT('-----')
1-----')
230 CONTINUE
IF(ABS(TC1).GE.TCA) GOTO 320
IF(DD.NE.1) GOTO 290
231 WRITE(6,232)PRT,PRW,PRA,PF,SS
232 FORMAT(2X,'PRT=',F8.5,1X,'Z',2X,'PRW=',F8.5,1X,'Z',2X,'PRA=',F8.5,
12X,'PS=',F12.2,2X,'S=',F12.2)
290 CONTINUE
GOTO 550
300 WRITE(6,310)
310 FORMAT(2X,'STRIP BREAKS AT THIS SPEED')
GOTO 550
320 WRITE(6,330)
330 FORMAT(2X,'-----CONDITION OF SLIP IS DETECTED -----')
DO 540 I=1,50
VEL=VEL
DO 430 J=2,N
STEP10=1E-03
REM10=1E-05
B10=0.0
K10=0
X(1)=X1
V(1)=VEL
340 B10=B10+STEP10
K10=K10+1
BB10=(W1/T1)*B10
X(J)=X(J-1)+DX
HH(J)=HH(J-1)+0.5*BB10*DX
W(J)=W(J-1)-(BB10*DX)
T(J)=T(J-1)-(B10*DX)
IF(T(J).LT.0)GOTO 300
IF(W(J).LT.0) GOTO 300
H(J)=H(J-1)+(0.5*B10*DX)
V(J)=V(J-1)*((W(J-1)*T(J-1))/(W(J)*T(J)))
SRS=0.0
IF(AA.NE.1)GOTO 350
MSR=V(J)*((ALOG((W(J-1)*T(J-1))/(W(J)*T(J))))/DX
SRS=(MSR/SR)**(1/SC)
350 Y(J)=(1+SRS)*(Y0+A*(ALOG((W1*T1)/(W(J)*T(J))))**F)
S(J)=(Y(J)*((T(J-1)/T(J))+W(J-1)/W(J))-2))+2*ABS(TC1)*DX/T(J))+
12*ABS(TC3)*DX/W(J))+S(J-1)
PS(J)=P(J)+S(J)
RES10=PS(J)-Y(J)
E10(K10)=ABS(RES10)
RES20=E10(K10)-E10(K10-1)

```

```

IF(ABS(RES10).LT.1E05) GOTO 361
IF(ABS(RES20).LE.REM10) GOTO 361
IF(RES10)360,361,340
360 B10=B10-STEP10
STEP10=STEP10/10
GOTO 340
361 PRT=(1-(T(J)/T1))*100
PRW=(1-(W(J)/W1))*100
PRA=(1-((W(J)*T(J))/(W1*T1)))*100
H4=H(J)-H1+H2
PF=P(J)
SS=S(J)
362 IF(DD.EQ.1) GOTO 430
365 WRITE(6,366)VEL
366 FORMAT(2X,'VEL=',F5.3)
370 WRITE(6,380)P(J),S(J),Y(J),X(J),T(J),W(J)
380 FORMAT(2X,'P=',F12.2,2X,'S=',F12.2,2X,'Y=',F12.2,2X,'X=',F8.6,2X
1,'T=',F8.5,2X,'W=',F8.5)
WRITE(6,400)PRT,PRW,PRA,V(J),SD
400 FORMAT(2X,'PRT=',F8.5,2X,'PRW=',F8.5,1X,'Z',2X,'PRA=',F8.5,2X,'VD
1',F6.4,2X,'SD=',F16.3)
WRITE(6,410)
410 FORMAT(2X,'-----
1-----')
430 CONTINUE
IF(DD.NE.1)GOTO 436
431 WRITE(6,432)PRT,PRW,PRA,PF,SS,VEL
432 FORMAT(2X,'PRT=',F8.5,1X,'Z',2X,'PRW=',F8.5,1X,'Z',2X,'PRA=',F8.5
1,1X,'Z',2X,'PS=',F12.2,2X,'S=',F12.2,2X,'VEL=',F4.2)
WRITE(6,435)
435 FORMAT(2X,'*****
1*****')
436 VEL=VEL+0.02
IF(VEL.GT.0.51) GOTO 550
540 CONTINUE
550 WRITE(6,560)
560 FORMAT(2X,'TO RUN THIS PROGRAMME AGAIN TYPE 1')
READ(5,*)CC
IF(CC.EQ.1) GOTO 5
STOP
END

```

TECHNOLOGICAL SYSTEMS AND MODELLING

A MATHEMATICAL MODEL FOR PLASTO-HYDRODYNAMIC DRAWING OF NARROW STRIPS

G R Symmons*, A H Memon*, M S J Hashmi**

* Department of Mechanical and Production Engineering, Sheffield City Polytechnic, England

** Head of School of Mechanical Engineering, NIHE Dublin, Ireland

Abstract Plasto-hydrodynamic drawing of circular cross-section wire has been modelled previously. In this technique the deformation to the wire is caused by the combined effect of axial pull and radial pressure generated due to the hydrodynamic action of a viscous fluid. The extent of deformation is such that for a moderately viscous fluid with Newtonian characteristics fracture of the wire is predicted at drawing speeds in excess of about 5 m/s even though the smallest bore size of the hydrodynamic pressure unit is larger than the undeformed diameter of the wire.

In this study, a closed form mathematical model has been developed for predicting the reduction in area of a rectangular cross-section narrow strip pulled through a unit having stepped rectangular cavity which is filled with a viscous Newtonian fluid; the smallest section of the stepped cavity being greater than the section of the undeformed strip.

It is suggested that gross deformation and indeed fracture could take place in a strip of rigid strain hardening material at moderate drawing speeds even though no metal to metal contact occurs.

Key Words Strip drawing; Newtonian flow; Plasto-hydrodynamics; Plane strain; Strain hardening; Reduction in area.

INTRODUCTION

When a solid continuum is pulled through an orifice filled with a viscous fluid, shearing takes place at the interface of the fluid and the solid continuum. If the fluid film is converging in the direction of pull then, in addition to the shear force a hydrodynamic pressure is generated. The magnitude of the shearing and pressure depends upon the speed with which the continuum is pulled, the viscosity of the fluid and the geometrical configuration of the orifice which contains the fluid. The shearing causes a drag force on the continuum which combined with the effect of hydrodynamic pressure may be sufficient to initiate plastic yielding and produce permanent deformation to the continuum. This is enhanced by the use of a polymer melt as the fluid that has substantial value of viscosity.

Hashmi and Symmons (1983) presented analytical solution of the deformation process of a wire being drawn through a conical orifice in which the minimum bore was greater than the undeformed wire and no conventional reduction dies used. The mathematical model for the drawing of circular cross-section continuum indicated that deformation comparable to the conventional die system could be attained. Theoretical and experimental results by Symmons, Hashmi and Parvinmehr (1982) on a stepped bore orifice demonstrated that a percentage reduction in area of copper and mild steel wires of above 20% could be achieved using a low density polyethylene as the melt fluid.

This paper presents a mathematical model of a stepped bore rectangular orifice for the

deformation of narrow strip, for a Newtonian fluid, incorporating linear strain hardening property of the material.

Equations are derived for the pressure and shear stresses generated on the width face of the strip and the plasto-hydrodynamic compatibility equation is analytically solved to predict percentage reduction in thickness/area of the strip.

ANALYSIS

The analysis is based on the geometrical configuration of the process shown in figure 1a. The process is divided in three zones shown in figure 1b and are named as:

1. Inlet Zone, where the work piece is considered rigid and the viscous fluid is trapped into the space between the workpiece and the unit.
2. Deformation Zone, from the point where the workpiece deforms plastically up to the step.
3. Outlet Zone, beyond the step where it is assumed that the workpiece again becomes rigid.

In order to establish a mathematical formulation of the process the following assumptions are made.

1. Plane strain condition is assumed.
2. The viscous fluid has the characteristic of a Newtonian fluid.

3. Flow is axial and laminar.
4. Isothermal conditions exist.
5. The film thickness is small compared with the dimensions of the unit, hence the pressure is generated in X-direction only and acts normally across the width face of the strip causing reduction in thickness.
6. Shearing effect along the thickness face of the strip is considered to be negligible.
7. Deformation takes place before the step and no deformation takes place after the step.

For a Newtonian fluid

$$\tau = \mu \frac{\partial u}{\partial y} \quad (1)$$

and for equilibrium

$$\frac{\partial p}{\partial x} = \frac{\partial \tau}{\partial y} \quad (2)$$

Differentiating equation (1) with respect to y and substituting in (2) we obtain

$$\frac{\partial^2 u}{\partial y^2} = \frac{1}{\mu} \frac{\partial p}{\partial x} \quad (3)$$

Integrating equation (3) and applying boundary conditions that

$$u = v \text{ at } y = 0 \text{ (At the surface of strip)}$$

$$u = 0 \text{ at } y = h_1 \text{ (At the surface of unit wall)}$$

an expression for determining velocity at any point in the flow is given by

$$u = \frac{1}{2\mu} \left(\frac{\partial p}{\partial x} \right) (y^2 - h_1 y) + v(1 - y/h_1) \quad (4)$$

Differentiating equation (4) and combining with equation (1), it can be shown that

$$\tau = \frac{1}{2} \left(\frac{\partial p}{\partial x} \right) (2y - h_1) - \frac{\mu v}{h_1} \quad (5)$$

Equation (5) gives an expression for shear stress at any point in flow at the fluid and strip interface.

Using equation (4) and (5) the flow of the fluid and shear stress at the surface of the strip, when no deformation occurs, in the inlet and outlet zones can be defined by

$$Q_1 = - \frac{h_1^3}{12\mu} \left(\frac{\partial p}{\partial x} \right)_1 + \frac{v h_1}{2} \quad (6)$$

$$Q_1 = - \frac{h_1^3}{12\mu} \left(\frac{\partial p}{\partial x} \right)_2 + \frac{v h_2}{2} \quad (7)$$

$$\tau_1 = - \frac{h_1}{2} \left(\frac{\partial p}{\partial x} \right)_1 - \frac{\mu v}{h_1} \quad (8)$$

$$\tau_2 = - \frac{h_2}{2} \left(\frac{\partial p}{\partial x} \right)_2 - \frac{\mu v}{h_2} \quad (9)$$

Now from steady state flow of the fluid it can be shown that

$\left(\frac{\partial p}{\partial x} \right) = \text{constant}$, and for a stepped configuration the maximum pressure is at the step hence, $\left(\frac{\partial p}{\partial x} \right)_1 = \frac{P_m}{L_1}$ and $\left(\frac{\partial p}{\partial x} \right)_2 = \frac{P_m}{L_2}$

The parameter P_m for the case when no deformation occurs can be determined by considering the continuity of flow and is given by

$$P_m = \frac{6\mu v(h_1 - h_2)}{(h_1^3/L_1 + h_2^3/L_2)} \quad (10)$$

Extent of Inlet Zone

The axial distance X_1 from the entry point of the orifice where plastic yielding takes place in the strip may be determined by considering the Plasto-hydrodynamic compatibility equation.

Using the Tresca Yield Criteria for plane strain condition

$$\sigma_{x_1} + P_1 = S_0 \quad (11)$$

where

$$\sigma_{x_1} = \frac{2\tau_1 X_1}{L_1}$$

Substituting values of σ_{x_1} and P_1 in equation (11) we obtain

$$X_1 = \frac{S_0}{\frac{2\tau_1}{L_1} + \frac{P_m}{L_1}} \quad (12)$$

Deformation Zone

Considering the geometrical shape in the orifice after the commencement of the plastic yielding it is assumed that deformation takes place linearly so that film thickness at any point in deformation zone can be defined by

$$h_p = h_1 + bx$$

and the deformation profile may be described by

$$t_p = t_1 - 2bx$$

also $v = v_x$

where 'b' is the constant and is slope of deformation line with x.

Referring to fig 1-c which depicts the deformation mode, Reynold's equation for a Newtonian fluid may be written as

$$\frac{\partial}{\partial x} (h_p^3 \frac{\partial p}{\partial x})_p = \frac{\partial}{\partial x} (b\mu v h) \quad (13)$$

Now for given fluid viscosity μ , the equation (13) can be written in the form

$$\frac{\partial}{\partial x} (h^3 \frac{\partial p}{\partial x}) = 6\mu v_x \left(\frac{\partial h}{\partial x} \right) + 6\mu h \left(\frac{\partial v_x}{\partial x} \right) \quad (14)$$

But

$$\frac{\partial h}{\partial x} = b \text{ (Refer fig 1-c)}$$

And from volume constancy it can easily be shown that

$$v_x = \frac{v t_1}{t_1 - 2bx}$$

$\therefore \text{Let } v t_1 = D$

$$\therefore v_x = \frac{D}{(t_1 - 2bx)}$$

$$\therefore \frac{\partial v_x}{\partial x} = \frac{2bD}{(t_1 - 2bx)^2}$$

Substituting values of $\frac{\partial h}{\partial x}$, v_x and $\frac{\partial v_x}{\partial x}$

Equation (14) becomes

$$\frac{\partial}{\partial x} \left(\frac{\partial P}{\partial x} h^3 \right) = \frac{M}{(t_1 - 2bx)^2} \quad (15)$$

where $M = 12\mu b D h_1 + 6\mu b D t_1$

Integrating equation (15) with respect to x we obtain

$$\left(\frac{\partial P}{\partial x} \right) h_p^3 = \frac{M}{2b(t_1 - 2bx)} + C_1 \quad (16)$$

where C_1 is constant of integration, and applying boundary conditions that at $x = 0$,

$\frac{\partial P}{\partial x} = \frac{P_m}{L_1}$, $h_p = h_1$; value of C_1 can be determined which on substituting in equation (16) gives

$$\left(\frac{\partial P}{\partial x} \right) h_p^3 = \frac{M}{2b(t_1 - 2bx)} + \frac{P_m h_1^3}{L_1} - \frac{M}{2bt_1}$$

substituting value of h_p we obtain

$$\left(\frac{\partial P}{\partial x} \right) = \frac{M}{2b(t_1 - 2bx)(h_1 + bx)^3} - \frac{P_m h_1^3}{L_1(h_1 + bx)^3} - \frac{M}{2bt_1(h_1 + bx)^3} \quad (17)$$

Using partial fractions, integrating equation (17) we obtain

$$P_p = -\frac{2M \ln(t_1 - 2bx)}{b^2(t_1 + 2h_1)^2} - \frac{M}{4b^2(t_1 + 2h_1)(h_1 + bx)^2} - \frac{M}{b^2(t_1 + 2h_1)^2(h_1 + bx)} + \frac{2M \ln(h_1 + bx)}{b^2(t_1 + 2h_1)^2} - \frac{P_m h_1^3}{2bL_1(h_1 + bx)^2} + \frac{M}{4b^2 t_1 (h_1 + bx)^2} + C_2 \quad (18)$$

Applying boundary conditions at the point where deformation starts $x = 0$, $P_p = P_1 = \frac{P_m x_1}{L_1}$.

Value of Constant C_2 can be determined which on back substitution in equation (18) gives

$$P_p = \frac{2M}{b^2(t_1 + 2h_1)^2} \left[\ln\left(\frac{t_1}{t_1 - 2bx}\right) \right] + \frac{M}{4b^2(t_1 + 2h_1)} \times \left[\frac{1}{h_1^2} - \frac{1}{(h_1 + bx)^2} \right] + \frac{M}{b^2(t_1 + 2h_1)^2} \times \left[\frac{1}{h_1} - \frac{1}{(h_1 + bx)} \right] + \frac{2M}{b^2(t_1 + 2h_1)^2} \times \left[\ln\left(\frac{h_1 + bx}{h_1}\right) \right] + \frac{P_m}{L_1} \left[x_1 + \frac{h_1}{2b} - \frac{h_1^2}{2b(h_1 + bx)^2} \right] + \frac{M}{4b^2 t_1} \left[\frac{1}{(h_1 + bx)^2} - \frac{1}{h_1^2} \right] \quad (19)$$

Equation (19) gives hydrodynamic pressure distribution along the deformation zone

starting from x_1 to $(L_1 - x_1)$

Now if ' h_1 ' is replaced by ' h_p ' and V by ' v_x ' equation (8) will give the shear stress at the surface of strip in deformation zone.

$$\therefore \tau_p = -\frac{(h_1 + bx)}{2} \left(\frac{\partial P}{\partial x} \right) - \frac{\mu v_x}{h_1 + bx}$$

Substituting values of $\left(\frac{\partial P}{\partial x} \right)$ and v_x , we obtain

$$\tau_p = -\frac{1}{2(h_1 + bx)^2} \left[\frac{M}{2b(t_1 - 2bx)} + \frac{P_m h_1^3}{L_1} - \frac{M}{2bt_1} \right] - \frac{\mu D}{(t_1 - 2bx)(h_1 + bx)} \quad (20)$$

Now axial force equilibrium conditions for a small element in deformation zone, as shown in fig: 1-c gives

$$d\sigma_x p = -\frac{dt}{t_p} [S + \tau_p \cot\theta] \quad (21)$$

But $t_p = t_1 - 2bx$ $\therefore dt = -2bdx$

and $\cot\theta = -\frac{1}{b}$ (fig: 1 -c)

Assuming material property to be rigid linearly strain hardening so that $S = S_0 + K\epsilon$

$$\text{where } \epsilon = \ln \frac{t_1}{t_p} = \ln \frac{t_1}{(t_1 - 2bx)}$$

Substituting values of dt , $\cot\theta$, τ_p and S , equation (21) gives

$$d\sigma_x = \frac{2bS_0 dx}{(t_1 - 2bx)} + \frac{2bK \ln \left\{ \frac{t_1}{(t_1 - 2bx)} \right\} dx}{(t_1 - 2bx)} + \frac{M dx}{2b(t_1 - 2bx)^2 (h_1 + bx)^2} + \left(\frac{P_m h_1^3}{L_1} - \frac{M}{2bt_1} \right) \left\{ \frac{1}{(t_1 - 2bx)(h_1 + bx)^2} \right\} dx + \frac{2\mu D dx}{(t_1 - 2bx)^2 (h_1 + bx)} \quad (22)$$

Using partial fractions integration of equation (22) gives

$$\sigma_x p = -S_0 \ln(t_1 - 2bx) + \frac{K}{2} \left[\ln\left(\frac{t_1}{t_1 - 2bx}\right) \right]^2 + \frac{M}{2b} \left[-\frac{4 \ln(t_1 - 2bx)}{b(t_1 + 2h_1)^2} + \frac{2}{b(t_1 + 2h_1)^2 (t_1 - 2bx)} \right] + \frac{4 \ln(h_1 + bx)}{b(t_1 + 2h_1)^2} - \frac{1}{b(t_1 + 2h_1)^2 (h_1 + bx)} + \left(\frac{P_m h_1^3}{L_1} - \frac{M}{2bt_1} \right) \left[-\frac{2 \ln(t_1 - 2bx)}{b(t_1 + 2h_1)^2} \right] + \frac{2 \ln(h_1 + bx)}{b(t_1 + 2h_1)^2} - \frac{1}{b(t_1 + 2h_1)(h_1 + bx)} + \left[2\mu D \right] \left[-\frac{\ln(t_1 - 2bx)}{b(t_1 + 2h_1)^2} + \frac{1}{b(t_1 + 2h_1)(t_1 - 2bx)} \right]$$

$$+ \frac{\ln(h_1+bx)}{b(t_1+2h_1)^2} \Big] + C_1 \quad (23)$$

Applying boundary conditions that at $x = 0$,

$$\sigma_p = \sigma_{x_1} = \frac{2\tau_1 X_1}{t_1}$$

Value of constant C_1 can be determined which on substituting in equation (23) we get

$$\begin{aligned} \sigma_{x_p} = & S_0 \ln\left(\frac{t_1}{t_1-2bx}\right) + \frac{K}{2} \left\{ \ln\left(\frac{t_1}{t_1-2bx}\right) \right\}^2 \\ & + \frac{M}{2b} \left[\frac{4 \ln\left(\frac{t_1}{t_1-2bx}\right)}{b(t_1+2h_1)^2} + \left\{ \frac{2}{b(t_1+2h_1)^2} \right\} \right. \\ & \times \left. \left\{ \frac{1}{(t_1-2bx)} - \frac{1}{t_1} \right\} + \frac{4 \ln\left(\frac{h_1+bx}{h_1}\right)}{b(t_1+2h_1)^2} \right. \\ & \left. + \left\{ \frac{1}{b(t_1+2h_1)^2} \right\} \left\{ \frac{1}{h_1} - \frac{1}{h_1+bx} \right\} \right] \\ & + \left[\frac{P_m h_1}{L_1} - \frac{M}{2bt_1} \right] \left[\frac{2 \ln\left(\frac{t_1}{t_1-2bx}\right)}{b(t_1+2h_1)^2} \right. \\ & \left. + \frac{2 \ln\left(\frac{h_1+bx}{h_1}\right)}{b(t_1+2h_1)^2} \right. \\ & \left. + \left\{ \frac{1}{b(t_1+2h_1)^2} \right\} \left\{ \frac{1}{h_1} - \frac{1}{h_1+bx} \right\} \right] \\ & + (2\mu D) \left[\frac{\ln\left(\frac{t_1}{t_1-2bx}\right)}{b(t_1+2h_1)^2} + \left\{ \frac{1}{b(t_1+2h_1)^2} \right\} \times \right. \\ & \left. \left\{ \frac{1}{(t_1-2bx)} - \frac{1}{t_1} \right\} + \frac{\ln\left(\frac{h_1+bx}{h_1}\right)}{b(t_1+2h_1)^2} \right] \\ & + \frac{2\tau_1 X_1}{t_1} \quad (24) \end{aligned}$$

Equation (24) is an expression for determining the axial stress at a point distant x from the point of yielding.

Once the plastic yielding takes place the deformation will continue as long as the yield criteria

$$P_p + \sigma_{x_p} = S$$

$$\text{or } P_p + \sigma_{x_p} - S = 0 \quad (25)$$

is satisfied.

It has been assumed that the deformation stops at the step where $x = L_1 - X_1$ and $t_p = t_1 - 2bx$. Keeping these values in equation (19) and (24), it can be shown that the only unknown parameter is 'b'. For a given drawing speed the value of 'b' may be determined using iteration process to satisfy equation (25). Once the value of 'b' is established the reduction in thickness at any point for $X_1 \ll L_1$ is given by $t = t_1 - 2bx$. Thus the percentage reduction in thickness/area of the strip can be determined by $(1 - \frac{t_p}{t_1}) \times 100$.

Results

In order to demonstrate the implication of the theoretical analysis, a number of sample calculations have been made. The calculations of different parameters were made using the equations derived in the previous section. The standard values of the parameters were assumed to be as follows:

Viscosity of the fluid $\mu = 100 \text{ NSm}^{-2}$

Initial gap $h_1 = 0.5 \text{ mm}$

Final gap $h_2 = 0.025 \text{ mm}$

Inlet length of DRU (before step)
 $L_1 = 90 \text{ mm}$

Outlet length of DRU (after step)
 $L_2 = 30 \text{ mm}$

Original thickness of strip $t_1 = 1.6 \text{ mm}$

Initial yield stress of the strip
material $S_0 = 50 \text{ MNm}^{-2}$

Strain hardening factor of the strip
material $K = 380 \text{ MNm}^{-2}$

The effect of the changes on these parameters on the point X_1 , where plastic deformation commences and on the percentage reduction in thickness/area (PRA) is demonstrated graphically in figures: 2-7.

Discussion

Figures (2) and (3) show the variation of hydrodynamic pressure and axial stress respectively for the various drawing speeds with the standard geometric size of DRU. They show a linear relationship with distance x up to the point where deformation starts. Significant values of the pressure and axial stress are developed at the step.

The effect of the gap ratio h_1/h_2 on X_1 and PRA is shown in figures (4a) and (4b) respectively. These graphs show that initial gap has significant effect on both the point of initiation of yielding and the amount of reduction. For smaller values of initial gap the deformation occurs further away from the step and a larger reduction in area is achieved even at a slow speed. These graphs demonstrate that with a smaller gap ratio of 10 the deformation is of such an extent that strip fracture can occur at a slow speed of $.25 \text{ ms}^{-1}$. For higher gap ratio of 50, deformation takes place to a lesser extent at higher drawing speed.

Figure (5) shows the effect of fluid viscosity on PRA. This figure suggests that at slow drawing speed max reduction could be achieved by using more viscous fluid. The strip fractures at a speed greater than 0.5 ms^{-1} with a fluid viscosity of 150 NSm^{-2} . For higher drawing speeds low viscosity fluid should be used. Figure (6) shows the effect of initial yield stress on PRA. This graph suggests that larger permanent deformation could be achieved with lower yield stress at a speed lower than 0.8 ms^{-1} . The figure also demonstrates that higher yield stress has no significant effect on the attainable deformation except that of drawing speed.

The effect of inlet length L_1 of the DRU on PRA is shown in figure (7). From this figure it is evident that the extent of inlet length limits the range of working speed. With longer inlet length the deformation range occurs at the lower drawing speeds.

Conclusion

It is evident that it should be possible in practice to affect gross permanent deformation of narrow strip with this process without using conventional die.

From the above discussion it is obvious that initial gap has significant effect on the performance of the system and with a smaller gap of .2 mm, maximum reduction of about 45% can be achieved at a slower speed of .25 ms^{-1} . An increase in the first land and viscosity have direct effect on the reduction of the area.

Notations

- h = Gap between strip and unit wall
- L = Length of unit
- t = Thickness of strip
- W = Width of strip
- b = Factor determining theoretical profile
- K = Material constant
- P = Hydrodynamic pressure
- τ = Shear stress
- σ_x = Axial stress
- V = Drawing velocity
- μ = Dynamic viscosity of fluid
- Q = Flow rate of fluid
- X_1 = Distance from inlet to the point at which deformation starts
- S_0 = Initial yield stress in plane strain condition
- P_m = Maximum pressure in the unit at step if no deformation occurs

Subscripts

- 1, refer to the inlet zone when no deformation occurs
- 2, refer to the outlet zone when no deformation occurs
- p, refer to the deformation zone
- C_1, C_2, C_3 , Coefficients of integration

References

Hashmi, M S J and Symmons, G R S (1983)
 A mathematical model for the drawing of a solid continuum through Newtonian fluid filled tubular orifice.

4th Int conference Mathematical Modelling in Science and Technology, Zurich 1983.

Symmons, G R S, Hashmi, M S J and Parvinmehr, H. (1982)

Plasto hydrodynamic, dieless wire drawing

Theoretical treatment and experimental results.

International Conference on Development in Drawing of Metals, Metal Society 1982

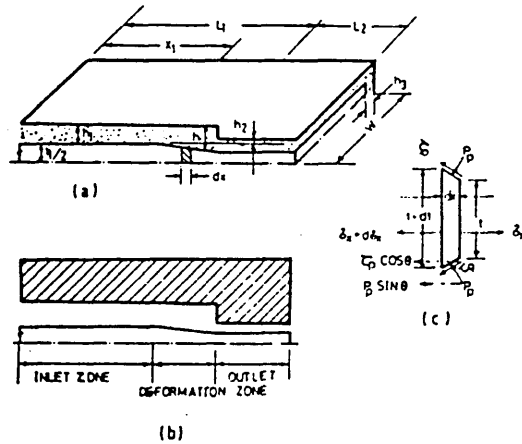


Fig: 1 (a) Schematic diagram of the process
 (b) Assumed zones for the analysis
 (c) Stresses acting on a small element of the strip

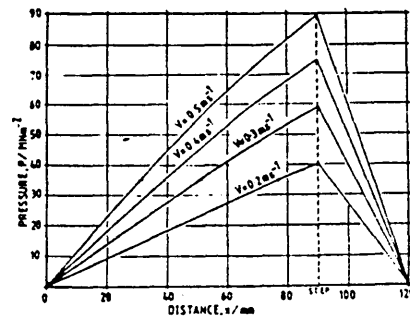


Fig: 2 Variation in hydrodynamic pressure along DRU

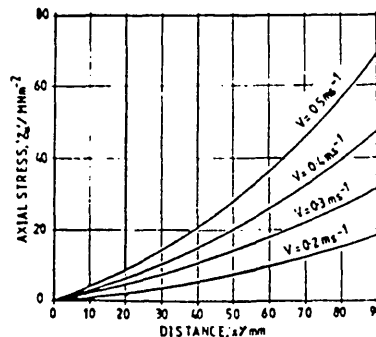


Fig: 3 Variation in axial stress along DRU

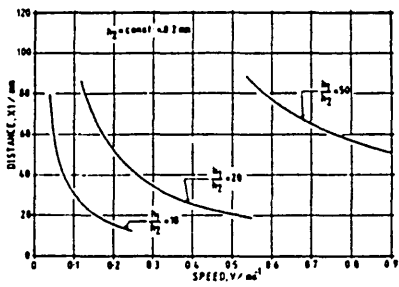


Fig: 4 (a) Effect of gap ratio on X_1 v/s speed

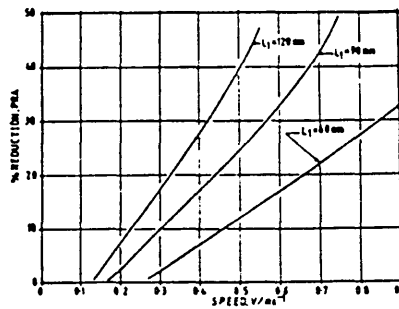


Fig: 7 Effect of inlet length on PRA v/s speed

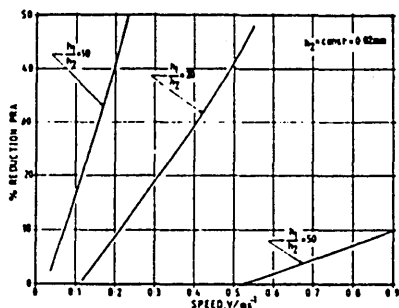


Fig: 4 (b) Effect of gap ratio on PRA v/s speed

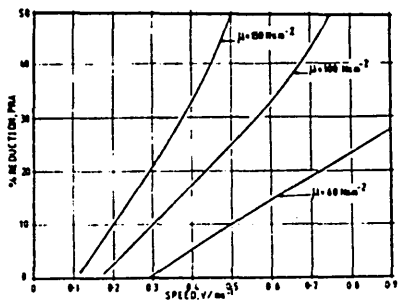


Fig: 5 Effect of fluid viscosity on PRA v/s speed

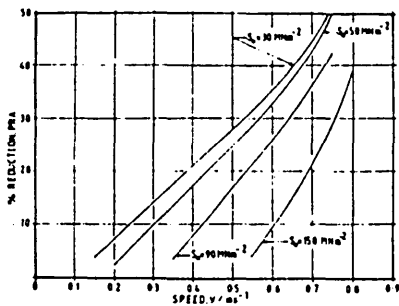


Fig: 6 Effect of initial yield stress on PRA v/s speed

A NEWTONIAN MODEL OF A PLASTO HYDRODYNAMIC DRAWING PROCESS OF A RECTANGULAR CROSS-SECTIONAL CONTINUUM

G R Symmons*, A H Memon*, M S J Hashmi^x

* Department of Mechanical and Production Engineering, Sheffield City Polytechnic, England

^x School of Mechanical Engineering, NIHE Dublin, Ireland

ABSTRACT Plasto-hydrodynamic drawing of narrow strip has been modelled where the deformation to the strip is caused by combined effect of axial pull and the pressure generated due to hydrodynamic action of a viscous fluid. The process is novel in that no conventional dies are used. A mathematical model has been developed for predicting the reduction in area of a rectangular cross-sectional strip pulled through a chamber filled with a viscous fluid and a unit having a stepped rectangular cavity. The model assumes the fluid behaves as a Newtonian fluid and the strip hardens with deformation and includes the effects of three dimensional deformation.

Computer results from the model are presented which show the influence of the geometry of the hydrodynamic unit and fluid viscosity on the deformation of the strip.

Keywords: Strip drawing, Plasto-hydrodynamics, Newtonian flow, strain hardening.

INTRODUCTION

When a solid continuum is pulled through an orifice filled with a viscous fluid, shearing takes place at the interface of the fluid and the solid continuum. If the fluid film is converging in the direction of the pull then, in addition to the shear force a hydrodynamic pressure is generated. The magnitude of the shearing and pressure depends upon the speed with which the continuum is pulled, the viscosity of the fluid and the geometrical configuration of the orifice. The shearing causes a drag force on the continuum which combined with the effect of hydrodynamic pressure may be sufficient to initiate plastic yielding and produce permanent deformation to the continuum. This is enhanced by the use of a polymer melt as the fluid that has substantial value of viscosity.

G R Symmons et al (1, 2) and M S J Hashmi et al (3, 4) have presented models for deformation process of wire and circular continuum using conical and stepped bore orifices.

This paper presents a Newtonian model of a stepped bore rectangular orifice for the deformation of narrow strip. The strain hardening effect of the material yield strength and the deformation in both the thickness and width of the strip is included in the analysis. Computer solutions are presented for the pressure, axial stress and reduction in area of the strip for a wide range of drawing conditions. The results show the influence of the orifice geometry and fluid viscosity on the performance of this novel deformation process.

ANALYSIS

The analysis is based on the schematic diagram shown in Fig 1a, b and the following assumptions have been taken into account:

- 1 Viscous fluid has Newtonian characteristics;
- 2 Flow is laminar axial and isothermal condition

exists;

- 3 No deformation takes place after step;
- 4 Hydrostatic condition is developed after the generation of hydrodynamic pressure.

Inlet Zone

Fig 1c depicts a section of the inlet zone. This section is divided into two sub-sections 'A' and 'B'. Section A refers to the flow along width face and the section B refers to the thickness face of the strip.

Reynolds equation for one dimensional flow, assuming viscosity to remain constant is given by

$$\frac{\partial}{\partial x} \left[h^3 \left\{ \frac{\partial p}{\partial x} \right\} \right] = \frac{\partial h}{\partial x} (6\mu v) \quad (1)$$

According to the geometrical configuration of the unit gap 'h' is constant in section B and the gap 'h' varies along x in section A. Therefore the pressure is generated only in section 'A'. If we consider the taken section instantaneously, the hydrostatic condition could be assumed. Hence in the analysis the pressure generated on section A is assumed to act equally in the section B.

For the stepped configuration the maximum pressure 'P_m' at the step, when no deformation occurs can be worked out from continuity of flow and, is given by

$$P_m = \frac{6\mu v(h_1 - h_2)}{\left[\frac{h_1^3}{L_1} + \frac{h_2^3}{L_2} \right]} \quad (2)$$

And the shear stresses on the surface of strip in section A and B are given by

$$\tau_1 = -\frac{h_1}{2} \left\{ \frac{P_m}{L_1} \right\} - \frac{\mu v}{h_1} \quad (3)$$

$$\tau_2 = -\frac{h_2}{2} \left\{ \frac{P_m}{L_1} \right\} - \frac{\mu v}{h_2} \quad (4)$$

Plastic Onset

For the present situation Von Mises yield criteria takes the form

$$P_1 + \sigma x_1 = y_1 \quad (5)$$

Let the deformation take place at a point distant x₁ from entry, the force equilibrium in inlet zone with combination to equation (5) gives

$$x_1 = \frac{y_1}{\frac{2\tau_1}{t_1} + \frac{2\tau_2}{w_1} + \frac{P_m}{L_1}}$$

PLASTIC REGION

Hydrodynamic Pressure and Shear Stresses

Assuming linear profile of deformation, the deformation geometry shown in Fig 1a, b

$$h_i = h_1 + bx \quad (7)$$

$$h'_i = h_1 + b'x \quad (8)$$

$$t_i = t_1 - 2bx \quad (9)$$

$$w_i = w_1 - 2b'x \quad (10)$$

Referring to Fig 1, equation (1) could be written in the form

$$\frac{\partial}{\partial x} [h_i^3 \left(\frac{\partial p}{\partial x}\right)_i] = 6\mu v b \quad (11)$$

The expression for hydrodynamic pressure 'P_i' at any point in deformation zone could be obtained by taking double integration wrt x of equation (11) and is

$$P_i = \frac{6\mu v}{b} \left[\frac{h_1}{2h_i^2} - \frac{1}{h_i} + \frac{1}{2h_1} \right] + \frac{P_m}{L_1} \left[x_i + \frac{h_1}{2b} - \frac{h_1}{2bh_i^2} \right] \quad (12)$$

And expressions for shear stress in this region are

$$\tau_i = -\frac{\mu v}{h_i^2} \left[4bx + h_1 + \frac{P_m h_1^2}{2\mu v L_1} \right] \quad (13)$$

$$\tau'_i = -\frac{h_1}{2} \left[\frac{6\mu v b x}{h_i^3} + \frac{P_m h_1^2}{L_1 h_i^3} \right] - \frac{\mu v}{h_i} \quad (14)$$

Axial Stress

$$\text{Assuming } P'_i = P_i \quad (15)$$

Levy-Mises flow rule gives

$$\frac{dt}{t_i} = \frac{dw}{w_i} \quad (16)$$

Consider a small element in the deformation zone as shown in Fig 2. The equilibrium of forces in x direction, in combination with equations (15) and (16) yields

$$d\sigma_x = \frac{2b dx}{t_i} \left[2y_i - \frac{\tau_i}{b} - \frac{\tau'_i}{b'} \right] \quad (17)$$

Equation (17) is the governing equation to determine the axial stress in the deformation zone.

From equations (9), (10) and (16)

$$b' = mb$$

where 'm' is constant and equal to the ratio of initial width to initial thickness.

Plastic Deformation

The material will continue to deform plastically until the yield criterion

$$P_i + \sigma x_i = y_i$$

is satisfied.

Assuming linear strain hardening

$$y_i = y_1 + kc$$

$$\text{where } c = \ln \left\{ \frac{A_1}{A_2} \right\} = 2 \ln \left\{ \frac{t_1}{t_2} \right\}$$

$$\therefore y_i = y_1 + 2k \ln \left\{ \frac{t_1}{t_i} \right\}$$

Substituting values of y_i, τ_i and τ'_i into equation (17), using partial fraction and applying boundary conditions the integration of the equation wrt x will give an expression to determine the axial stress 'σx_i' at any point in the deformation zone. In the simplified form it takes the form

$$\sigma x_i = \frac{1}{b} \left[\frac{B_1}{2} \ln \left\{ \frac{t_1}{t_i} \right\} + B_2 \ln \left\{ \frac{h_i}{h_1} \right\} + B_3 \left\{ \frac{1}{h_1} - \frac{1}{h_i} \right\} + \frac{B_4}{2} \left\{ \frac{1}{h_1} - \frac{1}{h_i^2} \right\} + \frac{B_5}{b'} \ln \left\{ \frac{h_i}{h_1} \right\} + \frac{B_6}{4b} \left[\ln \left\{ \frac{t_1}{t_i} \right\} \right]^2 + \sigma x_1 \right]$$

where

$$B_1 = \frac{2t_1 A_1 + 4(A_2 + A_3)}{(t_1 + 2h_1)^2} + \frac{4t_1(A_4 + A_5) + 2t_1^2 A_5 + 8A_6}{(t_1 + 2h_1)^3} + \frac{2A_7 b}{(b't_1 + 2bh_1)} + 4by_1$$

$$B_2 = \frac{t_1 A_1 + 2(A_2 + A_3)}{(t_1 + 2h_1)^2} + \frac{2t_1(A_4 + A_5) + t_1^2 A_5 + 4A_6}{(t_1 + 2h_1)^3}$$

$$B_3 = \frac{(A_2 + A_3) - h_1 A_4}{(t_1 + 2h_1)} + \frac{t_1(A_4 + A_5) - 2h_1(t_1 + h_1)A_5 + 2A_6}{(t_1 + 2h_1)^2}$$

$$B_4 = \frac{A_6 + h_1^2 A_5 - h_1(A_4 + A_5)}{(t_1 + 2h_1)}$$

$$B_5 = \frac{b'A_7}{b't_1 + 2bh_1}, \quad B_6 = 8bk$$

$$A_1 = 8\mu v, \quad A_2 = 2\mu v h_1, \quad A_3 = \frac{P_m h_1}{L_1}$$

$$A_4 = \frac{6\mu v h_1 b}{b'}, \quad A_5 = 6\mu v, \quad A_6 = \frac{P_m h_1^2 h_1 b}{b'L_1}$$

$$A_7 = \frac{2\mu v b}{b'}$$

RESULTS

A number of sample calculations have been made using equations derived in foregoing section to show,

(a) the dependence of pressure generation and other parameters on geometry of the unit

(b) the influence of fluid viscosity and drawing speed on the process

The standard input data used was

Inlet length, L₁ = 90 mm; Outlet length, L₂ = 30 mm;

Initial thickness, t₁ = 1.58 mm; Initial width,

w₁ = 12.68 mm

Initial gap, h₁ in section A = 0.5 mm

Final gap, h₂ in section A = 0.02 mm

Initial and final gap, h, in section B = 0.5 mm

Initial yield stress, y₁ = 50 MNm⁻²

Material strain hardening constant, K = 700 MNm⁻²

Initial viscosity, μ = 100 NSm⁻²

Discussion

Figures 3, 4, 5 demonstrate the effect of fluid viscosity on the generated maximum pressure, initiation of yielding and the percentage reduction in area of the strip respectively. These figures suggest that using a more viscous fluid the plastic region could be increased and which in turn will cause significantly more deformation.

The effect of gap ratio (initial gap) on the percentage reduction in area is presented in Fig 6. These results demonstrate that variation in gap ratio has little effect on the total attainable reduction in area but it limits the range of drawing speeds. The distribution of axial stress at various drawing speeds is presented in Fig 7.

Conclusion

- 1 The predicted combined effect of hydrodynamic pressure and axial stress are sufficiently high enough to induce plastic yielding of the material.
- 2 The achieved reduction in area is dependent on the geometry of DRU and the viscosity of the pressure medium.

Finally the analysis presented in this paper leads to the prediction that a reduction in area of rectangular and square sections in the excess of 40 percent could be achieved by using this novel technique.

REFERENCES

- 1 G R Symmons, M S J Hashmi and H Parvinmehr. 'Plasto hydrodynamic, dieless wire drawing. Theoretical treatment and experimental results'.
 - International Conference on Development in Drawing of Metals, Metal Society, 1982, London.
 - 2 G R Symmons, M S J Hashmi and Y Xie. 'The optimisation of a plasto hydrodynamic wire drawing process'
 - Proc IASTED Int Symp Identification, Modelling and Simulation, Paris, June 22-24, 1987.
 - 3 M S J Hashmi and G R Symmons. 'A mathematical model for the drawing of a solid continuum through Newtonian fluid filled tubular orifice'.
 - 4th International Conference Mathematical Modelling in Science and Technology, Zurich, 1983.
 - 4 M S J Hashmi, G R Symmons and H Parvinmehr. 'A novel technique of wire drawing'.
- J of Mech Eng Science. Vol: 24, No 1, 1982.

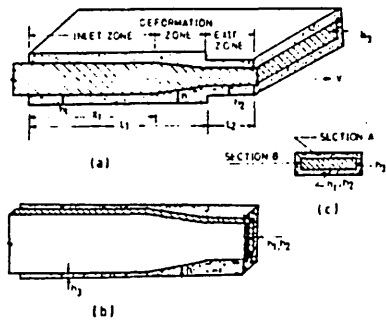


FIG.1 Schematic diagram of the process
 (a) Zones and deformation profile for thickness
 (b) Deformation profile for width
 (c) Sections A and B

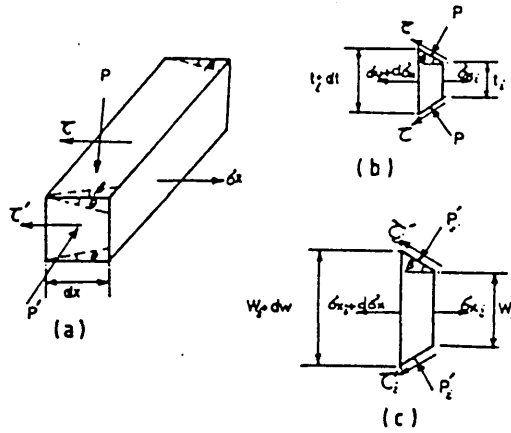


FIG.2
 (a) Stresses acting on a small element
 (b) Stresses acting on width face
 (c) Stresses acting on thickness face

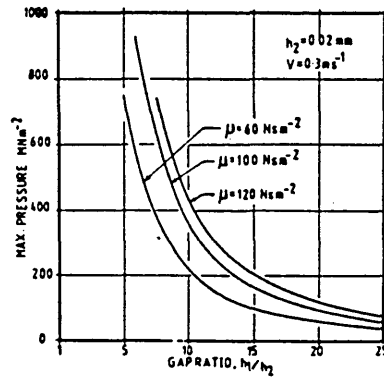


FIG.3 Effect of Viscosity on maximum pressure vs Gap ratio

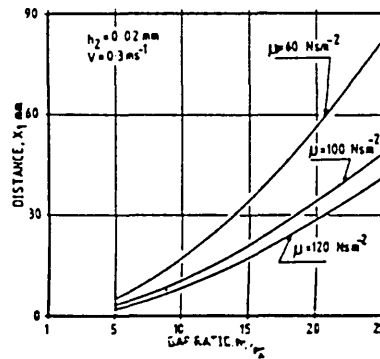


FIG.4 Effect of viscosity on yielding point vs gap ratio

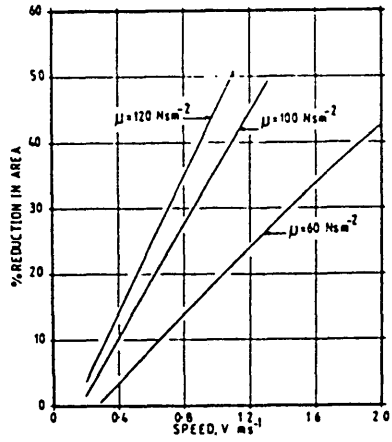


FIG.5 Effect of Viscosity on percentage reduction in Area vs Speed

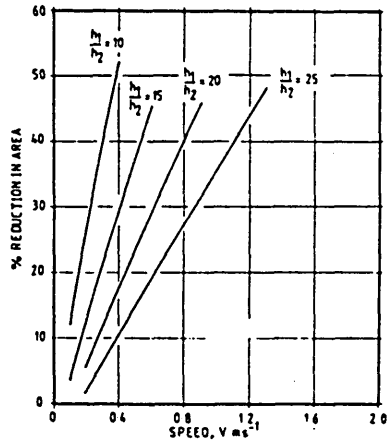


FIG.6 Effect of gap ratio on percentage reduction in area vs speed

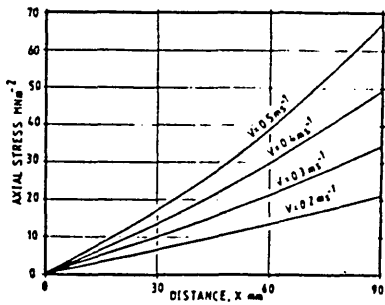


FIG.7 Effect of speed on axial stress along the unit

THERMAL EFFECT ON A PLASTO-HYDRODYNAMIC STRIP DRAWING PROCESS
USING A POLYMER MELT

G R SYMMONS*, A H MEMON*, R CRAMPTON*, M S J HASHMI+

* Department of Mechanical and Production Engineering
Sheffield City Polytechnic, England.

+ School of Mechanical Engineering
National Institute of Higher Education, Dublin, Ireland

ABSTRACT

Plasto-hydrodynamic drawing of circular cross-sectional wire has been modelled in references (1,3&4). The deformation of the wire in this novel process is caused by combined effect of axial pull and radial pressure generated due to hydrodynamic action of a polymer melt. No conventional dies are used in this process and the smallest bore size of the hydrodynamic pressure unit is larger than the undeformed wire, hence no metal to metal contact takes place.

In this study, a mathematical model has been developed to predict the reduction in area of a rectangular cross-sectional narrow strip pulled through a hydrodynamic unit. The effect of the heat generated by mechanical dissipation on the polymer melt during the drawing process is considered by coupling the energy equation into the analysis and allowing the polymer viscosity to be dependant on temperature.

The analytical results enable predictions to be made of the deformation of the strip and the effects of geometry of the hydrodynamic unit and

viscosity of the melt.

INTRODUCTION

Elasto-hydrodynamic drawing is a novel process in which the cross-sectional area of a solid continuum can be reduced and polymer coated without using any conventional reduction die. One of the features of the process is that it is possible to vary the magnitude of the reduction in area of the continuum by changing the drawing speed. In this novel technique the material is deformed plastically by the combined effect of drag force and hydrodynamic pressure generated by the converging flow of a viscous fluid, which is enhanced by using a polymer melt. The dimensions of the reduction unit are larger than the undeformed continuum, hence there is no metal to metal contact, eliminating the problem of frictional wear.

Symmons et al (1) have analysed the process of wire drawing using a stepped bore orifice in conjunction with a polymer melt as a pressure medium. It was assumed that the Polymer melt behaves like a Newtonian fluid and isothermal conditions exist. Hashmi et al (2) presented a paper for drawing a solid continuum through a tapered tubular orifice. Parvinmehr et al (3) developed a non-Newtonian analysis for die-less wire drawing introducing a critical shear stress limit in his analysis. Symmons et al (4) modified analysis presented in reference 1 and included the pressure dependence of the melt viscosity of exponential form. Memon (5) conducted a theoretical treatment of the process for a rectangular cross-sectional strip drawing, assuming Newtonian fluid flow and isothermal conditions to exist.

In all previous theoretical models reviewed above, the assumption of isothermal conditions prevails, and the effect of the heat generation due to plastic deformation of the material and viscous shear friction had been ignored. This is of importance in many cases where the heat generated may produce significant temperature variations and associated large viscosity variations. The viscosity of the melt is a vital factor affecting shear stress and hydrodynamic pressure, which in turn will effect the obtainable reduction in area and polymer coating thickness.

It can be seen from the data (reference 6) indicating the temperature dependence of polymer melt viscosity at a constant stress and pressure that increasing a temperature by 40° C the melt viscosity of different polymers is changed by a factor from 2-15.

An attempt has been made in the present investigation to include the viscosity-temperature dependence and the process has been analysed theoretically for strip drawing. The main assumptions regarding to the mode of plastic deformation are the same as used in reference 5.

The theoretical results are presented in graphical form demonstrating the effect of different operating conditions on the hydrodynamic pressure, the axial stress in the strip and the reduction in area.

ANALYSIS

The analysis is based upon the geometrical configuration shown in figure 1. To formulate the expressions for different parameters the following assumptions were made in addition to those used in reference 5.

1. The temperature in the fluid is constant along the direction of flow but varies in the section of polymer melt that is

$$T = T(y) \text{ in Section A and } T = T(z) \text{ in Section B.}$$

2. The viscosity temperature dependence is given by equation

$$\mu = \mu_0 e^{-\alpha T}$$

where μ_0 is the initial viscosity at a reference temperature.

Determination of maximum pressure prior to deformation

The basic equations for a Newtonian flow are

$$\tau = \mu \frac{\partial u}{\partial y} \quad \text{-----} \quad (1)$$

$$\frac{\partial p}{\partial x} = \frac{\partial \tau}{\partial y} \quad \text{-----} \quad (2)$$

$$\therefore \frac{\partial u}{\partial y} = \frac{1}{\mu} \frac{\partial p}{\partial x} + \frac{C_1}{\mu} \quad \text{-----} \quad (3)$$

Combining equations (1) and (2), the velocity distribution equation, introducing viscosity as a function of 'y' ie $\mu = \mu(y)$, is given by

$$u = \left(\frac{\partial p}{\partial x}\right)_1 \int_0^{y'} \frac{y'}{\mu(y')} dy' + C_1 \int_0^{y'} \frac{dy'}{\mu(y')} + C_2 \quad \text{-----} \quad (4)$$

where C_1 and C_2 are constants of integration and can be evaluated by applying boundary conditions that $u = 0$ at $y = h_1$ and $u = U_1$ at $y = 0$.

The flow rate in the inlet zone is given by

$$Q_1 = \left(\frac{\partial p}{\partial x}\right)_1 (h_1 K_1 - K_2) + C_1 (h_1 K_0 - K_1) + U_1 h_1 \quad \text{-----} \quad (5)$$

$$\text{where } C_1 = - \frac{U_1 + K_1 \left(\frac{\partial p}{\partial x}\right)_1}{K_0} \quad \text{-----} \quad (6)$$

$$\text{and } K_n = \int_0^{h_1} \frac{y'^n dy'}{\mu(y')} \quad , n = 0, 1, 2 \quad \text{-----} \quad (7)$$

from steady state flow it can be shown that

$$\left(\frac{\partial p}{\partial x}\right)_1 = \frac{P_m}{L_1} \quad \text{-----} \quad (8)$$

In the similar way equation for flow rate Q_2 in exit zone can be determined and by equating $Q_1 = Q_2$ the equation for maximum pressure P_m at step when no deformation occurs can be determined and is given by

$$P_m = \frac{U_1 L_1 L_2 (K_1' K_0 - K_1 K_0')}{K_0' L_2 (K_1^2 - K_2 K_0) + K_0 L_1 (K_1'^2 - K_2' K_0')} \quad \text{-----} \quad (9)$$

$$\text{where } K_n' = \int_0^{h_2} \frac{y'^n dy'}{\mu(y')} \quad , n = 0, 1, 2 \quad \text{-----} \quad (10)$$

From equations (1) and (2), the equation for shear stress in the inlet zone at the surface of strip can be established by using boundary conditions that $\tau = \tau_1$ at $y = 0$

$$\tau_1 = - \frac{1}{K_0} \left(U_1 + \frac{K_1 P_m}{L_1} \right) \quad \text{-----} \quad (11)$$

To determine the parameter K_n and K'_n , the energy equation has been used which in reduced form considering thermal energy generated by viscous friction is given by

$$H \frac{d^2 T}{dy^2} = - \mu \left(\frac{du}{dy} \right)^2 \quad \text{-----} \quad (12)$$

Substituting for C_1 equation (3) gives

$$\frac{du}{dy} = \frac{1}{\mu} \left(\frac{dp}{dx} \right) y - \frac{U_1 + K_1 \left(\frac{\partial p}{\partial x} \right)}{\mu K_0} \quad \text{-----} \quad (13)$$

For the present applications, here the following assumptions are made that $U_1 \gg K_1 \frac{\partial p}{\partial x}$ and $U_1 \gg \frac{1}{\mu} \frac{\partial p}{\partial x} y$ hence from equation (13)

$$\therefore \frac{du}{dy} = - \frac{U_1}{\mu K_0}$$

Substituting this value of $\frac{du}{dy}$ into equation (12)

$$\frac{d^2 T}{dy^2} = - \frac{U_1^2}{H \mu K_0^2} \quad \text{-----} \quad (14)$$

Integrating the above equation, and introducing viscosity - temperature relationship with a boundary condition that $T = 0$ at $y = h_1$

$$\left(\frac{dT}{dy} \right)^2 = D_1 (B - e^{\alpha T}) \quad \text{-----} \quad (15)$$

$$\therefore \frac{dT}{dy} = + \sqrt{D_1} (B - e^{\alpha T})^{\frac{1}{2}} \quad 0 < y < \frac{h_1}{2} \quad \text{-----} \quad (16)$$

$$\frac{dT}{dy} = - \sqrt{D_1} (B - e^{\alpha T})^{\frac{1}{2}} \quad h_1 < y < h_1 \quad \text{-----} \quad (17)$$

$$\text{where } D_1 = \frac{2U_1^2}{\alpha H \mu_0 K_0^2} \quad \text{-----} \quad (18)$$

$$B = 1 + \frac{\alpha \mu_0 U_1^2}{8H} \quad \text{-----} \quad (19)$$

by symmetry $\frac{dT}{dy} = 0$ at $y = \frac{h_1}{2}$ ie T reaches maximum value T_m Hence from equation (15)

$$T_m = \frac{1}{\alpha} \ln B \quad \text{-----} \quad (20)$$

Rearranging equation (16) and integrating

$$\frac{1}{\alpha \sqrt{B}} \ln \left| \frac{\sqrt{B-e^{\alpha T}} - \sqrt{B}}{\sqrt{B-e^{\alpha T}} + \sqrt{B}} \right| = \sqrt{D_1} y + C_3 \quad \text{----- (21)}$$

Applying boundary condition that $T = T_m$ at $y = \frac{h_1}{2}$

$$C_3 = -\frac{h_1}{2} \sqrt{D_1} \quad \text{----- (22)}$$

Again applying boundary condition that $T = 0$ at $y = 0$

$$C_3 = \frac{1}{\alpha \sqrt{B}} \ln \left| \frac{\sqrt{B-1} - \sqrt{B}}{\sqrt{B-1} + \sqrt{B}} \right| \quad \text{----- (23)}$$

Equating equations (22) and (23) and simplification gives

$$\frac{h_1}{2} = -\frac{1}{\alpha \sqrt{D_1 B}} \ln \left| \frac{\sqrt{B-1} - \sqrt{B}}{\sqrt{B-1} + \sqrt{B}} \right| \quad \text{----- (24)}$$

Substituting value of A_1 from equation (18) into equation 24 gives

$$K_0 = \frac{\sqrt{\frac{BU^2_1 h^2 \alpha}{2H \mu_0}}}{\ln \left| \frac{\sqrt{B-1} + \sqrt{B}}{\sqrt{B-1} - \sqrt{B}} \right|} \quad \text{----- (25)}$$

Substituting value for C_3 from equation (23) into equation (21)

$$y = \frac{1}{\alpha \sqrt{D_1 B}} \ln \left| \frac{\sqrt{B-e^{\alpha T}} - \sqrt{B}}{\sqrt{B-e^{\alpha T}} + \sqrt{B}} \right| - \frac{1}{\alpha \sqrt{D_1 B}} \ln \left| \frac{\sqrt{B-1} - \sqrt{B}}{\sqrt{B-1} + \sqrt{B}} \right| \quad \text{----- (26)}$$

for $0 < y < \frac{h_1}{2}$

In similar way from equation (17) with boundary condition $T = 0$ at $y=h_1$.

$$y = -\frac{1}{\alpha\sqrt{D_1B}} \ln \left| \frac{\sqrt{B-e^{\alpha T}} - \sqrt{B}}{\sqrt{B-e^{\alpha T}} + \sqrt{B}} \right| - \frac{1}{\alpha\sqrt{D_1B}} \ln \left| \frac{\sqrt{B-1} - \sqrt{B}}{\sqrt{B-1} + \sqrt{B}} \right| \quad \text{-----} \quad (27)$$

for $\frac{h_1}{2} < y < h_1$

From equation (6)

$$K_1 = \int_{\frac{h_1}{2}}^{h_1} \frac{y \, dy}{\mu(y)} + \int_{\frac{h_1}{2}}^{h_1} \frac{y \, dy}{h_1 \mu(y)} \quad \text{-----} \quad (28)$$

$$K_2 = \int_{\frac{h_1}{2}}^{h_1} \frac{y^2 \, dy}{\mu(y)} + \int_{\frac{h_1}{2}}^{h_1} \frac{y^2 \, dy}{h_1 \mu(y)} \quad \text{-----} \quad (29)$$

Substituting value of $\mu = \mu_0 e^{\alpha T}$ and for dy from equation (16), y from equation (26) in the first term; for dy from equation (17) and y from equation (27) in the second term; the integration of the equation (28) with the appropriate limits gives

$$K_1 = \frac{4\sqrt{B-1}}{\alpha^2 \mu_0 D_1 \sqrt{B}} \ln \left| \frac{\sqrt{B-1} + \sqrt{B}}{\sqrt{B-1} - \sqrt{B}} \right| \quad \text{-----} \quad (30)$$

Similarly substituting the respective values of μ , y , dy into equation (29), simplifying and integrating

$$K_2 = 2 \int_0^{T_m} \frac{e^{\alpha T}}{\sqrt{D_1} \sqrt{B-e^{\alpha T}} \alpha^2 \mu_0 D_1 B} \left[\ln \left| \frac{\sqrt{B-e^{\alpha T}} - \sqrt{B}}{\sqrt{B-e^{\alpha T}} + \sqrt{B}} \right| \right]^2 dT$$

$$+ \frac{4\sqrt{B-1}}{\alpha^3 D_1 B \sqrt{D_1} \mu_0} \left[\ln \left| \frac{\sqrt{B-1} - \sqrt{B}}{\sqrt{B-1} + \sqrt{B}} \right| \right]^2 \quad \text{-----} \quad (31)$$

The first part of the equation (31) on right hand side could be solved by numerical integration. Similarly values for K_A^H and K_B^H can be obtained for exit zone in Section A and for Section B respectively.

Shear Stress in Section B is given by

$$\tau_3 = -\frac{1}{K_0''} \left(U_1 + \frac{K_1' P_m}{L_1} \right) \quad \text{-----} \quad (32)$$

Prediction of Yielding Point

Assuming that generated hydrodynamic pressure acts equally in both directions, Von-Mises yield criteria gives

$$\sigma_{x1} + P_1 = y_0 \quad \text{-----} \quad (33)$$

Suppose that yielding starts at a point X_1 distance from entry point. The equilibrium of forces in X direction at this point gives

$$\sigma_{x1} = \frac{2\tau_1 X_1}{t_1} + \frac{2\tau_2 X_1}{W_1} \quad \text{-----} \quad (34)$$

$$\text{Also } P_1 = \frac{P_m}{L_1} X_1 \quad \text{-----} \quad (35)$$

Substituting values of σ_{x1} and P_1 equation (33) will give

$$X_1 = \frac{y_0}{\frac{P_m}{L_1} + \frac{2\tau_1}{t_1} + \frac{2\tau_2}{W_1}} \quad \text{-----} \quad (36)$$

Hydrodynamic Pressure in deformation zone

From equation (5), for gap h_i in deformation zone

$$\frac{d}{dx} \left[h_i^3 \frac{(I_1^2 - I_0 I_2) \left(\frac{dp}{dx} \right)_i}{I_1} \right] = -U_1 \frac{dh_i}{dx} \quad \text{-----} \quad (37)$$

$$\text{Where } J_n = h_i^{n+1} I_n \quad n = 0, 1, 2$$

$$\text{and } J_n = \int_0^{h_i} \frac{y^n dy}{\mu(y)}$$

$$\text{Define } \mu^* = -\frac{I_1}{6(I_1^2 - I_0 I_2)} \quad \text{-----} \quad (38)$$

Equation (37) can be written in the form

$$\frac{d}{dx} \left[h^3 \frac{dp}{dx} \right]_i = 6\mu^* U_1 \frac{dh_i}{dx} \quad \text{-----} \quad (39)$$

Equation (39) is the reduced form of Reynold's equation with variable viscosity μ^* which is assumed to remain constant along the length of unit.

It has been further assumed that the values of J_n and I_n in the deformation zone are same as those before deformation. With these assumptions the value of μ^* can be calculated from equation (38)

Defining the deformation profile be given by

$$h_i = h_1 + bx \quad \text{-----} \quad (40)$$

Integration of equation (39) with appropriate boundary conditions will give

$$P_i = \frac{6\mu^* U_1}{b} \left[\frac{h_1}{2(h_1+bx)^2} - \frac{1}{(h_1+bx)} + \frac{1}{2h_1} \right] + \frac{P_m}{L_1} \left[XI + \frac{h_1}{2b} - \frac{h_1^2}{2b(h_1+bx)^2} \right] \quad \text{-----} \quad (41)$$

Axial Stress in deformation zone

$$\text{Now } h_i = h_1 + bx \quad \text{-----} \quad (42)$$

$$h'_i = h_3 + b'x \quad \text{-----} \quad (43)$$

$$t_i = t_1 - 2bx \quad \text{-----} \quad (44)$$

$$W_i = W_1 - 2b'x \quad \text{-----} \quad (45)$$

Figure (2a) shows a small element isolated from the deformation zone.

With the assumption $p_i = p'_i$, Von-Mises flow rule will give

$$\frac{dw}{W_i} = \frac{dt}{t_i} \quad \text{-----} \quad (46)$$

$$\text{and } b' = mb \quad \text{-----} \quad (47)$$

$$\text{where } m = \frac{W_1}{t_1}$$

The equation for velocity distribution in the deformation zone is

$$u = \frac{1}{\mu^*} \left(\frac{\partial p}{\partial x} \right)_i \frac{y^2}{2} + \frac{C_4}{\mu^*} + C_5 \quad \text{-----} \quad (48)$$

Where C_4 and C_5 are constants and can be obtained by applying boundary conditions, and shear stress at the surface of strip along width face in deformation zone is given by

$$\tau_i = -\frac{h_i}{2} \left(\frac{\partial p}{\partial x} \right)_i - \frac{\mu^* U_1}{h_i} \quad \text{-----} \quad (49)$$

Substituting values of h_i and $\left(\frac{\partial p}{\partial x} \right)_i$ from equations (42) and (39) respectively into equation (49)

$$\tau_i = -\frac{\mu^* U_1}{(h_1 + bx)^2} \times \left(4bx + h_1 + \frac{Pmh^3_1}{2\mu^* U_1 L_1} \right) \quad \text{-----} \quad (50)$$

And the shear stress along thickness face is given by

$$\tau'_i = -\frac{(h_1 + bx)}{2} \left[\frac{6\mu^* U_1 bx}{(h_1 + bx)^3} + \frac{Pm(h^3_1)}{L_1 (h_1 + bx)^3} \right] - \frac{\mu^* U_1}{(h_1 + bx)} \quad \text{-----} \quad (51)$$

The force equilibrium in x-direction for small element shown in figure (2) gives

$$d\sigma_{x_i} = \frac{2b dx}{t_1 - 2bx} \left[2Y_i - \frac{\tau_i}{b} - \frac{\tau'_i}{b'} \right] \quad \text{-----} \quad (52)$$

Where Y_i is the current value of yield stress.

Assuming non-linear strain hardening

$$Y_i = y_0 + A \epsilon^n = y_0 + A \left[\ln \left(\frac{a}{a_i} \right) \right]^n = y_0 + 2^n A \left[\ln \left(\frac{t_1}{t_i} \right) \right]^n \quad \text{-----} \quad (53)$$

Substituting for Y_i , τ_i , τ'_i integration w.r.to x of equation (52) will give

$$\begin{aligned} \sigma_{x_i} = & \frac{B_1}{2b} \ln \left(\frac{t_1}{t_i} \right) + \frac{B_2}{b} \ln \left(\frac{h_i}{h_1} \right) + \frac{B_3}{b} \left(\frac{1}{h_1} - \frac{1}{h_i} \right) + \frac{B_4}{2b} \left(\frac{1}{h_1^2} - \frac{1}{h_i^2} \right) \\ & + \frac{B_5}{b'} \ln \left(\frac{h_i'}{h_3} \right) + \frac{B_6}{2b(n+1)} \left[\ln \left(\frac{t_1}{t_i} \right) \right]^{n+1} + \sigma_{x_1} \quad \text{-----} \quad (54) \end{aligned}$$

$$\text{where } B_1 = \frac{2t_1 A_1 + 4(A_2 + A_4)}{(t_1 + 2h_1)^2} + \frac{4t_1(A_4 + A_7) + 2t_1^2 A_5 + 8A_6}{(t_1 + 2h_1)^3} + \frac{2bA_8}{bt_1 + 2bh_3} + A_9$$

$$B_2 = \frac{t_1 A_1 + 2(A_2 + A_4)}{(t_1 + 2h_1)^2} + \frac{2t_1(A_4 + A_7) + t_1^2 A_5 + 4A_6}{(t_1 + 2h_1)^3}$$

$$B_3 = \frac{A_2 + A_4 - A_1 h_1}{(t_1 + 2h_1)} + \frac{t_1(A_4 + A_7) - 2A_5 h_1(t_1 + h_1) + 2A_6}{(t_1 + 2h_1)^2}$$

$$B_4 = \frac{A_6 + A_5 h_1^2 - (A_4 + A_7) h_1}{(t_1 + 2h_1)}$$

$$B_5 = \frac{b' A_8}{(b' t_1 + 2bh_3)} \quad , \quad B_6 = 2^{n+2} bA$$

$$\text{And } A_1 = 8\mu^* U_1$$

$$A_2 = 2\mu^* U_1 h_1$$

$$A_3 = \frac{Pmh^3_1}{L_1}$$

$$A_4 = \frac{6\mu^* U_1 b h_3}{b'}$$

$$A_5 = 6\mu^* U_1$$

$$A_6 = \frac{Pmh^3_1 h_3 b}{b' L_1}$$

$$A_7 = \frac{Pmh^3_1}{L_1}$$

$$A_8 = \frac{2\mu^* U_1 b}{b'}$$

$$A_9 = 4bY_0$$

Prediction of Percentage reduction in area

Again using Von-Mises yield criteria, the deformation will occur when the equation

$$P_i + \sigma x_i = Y_i \quad \text{-----} \quad (55)$$

is satisfied.

It is assumed that the deformation ceases at $x = L_1 - X_1$, the values of P_i and σx_i and Y_i are substituted into equation (55) from equations (41) and (54) and (53) respectively. The parameter 'b' is the only unknown parameter for a given drawing speed and the unit geometry. Equation (55) may be iterated to establish the value of b: Once this value is established, the reduction in area at any point for $X_1 < X < L_1$ is given by

$$\text{PRA} = \left(1 - \frac{W_i t_i}{W_1 t_1}\right) \times 100 \quad \text{-----} \quad (56)$$

RESULTS AND DISCUSSION

Equations derived in previous section were solved on computer using the following data

$$\begin{array}{lll} h_1 = 0.24\text{mm} & , & h_2 = 0.02\text{mm} & , & h_3 = 0.3\text{mm} \\ L_1 = 120\text{mm} & , & L_2 = 30\text{mm} & , & \mu_0 = 100 \text{ Nsm}^{-2} \\ y_0 = 6 \text{ MNm}^{-2} & , & A = 70 \text{ MNm}^{-2} & , & n = 0.54 \\ \tau_1 = 1.59\text{mm} & , & W_1 = 12.5\text{mm} & , & \alpha = 0.3/\text{K} \\ H = 0.2 \text{ W/mK} & & & & \end{array}$$

Results obtained from computer were in tabular form and are presented in graphical form in figures(3-9).

The predicted percentage reduction in area of strip is shown in figures (3-5). The characteristic feature of these figures is a critical speed for each set of conditions. Any increase in the speed beyond that value causes a decrease in obtainable reduction. These figures also demonstrate the possible effect of the gap ratio, thermal conductivity and temperature dependance coefficient on the attainable reduction.

Figures (6-9) present the results showing the effect of thermal conductivity and temperature dependence coefficient of the polymer melt on pressure and axial stress at the step. These figures suggest that these parameters have little effect on the pressure but they effect significantly on the axial stress, which is consistent with the obtainable reduction in area.

Conclusions

The results obtained from the present analysis suggest that

- 1 It is possible to get a reduction of more than 30% in area of the strip by applying this novel technique.
- 2 There is a critical value of speed and beyond that value the achieved reduction starts to decrease.
- 3 More reduction could be achieved using a fluid of higher thermal conductivity and lower value of temperature dependence coefficient.

Notations

L	=	Length of unit
h	=	Gap between the strip and die less unit
t	=	Thickness of the strip
W	=	Width of the strip
x	=	Distance along the unit
μ	=	Viscosity of the polymer
μ^*	=	Viscosity in the reduced Reynolds equation
α	=	Viscosity temperature dependency constant
H	=	Thermal conductivity of polymer melt
Y	=	Yield stress of the strip material
A	=	Strain hardening constant
n	=	Strain hardening index
u	=	Polymer melt velocity
P	=	Pressure at any point within DRU
τ	=	Shear stress on strip surface

σ_x = Axial Stress
 b = Factor determining theoretical deformation profile for thickness
 b' = Factor determining theoretical deformation profile for width
 X_1 = Point of yielding
 RH = Gap ratio, h_1/h_2
 PRA = Percentage reduction in area
 subscript i = relates to deformation zone
 C_1, C_2, \dots, C_6 are constants of integration
 $Kn, K\dot{\epsilon}, KH, B, D_1$ and I_n are computation variables

References

- 1 G R Symmons, M S J Hashmi and H Parvinmehr
 'Plasto hydrodynamic die less wire drawing: Theoretical treatment and experimental results.'
 Proc. Int. Conf. on developments in drawing of metal, Metal Society, London May 1983.
- 2 M S J Hashmi, G R Symmons
 'A mathematical model for drawing of a solid continuum through Newtonian fluid filled tubular orifice.'
 Proc. 4th Int. Conf. on Mathematical modelling, Zurich August 1983.
- 3 H Parvinmehr, G R Symmons and M S J Hashmi
 'A Newtonian plasto hydrodynamic analysis of die less wire drawing process using a stepped bore unit.'
 Int. Jr. Mech. Sci. Vol. 29 No 4, 1987.
- 4 G R Symmons, M S J Hashmi, Y D Xie
 'The optimisation of a plasto hydrodynamic wire drawing process.'
 Presented at sixth IASTED conference, Paris June 1987.

- 5 G R Symmons, A H Memon, M S J Hashmi
'A Newtonian model of a plasto hydrodynamic drawing process of a
rectangular cross-sectional continuum.'
Presented at seventh IASTED conference
February 17-19 Grindelwald, Switzerland, 1988
- 6 Thermoplastics Properties and Design,
A collective work by ICI Plastics division
by R M Ogorockiewicz, p. 185.

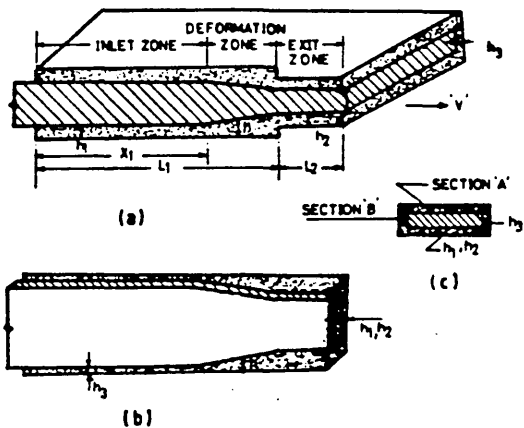


FIG 1 Schematic diagram of the process

- (a) Zones and deformation profile for thickness
- (b) Deformation profile for width
- (c) Sections A and B

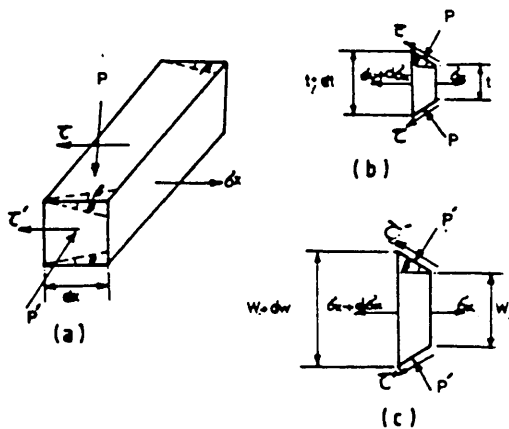


FIG 2 Stresses acting on a small element

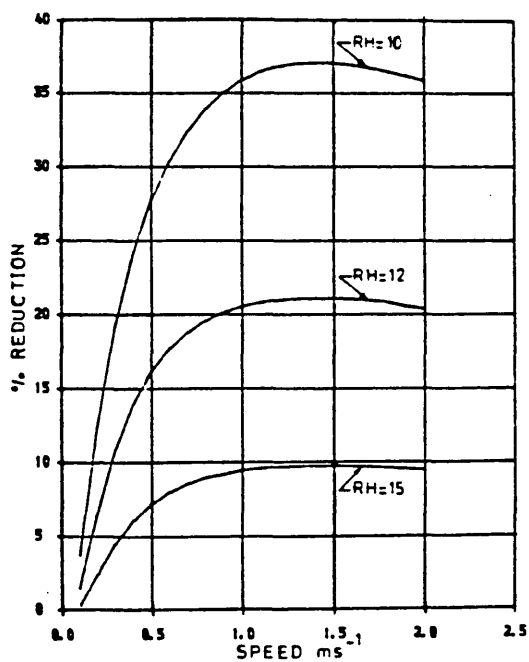


FIG 3 Effect of gap ratio, RH, on percentage reduction in Area v/s speed

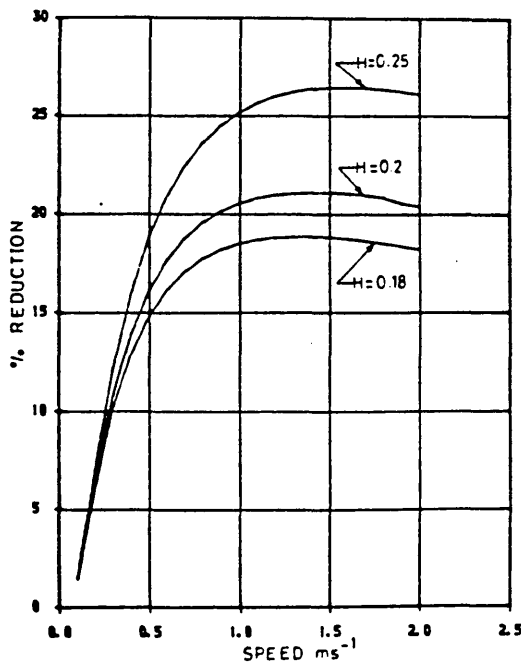


FIG 4 Effect of thermal conductivity, H, on percentage reduction in Area v/s speed

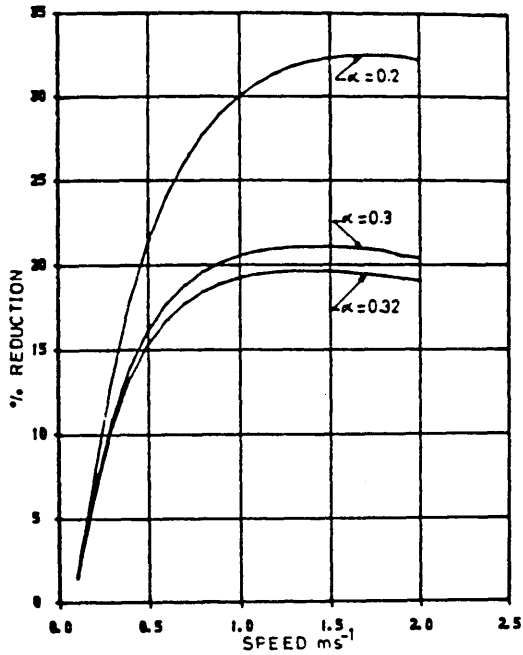


FIG 5 Effect of temperature dependence coefficient, α , on percentage reduction in Area v/s speed

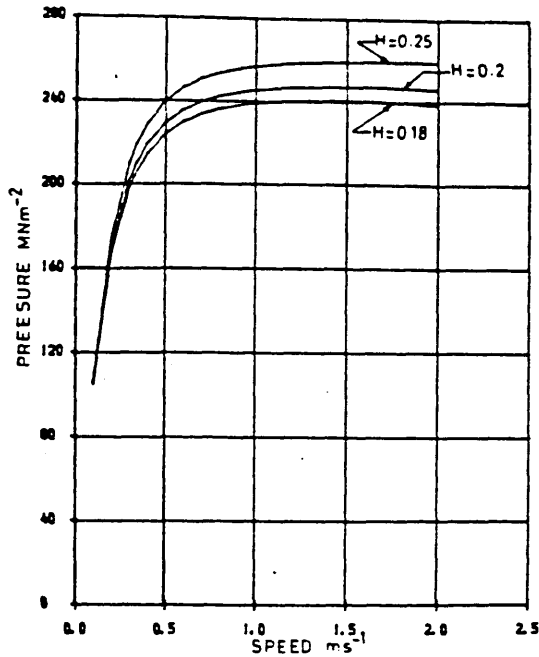


FIG 6 Effect of thermal conductivity, H , on maximum pressure at step after deformation v/s speed

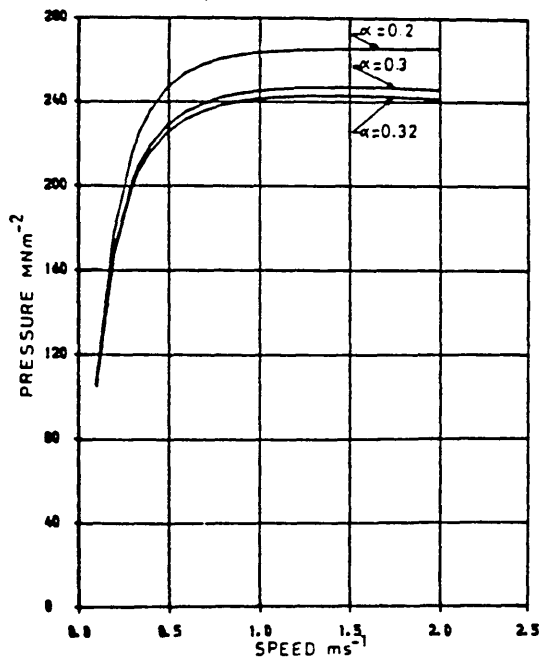


FIG 7 Effect of temperature dependence coefficient, α , on maximum pressure and step after deformation v/s speed.

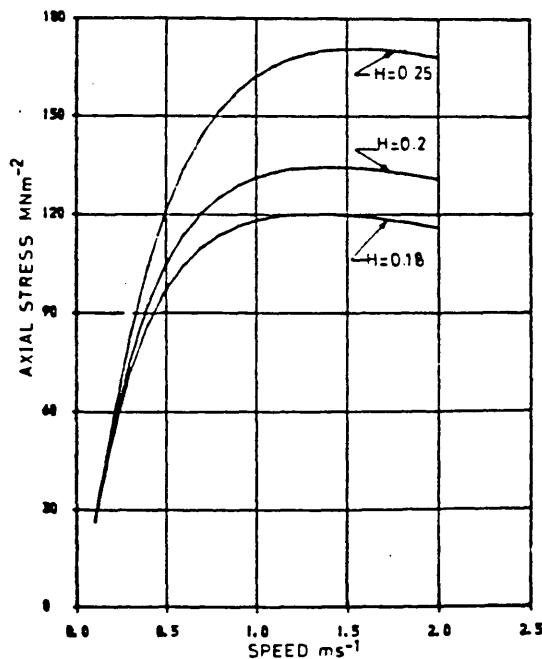


FIG 8 Effect of thermal conductivity, H , on axial stress at step v/s speed

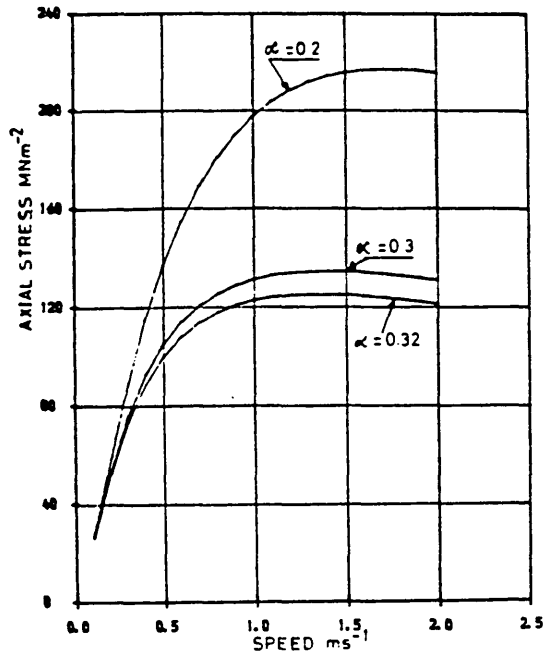


FIG 9 Effect of temperature dependence coefficient, α , on axial stress at step v/s speed